



University  
of Glasgow

<https://theses.gla.ac.uk/>

Theses Digitisation:

<https://www.gla.ac.uk/myglasgow/research/enlighten/theses/digitisation/>

This is a digitised version of the original print thesis.

Copyright and moral rights for this work are retained by the author

A copy can be downloaded for personal non-commercial research or study,  
without prior permission or charge

This work cannot be reproduced or quoted extensively from without first  
obtaining permission in writing from the author

The content must not be changed in any way or sold commercially in any  
format or medium without the formal permission of the author

When referring to this work, full bibliographic details including the author,  
title, awarding institution and date of the thesis must be given

Enlighten: Theses

<https://theses.gla.ac.uk/>  
[research-enlighten@glasgow.ac.uk](mailto:research-enlighten@glasgow.ac.uk)

**DESIGN APPROXIMATIONS FOR  
OFFSHORE TUBULARS AGAINST COLLISIONS**

**Volume I**

by

**Sang - Rai Cho**

**B.Sc., M.Sc., C. Eng., MRINA**

**A Thesis Submitted for the Degree of  
Doctor of Philosophy  
in the Faculty of Engineering in Glasgow University**

**December, 1987**

ProQuest Number: 10997383

All rights reserved

INFORMATION TO ALL USERS

The quality of this reproduction is dependent upon the quality of the copy submitted.

In the unlikely event that the author did not send a complete manuscript and there are missing pages, these will be noted. Also, if material had to be removed, a note will indicate the deletion.



ProQuest 10997383

Published by ProQuest LLC (2018). Copyright of the Dissertation is held by the Author.

All rights reserved.

This work is protected against unauthorized copying under Title 17, United States Code  
Microform Edition © ProQuest LLC.

ProQuest LLC.  
789 East Eisenhower Parkway  
P.O. Box 1346  
Ann Arbor, MI 48106 – 1346

## To the Memory of my Mother



## Acknowledgements

My warmest thanks are due

- To my supervisor, Prof. Douglas Faulkner, Head of the Department of Naval Architecture and Ocean Engineering, for his guidance and care throughout the course and for his help to get a research scholarship of Glasgow University,
  - To Dr. Paul A. Frieze, formerly senior lecturer in the Department of Naval Architecture and Ocean Engineering, for his supervision in the early stage of this work and for his concern after leaving the department,
  - To Messrs. Cameron Miller and Robert McLetchie, technicians of the Mechanical Workshop, and Mr. Robert B. Christison, chief technician of the Hydrodynamics Laboratories, for their assistance during the execution of the experimental programme and Mrs. Ruth Young, tracer of the Faculty of Engineering, for her preparing many of the figures,
  - To my colleagues at Ulsan University and all of my friends for their continual encouragement,
- And finally,
- To all of my families for their endurance and financial and vital moral support.

Sang-Rai Cho,  
Glasgow,  
December 1987.

## CONTENTS

<b>Volume I</b>	<b>page</b>
<b>Acknowledgements</b>	<b>iii</b>
<b>Summary</b>	<b>1</b>
<b>Notation</b>	<b>3</b>
<b>Chapter 1 INTRODUCTION AND LITERATURE REVIEW</b>	<b>10</b>
1.1 Introduction	10
1.2 Literature Review	12
1.2.1 Probability of Collision	13
1.2.1.1 Historical Records	13
1.2.1.2 Prediction Model	14
1.2.2 Collision Mechanics	17
1.2.2.1 Static Approach	17
1.2.2.2 Dynamic Approach	18
1.2.3 Dynamic Response of a Beam	19
1.2.4 Force-Deformation Characteristics of Platform	22
1.2.4.1 Theoretical Works	22
1.2.4.2 Experimental Works	24
1.2.5 Residual Strength of Damaged Structures	25
1.2.6 Design Codes	28
1.3 Aim of the Thesis	30
1.4 Layout of the Thesis	31
<b>Chapter 2 LATERAL IMPACT TESTS</b>	<b>33</b>
2.1 Introduction	33
2.2 Test Models and Pre-Test Measurements	34
2.2.1 Choice of Model Parameters	34
2.2.2 Heat-Treatment	35
2.2.3 Pre-Test Measurements	36
2.3 Lateral Impact Tests	41
2.3.1 Test Rig	41

2.3.2	Measurements and Recording	42
2.3.3	Model Installation	44
2.3.4	Extent of Damage Measurements	44
2.4	Results	45
2.4.1	Pre-Test Measurements	45
2.4.2	Impact Tests	49
2.5	Geometric Configuration of Damaged Tubulars	59
2.5.1	Description of Dent Section	60
2.5.2	Extent of Damage	64
2.6	Discussion	66
 <b>Chapter 3 DYNAMIC RESPONSE OF A TUBULAR UNDER LATERAL IMPACT</b>		 71
3.1	Introduction	71
3.2	Spring-Mass Model with Two Degree-of-Freedom	76
3.2.1	Equations of Motion	76
3.2.2	Integration of Equation of Motion	79
3.3	Equivalent Masses and Equivalent Spring Coefficients	84
3.3.1	Equivalent Masses	84
3.3.2	Equivalent Spring Coefficients	85
3.3.2.1	Spring Coefficient for Local Denting	85
3.3.2.2	Spring Coefficient for Overall Bending	87
3.3.3	Modification Factor for Dynamic Effects	91
3.4	Solution Scheme	94
3.4.1	Algorithm for Step by Step Solution	94
3.4.2	Selection of Time Step	96
3.5	Results and Discussion	97
 <b>Chapter 4 ULTIMATE STRENGTH TESTS</b>		 111
4.1	Introduction	111
4.2	Models and End Fittings	112
4.2.1	Extent of Damage Range	114
4.2.2	Strain-Gauging	114
4.2.3	End Fittings	116

4.3	Testing Procedures and Measurements	116
4.3.1	Axial Compression Tests	116
4.3.2	Combined Axial Compression and hydrostatic Pressure Tests	118
4.4	Results and Discussion	121
4.4.1	Collapse Loads	123
4.4.2	LVDT and Strain-Gauge Results	124
4.4.3	Shape of Collapsed Models	151
4.4.4	Collapse Strength of Undamaged Models	151
<b>Chapter 5</b>	<b>RESIDUAL STRENGTH OF DAMAGED TUBULARS</b>	<b>155</b>
5.1	Introduction	155
5.2	$M - P_{ext} - Q_H - \Phi$ Relationships for Dented Tubular Sections	157
5.2.1	Geometry of Dented Cross-Section and Residual Stresses	157
5.2.2	Effect of Hydrostatic Pressure	160
5.2.3	Tangent Stiffness Formulation	162
5.2.4	$M - P_{ext} - Q_H - \Phi$ Data Generation	167
5.2.5	Derivation of Approximate Equations	169
5.3	Residual Strength	170
5.3.1	Effect of Local Shell Deformation	170
5.3.2	Newmark's Integration Method	173
5.4	Correlation Study and Discussion	178
5.4.1	Available Test Data	178
5.4.2	Results of Correlation Study	181
5.4.3	Effect of Local Shell Deformation	183
5.4.4	Effect of Damage Location	185
5.4.5	Effect of Dent Shape	186
<b>Chapter 6</b>	<b>DERIVATION OF DESIGN FORMULAE</b>	<b>187</b>
6.1	Introduction	187
6.2	Extent of Damage due to Lateral Impact	189
6.2.1	Parametric Study	189
6.2.2	Design Equations	190
6.3	Residual Strength of Damaged Tubulars	193
6.3.1	Parametric Study	193

6.3.2	Design Formula	193
6.4	Discussion	195
6.4.1	Extent of Damage	195
6.4.1.1	Proposed Equations	195
6.4.1.2	End Conditions	195
6.4.1.3	Size Effect	196
6.4.1.4	Application Limit	196
6.4.2	Residual Strength	197
6.4.2.1	Proposed Formula	197
6.4.2.2	End Conditions	200
6.4.2.3	Effects of Residual Stresses due to Cold-Rolling and Welding	200
6.4.2.4	Ultimate Strength of Undamaged Tubulars	202
<b>Chapter 7</b>	<b>CONCLUSIONS AND PROPOSALS FOR FUTURE WORK</b>	<b>203</b>
7.1	Conclusions	203
7.2	Proposals for Future Work	210
<b>References</b>		<b>212</b>
<b>Appendix 1</b>	<b>Approximate Equation for Bending Moment - External Axial Compression - Hydrostatic Pressure - Curvature Relationships of Damaged Tubular Cross-Sections</b>	<b>228</b>
<b>Appendix 2</b>	<b>Approximate Formula for Elastic Buckling Pressure of Circular Cylinder under Radial Pressure alone</b>	<b>232</b>
<b>Appendix 3</b>	<b>Derivation of a Strength Formulation for Ring-Stiffened Cylindrical Shells Subjected to Combined Axial Loading and Radial Pressure</b>	<b>238</b>

## Summary

The aim of this study is to derive simple design formulae for estimating the probable extent of damage to offshore tubular members due to lateral impacts, and for evaluating the residual strength of damaged tubular members subjected to combined axial compression and hydrostatic pressure.

Existing models and methods are reviewed for predicting the probability of offshore collisions and consequential probable extents of damage, and for evaluating the residual strength of damaged members.

Lateral impact tests are reported conducted on small-scale tubes having simply supported roller end conditions. The aim of the tests was to provide more realistic experimental information for local denting deformation of the tube wall at the point of impact and overall bending deformation of the tubular member as a beam under lateral impact. A simple numerical model is developed for simulating the dynamic response of a tubular member having simply supported roller end conditions. In the analysis, the tubular member is reduced to a spring-mass system with two degrees-of-freedom, one for local denting and the other for overall bending. Strain-rate sensitivity of the material and other dynamic effects upon the response of the tubular member have been considered by multiplying an empirically derived modification factor to the spring coefficient for overall bending.

Combined axial compression and hydrostatic pressure loading tests are also conducted on damaged tubes whose form of damage are realistic. An analytical method is also developed to evaluate the residual strength of damaged tubular members under combined axial compression and hydrostatic pressure. The method involves two separate phases of calculation : derivation of bending moment - external axial compression - hydrostatic pressure - curvature relationships for dented tubular cross-

sections using the tangent stiffness method; and determination of the residual strength of a damaged tubular member using the bending moment - curvature relationship based on the Newmark integration method.

Rigorous parametric studies are performed using the theoretical models which have been validated with the experimental results obtained from the tests conducted as part of this study and other test data available in the literature. Finally, simple design formulae are derived using the parametric study results. A direct fit is attempted for design equations to predict the probable extent of damage to unstiffened tubular members subjected to lateral impacts, while the Perry formula is adopted as the basis of a formulation to estimate the residual strength of damaged tubular members under combined axial compression and hydrostatic pressure.

Conclusions regarding the experimental and theoretical studies and the proposed design formulae are included, and an extension to this study is proposed in order for the design formulae to directly be applicable to the design of offshore structures against collisions.

An approximate equation is presented in Appendix 1 for bending moment - external axial compression - hydrostatic pressure - curvature relationships of damaged tubular cross-sections.

In Appendix 2 an approximate expression is derived for von Mises elastic buckling pressure of circular cylinder under pure radial pressure

Appendix 3 describes the derivation procedure of a strength formulation for ring-stiffened cylindrical shells under combined axial loading and radial pressure, where the quadratic Merchant - Rankine formula in generalised form is adopted as the basis of the formulation.

Volume II of this thesis is ref.82 and contains the full experimental report and test data for the lateral impact tests.

## Notation

$B$	length of the flattened part of a damaged tubular
$C_s$	correction factor for shell effects defined as eqn.(5.32)
$D$	diameter to mid-thickness of a tube
$D_o$	outside diameter of a tube
$D_{d_{max}}$	maximum outside diameter of a dented section
$D_{d_{min}}$	minimum outside diameter of a dented section
$D_{max}$	maximum diameter to mid-thickness of a tube
$D_{mean}$	mean diameter to mid-thickness of a tube
$D_{min}$	minimum diameter to mid-thickness of a tube
$E$	Young's modulus
$E_D$	energy dissipated plastically due to damage on the struck object, $E_{D_d} + E_{D_b}$
$E_{D_b}$	energy dissipated plastically due to overall bending damage
$E_{D_d}$	energy dissipated plastically due to local denting damage
$E_{D_u}$	maximum possible energy dissipated plastically due to damage on the struck object, $1/2 M_s V_i^2 - 1/2 M_s V_r^2$
$E_e$	maximum possible elastic strain energy of the beam $1/2 (M_p^2 L)/(EI)$
$E_{eff}$	'effective' modulus defined as eqn.(5.19)
$E_k$	initial kinetic energy of the striker, $1/2 M_s V_i^2$
$E_p$	energy absorbed by the platform
$E_s$	energy absorbed by the ship
$E_{sb}$	strain energy absorbed during the formation of local denting
$E_{sd}$	strain energy absorbed during the formation of overall bending
$E_T$	total system energy, defined as eqns.(3.37a) and (3.37b)
$F$	concentrated lateral load applied at midspan
$F_{I1}$	inertia force of mass $M_1$ , increment $\Delta F_{I1}$
$F_{I2}$	inertia force of mass $m_2$ , increment $\Delta F_{I2}$
$F_{sb}$	spring forces for overall bending deformation, increment $\Delta F_{sb}$



$F_{sd}$	spring forces for local denting deformation, increment $\Delta F_{sd}$
$F_{sbm}, F_{sdm}$	maximum values for $F_{sb}$ and $F_{sd}$ respectively
$F_{sm}$	mean of $F_{sbm}$ and $F_{sdm}$
$I$	moment of inertia of the cross-section of a beam
$L$	length of a tube
$L_i$	length of a tube for the lateral impact test, $L - 50$ mm
$M$	bending moment
$M_p$	plastic bending moment capacity of an intact cross-section of a tubular
$M_{pc}$	fully plastic bending moment of a tubular's cross-section for the presence of axial force
$M_{pd}$	plastic bending moment capacity of a dented cross-section of a tubular
$M_s$	mass of the ship including added mass or of the striker
$M_u$	ultimate strength of a damaged tubular under bending moment
$M_z$	bending moment about z-axis, increment $dM_z$
$M_1$	$m_1 + M_s$ ; during impact, $M_s$ ; after separation, or linear limit bending moment
$M_{1i}$	mass $M_1$ at time $t = t_i$
$N_D$	number of segments in damaged part
$N_s$	number of total stations, $N_1 + N_D + N_2 + 1$
$N_1$	number of segments in upper undamaged part
$N_2$	number of segments in lower undamaged part
$P_{ext}$	externally applied axial force
$P_H$	axial force due to hydrostatic pressure, $\pi/4 Q_H (D + t)^2$
$P_t$	total applied axial force, $P_{ext} + P_H$ , increment $dP_t$
$P_Y$	axial force at fully yield condition of a tubular's cross-section, $\pi \sigma_Y D t$
$Q_H$	hydrostatic pressure
$Q_{Hcr}$	elastic buckling pressure of a 'long' tube under hydrostatic pressure
$Q_{ij}$	element of tangent stiffness matrix $[Q]$ defined as eqn.(5.22)
$R$	mean radius of the tube, or radius of curvature of a finite shell element before denting deformation
$R'$	radius of curvature of a finite shell element after denting deformation

$R_d$	distance of the plastic neutral axis of a dented cross-section from the opposite side of that of the dent, see Fig. 2.9
$R_E$	energy ratio, $E_k/E_e$
$R_k$	initial static stiffness ratio, $(k_{ds})_{\delta_d=0.001}/(k_{bs})_{\delta_o=0}$
$R_m$	initial mass ratio, $(M_1)_{t=0}/(m_2)_{t=0}$
$R_v$	non-dimensionalised impact velocity, $V_i/(L/T_b)$
$R_1, R_2$	radii defined in Fig. 2.9
$S$	circumferential force per unit length due to hydrostatic pressure, eqn.(5.10)
$S_f$	width of the flattened segment of a dented cross-section
$T_D$	impact duration
$T_b$	natural period of a beam flexural vibration
$T_c$	natural period of a tube overall shell vibration
$T_l$	natural period of the local shell denting vibration of a tube, defined as eqn.(3.38)
$T_s$	natural period of a tube wall stretch vibration
$T_t$	natural period of a tube wall shear vibration
$T_1$	duration of the elastic-plastic deformation stage of a impact
$V_i$	impact velocity, i.e. velocity of the striker immediately before impact
$V_r$	rebound velocity of the striker

$c$	wave propagation speed, $\sqrt{E/\rho}$
$d_d$	depth of dent at the point of impact, or $d_1 - d_2$
$d_{dx}$	depth of dent at a distance $x$ from the point of impact
$d_{oi}$	initial out-of-straightness of the tube
$d_{opk}$	peak bending deformation of a tubular due to impact
$d_{o1}$	out-of-straightness of a damaged tube at the dent side, or elastic limit lateral deflection
$d_{o2}$	out-of-straightness of a damaged tube at the opposite side of that of dent
$d_1$	absolute displacement of mass $M_1$ from its initial position, increment $\Delta d_1$
$d_2$	absolute displacement of mass $m_2$ from its initial position, increment $\Delta d_2$

$\Delta d_{1i}, \Delta d_{2i}$	incremental values for $d_1$ and $d_2$ at time $t = t_i$ respectively
$\dot{d}_1$	velocity of mass $M_1$ , increment $\Delta \dot{d}_1$
$\dot{d}_2$	velocity of mass $m_2$ , increment $\Delta \dot{d}_2$
$\Delta \dot{d}_{1i}, \Delta \dot{d}_{2i}$	incremental values for $d_1$ and $d_2$ at time $t = t_i$ respectively
$\ddot{d}_1$	acceleration of mass $M_1$ , increment $\Delta \ddot{d}_1$
$\ddot{d}_2$	acceleration of mass $m_2$ , increment $\Delta \ddot{d}_2$
$\Delta \ddot{d}_{1i}, \Delta \ddot{d}_{2i}$	incremental values for $d_1$ and $d_2$ at time $t = t_i$ respectively
$f_D$	modification factor for dynamic effects, defined as eqns.(3.29a,b and c)
$f_{D1}$	coefficient of $f_D$ for elastic-plastic deformation stage
$f_{D2}$	coefficient of $f_D$ for elastic spring-back stage
$f_{\max}$	non-dimensionalised ultimate lateral load
$f_1$	non-dimensionalised elastic limit lateral load
$k$	constant for the fundamental mode of the flexural vibration of a beam
$k_b$	spring coefficient for overall bending deformation
$k_{bi}$	spring coefficient for overall bending deformation at time $t = t_i$
$k_{bs}$	static spring coefficient for overall bending deformation
$k_d$	spring coefficient for local denting deformation
$k_{di}$	spring coefficient for local denting deformation at time $t = t_i$
$k_{ds}$	static spring coefficient for local denting deformation
$l_d$	extent of denting on either side of the point of impact
$l_i$	length of the $i$ th segment of a damaged tubular
$m$	mass of a tube, or non-dimensionalised value for $M_z$ , $M_z/M_p$
$m_p$	plastic moment resultant of the tube wall, $1/4 \sigma_Y t^2$
$m_{pc}$	non-dimensionalised value for $M_{pc}$ , $M_{pc}/M_p$
$m_1$	equivalent mass of a tube wall for local denting deformation
$m_2$	equivalent mass of a tube wall for overall bending deformation
$m_{2i}$	equivalent mass of a tube wall for overall bending deformation at time $t = t_i$
$n$	imperfection index, see eqn.(6.3)
$p$	non-dimensionalised value for $P_{ext}$ , $P_{ext}/P_c$
$q$	non-dimensionalised value for $Q_H$ , $Q_H/Q_{Hc}$
$t$	thickness of a tube, or time

$\Delta t$	time increment
$t_i$	time at the $(i - 1)$ th time increment
$w$	total deflection, $w_i + w_a$
$w_o$	radial deviation of a dented cross-section from the perfect circle, $D/2 - \sqrt{y^2 + z^2}$ , see Fig.5.2
$w_a$	deflection amplified by externally applied axial force
$w_a'$	newly obtained value for $w_a$
$(w_a')_i$	newly obtained value for $w_a$ at the $i$ th station
$w_i$	initial deflection, i.e. initial out-of-straightness
$x$	co-ordinate axis along the tubular, see Fig.5.3
$x_d$	axial location of dent centre
$y$	co-ordinate axis normal to the tubular, see Fig.5.3
$y'$	distance from the middle surface of a tubular: (+); outwards, (-); inwards
$z$	co-ordinate axis normal to the tubular, see Fig.5.3
$\Phi$	curvature of a cross-section
$\Phi_i$	curvature of a cross-section at the $i$ th station
$\Phi_Y$	curvature at initial yield state of an intact cross-section, $2 \sigma_Y/E/D$
$\Phi_z$	curvature with respect to $z$ -axis, increment $d\Phi_z$
$\bar{\alpha}_i$	equivalent concentrated curvature at the $i$ th station
$\beta$	$(1 - \sigma_{pd}/\sigma_Y) \delta_d^{1/2}$
$\delta_d$	non-dimensionalised depth of dent at the point of impact of a tube, $d_d/D$ or $(d_{d1} - d_{d2})/D$
$\delta_{df}$	non-dimensionalised permanent depth of dent, $d_{df}/D$
$\delta_{do}$	non-dimensionalised local denting deformation when $F = 0$ , $d_{do}/D$
$\delta_{dp}$	non-dimensionalised local denting deformation at which unloading starts, $d_{dp}/D$

$\delta_{dx}$	non-dimensionalised depth of dent at a distance $x$ from the point of impact, $d_{dx}/D$
$\delta_o$	non-dimensionalised out-of-straightness of a damaged tube, $d_o/L$ or $d_2/L$
$\delta_{of}$	non-dimensionalised permanent out-of-straightness of a damaged tube, $d_{of}/L$
$\delta_{opk}$	non-dimensionalised peak overall bending deformation of a tube due to impact, $d_{opk}/L_i$
$\delta_{o1}$	non-dimensionalised elastic limit deflection of a tube, $d_{o1}/L$
$\epsilon_x$	axial strain, increment $d\epsilon_x$
$\epsilon_{xo}$	axial strain on $z$ -axis, increment $d\epsilon_{xo}$
$\epsilon_{\theta r}$	circumferential residual strain due to denting damage
$\phi$	non-dimensionalised curvature with respect to $z$ -axis, $\Phi_z/\Phi_Y$
$\phi_o$	non-dimensionalised curvature with respect to $z$ -axis due to external axial force and/or hydrostatic pressure
$\phi_1$	non-dimensionalised curvature with respect to $z$ -axis corresponding to $m_1$
$\bar{\lambda}$	reduced slenderness ratio of a column, $\sqrt{\sigma_Y/\sigma_{cr}}$
$\lambda_{PR}$	Perry - Robertson 'imperfection' parameter
$\lambda_{PRH}$	equivalent imperfection parameter for hydrostatic pressure
$\lambda_{PRL}$	equivalent imperfection parameter for local denting damage
$\lambda_{PRO}$	overall straightness imperfection parameter
$\nu$	Poisson's ratio
$d\theta$	central angle of a finite shell element before denting deformation
$d\theta'$	central angle of a finite shell element after denting deformation
$\theta_o$	$\pi/2(D_o/D_{dmin})$ , see Fig.2.9
$\theta_1, \theta_2$	circumferential angles of the segments of radii $R_1$ and $R_2$ of a dented cross-section respectively, see Fig.2.9
$\rho$	material density
$\rho_x$	axial compression elasto-plastic knockdown factor
$\rho_\theta$	radial pressure elasto-plastic knockdown factor
$\sigma_{cr}$	Euler column buckling strength
$\sigma_{crL}$	local elastic buckling strength

$\sigma_e$	von Mises equivalent stress, $\sqrt{\sigma_x^2 + \sigma_\theta^2 - \sigma_x \sigma_\theta}$
$\sigma_{pd}$	$\sigma_Y D/t [(4/3 \delta_d)^2 + (t/D)^{1/2}]^{1/2} - 4/3 \delta_d$
$\sigma_u$	ultimate strength of a column under axial compression
$\sigma_x$	axial stress, increment $d\sigma_x$
$\sigma_{xcr}$	elastic buckling stress of an ideal shell structure under axial compression
$\sigma_Y$	static yield stress
$\sigma_{Yc}$	compressive static yield stress
$\sigma_\theta$	circumferential stress
$\sigma_{\theta cr}$	elastic buckling stress of an ideal shell structure under radial pressure
$\sigma_{\theta H}$	circumferential stress due to hydrostatic pressure
$\{ f \}$	generalised force vector, increment $d\{ f \}$
$\{ x \}$	generalised deformation vector, increment $d\{ x \}$
$[ Q ]$	tangent stiffness matrix, defined as eqn.(5.22)
$( \cdot )$	differentiation with respect to time

## **Chapter 1**

# **INTRODUCTION AND LITERATURE REVIEW**

### **1.1 Introduction**

In the late 1890s the offshore oil industry began off the coast of California<sup>[1]</sup>. The first hole over water was drilled as an extended land operation out by means of a wharf. Drilling from timber platforms in Lake Maracaibo began in the 1920s and in the Gulf of Mexico in the 1930s. The first steel platform was installed in Louisiana in 1946 and in the 1950s fixed steel platforms, steel framed structures (jackets) and self-elevating platforms (jack-ups), began to make their appearance<sup>[2]</sup>. In the early 1960s exploration began in the North Sea, which drew offshore engineers' interests to floating semi-submersible platforms. In the last two decades the new 'compliant' concepts for deeper waters and stormier conditions were proposed, developed and some of them were already realised. They consisted of Guyed Towers (GT), Tension Leg Platforms (TLP) and Articulated Buoyant Columns (ABC) and their attractions and disadvantages are clearly discussed in ref.3.

Despite its less than a hundred years history, very briefly summarised above, the technological developments achieved in offshore structures can be compared with those made in ships structures which has been dominant among marine structures possibly since the beginning of the mankind's history. Among others, one of their contributions to the technical developments can be the application of reliability design concepts to marine structures, with which any innovative marine structures can possibly be designed. Of course, the reliability design concepts was not new to ships structure designers. After the recognition of the possibilities of applying these ideas to

ships structures some twenty years ago<sup>[4]</sup>, subsequent developments were followed by, Mansour<sup>[5]</sup>, Faulkner<sup>[6]</sup> and by others. Despite those efforts its progress in ships structure designs cannot be compared with that for offshore structures and still most of ships structures are designed to satisfy classification society requirements which strongly rely on conventional, deterministic margins of safety.

Drilling for North Sea oil and gas posed many new problems that had been rather insignificant in shallow and less rough waters. Collision with ships is among them<sup>[7,8]</sup> and which is the problem that should be rationalised in terms of the probability of the event and the likely effect of such an occurrence. Even though collisions in the North Sea to date have been relatively minor<sup>[9,10,11,12]</sup>, there has been a considerable growth of interest in offshore collision problems probably because of the significance of their consequences, e.g. lives at risk, capital cost and potential environmental pollution. The risk from collision is also significant to floating rigs as well as fixed ones since the elements of floating rigs tend to be far more slender due to the inherent savings in weight required of a floating design and secondly there is often very little or even no effective redundancy if one of the main members were to be significantly damaged<sup>[13]</sup>.

A collision with an offshore platform can be categorised as major or minor based on the extent of the damages to the structure. A minor collision will result in only repairable local damage of the structure and probably will not call for cease of operation. A major collision on the other hand will damage the platform globally and will certainly require a cease of operations. However, it seems extremely uneconomical to design a platform to withstand a major collision and remain operational and it also seems that an attempt to eliminate all collisions can be impractical. Therefore, in order to practically while at the same time economically solve the offshore collision problems the probability of major collisions should be kept at a low level by defining adequate preventive measures and minor ones should be considered in the design stage of the platform.



The precautionary safety measures presently adopted in the North Sea include 500 metres radius of safety zone, marking of these zone for permanent platforms on navigation charts, identification of the installations themselves and others<sup>[14]</sup>. The total number of offshore platform collisions with ships in the British sector of the North Sea reported during from 1976 to 1982 was 107 and most of them were by supply vessels<sup>[11]</sup>. Furthermore, the most serious cases of damage to offshore platforms selected from boat impact survey records reported on Lloyd's Register Certified or Classed installations operating in the North Sea can be catagorised as minor collisions<sup>[12]</sup>. These data may indicate that, as far as North Sea platforms are concerned, the above safety measures have very positive results. Even though the probability of occurrence of major collisions is acceptably low, such collisions may still happen. Therefore, it is necessary to give due consideration to the protection of human lives<sup>[15]</sup>.

Provided that the probability of major offshore collisions can be kept at a low level by means of adequate preventive measures and due considerations are given to protections of human lives, then the problem remains to be solved is how to efficiently design the offshore structure considering minor offshore collisions, which will result in only repairable damage of the structure and probably will not require any cease of operations, and in which optimising building/repair costs can be the objective. For this purpose it is necessary to be able to predict the probability of minor collisions, the probable extents of damage due to minor collisions and the residual strengths of the damaged structures as a basis for repair decisions. In the following section a literature review on offshore collisions is presented.

## 1.2 Literature Review

A concise review on offshore collisions with regards to methods and principles for design against damage is readily available in ref.15, so only a few pertinent papers will be mentioned here and what would be necessary for more efficient design of

offshore structures against collisions will be identified.

### 1.2.1 Probability of Collision

Like other probability of accident estimation problems, there are two basic types of estimation for offshore collision probability. One is backward estimates which depend upon collision records and the other is forward estimates using simulation methods. Historical records are vital for the former and also necessary for the latter to select representative scenarios of the majority of collisions and to validate any predictive models.

#### 1.2.1.1 Historical Records

In ref. 10, mostly based on Lloyds' List and DnV Offshore Accidents Databank worldwide statistics on offshore accidents in the period 1970-1981 are summarised according to type of accident, degree of structural loss, operation mode and geographical location. Within the period 82 collision accidents for all platforms (fixed and mobile) were reported representing 16 % of the total accidents and second to weather accidents. Even though the number of collisions are high, the consequences are normally small and the number of lives lost by collisions are relatively small. The number of infringements of safety zones in the Norwegian sector in the North Sea from 1975 to 1981 is 91 and 157 infringements were reported in the UK sector in the period 1976-1980. For the both cases the infringements by fishing vessels are three quarters of the totals. Similar summaries can also be found in ref.16.

Offshore collision records in UK waters from 1976 to 1982 are provided in ref.11, which were the results of a survey of a number of offshore installation operators conducted in aiming to identify the nature of collisions that have been occurred in the past. As mentioned earlier the total number of incidents reported was 107 and most of them were by supply vessels. Classifying the types of operation leading to the incidents was attempted. 48 incidents occurred during loading alongside or in attendance, nearly half of the total, and 23 incidents happened when the vessels were approaching or departing. For the former category the mean wave height is about

3 m and approximately 17 % of the collisions are recorded as severe, requiring immediate repairs, while the mean wave height is 2 m and the proportion of severe collisions is about 30 % for the latter.

In refs.17 and 12, the extents of damage and the damage types are given for twenty-four damaged tubular members involved in eleven most severe collision accidents selected among the records reported on Lloyd's Register Certified or Classed platforms operating in the North Sea. The ranges of non-dimensionalised depth of dent ( $\delta_d = d_d/D$ ) and out-of-straightness ( $\delta_o = d_o/L$ ) are 0.012-0.449 and 0.0052-0.097 respectively. Local denting and/or overall bending damage is common to all the cases, and punching shear failure at joints for four cases and weld pull-out at joint for three cases were reported.

A review of the records is provided in ref.18 of safety zone infringements in UK waters from 1973 to 1980 mostly based on the UK Department of Energy Records. The number of infringements is 53 which is much smaller than that in the period 1976-1980 given in ref.10. The results of the shipping route surveys for the North Sea are also presented.

#### 1.2.1.2 Prediction Models

As far as offshore collisions are concerned the marine traffic may be divided into three groups :

- authorised vessels servicing the installations;
- tankers for offshore loading in the area; and
- passing vessels including drifting vessels.

Various prediction models are available to predict the probability of collisions of offshore installations by passing vessels[9,18], by loading tankers[19] and by attendant vessels[9,11].

In ref.9, methods are proposed for predicting the collision probability of offshore installations in a certain area by service vessels and by passing vessels on the

basis of recorded incidents, density of shipping, infringements and significant wave heights and estimated number of visits. However, since collisions are the events hoped to be rare, historical data should be expected to be sparse. In order to overcome this contradiction more advanced models have been proposed based on experienced data whose occurrence probabilities are generally much greater and thus which are more reliable than those of the final events.

Furnes and Amdahl<sup>[19]</sup> developed a simulation technique to obtain the relative probability of loading tanker collisions and suggested to calculate the actual probability of the collisions by multiplying the rate of loss of propulsion, lock of rudder in the instantaneous position etc. which can hopefully be determined using experienced data. In ref.18 passing vessels are subdivided into errant, blind and drifting vessels and models are proposed for errant and blind vessel collisions and for drifting vessel collisions. The total number of traffic per year for shipping lanes near the platform, their distribution about the centre lines of the lanes, proportion of errant and blind vessels among the traffic etc. are necessary as input data of the model for passing vessel collisions. For the case of drifting vessel collisions the expected frequency of major propulsive or steering breakdown instead of the proportion of errant and blind vessels and wind direction data are required.

Standing and Brending<sup>[11]</sup> provided probable ranges of the collision velocity for four scenarios modelled based on the results of the survey of offshore operators. In calculating vessel motions, the probable weather conditions, corresponding wave data and current data of the area were considered. The results of this study is summarised in Table 1.1 and the distribution of collision velocity was found to be insensitive to vessel size.

In ref.12 a mass distribution for supply vessels is provided covering a worldwide record of vessels classed as 'supply' or 'supply/tug', which shows that the displacement tonnages for 85 percent of the vessels are less than 2500 tonnes and

displacement of 5000 tonnes covers more than 95 percent of the vessels. However, the tendency of modern supply vessels towards increase of the size<sup>[11]</sup> needs to be considered and the correlation of the mass distribution of worldwide supply vessels to a specific offshore installation remains questionable.

Table 1.1 Mean and 10 % Exceedance Collision Velocities for most Probable Operation Types of Offshore Attendant Vessels (from ref.11)

Scenario	Mean Collision Velocity (m/s)	10 % Exceedance Collision Velocity (m/s)
• Heave Collision at the Stern	0.83	1.53
• Collision when Alongside :		
a) Stern Surge Collision	0.39	0.73
b) Stern Sway Collision	0.37	0.70
c) Side Sway Collision	0.28	0.54
• Collision when Manoeuvring	0.74	1.29
• Collision of Drifting Vessel :		
a) Sideways Drifting ; Impact amidships	0.76	0.98
b) Sideways Drifting ; Bow or Stern Impact	0.83	1.44
c) Foreward Drifting ; Bow Impact	1.18	1.82

As reviewed in this section, in general, the collision statistics available so far are not detailed enough for collision consequences calculations and it is still premature to predict the actual collision probability using the proposed models. Nevertheless, the models proposed for predicting the probability of tank loading collisions<sup>[19]</sup> and passing vessel collisions<sup>[18]</sup> can be useful for positioning a structure at an alternative locations and the probable ranges of collision velocity for attendant vessel collisions provided in ref.11 should be of some use for collision consequence calculations and for

cost-benefit studies of offshore collision problems.

## 1.2.2 Collision Mechanics

### 1.2.2.1 Static Approach

Assuming that a collision results in purely translational motion the following equation, eqn (1.1) for a collision against a fixed unfendered platform can be obtained from the energy conservation law.

$$E_k = E_p + E_s \quad (1.1)$$

where  $E_k$  : kinetic energy of the ship immediately before impact,  $\frac{1}{2} M_s V_i^2$   
 $E_p$  : energy absorbed by the platform  
 $E_s$  : energy absorbed by the ship  
 $M_s$  : mass of the ship including added mass  
 $V_i$  : impact velocity

In fact, the amount of energy that has to be absorbed as strain energy in the colliding bodies can be determined by the masses, impact velocity, impact geometries among other factors. However, provided that dynamic effects, e.g. motion and vibration of the impacting bodies, strain-rate sensitivity of the material, etc., are insignificant the energies,  $E_p$  and  $E_s$ , can then be determined by integrating the static force-deformation curves satisfying eqn (1.1) and maintaining force equilibrium. Assuming further that the elastic strain energy stored in both the striking vessel and platform are negligible, i.e. the ship will be totally stopped by the platform, the absorbed energies  $E_p$  and  $E_s$  then can be estimated from the corresponding areas of the force-deformation curves up to the maximum impact force. The procedure described above is a brief outline of the static approach adopted in refs.19 - 24. In adopting the static approach for predicting the associated damage of the colliding structures, the problem remains to be solved is how to construct the force-deformation relationships for the ship and platform.

The pioneering work on the mechanical properties of ship hulls in collision was

carried out by Minorsky<sup>[25]</sup> and works conducted in the field of ship collisions have been reviewed by Jones<sup>[26,27]</sup> and by others<sup>[29,30]</sup>. However, in practice, if the energy absorption capability of the platform is an important aspect, the energy absorbed by the ship  $E_s$  is usually neglected due to the lack of reliable data for energy absorption in ships, leading to a conservative design of platform structure. Thus, in this literature review the emphasis is on the force-deformation relationship of platforms. Existing methods to estimate the energy absorption capability of platforms will be mentioned later.

#### 1.2.2.2 Dynamic Approach

As mentioned above the assumptions commonly adopted in the static approach are that dynamic effects are insignificant and the elastic strain energy stored in the colliding bodies is negligible. However, the validity of these assumptions has not been investigated properly as yet. Furthermore, according to the results of recently published works these assumptions cannot be valid at least for the cases investigated.

In an experimental and theoretical study by Arochiasamy et al.<sup>[30]</sup> on the response of a hydro-elastic semi-submersible to bergy-bit impacts, it was observed that the rebound velocity of the bergy-bit after impact was approximately 70 to 75 % of the impact velocity. In other words, about a half of the initial kinetic energy of the bergy-bit was spent on the motion and vibration of the semi-submersible. Nataraja and Pemsing<sup>[12]</sup> evaluated the energy distribution of an offshore fixed platform based on the measured extents of damage and the estimated impact velocity, which showed that the elastic strain energy stored in the whole platform is greater than that absorbed by the impacted structural elements.

Of course, it is premature to draw any firm conclusions from the results of the limited cases mentioned here, but it can be suggested that dynamic elastic-plastic analyses must be employed at least for some cases to avoid excessive conservatism in predicting the consequences of offshore collisions. Probably owing to the complexity of the problem and the uncertainty in the nature of offshore collisions, various

simplified dynamic models have been proposed in the literature.

Petersen and Pedersen<sup>[31]</sup> presented a time simulation model considering the variation of the hydrodynamic pressure on the ship hull, the overall dynamic behaviour of the platform and the actual load-penetration relation at the impact zone. Davies and Mavrides<sup>[32]</sup> developed a spring-mass model, in which the ship deformation and the local deformation of the platform are considered, for computing the force function arising in supply vessel - concrete platform collisions and this force function was used in the structural analysis of the whole caisson later. In ref.14 a simple lumped mass model of two degrees-of-freedom is proposed for fully plastic collisions where one degree-of-freedom is for the motion of the ship and the other is for that of the platform. Recently, Ueda et al.<sup>[33]</sup> suggested a spring-mass model of multi degrees-of-freedom for elastic collisions and provided some analysis results of an isolated tubular member under impacts. In the analysis of a single tubular member, the overall bending deformation as a beam and the local denting deformation of the tube wall were considered.

As reviewed here, not much work on offshore collisions using dynamic approaches has been carried out in the literature. However, the response of a single structural element under dynamic loads has relatively extensively been investigated. Therefore, at this juncture, it may be worthwhile to survey the literature on the response of a beam under impacts due to collisions.

### 1.2.3 Dynamic Response of a beam

Since the early experimental works by Hodgkinson<sup>[34,35]</sup> the response of a beam under impacts due to moving objects and under impulsive loadings caused by explosions has been one of the problems of interest to the engineer. Experimental and theoretical investigations conducted in this field have been reviewed by Timoshenko<sup>[36]</sup> for early works and by Rawlings<sup>[37,38]</sup> and Jones<sup>[39,40]</sup> for recent progresses among others. Works on the behaviour of a beam under impacts due to collisions will be reviewed in the following.



· Early Work : Among early studies those of Cox, St. Venant and Timoshenko can be distinguished, who examined the problem of central impact of a ball striking a simply supported elastic beam having uniform cross-section. Cox<sup>[41]</sup> assumed that the impact might be divided into two stages: (a) A sudden alteration of velocity at the first instant of collision, and (b) the gradual transformation of the resulting kinetic energy into elastic energy of the deflected beam. Then he obtained the common velocity of the striking ball and struck beam immediately after impact and derived an expression for the maximum deflection of the beam with a further assumption that the deflected shape is that of the static deflection curve. The contributions of St. Venant and Timoshenko in this field can be found in refs. 36 and 42 respectively and the latter will be mentioned later. Mason<sup>[43]</sup> conducted impact tests on steel I-beams with a heavy spherical pendulum bob and measured the maximum flexural strain using a magnetic strain gauge and a mirror oscillograph to record the response. From the results of these tests it was concluded that the peak stresses were about double those predicted by the theory of Cox, and that an impact can consist of several blows in rapid succession.

· Timoshenko's Approach : In Timoshenko's approach to a central impact on elastic beams having simply supported boundaries, the contact force between the striking ball and the beam can be determined using the elastic reversible Hertz contact force equation. A governing integral equation can be derived combining the interactive force function and the central deflection due to forced vibration, which can be solved by a timewise step-by-step solution procedure. This approach has been approximated<sup>[42,45]</sup> and extended including other types of contact force relationship<sup>[44]</sup> and other boundaries<sup>[44,45]</sup>.

In an attempt to avoid lengthy and tedious numerical computation works, Lee<sup>[42]</sup> developed an approximate procedure for Timoshenko's approach assuming that the duration of contact is small in comparison with the period of the fundamental mode of vibration of the beam, and that only the fundamental mode of oscillation of the

beam need to be considered. The accuracy of this approximate solutions was checked by examining the proportion of the energy attributable to the fundamental mode. Barnhart and Goldsmith<sup>[44]</sup> investigated the influence of linear elastic boundary conditions of the beams and of various contact force relationships on the calculated stress history. Hoppmann<sup>[45]</sup> extended Timoshenko's approach to a simply supported beam on an elastic foundation. An expression was derived for the coefficient of restitution which is essential in calculating the deflections and the strains and criteria were proposed for determining the cases in which the beam may be considered as a single degree-of-freedom.

· Inelastic Response : Bohnenblust et al.<sup>[46]</sup> developed a theoretical method for predicting the elastic response of an infinitely long beam to impacts by extending Boussinesq's method for elastic analysis. In the method the bending moment is assumed to depend on the curvature according to a function that is obtained from the stress-strain curve of the material and the effects of shear and rotatory kinetic energy are ignored. The predictions by the theory were compared with the results of a series experiment conducted on long simply supported beams having rectangular solid cross-section. Experimental and theoretical deflection curves show negative curvature away from the impact point, and the results of cold-rolled low-carbon steel models exhibited that plastic deflection is localised at the point of impact.

Rigid-plastic analysis was carried out by Conroy<sup>[47]</sup> for long beams under impact subsequent to Bohnenblust's method neglecting elastic strains and by Lee and Symonds<sup>[48]</sup> for free beams of finite length subjected to specified impulsive loads. Parkes<sup>[49]</sup> conducted a series of mild steel cantilevers and encastre beams struck by moving masses. The experimental results were then compared with the predictions by a rigid-plastic analysis based on the concept of a constant dynamic plastic bending moment.

As reviewed here most of the works are of compact section, particularly of rectangular solid one, for which the initial or given sectional configuration can be

assumed to be unchanged throughout the period of impact, and strain-rate effects are not considered or treated indirectly in inelastic analyses.

#### 1.2.4 Force-Deformation Characteristics of Platform

As mentioned earlier in section 1.2.2, applying static approaches to ship-offshore platform collisions it is essential to derive the force-deformation relationship of the platform in order to estimate the amount of energy absorbed by the platform. Even for simplified dynamic approaches the stiffness coefficient of the platform can possibly be approximated by the slope of this relationship. The deformation modes of the platform due to collisions with vessels consist of local denting and overall bending of impacted structural members and global deflection of the whole structure. Since, in most cases, the global deflection is elastic<sup>[12]</sup>, the force-global deflection curve can be obtained from a linear frame analysis. However, the other two modes, i.e. local denting and overall bending of impacted members, involve considerable plastic deformation and, in general, the interaction between the two modes makes the problem more complex. Theoretical and experimental investigations of the local denting and overall bending characteristics of tubular members will be reviewed in the following.

##### 1.2.4.1 Theoretical Works

de Oliveira<sup>[50,51]</sup> suggested a simple method for estimating the local denting and overall bending damages resulting from a supply vessel collision. For local denting damage, assuming that all the energy is dissipated through the plastic bending of the surface, the energy absorbed by local denting is estimated from the final deformed configuration of the dent. In the estimation, the rotation of surface at yield lines and flattening of the cylindrical surface to a central rectangular area are considered. While for overall bending damage, assuming that a plastic hinge forms at the point of application of the load, an analytical expression has been derived for the lateral force-deflection relationship of a rigid-plastic intact tubular member. In the analysis the membrane forces due to large displacement are considered, and the varying degree of axial and rotational restraint of the end boundaries is included.

For local denting mode, another method has been proposed by Furnes and

Amdahl<sup>[52]</sup> incorporating the plastic effects from the rotation of yield lines, flattening of the surface between yield lines and tension work due to elongation of generatrices. The predictions by this method show good agreements with experimental results of clamped tubes at small indentation, whereas the deviations increase when the tube starts undergoing global deformations. While for overall bending mode, Soreide and Amdahl<sup>[53,22]</sup> provide a simple analytical force-deflection relationship for a centrally loaded intact tubular beam having fully fixed ends. The relationship was derived using a rigid-plastic method of analysis under the assumption that no buckling of the tube wall takes place so that the full plastic capacity of the cross section is retained during deformation.

Ellinas and Walker<sup>[54]</sup> derived an empirical expression for the relationship between lateral load and local denting damage. They also proposed a method to evaluate the ultimate lateral load carrying capacity of a damaged tube having rotationally fixed but axially free boundaries. Using this method the overall bending damage can be estimated under the assumption that a pure local denting phase is followed by a pure overall bending phase until absorbing all the kinetic energy released in the course of a collision.

Recently, Wierzbicki and Suh<sup>[55]</sup> proposed a simplified shell model consisting of a series of unconnected rings and a bundle of unconnected generatrices for deriving the lateral force-lateral displacement relationship of tubes having various boundary conditions and end actions. In the model, it is assumed that the rings are rigid-plastic and inextensible, and that the generatrices are rigid-plastic beams. The dissipated energy is then obtained by summing up the work-done by circumferential bending of the rings, by stretching or compression of the generatrices and by rotation of plastic hinge in the ring. More improved results upon previous studies are presented in ref.55, but the proposed model can underestimate the actual strength of a tube by roughly 30-40 %.

#### 1.2.4.2 Experimental Works

Recently, a number of tests have been conducted on small-scale tubular members under lateral concentrated load applied with a sharp or rectangular indenter. The results of these tests can be found in refs. 56, 52, 56 and 22. In the following the test conditions, geometric parameters of the specimens and their deformation history of these tests will be summarised.

Thomas et al.[56] conducted tests on short simply supported aluminum and steel tubes under the action of quasi-static transverse loading applied through a wedge-shaped indenter. The ranges of diameter to thickness ratios( $D/t$ ) and length to diameter ratios( $L/D$ ) of the tubes were 24-37 and 1.5-11 respectively. In-the tests it was observed that three phases of deformation were apparent as pure crumpling, followed by bending and crumpling and finally complete structural collapse of the tube. The principal effect of increasing the length was also found that the amount of deformation experienced by the tube in the first phase of deformation is greatly reduced by an increase in the length. In ref.52 the results are provided of tests on fully fixed steel tubes loaded with rectangular indentors having different breadths. The ranges of  $D/t$  and  $L/D$  were 30-45 and 4-6 respectively. Local denting deformation was dominant until the depth of dent was about 0.7 times the radius of the tube, and after that the tube started defecting like a beam and high axial forces were developed. Failure at supports was caused by these high axial forces.

In ref.21 and 22 the results are reported of a series of tests conducted on relatively long steel tubulars whose non-dimensionalised geometric parameters are similar to those of offshore tubulars. The results of tests on simply supported tubes, whose  $D/t$  and  $L/D$  ratios were 27-49 and 9-25 respectively, are summarised in ref.21.

Contrary to the phases of deformation observed in the tests on short tubes described above, the following deformation history was exhibited for all the specimens:

stage 1; elastic bending of the tubular as a beam

stage 2; further elastic bending and simultaneous local indentation at loaded position

stage 3; localised plastification at dent

It was also observed that the bending stresses created by the lateral force made the lateral load induced dent propagate.

Soreide and Amdahl[22] presented the results of tests on steel tubes whose  $D/t$  and  $L/D$  ratios were 22-61 and 10-20 respectively. The end conditions simulated in the tests were axially free but rotationally restrained as well as fully fixed. Lateral load was applied with a rectangular indenter at two different displacement rates, 0.15 mm/s and 54 mm/s. The specimens loaded at the higher indenter displacement rate showed an increase in load carrying capacity of about 10 percent as compared with those loaded at the lower rate. Axially restrained tubes were collapsed by fracture occurred at tension sides at the ends, whereas local crippling of tube wall on the compression sides of ends caused the failure of axially free ones.

As reviewed in this section, recently, various theoretical methods have been proposed for estimating the force-deformation characteristics of a tubular member in the literature and quite a number of tests have been conducted to provide experimental information of the load carrying capacity of tubular members under concentrated lateral load. However, the interaction between local denting and overall bending deformations have not fully been investigated theoretically, and local buckling, which possibly occurs at joints with adjacent members, is not considered in the proposed methods. Furthermore, in the literature, no experimental works have been reported on the structural response of a tubular member under dynamic load like the impacts arising in ship-offshore structure collisions.

#### 1.2.5 Residual Strength of Damaged Tubulars

For the last ten years, there has been a considerable growth of interest in the structural behaviour of damaged unstiffened tubulars and damaged stiffened cylinders. In the following experimental and theoretical works on the ultimate and post-ultimate strength of damaged tubulars will be reviewed. The works on the resistance of intact stiffened cylinders under lateral concentrated loads and residual strength of damaged

stiffened cylinders can be found in refs. 57-61, 63 and 64 for ring-stiffened cylinders and in refs. 62, 63 and 64 for orthogonally-stiffened cylinders.

Smith, Kirkwood and Swan<sup>[65]</sup> conducted sixteen axial compression tests on undamaged and slightly damaged small-scale tubes. Parametric study results are also provided of an incremental finite element beam-column analysis of axially compressed tubular members having overall bending damage. The influences of initial out-of-straightness and residual stresses due to cold bending and welding in fabrication on the load carrying capacity of undamaged tubulars were also investigated in the theoretical work. Loss of strength caused by initial out-of-straightness and residual stress was found to be greatest in tubes whose elastic buckling strength and squash loads are approximately equal. However, the residual stress effect diminishes as initial out-of-straightness increases.

Taby, Moan and Rashed<sup>[66]</sup> presented the results of twenty one axial compression tests on damaged small-scale tubes. The damage was in the form of slight overall bending and moderate local denting. A method of analysis was also suggested to evaluate the ultimate strength and post ultimate behaviour of dented tubular members subjected to axial compression. In the analysis, a yield line collapse mechanism was introduced in the dented zone, and the ultimate strength was considered as the load when yielding was detected in the undamaged part of the dented portion.

Smith, Somerville and Swan<sup>[67]</sup> reported the results of tests on four full-scale tubes and four small-scale tubes whose geometric parameters were nominally identical with those of the corresponding full-scale tubes. The full-scale tubes were obtained from a removed North Sea platform following completion of service. The two tubes from each group were tested in an undamaged condition while the others were tested following application of damage. They also introduced in non-linear finite element beam-column analysis the concept of effective yield stress and effective modulus of elasticity of the fibres in the dent to account for the residual stresses resulting from dent

formation and the eccentricity acting at the dented portion of the damaged tube. It was found that the collapse loads for large and small-scale tubes were in reasonable agreement.

Ellinas and Walker<sup>[54,68]</sup>, using a first-yield failure criterion similar to that proposed in ref. 66, developed a simple design-oriented analytical expression to estimate the lower-bound of the ultimate strength of tubular members having overall bending and local denting damage subjected to axial compression.

Smith<sup>[69]</sup> reported the results of twelve axial compression tests on small-scale tubes to investigate the influences of dent location and dent shape on the damage effect. He also provided an empirical reduction factor for the effective strength and stiffness of the fibres in the dent and presented data curves defining the mean and lower-bound residual strength of axially compressed damaged tubes. It was found that the loss of strength due to damage depends critically on dent depth and amplitude of out-of-straightness. In other words, the loss of strength is insensitive to the shape and location of dents and the shape of bending damage.

Ueda and Rashed<sup>[70]</sup> reported the results of eighteen tests on welded tubes to investigate the effects of local denting damage on the ultimate strength of tubulars subjected to pure bending. They also constructed an analytical model deriving an ultimate strength interaction relationship between axial force and biaxial bending moments for a dented cross section. Influence of dent damage was found to be insignificant for the case where the dent was placed at the neutral axis of bending or in tension side. Whereas, when the dent was in compression side, the loss of strength due to local denting damage was remarkable. The theoretical model is found to be in satisfactory agreement with experimental results, but the predictions using the model can be non-conservative for deeply dented thinner tubes and the opposite is true for thicker tubes having shallow dent.

Taby and Moan<sup>[71,72]</sup> derived an empirical correction factor for the analytical



model suggested in ref.66 to accommodate the underestimation of the load carrying capacity for the tubes whose  $D/t$  ratios are less than 50. In refs.71 and 72, forty eight axial compression tests with simply supported boundaries and ten tests with clamped ones on damaged tubulars are reported, but unfortunately their results are not available. However, it was found that the post-ultimate strength is to a large extent influenced by increasing distortion of the cross-section during loading, and that the effective buckling length concept, normally employed for undamaged tubular columns, yields conservative estimations for damaged tubular columns.

Richards and Andronicou<sup>[73]</sup>, adopting the reduction factor for the fibres in the dent given in ref.69, developed a numerical method to evaluate the ultimate and post-ultimate strength of an axially compressed damaged tubular using a finite segment technique. Yao et al.<sup>[74]</sup>, employing the analytical model suggested in ref.66 together with the correction factor derived in ref.71 and 72, proposed a method of analysis to simulate the structural behaviour of an axially compressed damaged tubular using an elastic-plastic matrix method.

As reviewed above research works reported in the literature have been focused on developing analytical and numerical methods to evaluate the ultimate strength and the post-ultimate behaviour of damaged tubulars under axial compression and bending moment. And reasonably accurate predictions of the strength of axially compressed damaged tubulars can be obtained using the proposed methods. However, in spite of the possibility of damage onto underwater members of offshore structures as a result of collisions, dropped objects and other accidental impacts occurring in service or during fabrication or installation no research works on the structural behaviour of damaged tubulars under combined loadings including hydrostatic pressure have been reported in the literature.

#### 1.2.6 Design Codes

In the traditional design codes for offshore structures such as API Code for

fixed platforms<sup>[75]</sup> it is simply stated that the impact caused by a vessel berthing against a platform is required to be considered in the assessment of dynamic loads. However, a recently published API Code for tension leg platforms<sup>[76]</sup> recommends to consider the impact from ship collisions as an accidental loads, and to design the platform to be able to resist functional and reduced extreme environmental loads after having consequential damage due to collisions.

In British codes such as Department of Energy (DEn) Guidance<sup>[77]</sup> and British Standard Institution Code (BS 6235)<sup>[78]</sup> a little bit more detailed guidance can be found. DEn Guidance requires that there should be fendering adequate to withstand the impact caused by a ship of 2500 tonnes displacement coming into contact at 0.5 m/s. In BS 6235 localised damage due to ship collisions is accepted but the impact from a vessel of 2500 tonnes travelling at 0.5 m/s is specified as the minimum impact which the primary structure should withstand safely. However, it is allowed in the BSI Code to use suitable computational methods, e.g. a solution of the equations of motion based on an impulse-momentum approach, for the design calculations of the energy to be absorbed by the structure, but otherwise all of the impact energy should be absorbed by the structure non by the ship.

In DnV Technical Notes for fixed platforms<sup>[79,80]</sup> and Rules for mobile units<sup>[81]</sup> more detailed guidance is provided than in those mentioned above. According to DnV Technical Note TNA 202<sup>[80]</sup> the impact resulting from collisions with supply vessels are recommended to be considered in two levels, i.e. as an operational impact load and accidental impact load. An operational ship impact load, which should be considered as a live load, the load caused by the maximum authorised vessel travelling at 0.5 m/s. On the other hand for an accidental impact load is defined as the load caused by the maximum authorised vessel travelling at a velocity given as  $V_i$  (m/s) =  $0.5 H_s$ (m), where  $H_s$  is the maximum significant wave height in metres for operation at the structure. However, for North Sea conditions the accidental impact velocity is required not to be assumed less than 2.0 m/s. And if no restrictions on the authorised vessel sizes are specified in the operations manual of the structure, the

displacement of the servicing vessel should not be taken less than 5000 tonnes. An added mass coefficient of 0.4 is recommended for broad side collision and of 0.1 for bow and stern collision. Furthermore, for a platform having the damages resulting from an accidental impact is recommended to withstand the environmental loads corresponding to a recurrence period three times the anticipated repair time or at least one year<sup>[24]</sup>. In ref.80 force indentation characteristics for energy absorption at ships are provided, which can be used in lack of more relevant data. It is also required that no rotational dissipation of energy should be assumed in any cases.

As reviewed here some guidance on determining design collision loads can be found in BSI Code<sup>[78]</sup> and DnV Rules<sup>[81]</sup> and Technical Notes<sup>[79,80]</sup>, but their corresponding probabilities of occurrence are not specified. No specific guidance is given anywhere on estimating the resistance of structures against impact loads and the consequential damage, and on methods to evaluate the residual strength of damaged members or structures.

### 1.3 Aim of the Thesis

The objective of the work presented in this thesis is to derive simple design formulae for estimating the probable extent of damage to offshore tubular members due to lateral impacts, and for evaluating the residual strength of damaged tubular members subjected to combined axial compression and hydrostatic pressure.

As part of the work, lateral impact tests were to be conducted on small-scale tubes having simply supported roller conditions. And combined axial compression and hydrostatic pressure loading tests were to be followed on damaged tubes whose form of damage were realistic. Then, a simple numerical procedure was to be developed to simulate the dynamic response of tubular members under lateral impacts. A theoretical method was also to be developed to evaluate the residual strength of damaged tubular members under combined axial compression and hydrostatic pressure based on the Newmark integration method. Rigorous parametric studies were to be performed using

the theoretical models which were validated with the experimental results obtained from the tests conducted as part of this study.

Finally, simple design formulae were to be derived using the parametric study results.

#### 1.4 Layout of the Thesis

In chapter 2, description of the testing procedures and results are presented of lateral impact tests conducted on stress-relieved seamless cold-drawn tubes.

In chapter 3, a simple numerical procedure is developed for simulating the dynamic response of a tubular member having simply supported roller conditions. In the analysis the tubular member is reduced to a spring-mass system with two degrees-of-freedom.

In chapter 4, details of testing procedure are described and results are presented of axial compression and hydrostatic pressure loading tests on damaged tubes. Those of axial compression tests on undamaged tubes are also provided from which an experimental technique can hopefully be developed for the determination of the actual effective lengths of undamaged tubes in the tests.

In chapter 5, an analytical method is developed for evaluating the residual strength of damaged tubular members under axial compression and hydrostatic pressure. The analytical method involves two separate phases of calculation : (a) The moment - external axial compression - hydrostatic pressure - curvature relationships for damaged cross-sections are derived using the tangent stiffness formulation ; and then (b) using <sup>these</sup> relationships the residual strength of the damaged tubular is determined.

In chapter 6, parametric studies are performed using the developed theoretical

models, and then using the parametric study results simple design formulae are derived. In the derivation the Perry formula is adopted as a basis of the formula to estimate the residual strength.

Finally, chapter 7 contains the conclusions and proposals for future work.

In Appendix 1, approximate equation for bending moment - external axial compression - hydrostatic pressure - curvature relationships of damaged tubular cross-sections is included in an attempt to keep the main text concise.

In Appendices 2 and 3, an approximate formula for elastic buckling pressure of circular cylinder under pure radial pressure, and a strength formulation for ring-stiffened cylindrical shells under combined axial loading and radial pressure are derived respectively.

## Chapter 2

### LATERAL IMPACT TESTS

#### 2.1 Introduction

The response of an offshore structure to boat or dropping object impacts may include :

- local denting deformation of the tube wall at the point of impact ;
- bending deformation of the struck member as a beam ;
- tearing of the joint weld at tension side ;
- crippling of the compression side near the joints ;
- shear failure of the struck member at the joints ;
- punching shear deformation of the wall of supporting structures ; and
- overall deformation of the platform.

As reviewed in section 1.2.4.2, most of the reported experimental works relevant to the offshore collision problems were conducted under quasi-static loads. Therefore the structural behaviour of offshore tubulars under dynamic load like impact has not been fully investigated yet. In aiming to provide more realistic experimental information for the first two modes above, lateral impact tests have been conducted as a part of this study.

In this chapter the description of testing procedures and summaries of the results are presented of twenty four lateral impact tests conducted on small scale tubulars having simply supported roller conditions. Only some typical detailed results are provided herein. All the details of the measurements and results were reported separately in ref.82. Using the extent of damage measurement results simple

mathematical expressions for the geometric configuration of damaged tubulars have been derived. The general response of a tubular under lateral impact is identified and a comparison of its detailed deformation procedure with those of under quasi-static loads is provided. Finally, the extent of damage measured in the tests is compared with the predictions using existing formulae.

## 2.2 Test Models and Pre-Test Measurements

Ideally the model parameters chosen for a test series should cover what is considered to be the practical range of geometries, material properties and fabrication sequences of actual unstiffened cylindrical members of offshore structures. Also the real damage situations and the boundary conditions should be simulated in the test set-up. However, because of testing facility limitations and budget constraints, it was decided to perform dry tests on small scale tubes.

Fabricated tubes, which are generally formed by cold-rolling and welding of flat plates, are used for the unstiffened cylindrical members of offshore platforms. It is virtually impossible to simulate correctly scaled distortions and residual stresses on small scale tubes. Therefore, the specimens were formed from CDS-24 cold-drawn seamless tube.

### 2.2.1 Choice of Model Parameters

Characteristic cross-sectional dimensions of bracing elements in the water-plane of jackets and semi-submersibles are in the range:

$$20 < D/t < 100$$

$$10 < L/D < 40$$

However, the structural framework of most offshore platform is formed by long unstiffened tubular members whose diameter/thickness ratio ( $D/t$ ) is usually chosen to be less than 50-60 in order to avoid unfavourable local buckling of the tube walls. Hence, 50.80 mm x 1.22 mm (nominal outside diameter x thickness) and 50.80 mm x 2.03 mm tubes whose nominal diameter/thickness ratios( $D/t$ ) are 40.6 and 20.0

respectively were chosen for the models. For the length(L) of the models, 1.0, 1.4 and 1.8 m, whose approximate nominal length/diameter ratios(L/D) are 20.3, 28.5 and 36.6 respectively, were selected, dictated primarily by the available test facilities.

The yield stress of normally fabricated offshore tubulars is in the range 250-400 N/mm<sup>2</sup>. However, the tube material procured for the present test was found to be variable and to have a much higher yield stress of 500-600 N/mm<sup>2</sup>[82]. In order to achieve yield strengths in the practical range, it was decided that the tubes should be subjected to heat-treatment.

### 2.2.2 Heat-Treatment

The factors which can influence the yield strength of heat-treated material are the heating temperature, the warming-up time(heating rate), the holding time, and the cooling-down time(cooling-rate) of the heat-treatment and the original yield stress. Some heat-treatments, whose aims were to eliminate the residual stresses associated with fabrication or cold-drawing procedures and/or to reduce the yield strength of cold-formed material by removing the work-hardening effect, were reported in refs.65, 67, 66, 69 and 83.

However, it proved impossible to derive any relationship between the aforementioned factors and the final yield strength from the data given in these references because the heat-treatment procedures were not fully described except in ref.83. The heating temperatures ranged from 550°C to 800°C while very slow cooling was common. Hence a series of systematic preliminary heat-treatments was proposed to select the appropriate procedure for the current models. Firstly, six 300 mm length tensile specimens were cut from each parent tube and flattened(the effect of flattening on the static tensile yield strength is discussed later). Secondly, the specimens were heat-treated in a sand box inside the University's Hedin Electric Furnace whose chamber volume is 43,000 cm<sup>3</sup> to various heating temperatures in the range 350°C to 750°C with various holding times between 0 and 3 hours. Finally the



furnace was allowed to cool overnight to ambient conditions.

Results of the preliminary heat-treatment are presented in Figs.2.1, 2.2(a) and 2.2(b). In Fig.2.1 the effect of heat-treatment on the material properties of cold drawn seamless tube is clearly shown. As can be seen in the figure the yield strength can be reduced to a required value and the residual stress can be removed through a heat-treatment. However, the Young's modulus remains nearly constant irrespectively. In Figs.2.2(a) and 2.2(b) the variation of yield stress with heating temperature and holding time are plotted respectively. From these results, a temperature of 550°C and two hours of holding time were selected for the first main heat-treatment, while 550°C and three hours of holding time were selected for the second, the aim being to reduce the yield stress to some 250 N/mm<sup>2</sup> while also avoiding the development of thick scale.

The two main heat-treatments were conducted by an independent firm. However, the results of these showed the yield stress to be higher than expected, by some 200 N/mm<sup>2</sup>. The much shorter warming-up time(see Fig 2.3) which could not be simulated in the preliminary heat-treatments seemed to be the main cause of the difference. The scale effect arising from the difference in furnace sizes may also have been a contributing factor. It is suggested that warming-up time is an important factor in determining heat-treatment effects.

### 2.2.3 Pre-Test Measurements

The procured tubes were cut in accordance with the schedule shown in Fig.2.4. Both ends of each model were machined flat. Models B1, B3, D4, E3 and H1 were sent off for the first main heat-treatment and the others for the second one. The detailed procedure of both main heat-treatments is described in the previous section. Following heat-treatment all models were marked with a grid using a steel pin. The grid was to assist in the measurements described below.

After grid-marking, the thickness, circularity and straightness of each tube was surveyed. Also their static tensile yield stress and Young's modulus were measured.

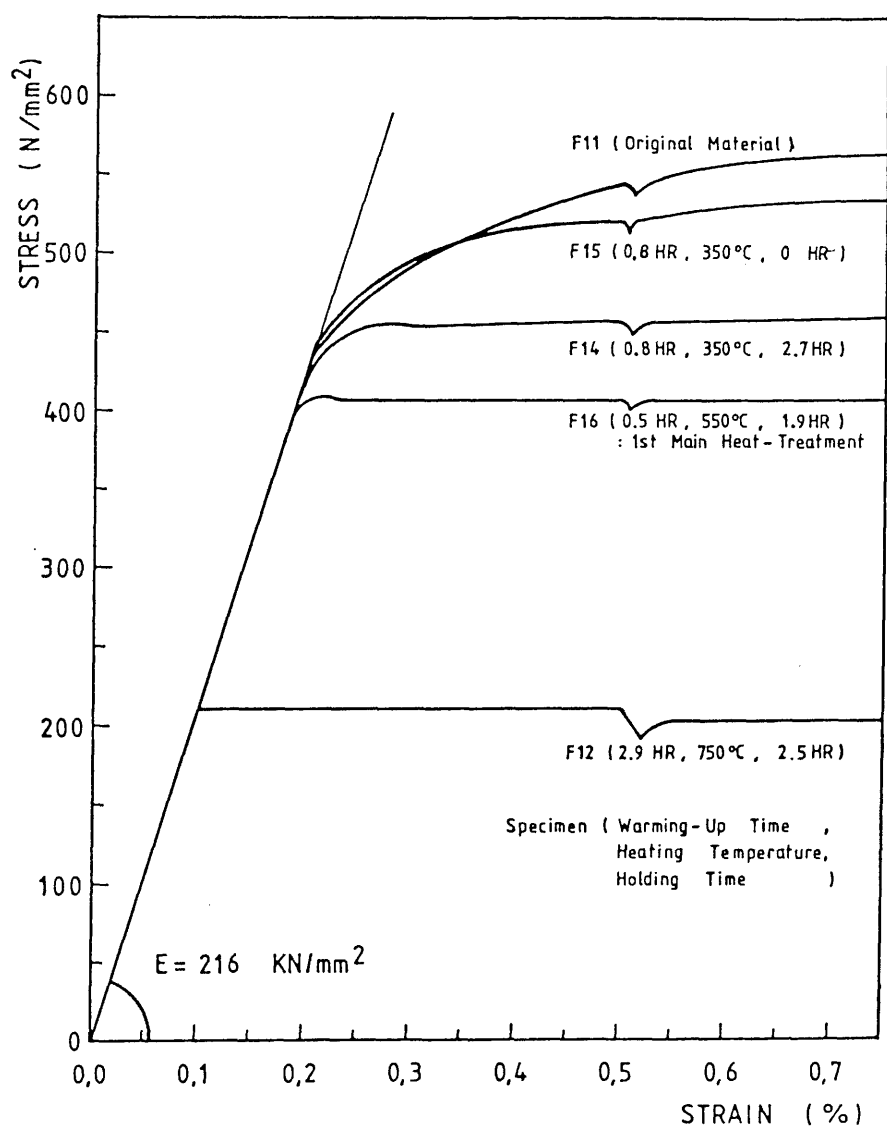


Fig. 2.1 Effect of Heat-Treatment on Material Properties  
of Cold-Drawn Seamless Tube

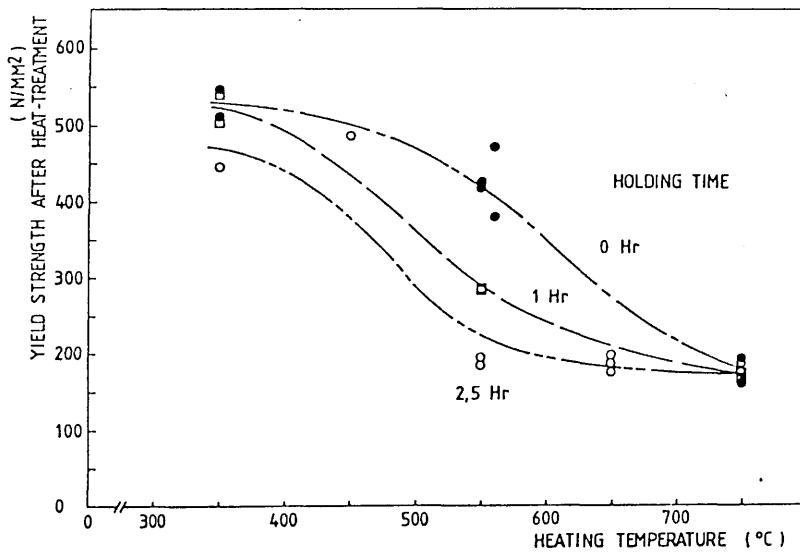


Fig. 2.2(a) Effect of Heating Temperature on Yield Strength of Cold-Drawn Seamless Tube

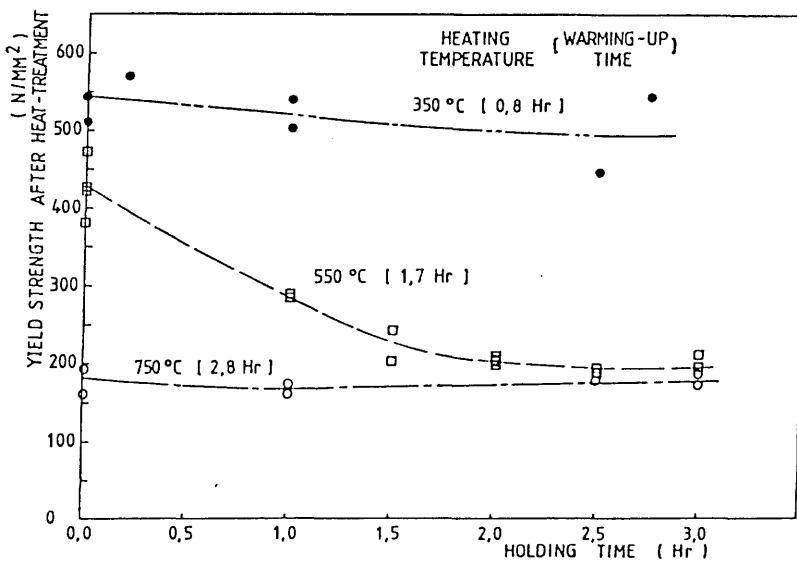


Fig. 2.2(b) Effect of Holding Time on Yield Strength of Cold-Drawn Seamless Tube

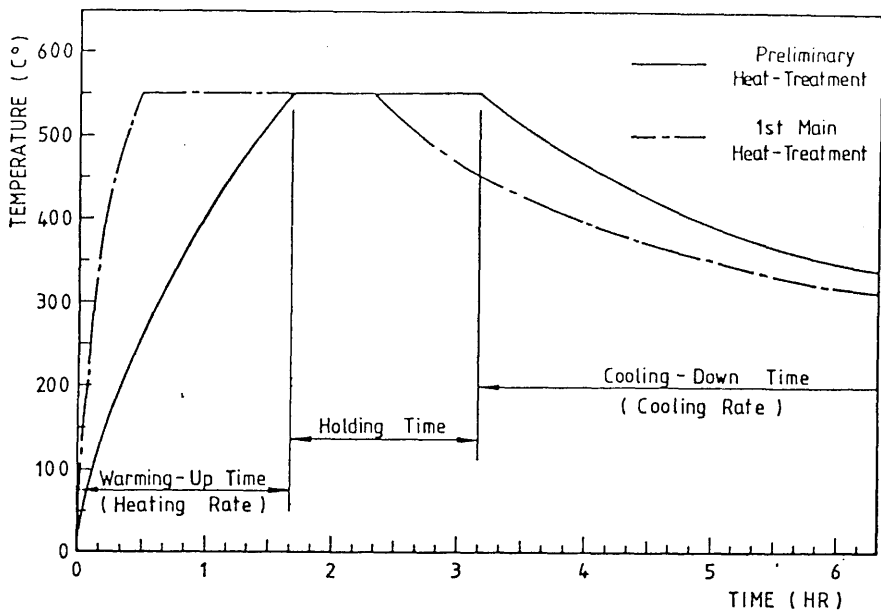


Fig. 2.3 Typical Temperature History of Heat-Treatments

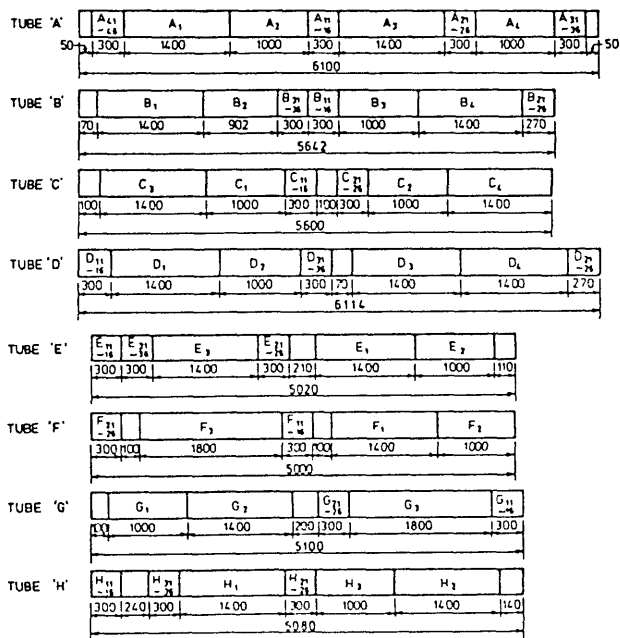


Fig. 2.4 Tube Cutting Plan

· Geometries : Thickness was measured at 60 points along each tube using a Krautkramer-Branson CL204 ultrasonic thickness probe with a grease couplant. Records were taken at the ends, the quarter points and the mid-length of each model every 30° around the circumference. The measurements were checked against micrometer readings taken at the tube ends. Outside diameter was measured at these same positions using a vernier caliper.

Five LVDTs were used for the measurement of initial out-of-straightness. Their output was logged using a Solatron 3510 Integrated Measuring System in conjunction with an Apple micro-computer. Prior to the model measurements, the LVDT gauge factors were checked with slip gauges and the reference points for the LVDTs were determined using a solid, straight and round datum bar whose straightness had checked with a straight edge and circularity with a vernier caliper.

The datum bar, whose measured mean diameter was 50.55 mm, was positioned in a lathe. Five LVDTs were placed at positions selected according to tube length and the bar position. The reference point of each LVDT, which was distant 25.27 mm from the centre of the lathe, was then found by taking the mean of the corresponding results. With the reference points established, the datum bar was replaced by a model. The distances between the reference points and the corresponding points on the model were then recorded every 30° around the circumference. The initial out-of-straightness was then found by calculating the deviations at mid-length and quarter points from the straight line joining the end points. The average initial out-of-straightness was determined by taking the mean of the two deviations in the same plane.

· Material properties : Material properties were determined from at least six tensile tests from each parent tube. Test specimens were prepared in accordance with ref.84 and tests were conducted more or less according to the procedure recommended in ref.85. Tests were performed in a Tinius-Olsen 0-20,000 lb testing machine. The speed of cross-head separation is recommended to provide a rate of strain in the specimen of 300 micro-strain per minute in the plastic range of the test. For the purpose of these tests,

however, the specimens were loaded steadily at a rate of strain such that it took about five minutes to pass the yield point and at a strain of 5000 micro-strain the cross-head was stopped for two minutes. The minimum value recorded during this period was taken as the corresponding static tensile yield stress. Young's modulus was obtained from the initial slope of the stress-strain curve.

## 2.3 Lateral Impact Tests

### 2.3.1 Test Rig

· Striker and Runway : In order to bring a rigid striker, having a pre-determined amount of kinetic energy, into violent contact with a deformable model, it was decided to use an existing runway and striker (see Fig.2.5). The striker consisted of a box mounted on four wheels having a vertical aluminum wedge, whose angle was  $45^\circ$  and tip was sharp, mounted on the front of the box. The light weight of the striker was 18.8 kgf which could be increased to 50.0 kgf by the addition of weights in the box. The runway was constructed from a pair of angled rails mounted on a frame. It consisted of a straight path inclined at  $30^\circ$  which was joined to a horizontal one by a curved segment. By releasing the striker from different heights on the inclined section of the runway, the speed of the striker could be varied up to approximately  $3.0 \text{ ms}^{-1}$ . Further details are given in ref.29.

· Test Rig : In aiming to avoid the possibility of fracture of the tension side and local crippling of the compression side of the model ends, it was decided to adopt simply supported roller conditions. This would allow free rotation and axial movement of the ends of the specimens but no lateral movement. This configuration was achieved with a test rig which consisted of a pair of rigid frames bolted to the laboratory floor and a pair of model holders. Each model holder was doubly-hinged, created by two carefully machined pins, and was mounted on the rear face of the front member of the rigid frame (see Fig.2.5). The width of the model holders was 50 mm and their insides were lined with rubber in order to prevent unfavourable scratching of the model surface during installation and testing.

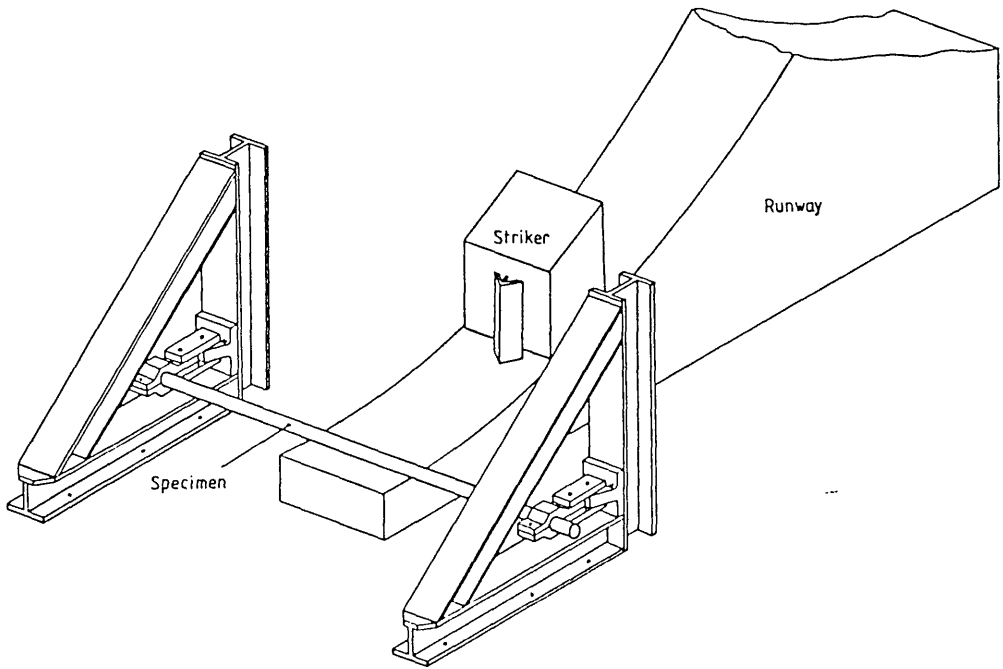


Fig. 2.5 Arrangement of Runway and Test Rig for Lateral Impact Test

### 2.3.2. Measurements and Recording

· Light Emitting Diode and Detector : For recording of the displacement history of the striker and the overall bending deformation history of the struck model, a light emitting diode (LED 1) was attached to the top of the front wall of the striker and to the mid- and quarter-points of the model (LED 2 and 3 respectively) and a light detector was attached to a beam of the laboratory ceiling. The principle on which the system is based is that when infra-red light from an LED is focussed onto the detector surface, a photocurrent divided among 4 electrodes occurs which is then used to obtain 2 signals linearly related to the coordinates of the LED on a plane parallel to the detector surface. The velocities of the striker immediately before and after impact were obtained from the slopes of the displacement curve of the LED on the striker.

- Infra-Red Switches : Two infra-red switches were placed 110 mm apart near the bottom end of the runway to confirm the striker velocity obtained from the LED on the striker. The first one was set to start a timer and the second to stop it as the striker passed in front of each. The impact speed was estimated as the ratio of the distance between the two infra-red switches to the time recorded.
- Mass of Striker : The mass of the striker including the vertical wedge and any added lead weight was measured using a weight scale.
- Strain-Gauging : All the models were gauged with nine or ten quarter bridge strain gauges to recorded the strain histories during and after impact and their residual strains (Fig.2.6).

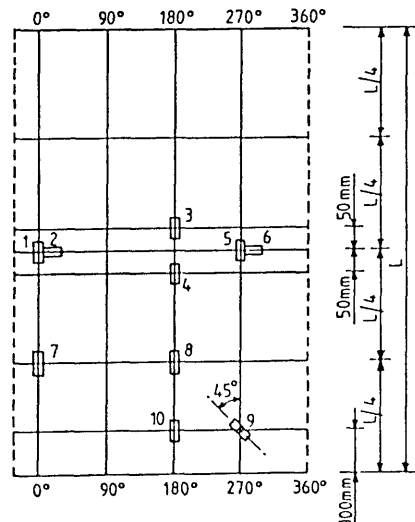


Fig. 2.6 Strain Gauge Arrangement for Lateral Impact Test



· High Speed Tape Recorder : In order to store the output from the three LEDs and four strain gauges during the impact tests a seven channel high speed tape recorder was used in conjunction with four strain amplifiers. The tape speed was set to 60 inches per second for recording and to 15/16 inches per second for realisation of the recorded data using a four channel pen-recorder.

A preliminary test on a dummy model was made to measure the deceleration of the striker during impact using an accelerometer attached to the dummy in order to establish the history of the interactive force between the striker and the model. However, from the recorded results it was not possible to separate the rigid body acceleration of the striker from the vibrations of the member on which the instrument was mounted. Hence, the accelerometer was not used any more in the main tests. A video tape recording was made of the first three tests in the hope of developing a better understanding of the sequence of local denting and overall bending damage which occurred during the impact. However, it was not used further because the recording speed of 25 frames per second was not fast enough for this purpose.

### 2.3.3 Model Installation

The model was carefully positioned in the test rig such that first contact by the striker would occur at mid-length and at the 180° position on the circumference. Both ends of the model were then gripped firmly in the model holders. After installation of the model, wiring of the strain gauges and fixing of the LEDs, the striker with added weights if necessary was released at particular heights on the runway to acquire the required speed.

### 2.3.4 Extent of Damage Measurements

The same technique which was established for the initial out-of-straightness measurements (see section 2.2.3) was employed to measure the overall bending damage on the struck model. The deviation from the straight line joining the two end points were measured on the opposite side to that of the dent at the mid- and quarter-

length positions. Measurement was also made at the dent centre when the dent centre was off mid-length. The overall bending damage of the specimen centroid was then calculated by adding the change of the distance between the specimen centroid and the opposite to that of the dent (for details see section 2.5)

For the local denting damage measurements, the outside diameter of the struck model was measured using a vernier caliper. Measurements were performed in the axial plane coinciding with the position of maximum indentation along the longitudinal centre line of the dent every 5 mm up to points 50 mm away from the transverse centre line and every 10 mm beyond these points. The dent depths were estimated by subtracting these values from the initial outside diameter measurements of the model.

## 2.4 Results

### 2.4.1 Pre-Test Measurements

Detailed results of all the pre-test measurements are presented in Appendix B of ref. 82. They include the thickness, outside diameter and initial out-of straightness measurements including initial out-of-straightness plots, yield strength and Young's modulus values with at least one typical stress-strain curve per each parent tube. In Table 2.1, a summary of mean model geometry and material properties is given including some corresponding COVs and geometric parameters.

- Initial Out-of-Roundness : In Table 2.1, the initial out-of-roundness in the form of initial ovality,  $(D_{\max} - D_{\min}) / D_{\text{mean}} \times 10^2$ , is presented. For most of the models the initial ovality at both ends is much higher than in the middle. Also the ovality of some thinner models (nominal thickness = 1.22 mm) is higher than that of the remaining specimens. The initial ovality of models A4, B4 and C4 is higher than the limit of 1.00 specified in the DnV-OS Rules[86].
- Initial Out-of-Straightness : Initial out-of-straightness was determined by averaging the values in each plane, i.e. 0°-180° and so on, of the model. The initial out-of-straightness of models C3, F3 and H2 is higher than the limit  $(d_{oi}/L \times 10^3 = 1.5)$  specified in ref. 86.

Table 2.1 Measured Model Geometry and Material Properties

Model	Length(mm)		Outside Diameter		Diameter to Mid-Thickness		Thickness		Maximum Initial Out-of-Straightness		Heat Treatment		Static Tensile Yield Stress		Young's Modulus		d <sub>oi</sub> /L  x10 <sup>3</sup>
	Actual	Impact	D <sub>O</sub>	Mean	COV	D	t	Mean	COV	d <sub>oi</sub>	Straightness	Treatment	Mean	COV	Mean	COV	
L	L <sub>i</sub>	(mm)	(mm)	(%)	(mm)	(mm)	(%)	(mm)	(mm)	(mm)	(mm)		(N/mm <sup>2</sup> )	(%)	(N/mm <sup>2</sup> )	(%)	
A3	1400	1350	50.88	0.12	49.65	1.23	1.46	0.37	2nd	472	4.25	200000	4.73	40.4	27.2	0.26	
A4	1000	950	50.89	0.35	49.69	1.20	1.41	0.28	2nd	472	4.25	200000	4.73	41.4	19.1	0.28	
B1	1400	1350	50.86	0.15	49.66	1.20	2.18	0.72	1st	491	2.52	205000	8.20	41.4	27.2	0.51	
B3	1000	950	50.92	0.11	49.72	1.20	0.70	0.50	2nd	482	2.36	204000	9.99	41.4	19.1	0.50	
B4	1400	1350	50.86	0.22	49.66	1.20	1.03	0.28	2nd	482	2.36	204000	9.99	41.4	27.2	0.20	
C1	1000	950	50.97	0.21	49.76	1.21	1.59	0.91	2nd	441	3.00	232000	12.5	41.1	19.1	0.91	
C2	1000	950	50.91	0.18	49.69	1.22	1.81	0.31	2nd	441	3.00	232000	12.5	40.7	19.1	0.31	
C3	1400	1350	50.86	0.14	49.64	1.22	1.79	3.68	2nd	441	3.00	232000	12.5	40.7	27.2	2.63	
C4	1400	1350	50.85	0.24	49.63	1.22	1.71	0.25	2nd	441	3.00	232000	12.5	40.7	27.2	0.18	
D1	1400	1350	50.91	0.09	49.71	1.20	1.71	0.43	2nd	480	2.56	211000	6.77	41.4	27.2	0.31	
D2	1000	950	50.98	0.10	49.77	1.21	1.18	0.14	2nd	480	2.56	211000	6.77	41.1	19.1	0.14	
D3	1400	1350	50.91	0.08	49.70	1.21	1.57	0.64	1st	485	3.07	210000	7.83	41.1	27.2	0.46	
D4	1400	1350	50.90	0.14	49.69	1.21	1.70	0.28	1st	485	3.07	210000	7.83	41.1	27.2	0.20	

(cont'd)

Table 2.1 Measured Model Geometry and Material Properties(cont'd)

Model	Length(mm) for		Outside Diameter		Diameter to Mid- Thickness		Thickness		Maximum Initial Out-of- Straightness		Heat Treatment		Static Tensile Yield Stress		Young's		d <sub>oi</sub> /L  x10 <sup>3</sup>																																																																																																																																																																																																																																																																																																																																																																																																																																																																																																																																																																																																																																																																																																																																																																																																																																																																																																																																																																																																																																																																																																																																																																																																																																																																																																																																																								
	Actual	Impact test	D <sub>O</sub>  Mean	COV  (%)	D  (mm)	t  Mean	COV  (%)	d <sub>oi</sub>  (mm)	Straightness	1st	2nd	2nd	2nd	2nd	2nd	2nd		2nd																																																																																																																																																																																																																																																																																																																																																																																																																																																																																																																																																																																																																																																																																																																																																																																																																																																																																																																																																																																																																																																																																																																																																																																																																																																																																																																																																							

- Notes :
- The nominal outside diameter of all of the models is 50.80 mm, and the nominal thicknesses are 1.22 mm (A3 to D4) and 2.03 mm (E3 to H3).
  - The geometry and material properties of model F1p are the same as model F1.
  - Details of 1st and 2nd heat-treatments are given in section 2.2.2

· Yield Strength and Young's Modulus : Most of the tensile test specimens were cut from 300 mm long heat-treated stubs and then flattened and machined. Initially, the influence of flattening on the yield strength was investigated by comparing the mean yield strength of flattening specimens with that of curved specimens. The results are given in Table 2.2.

Table 2.2 Effect of Flattening of Tensile Test Specimen on Yield Strength

Nominal Thickness (mm)	Curved		Flattened		
	Specimen	Mean Yield Strength (N/mm <sup>2</sup> )	Specimen	Mean Yield Strength (N/mm <sup>2</sup> )	Change
1.22	A21, A23, A25	498	A22, A24, A26	465	- 7 %
	B34, B35, B36	497	B31, B32, B33	485	- 2 %
2.03	G21, G23, G25	422	G22, G24, G26	436	+ 3 %
	H34, H35, H36	425	H31, H32, H33	438	+ 3 %

From the table, it seems likely that the values of yield strength obtained from the flattened specimens can be used as a measure of the yield stress in the corresponding model because the changes due to flattening are within the variation expected of a variable having a COV of 5-6 %. The tests on the curved specimens demonstrated typical elastic-rigid-plastic stress-strain responses, which confirmed the unknown residual stresses due to cold forming had been removed by the heat treatment, while those on the flattened specimens demonstrated a 'rounded' response. Most of the specimens demonstrated a 1-4 % COV in yield strength (see Table 2.1) while the mean yield strength of the thinner models (nominal thickness = 1.22 mm) was greater than that of thicker specimens (nominal thickness = 2.03 mm) by some 40 N/mm<sup>2</sup>. Of the

total number of 82 specimens, a mean of  $2.12 \times 10^5 \text{ N/mm}^2$  together with an 8.8 % COV was obtained for Young's modulus. The dubious accuracy of drawing tangential lines to rounded stress-strain curves contributes to the scatter found for this material constant.

#### 2.4.2 Impact Tests

From recordings made during the impact tests, the following tables and figures have been prepared and are presented for each model in turn in Appendix C of ref. 82:

- the mass and impact speed of the striker and the residual strains in the struck model ;
- the dynamic recording of the LEDs and the strain gauges ;
- measurements of the extent of damage ; and
- plots of the extent of damage.

A summary of the test results is given in Table 2.3. They include the striker's mass and the velocities immediately before and after impact, the extent of damage of the struck model together with their non-dimensionalised values, impact duration and the period of elastic vibration after impacts.

Model F1 was tested again with a different mass and velocity for the striker because only negligible residual strains were generated by the original test: the second test has been designated F1p. During the test on model B4 the high speed tape recorder was not operated properly so that its dynamic recording results were lost. For the test on model H1 the wire connecting LED1, which was fixed to the striker, was cut due to its significant lateral movement.

· LED Results : The velocity of the striker immediately before and after impact were measured from the slopes of displacement history of LED1. The result was then compared with the value measured using the infra-red switches. All the velocities measured using LED1 were smaller than those found from the infra-red switches, except that of model F2. The difference between the result of the two methods is probably due to the deceleration of the striker during its passage over the distance of some 300 mm between the infra-red switches and the model.

Table 2.3 Lateral Impact Test Results

Model	Mass of Striker $M_s$ (kg)	Initial Velocity of Striker $V_i$ (m/s)	Rebound Velocity of Striker $V_r$ (m/s)	Peak Bending Deformation $d_{opk}$ (mm)	Extent of Damage		Centre of Impact		$d_{opk}/L_i$	$d_d/D$	$d_o/L$	Impact Duration	Period of Elastic Vibration after Impact
					Depth of Dent $d_d$ (mm)	Out-of-Straightness $d_o$ (mm)	Longi. (x $1/L_i$ )	Circum. (deg.)	$\delta_{opk} \times 10^3$	$\delta_d \times 10^2$	$\delta_o$	$T_D$ (ms)	$T_E$ (ms)
A3	18.8	2.34 (2.42)	0.94	19.8	3.5	4.12	- 0.003	179	14.7	7.1	2.9	33.6	18.0
A4	18.8	2.43 (2.77)	1.16	12.4	4.6	3.51	0.011	190	13.1	9.3	3.5	25.0	12.7
B1	23.5	2.52 (2.63)	1.47	19.5	3.1	3.90	0.005	170	14.4	6.2	2.8	37.8	17.5
B3	28.3	1.57 (1.75)	0.89	6.5	2.8	1.69	0.000	177	6.8	5.6	1.7	28.0	12.8
B4	28.3	--- (2.63)	---	---	2.2	2.37	0.005	173	---	4.4	1.7	---	---
C1	41.1	1.18 (1.26)	0.53	16.8	2.0	1.13	0.000	185	17.7	4.0	1.1	31.3	13.1
C2	41.1	2.32 (2.64)	0.84	24.3	10.4	14.96	0.000	169	25.6	20.9	15.0	51.4	13.3
C3	41.1	0.92 (1.07)	0.69	11.6	0.5	0.17	0.001	178	8.6	1.0	0.1	45.6	15.5
C4	41.1	2.06 (2.15)	1.04	24.3	6.8	12.03	0.009	180	18.0	13.7	8.6	61.7	15.5
D1	28.3	1.16 (1.15)	1.04	10.1	0.2	0.52	0.000	175	7.5	0.4	0.4	37.8	17.2
D2	28.3	2.52 (2.83)	1.12	---	6.2	5.87	0.013	177	---	12.5	5.9	30.5	9.2
D3	28.3	2.55 (2.84)	1.24	25.0	5.3	7.78	0.012	180	18.5	10.7	5.6	41.9	17.3
D4	41.1	2.59 ( --- )	1.09	36.4	9.1	20.70	0.000	172	27.0	18.3	14.8	69.7	19.5

(cont'd)

Table 2.3 Lateral Impact Test Results(cont'd)

Model	Mass of Striker $M_S$ (kg)	Initial Velocity of Striker $V_i$ (m/s)	Rebound Velocity of Striker $V_r$ (m/s)	Peak Bending Deformation $d_{opk}$ (mm)	Extent of Damage		Centre of Impact		$d_{opk}/L_i$	$d_d/D$	$d_o/L$	Impact Duration	Period of Elastic Vibration after Impact
					Depth of Dent $d_d$ (mm)	Out-of-Straightness $d_o$ (mm)	Longi. Circum. (x $1/L_i$ )		$\delta_{opk} \times 10^3$	$\delta_d \times 10^2$	$\delta_o$	$T_D$ (ms)	$T_E$ (ms)
E3	28.3	2.49 (2.66)	2.14	16.3	0.4	0.51	0.011	183	12.1	0.8	0.4	30.5	15.9
F1	50.0	0.55 (0.82)	0.31	4.4	0.0	0.00	0.000	180	3.3	0.0	0.0	39.8	14.1
F1p	41.1	1.91 (1.97)	1.13	18.1	0.8	1.13	0.000	191	13.4	1.6	0.8	36.1	15.9
F2	41.1	1.78 (1.65)	1.45	8.9	2.1	1.99	-0.009	197	9.4	4.3	2.0	23.4	6.1
F3	28.3	2.53 (2.99)	1.70	44.4	1.2	2.76	0.003	182	25.4	2.5	1.5	42.2	23.9
G1	28.3	2.24 (2.73)	1.34	10.4	1.7	1.73	0.011	180	10.9	3.5	1.7	11.4	5.9
G2	28.3	2.59 (2.81)	1.84	22.2	1.8	3.40	0.000	192	16.4	3.7	2.4	32.0	15.9
G3	41.1	1.69 (1.86)	1.41	23.7	0.2	-0.54	0.000	192	13.5	0.4	-0.3	52.2	24.1
H1	18.8	2.90 (2.96)	--	17.5	0.3	0.40	0.014	183	13.0	0.6	0.3	25.3	16.1
H2	41.1	2.55 (2.55)	1.39	23.4	3.2	6.06	0.000	173	17.3	6.5	4.3	39.1	15.9
H3	41.1	1.08 (1.16)	0.64	5.9	0.0	0.01	0.000	180	6.2	0.0	0.0	23.1	10.2

Notes : · Initial velocities in parentheses were measured using Infra-Red Switches.

· Minus sign of out-of-straightness denotes opposite direction.

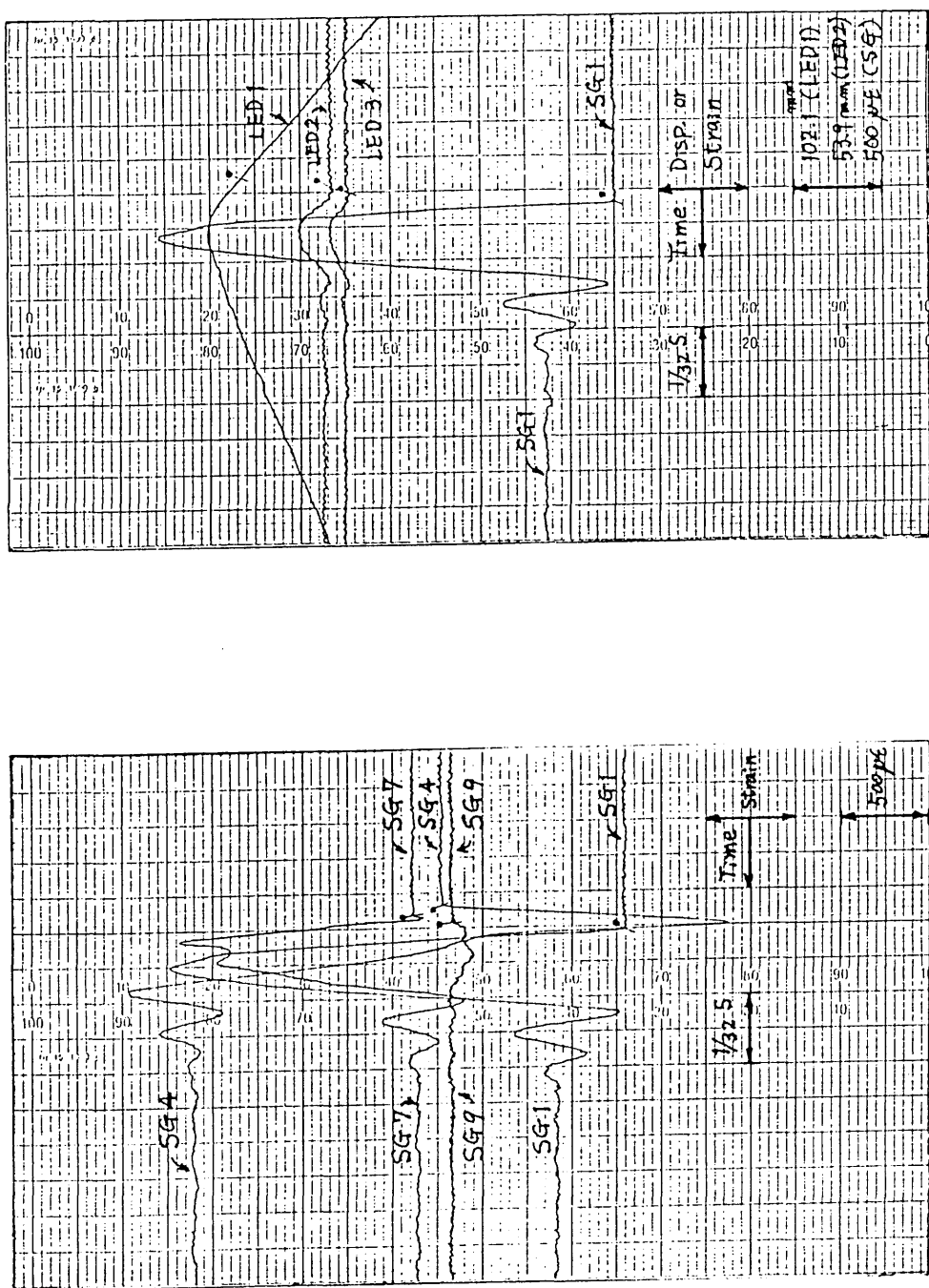
· Longitudinal location of the centre of impact was measured from the mid-length, (+): towards top, (-): towards bottom.



The outputs from LED2 and 3, attached at the mid- and quarter-lengths of the model respectively, were found to be very useful in understanding the overall bending behaviour of the model during and after impact. Some delay in their movement after the beginning of contact between the striker and the model indicated that the purely local denting occurred before overall bending together with some additional local denting deformation. Most of the output from LED2 and 3 showed that elastic overall bending vibrations occurred after impact, but some of these were more clearly demonstrated by the strain gauges.

· Strain Gauge Results : Most of the strain history curves obtained from the output of the four strain gauges monitored during each test initially have sharp knees which can be used to indicate the beginning of contact between the striker and the model and then very apparent elastic vibrations following impact. They proved to be very useful in the determination of both the impact duration and the period of elastic vibration after impact. Impact duration was determined by measuring the time from the beginning of contact to the start of elastic vibration. There is some disagreement between the results for residual strain found by using the strain meter and from the strain amplifier, especially for the first three tests on models A3, B1 and C3, in which proper strain gauge wire terminals were not used.

In Figs.2.7(a)-2.7(e) the dynamic records of output from three LEDs and four strain gauges are presented for A3, C4, D3, E3 and F3 in turn. A similar shape to those for LED 2 and LED 3 was obtained from the output of strain gauge no.1, which shows monotonic increase and decrease of strain followed by a damped free vibration. However, the output from strain gauges no.5, no.7, no.8 and no.10 displays a double peak or plateau and in the very early stage of the strain history obtained from strain gauges no.7, no.8 and no.10 negative strains can be perceived. Interestingly, a peculiar shape was demonstrated by the output from strain gauges no.3 and no.4, which shows the transition from bending of the tube wall to membrane action in the dent side.



/ denotes beginning of contact

Fig. 2.7(a) Dynamic Results of Lateral Impact Tests : model A3

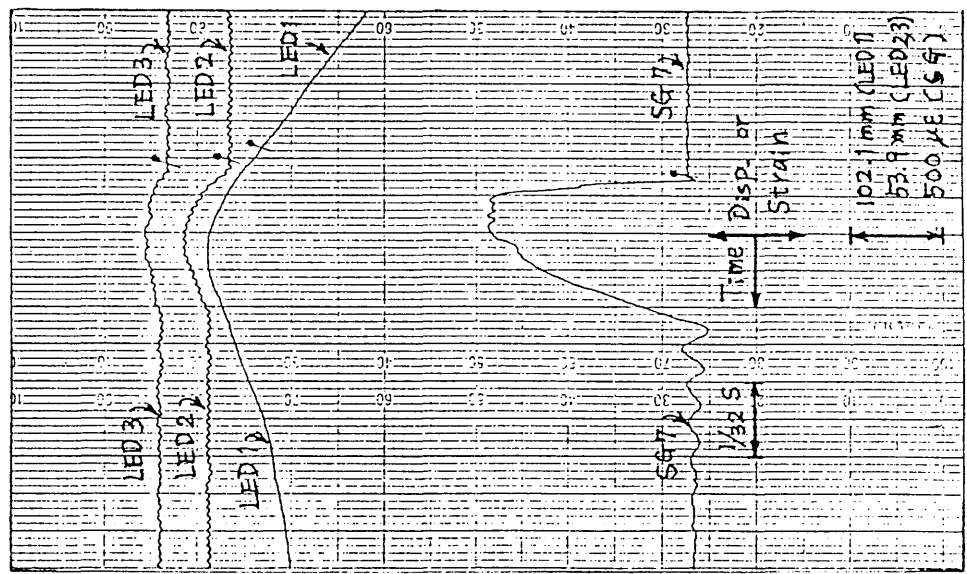
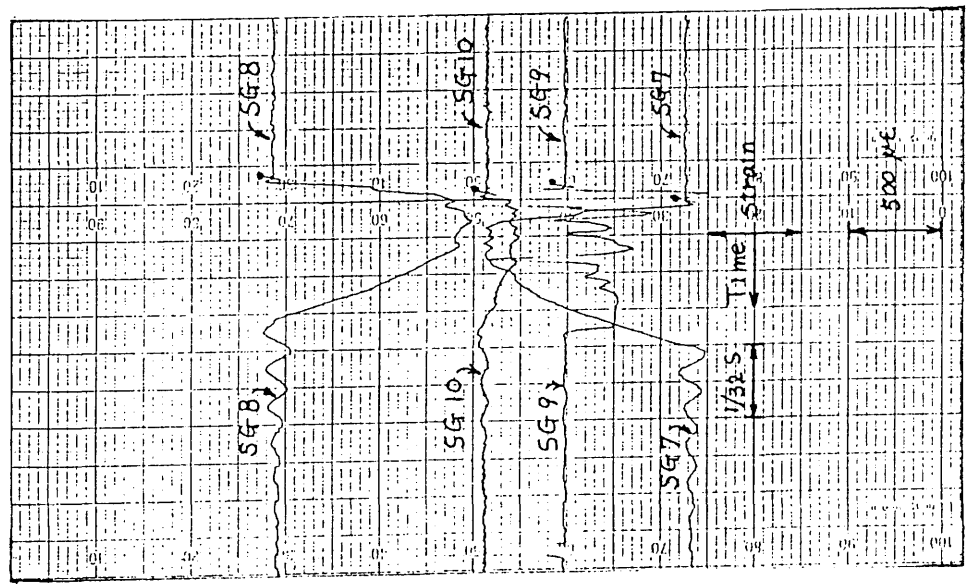
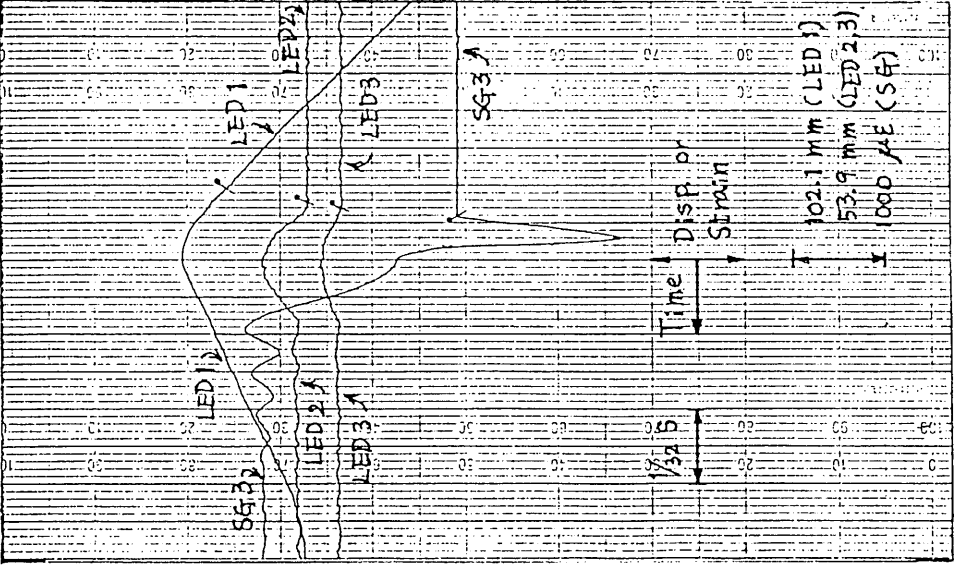
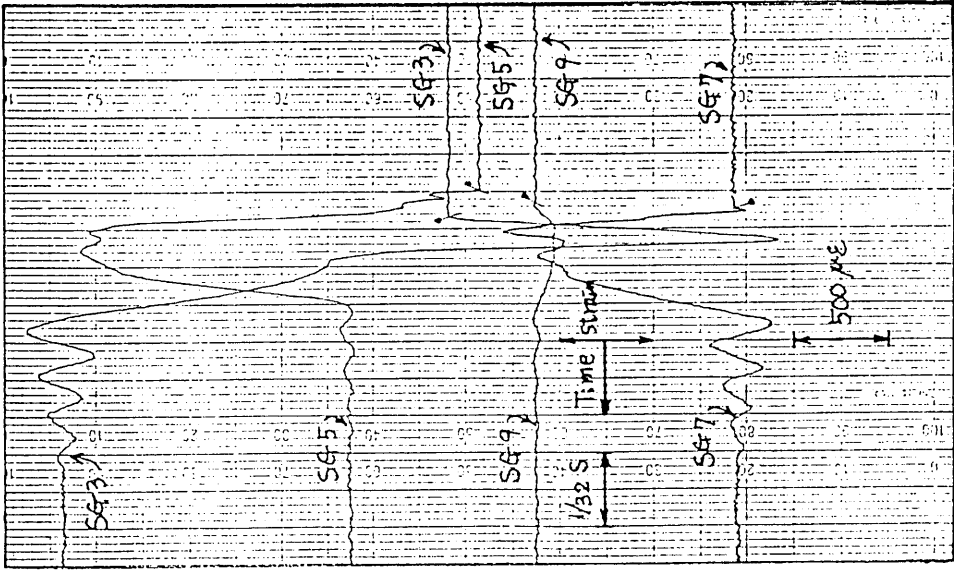
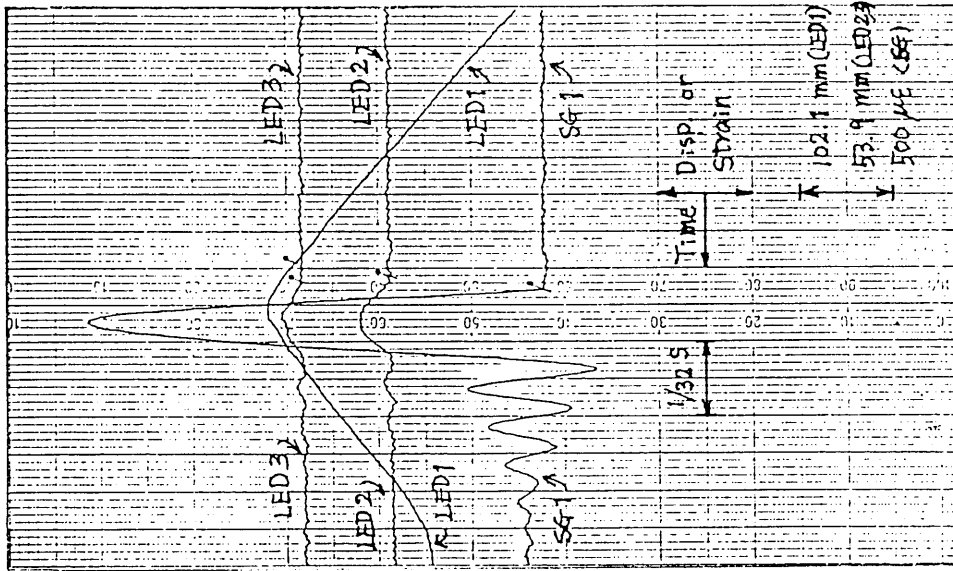
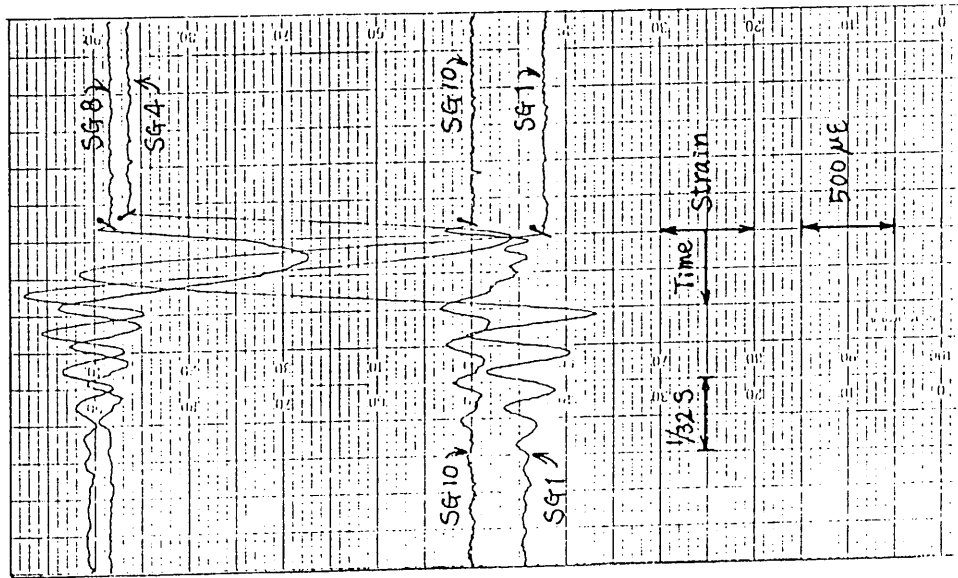


Fig. 2.7(b) Dynamic Results of Lateral Impact Tests : model C4



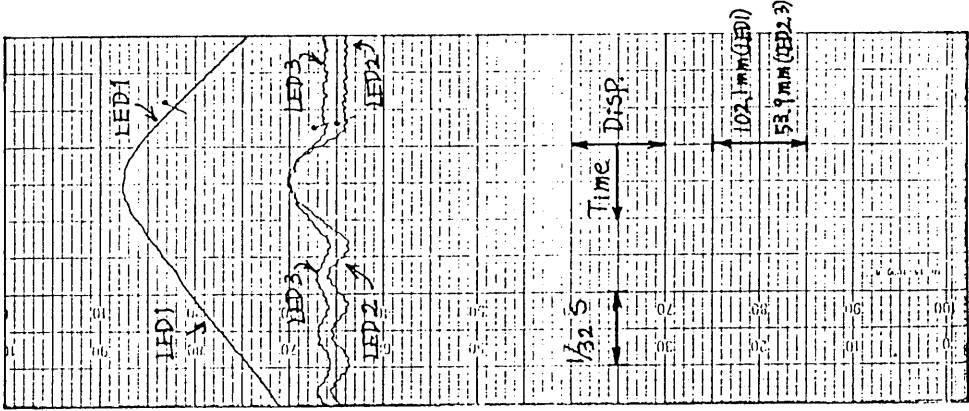
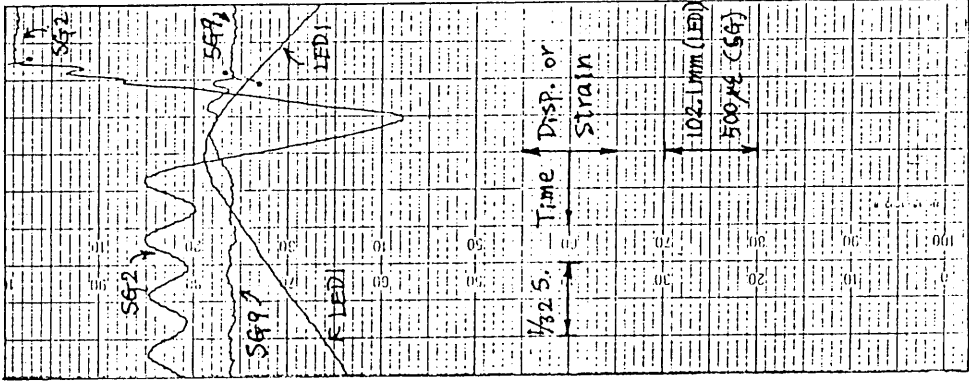
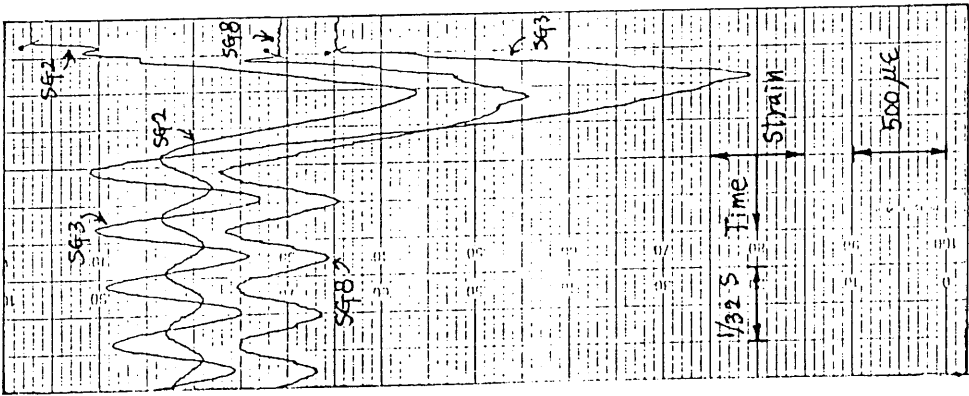
↑ denotes beginning of contact

Fig. 2.7(c) Dynamic Results of Lateral Impact Tests : model D3



denotes beginning of contact

Fig. 2.7(d) Dynamic Results of Lateral Impact Tests : model E3



↑ denotes beginning of contact

Fig. 2.7(e) Dynamic Results of Lateral Impact Tests : model F3

· Extent of Damage : The locations of the centre of impact are given in Table 2.3. In some tests the striker unexpectedly impacted off centre both longitudinally and circumferentially due to its lateral movement and bounce. The depth of dent and out-of-straightness plots show a corresponding asymmetry. Interestingly, the tests on models C3 and G3 showed a negative out-of-straightness, i.e. towards the striker. The reason for this is not obvious. The depth of dent and out-of-straightness non-dimensionalised with respect to model diameter and length respectively are given in Table 2.3. The plots of extent of damage for models A3 and C2, which show very sharp dents and dog-leg type bows, are given in Figs.2.8(a) and 2.8(b) respectively.

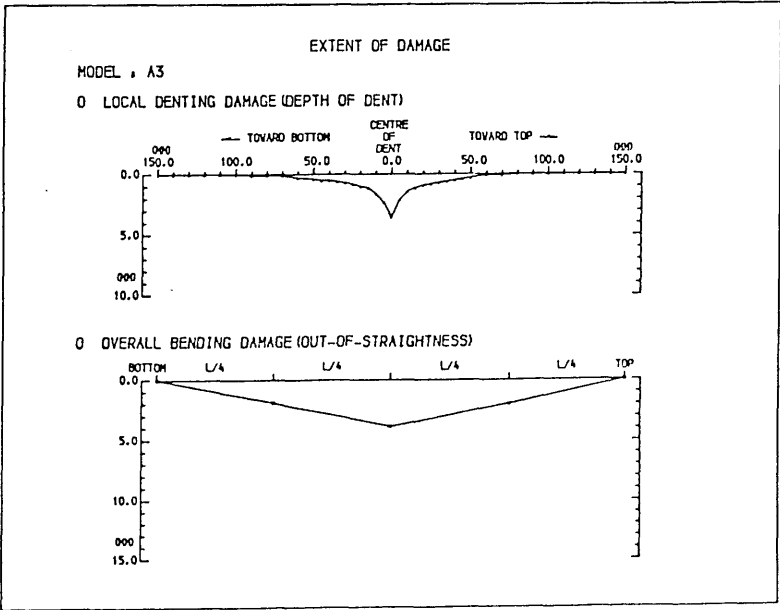


Fig. 2.8(a) Plot of Extent of Damage : model A3

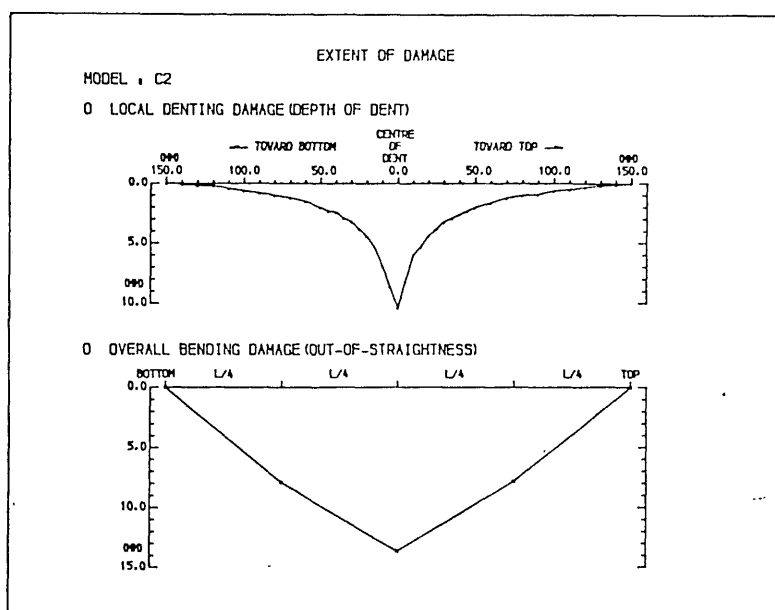


Fig. 2.8(b) Plot of Extent of Damage ; model C2

## 2.5 Geometric Configuration of Damaged Tubulars

In most of analytical methods to predict the structural behaviour of damaged tubulars a somewhat unrealistic assumption has been adopted for the cross-sectional geometry of damaged tubulars. In refs.66, 68, and 70, the damaged cross-section was assumed to consist of a flattened segment and undeformed one. However, strictly speaking, no part of the section can remain undeformed and consequently the radius of unflattened segment can be increased at least partly. Therefore this assumption can lead to overestimation of the residual strength especially for deeply dented cases.

On the other hand for the longitudinal variation of depth of dent the relationship, given as eqn (2.1), was employed in refs.54 and 51. The equation was empirically derived using the test results of aluminum and mild steel tubes, whose diameter to thickness ratio was 31.25, loaded transversely by opposed wedge shaped



indentors[87].

$$\delta_{dx} = \delta_d \exp (-1.3 x/D) \quad (2.1)$$

where  $\delta_d$  : non-dimensionalised depth of dent at the point of impact

$\delta_{dx}$  : non-dimensionalised depth of dent at a distance  $x$  from the point of impact

The extent of denting in the longitudinal direction,  $l_d$ , was approximated to be

$$l_d = 3.5 D \quad (2.2)$$

on either side of the point of impact where the dent depth becomes less than 1% of that of impact point. Therefore it seems necessary to provide more realistic and relevant relationships for the geometric configuration of damaged tubulars.

Furthermore, in hostile offshore environments, it is often not easy to measure promptly the extent of damage of stuck tubulars. Hence it is desirable to provide a simple procedure by which the local dent and overall bending damage, by which the residual strength can be predicted, can be measured. In fact, ambiguity could arise in seeking to define the overall bending damage because it is not clearly stated in any rules or regulations. In this study the overall bending damage is defined as the maximum deviation of the plastic neutral axis along the length from the line joining these of both end sections.

#### 2.5.1 Description of Dented Section

A dented section is assumed to consist of one flattened segment, two segments of radius  $R_2$  and circumferential angle  $\theta_2$ , and one segment of radius  $R_1$  and circumferential angle  $2\theta_1$  (Fig.2.9). That assumption can violate the continuity of slope requirement at both ends of the flattened segment (this will be discussed later.).

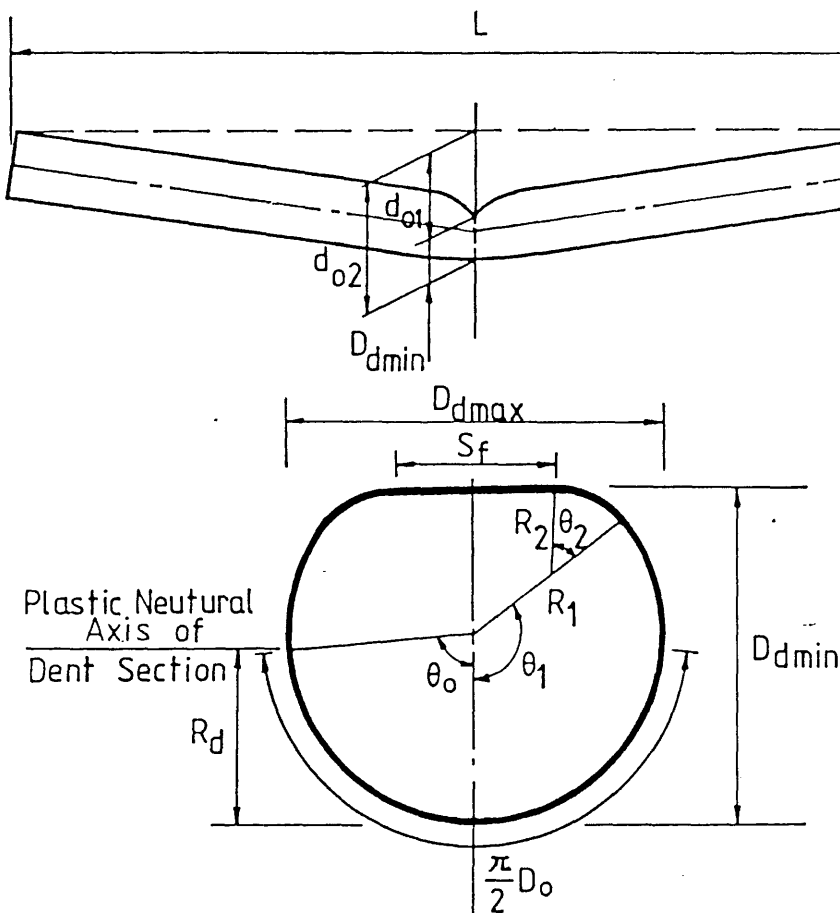


**Fig. 2.9 Geometry of Damaged Tubular Member**

From Fig.2.9, the following equations can be obtained:

$$\frac{\pi}{2} D_o = R_1 \theta_1 + R_2 \theta_2 + \frac{1}{2} S_f \quad (2.3)$$

$$\frac{1}{2} S_f = R_2 \sin(\theta_1 + \theta_2) + (R_1 - R_2) \sin \theta_1 \quad (2.4)$$

$$D_{dmin} = R_1 - R_2 \cos(\theta_1 + \theta_2) - (R_1 - R_2) \cos \theta_1 \quad (2.5)$$

$$\left. \begin{aligned} \frac{1}{2} D_{dmax} &= R_1 & ; \pi/2 \leq \theta_1 < \pi \\ &= R_2 + (R_1 - R_2) \sin \theta_1 & ; 0 < \theta_1 < \pi/2 \end{aligned} \right\} \quad (2.6)$$

If the measured values of  $D_o$ ,  $S_f$ ,  $D_{dmin}$  and  $D_{dmax}$  are provided, the shape of the dented section can be mathematically defined by solving simultaneously eqns (2.3), (2.4), (2.5) and (2.6).

It is desirable to reduce the number of values measured to determine the extent of damage for full-scale damaged tubulars. Therefore a relationship between  $D_{dmax}$  and  $D_{dmin}$ , given as eqn (2.7), has been derived empirically using the small-scale test results (see Fig.2.10).

$$\frac{D_{dmax}}{D_o} = 1 + 2.45 \left( \frac{1}{D_{dmin}/D_o} - 1 \right) \exp\{-2.4 (D_{dmin}/D_o)\} \quad (2.7)$$

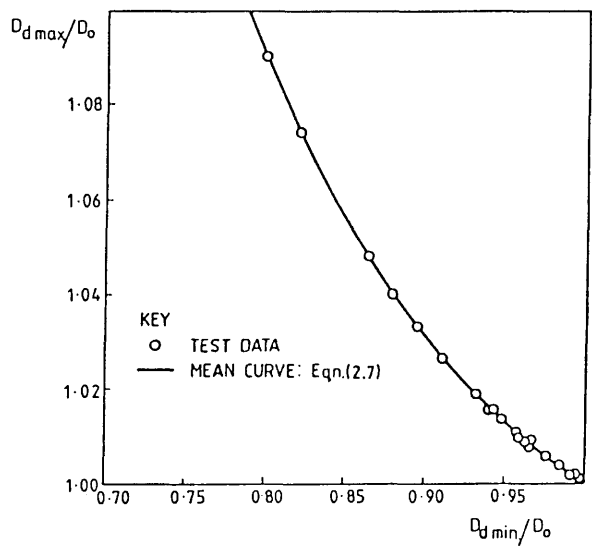


Fig. 2.10 Relationship between  $D_{dmax}$  and  $D_{dmin}$

Using the measured values of  $D_o$ ,  $S_f$ ,  $D_{dmin}$  and  $D_{dmax}$  for twenty three small-scale models whose range of  $\delta_d$  and  $\delta_o$  were 0.001-0.201 and 0.00001-0.015 respectively, the shapes of dented sections were mathematically defined: their results are given in Table 2.4.

Table 2.4 Mathematical Presentation of Geometric  
Configuration of Damaged Section

dimensions : mm, rad.

Model	<u>Measured Values</u>				<u>Calculated Value</u>				
	D <sub>o</sub>	D <sub>dmax</sub>	D <sub>dmin</sub>	S <sub>f</sub>	R <sub>1</sub>	$\theta_1$	R <sub>2</sub>	$\theta_2$	$\theta_1 + \theta_2$
A3	50.88	51.80	47.40	25.3	25.9	2.49	4.7	0.60	3.09
A4	50.89	52.20	46.30	29.3	26.1	2.39	4.1	0.68	3.07
B1	50.86	51.60	47.80	23.2	25.8	2.52	5.5	0.58	3.10
B3	50.92	51.60	48.30	21.5	25.8	2.56	5.8	0.55	3.11
B4	50.86	51.40	48.70	19.3	25.7	2.61	6.4	0.51	3.12
C1	50.97	51.45	49.15	17.9	25.7	2.65	6.5	0.47	3.12
C2	50.91	51.50	40.65	44.0	27.8	1.98	3.1	0.95	2.93
C3	50.86	50.85	50.50	6.3	25.4	2.93	10.5	0.21	3.14
C4	50.85	53.30	44.00	36.5	26.7	2.22	3.1	0.77	2.99
D1	50.91	50.95	50.80	3.8	25.5	2.99	12.9	0.15	3.14
D2	50.98	53.00	44.85	34.5	26.5	2.28	3.2	0.74	3.02
D3	50.91	52.60	45.60	32.0	26.3	2.34	3.6	0.70	3.04
D4	50.90	54.70	41.80	42.0	27.4	2.07	2.7	0.86	2.93
E3	50.91	50.90	50.40	7.7	25.5	2.89	9.8	0.25	3.14
F1p	50.91	51.10	50.15	10.5	25.6	2.79	9.9	0.34	3.13
F2	50.90	51.45	48.90	19.0	25.7	2.63	6.1	0.49	3.12
F3	50.86	51.20	49.70	14.0	25.6	2.73	7.8	0.40	3.13
G1	50.95	51.40	49.25	16.7	25.7	2.65	7.7	0.47	3.12
G2	50.92	51.30	49.20	17.2	25.7	2.67	6.3	0.45	3.12
G3	50.93	51.03	50.95	2.8	25.5	3.03	12.9	0.11	3.14
H1	50.90	51.00	50.60	7.0	25.5	2.92	9.4	0.22	3.14
H2	50.92	51.70	48.00	23.0	28.9	2.53	5.3	0.56	3.09
H3	50.94	51.03	50.95	2.8	25.5	3.03	12.9	0.11	3.14

In the table, all values of  $\theta_1$  are greater than  $\pi/2$ , and the sums of  $\theta_1$  and  $\theta_2$  approach  $\pi$  for shallow dented sections while the sum is about  $0.95\pi$  when  $\delta_d$  is 0.2 where

$R_1/0.5D_o$  is about 0.12. Hence eqn (2.8) can be used to determine  $R_d$  since the slope discontinuity at the both ends of the flattened segment is negligible.

$$\begin{aligned} R_d &= R_1 (1 - \cos \theta_o) \\ &= \frac{1}{2} D_{dmax} (1 - \cos \theta_o) \end{aligned} \quad (2.8)$$

where  $\theta_o = \frac{\pi}{2} \frac{D_o}{D_{dmax}}$

### 2.5.2 Extent of Damage

Using the measurement results of depth of dent along the length, given in Appendix C of ref.82, the equation for the longitudinal variation of depth dent was obtained as

$$\delta_{dx} = \delta_d \exp(-b x/D) \quad (2.9)$$

where  $b = 1.4 + 3.5 \exp(-18 \delta_d)$

Consequently, the length of damaged part on either side of the point of impact can be approximated as

$$l_d = \frac{4.6 D}{1.4 + 3.5 \exp(-18 \delta_d)} \quad (2.10)$$

beyond which the dent depth becomes less than  $0.01 \delta_d$ . A comparison of eqns (2.9) and (2.1) with the measured values for models A1 and C2 is presented in Fig. 2.11. As demonstrated in the figure when using eqn (2.1) the predicted depth of dent along the length is greater than the test data especially for shallow dents and consequently the length of damaged part,  $l_d$ , can be overpredicted. This is probably because eqn (2.1) is based on the data obtained by loading statically through opposed indentors.

In conclusion the non-dimensionalised depth of dent at impact point,  $\delta_d$ , the non-dimensionalised out-of-straightness,  $\delta_o$ , and the length of damaged part,  $l_d$ , can be assessed from eqns (2.11), (2.12) and (2.10) respectively only using the measured values of  $d_{o2}$ (see Fig.2.9) and  $D_{dmin}$  together with eqns (2.7) and (2.8).

$$\delta_d = \frac{D_o - D_{dmin}}{D} \quad (2.11)$$

$$\delta_o = \frac{(d_{o2} - D_o) + (\frac{1}{2}D_o - R_d)}{L} \quad (2.12)$$

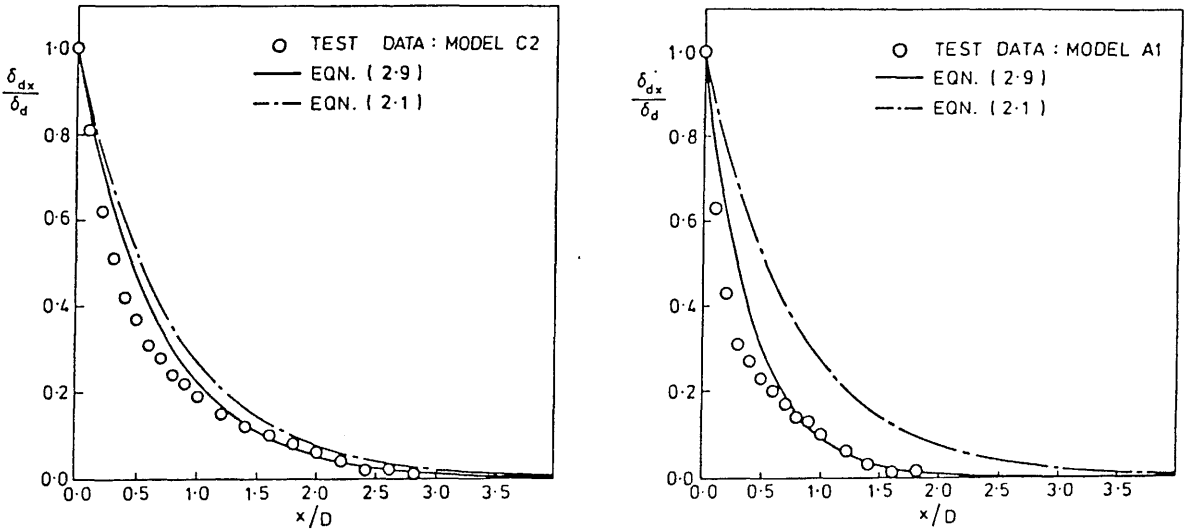


Fig. 2.11 Comparison of Eqns (2.9) and (2.1) with Test Data

## 2.6 Discussions

· General Response : As can be seen in the deflection and strain histories, provided in Figs. 2.7(a)-(e), the dynamic response of a tubular under lateral impact may be divided into three stages, namely,

stage 1 ; elastic-plastic deformation

stage 2 ; elastic spring-back

stage 3 ; free elastic vibration

where for the case of very low energy impact the elastic-plastic stage can be replaced by a pure elastic one. The elastic-plastic deformation stage may continue until the velocity of the striker reaches zero when all the initial kinetic energy of the striker is virtually converted into the elastic-plastic strain energy in the object. Then during the elastic spring-back stage the elastic strain energy stored in the previous stage can be dissipated through accelerating the striker and the struck object backwards. The second stage comes to an end when the acceleration approaches to zero, i.e. no interactive force between the striker and the object, and the deceleration of the struck body starts due to the occurrence of reverse elastic strain. At this moment retaining a rebound velocity the striker separates from the tubular and the struck object enters the free elastic vibration stage. Therefore the predicted extent of damage can be obtained from the displacements when the separation occurs.

· Deformation procedure : In ref.56 the test results are presented of short simply supported tubes under the action of quasi-static transverse loading. In the tests aluminum and steel tubes, whose ranges of diameters, diameter to thickness ratios and span between supports to diameter ratios were 25-50 mm, 24-37 and 1.5-11.0 respectively, were used and the loading was applied through a wedge-shaped indenter. It was found that three phases of deformation were apparent as pure crumpling, followed by bending and crumpling and finally complete structural collapse of the tube. The principal effect of increasing the span was also found that the amount of deformation experienced by the tube in the first phase of deformation is greatly reduced by an increase in the span.

Similar tests on relatively long simply supported steel tubulars, whose non-dimensionalised geometric parameters are similar to those of offshore tubulars, are briefly summarised in ref.21. The diameters of the specimens were 50 mm and 70 mm and the ranges of diameter to thickness ratios and length to diameter ratios were 27-49 and 9-25 respectively. Contrary to the phases of deformation observed in the tests on short tubes, the following deformation history was exhibited for all the specimens:

stage 1; elastic bending of the tubular as a beam

stage 2; further elastic bending and simultaneous local indentation at loaded position

stage 3; localised plastification at dent

It was also observed that the bending stresses created by the lateral force made the lateral load induced dent propagate.

However, the dynamic tests on simply supported steel tubes reported herein showed a somewhat different deformation procedure. As given in Table 2.1 the diameter of the specimens was approximately 50 mm and the diameter to thickness ratios were 20 and 41. The range of supported length to diameter ratios were 19-35. In the tests purely local denting deformation occurred before overall bending together with additional local denting, which is similar to the deformation history observed in the static tests on short tubes.

Higher Mode Effect : On top of the strain-rate effect localised bending<sup>[88]</sup> and higher flexural vibration mode can be another factors which distinguish the response of beam-like structures under dynamic loads from that under static ones. The phenomenon of localised bending may be observed in the impact of a projectile travelling at a high velocity because structures as a whole owing to their inertia do not have time to react to the sudden blow. Hence, when localised bending occurred a reduced span length has to be considered rather than the actual span in calculating its bending stiffness. However, having carefully observed the strain history monitored from strain gauges no.7, no.8 and no.10 it was found that the deformations in the vicinity of supports were accompanied from the very beginning of the impact and reverse curvatures were



demonstrated in the early stage. Therefore it seems possible to draw a conclusion from the phenomena observed that for the problems of low velocity impact considered in this study the influence of localised bending on the gross structural response may be negligible but the higher mode effect substantiated by the reverse curvatures may play a role for the flexural behaviour of the beam.

· Comparison with Predictions by Existing Formulae : Even though a number of studies on the plastic dynamic behaviour of structures have been reported, only a few are available to predict the extent of damage of unstiffened tubulars suffering from impacts. Those available are briefly reviewed here together with their assumptions.

In ref.54, Ellinas and Walker proposed a semi-analytical method both for the local denting and overall bending damage of fully flexurally restrained tubes. The depth of dent is obtained by solving eqns (2.13) and (2.14) simultaneously.

$$F_b = 150 m_p \delta_d^{1/2} \tag{2.13}$$

$$\text{where } F_b = \text{lateral load at which the overall bending deformation starts} \tag{2.14}$$

$$\begin{aligned} m_p &= \text{plastic moment resultant of the tube wall, } 1/4 \sigma_Y t^2 \\ \delta_d &= \text{non-dimensionalised dent depth, } d_d/D \\ M_p &= \text{plastic moment capacity of the undamaged tube cross-section, } D^2 t \sigma_Y \\ \beta &= (1 - \sigma_{pd}/\sigma_Y) \delta_d^{1/2} \\ \sigma_{pd} &= \sigma_Y D/t [ \{ (4/3 \delta_d)^2 + (t/D)^2 \}^{1/2} - 4/3 \delta_d ] \\ \sigma_{pd} &= \sigma_Y D/t [ \{ (4/3 \delta_d)^2 + (t/D)^2 \}^{1/2} - 4/3 \delta_d ] \end{aligned}$$

For overall bending damage, eqn (2.15) was derived by assuming that all the kinetic energy of the striker,  $E_k$ , was absorbed by the tube developing deformations in both the local denting and overall bending modes.

$$\delta_o = \frac{E_k - E_{Dd}}{4 M_p (1 + \cos \beta - \beta)} \quad (2.15)$$

where  $\delta_o$  = non-dimensionalised out-of-straightness,  $d_o/L$

$E_k$  = initial kinetic energy of the striker,  $1/2 M_s V_i^2$

$M_s$  = mass of the striker

$V_i$  = speed of the striker immediately before impact

$E_{Dd}$  = energy absorbed during the formation of the local dent,  $100 m_p D \delta_d^{3/2}$

For overall bending damage only, de Oliveira<sup>[89]</sup> derived eqn (2.16) using a mode approximation technique based on the assumptions of a rigid-plastic hollow circular section member which is perfectly clamped and fully restrained axially at both ends, and that geometry changes are disregarded :

$$\delta_o = \frac{1}{2} \frac{E_k}{P_Y D} \frac{1}{1 + \frac{m}{3 M_s}} \quad (2.16)$$

where  $P_Y$  = fully plastic axial force,  $\pi \sigma_Y D t$

$m$  = mass of the tube

Ellinas et al<sup>[90]</sup> suggested another very simple formula, eqn (2.17), for the local denting damage prediction. The tube was assumed to be sufficiently stiff in bending that all the impact energy was absorbed by the local denting mode.

$$\delta_d = \left\{ \frac{0.051 E_k}{D t^2 \sigma_Y} \right\}^{2/3} \quad (2.17)$$

A comparison between predictions by the existing formulae and the present test results is illustrated in Fig.2.12. The method suggested in ref.54 to predict both modes

of damage appears to suffer from the following shortcomings :

- for the local denting damage, the predicted values are constant in relation to the geometry and the material properties of the struck models irrespective of the striker's mass and speed because eqns (2.13) and (2.14) contain no terms to represent the kinetic energy of the striker ; and
- for the overall bending damage, the lack of consistency shown in Fig.2.12 is due to the too conservative estimate of the extent of local denting.

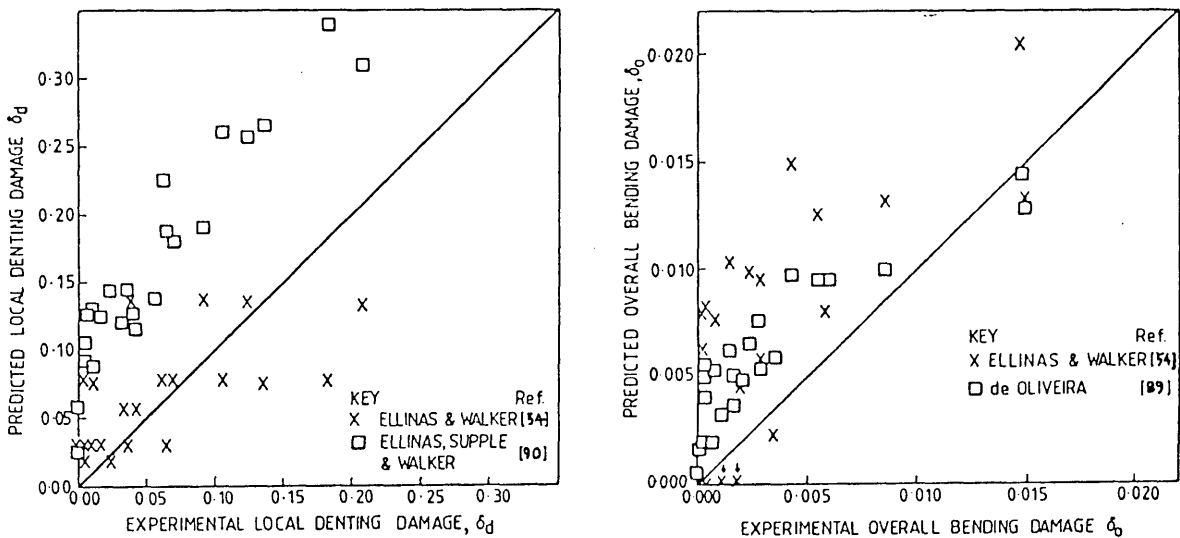


Fig. 2.12 Comparison between Predictions of Existing Formulae and Test Results for Extent of Damage

The formulae suggested in refs.90 and 89, although they overpredict the experimental results, especially in the ranges  $\delta_d$  of 0.01-0.05 and  $\delta_o$  of 0.0015-0.002 where the detrimental effect of damage on the ultimate strength of the damaged tubes is most sensitive[69,54], can be seen in Fig.2.12 to demonstrate some consistency with the measured values for the larger extents of damage of interest.

## Chapter 3

### DYNAMIC RESPONSE OF A TUBULAR MEMBER UNDER LATERAL IMPACT

#### 3.1 Introduction

The ductile response of unstiffened tubular members under lateral impacts can be divided into local denting of the cylinder wall and overall bending of the member as a beam. Some combination of these two modes is the most likely outcome for offshore tubulars. As reviewed in section 1.2 the dynamic behaviour of beams, particularly of rectangular solid section, under transverse impulsive loadings or impacts has been examined extensively by many investigators. In most analyses local effects, i.e. the local deformation surrounding the region where a striker impinges on a structure, are neglected and consequently the initial or given transverse sectional configuration is assumed to be unchanged throughout the period of impact. As far as offshore tubulars are concerned it is, however, unlikely that the local deformation can be neglected in the analysis not only because roughly 10 to 15% of the total available energy would be locally dissipated<sup>[50]</sup> but because the dent depth of a damaged tubular is one of the most influential factors upon its ultimate strength<sup>[69, 68, 91]</sup>.

A question may be raised whether collisions of offshore structures by attendant vessels can be considered as quasi-static or dynamic phenomena. It has been suggested that quasi-static methods of plastic analysis should suffice for predicting the structural damage if the duration of a dynamic load is long compared with the corresponding natural period of elastic vibration. The natural periods of local vibration modes were estimated for concrete and steel tubular members by Sorensen<sup>[92]</sup> and de Oliveira<sup>[50]</sup>

respectively. In ref.50, the natural periods for tube wall stretch ( $T_t$ ), tube wall shear ( $T_s$ ), and overall shell ( $T_c$ ) modes are considered and the ranges of these periods for a typical offshore steel tubular member are given as follows:

$$\begin{aligned} 0.007 \times 10^{-3} < T_t < 0.101 \times 10^{-3} \text{ s} \\ 0.013 \times 10^{-3} < T_s < 0.189 \times 10^{-3} \text{ s} \\ 15 \times 10^{-3} < T_c < 400 \times 10^{-3} \text{ s} \end{aligned}$$

Besides these three modes, the flexural vibration of the tubular as a beam can be taken into consideration. The natural period,  $T_b$ , of a uniform thin-walled circular section beam is given in ref.93 as follows:

$$T_b = \frac{2\sqrt{2}}{k} \sqrt{\frac{\rho}{E}} \frac{L^2}{D} \quad (3.1)$$

where

$E$  = Young's modulus

$\rho$  = density of the material

$k$  = constant depending upon the mode of vibration and the end constraints  
for the fundamental mode;

$k = 1.57$ , simply supported end conditions

$k = 3.56$ , built-in end conditions

Assuming built-in end conditions, the range of the natural periods of a typical offshore steel tubular member is then found to be

$$15.4 \times 10^{-3} < T_b < 1000 \times 10^{-3} \text{ s}$$

In ref.94 the impact duration of collisions between supply vessels and platforms is estimated to be lying in the interval 0.2 to 2.0 seconds. However, the natural periods of the aforementioned three local modes are reasonably shorter than the estimated impact duration but the natural period of flexural mode is nearly the same order as the

impact duration. Therefore it seems likely that a dynamic analysis is necessary for the minor supply vessel-platform collision problem.

In quasi-static analyses of offshore collision a common assumption adopted is that the initial kinetic energy of the striker can be absorbed through the plastic deformation of the offshore structure. An experimental and theoretical study<sup>[30]</sup> on the response of a semi-submersible to bergy-bit impacts, however, showed that the rebound velocity of the bergy-bit after impact was approximately 70 to 75 % of the impact velocity. Even though this rebound velocity can be the upper bound since the plastic deformation of the struck body was not considered in the study, the results of this hydro-elastic analysis may indicate that the common assumption adopted in the static analyses leads to too pessimistic predictions for extent of damage.

The difference of the deformation procedure of unstiffened tubulars under dynamic loading from that under static loading can be another reason for the necessity of dynamic analysis. As discussed in section 2.6, contrary to the phase of deformation observed in the static tests<sup>[21]</sup>, purely local denting deformation occurred before overall bending together with additional local denting in the lateral impact tests.

A rigid-plastic method employing a rigid-perfectly plastic constitutive equation leads to significant simplification for many dynamic structural problems. A criterion for the validity of the rigid-plastic analysis of beams under impact and dynamic loading was studied by Lee and Symond<sup>[48]</sup>. In ref.95 a comparison between elastic-plastic and rigid-plastic solutions is illustrated by a simple mass-spring system. Experimental and theoretical findings on the plastic deformation of steel and aluminum alloy cantilever beams under impulsive loadings are reported in ref.96. It is concluded in the paper that elastic vibrations do not have much effect on the results when the energy ratio  $R_E$  is greater than about 10 and for some cases the results can reasonably free from elastic effects even for  $R_E$  about 3 where energy ratio  $R_E$  is defined as

$$R_E = \frac{\text{kinetic energy input}}{\text{maximum possible elastic strain energy}} = \frac{E_k}{E_e} \quad (3.2)$$

In a beam problem  $E_e$  can conveniently be taken as

$$\frac{M_p^2 L}{2EI}$$

where

$M_p$ ; fully plastic moment of the beam cross-section

$L$  ; beam length

$E$  ; Young's modulus

$I$  ; moment of inertia of the beam cross-section

It may be interesting at this juncture to have an idea what the energy ratio  $R_E$  can be for typical offshore unstiffened tubular members and the design load for collision specified in relevant offshore rules. We can assume a collision between a supply vessel of 2500 tonnes, travelling at 0.5 m/s and a bracing member whose length, diameter and thickness are about 8 m, 0.4 m and 0.01 m respectively. Here the mass and velocity of the striker is the design criteria adopted in the BSI code for fixed offshore structures[78] and geometry of the bracing is the same as the one obtained from the BP West Sole platform WE[67]. Assuming the added mass to be equal to 10 % of the ship's mass, Young's modulus of  $207 \times 10^3 \text{ MN/m}^2$  and yield stress of  $300 \text{ MN/m}^2$ , eqn (3.2) leads to an energy ratio  $R_E$  of 19.4. Another example is a collision of a tubular, whose length, diameter and thickness are 38 m, 1.8 m and 0.028 m respectively, by a supply vessel of 5000 tonnes displacement with impact speed 2 m/s. For this case the collision load is that of specified in the DnV Rules for Mobile Offshore Units[81] and the geometry of the tubular is representing a bracing of the semi-submersible drilling rig, AKER H-42[97]. Assuming the same values for the added mass, Young's modulus and yield stress as above leads to an  $R_E$  of 10.4.

Provided that the findings of the dynamic analyses for beams of rectangular solid section under impulsive loadings are applicable to offshore tubulars, a rigid plastic

analysis seems to suffice for the collision load specified in the offshore rules. However, as reviewed in section 1.2, according to the theoretical predictions presented by Standing and Brending<sup>[11]</sup> the mean collision velocity can vary between 0.28 and 1.18 m/s. Considering the random nature of collision loads and hoping to provide a criteria for the validity of results obtained using a rigid-plastic analysis, it was decided to retain the material elasticity in the analysis.

Bracings and other members of offshore structures whose ductility is important for the development of full yielding reserve capacity are normally fabricated from mild steel. However, mild steel is highly strain-rate sensitive and the flow stress in a uniaxial test conducted at a strain rate of  $40 \text{ s}^{-1}$  is approximately twice the corresponding static uniaxial yield stress<sup>[39]</sup>. This property has been described as one of the major factors responsible for the excessive scatter of impact and impulsive loading test results which greatly exceeds the precision of measurements.

In order to fully take into account the local denting of cylinder wall and the influence of elastic vibrations and strain-rate sensitivity of the material on the permanent plastic deformations it seems inevitable to solve the problem using a dynamic elastic-viscoplastic numerical shell analysis with the aid of finite element method or finite difference technique. These numerical procedures are, however, expensive to operate, particularly for preliminary design studies and even for parametric studies to derive any simple design equations. Thus, it seems desirable to use such kinds of numerical methods as a learning tool to guide the formulation of simpler, less time-consuming prediction methods and to define realistically the conditions under which these simpler methods yield reliable predictions.

In the present study an attempt has been made to develop a simple numerical procedure in which the tubular member is reduced to a spring-mass system with two degrees-of-freedom. The results of the impact tests conducted in this study have been correlated with numerical analysis in order to achieve an empirical representation of the



strain-rate sensitivity and other dynamic effects upon the spring coefficient for bending deformation. Material strain hardening and the influence of transverse shear force and rotatory inertia are not considered.

### 3.2 Spring-Mass Model with Two Degree-of-Freedom

Provided that the transverse sectional shape of the beam does not change throughout the procedure, the dynamic flexural responses under lateral impact can be approximately investigated by reducing a given problem to a spring-mass system with one degree-of-freedom. In this simplification, the fundamental mode of vibration of the system under consideration needs to be estimated. The degree to which the single degree-of-freedom system represents the given structural system, which virtually has an infinite number of degrees-of-freedom, depends upon the accuracy with which the fundamental mode is approximated. In any case, the effects of higher modes of vibration which may somehow contribute the response will not be contained in the simplified model. Nevertheless, a single degree-of-freedom model with sufficient accuracy can be a very important tool for performing parametric studies of system behaviour and for developing design guidance because of its computing efficiency.

When considering the local denting deformation of the cylinder wall, the problem, however, becomes more complicated. In order to overcome this difficulty the local denting and the overall bending deformations are uncoupled and adopting a spring-mass model with two degrees-of-freedom, one for overall bending and the other for local denting, the problem can be reduced to a practically tractable one.

#### 3.2.1 Equations of Motion

In Fig. 3.1 the analytical system model is illustrated. It is assumed in the system that damping is negligible. Thus the dynamic equilibrium in the system is established by equating to zero the sum of the inertial forces and the spring forces. At time  $t_i$  the equilibrium of these forces can be written as follows:

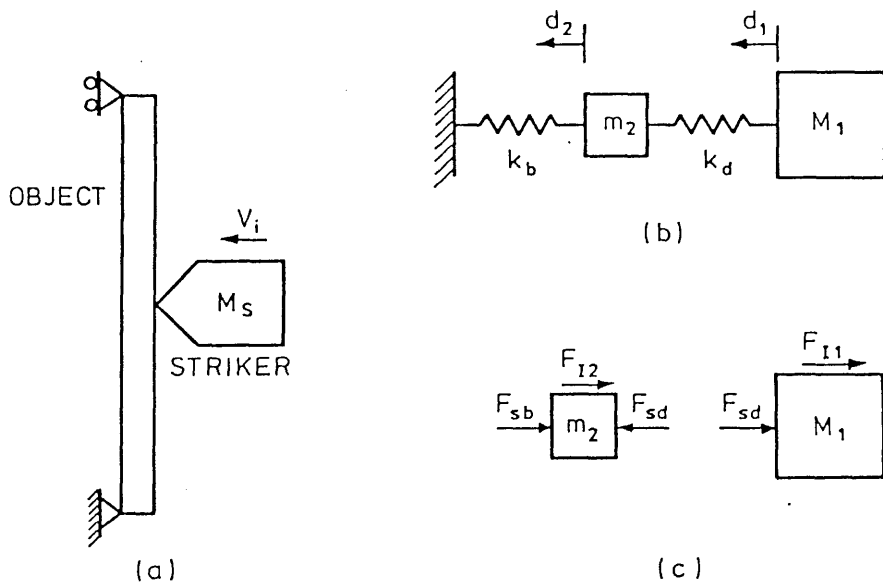


Fig. 3.1 (a) Physical System (b) Mathematical Model  
(c) Free Body Diagram

for mass  $M_1$ ;  $F_{I1}(t_i) + F_{sd}(t_i) = 0$  (3.3a)

for mass  $M_2$ ;  $F_{I2}(t_i) + F_{sb}(t_i) - F_{sd}(t_i) = 0$  (3.3b)

where

$F_{I1}, F_{I2}$  ; inertia forces of the masses  $M_1$  and  $m_2$  respectively

$F_{sd}, F_{sb}$  ; spring forces for local denting deformation and overall bending deformation respectively

$M_1$  ;  $m_1 + M_s$ , during impact  
 $m_1$ , after separation

$m_1$  ; equivalent mass of the tube wall for local denting mode

$m_2$  ; equivalent mass of the tube for overall bending mode

$M_s$  ; mass of the striker

The dynamic equilibrium at short time  $\Delta t$  later can be expressed as

$$F_{I1}(t_i + \Delta t) + F_{sd}(t_i + \Delta t) = 0 \quad (3.4a)$$

$$F_{I2}(t_i + \Delta t) + F_{sb}(t_i + \Delta t) - F_{sd}(t_i + \Delta t) = 0 \quad (3.4b)$$

Subtracting eqns(3.3a) and (3.3b) from eqns(3.4a) and (3.4b) respectively results in the differential equations of motion in terms of increments, namely

$$\Delta F_{I1} + \Delta F_{sd} = 0 \quad (3.5a)$$

$$\Delta F_{I2} + \Delta F_{sb} - \Delta F_{sd} = 0 \quad (3.5b)$$

where the incremental forces in these equations are defined as follows:

$$\Delta F_{I1} = F_{I1}(t_i + \Delta t) - F_{I1}(t_i) \quad (3.6a)$$

$$\Delta F_{I2} = F_{I2}(t_i + \Delta t) - F_{I2}(t_i) \quad (3.6b)$$

$$\Delta F_{sd} = F_{sd}(t_i + \Delta t) - F_{sd}(t_i) \quad (3.6c)$$

$$\Delta F_{sb} = F_{sb}(t_i + \Delta t) - F_{sb}(t_i) \quad (3.6d)$$

It is assumed here that the spring force  $F_{sd}$  is a function of the displacement of mass  $M_1$  relative to  $m_2$  while  $F_{sb}$  is a function of the absolute displacement of mass  $m_2$ . In addition, the inertia forces are proportional to the corresponding accelerations and the masses  $M_1$  and  $m_2$  and the spring coefficients  $k_d$  and  $k_b$  remain constant during the interval  $\Delta t$ . On these assumptions the incremental forces in eqns(3.6a-d) can be expressed as

$$\Delta F_{I1} = M_1(t_i) \Delta \ddot{d}_{1i} \quad (3.7a)$$

$$\Delta F_{I2} = m_2(t_i) \Delta \ddot{d}_{2i} \quad (3.7b)$$

$$\Delta F_{sd} = k_{di} (\Delta d_{1i} - \Delta d_{2i}) \quad (3.7c)$$

$$\Delta F_{sb} = k_{bi} \Delta d_{2i} \quad (3.7d)$$

where the incremental displacements  $\Delta d_1$  and  $\Delta d_2$ , and the incremental accelerations  $\Delta \ddot{d}_1$  and  $\Delta \ddot{d}_2$  are given by .

$$\Delta d_{1i} = d_1(t_i + \Delta t) - d_1(t_i) \quad (3.8a)$$

$$\Delta d_{2i} = d_2(t_i + \Delta t) - d_2(t_i) \quad (3.8b)$$

$$\Delta \dot{d}_{1i} = \dot{d}_1(t_i + \Delta t) - \dot{d}_1(t_i) \quad (3.8c)$$

$$\Delta \dot{d}_{2i} = \dot{d}_2(t_i + \Delta t) - \dot{d}_2(t_i) \quad (3.8d)$$

where dots denote differentiations with respect to time and

$d_1, d_2$  ; absolute displacements of the masses  $M_1$  and  $m_2$  respectively  
from their initial position

The spring coefficients  $k_{di}$  in eqn (3.7c) and  $k_{bi}$  in eqn (3.7d) are defined as the current evaluation for the derivatives of the spring forces with respect to the corresponding displacements, namely,

$$k_{di} = \left\{ \frac{d(F_{sd})}{d(d_d)} \right\} d_d = d_{di} \quad (3.9a)$$

$$k_{bi} = \left\{ \frac{d(F_{sb})}{d(d_2)} \right\} d_2 = d_{2i} \quad (3.9b)$$

where  $F_{sd}$  and  $F_{sb}$  are the spring forces for local denting and overall bending deformations respectively and  $d_d = d_1 - d_2$ .

Substituting eqns (3.7a-d) into eqns (3.5a) and (3.5b) convenient forms for the incremental equations of motion can be obtained as follow:

$$M_{1i} \Delta \dot{d}_{1i} + k_{di} (\Delta d_{1i} - \Delta d_{2i}) = 0 \quad (3.10a)$$

$$m_{2i} \Delta \dot{d}_{2i} + k_{bi} \Delta d_{2i} - k_{di} (\Delta d_{1i} - \Delta d_{2i}) = 0 \quad (3.10b)$$

### 3.2.2 Integration of Equation of Motion

Among the many methods available for the solution of the non-linear equations of motion, probably one of the most effective is the step-by-step integration method. In this method, the response is evaluated at successive increments  $\Delta t$  of time, usually

taken of equal length of time for computational convenience. The non-linear characteristics of the masses  $M_1$  and  $m_2$  and the spring coefficients  $k_d$  and  $k_b$  are considered in the analysis by reevaluating at the beginning of each time increment. At the beginning of each interval, the condition of dynamic equilibrium is established. The response is then obtained using the displacement and velocity calculated at the end of the time interval as the initial conditions for the next time step. The masses and spring coefficients are evaluated at the initiation of the interval but are assumed to remain constant until the next step, thus the non-linear behaviour of the system is approximated by a sequence of successively changing linear systems.

In this study, the linear acceleration method<sup>[98]</sup> is adopted in performing the step-by-step integration of eqns (3.10a) and (3.10b). It is assumed in the linear acceleration method that the acceleration may be expressed by a linear function of time during the time interval  $\Delta t$ . Let  $t_i$  and  $t_{i+1} = t_i + \Delta t$  be, respectively, the designation for the time at the beginning and at the end of the time interval  $\Delta t$ . Then, the acceleration during a small time increment can be expressed as

$$\ddot{d}_1(t) = \ddot{d}_{1i} + \frac{\Delta \ddot{d}_{1i}}{\Delta t} (t - t_i) \quad (3.11a)$$

$$\ddot{d}_2(t) = \ddot{d}_{2i} + \frac{\Delta \ddot{d}_{2i}}{\Delta t} (t - t_i) \quad (3.11b)$$

where  $\Delta \ddot{d}_{1i}$  and  $\Delta \ddot{d}_{2i}$  are given by eqns (3.8c) and (3.8d) respectively. Integrating eqns (3.11a) and (3.11b) twice with respect to time between the limits  $t_i$  and  $t$  yields

$$\dot{d}_1(t) = \dot{d}_{1i} + \ddot{d}_{1i} (t - t_i) + \frac{1}{2} \frac{\Delta \ddot{d}_{1i}}{\Delta t} (t - t_i)^2 \quad (3.12a)$$

$$\dot{d}_2(t) = \dot{d}_{2i} + \ddot{d}_{2i} (t - t_i) + \frac{1}{2} \frac{\Delta \ddot{d}_{2i}}{\Delta t} (t - t_i)^2 \quad (3.12b)$$

$$d_1(t) = d_{1i} + \dot{d}_{1i}(t - t_i) + \frac{1}{2}\ddot{d}_{1i}(t - t_i)^2 + \frac{1}{6}\frac{\Delta\ddot{d}_{1i}}{\Delta t}(t - t_i)^3 \quad (3.13a)$$

and

$$d_2(t) = d_{2i} + \dot{d}_{2i}(t - t_i) + \frac{1}{2}\ddot{d}_{2i}(t - t_i)^2 + \frac{1}{6}\frac{\Delta\ddot{d}_{2i}}{\Delta t}(t - t_i)^3 \quad (3.13b)$$

The evaluation of eqns (3.12a), (3.12b), (3.13a) and (3.13b) at time  $t = t_i + \Delta t$  gives

$$\Delta\dot{d}_{1i} = \ddot{d}_{1i}\Delta t + \frac{1}{2}\Delta\ddot{d}_{1i}\Delta t \quad (3.14a)$$

$$\Delta\dot{d}_{2i} = \ddot{d}_{2i}\Delta t + \frac{1}{2}\Delta\ddot{d}_{2i}\Delta t \quad (3.14b)$$

$$\Delta d_{1i} = \dot{d}_{1i}\Delta t + \frac{1}{2}\ddot{d}_{1i}\Delta t^2 + \frac{1}{6}\Delta\ddot{d}_{1i}\Delta t^2 \quad (3.15a)$$

and

$$\Delta d_{2i} = \dot{d}_{2i}\Delta t + \frac{1}{2}\ddot{d}_{2i}\Delta t^2 + \frac{1}{6}\Delta\ddot{d}_{2i}\Delta t^2 \quad (3.15b)$$

where  $\Delta d_{1i}$  and  $\Delta d_{2i}$  are defined in eqns (3.8a) and (3.8b) respectively and  $\Delta\dot{d}_{1i}$  and  $\Delta\dot{d}_{2i}$  are given by

$$\Delta\dot{d}_{1i} = \dot{d}_1(t_i + \Delta t) - \dot{d}_1(t_i) \quad (3.16a)$$

$$\Delta\dot{d}_{2i} = \dot{d}_2(t_i + \Delta t) - \dot{d}_2(t_i) \quad (3.16b)$$

Comparing the coefficients of the acceleration terms in eqns (3.14a), (3.14b), (3.15a) and (3.15b) it can be noted that these expressions are equivalent to the Newmark  $\beta$  Method<sup>[99]</sup> with  $\beta = 1/6$  and  $\gamma = 1/2$ . Using a value of  $\gamma = 1/2$  implies that no spurious damping is introduced into the system by the numerical procedure.

Now to use the incremental displacements  $\Delta d_1$  and  $\Delta d_2$  as the basic variables in the analysis, eqns (3.15a) and (3.15b) are solved for the incremental accelerations  $\Delta\ddot{d}_1$  and  $\Delta\ddot{d}_2$  and then substituted respectively into eqns (3.14a) and (3.14b) to obtain

$$\Delta \ddot{d}_{1i} = \frac{6}{\Delta t^2} \Delta d_{1i} - \frac{6}{\Delta t} \dot{d}_{1i} - 3 \ddot{d}_{1i} \quad (3.17a)$$

$$\Delta \ddot{d}_{2i} = \frac{6}{\Delta t^2} \Delta d_{2i} - \frac{6}{\Delta t} \dot{d}_{2i} - 3 \ddot{d}_{2i} \quad (3.17b)$$

$$\Delta \dot{d}_{1i} = \frac{3}{\Delta t} \Delta d_{1i} - 3 \dot{d}_{1i} - \frac{\Delta t}{2} \ddot{d}_{1i} \quad (3.18a)$$

and

$$\Delta \dot{d}_{2i} = \frac{3}{\Delta t} \Delta d_{2i} - 3 \dot{d}_{2i} - \frac{\Delta t}{2} \ddot{d}_{2i} \quad (3.18b)$$

The substitution of eqns (3.17a) and (3.17b) into eqns (3.10a) and (3.10b) respectively leads to the following simultaneous equations for  $\Delta d_{1i}$  and  $\Delta d_{2i}$  :

$$A_{1i} \Delta d_{1i} - k_{di} \Delta d_{2i} - B_{1i} = 0 \quad (3.19a)$$

$$-k_{di} \Delta d_{1i} + A_{2i} \Delta d_{2i} - B_{2i} = 0 \quad (3.19b)$$

where

$$A_{1i} = \frac{6 M_{1i}}{\Delta t^2} + k_{di} \quad (3.20a)$$

$$A_{2i} = \frac{6 M_{2i}}{\Delta t^2} + k_{di} + k_{bi} \quad (3.20b)$$

$$B_{1i} = 3 M_{1i} \left( \frac{2}{\Delta t} \dot{d}_{1i} + \ddot{d}_{1i} \right) \quad (3.20c)$$

and

$$B_{2i} = 3 M_{2i} \left( \frac{2}{\Delta t} \dot{d}_{2i} + \ddot{d}_{2i} \right) \quad (3.20d)$$

Eqns (3.19a) and (3.19b) may be solved for the incremental displacements  $\Delta d_{1i}$  and  $\Delta d_{2i}$  :

$$\Delta d_{1i} = \frac{k_{di} B_{2i} + A_{2i} B_{1i}}{A_{1i} A_{2i} - k_{di}^2} \quad (3.21a)$$

$$\Delta d_{2i} = \frac{k_{di} B_{1i} + A_{1i} B_{2i}}{A_{1i} A_{2i} - k_{di}^2} \quad (3.21b)$$

The displacements  $d_{1\ i+1}$  and  $d_{2\ i+1}$  at time  $t = t_i + \Delta t$  can be obtained by substituting eqns (3.21a) and (3.21b) into eqns (3.8a) and (3.8b) as

$$d_{1\ i+1} = d_{1i} + \Delta d_{1i} \quad (3.22a)$$

$$d_{2\ i+1} = d_{2i} + \Delta d_{2i} \quad (3.22b)$$

Then the incremental velocities  $\Delta \dot{d}_{1i}$  and  $\Delta \dot{d}_{2i}$  are obtained respectively from eqns (3.18a) and (3.18b) and the velocities at time  $t_{i+1}$  from eqns (3.16a) and (3.16b) as

$$\dot{d}_{1\ i+1} = \dot{d}_{1i} + \Delta \dot{d}_{1i} \quad (3.23a)$$

$$\dot{d}_{2\ i+1} = \dot{d}_{2i} + \Delta \dot{d}_{2i} \quad (3.23b)$$

Finally the accelerations  $\ddot{d}_{1\ i+1}$  and  $\ddot{d}_{2\ i+1}$  at the end of the time step are directly obtained from eqns (3.3a) and (3.3b) after setting  $F_{I1}(t_{i+1}) = M_1(t_{i+1}) \ddot{d}_{1\ i+1}$  and  $F_{I2} = m_2(t_{i+1}) \ddot{d}_{2\ i+1}$ :

$$\ddot{d}_{1\ i+1} = \frac{F_{sd}(t_{i+1})}{M_1(t_{i+1})} \quad (3.24a)$$

$$\ddot{d}_{2\ i+1} = \frac{F_{sd}(t_{i+1}) - F_{sb}(t_{i+1})}{m_2(t_{i+1})} \quad (3.24b)$$

where  $F_{sd}(t_{i+1})$  and  $F_{sb}(t_{i+1})$  can be obtained by substituting eqns (3.7c) and (3.7d)



into eqns (3.6c) and (3.6d) respectively.

It is noteworthy here that in order to minimise accumulated errors the accelerations are calculated from the dynamic equilibrium equations rather than using the equations for the incremental accelerations, eqns (3.17a) and (3.17b).

After having determined the displacements, velocities and accelerations at time  $t_{i+1}$ , the outlined procedure is repeated to calculate these quantities at the following time step  $t = t_{i+1} + \Delta t$  and the process is continued to any desired final value of time. In the analysis there still remains the problems of the selection of the proper time increment  $\Delta t$  and the evaluation of the spring coefficients,  $k_d$  and  $k_b$ , and the masses,  $M_1$  and  $m_2$ . A detailed explanation of each of these is given in the following sections.

### 3.3 Equivalent Masses and Equivalent Spring Coefficients

#### 3.3.1 Equivalent Masses

In the step-by-step integration of the non-linear equations of motion described in the previous section the equivalent masses and stiffness properties of the system need to be evaluated at the initiation of each time increment. In the analysis the mass  $M_1$  is assumed to be the sum of the striker's mass  $M_s$  and the equivalent mass of locally deformed tube wall,  $m_1$ , during impact and to be the mass  $m_1$  alone after the separation of the striker from the struck model. For overall bending deformation Cox<sup>[41]</sup> obtained an equivalent mass,  $m_2$ , equal to 17/35 of the beam's mass under the assumption that the deflection curve of the beam during impact does not differ much from the elastic curve produced by static concentrated load at its mid-length and the velocity distribution along the length has the same form as that of deflection. When considering the fundamental mode shape of elastic vibration of the beam the equivalent mass equal to 1/2 of that of the beam can be obtained (see chapter 5 of ref 100).

For most of the practical cases the mass of the striker  $M_s$  can be much greater than the mass  $m_1$ . Thus the influence of  $m_1$  on the mass  $M_1$ , and consequently on the extent of damage, seems negligible. But the accuracy in determining  $m_1$  can be

transferred in the prediction of the local shell elastic vibration after the separation of the striker, which is not of importance from practical design viewpoints. In the present study, however, the equivalent mass for local denting deformation,  $m_1$ , is approximated to be a half of the mass of locally deformed tube wall, while the equivalent mass for overall bending deformation,  $m_2$ , is assumed to be a half of the mass of the tube.

### 3.3.2 Equivalent Spring Coefficients

In order to evaluate the stiffness properties of the system the force-displacement curves for overall bending deformation under static lateral loads have numerically been derived, while for local denting deformation an empirical representation of the relationships has been attempted. Then the spring coefficients are obtained from the slope of these curves. It seems highly likely that strain-rate and higher mode effects are attributable for the difference of the structural behaviours of beam-like structures under moderate dynamic loads from those under static actions. In hoping to consider these dynamic effects in the analysis an attempt has made to multiply a modification factor to the spring coefficient for overall bending deformation. The modification factor is obtained from an empirical correlation with the experimental data.

#### 3.3.2.1 Spring Coefficient for Local Denting

The force-deformation relationship for a circular thin-walled cylinder under a transverse concentrated load was theoretically investigated among others by Mavrikios and de Oliveira<sup>[14]</sup> and Wierzbicki and Suh<sup>[55]</sup>. In ref.14 the analysis method involving the concept of the isometric transformation of surfaces provides overestimating results for the crushing load by approximately a factor of three. Wierzbicki and Suh adopted in their analysis a simplified shell model consisting of a series of unconnected rings and a bundle of unconnected generators. More improved results upon previous studies are presented in ref.55, but the proposed model can underestimate the actual strength of a tube by roughly 30-40 %.

It seems difficult to predict the force-deformation relation with reasonable

accuracy using any of the reported theoretical methods. It is, therefore, decided to empirically derive the spring coefficient for local deformation using published experimental data. There have been five load-indentation curves reported so far in the literature. Three curves were presented by Smith<sup>[67,69]</sup> and the other two by Ueda and Rashed<sup>[70]</sup>. In all the tests a quasi-static lateral load was applied at midspan through a solid knife-edge with a tip of small radius. The back of the tube at midspan was supported in a soft cylindrical cradle except for specimen P<sub>1A</sub> in ref.69 where two cradles, located opposite positions to midspan, were employed.

The equation of force-indentation relation for loading has been obtained using a least-square method to provide a best fit to experimental data. Then the equation for spring coefficient is obtained by differentiating the force-indentation equation with respect to displacement. But for unloading the equation for the spring coefficient is directly derived using the test results and then the force-indentation relation is obtained by integrating this equation. The equations for reloading up to the indentation at which the unloading starts is assumed to be the same as those for unloading. The equations for force-indentation relation and spring coefficient are given as follows:

#### force-indentation relationship

$$F = 2.5 m_p (D/t)^{0.2} (E/\sigma_Y)^{0.5} \delta_d^{0.5} \quad ; \text{ for loading} \quad (3.25a)$$

$$= 5.0 m_p (E/\sigma_Y) (\delta_{dp} - \delta_{do}) \left\{ \frac{3}{5} \left( \frac{\delta_d - \delta_{do}}{\delta_{dp} - \delta_{do}} \right)^5 + \frac{2}{5} \left( \frac{\delta_d - \delta_{do}}{\delta_{dp} - \delta_{do}} \right) \right\}$$

$$; \text{ for unloading} \quad (3.25b)$$

#### spring coefficient for local denting

$$k_{ds} = 1.25 \frac{m_p}{D} (D/t)^{0.2} (E/\sigma_Y)^{0.5} \delta_d^{-0.5} \quad ; \text{ for loading} \quad (3.26a)$$

$$= 5.0 \frac{m_p}{D} (E/\sigma_Y) \left\{ 3 \left( \frac{\delta_d - \delta_{do}}{\delta_{dp} - \delta_{do}} \right)^4 + \frac{2}{5} \right\} \quad ; \text{ for unloading} \quad (3.26b)$$

where

$F$  ; concentrated lateral load applied at midspan

$m_p$  ; plastic moment resultant of the tube wall,  $1/4 \sigma_Y t^2$

$D$  ; diameter to mid-thickness of the tube

$t$  ; thickness of the tube

$\sigma_Y$  ; static yield stress

$\delta_d$  ; non-dimensionalised depth of dent,  $d_d/D$  or  $(d_1 - d_2)/D$

$\delta_{dp}$  ; non-dimensionalised depth of dent at which unloading starts

$\delta_{do}$  ; non-dimensionalised depth of dent when  $F = 0$ ,

$$\delta_{dp} - 1/2 (D/t)^{0.2} (E/\sigma_Y)^{-0.5} \delta_{dp}^{0.5}$$

$k_{ds}$  ; static spring coefficient for local denting

In deriving eqn (3.26b) the slope of the straight line joining the point at which the unloading starts and the completely unloaded point is calculated and then the term in the curly brackets in the equation is multiplied to accommodate the deviation of the straight line from the concave experimental results. The comparisons of eqns (3.25a) and (3.25b) with the experimental relations are presented in Fig. 3.2. Despite the simplicity in the form of the equations, reasonably accurate fitting has been achieved in the figure.

### 3.3.2.2 Spring Coefficient for Overall Bending

Provided that the depth of dent of the tube does not increase during overall bending deformation, the force and midspan lateral deflection relation of the simply supported beam under concentrated load at midspan can be computed using the Newmark integration method[101]. The elastic plastic moment - thrust - curvature relationships allowing for local denting deformation and hydrostatic pressure have been

computed and their approximate equations have been derived in this study. The details of the procedures of obtaining these relationships and equations are described in chapter 5.

The bending moment at any section along the beam can be easily determined from static equilibrium conditions and the curvature along the beam can then be calculated using the approximate equations for moment-curvature relationships. The deflection at midspan for given lateral load can be obtained by integrating twice the curvature with respect to beam length. Increasing the lateral force incrementally up to ultimate value the non-linear force-deflection relations have been established.

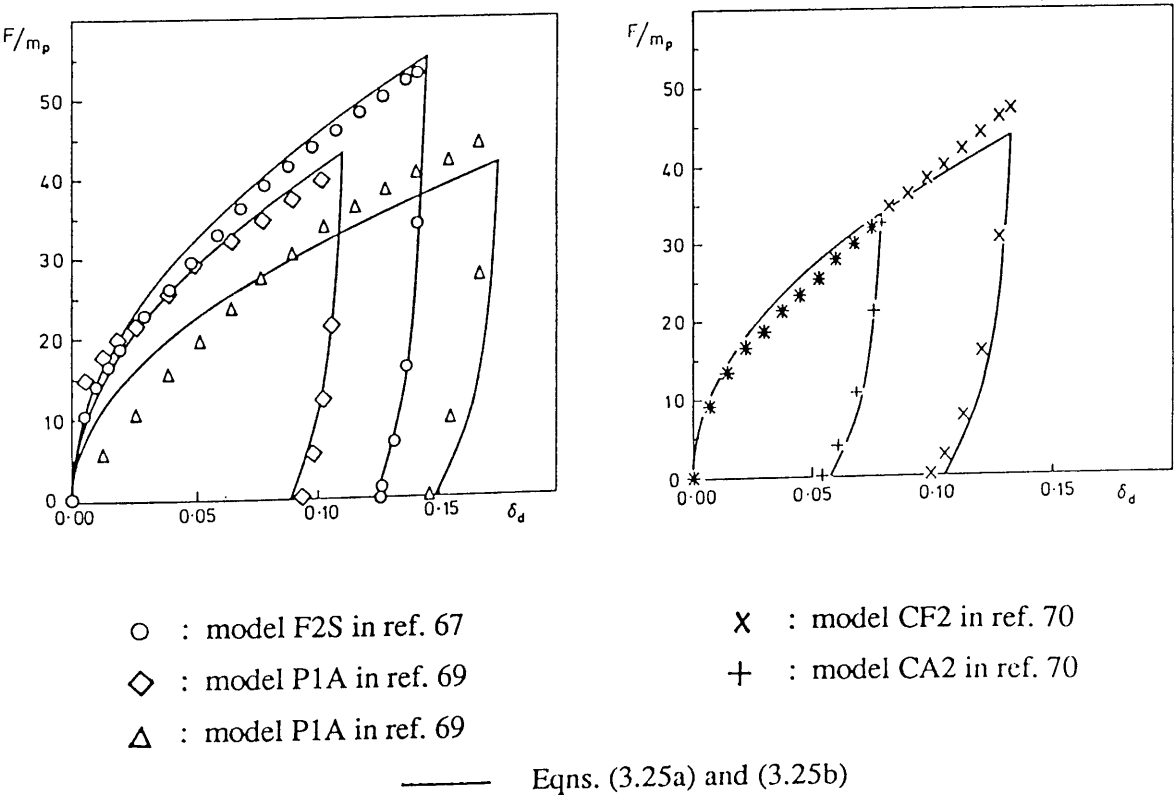


Fig. 3.2 Force-Indentation Relationship as Derived from Test Data

Using a computer program based on the procedure described above an extensive parametric study has been carried out for the ranges of  $L/D = 10-40$ ,  $D/t = 20-60$  and  $\delta_d = 0.00-0.20$ . The force-deflection curves resulting from the parametric study were then approximately represented by a linear equation up to the elastic limit and by an exponential equation for the elastic plastic regime. The approximate equations for the relation of lateral force and lateral deflection at midspan obtained by a regression are as follows:

force-deflection relationship

$$F = 4 \frac{M_p}{L} a \delta_d \quad ; \text{ for elastic regime } \quad (3.27a)$$

$$= 4 \frac{M_p}{L} \left\{ f_{\max} - (f_{\max} - f_1) \exp\{c_1(\delta_o - \delta_{o1})^{c_2}\} \right\} \quad ; \text{ for elastic plastic regime } \quad (3.27b)$$

where

- $F$  ; concentrated lateral load at midspan
- $M_p$  ; fully plastic moment of the intact tubular section,  $t D^2 \sigma_Y$
- $\delta_o$  ; non-dimensionalised bending deflection or overall bending deformation,  $d_o/L$  or  $d_1/L$
- $\delta_{o1}$  ; non-dimensionalised elastic limit bending deflection,  $f_1/a$
- $f_{\max}$  ; non-dimensionalised ultimate lateral load,  $F_{\max}/(4 M_p/L) \exp(f_{\max}')$
- $f_1$  ; non-dimensionalised elastic limit lateral load,  $F_1/(4 M_p/L) \pi/4 \exp(f_1')$
- $a$  ; initial slope of non-dimensionalised lateral force - deflection curve,  $3/2 \pi (E/\sigma_Y)/(L/D) \exp(a')$
- $c_1$  =  $1/(L/D) \exp(c_1')$
- $c_2$  =  $\exp(c_2')$
- $a'$  =  $-0.347\delta_d^{0.7} - 1.05\delta_d^{1.4} + 0.00358(L/D)\delta_d^{0.5} + 0.00279(L/D)\delta_d$

$$f_{\max}' = -0.01 - 0.2\delta_d^{0.5} - 2.95\delta_d + 6.72\delta_d^{2.5} - 453\delta_d^5 \\ + \{1 - 0.25(D/t)\}(0.186 + 0.107\delta_d^{0.5}) - \{1 - 0.25(D/t)\}^2(0.332 + 0.86\delta_d^{0.1} \\ - 0.727\delta_d) + 4.27\delta_d^{0.2}\{1 - 0.25(D/t)\}$$

$$f_1' = -0.0069 - 0.519\delta_d^{0.5} + 1.31\delta_d - 5.33\delta_d^{1.5} - 151\delta_d^3 \\ + \{1 - 0.025(D/t)\}(0.152 + 0.00784\delta_d^{0.5} + 4.8\delta_d - 14.4\delta_d^{1.5} - 178\delta_d^3) \\ - \{1 - 0.025(D/t)\}^2(0.279 - 2.01\delta_d^{0.5} + 14.6\delta_d - 6.98\delta_d^{1.5} - 51.8\delta_d^3)$$

$$c_1' = 11.1 + 1.64\delta_d^{0.5} + 19.4\delta_d - 86.8\delta_d^2 - 8250\delta_d^5 + 28200000\delta_d^{10} \\ + (L/D)^{0.1}(1.5 - 75\delta_d^{2.5} + 229\delta_d^5) - (L/D)^{0.2}(1.11 - 3250\delta_d^5 + 1130000\delta_d^{10}) \\ - (L/D)^{0.5}(0.263\delta_d^{0.1} - 0.583\delta_d) - (L/D)(0.033\delta_d^{0.1} + 0.0679\delta_d^{0.2} + 0.0212\delta_d^{0.5} \\ + 0.155\delta_d - 0.866\delta_d^2) + (L/D)^2(0.00212\delta_d^{0.2} - 0.00158\delta_d - 0.029\delta_d^2) \\ + \{1 - 0.025(D/t)\}\{0.50 + 4.33\delta_d^{0.5} - 11.4\delta_d + 1.34\delta_d^2 + 5910\delta_d^5 - 22000000\delta_d^{10} \\ + (L/D)^{0.1}(1.55\delta_d + 202\delta_d^5) - (L/D)(0.0011 + 0.00821\delta_d^{1.1} + 57.5\delta_d^5)\} \\ + \{1 - 0.025(D/t)\}^2\{-3.24 + 59.1\delta_d^{0.5} - 185\delta_d + 305\delta_d^2 - 5470\delta_d^5 \\ + 22600000\delta_d^{10} - (L/D)^{0.1}(2.16 - 8630\delta_d^5) + (L/D)^{0.2}(0.409\delta_d^2 - 324000\delta_d^{10}) \\ + (L/D)^{0.3}(1.59\delta_d^{0.1} - 7.35\delta_d^{1.5}) + (L/D)(0.0189\delta_d^{0.1} - 0.199\delta_d) \\ + (L/D)^2(0.000192 + 0.0000704\delta_d^{0.2} + 6670\delta_d^{10})\} \\ + \{1 - 0.025(D/t)\}^4\{(L/D)^{0.2}(6.12 - 83800000\delta_d^{10}) - (L/D)^{0.6}(2.95\delta_d^{0.2} - 143\delta_d^3) \\ - (L/D)^2(0.00253\delta_d^{0.2} + 0.116\delta_d^2)\}$$

$$c_2' = 0.191 + 0.106\delta_d^{0.5} + 0.388\delta_d + 2.38\delta_d^2 - 16.5(L/D)^{0.1}\delta_d^3 \\ + (L/D)^{0.2}(0.251\delta_d^{0.7} + 1700\delta_d^6) - 0.548(L/D)^{0.4}\delta_d^{1.4} \\ - (L/D)(0.00479\delta_d^{0.1} + 0.0219\delta_d) + (L/D)^2(0.000322\delta_d^{0.2} - 0.00391\delta_d^2) \\ + \{1 - 0.025(D/t)\}\{0.0727 - 0.382\delta_d^{0.5} + 2.75\delta_d - 4.69\delta_d^2 - 86.2(L/D)^{0.5}\delta_d^5\} \\ - \{1 - 0.025(D/t)\}^2\{0.385 - 3.73\delta_d^{0.5} + 7.3\delta_d + 1.98\delta_d^2 - 0.715(L/D)^{0.1}\delta_d^{0.1} \\ - 49400(L/D)\delta_d^{10}\} - 2.62\{1 - 0.025(D/t)\}^4(L/D)^{0.2}\delta_d^{0.2}$$

The spring coefficient for overall bending deformation obtained from the slopes of the force-deflection relations are given as follows:

spring coefficient for overall bending

$$k_{bs} = 4 \frac{M_p}{L^2} a \quad ; \text{ for elastic regime} \quad (3.28a)$$

$$= 4 \frac{M_p}{L^2} c_1 c_2 (\delta_o - \delta_{ol})^{c_2-1} (f_1 - f_{\max}) \exp\{c_1 (\delta_o - \delta_{ol})^{c_2}\}$$

; for elastic plastic regime (3.28b)

For unloading and reloading up to the deflection at which the unloading starts the spring coefficient is assumed to be the same as that for the elastic regime. In Fig. 3.3 the comparisons are presented of the approximate equations, eqns (3.27a) and (3.27b), with the computed results. As can be seen in the figures, in spite of the number of the independent variables reasonably accurate approximations have been achieved for the force-deflection relations of the tubular beams with local denting damage except for some extreme cases. Taking into consideration the computing efficiency of using these equations, when compared with the alternative method for interpolating the computed results, however, the minor inaccuracy in the approximation is justified.

### 3.3.3 Modification Factor for Dynamic Effects

It is well known that the strain-rate sensitivity of the material can significantly increase the bending stiffness of beam-like structures subjected to severe dynamic loadings. On top of that localised bending[88] the higher flexural vibration mode can also raise the spring coefficient for bending deformation based on the force-deflection relation under static load. As discussed in section 2.6 for the low velocity impacts considered in this study the influence of localised bending on the gross structural response can be negligible but the higher modes can affect the flexural behaviour of the beam especially in the early stage of the impact.



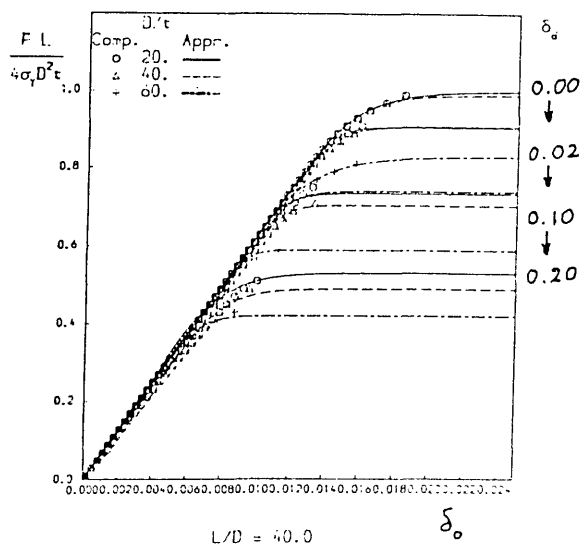
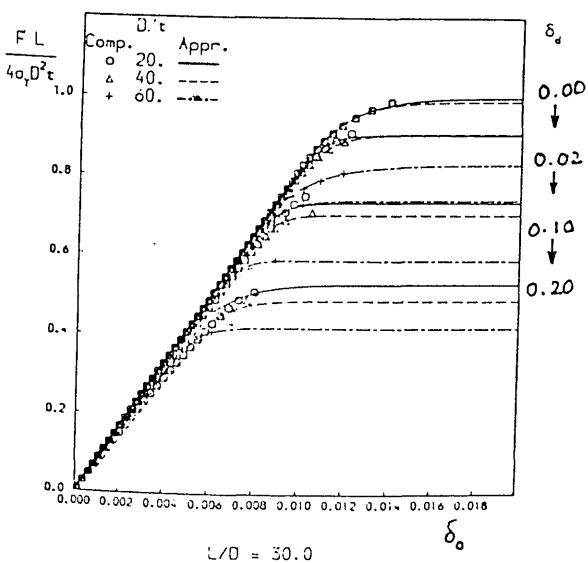
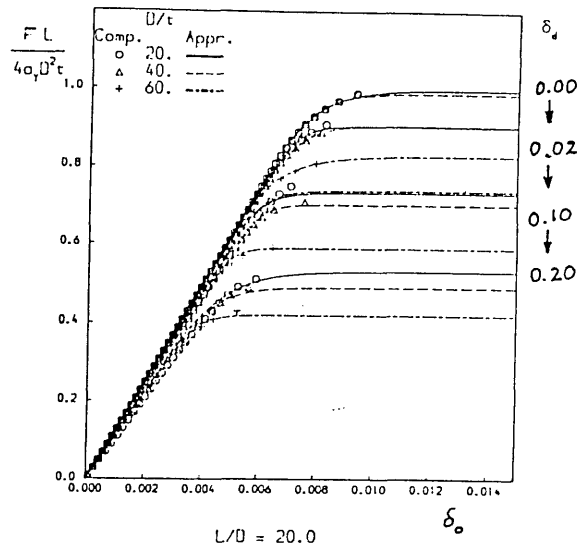
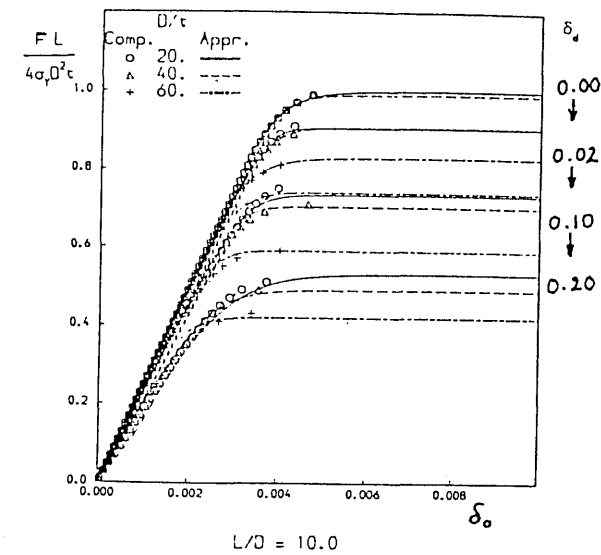


Fig. 3.3 Lateral Force - Midspan Deflection Relationships as Derived from  
computed Results for Simply Supported Damaged Tubulars

In this study the dynamic effects, especially the strain-rate sensitivity and higher mode effects, are roughly accounted for by multiplying an empirically derived modification factor,  $f_D$ , by the spring coefficient for bending deformation obtained from static load - deflection relationships. Generally, the response of a tubular under lateral impact may consist of elastic-plastic deformation ( $0 < t \leq T_1$ ), elastic spring-back ( $T_1 < t \leq T_D$ ) and free elastic vibration ( $t > T_D$ ) stages, which is described in detail in section 2.6. Having considered the nature of each stage it was decided to adopt different values of  $f_D$  for the first and second stages but no modification factor for the elastic vibration stage and to assume the form of the equation for  $f_D$  to be

$$f_D = 1 + f_{D1} \left\{ \frac{d_1(t)}{V_i} \right\}^{1/2} \quad ; \quad 0 < t \leq T_1 \quad (3.29a)$$

$$= 1 + f_{D2} \left\{ \frac{d_1(t)}{V_i} \right\}^{1/2} \quad ; \quad T_1 < t \leq T_D \quad (3.29b)$$

$$= 1 \quad ; \quad t > T_D \quad (3.29c)$$

The analysis procedure described in the following section was correlated with the experimental data of impact tests provided in chap.2, modification factors being varied in an attempt to find values which would give a satisfactory estimate of extent of damage. It was found in this correlation work that the local denting damage, i.e. permanent depth of dent, can be determined by the value of  $f_{D1}$  irrespective of  $f_{D2}$ . Thus for each test case a value of  $f_{D1}$  was first identified for which theoretical and experimental local denting damage were equal. Parameters which might influence  $f_{D1}$  were judged to be

$$R_k : \text{initial static stiffness ratio, } \frac{(k_{ds})_{\delta_d=0.001}}{(k_{bs})_{\delta_0=0}}$$

$$R_m : \text{initial mass ratio, } \frac{(M_1)_{t=0}}{(m_2)_{t=0}} \text{ or } \frac{M_s}{\frac{1}{2} \rho \pi D t L}$$

$R_v$  : non-dimensionalised impact velocity,  $V_i/(L/T_b)$

and

$R_E$  : energy ratio defined as eqn (3.2)

where the initial static stiffness for local denting is taken for  $\delta_d = 0.001$  rather than for  $\delta_d = 0.0$  due to a mathematical difficulty and  $T_b$  is the natural period of the flexural beam vibration of the intact tubular,  $2\pi \sqrt{(m_2)_{t=0} / (k_{bs})_{\delta_0=0}}$

A non-linear regression equation of the form

$$f_{D1} = \alpha_0 R_k^{\alpha_1} R_E^{\alpha_2} R_m^{\alpha_3} R_v^{\alpha_4} \quad (3.30)$$

was assumed and the values of  $\alpha_0, \alpha_1, \alpha_2, \alpha_3$  and  $\alpha_4$  were found to provide a best fit to the identified values for  $f_{D1}$ . Parameters  $R_m$  and  $R_v$  were found to be negligible and then the equation finally obtained was

$$f_{D1} = 0.08 R_k R_E \quad (3.31)$$

Using the experimental values for overall bending damage together with eqn (3.31) a value of  $f_{D2}$  for each test was identified and then following a similar procedure to that for  $f_{D1}$  the equation of  $f_{D2}$  was found as

$$f_{D2} = f_{D1} \exp(0.07 R_v R_m^2) \quad (3.32)$$

Different values for the exponent of  $d_1(t)/V_i$  were investigated but found not to offer better results.

### 3.4 Solution Scheme

#### 3.4.1 Algorithm for Step by Step Solution

The algorithm for step by step solution of the non-linear spring-mass model

with two degrees-of-freedom involves initial calculations and calculations for each time step. Details of these calculations are described herein.

(A) Initial Calculation

1. Geometric, material and sectional property parameters :  $L/D$ ,  $D/t$ ,  $E/\sigma_Y$ ,  $M_p$ ,  $m_p$
2. Basic system parameters :  $R_K$ ,  $R_E$ ,  $R_m$  and  $R_v$
3. Initial conditions:
  - $d_1 = V_i$  0,
  - equivalent masses ;  $M_1 = M_s$ ,  $m_2 = 1/2 \pi \rho D t L$
  - spring forces ;  $F_{sd} = F_{sb} = 0$
  - strain energies and total system energy ;  $E_{sd} = E_{sb} = 0$ ,  $E_T = 1/2 M_s V_i^2$
  - strain energies and total system energy ;  $E_{sd} = E_{sb} = 0$ ,  $E_T = 1/2 M_s V_i^2$
4. Time step  $\Delta t$

(B) Calculations for Each Time Step

1. Dynamic spring coefficients,  $k_d$  and  $k_b$ , using eqns.(3.26a,b), and eqns.(3.28a,b) together with eqns.(3.29a,b,c) respectively
2. Incremental displacements,  $\Delta d_{1i}$  and  $\Delta d_{2i}$ , using eqns (3.21a) and (3.21b) respectively
3. Incremental velocities,  $\Delta \dot{d}_{1i}$  and  $\Delta \dot{d}_{2i}$ , using eqns (3.18a) and (3.18b) respectively
4. Displacements and velocities at the end of time interval,  $d_{1\ i+1}$ ,  $d_{2\ i+1}$ ,  $\dot{d}_{1\ i+1}$  and  $\dot{d}_{2\ i+1}$ , using eqns (3.22a), (3.22b), (3.23a) and (3.23b) respectively
5. Spring forces,  $F_{sd}$  and  $F_{sb}$ , at  $t = t_i + \Delta t$

$$F_{sd}(t_i + \Delta t) = F_{sd}(t_i) + k_{di} (\Delta d_{1i} - \Delta d_{2i}) \quad (3.33)$$

$$F_{sb}(t_i + \Delta t) = F_{sb}(t_i) + k_{bi} \Delta d_{2i} \quad (3.34)$$

6. Equivalent masses,  $M_{1\ i+1}$  and  $m_{2\ i+1}$

7. Accelerations,  $\ddot{d}_{1\ i+1}$  and  $\ddot{d}_{2\ i+1}$ , using eqns (3.24a) and (3.24b) respectively
8. Strain energies,  $E_{sd}$  and  $E_{sb}$ , and total system energy,  $E_T$ , at  $t = t_i + \Delta t$

$$E_{sd}(t_i + \Delta t) = E_{sd}(t_i) + F_{sd}(t_i + \Delta t) (\Delta d_{1i} - \Delta d_{2i}) \quad (3.35)$$

$$E_{sb}(t_i + \Delta t) = E_{sb}(t_i) + F_{sd}(t_i + \Delta t) \Delta d_{2i} \quad (3.36)$$

$$E_T(t_i + \Delta t) = E_{sd}(t_i + \Delta t) + E_{sb}(t_i + \Delta t) + 1/2 M_1 \dot{d}_1^2 + 1/2 m_2 \dot{d}_2^2 \quad (3.37a)$$

$$E_{sd}(t_i + \Delta t) + E_{sb}(t_i + \Delta t) + 1/2 M_s V_r^2 + 1/2 m_1 \dot{d}_1^2 + 1/2 m_2 \dot{d}_2^2 \quad (3.37b)$$

where  $V_r$  is the rebound velocity of the striker, i.e.  $V_r = -\dot{d}_1(t)_{t=T_D}$ .

### 3.4.2 Selection of Time Step

As in any numerical method the accuracy of the step-by-step integration method depends upon the magnitude of the time increment selected. Generally, the natural period of the structure, the rate of variation of the loading function and the complexity of the stiffness and damping functions can be considered in the selection of time step  $\Delta t$ . In this study the sensitivity of the predicted extent of damage to  $\Delta t$  was investigated for the cases of models A<sub>3</sub> and F<sub>3</sub>. In Fig. 3.4 plots are presented of the predicted extent of damage against non-dimensionalised  $\Delta t$  divided by  $T_1$  which is the natural period for local denting vibration, i.e.

$$T_1 = 2\pi \sqrt{\frac{M_s}{(k_{sd})_{\delta_d=0.001}}} \quad (3.38)$$

For both the models, as the incremental time step  $\Delta t$  decreases, the local denting damage increases while the overall bending damage decreases but each one is approaching a certain value. However, the predicted overall bending damage is relatively insensitive to the time step for the range  $0.00003T_1 - 0.0005T_1$ . Compromising the accuracy of prediction and the computing efficiency, the incremental

time step finally selected to carry out the correlation study and parametric study was  $0.0001T_1$ .

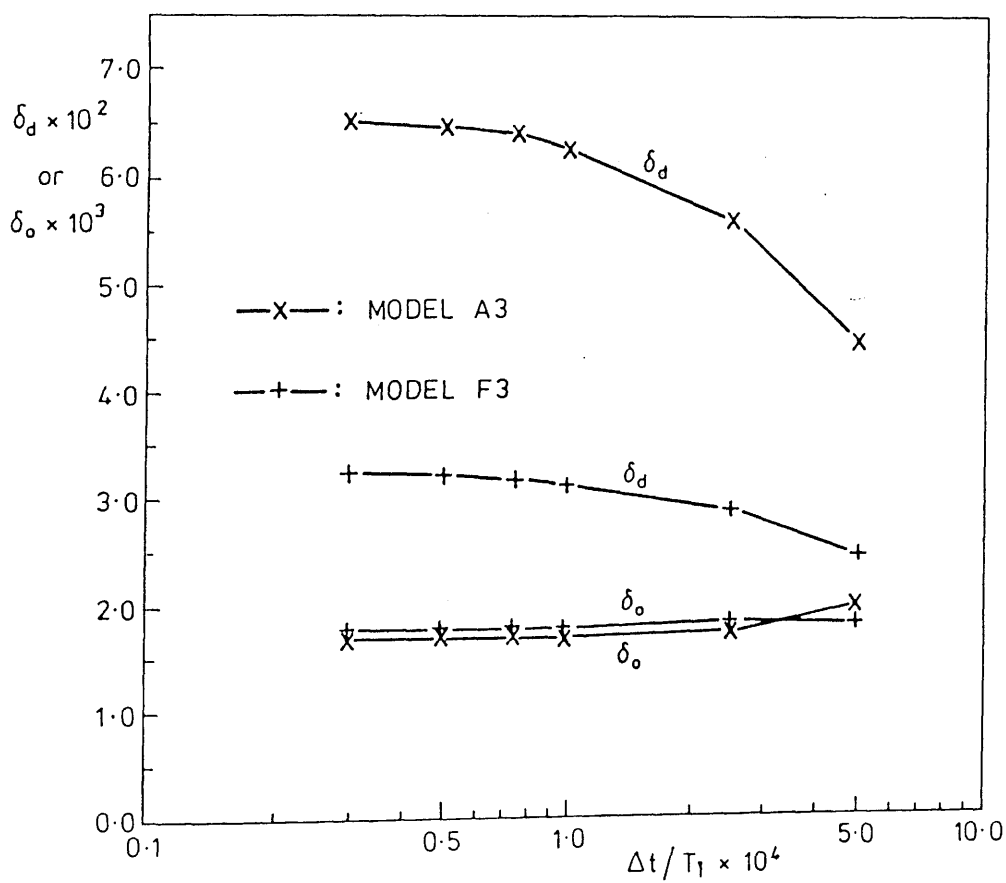


Fig. 3.4 Sensitivity of Predicted Extent of Damage to Time Increment Step  $\Delta t$

### 3.5 Results and Discussion

Following the solution procedures described above the analysis has been carried out for the twenty-four test cases. In Figs. 3.5(a)-3.5(g) the history of displacements  $d_1$ ,  $d_2$  and  $d_d(= d_1 - d_2)$ , velocities and accelerations for masses  $M_1$  and  $m_2$  are

illustrated in turn for models A3, B3, C2, D1, F1, F3 and H2. The history is also presented in the figures of the non-dimensionalised spring forces divided by maximum static lateral load,  $4 M_P/L$ , and of the non-dimensionalised energies divided by impact energy,  $E_k (=1/2 M_s V_i^2)$ .

The characteristics of the impact history curves shown in Figs.3.5(a)-3.5(g) can be specified as follows:

- purely local denting deformation is followed by overall bending together with additional local denting ;
- bending deformation dominates in the elastic vibration stage and a smooth curve has been demonstrated by the total displacement  $d_1$  ;
- in the purely local denting phase very high acceleration due to high local denting stiffness is imposed on mass  $m_2$ , which consequently develops the velocity of  $m_2$  greater than the initial impact velocity ;
- a high frequency local shell vibration is apparent in the elastic vibration stage, i.e. after separation of the striker from the struck model ;
- maximum spring force can far surpass the maximum static lateral load,  $4M_P/L$ , and the spring force  $F_{sb}$  is the basis of the oscillation of the spring force  $F_{sd}$  ;
- the change of the strain energy of denting deformation in the elastic spring-back and elastic vibration stages is negligible ; and
- despite the fact that dynamic force equilibrium only is retained in the formulation, energy conservation has been achieved throughout the procedure with a negligible violation in the purely local denting phase.

A summary of the theoretical estimates is made in Table 3.1, which includes the extent of damage,  $\delta_d$  and  $\delta_o$ , peak bending deformation,  $\delta_{opk}$ , impact duration,  $T_D$ , rebound velocity,  $V_r$ , energy absorbed plastically in the struck model,  $E_D$ , and maximum spring force for all test cases together with their parameters and experimental results. All the values are non-dimensionalised in the table except the impact duration.

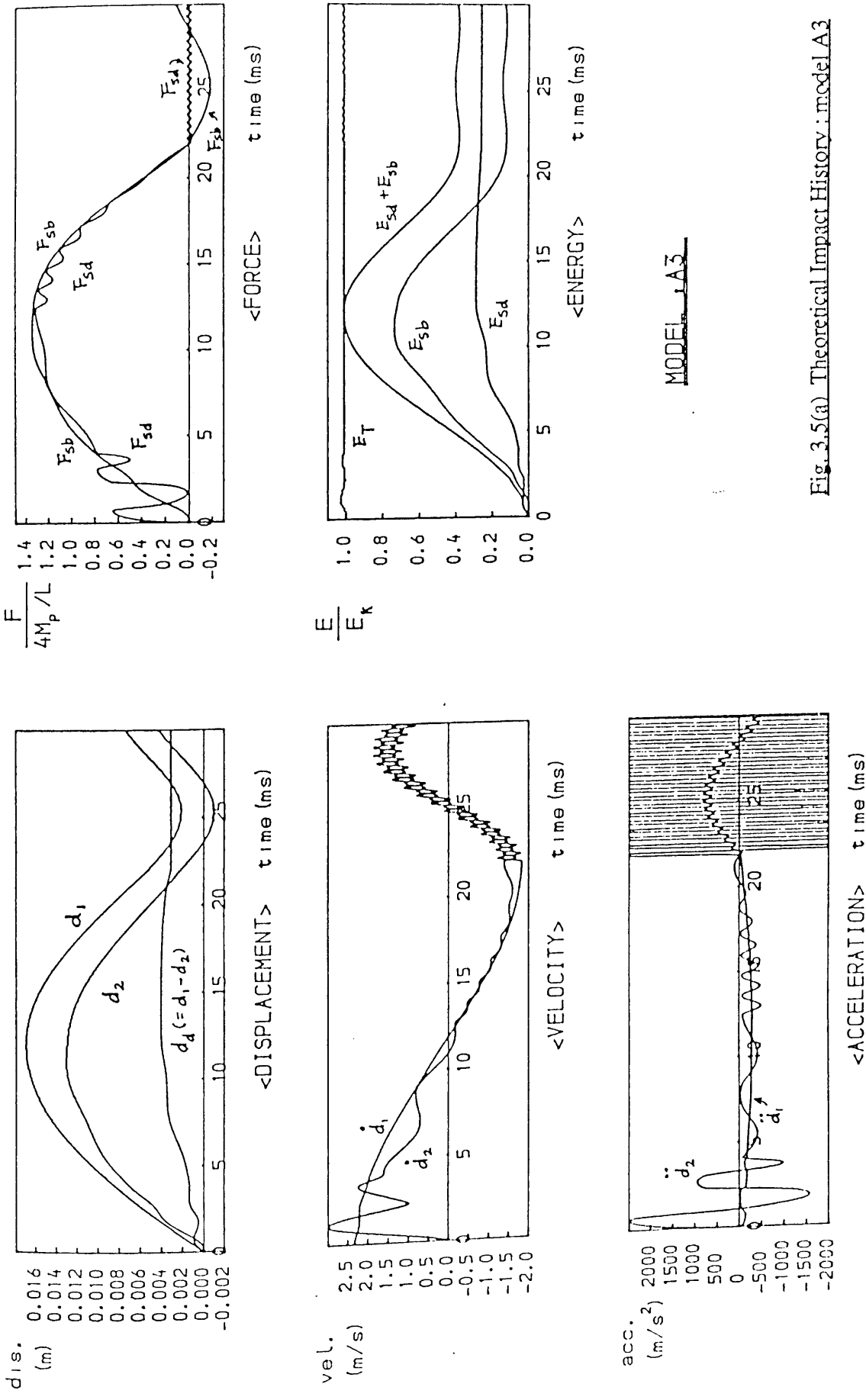
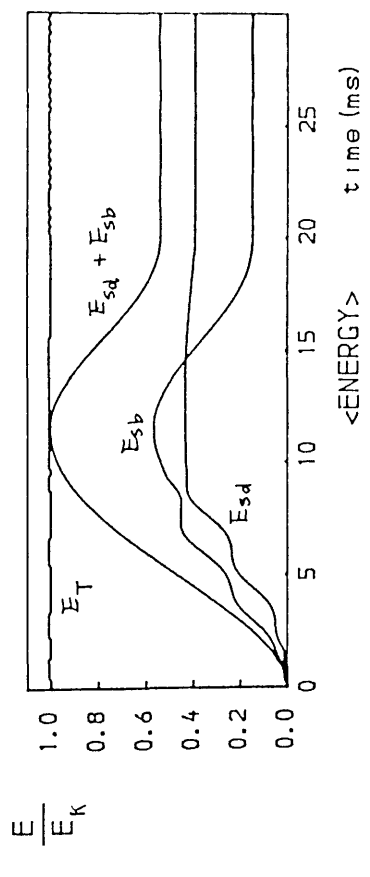
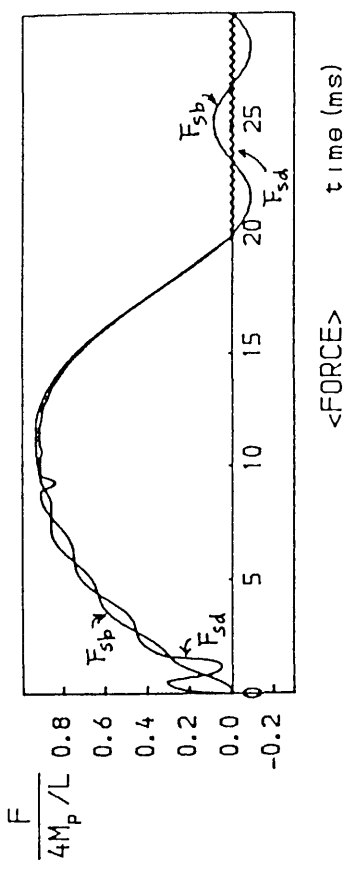
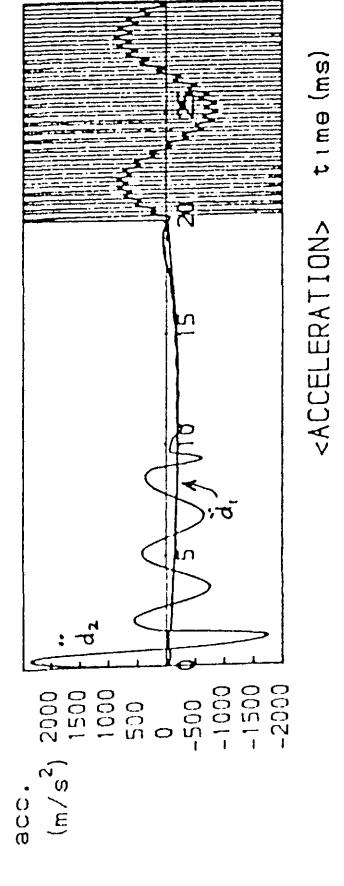
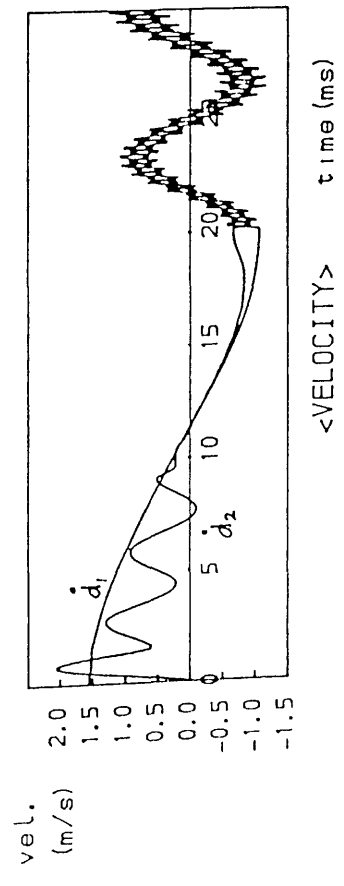
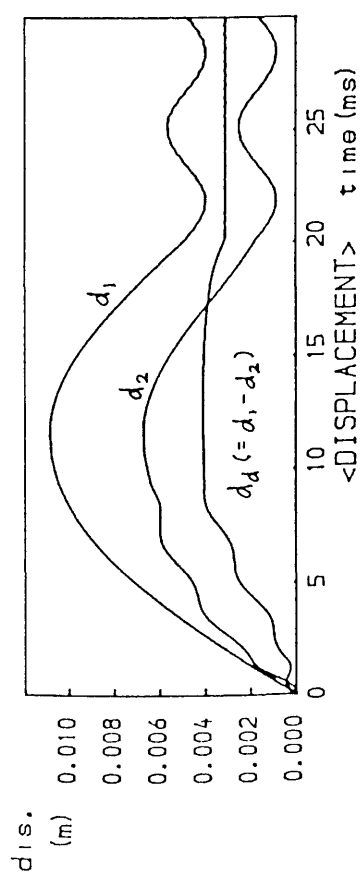


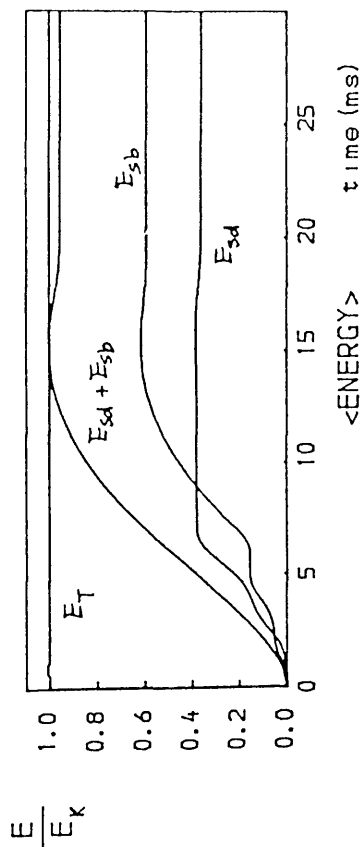
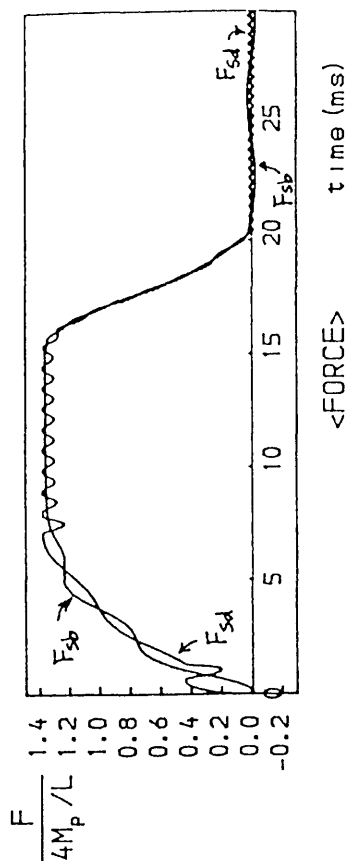
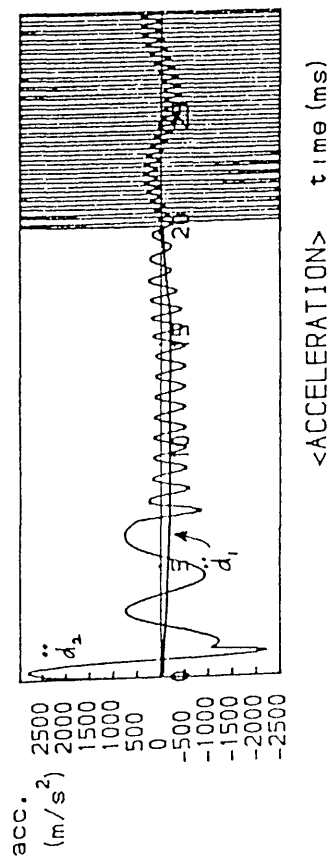
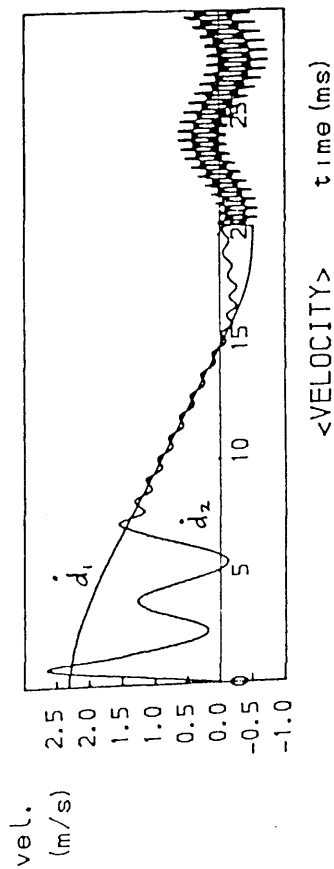
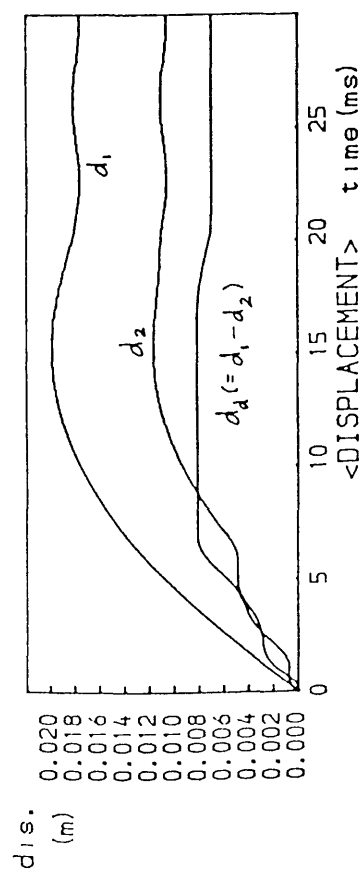
Fig. 3.5(a) Theoretical Impact History : model A3





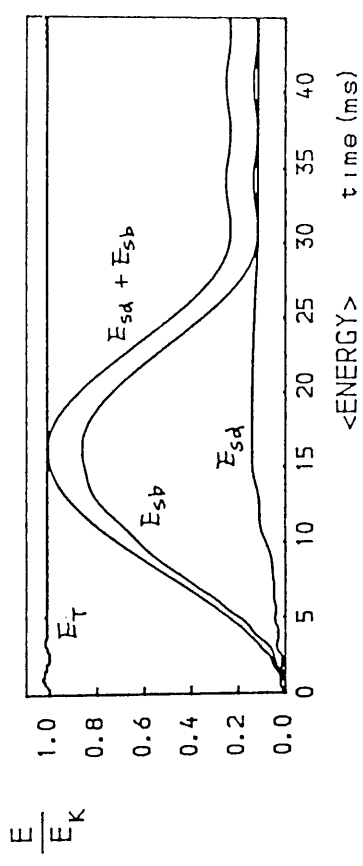
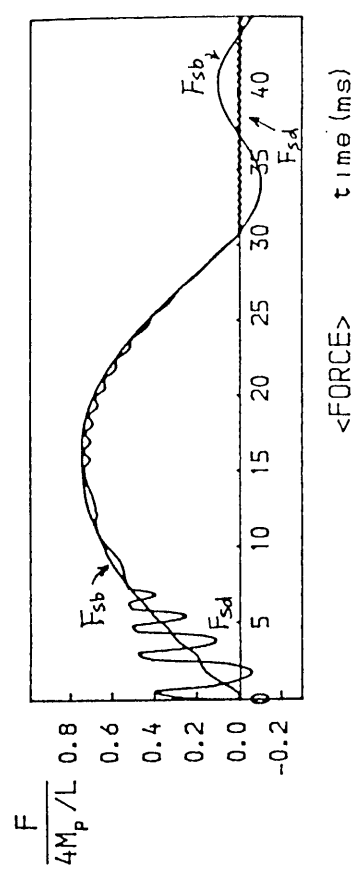
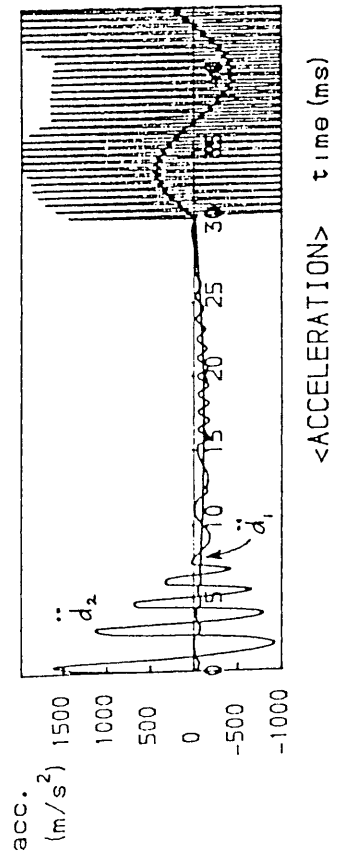
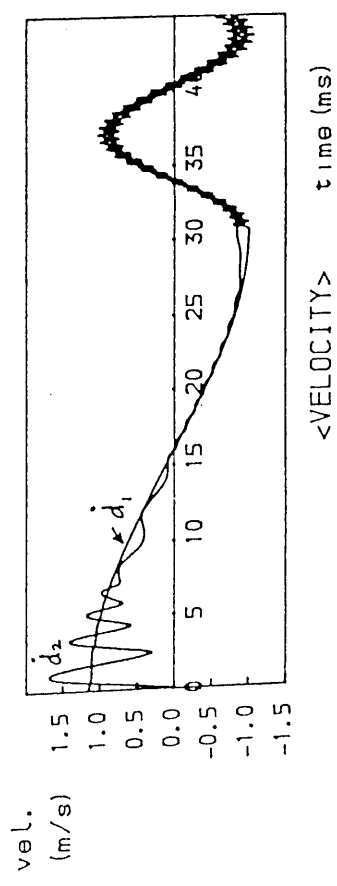
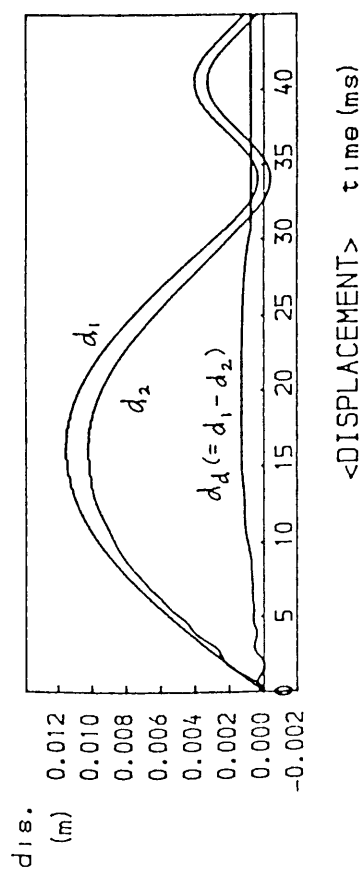
MODEL B3

Fig. 3.5(b) Theoretical Impact History : model B3



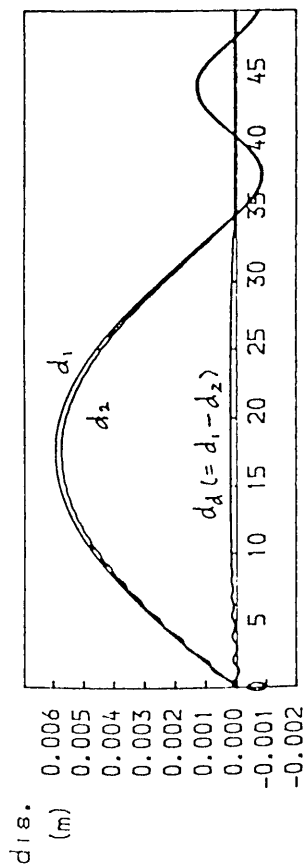
MODEL C2

Fig. 3.5(c) Theoretical Impact History : model C2

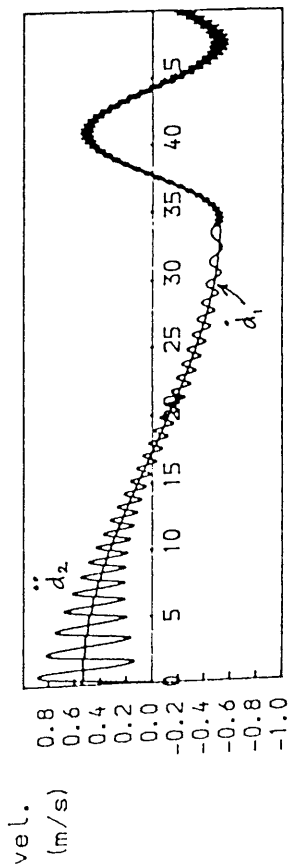


MODEL D1

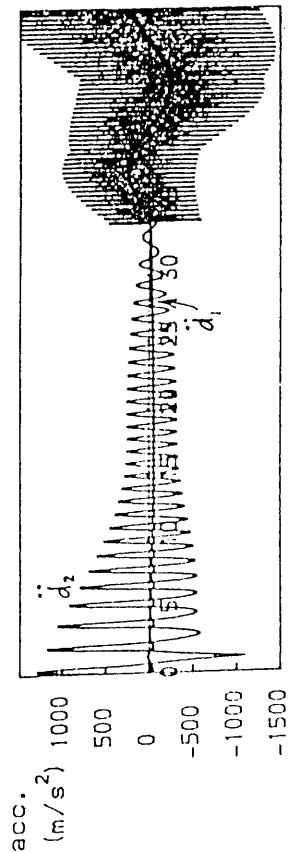
Fig. 3.5(d) Theoretical Impact History : model D1



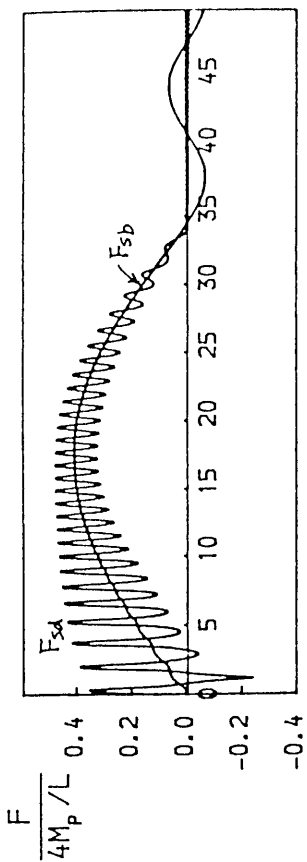
<DISPLACEMENT>



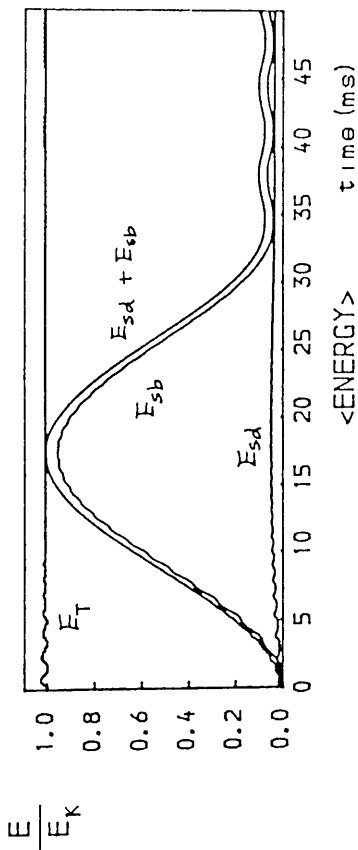
<VELOCITY>



<ACCELERATION>



<FORCE>



<ENERGY>

MODEL F1

Fig. 3.5(e) Theoretical Impact History : model F1

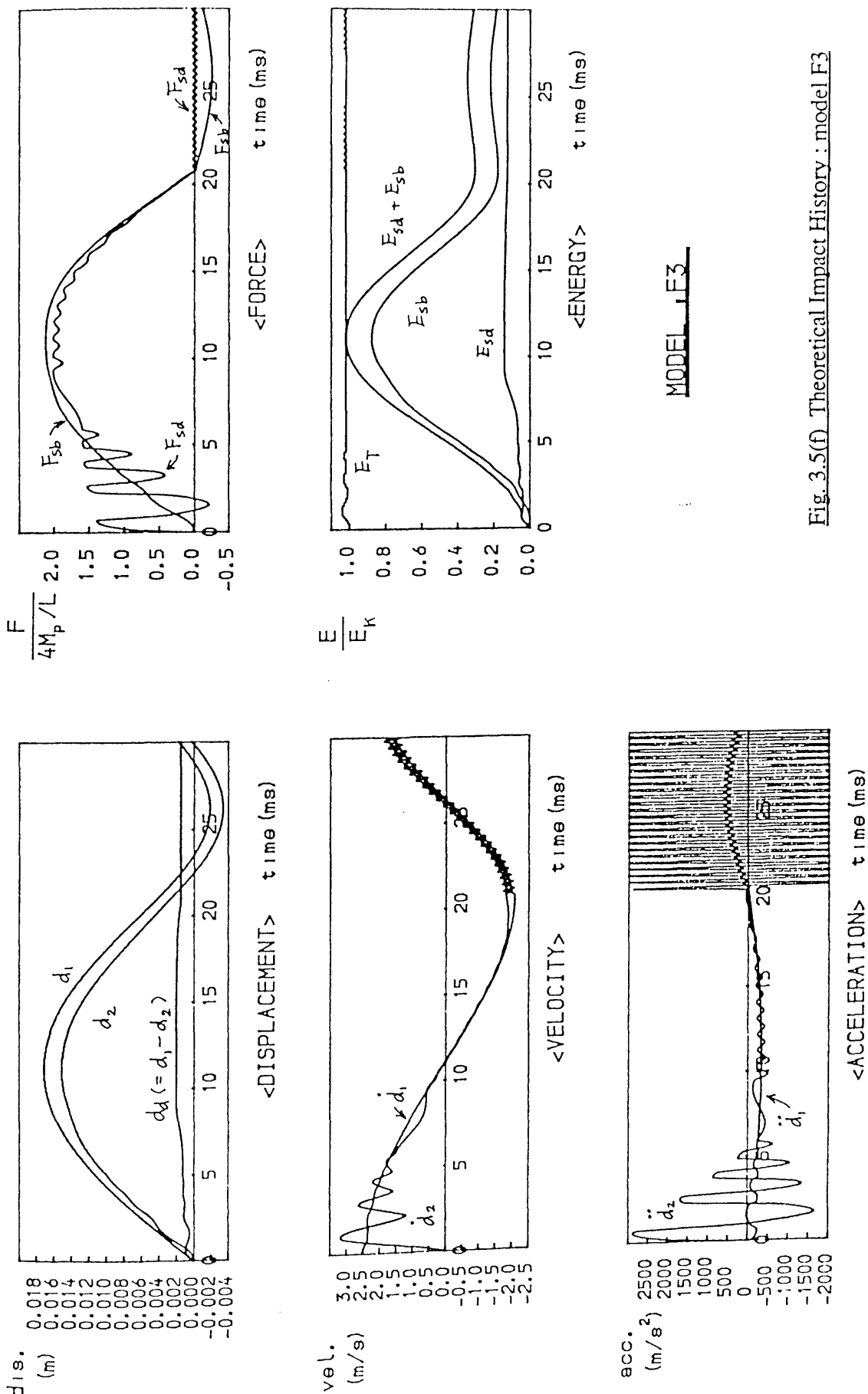


Fig. 3.5(f) Theoretical Impact History : model F3

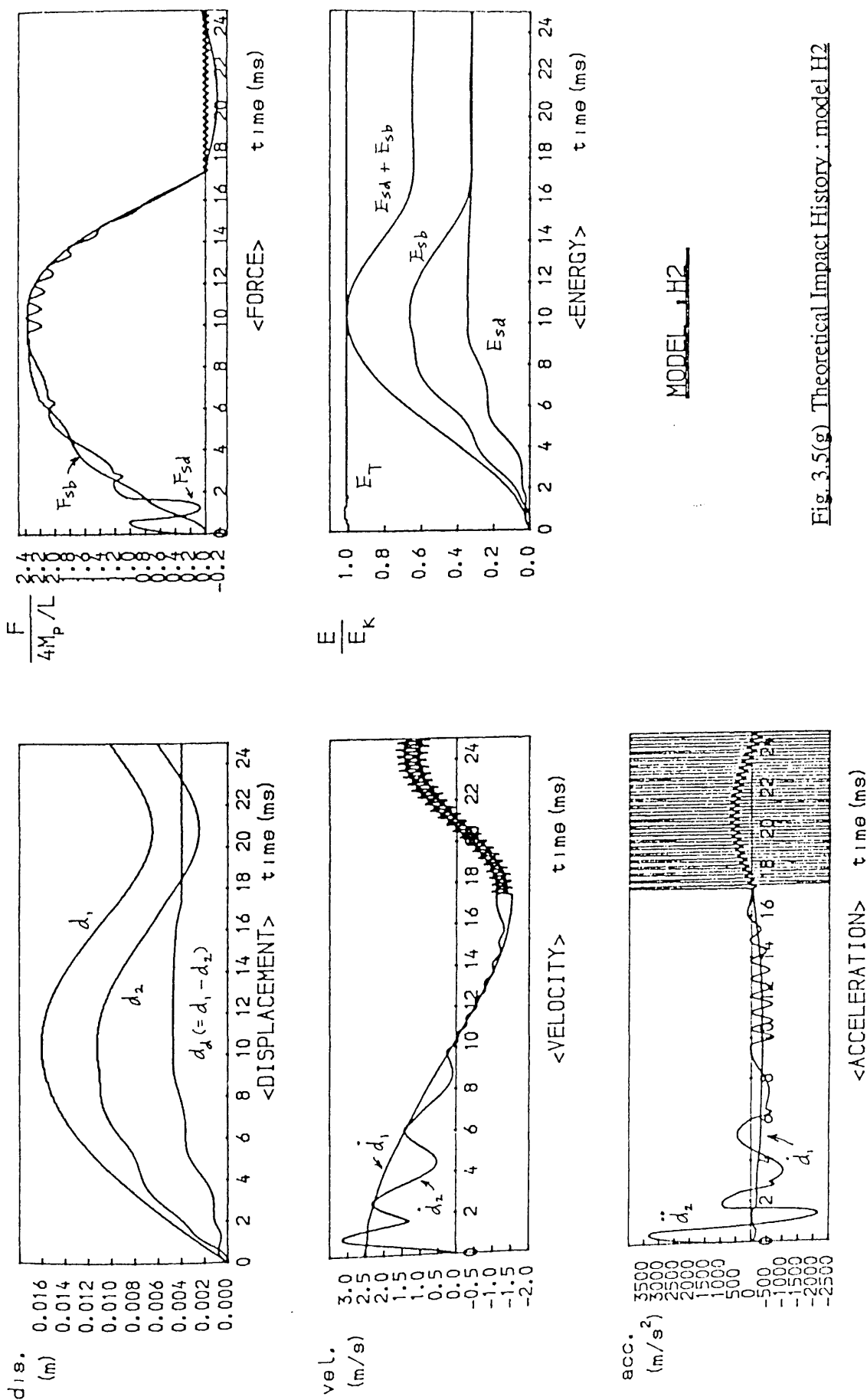


Fig. 3.5(g) Theoretical Impact History : model H2

Table 3.1 Comparison between Experimental and Theoretical Results

Model	Test Parameters				Results													
					Experimental							Theoretical						
	$R_k$	$R_E$	$R_m$	$R_v$	$\delta_d \times 10^2$	$\delta_o \times 10^3$	$\delta_{opk} \times 10^3$	$T_D$ (ms)	$V_r$	$E_{Du}$	$E_k$	$\delta_d \times 10^2$	$\delta_o \times 10^3$	$\delta_{opk} \times 10^3$	$T_D$ (ms)	$\frac{V_r}{V_i}$	$\frac{E_D}{E_k}$	$\frac{F_{sm}}{4Mp/L_i}$
A3	25.2	0.47	19.1	2.22	7.1	2.9	14.7	33.6	0.40	0.84		6.26	1.71	9.7	21.9	0.781	0.380	1.347
A4	8.8	0.73	27.1	1.62	9.3	3.5	13.1	25.0	0.48	0.77		8.90	2.91	8.8	16.8	0.599	0.641	1.080
B1	25.9	0.64	23.8	2.39	6.2	2.8	14.4	37.8	0.58	0.66		9.40	3.53	10.2	22.3	0.664	0.558	1.556
B3	8.9	0.44	40.8	1.05	5.6	1.7	6.8	28.0	0.57	0.68		6.30	1.84	7.1	20.1	0.681	0.535	0.937
B4	25.7	0.64	28.7	2.16	4.4	1.7	---	---	---	---		9.80	4.43	9.9	23.7	0.606	0.633	1.593
C1	8.6	0.42	58.6	0.79	4.0	1.1	9.4	31.3	0.45	0.80		5.87	2.82	6.4	22.9	0.600	0.641	0.917
C2	8.7	1.63	58.2	1.55	20.9	15.0	25.6	51.4	0.36	0.87		14.10	11.59	12.3	20.3	0.225	0.953	1.386
C3	24.9	0.18	41.0	0.88	1.0	0.1	8.6	45.6	0.45	0.80		1.57	1.88	7.2	35.1	0.813	0.334	0.774
C4	24.9	0.90	41.0	1.96	13.7	8.6	18.0	61.7	0.51	0.75		12.34	7.40	9.6	24.1	0.392	0.850	1.844
D1	25.5	0.17	28.7	1.10	0.4	0.4	7.5	37.8	0.90	0.20		1.50	1.13	7.6	30.6	0.870	0.233	0.747
D2	8.9	1.12	40.4	1.68	12.5	5.9	---	30.5	0.44	0.80		12.52	7.62	10.7	18.7	0.400	0.843	1.261
D3	25.8	0.80	28.5	2.42	10.7	5.6	18.5	41.9	0.49	0.76		11.22	5.72	10.4	22.4	0.546	0.704	1.699
D4	25.9	1.19	41.3	2.46	18.3	14.8	27.0	69.7	0.42	0.82		15.42	10.19	11.6	22.7	0.293	0.917	1.987

(cont'd)

Table 3.1 Comparison between Experimental and Theoretical Results(cont'd)

Model	Test Parameters		Results													
			Experimental							Theoretical						
	$R_k$	$R_E$	$R_m$	$R_v$	$\delta_d$	$\delta_o$	$\delta_{opk}$	$T_D$	$V_r$	$E_{Du}$	$\delta_d$	$\delta_o$	$\delta_{opk}$	$T_D$	$V_r$	$F_{sm}$
				$\times 10^2$	$\times 10^{-2}$	$\times 10^3$	$\times 10^3$	(ms)	$V_i$	$E_k$	$\times 10^2$	$\times 10^3$	$\times 10^3$	(ms)	$V_i$	$E_k$
E3	41.3	0.49	17.1	2.40	0.8	0.4	12.1	30.5	0.86	0.26	3.44	1.87	9.1	17.8	0.809	0.332
F1	39.0	0.05	30.5	0.53	0.0	0.0	3.7	39.8	0.56	0.68	0.10	0.38	4.3	33.8	0.953	0.079
F1p	39.0	0.51	25.0	1.84	1.6	0.8	13.4	36.1	0.59	0.65	3.61	2.84	8.4	20.5	0.738	0.450
F2	13.6	0.64	35.5	1.22	4.3	2.0	9.4	23.4	0.81	0.35	4.62	2.90	7.6	15.9	0.651	0.575
F3	84.9	0.48	13.4	3.17	2.5	1.5	25.4	42.2	0.67	0.55	3.12	1.77	8.6	20.8	0.822	0.304
G1	13.7	0.67	24.4	1.52	3.5	1.7	10.9	21.4	0.60	0.64	4.79	1.92	7.8	13.8	0.704	0.501
G2	39.5	0.63	17.1	2.50	3.7	2.4	16.4	32.0	0.71	0.50	4.39	2.03	8.7	16.9	0.773	0.392
G3	85.6	0.30	19.2	2.11	0.4	0.3	13.5	52.2	0.83	0.30	1.33	2.27	8.3	27.7	0.820	0.313
H1	39.5	0.52	11.4	2.80	0.6	0.3	13.0	25.3	---	---	3.57	0.77	8.7	15.1	0.849	0.253
H2	38.6	0.93	25.1	2.46	6.5	4.3	17.3	39.1	0.55	0.70	8.22	4.00	8.4	17.3	0.598	0.641
H3	13.5	0.24	35.5	0.73	0.1	0.0	6.2	23.1	0.59	0.65	1.52	0.64	5.6	18.2	0.852	0.267



In Fig. 3.6 the predictions for the extent of damage are compared with the test results. A reasonably good correlation can be seen in the figure except for the two most severely damaged cases, i.e. for models C2 and D4. For those two cases the analysis method provides underestimated extents of damage. Another shortcoming of the method can be found in the skewness of the predicted impact durations,  $T_D$ , and peak bending deformations,  $\delta_{opk}$ , which is illustrated in Fig. 3.7. The underestimation both of  $T_D$  and  $\delta_{opk}$  is becoming more apparent as the value of  $R_k R_E R_v R_m$  increases. Among other factors the consideration of overall bending damage in the derivation of the spring coefficient for denting deformation seems to improve these shortcomings. As described in section 3.3.2 the derived force-indentation relationship is based on the results of tests conducted with supports at the back of the dent centre which minimises the overall bending deformation. Therefore when the bending deformation is large an overestimated spring coefficient is obtained from the relationship

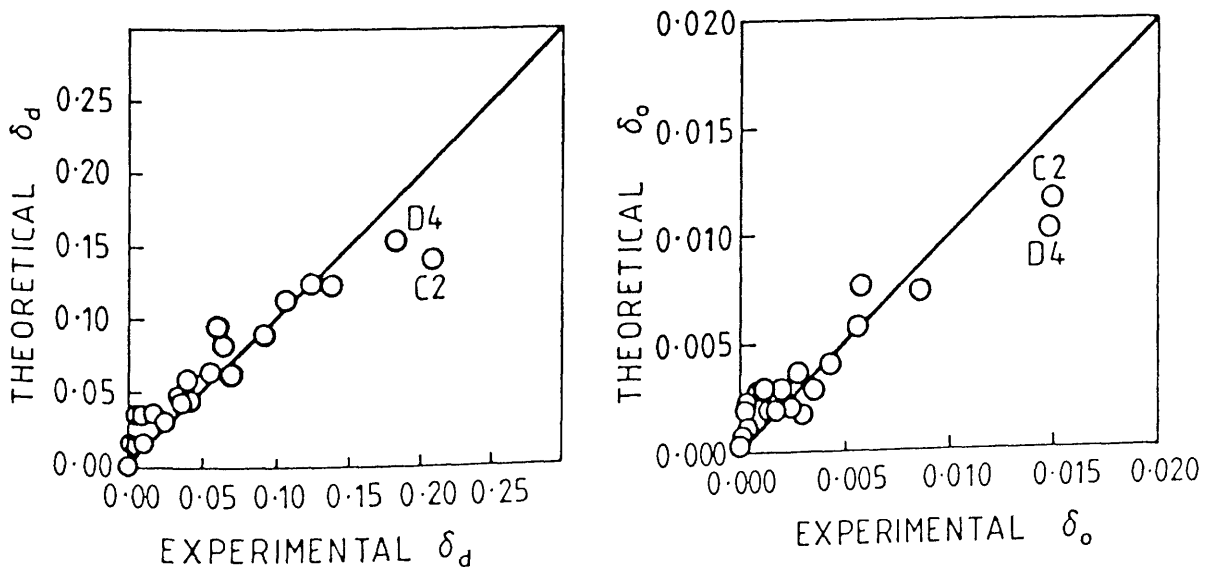


Fig. 3.6 Comparison between Theoretical Predictions  
and Test Results for Extent of Damage

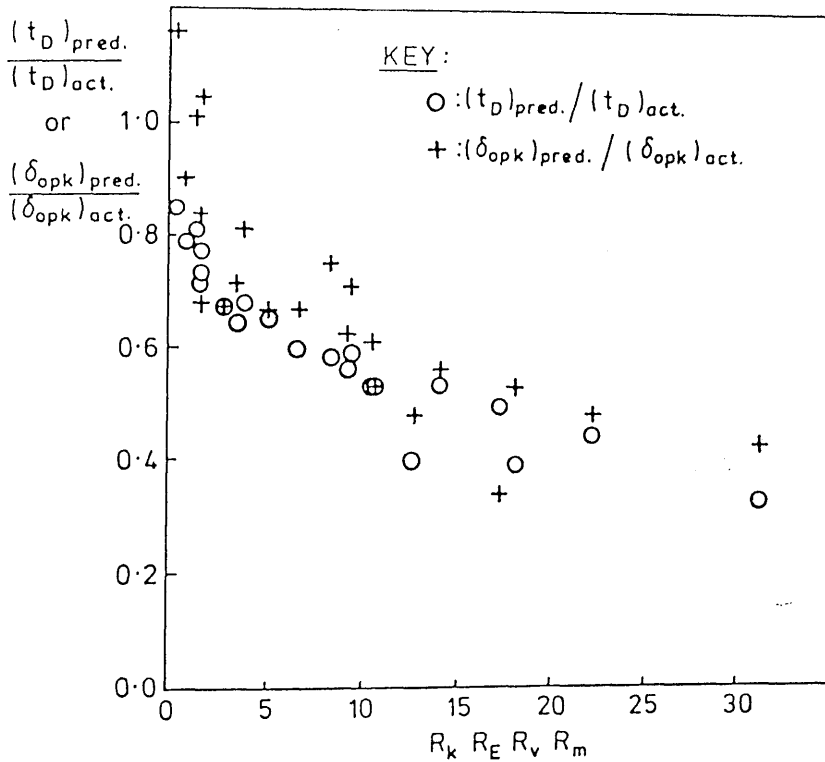


Fig. 3.7 Skewness of Predicted Impact Duration ( $T_D$ )  
and Peak Bending Deformation ( $\delta_{opk}$ )

The experimental values for rebound velocity  $V_R$  and the difference of kinetic energy of the striker immediately before and after impact,  $E_{Du}(= 1/2 M_S V_i^2 - 1/2 M_S V_R^2)$  also are presented in the table. It might be meaningless to directly compare these values with those of the theory since the energy absorbed by the striker itself and by elastic vibrations of the model supporting frames was not taken into account in the analysis. Nevertheless,  $E_{Du}$  can be a very rough upper bound for the energy dissipated plastically in the struck model,  $E_D$ . For most cases the predicted rebound velocity,  $V_R$ , and absorbed energy,  $E_D$ , are less than their corresponding experimental values. However, the opposite is found for the cases of models C2, C4, D2, D4, E2 and F2. It seems likely that the overestimation of denting stiffness explained above and the uncertainty in the experimental velocity, which was obtained from the tangential

line of the displacement history curve for the striker, can be attributable to the overprediction of absorbed energy.

The predictions for fourteen cases, whose extents of damage exceeded the tolerance specifications given in ref.86, provide a 20.9 % COV with a mean of 1.080 and a 25.3 % COV with a mean of 0.993 for local denting damage and overall bending damage respectively. It seems that these COVs are somewhat higher than those of static structural problems. However, considering the complexity of the dynamic problem and the computing efficiency the usefulness of the proposed method can be justified.

## Chapter 4

### ULTIMATE STRENGTH TESTS

#### 4.1 Introduction

Since the pioneering work of Smith et al.[65] the residual strength of damaged tubulars under axial compression has extensively been investigated particularly in the UK[67,68,54,69,73] and Norway[66,71]. Recently a study on the effect of local denting damage upon the load carrying capacity of tubular members under pure bending was reported in ref.70. However, in spite of the possibility of damage onto underwater members of offshore structures as a result of collisions, dropped objects and other accidental impacts occurring in service or during fabrication or installation no research works on the structural behaviour of damaged tubulars under combined loadings including hydrostatic pressure have been reported in the literature. In aiming to provide experimental information for the effect of hydrostatic pressure on the residual strength of damaged tubulars, combined axial compression and hydrostatic pressure loading tests have been conducted as a part of this study.

A problem in column tests having pin-ended support conditions is the rotational restraint of the supports due to unavoidable frictional resistance of the normally employed spherical end blocks, which leads to an overestimation of load carrying capacity especially for intermediate length columns unless the actual effective length is considered in the interpretation of its result. Another problem in column tests is the eccentricity of applied loads, which results in additional moments. Therefore, in column tests it seems necessary to provide experimental information from which the effective length of the model and the eccentricity of applied load can be estimated.

As part of the process of evaluating the deteriorating effect of damage on the load carrying capacity of tubulars subjected to axial compression, it is worthwhile to reappraise experimental results of column tests on intact tubulars having pin-ended supports. Therefore, besides four combined axial compression and hydrostatic pressure loading tests on damaged tubes five pure axial compression tests on undamaged tubes were conducted in aiming to provide test material from which the actual effective lengths of undamaged models can be evaluated. Another eight axial compression tests have also been conducted on damaged tubes with the view to broaden the damage extent range of available test data and to validate the test rig which was to be used for combined axial compression and hydrostatic pressure tests by comparing the axial compression test results with those of other investigators. In this chapter details of test procedures are described and test results are presented.

## 4.2 Models and End Fittings

The models were formed from CDS-24 cold-drawn seamless tubes with a nominal outside diameter of 50.80 mm, and thicknesses of 1.22 mm and 2.03 mm. Both ends of each model were machined flat after cutting. In order to achieve yield strengths in the practical range and to eliminate unknown residual stresses caused by cold-drawing heat-treatments were carried out.

Following heat-treatment, the thickness, circularity and straightness of each tube were surveyed and material properties were determined from at least six tensile tests from each heat-treated parent tube. In the tensile tests the minimum value recorded during a two minute stoppage at a strain of 5000 micro-strain was taken as the corresponding static tensile yield stress. Compressive yield stress was taken to be 5 % higher than the measured tensile values[85]. Young's modulus was obtained from the initial slope of the stress-strain curve. The geometric and material properties of test models are summarised in Table 4.1. It must be noted here that  $\delta_o$  in the table refers to total out-of-straightness, whereas in Table 2.3 in chapter 2 it related to impact-generated overall damage.

Table 4.1 Measured Model Geometry and Material Properties

<u>Model</u>	<u>Length</u>		<u>Outside Diameter</u>		<u>Diameter to Mid-Thickness</u>		<u>Static Yield Stress</u>			
	<u>L(mm)</u>		<u>D<sub>o</sub></u>		<u>D(mm)</u>		<u>Tensile</u>		<u>Compressive</u>	
			<u>Mean COV</u>		<u>Mean COV</u>		<u>Mean COV</u>		<u>σ<sub>Yc</sub></u>	
			<u>(mm) (%)</u>		<u>(mm) (%)</u>		<u>(N/mm<sup>2</sup>) (%)</u>		<u>(N/mm<sup>2</sup>)</u>	
A1*	1400		50.89	0.12	49.69	1.20 1.46	481	0.46	505	
A2*	1000		50.91	0.10	49.71	1.20 1.45	481	0.46	505	
B1	1400		50.86	0.15	49.66	1.20 2.18	491	2.52	516	
B2*	902		50.94	0.16	49.74	1.20 0.84	482	2.36	506	
C2	1000		50.91	0.18	49.69	1.22 1.81	441	3.00	463	
C4	1400		50.85	0.24	49.63	1.22 1.71	441	3.00	463	
D2	1000		50.98	0.10	49.77	1.21 1.18	480	2.56	504	
D3	1400		50.91	0.08	49.70	1.21 1.57	485	3.07	509	
D4	1400		50.90	0.14	49.69	1.21 1.70	485	3.07	509	
E1*	1400		50.92	0.08	48.87	2.05 3.17	461	3.06	484	
E2*	1000		50.92	0.11	48.88	2.04 2.81	461	3.06	484	
F1p	1400		50.91	0.09	48.88	2.03 1.48	425	1.40	446	
F2	1000		50.90	0.12	48.87	2.03 1.97	425	1.40	446	
G1	1000		50.95	0.14	48.91	2.04 1.37	429	1.96	450	
G2	1400		50.92	0.05	48.87	2.05 1.24	429	1.96	450	
H1	1400		50.90	0.07	48.86	2.04 1.44	431	3.01	453	
H2	1400		50.92	0.16	48.90	2.02 3.06	421	3.29	442	

Note : \* denotes undamaged model.

In order to realistically simulate the damage conditions associated with offshore structure impacts, damage was imposed via lateral impact tests conducted using an existing runway and striker. Following these tests, extent of damage measurements were carried out. Details of the heat-treatments, geometric and material property

measurements and lateral impact tests are given in chapter 2.

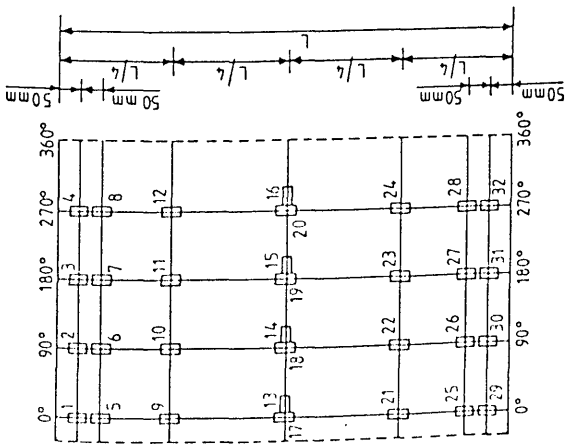
#### 4.2.1 Extent of Damage Range

For pure axial compression load the range of extent of damage for forty five existing test data from refs.65, 67, 66 and 69 are  $\delta_d = 0.001-0.128$ ,  $\delta_o = 0.0001-0.0055$  and  $\sqrt{\delta_d \delta_o} = 0.0022-0.0259$ . Models B1, D3, F2 and G1 were chosen to verify the adequacy of the testing rig by comparing their axial compressive strengths with the results of other investigators. In aiming to broaden the range of extent of damage, models C2, D2, F1p and H1, whose  $\sqrt{\delta_d \delta_o}$  were 0.0559, 0.0269, 0.0032 and 0.0017 respectively, were chosen.

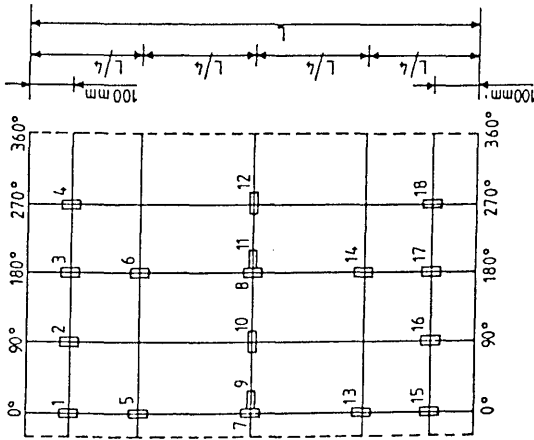
It has theoretically been shown by Toma et al.[103] that the effect of hydrostatic pressure on maximum strength of an intact tube can be amplified by larger initial out-of-roundness. Therefore, in order to clearly demonstrate the effect of hydrostatic pressure on the load carrying capacity of a damaged tube under axial compression more severely damaged models, i.e. models C4, D4, G2 and H2, were chosen for combined axial compression and hydrostatic pressure tests. The extent of damage and the dent centre location of the models are given in Table 4.3.

#### 4.2.2 Strain-Gauging

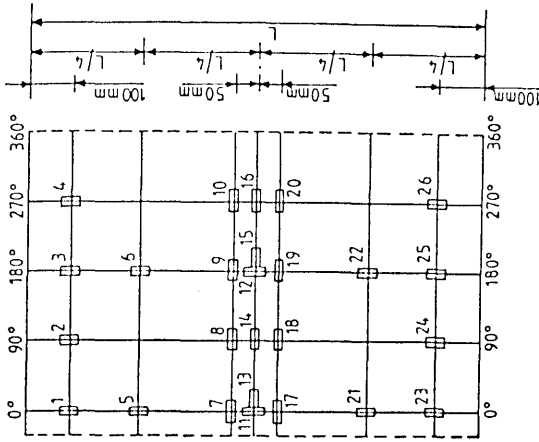
In order to achieve concentricity of applied load and to obtain information from which actual effective lengths for undamaged models could be accurately evaluated, thirty two strain-gauges were used to the undamaged tubes. In the case of damaged models eighteen strain-gauges were bonded for axial compression tests, while twenty six gauges for combined axial compression and hydrostatic pressure tests. Since it is not easy to predict the buckling direction of an undamaged tubular column more strain gauges were used for the undamaged models. In the combined load tests the strain-gauges and strain-gauge terminals were covered with silicon rubber. The strain-gauge arrangements are presented in Fig.4.1. On model E2 strain-gauges no.9 to no.12 were incorrectly installed 200 mm distant from the top rather than 250 mm(L/4).



(for Axial Compression Tests  
on Undamaged Models)



(for Axial Compression Tests  
on Damaged Models)



(for Combined Axial Compression  
and Hydrostatic Pressure Tests on  
Damaged Models)

Fig. 4.1 Strain-Gauge Arrangements



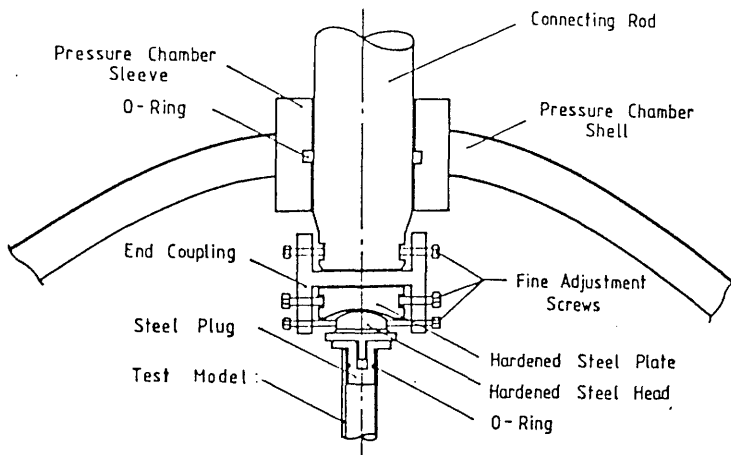


Fig. 4.2 Details of Tube Head Support Arrangement

### 4.2.3 End Fittings

As shown in Fig.4.2 each tube was fitted at its ends with steel plugs, designed to transmit compressive load as uniformly as possible and to provide some support against premature local buckling in the case of any non-uniformity of the compressive stress. Also 70 mm radius spherical heads of hardened steel were used to simulate simple supports. Hardened steel plates, of 200 mm radius concave, and spherical heads were employed to prevent any lateral movement of the models during mounting and to minimise distortions of both fittings due to stress concentrations.

## 4.3 Testing Procedures and Measurements

### 4.3.1 Axial Compression Tests

· Model Alignment : The tubes were mounted in a Tinius-Olson 0-20,000 lb testing machine. For the axial compression tests it was not necessary to use a pressure chamber. After mounting a tube, 0.5-1.0 KN axial load was applied and the strains recorded. When the strain distributions at positions 100 mm from both ends were not satisfactory, the tube positions were adjusted using the 'fine position' screws (see Fig.4.2). This procedure was repeated until the alignment was acceptable.

Table 4.2 Positions of LVDTs in Axial Compression Tests  
for Lateral Deflection Measurements

Model	LVDT Position (Distance from the top, Circumferential Angle)							
	no.3	no.4	no.5	no.6	no.7	no.8	no.9	no.1
A1*	0.26L, 0°	0.26L, 270°	0.49L, 0°	0.49L, 270°	0.49L, 180°	0.49L, 90°	0.74L, 0°	0.74L, 270°
A2*	0.27L, 0°	0.27L, 270°	0.49L, 0°	0.49L, 270°	0.49L, 180°	0.49L, 90°	0.73L, 0°	0.73L, 270°
B1	0.26L, 350°	0.26L, 170°	0.49L, 350°	0.49L, 170°	0.74L, 350°	0.74L, 170°	-- --	-- --
B2*	0.27L, 0°	0.27L, 270°	0.48L, 0°	0.48L, 270°	0.48L, 180°	0.48L, 90°	0.73L, 0°	0.73L, 270°
C2	0.26L, 349°	0.26L, 169°	0.49L, 349°	0.49L, 169°	0.73L, 349°	0.73L, 169°	-- --	-- --
D2	0.27L, 0°	0.27L, 180°	0.49L, 0°	0.49L, 180°	0.73L, 0°	0.73L, 180°	-- --	-- --
D3	0.26L, 0°	0.26L, 180°	0.49L, 0°	0.49L, 180°	0.74L, 0°	0.74L, 180°	-- --	-- --
E1*	0.26L, 0°	0.26L, 90°	0.49L, 0°	0.49L, 90°	0.49L, 180°	0.49L, 270°	0.74L, 0°	0.74L, 90°
E2*	0.27L, 0°	0.27L, 90°	0.49L, 0°	0.49L, 90°	0.49L, 180°	0.49L, 270°	0.73L, 0°	0.73L, 90°
F1p	0.26L, 11°	0.26L, 191°	0.49L, 11°	0.49L, 191°	0.74L, 11°	0.74L, 191°	-- --	-- --
F2	0.27L, 17°	0.27L, 197°	0.49L, 17°	0.49L, 197°	0.73L, 17°	0.73L, 197°	-- --	-- --
G1	0.26L, 0°	0.26L, 180°	0.49L, 0°	0.49L, 180°	0.73L, 0°	0.73L, 180°	-- --	-- --
H1	0.26L, 3°	0.26L, 183°	0.49L, 3°	0.49L, 183°	0.73L, 3°	0.73L, 183°	-- --	-- --

Note : \* denotes undamaged model.

- Displacement Measurements : In order to monitor axial displacements, two LVDTs and a Tinius Olson D-23 deflectometer were used. The signal from the deflectometer was fed into an X-Y plotter together with a load signal to provide autographic load-axial shortening curves. For lateral deflection measurements, four LVDTs near mid-height and two LVDTs near each quarter point were used for the undamaged tubes, while two LVDTs near mid-height and two LVDTs near each quarter point were used for the damaged tubes. Details of the LVDT positions for lateral deflection measurements are given in Table 4.2. The LVDTs were factory calibrated but their gauge factors were checked with slip gauges prior to testing. The output from the LVDTs and strain-gauges was logged using a Solatron Schlumberger 3530 Orion Data Logging System.

- Loading Procedure : Axial load was applied under displacement control at a crosshead approaching speed of some  $1.2 \times 10^{-5}$  mm/s with frequent stops for periods of 2-3 minutes during which load was allowed to drop until it was 'steady' and displacement and strain gauge reading were recorded together with corresponding applied load. Preselection of the load increments was based on previous test results and theoretical predictions of collapse loads. Up to about 10 % of the predicted collapse load, applied load was increased by about 1.0 KN. Between 10 to 70 % of the predicted collapse load, the increment was raised to about 2.5, 5.0 or 10.0 KN according to the magnitude of the predicted collapse load. Up to actual collapse load, the load increment was gradually decreased to 0.5 KN. Beyond collapse load, the load increment was determined according to the load-axial shortening curve plotted from the load and deflectometer signals. The test results show that the actual number of load increments was applied in the range of 68 to 147.

#### 4.3.2 Combined Axial Compression and Hydrostatic Pressure Tests

- Pressure Chamber : The chamber is shown in Figs.4.3(a) and 4.3(b). Rails were used to help position the chamber inside a Losenhausen UPS 2000 KN tension-compression universal testing machine. The chamber was a cylinder capped top and bottom by hemispheres, whose inside diameter and working pressure were 1331 mm and 13.79 N/mm<sup>2</sup> respectively. Connecting rods and the jaws of the testing machine

were joined by intermediate couplings. Sealing between the sleeves of the chamber and the connecting rods was achieved by the use of o-rings set into circumferential grooves in the sleeves. Careful machining of the rods was necessary to achieve a close fit in order to prevent leaking.

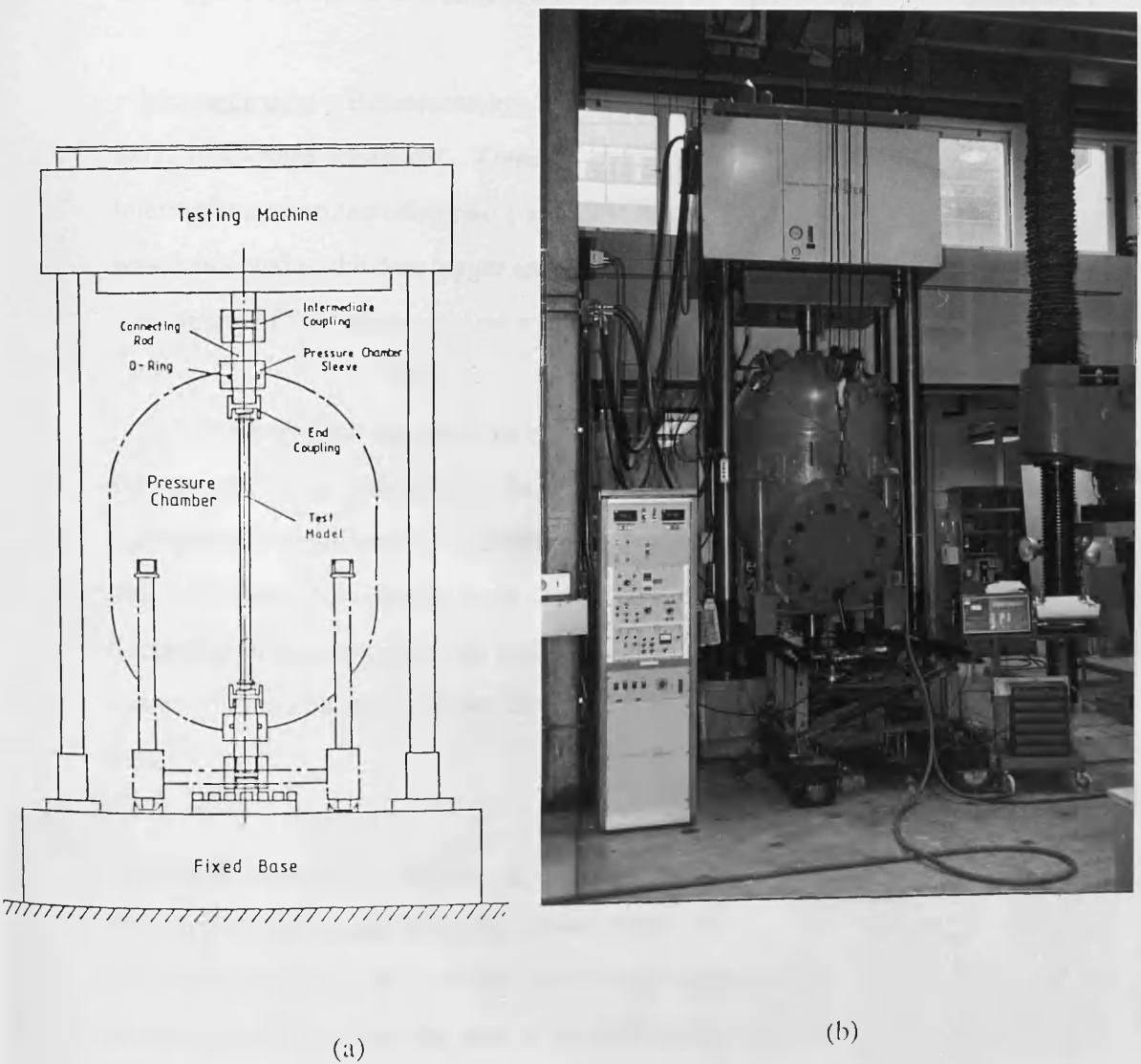


Fig. 4.3 (a) Sketch of Test Rig with a Test Model in Position

(b) Photograph of Test Rig during Filling Pressure Chamber with water

· Test Procedure : After placing the chamber in the position and joining the connecting rods with the jaws of the testing machine the alignment of the model was carried out following the same procedure for the axial compression tests described in the previous section. In order to seal between the model and the steel plugs and consequently to achieve an external hydrostatic pressure load a set of o-rings were inserted into circumferential grooves in the steel plugs. Before filling the chamber with water the access hole for wiring to strain-gauges was sealed with araldite and the manhole was tightly covered by a blind flange having an o-ring. After filling the chamber pressure was applied by means of a hand-operated pump.

· Measurements : Besides strains, overall end-shortening, water pressure and external axial load were measured. Overall shortening reads were taken from the upper intermediate coupling using two LVDTs mounted <sup>on</sup> top of the chamber. One LVDT was connected to the data logger and the output from the other was used by the servo-mechanism of the testing machine to control the axial load.

Pressure was measured by a pressure transducer activated by an independent voltage supply, but connected to the logging system. The measurements were checked against manometer readings. External axial loads were recorded from the output of a load cell located between the lower connecting rod and the lower intermediate coupling. Recording of the data from the strain-gauges, the LVDT and the pressure transducer was maintained by means of the same data logger used for the pure axial compression tests.

· Loading Procedure : Following the alignment of the model some 60-70 % of the estimated collapse axial load was applied incrementally. The chamber was then filled with water and pressure was also incrementally applied up to a target value. During pressurising the chamber the jaws of the testing machine remained at a fixed position. Maintaining the target pressure as possible as we can, further axial load was applied up to a collapse load. Beyond the collapse load the load increment was determined according to the axial shortening. Throughout the tests axial loads were applied under

displacement control with frequent stops for recording.

However, for model C4 a somewhat different loading procedure was attempted. In the test for model C4 about 30 % of the estimated collapse axial load was applied before filling the chamber with water and further axial load was applied in the pressurising procedure. In post-ultimate range a continuous operation of the hand pump was maintained in the test of model C4 to keep the pressure as close to the target value as possible, whereas the pump was intermittently operated for the other tests not allowing the pressure to drop under the value when the ultimate state occurred. Unloading started when the applied load was about a quarter of the ultimate value and depressurising of the chamber was followed.

It was found difficult to apply axial load following a predetermined increment schedule since the loading capacity of the testing machine was too big for such a small increment. A leakage occurred through the gap between the filling connection flange and its cover, where a rubber pad was inserted instead of a proper o-ring, was the main cause of the undesirable pressure drop during the tests. In addition, the increase in the water jacket volume due to further development of local denting seemed to be a minor cause for the fall in the pressure.

#### 4.4 Results and Discussion

A summary of the test results is given in Table 4.3. They include non-dimensionalised geometry and material property, extent of damage parameters, collapse load and collapse strength of each model. The location of the dent centre for damaged tubes and the longitudinal location of lobe (for models A1, A2, B2 and E2) or bow centre (for model E1) and the bow direction for undamaged tubes are also included in the table.

Table 4.3 Ultimate Strength Test Results

Model	D/t	L/r	$\bar{\lambda}^{**}$	$\delta_d$ ( $d_d/D$ )	$\delta_o$ ( $d_o/L$ )	Centre of Dent (longi., Circ.)	Collapse Load Axial Comp. (KN)	Hydro. Press. (N/mm <sup>2</sup> )	Collapse Strength $\sigma_u/\sigma_{Yc}$	$Q_H/Q_{Hcr}$
A1*	41.4	79.7	1.24	0.003	0.0005	(0.51L, 50° → 230°)	66.6	--	0.70	--
A2*	41.4	56.9	0.88	0.002	0.0002	(0.48L, 325° → 145°)	83.8	--	0.89	--
B1	41.4	79.7	1.25	0.062	0.0023	(0.50L, 170°)	43.1	--	0.45	--
B2*	41.5	51.3	0.80	0.004	0.0001	(0.49L, 75° → 255°)	77.5	--	0.82	--
C2	40.7	56.9	0.85	0.209	0.0149	(0.50L, 169°)	22.8	--	0.26	--
C4	40.7	79.8	1.19	0.137	0.0087	(0.50L, 180°)	23.7	0.98	0.27	0.143
D2	41.1	56.8	0.88	0.125	0.0058	(0.49L, 177°)	44.0	--	0.46	--
D3	41.1	79.7	1.24	0.107	0.0055	(0.49L, 180°)	36.2	--	0.36	--
D4	41.1	79.7	1.24	0.183	0.0147	(0.50L, 172°)	17.4	1.91	0.18	0.287
E1*	23.8	81.0	1.23	0.001	0.0004	(0.51L, 95° → 275°)	97.7	--	0.64	--
E2*	24.0	57.9	0.88	0.002	0.0003	(0.50L, 315° → 135°)	113.8	--	0.75	--
F1p	24.1	81.0	1.18	0.016	0.0006	(0.50L, 191°)	85.0	--	0.64	--
F2	24.1	57.9	0.85	0.043	0.0014	(0.51L, 197°)	108.0	--	0.78	--
G1	24.0	57.8	0.85	0.035	0.0016	(0.49L, 180°)	115.5	--	0.82	--
G2	23.8	81.0	1.19	0.037	0.0024	(0.50L, 192°)	76.3	1.94	0.54	0.057
H1	24.0	81.0	1.19	0.006	0.0005	(0.49L, 183°)	95.6	--	0.67	--
H2	24.2	81.0	1.18	0.065	0.0054	(0.50L, 173°)	54.1	2.98	0.39	0.092

Note : \* denotes undamaged model.

\*\* E is taken the mean of the tensile test results,  $2.12 \times 10^5$  N/mm<sup>2</sup>

#### 4.4.1 Collapse Loads

For the pure axial compression tests the collapse loads are the maximum recorded load before collapse. In those tests estimated collapse loads were also recorded, which was obtained by means of the extreme value indicating needle of the testing machine load indicator. However, the maximum recorded load was adopted as the failure load of a model partly because of the uncertainty in the estimated collapse load due to the inertial movement of the extreme value indicating needle especially for the undamaged and the slightly damaged models where catastrophic shortening of the models occurred at the collapse and partly because the small differences (1.5 % at most) between the recorded and estimated values.

In the combined load tests the external axial load ( $P_{\text{ext}}$ ) was obtained using eqn (4.1), i.e. by deducting the resultant axial force due to the hydrostatic pressure over the cross-section of the connection rod from the load applied through the lower jaw of the testing machine.

$$P_{\text{ext}} = P' - Q_H A_r \quad (4.1)$$

where  $P_{\text{ext}}$  : externally applied axial load  
 $P'$  : axial load applied through the lower jaw of the testing machine  
 $Q_H$  : hydrostatic pressure  
 $A_r$  : cross-sectional area of the connection rod

For the combined loading tests the maximum external axial load and together with the corresponding hydrostatic pressure was adopted as the collapse load. The collapse strength of each model is defined as the ratios of the average compressive stress calculated from the collapse axial load to the corresponding static compressive yield stress derived from the tensile tests and the normalised hydrostatic pressure with respect to the elastic buckling pressure ( $Q_{HCr}$ ) given as eqn (4.2).



$$Q_{Hcr} = \frac{2 E}{1 - \nu^2} (t / D)^3 \quad (4.2)$$

where  $Q_{Hcr}$  : elastic buckling pressure of a 'long' tube under hydrostatic pressure  
 $\nu$  : Poisson ratio of the material

#### 4.4.2 LVDT and Strain-Gauge Results

From the displacement and strain recordings made during the tests, the following figures have been prepared:

- axial load-axial shortening curves;
- axial load-lateral deflection curves; and
- axial load-strain curves.

In these curves applied axial load (external axial load for the combined loading tests) is normalised with respect to the corresponding static compressive yield capacity, while average axial strain and local strain is non-dimensionalised with respect to the corresponding yield strain. In the lateral deflection curves lateral displacement is non-dimensionalised with respect to the model length.

· Axial Load-Axial Shortening Curves : The load-axial shortening curves presented in Figs. 4.4 and 4.5 for the pure axial compression tests on the undamaged and damaged models respectively. In the pure axial compression tests tilting of the testing machine cross-head was observed at about 5 KN of applied load. Consequently the load-shortening curves initially behave non-linearly. Hence the load-shortening curves presented in Figs. 4.4 and 4.5 were derived by averaging the results of displacement records from the two LVDTs which were located on the testing machine cross-head at either sides to the model. For some undamaged models (models A1,A2 and E1) whose failure loads were far in excess of the DnV strength curve 'a'[86] (see Fig.4.15) and a slightly damaged model (model H1) apparent dynamic unloading can be seen in their axial shortening curves. For the other models, however, collapse occurred slowly.

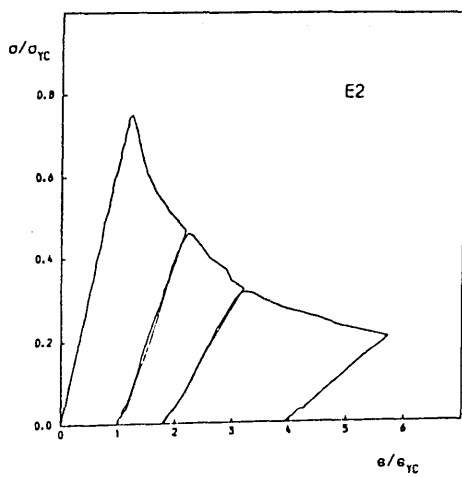
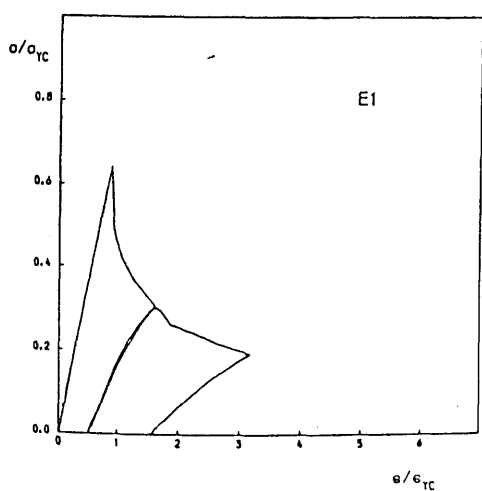
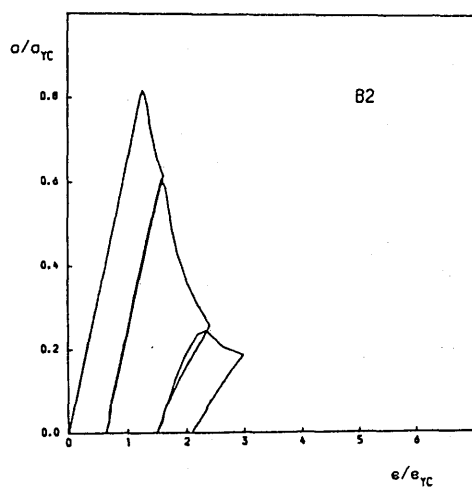
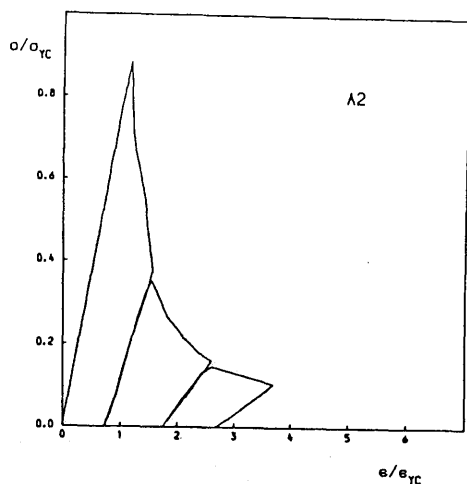
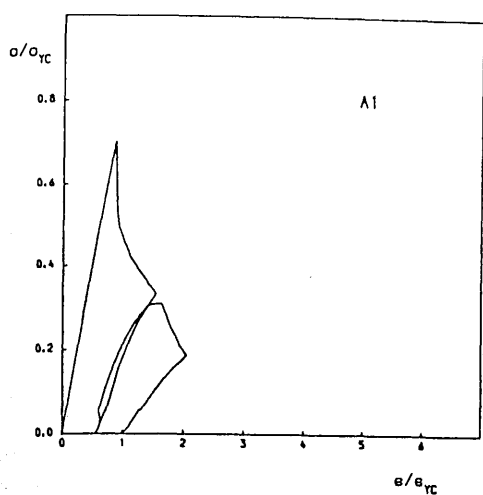


Fig. 4.4 Axial Compression - Axial Shortening Curves of Undamaged Models

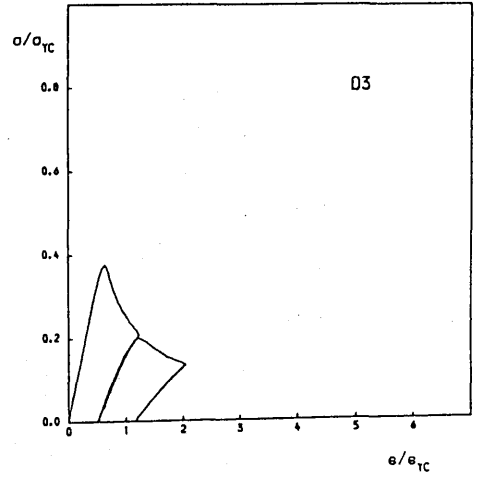
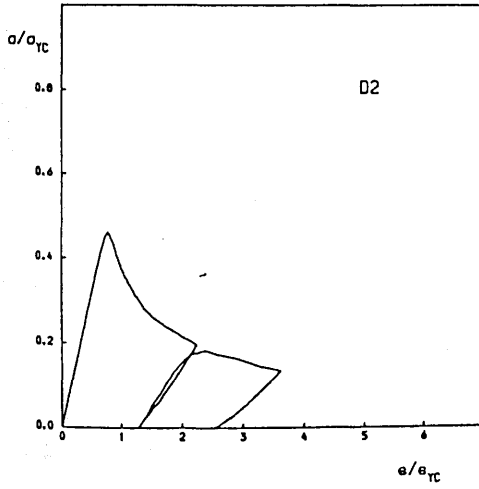
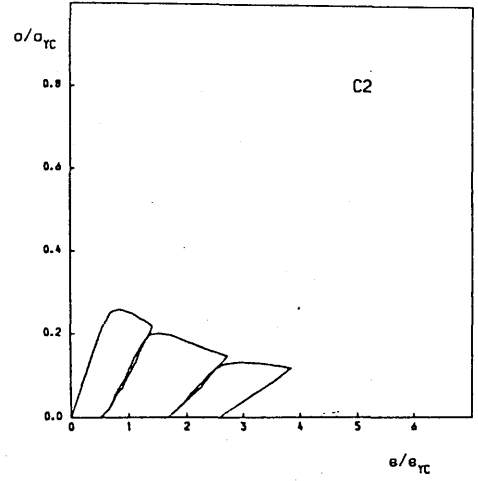
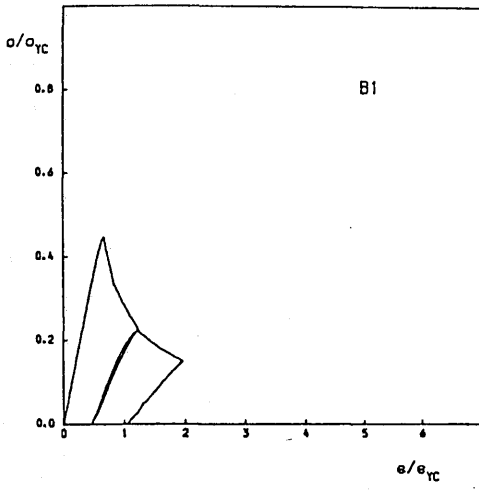


Fig. 4.5 Axial Compression - Axial Shortening Curves of Damaged Models(cont'd)

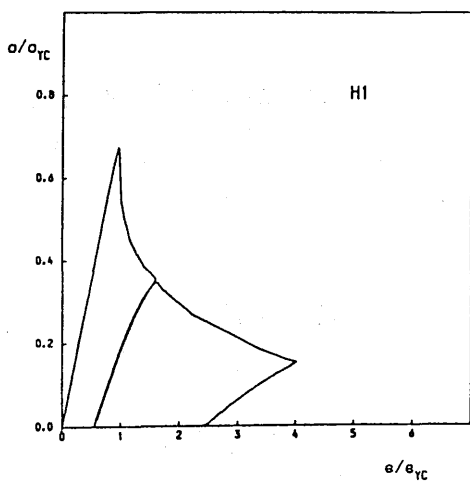
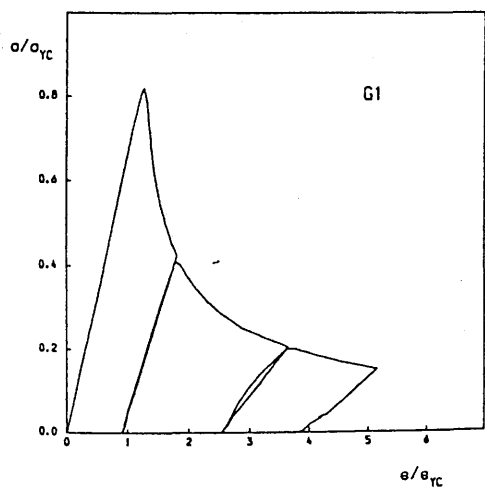
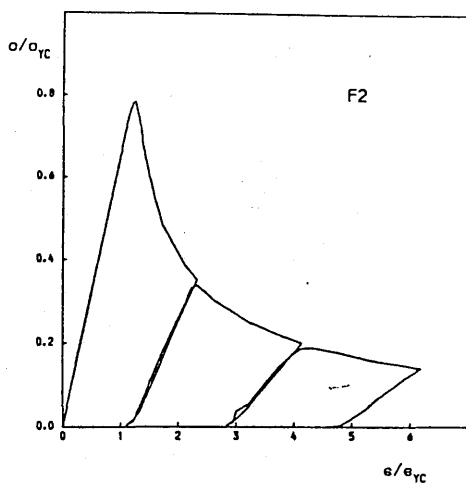
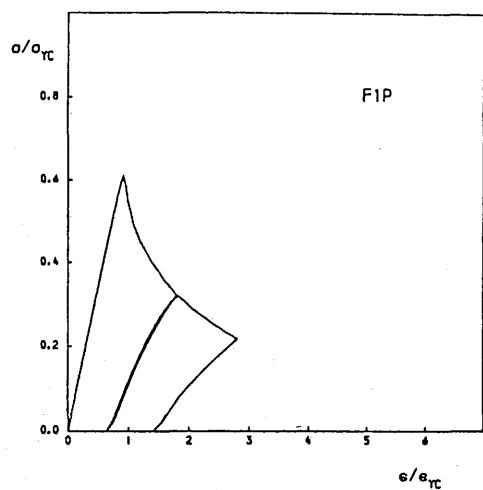
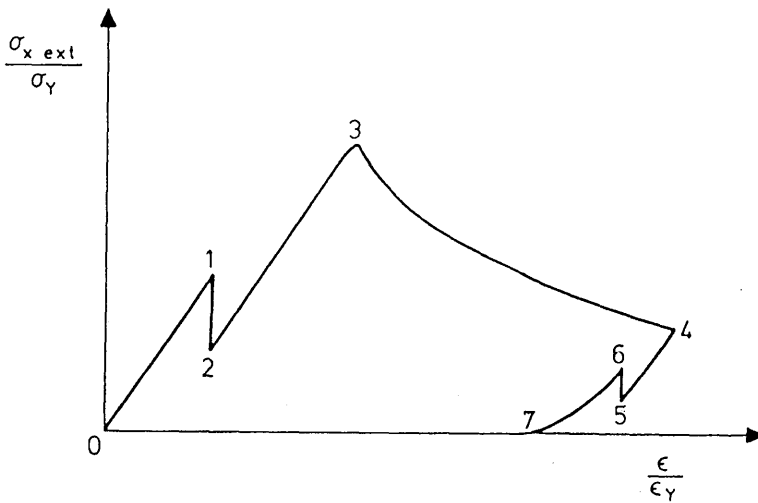


Fig. 4.5 cont'd



- 0 - 1 : Application of Pure Axial Compression
- 1 : Filling the Pressure Chamber with Water
- 1 - 2 : Pressurising the Chamber
- 2 - 3 : Further Application of Axial Compression under Hydrostatic Pressure
- 3 : Ultimate State
- 3 - 4 : Post-Ultimate State
- 4 - 5 : Unloading under Hydrostatic Pressure
- 5 - 6 : Depressurising the Pressure Chamber
- 6 - 7 : Further Unloading without Hydrostatic Pressure

Fig. 4.6 Loading Procedure for Combined Axial and Hydrostatic Pressure Tests on Damaged Models

In Fig.4.7 the load-axial shortening curves are provided of the damaged model under combined axial compression and hydrostatic pressure. However, unlike the curves for the axial compression tests, somewhat complicated features of the curves can be seen in the figures. Therefore, in order to assist a better understanding of the curves a typical example together with a supplementary explanation for each loading and unloading step is presented in Fig.4.6. The apparent saw-toothed response in the post-ultimate state of models D4, G2 and H2 were due to the intermittent operation of the hand-pump. For those models post-ultimate responses under the corresponding constant pressure are estimated in the figure with dotted lines.

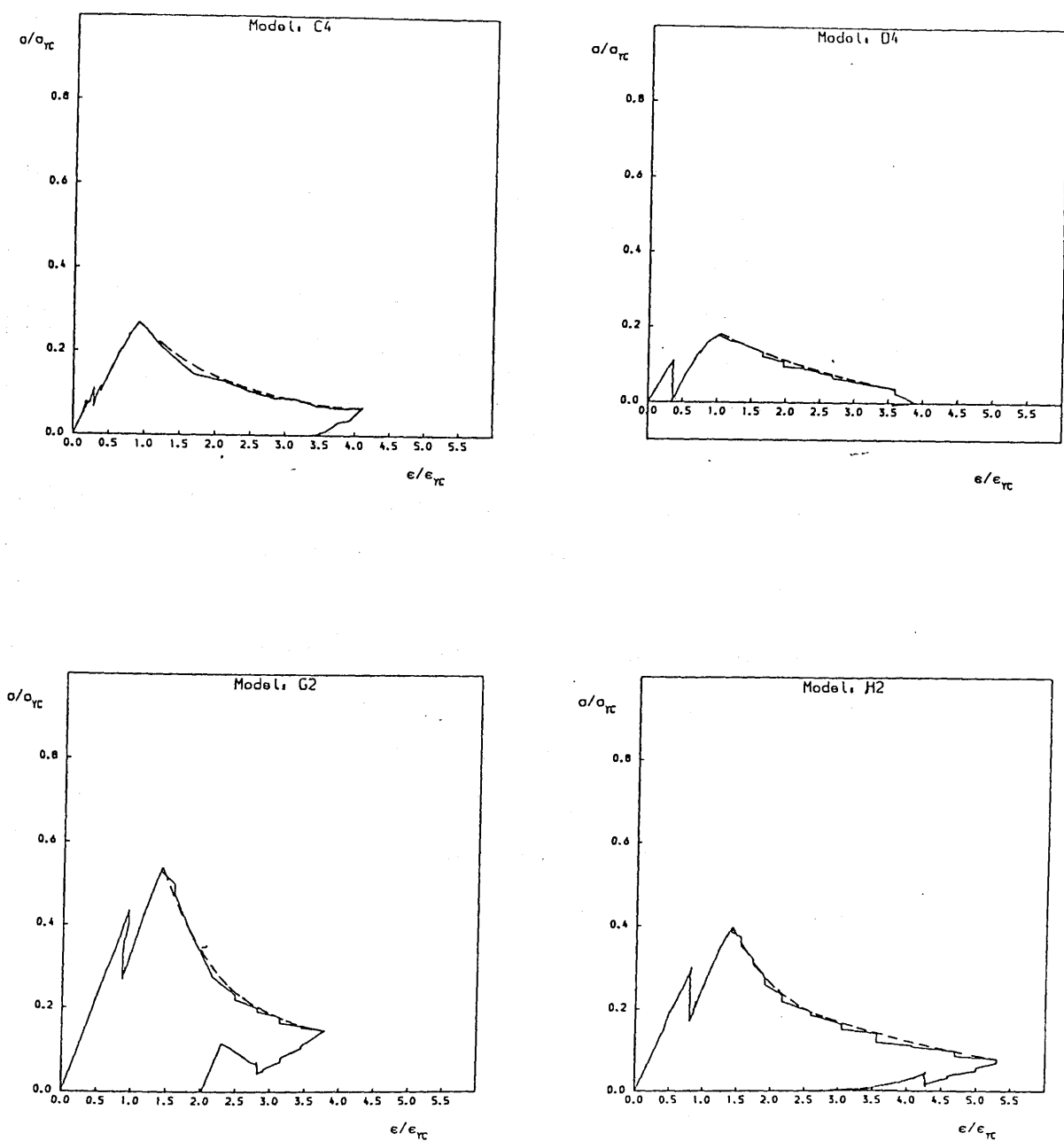


Fig. 4.7 External Axial Compression - Axial Shortening Curves of Damaged Models under Combined Axial Compression and Hydrostatic Pressure (post-ultimate behaviours under the corresponding constant hydrostatic pressure are estimated by dotted lines)

· Axial Load-Lateral Deflection Curves : All the load-lateral deflection curves obtained from the LVDT records made in the axial compression tests are presented in ref.91. Some typical curves are given in Figs.4.8 and 4.9(a,b) for undamaged and damaged models respectively. For the undamaged tubes, where prediction of the direction of bowing is difficult, it was not always possible to obtain reliable results after collapse (especially for models B2 and E2). In most of the lateral deflection curves except for model A2, non-linear behaviour was in evidence well before collapse whereas the axial shortening curves for all of the undamaged and slightly damaged models showed a linear increase nearly up to collapse load. This is probably due to the geometric non-linearity of the lateral movement. Unlike the results of fabricated tubular column tests[102] where the lateral movement was noted at approximately 70-80 % of the recorded maximum load, most of the undamaged models showed recognisable lateral deflection from about 30-40 % of the ultimate load.

· Axial Load-Strain Curves : In Figs.4.10(a)-(b) and 4.11(a)-(d) for undamaged and damaged models respectively, typical axial load-strain curves are presented obtained from the strain-gauge recordings made in the axial compression tests. Those curves for the other models under axial compression can be found in ref.91. The strain curves are given in Figs.4.12(a)-(d) for the damaged models under axial compression and hydrostatic pressure. Compressive strain is taken as positive in the curves.

For the undamaged models under axial compression the bow directions can clearly be seen in the curves well before collapse especially from those of strain-gauges no.17-no.20 bonded longitudinally at mid-height. However, the bow directions for the thicker models (models E1 and E2) coincided with the directions of their maximum initial out-of-straightness but the thinner models did not show such relevance. The occurrence of local buckling in the thinner models (models A1, A2 and B2) can be estimated from the curves of strain-gauges bonded at mid-height in post-ultimate range. For the case of model A1 the curves for strain-gauges no.13, no.14, no.19 and no.20 show a sharp knee or sudden change in slope at some 40 % of its ultimate load (see Fig.4.10a).

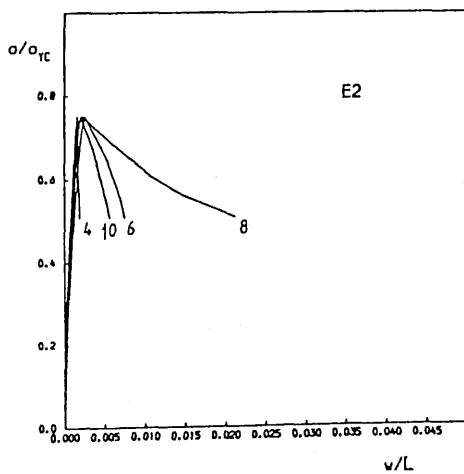
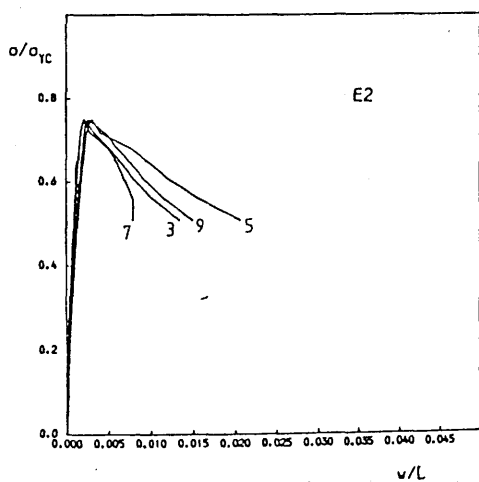
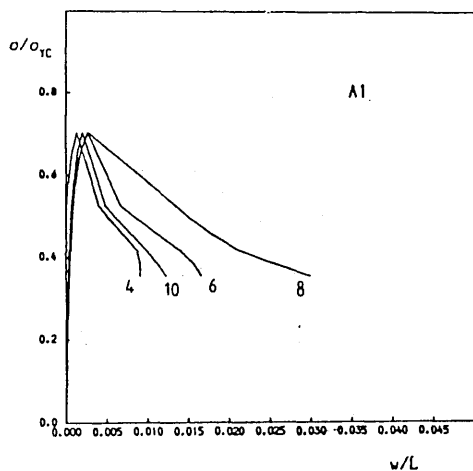
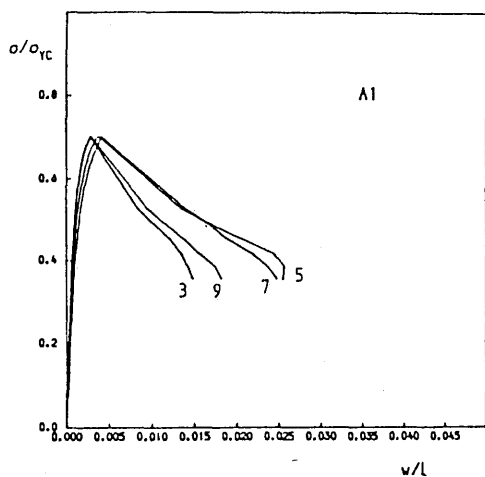


Fig. 4.8 Axial Compression - Lateral Deflection Curves of Undamaged Models  
(Results of LVDTs no.3 to no.10 for models A1 and E2)



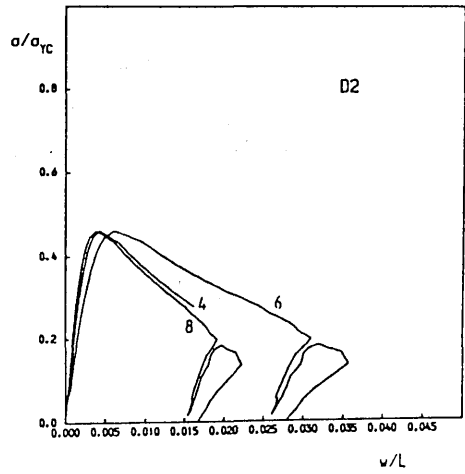
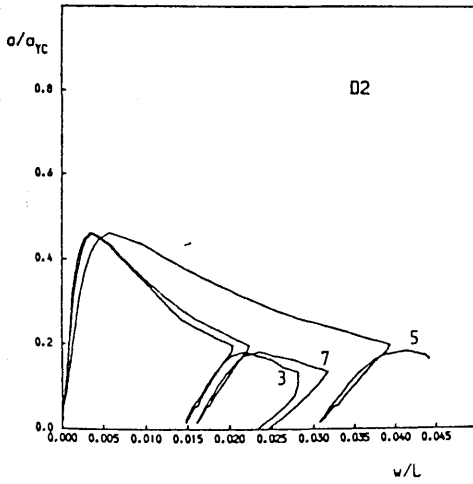
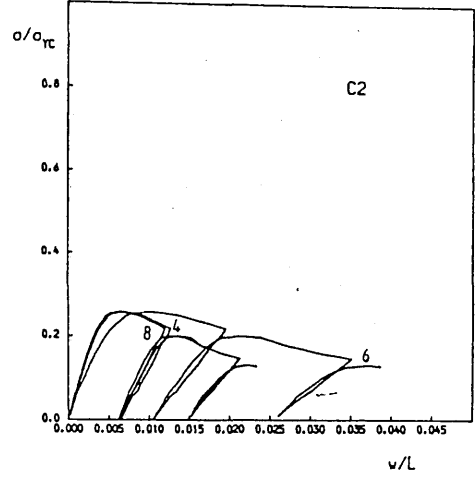
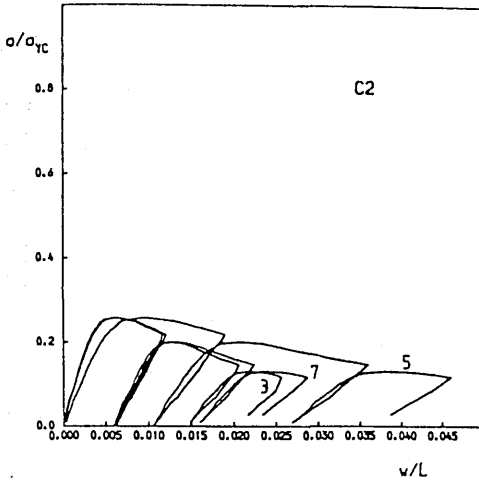


Fig. 4.9(a) Axial Compression - Lateral Deflection Curves of Damaged Models  
(Results of LVDTs no.3 to no.8 for models C2 and D2)

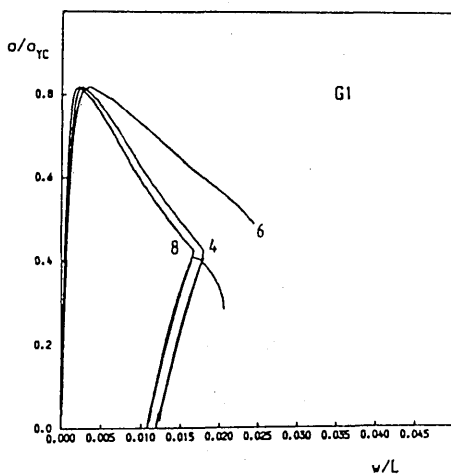
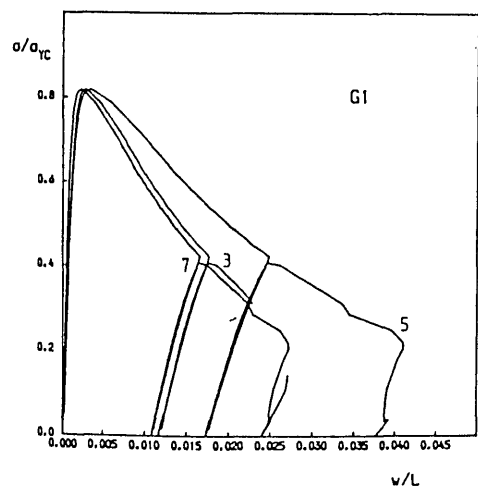
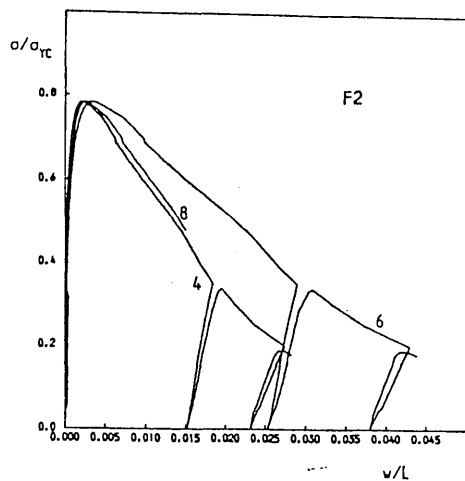
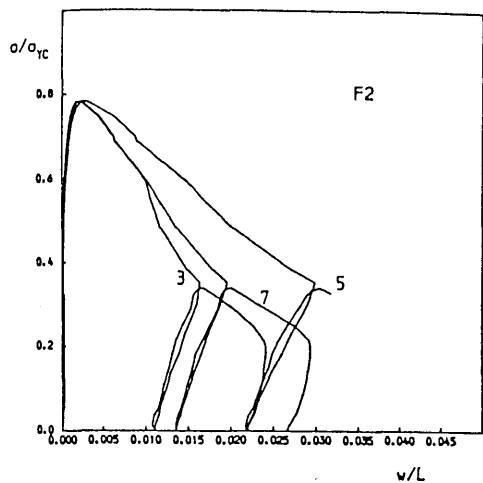


Fig. 4.9(b) Axial Compression - Lateral Deflection Curves of Damaged Models  
(Results of LVDTs no.3 to no.8 for models F2 and G1)

For the other thinner models, models A2 and B2, the occurrence of local buckling can be estimated at about 65 % and 75 % of their ultimate loads respective. Any attempt to approximate the actual effective column lengths for the undamaged models are not made in this study. However, hopefully, the strain and lateral deflection curves provided may be of some use in future research.

The results from the strain-gauges installed at mid-height of damaged models having relatively shallow dents showed linear behaviour under axial compression nearly up to their ultimate capacity, while the damaged parts of relatively severely dented models deformed non-linearly well before collapse. In ref.71 the measurement records of depth of dent growth under axial compression is provided for a model whose initial non-dimensionalised depth of dent ( $\delta_d$ ) was about 0.058 but whose diameter to thickness ratio ( $D/t$ ) is not given. The dent depth was almost constant up to ultimate load and increased thereafter. If it is possible to relate the depth of dent growth to the non-linear behaviour of damaged part, for deeply dented tubes notable increase of dent depth may occur before ultimate state. Some difference can be found in the records of strain-gauge no.11 of models F2 and G1 which were almost identical both in geometry and material property. The circumferential location of dent centre of model F2 ( $197^\circ$  rather than  $180^\circ$ ) may be attributable for the difference.

The plots of strain records against external axial compression are made for the damaged models under combined axial compression and hydrostatic pressure. Like the axial shortening curves for these models the strain curves appeared to be more complicated than those under pure axial compression. For model D4 the records of strain gauges no.11 and no.13 bonded opposite to dent showed apparently the local shell buckle at about 13.5 % of its ultimate external axial load (see Fig.4.12b). In the test a roaring sound was accompanied at that moment. The effect of hydrostatic pressure on the behaviour of the models before ultimate state was not apparent but the parallel shifting of the curves.

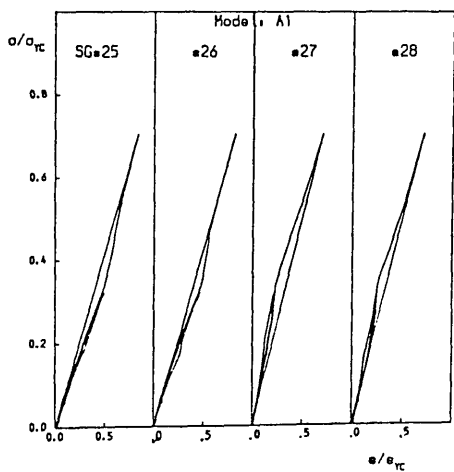
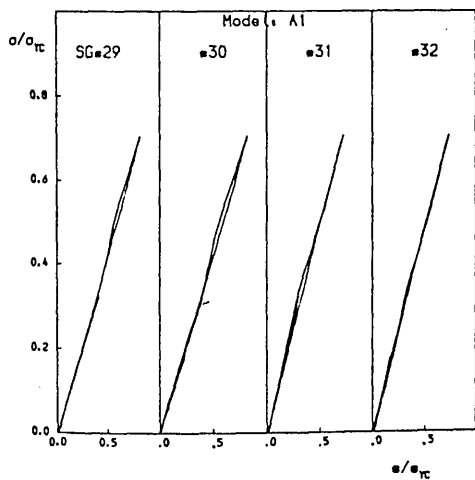
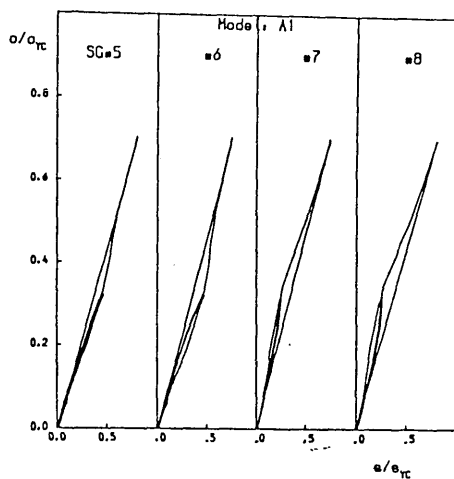
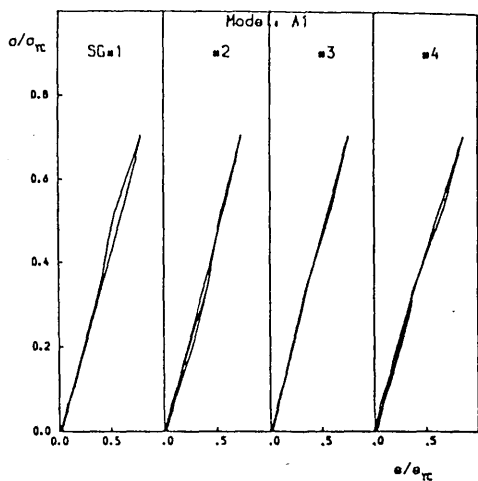


Fig. 4.10(a) Axial Compression - Axial Strain Curves of Undamaged Models  
(Results of Strain-Gauge Readings) : model A1 (cont'd)

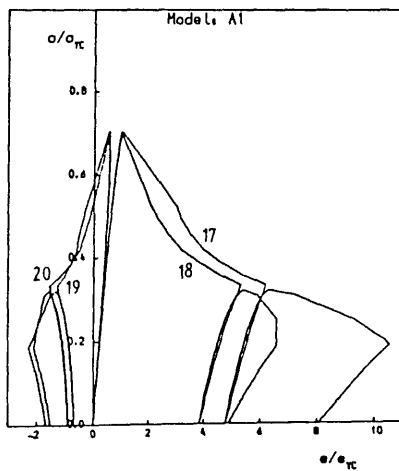
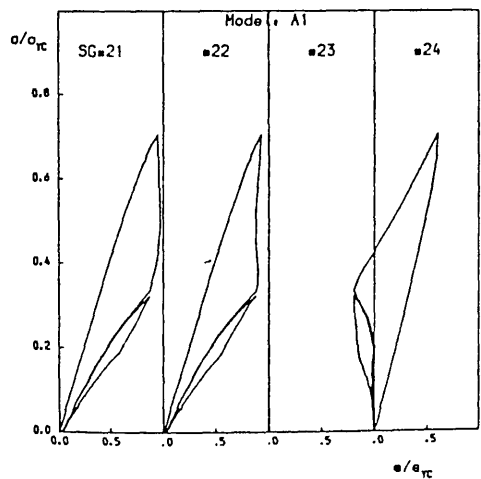
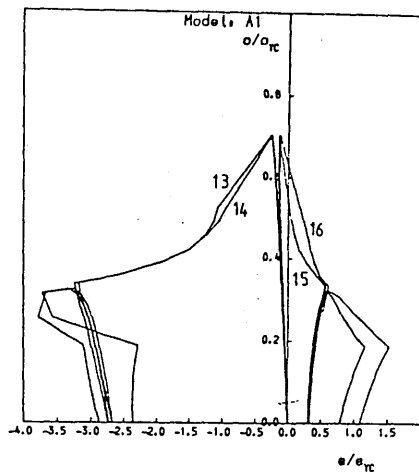
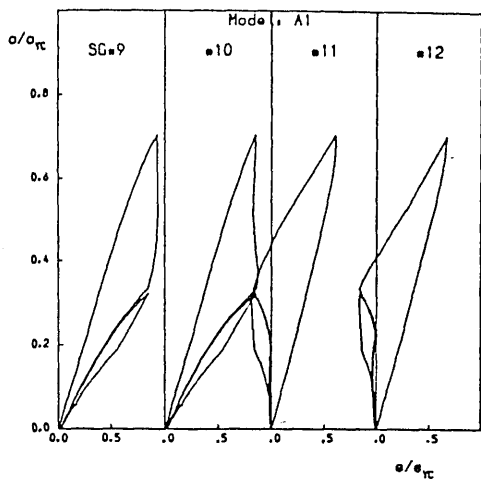


Fig. 4.10(a) cont'd

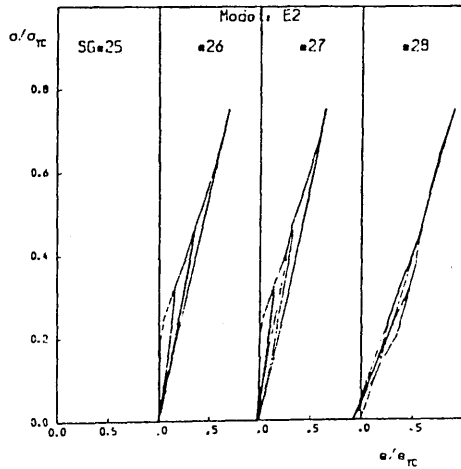
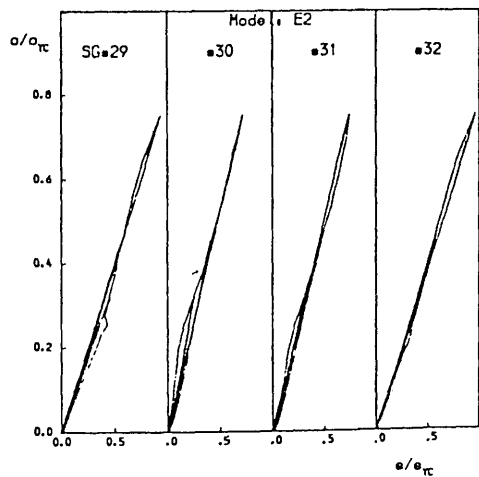
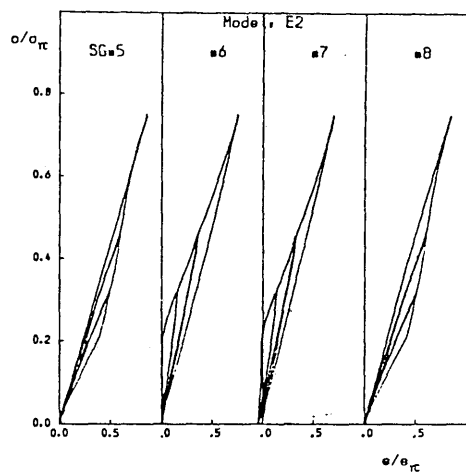
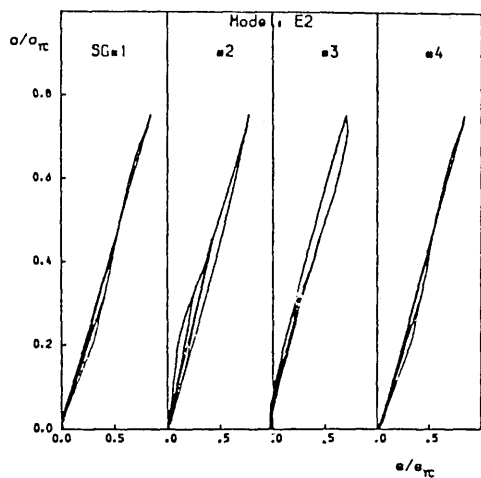


Fig. 4.10(b) Axial Compression - Axial Strain Curves of Undamaged Models  
(Results of Strain-Gauge Readings) : model E2 (cont'd)

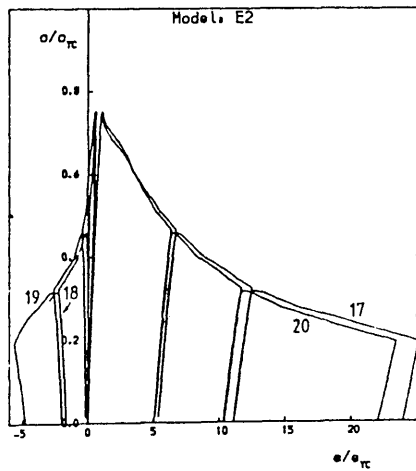
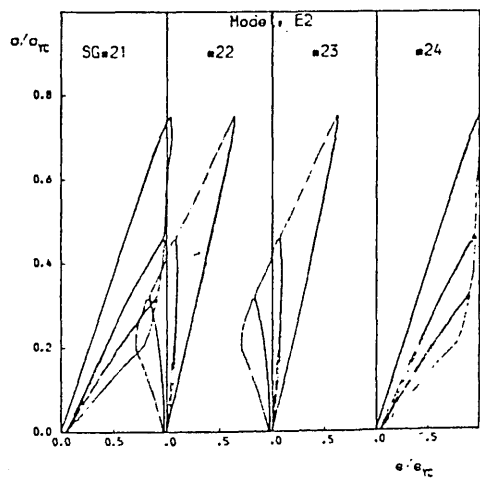
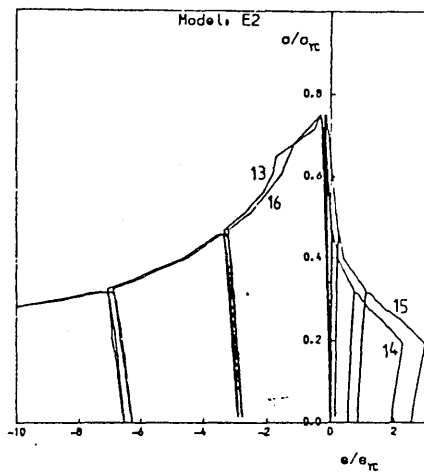
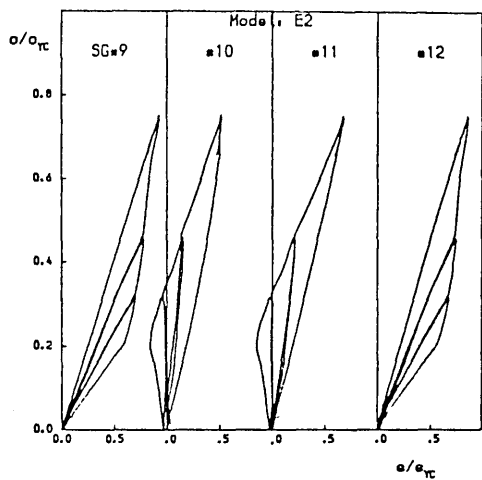


Fig. 4.10(b) cont'd

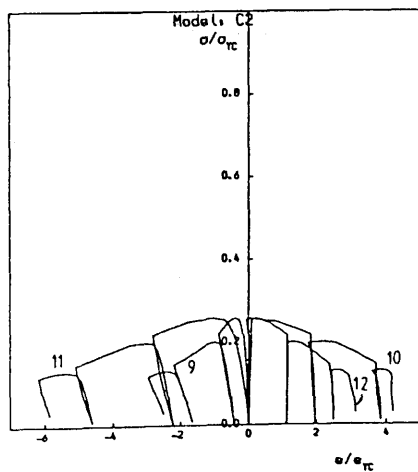
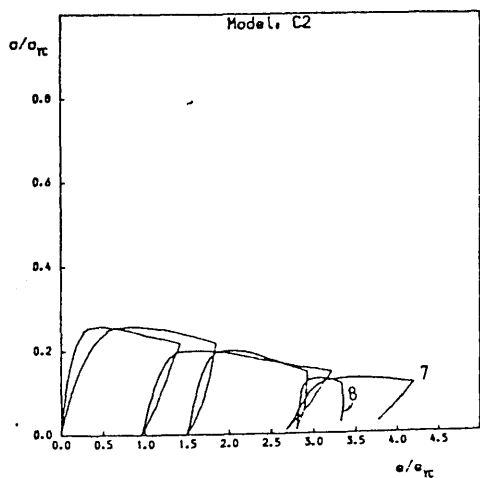
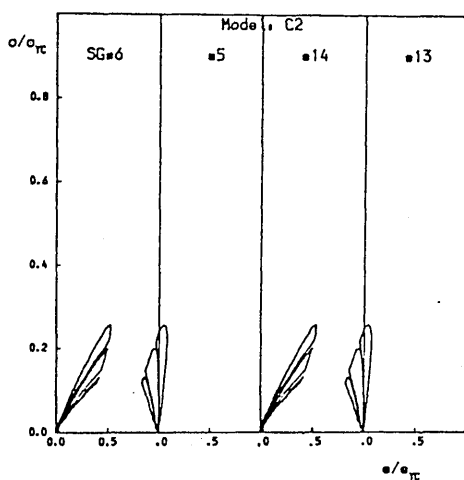
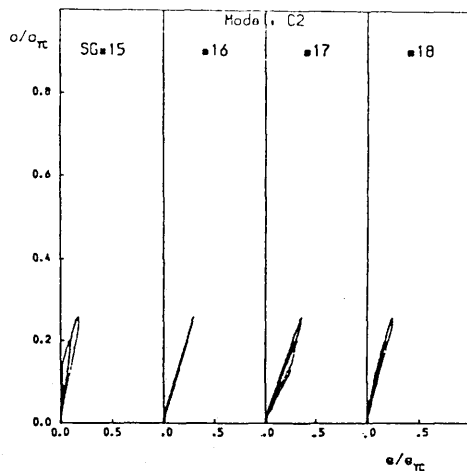
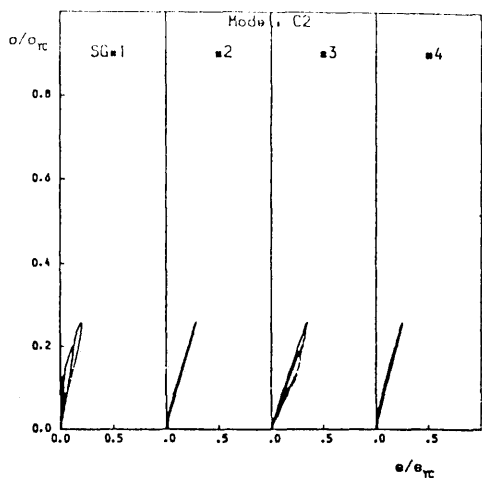


Fig. 4.11(a) Axial Compression - Axial Strain Curves of Damaged Models  
(Results of Strain-Gauge Readings) : model C2



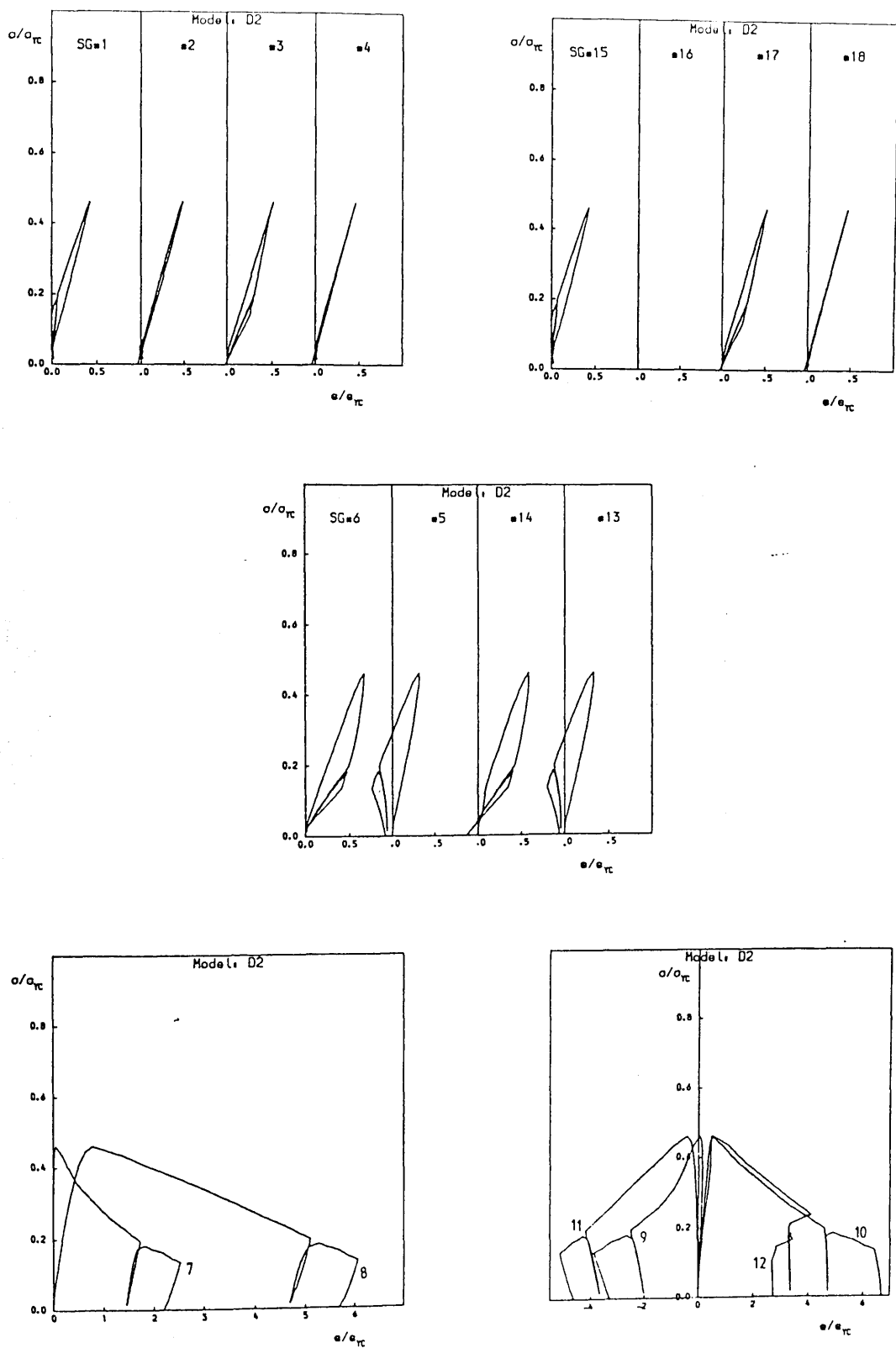


Fig. 4.11(b) Axial Compression - Axial Strain Curves of Damaged Models  
(Results of Strain-Gauge Readings) : model D2

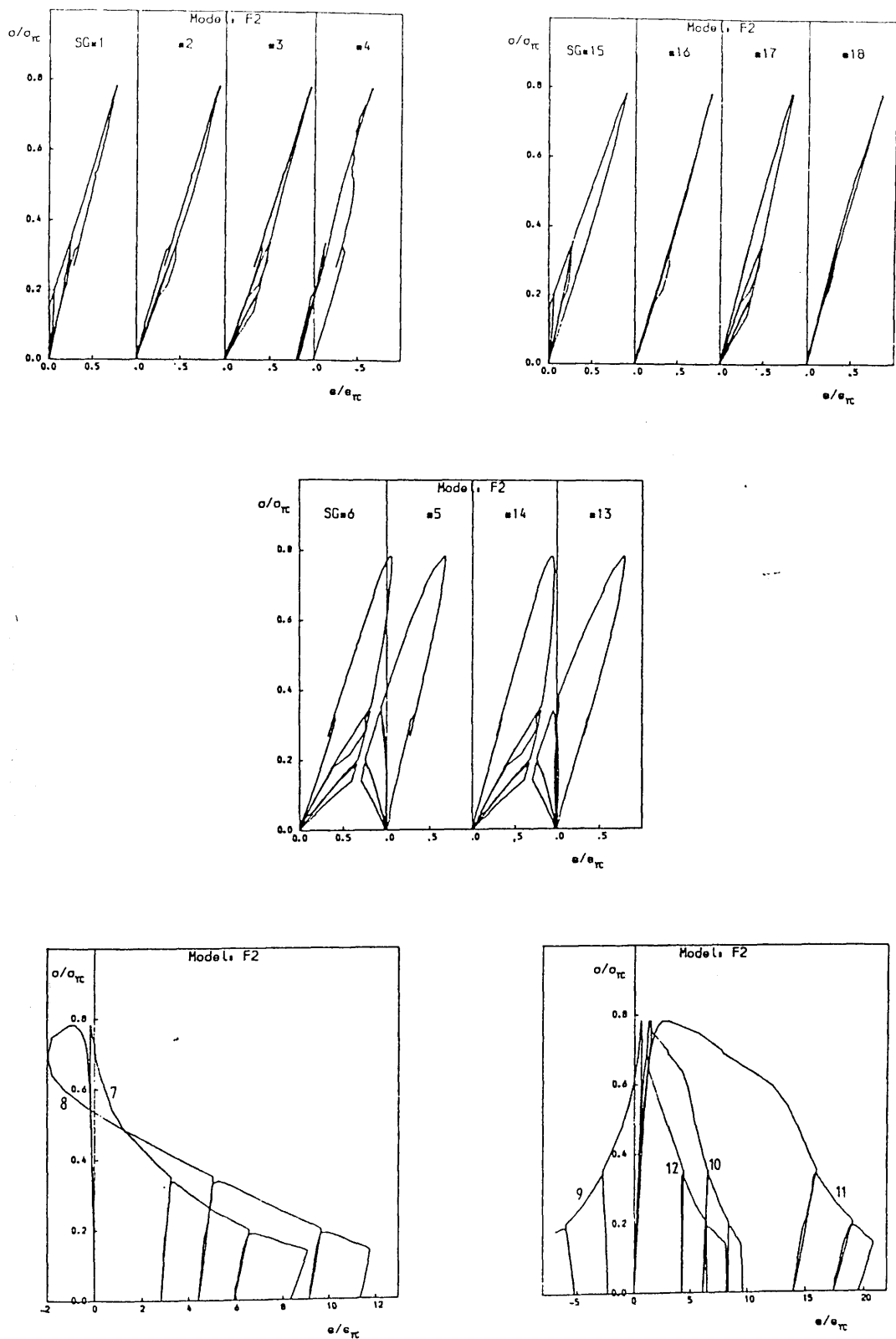


Fig. 4.11(c) Axial Compression - Axial Strain Curves of Damaged Models  
(Results of Strain-Gauge Readings) : model F2

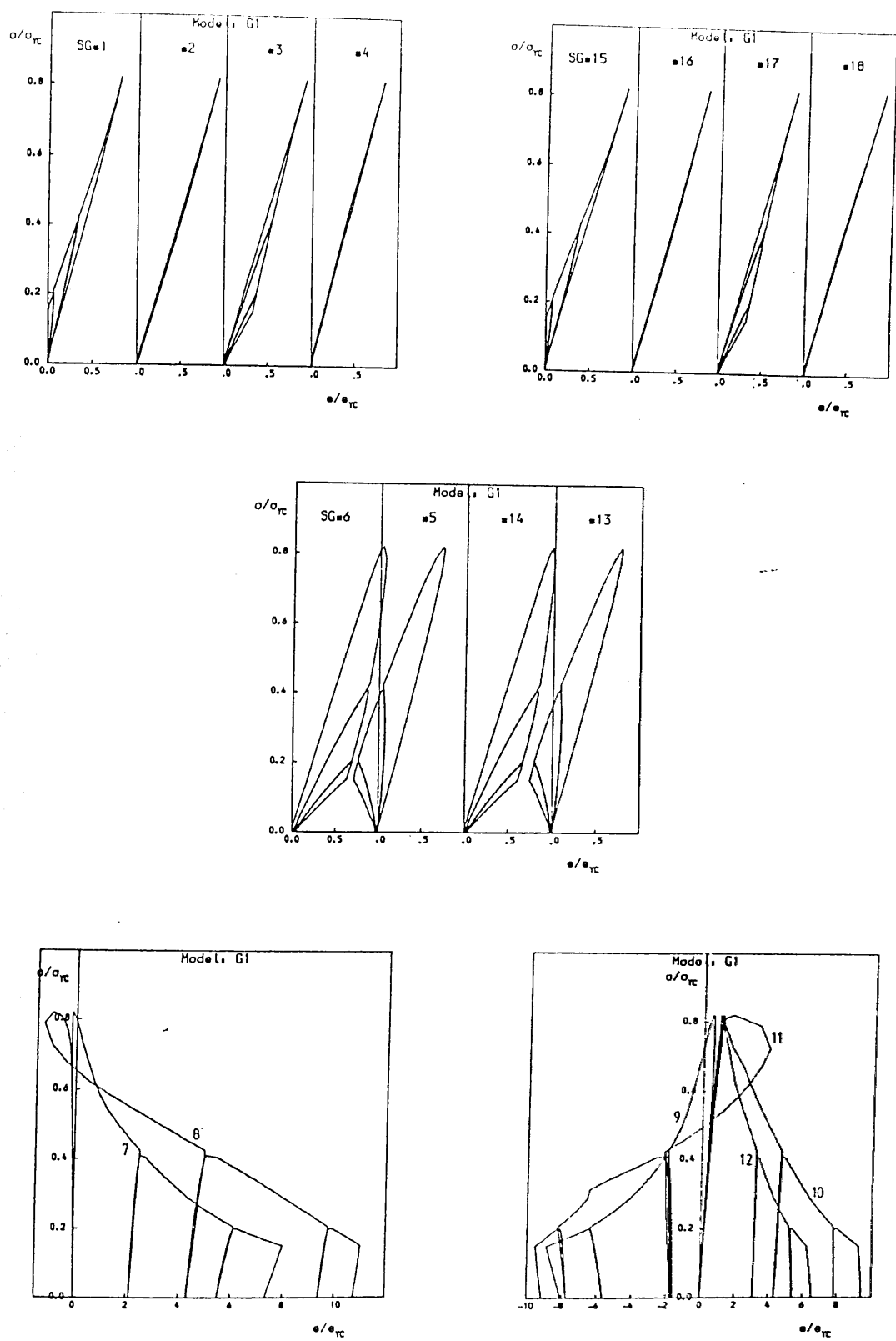


Fig. 4.11(d) Axial Compression - Axial Strain Curves of Damaged Models  
(Results of Strain-Gauge Readings) : model G1

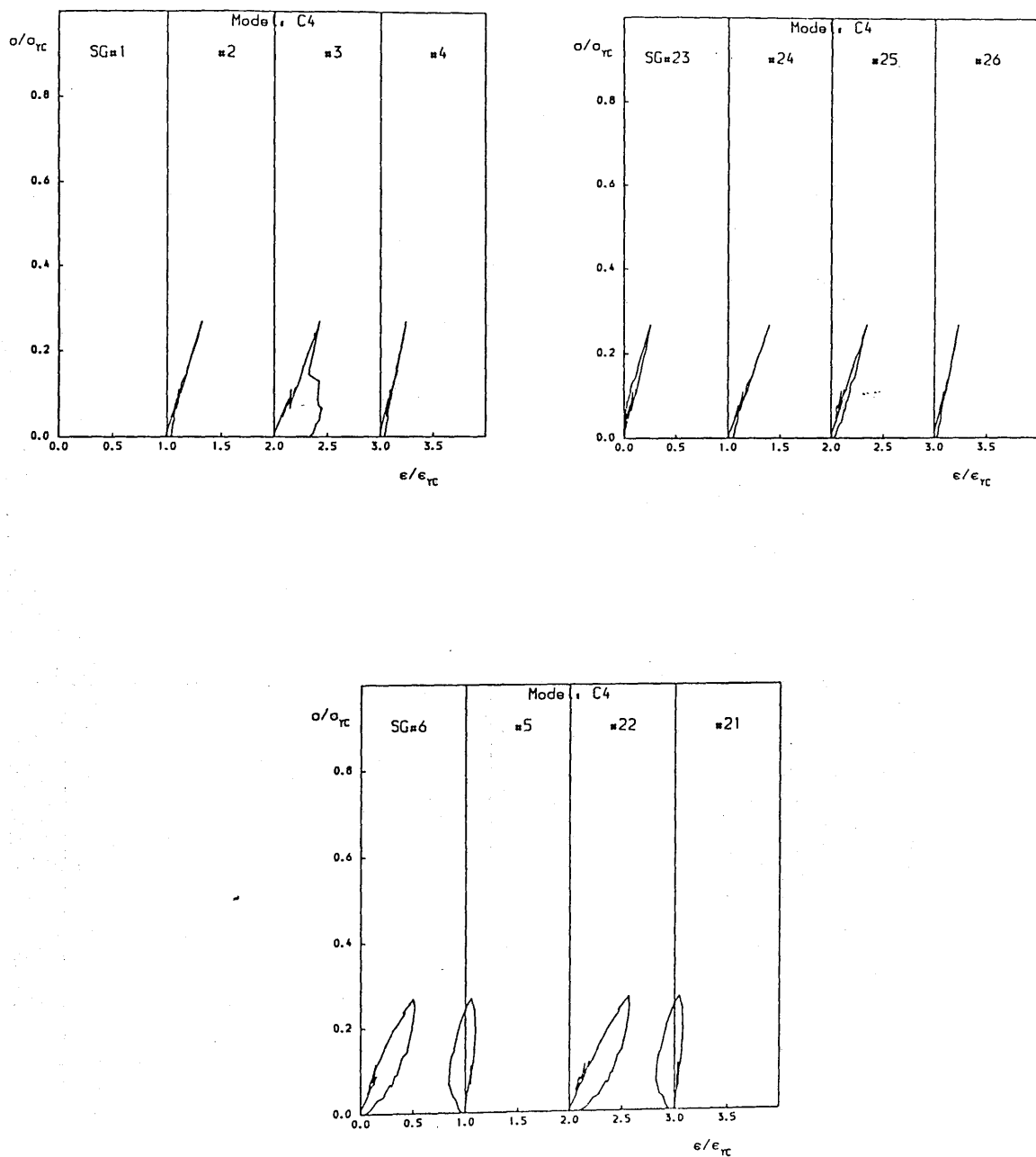


Fig. 4.12(a) External Axial Compression - Axial Strain Curves of Damaged Models  
under Combined Axial Compression and Hydrostatic Pressure  
(Results of Strain-Gauge Readings) : model C4 (cont'd)

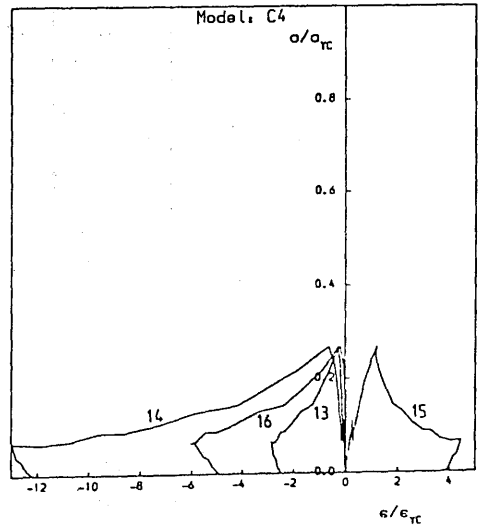
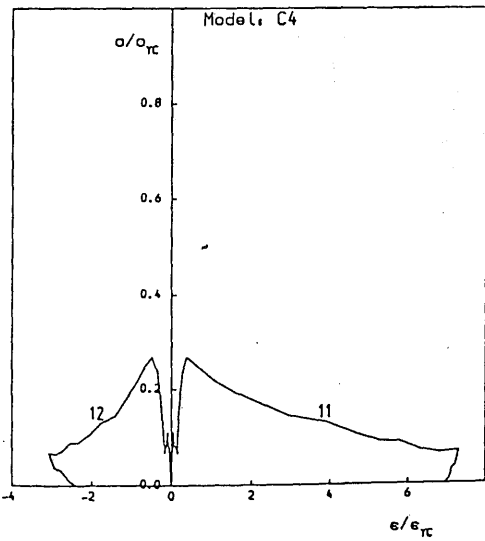
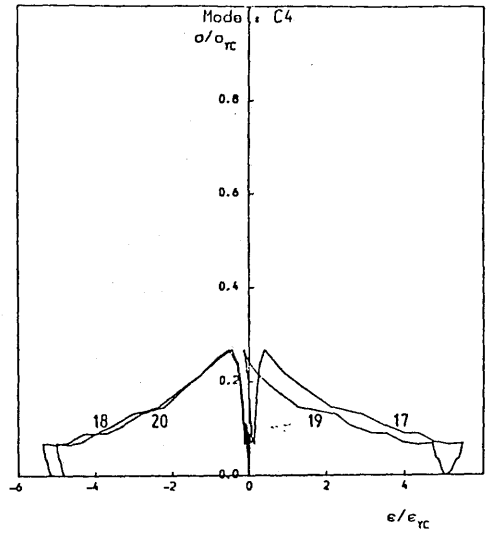
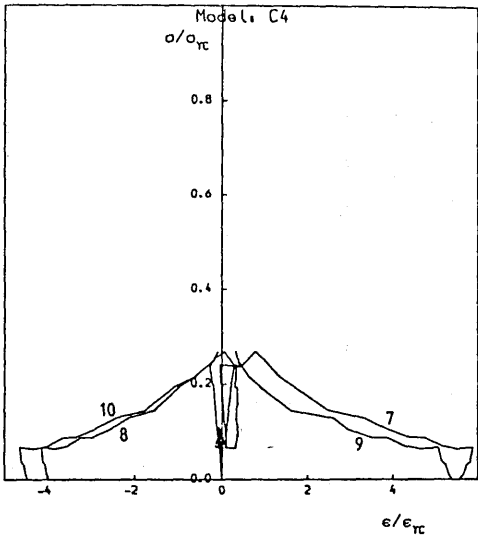


Fig. 4.12(a) cont'd

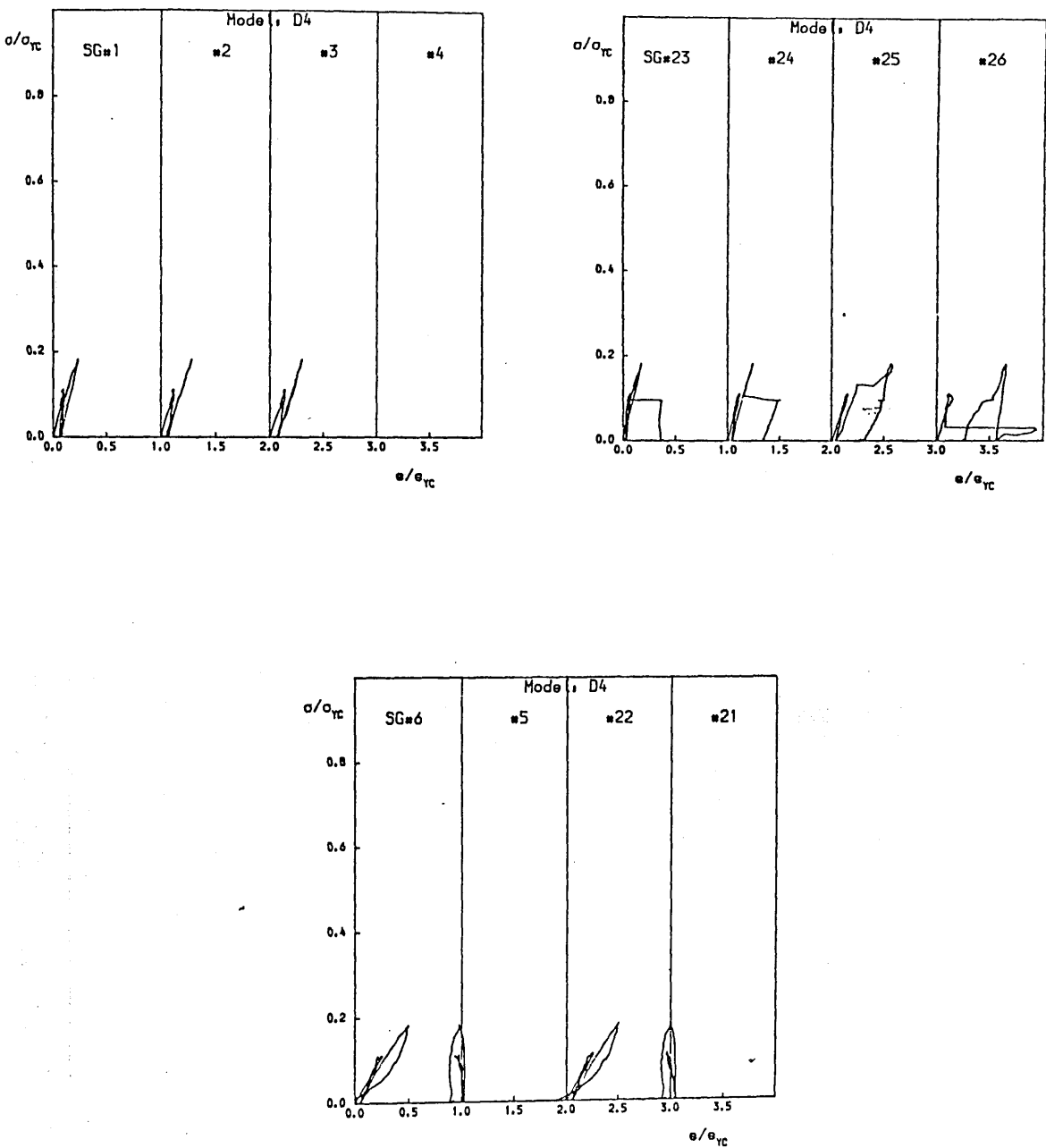


Fig. 4.12(b) External Axial Compression - Axial Strain Curves of Damaged Models  
under Combined Axial Compression and Hydrostatic Pressure  
(Results of Strain-Gauge Readings) : model D4 (cont'd)

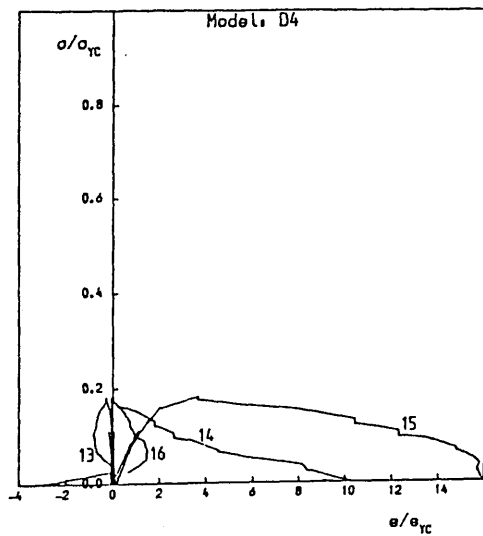
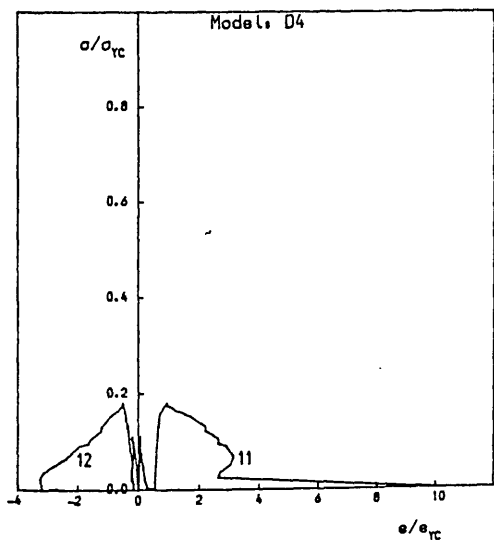
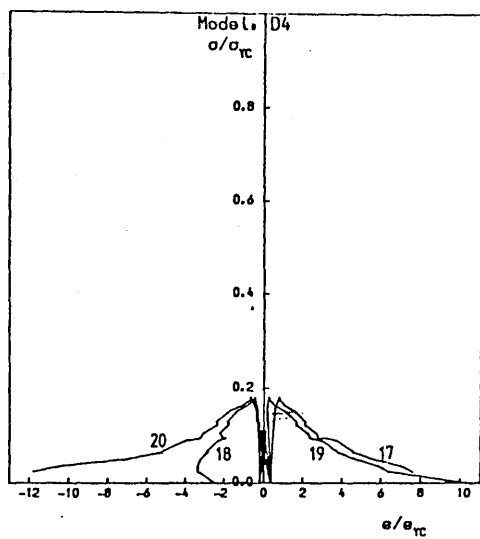
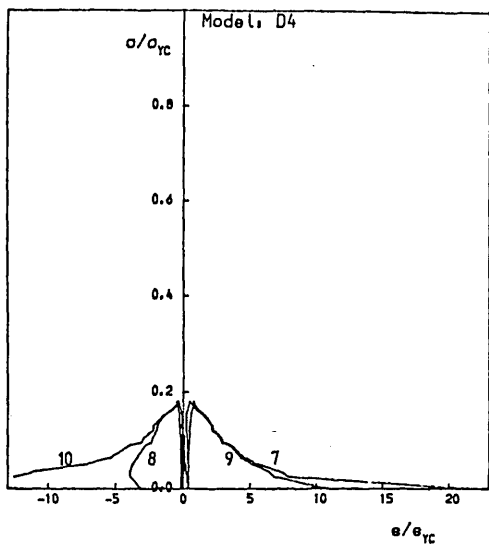


Fig. 4.12(b) cont'd

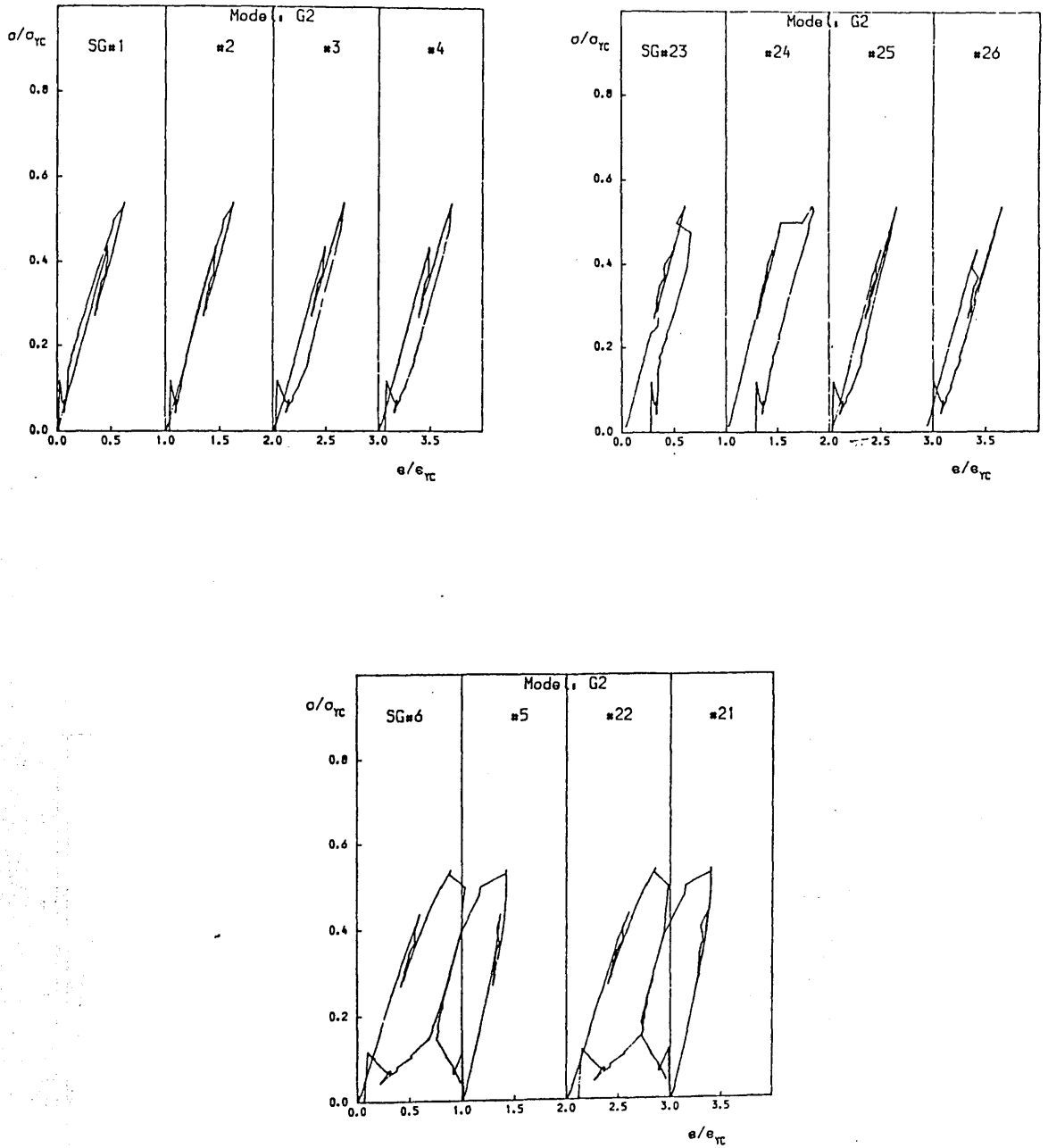


Fig. 4.12(c) External Axial Compression - Axial Strain Curves of Damaged Models  
under Combined Axial Compression and Hydrostatic Pressure  
(Results of Strain-Gauge Readings) : model G2 (cont'd)



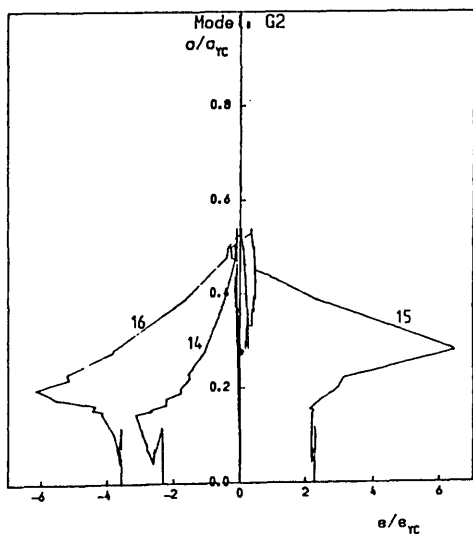
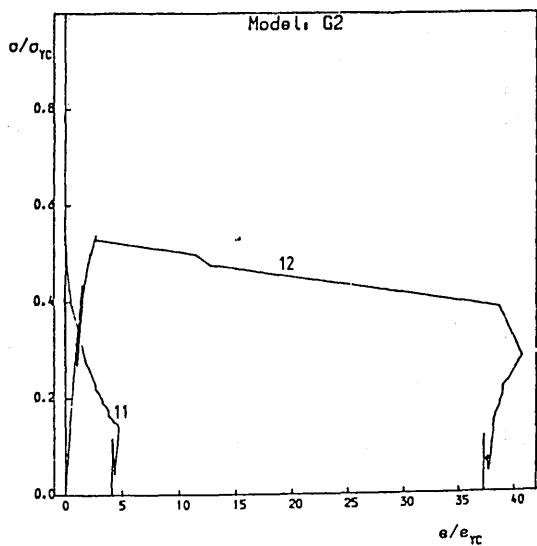
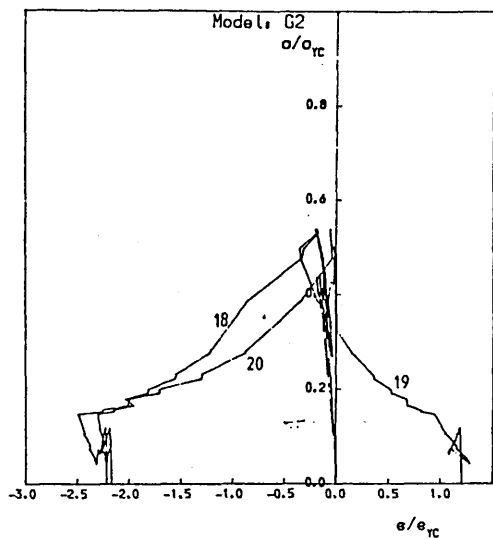
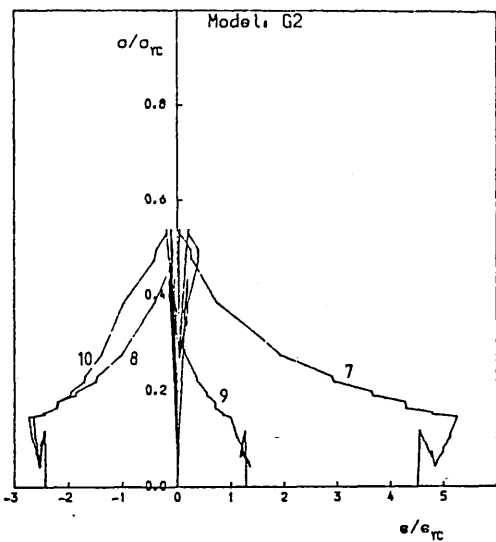


Fig. 4.12(c) cont'd

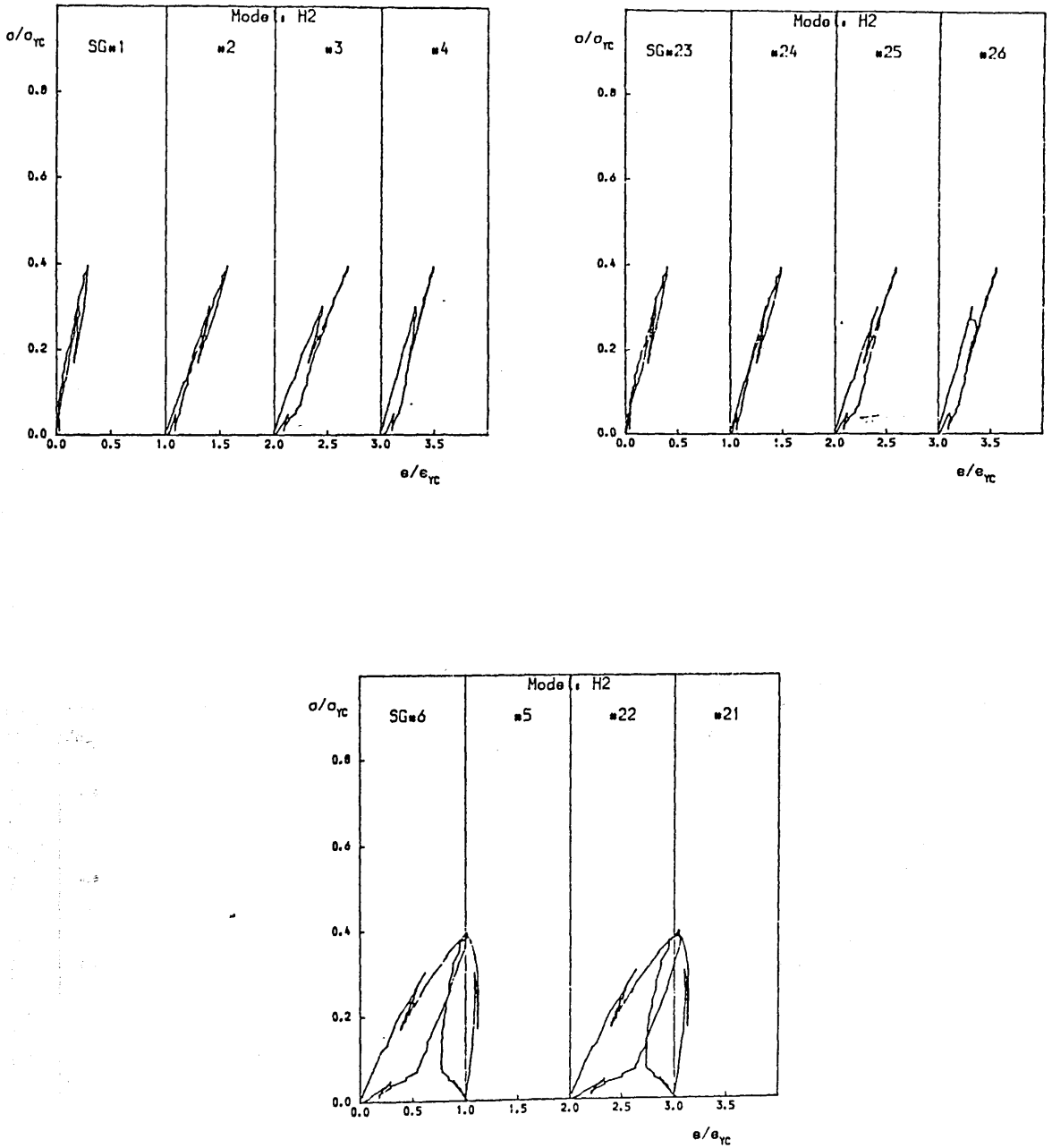


Fig. 4.12(d) External Axial Compression - Axial Strain Curves of Damaged Models under Combined Axial Compression and Hydrostatic Pressure (Results of Strain-Gauge Readings) : model H2 (cont'd)

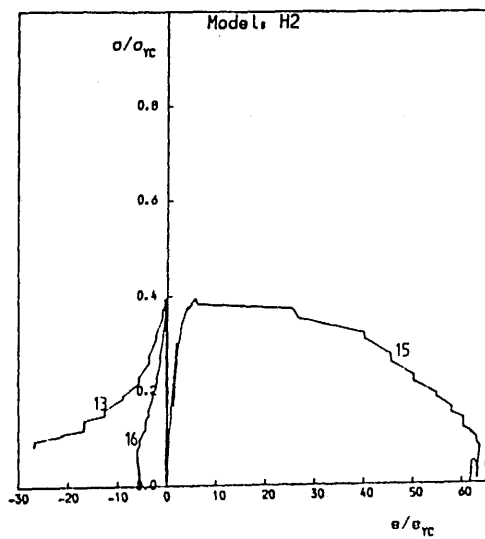
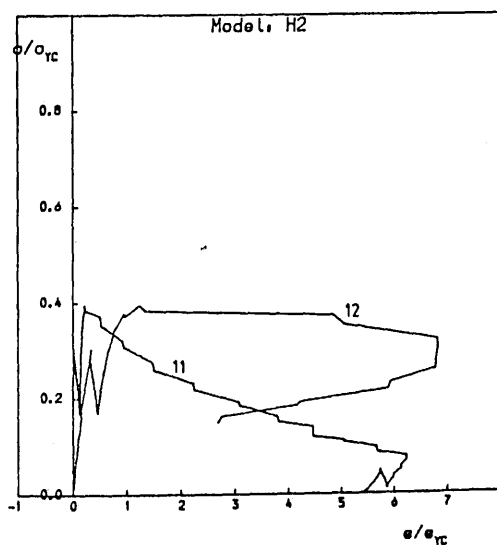
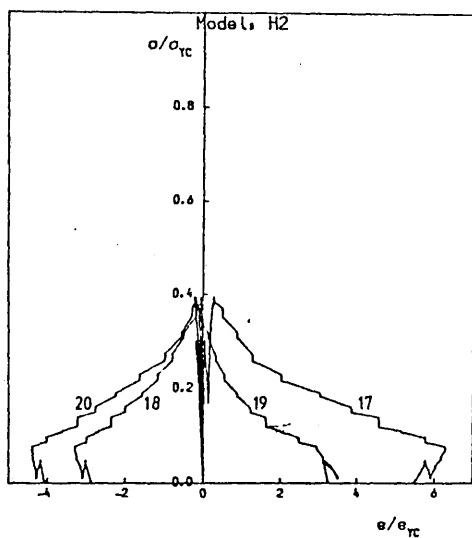
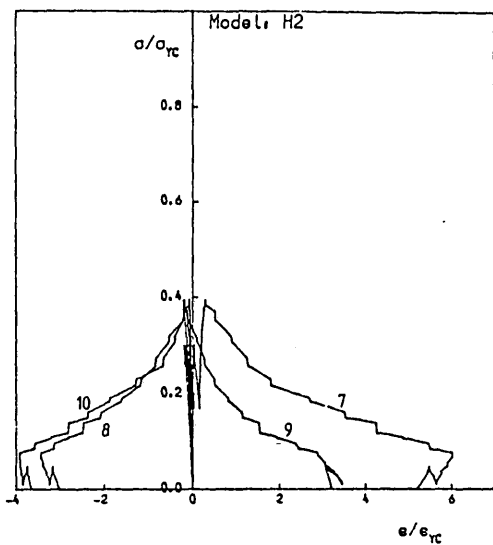


Fig. 4.12(d) cont'd

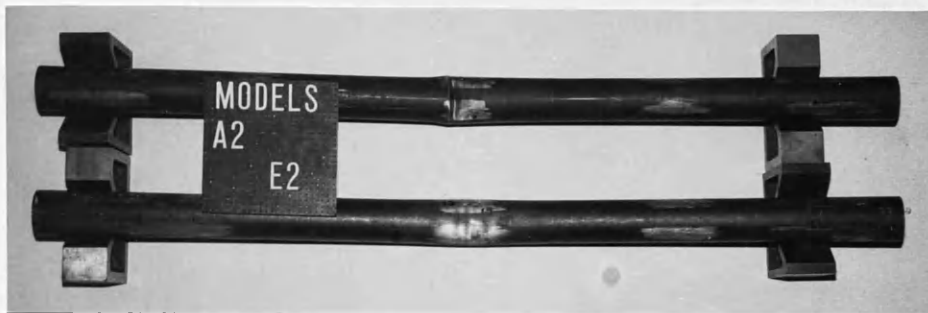
#### 4.4.3 Shape of Collapsed Models

Photographs of typical collapsed models under pure axial compression are presented in Fig.4.13. After collapse, a sharp single-lobe local buckle occurred in the thin-walled undamaged models (models A1,A2 and B2). However, for the thicker undamaged tubes a smooth single-lobe was formed in model E2 while there was no sign of post-collapse local buckling observed in model E1 but of remarkable ovalisation. For the damaged models, there was remarkable increase in both of depth of dent and out of straightness. For most of the undamaged and damaged models the overall shape was a dog-leg type.

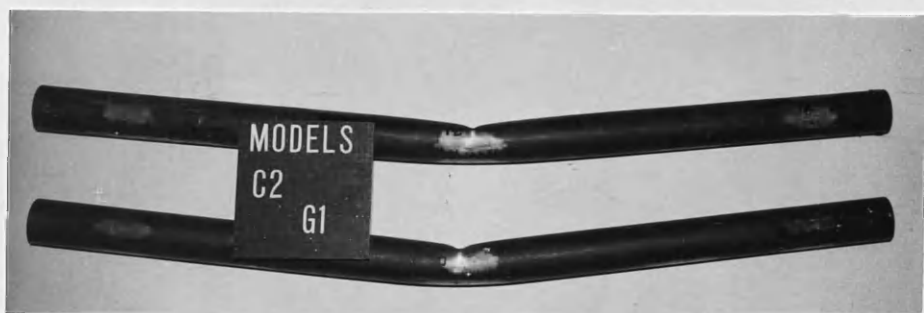
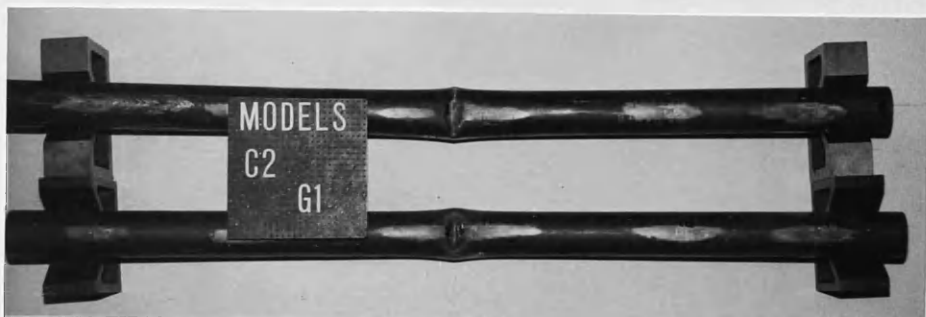
The effect of hydrostatic pressure on the cross-sectional shape of collapsed models can clearly be seen in Fig.4.14. In the damaged models under axial pure axial compression there was no recognisable change but the turning of the flattened segment in dent side into a very slightly concave one which is hardly seen in the figure. However, the damaged models under combined loading show somewhat different collapsed shapes. In the thicker model (model G2) an apparent concave shape can be seen in the dent side but no apparent change in shape in the other part, whereas the whole section of the thinner model (model D4) turned into a peanut shell-like shape which is similar to those of intact seamless tubes under combined axial load and external radial pressure<sup>[104]</sup>.

#### 4.4.4 Collapse Strength of Undamaged Models

The collapse strengths of the undamaged models are presented together with previous test data and relevant design curves in Fig.4.15. The collapse strength of model A1 is higher than the Euler buckling strength and those of models B2 and E2 are very close to the DnV strength curve 'a'. However, it can be seen that the results for the five models show the same trend as that of the test data given in refs.65 and 67. From the trend shown in the figure it seems possible that the actual effective length might be smaller than the model length not only for model A1 but for some of the other models. This finding can be supported by the comparison between the prediction of DnV curve 'a' and available test results for axially compressed tubulars provided in ref.105.

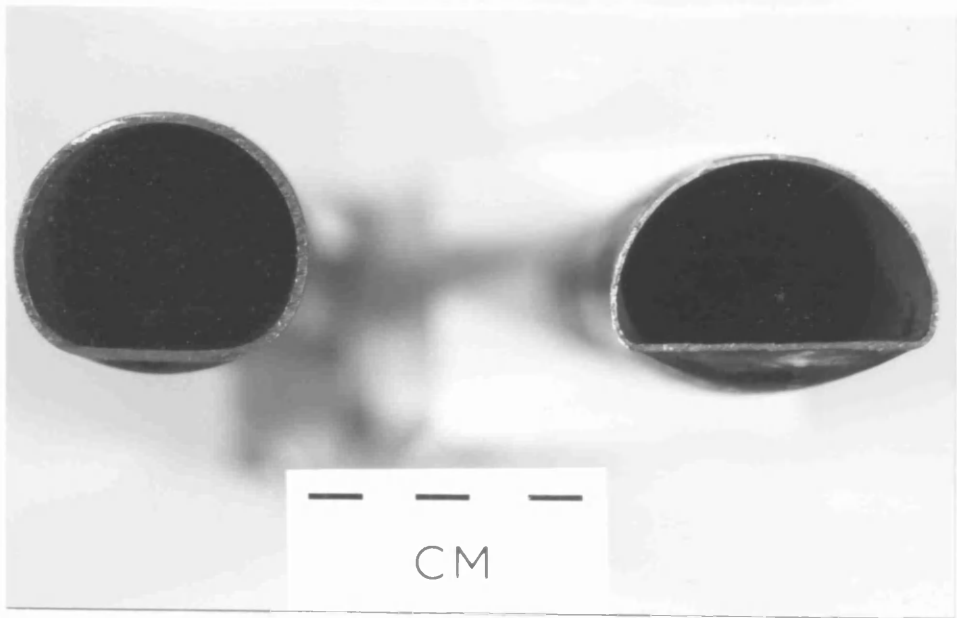


(a)

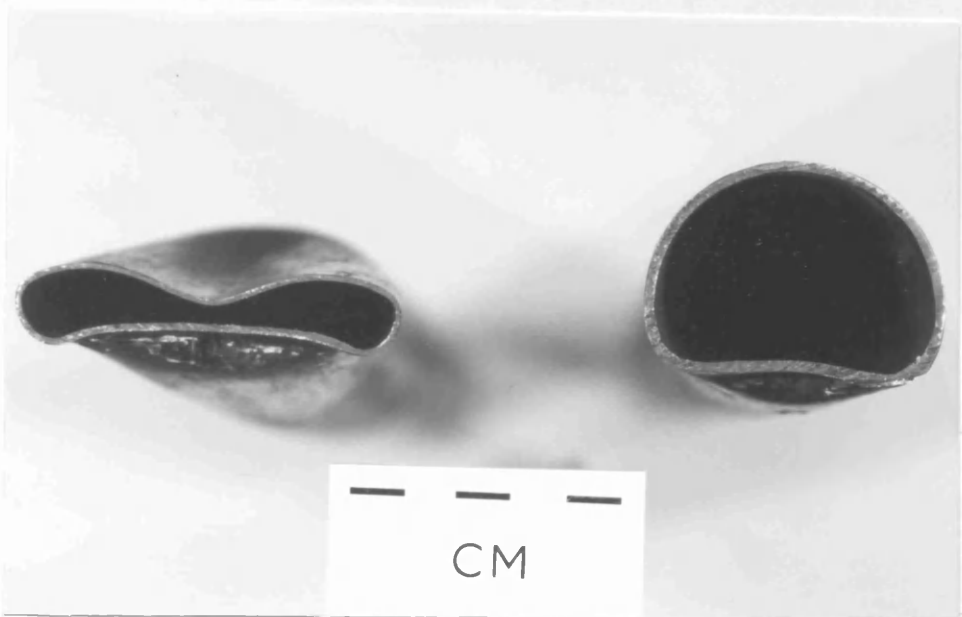


(b)

Fig. 4.13 Collapsed Models after Axial Compression Tests : (a) Undamaged Models : models A2 and E2,(b) Damaged Models : models C2 and G1



(a)



(b)

Fig. 4.14 Cross-sectional Shape of Collapsed Damaged Models :

(a) under Axial Compression ; models H1(l) and C2(r).

(b) under Combined Axial Compression and Hydrostatic Pressure ;  
models C2 and G1

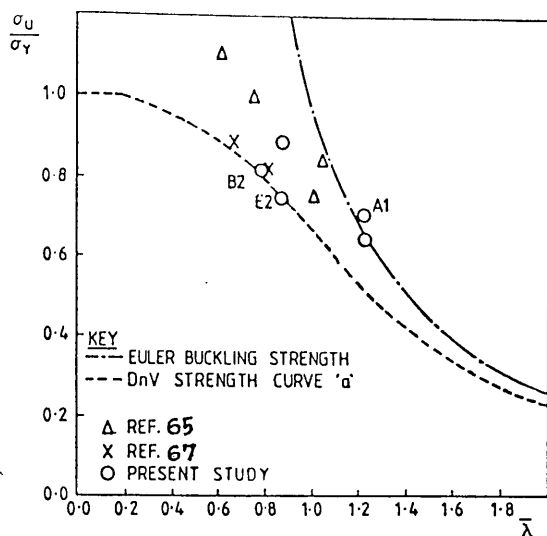


Fig.6. DESIGN CURVES AND TEST DATA  
FOR UNDAMAGED TUBULARS

Fig. 4.15 Design Curves and Test Data for Undamaged Tubulars

A plot of the ratios of predicted to actual strength against the reduced slenderness ratio of the column ( $\bar{\lambda}$ ) is presented in Fig.1 of the paper, which shows more uncertainty and larger bias in the range  $0.8 < \bar{\lambda} < 1.6$  probably due to the error in the tests rather than due to the inaccuracy of the formulation. Therefore, an accurate estimation of the effective length of the model seems crucial for a meaningful interpretation of tubular column test results.

## Chapter 5

### RESIDUAL STRENGTH OF DAMAGED TUBULARS

#### 5.1 Introduction

There are basically two models suggested for the evaluation of the ultimate strength and post-ultimate strength behaviour of damaged tubular members subjected to axial compression. In the method proposed by Taby, Moan and Rashed[66] the effective yield stress was introduced in the dented zone and the ultimate strength was considered as the load when yielding was first detected in the undamaged part of the dented portion. Dented section was assumed in the analysis to consist of a flattened segment and undamaged one. Later, the effective yield stress was corrected by an empirically derived factor to accommodate the underestimation of the load carrying capacity for the tubes whose  $D/t$  are less than 50[71]. This model was adopted in the ultimate strength analysis of dented tubulars under pure bending[70] and a similar method to the above was suggested by Ellinas[68].

Smith, Somerville and Swan introduced the concept of effective yield stress and effective modulus of elasticity of the fibres in the dent to account for the residual stresses resulting from dent formation and the eccentricity acting at the dented portion of the damaged tube. In ref.69, Smith presented an empirical reduction factor both for the effective strength and effective stiffness in terms of the dent size, yield stress and  $D/t$  ratio. This reduction factor was adopted by Richards and Andronicou[73] in their large displacement elasto-plastic analysis of damaged tubular columns.

However, it seems difficult to adopt any of the models described above for



combined axial compression and hydrostatic pressure loading not only because both of these models involve the empirical factors based upon test results of axially compressed damaged tubulars but because hypothetical stresses were used in the analyses rather than real occurring ones. In order to incorporate hydrostatic pressure in the analysis it seems necessary to develop a method by which real occurring stresses can be determined. In this study, therefore, the geometric configuration of dented portion is realistically simulated in the analysis by using the equations based on the lateral impact test results and the circumferential residual stresses due to denting deformation are considered. In other words the damaged tubular is treated as a beam-column having varying cross-sections and residual stresses.

For a long or intermediate length beam-column having initial crookedness the effect of lateral deflection which magnifies the primary moments by the axial load cannot be ignored in the analysis. Therefore, the ultimate strength of the beam-column should generally be determined from the stand point of load-deflection analysis. On top of that if the column fails beyond the elastic limit of the material the problem becomes more complicated and, thus, recourse must be made to numerical methods to obtain solutions. An incremental finite element method was employed by Smith and his coworkers<sup>[65, 67, 69]</sup> in their parametric studies for axially compressed damaged tubulars using non-linear beam-column elements. In ref.73 the pre- and post-ultimate behaviour of damaged tubular under axial compression was traced by means of a finite segment approach<sup>[106]</sup>.

The analytical method presented in this chapter, however, involves two separate phases of calculations:

- The moment-external axial compression-hydrostatic pressure-curvature ( $M - P_{ext} - Q_H - \Phi$ ) relationships for damaged cross sections are derived;
- then, using the relationships the residual strength of the damaged tubular is determined.

The  $M - P_{ext} - Q_H - \Phi$  relationships are computed using the tangent stiffness formulation<sup>[107]</sup> and the approximate equations for the relationships are then obtained

by fitting the computed data to non-linear multiple regression models. The ultimate strength is computed by using the Newmark integration method[101,108,109].

Finally, the predictions using the present method are compared with available experimental results including those conducted in this study to demonstrate their validity and accuracy.

## 5.2 M - P<sub>ext</sub> - Q<sub>H</sub> - Φ Relationships for Dented Tubular Sections

The M - P<sub>ext</sub> - Q<sub>H</sub> - Φ or generalised stress-strain relationships may be computed every time in need in the ultimate strength solution scheme. However, by using close-form approximate expressions for the relationships instead of computing the relationship in the solution scheme the computing time can considerably be reduced. As a starting point of the ultimate strength analysis, therefore, approximate equations were derived for a dented tubular cross-section subjected to a given value of external axial force and hydrostatic pressure.

### 5.2.1 Geometry of Dented Cross-Section and Residual Stresses

In this study a dented section is assumed to consist of one flattened segment, two segments of radius R<sub>2</sub> and circumferential angle θ<sub>2</sub>, and one segment of radius R<sub>1</sub> and circumferential angle 2θ<sub>1</sub> (see Fig.2.9). Besides the equation for the relationship between D<sub>dmax</sub> and D<sub>dmin</sub>, eqn (2.7), expressions for S<sub>f</sub> and θ<sub>1</sub> were also derived empirically using the test results given in Table 2.4. Hence, using eqns.(5.1) to (5.7) the geometric configuration of a dented tubular cross-section having a given non-dimensionalised depth of dent δ<sub>d</sub> can be defined straightforwardly.

$$D_{dmin} = D_o - \delta_d D \quad (5.1)$$

$$D_{dmax} = D_o \left\{ 1 + 2.45 \left( \frac{D_o}{D_{dmin}} - 1 \right) \exp (-2.4 D_{dmin}/D_o) \right\} \quad (5.2)$$

$$S_f = 1.64 D_o \left(1 - \frac{D_{dmin}}{D_o}\right)^{0.56} \exp(0.33 D_{dmin}/D_o) \quad (5.3)$$

$$\theta_1 = \pi \left\{ 1 - 1.47 \left(1 - \frac{D_{dmin}}{D_o}\right)^{0.4} \exp(-0.94 D_{dmin}/D_o) \right\} \quad (5.4)$$

$$\theta_2 = \pi - \theta_1 \quad (5.5)$$

$$R_1 = \frac{1}{2} D_{dmax} \quad (5.6)$$

$$R_2 = \frac{1}{2\theta_2} (\pi D_o - S_f - 2 R_1 \theta_1) \quad (5.7)$$

where eqn.(5.2) is identical with eqn.(2.7).

It seems not easy to accurately express the longitudinal and circumferential residual stresses in a tubular caused by the local denting and overall bending deformations due to lateral impact. In the present analysis, however, the residual stresses in circumferential direction only are simply approximated. By assuming that the denting of the cross-section is the result of irreversible and inextentional circumferential bending deformations, the circumferential strain ( $\epsilon_{\theta r}$ ) can be obtained by the equation (see Fig.5.1):

$$\begin{aligned} \epsilon_{\theta r} &= \frac{(R' + y') \frac{R}{R'} d\theta'}{(R + y') d\theta} - 1 \\ &= \frac{y' \left(\frac{R}{R'} - 1\right)}{R + y'} \end{aligned} \quad (5.8)$$

where  $\epsilon_{\theta r}$  : circumferential residual strain due to denting damage

$R$  : radius of curvature of the finite shell element before denting

$R'$  : radius of curvature of the finite shell element after denting

$y'$  : distance from the middle surface of the tube (+) ; outwards, (-) ; inwards

$d\theta$  : central angle of the finite element before denting

$d\theta'$  : central angle of the finite element after denting

Consequently, the circumferential residual stress due to denting damage can be obtained from eqn (5.9).

$$\sigma_{\theta r} = \begin{cases} \sigma_Y & ; \sigma_{\theta r} \geq \sigma_Y \\ E \frac{y'}{R + y'} \left( \frac{R}{R'} - 1 \right) & ; |\sigma_{\theta r}| < \sigma_Y \\ -\sigma_Y & ; \sigma_{\theta r} \leq -\sigma_Y \end{cases} \quad (5.9)$$

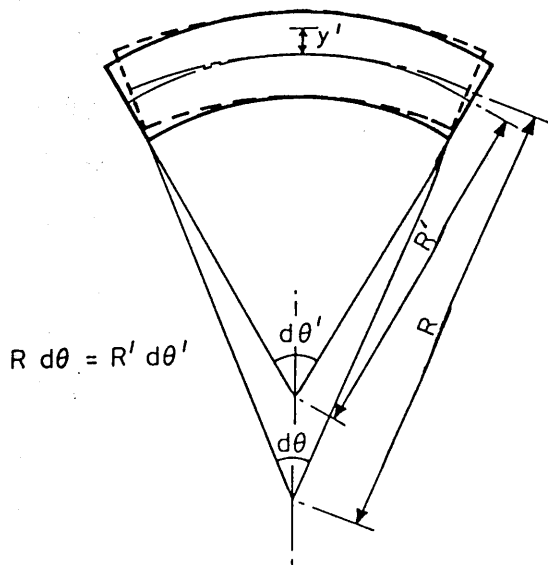


Fig. 5.1 Inextensional Circumferential Bending Deformation of a Tube Segment

### 5.2.2 Effect of Hydrostatic Pressure

When subjected to external hydrostatic pressure additional compressive axial stresses combined with hoop stresses occur in an axially compressed column. A question may be raised whether the end axial force due to hydrostatic pressure can introduce any secondary moment along the column. Breckenridge and Haynes<sup>[110]</sup> conducted on slender hollow straight and curved columns of stainless steel and aluminum under a high external hydrostatic pressure. The test results showed no evidence that the curved columns experienced bending. Thus it was concluded that hydrostatic pressure does not apply any effective loads to develop bending moment to the ends of columns. This experimental finding can also be explained by means of an equivalent resultant force concept. The magnitude of the equivalent resultant force acting on any cross-section of the column due to hydrostatic pressure is the same as the product of the hydrostatic pressure and the cross-sectional area. The direction of the resultant force is normal to the cross-section and its point of application is the centroid of the cross-section. Therefore, the hydrostatic pressure does not introduce any bending moment along the length, it does not contribute to the deflection and consequently not influence the theoretical elastic buckling strength of the column. It is accordingly necessary to distinguish the external axial compression ( $P_{ext}$ ) from the end force due to hydrostatic pressure. However, the axial and hoop stresses due to hydrostatic pressure may indirectly influence the failure load of a column in inelastic range.

Because of the lack of symmetry in the cross-section of a dented tubular the resultant hoop stress produced by hydrostatic pressure applies eccentrically causing an additional moment with respect to the middle surface of the wall. Furthermore, the eccentrically applied hoop stress can magnify the geometric imperfection, which in turn increase the bending stress in the circumference. In order to consider the magnification effect of hydrostatic pressure in the analysis it is assumed that the circumferential deformations are inextensional and that the internal circumferential forces in the dented tubular of unit length reduce to a constant circumferential force ( $S$ ) and a bending

moment ( $M$ ). The constant circumferential force and the bending moment can be obtained from eqns (5.10) and (5.11) respectively. In the equations the out of roundness is defined as the radial deviation of the dented section from a perfect circular form, and the magnification of the geometric imperfection due to the hydrostatic pressure is considered by multiplying the well-known amplification factor,  $1/(1 - Q_H/Q_{Hcr})$ . Finally, the circumferential stress ( $\sigma_{\theta H}$ ) due to hydrostatic pressure can be calculated from eqn (5.12).

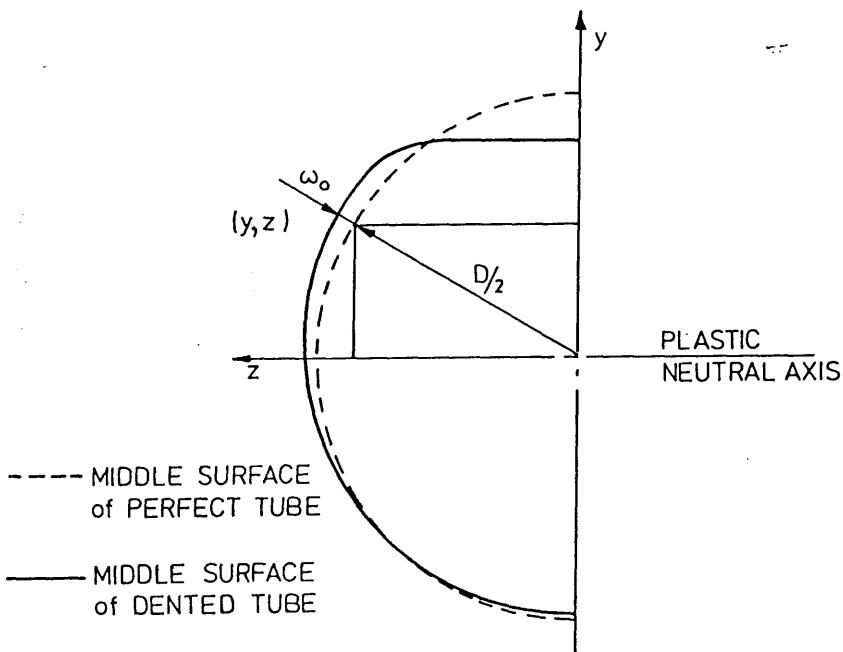


Fig. 5.2 Radial Deviation of Dented Cross-Section from Perfect Circle

$$S = Q_H \frac{D}{2} \quad (5.10)$$

$$M = S w_o \left( \frac{1}{1 - Q_H/Q_{Hcr}} \right) \quad (5.11)$$

$$\sigma_{\theta H} = \frac{Q_H D}{2 t} + w_o \left( \frac{1}{1 - Q_H / Q_{Hcr}} \right) \frac{6 y' Q_H D}{t^3} \quad (5.12)$$

where  $S$  : circumferential force per unit length due to hydrostatic pressure

$M$  : bending moment per unit length

$w_o$  : radial deviation of the dented cross-section from the perfect circle,  
 $D/2 - \sqrt{y^2 + z^2}$  (see Fig. 5.2)

### 5.2.3 Tangent Stiffness Formulation

Unlike for the cases of perfect thin-walled steel tubular members made of material with simple stress-strain curves and cross-section with simple geometry, it is difficult to derive any analytical expressions for the moment-curvature relationships for damaged tubulars having material and geometric imperfections. Therefore, recourse must be made to numerical procedures for a rigorous solution. In this study the tangent stiffness method, which has successfully been applied to the cases of fabricated tubulars[111,112,103,113] and other types of sections having residual stresses[107], is employed to obtain the  $M - P_{ext} - \Phi$  relations for damaged tubulars under hydrostatic pressure.

Mathematical Formulation In the tangent stiffness method the cross-section is divided into many small elements and the total axial force ( $P_t$ ) and bending moment ( $M_z$ ) can be obtained by summing up the effects of axial stresses. The generalised stresses ( $P_t, M_z$ ) and generalised strains ( $\epsilon_{x0}, \Phi_z$ ) are shown in Fig.5.3 in positive direction, where  $z$ -axis coincides with the plastic neutral axis of the cross-section and the cross-section is symmetric about  $y$ -axis.

$$P_t = \int_A \sigma_x dA \quad (5.13)$$

$$M_z = \int_A \sigma_x y dA \quad (5.14)$$

By assuming that plane remains plane after deformation the axial strain,  $\epsilon_x$ , at a point in the cross-section can be expressed in a linear form as

$$\epsilon_x = \epsilon_{x0} + y \Phi_z \quad (5.15)$$

where  $\epsilon_{x0}$  : axial strain on z-axis  
 $\Phi_z$  : curvature with respect to z-axis

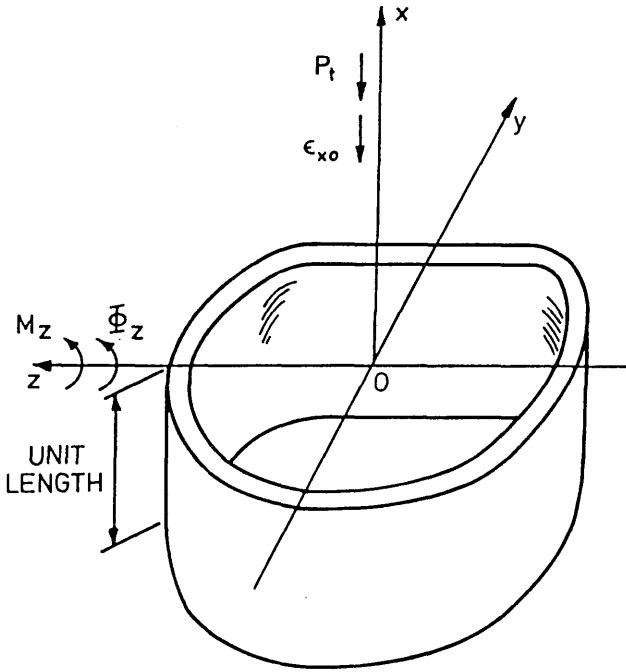


Fig. 5.3 Positive Vectors of Generalised Stresses and Generalised Strains

Because of the nonlinear character of the material property (the material is assumed to be elastic-perfectly plastic) it is necessary to establish incremental generalised stress equations. Changing eqns.(5.13) and (5.14) into incremental form eqns.(5.16) and (5.17) can be obtained.



$$dP_t = \int_A d\sigma_x dA \quad (5.16)$$

$$dM_z = \int_A d\sigma_x y dA \quad (5.17)$$

The rate of change of axial stress is then given as eqn.(5.18) by introducing 'effective' modulus  $E_{eff}$  defined as eqn.(5.19) in which yielding is monitored using the von Mises yield criteria.

$$d\sigma_x = E_{eff} d\epsilon_x \quad (5.18)$$

$$E_{eff} = \begin{cases} E & ; |\sigma_e| < \sigma_Y \\ 0 & ; |\sigma_e| \geq \sigma_Y \end{cases} \quad (5.19)$$

where  $\sigma_e$  : von Mises equivalent stress,

$$\sqrt{\sigma_x^2 + (\sigma_{\theta r} + \sigma_{\theta H})^2 - \sigma_x(\sigma_{\theta r} + \sigma_{\theta H})}$$

The equation for axial strain change rate is

$$d\epsilon_x = d\epsilon_{x0} + y d\Phi_z \quad (5.20)$$

By carrying out substitution eqns.(5.16) and (5.17) yield the following incremental relationship in matrix form:

$$d \begin{Bmatrix} M_z \\ P_t \end{Bmatrix} = \begin{bmatrix} Q_{11} & Q_{12} \\ Q_{21} & Q_{22} \end{bmatrix} d \begin{Bmatrix} \Phi_z \\ \epsilon_{x0} \end{Bmatrix} \quad (5.21)$$

where  $[Q]$  is called the tangent stiffness matrix whose elements  $Q_{ij}$  are defined as

$$\begin{aligned}
Q_{11} &= \int_A E_{\text{eff}} y^2 dA \\
Q_{12} &= Q_{21} = \int_A E_{\text{eff}} y dA \\
Q_{22} &= \int_A E_{\text{eff}} dA
\end{aligned} \tag{5.22}$$

Once the tangent stiffness matrix  $[Q]$  corresponding to a given state of stress can be evaluated, the path of generalised strains for a given path of generalised stresses can be determined through a step-by-step incremental calculation and an iteration procedure.

· Iteration Procedure : For a given state of increments of external forces the corresponding increments of deformations may be obtained approximately from eqn.(5.21) when all the information of stress and strain and the tangent stiffness matrix of the current state are known. However, the solution for a partly yielded section may deviate considerably from the exact value because the tangent stiffness matrix is that before the increments occur. Therefore an iteration procedure must be employed for inelastic problems.

The step-by-step iterative technique proposed in ref.107 is adopted in this study and its procedure is depicted in Fig.5.4. For convenience the following vectors of force and deformation are defined:

$$\{f\} = \begin{Bmatrix} M_z \\ P_t \end{Bmatrix}, \quad \{X\} = \begin{Bmatrix} \Phi_z \\ \epsilon_o \end{Bmatrix} \tag{5.23}$$

Following the definitions above eqn.(5.21) can be rewritten as

$$d\{f\} = [Q] d\{X\} \tag{5.24}$$

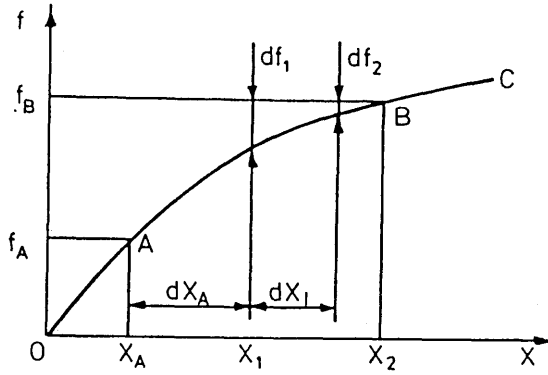


Fig. 5.4 Step-by-Step Iterative Technique (from ref.107)

In the figure the curve OABC is the true force-deformation curve. Let  $\{f_A\}$  and  $\{X_A\}$  be the vectors at state A which satisfy equilibrium and  $[Q_A]$  is the corresponding tangent stiffness matrix, which is equivalent to the slope at point A. The increment of force vector from A to B is

$$d\{f_A\} = \{f_B\} - \{f_A\} \quad (5.25)$$

With the increment of external force vector  $d\{f_A\}$  the increment of deformation is obtained from eqn.(5.24) as

$$d\{X_A\} = [Q_A]^{-1} d\{f_A\} \quad (5.26)$$

where  $[Q]^{-1}$  is the inverse of the matrix  $[Q_A]$ .

The first estimated deformation is given by the sum of  $\{X_A\}$  and  $d\{X_A\}$ .

$$\{X_1\} = \{X_A\} + d\{X_A\} \quad (5.27)$$

The deformation gives rise to incremental force  $\{f_1\}$  which is not in equilibrium with the external force  $\{f_B\}$ . The first unbalanced force  $d\{f_1\}$  is computed from

$$d\{f_1\} = \{f_B\} - \{f_1\} \quad (5.28)$$

The next step is to find a correction vector  $d\{X_1\}$  which will be added to  $\{X_1\}$  in order to eliminate the unbalanced force. Vector  $d\{X_1\}$  is obtained from

$$d\{X_1\} = [Q_1]^{-1} d\{f_1\} \quad (5.29)$$

where  $[Q_1]^{-1}$  is the inverse of the new tangent stiffness matrix  $[Q]^{-1}$  corresponding to the the state  $\{f_1\}$  and  $\{X_1\}$ . The procedure is repeated until the unbalanced force is within a prescribed error bound.

#### 5.2.4 M - P<sub>ext</sub> - Q<sub>H</sub> - Φ Data Generation

Based on the equations formulated a computer program was developed to provide numerical results from which approximate equations can be derived for damaged tubulars under hydrostatic pressure. In the development a subroutine listed in chapter 2 of ref.109 was used in a modified form. Using the computer program computations have been conducted for the following values of parameters:

$$\begin{aligned} D/t &= 20, 40, 60 \\ \delta_d &= 0.00, 0.01, 0.02, 0.05, 0.10, 0.15, 0.20 \\ Q_H/Q_{Hcr} &= 0.0, 0.1, 0.2, 0.3, 0.4, 0.5, 0.6 \\ P_{ext}/P_Y &= 0.0, 0.1, 0.2, 0.3, 0.4, 0.5, 0.6, 0.7, 0.8, 0.9 \end{aligned}$$

where  $P_Y$  : axial load at full yield condition of a section,  $\pi \sigma_Y D t$

In the computations a half of the damaged tubular cross-section was divided into fibres as shown in Fig.5.5 and diameter, Young's modulus and yield stress were

assumed to be 50 mm, 210000 N/mm<sup>2</sup> and 350 N/mm<sup>2</sup> respectively. Bending moment  $M_z$  was increased by 1 % of the fully plastic moment  $M_p$  when external axial force  $P_{ext}$  was less than 0.8  $P_Y$  and the increment was reduced to 0.5 % of  $M_p$  when  $P_{ext}$  is greater than or equal to 0.8  $P_Y$ .

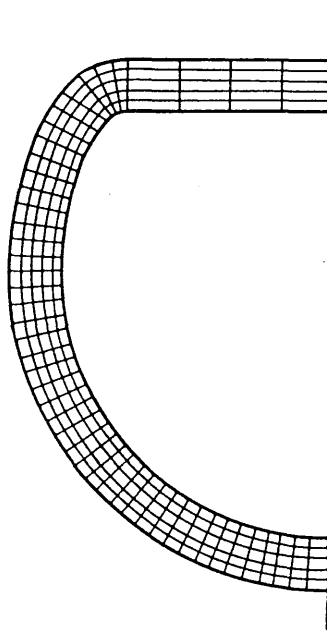


Fig. 5.5 Division of Damaged Cross-Section into Fibres

Total axial force  $P_t$  was calculated by :

$$P_t = P_{ext} + P_H \quad (5.30)$$

where  $P_H$  : axial force due to hydrostatic pressure,  $\pi/4 Q_H (D+t)^2$

Iteration was continued until both of the unbalanced values for  $P_t$  and  $M_z$  were less than 0.01 % of  $P_Y$  and  $M_{pd}$  respectively.  $M_{pd}$ , fully plastic bending moment of the

dedented section, was calculated numerically in the program. Fully plastic state of the section was defined when the determinant of the tangent stiffness matrix  $[Q]$  was not positive or when the curvature  $\Phi_z$  was greater than fifty times of  $\Phi_Y$ .

### 5.2.5 Derivation of Approximate Equations

The analyses of damaged tubular beam-column problems may considerably be simplified if an analytical expression can be found to reasonably approximate the numerically computed  $M - P_{ext} - Q_H - \Phi$  relationships. Using non-dimensionalised quantities,

$$q = Q_H/Q_{Hcr}, \quad p = P_{ext}/P_Y, \quad m = M_z/M_p, \quad \phi = \Phi_z/\Phi_Y \quad (5.30)$$

where  $M_p$ : plastic bending moment capacity of an intact tubular,  $\sigma_Y D^2 t$  and  
 $\Phi_Y$ : curvature at initial yielding,  $2 \sigma_Y / E / D$

the non-linear moment-curvature relationships may be approximately represented by :

$$m = \begin{cases} 0 & (\phi \leq \phi_0) \\ a (\phi - \phi_0) & (\phi_0 < \phi \leq \phi_1) \\ m_{pc} - (m_{pc} - m_1) \exp\{f(\phi)\} & (\phi_1 < \phi) \end{cases} \quad (5.31)$$

where  $a$  : slope of the linear part  
 $m_1$  : non-dimensionalised linear limit bending moment,  $M_1/M_p$   
 $m_{pc}$  : non-dimensionalised fully plastic bending moment reduced for  
the presence of axial load,  $M_{pc}/M_p$   
 $f(\phi) = -c_1 (\phi - \phi_1)^{c_2}$  and  
 $\phi_1 = m_1 / a + \phi_0$

The parameters  $a, \phi_0, c_1, c_2, m_1$  and  $m_{pc}$  which are functions of diameter to thickness ratio  $D/t$ , non-dimensionalised depth of dent  $\delta_d$ , non-dimensionalised hydrostatic pressure  $q$  and non-dimensionalised external axial compression  $p$ , were

determined using the computed results of the moment-curvature relationships. In the derivation the values of  $a$ ,  $\phi_0$ ,  $m_1$  and  $m_{pc}$  for each moment-curvature curve were first determined from the computed data and then a regression analysis was carried out for each of  $a$ ,  $\phi_0$ ,  $m_1$  and  $m_{pc}$ .

In the regression analysis all of the possible combination of the basic parameters, i.e.  $D/t$ ,  $\delta_d$ ,  $p$  and  $q$ , were considered as independent variables and most appropriate exponents together with a corresponding coefficient for each independent variable were then chosen by comparing the squares of deviation provided by them. The exponents were extended to non-integer numbers with a hope to reduce the number of terms in the approximate equations. For  $c_1$  and  $c_2$  the values for each moment-curvature curve were determined after substituting the derived equations for  $a$ ,  $\phi_0$ ,  $m_1$  and  $m_{pc}$  into eqn.(5.31) and then the same regression procedure described above was followed. The equations for  $a$ ,  $c_1$ ,  $c_2$ ,  $m_1$ ,  $m_{pc}$  and  $\phi_0$  are given in Appendix I.

The approximate equations together with the computed results are illustrated in Fig.5.6. Some inaccuracy of the equations can be found in the figure. However, the computing efficiency and convenience of using the equations in beam-column analysis can compensate the penalty in accuracy when comparing with an alternative to interpolate the more than 40,000 computed data.

### 5.3 Residual Strength

#### 5.3.1 Effect of Local Shell Deformation

In the derivation of the moment-curvature relationships for dented tubular sections the dented cross-section was assumed not to change, i.e. any further local deformation was not considered. As discussed in section 4.4.2 for deeply dented thin tubes a notable local shell deformation at damaged part, probably in the form of growth of dent depth, may occur before ultimate state and consequently the ultimate strength can be reduced.

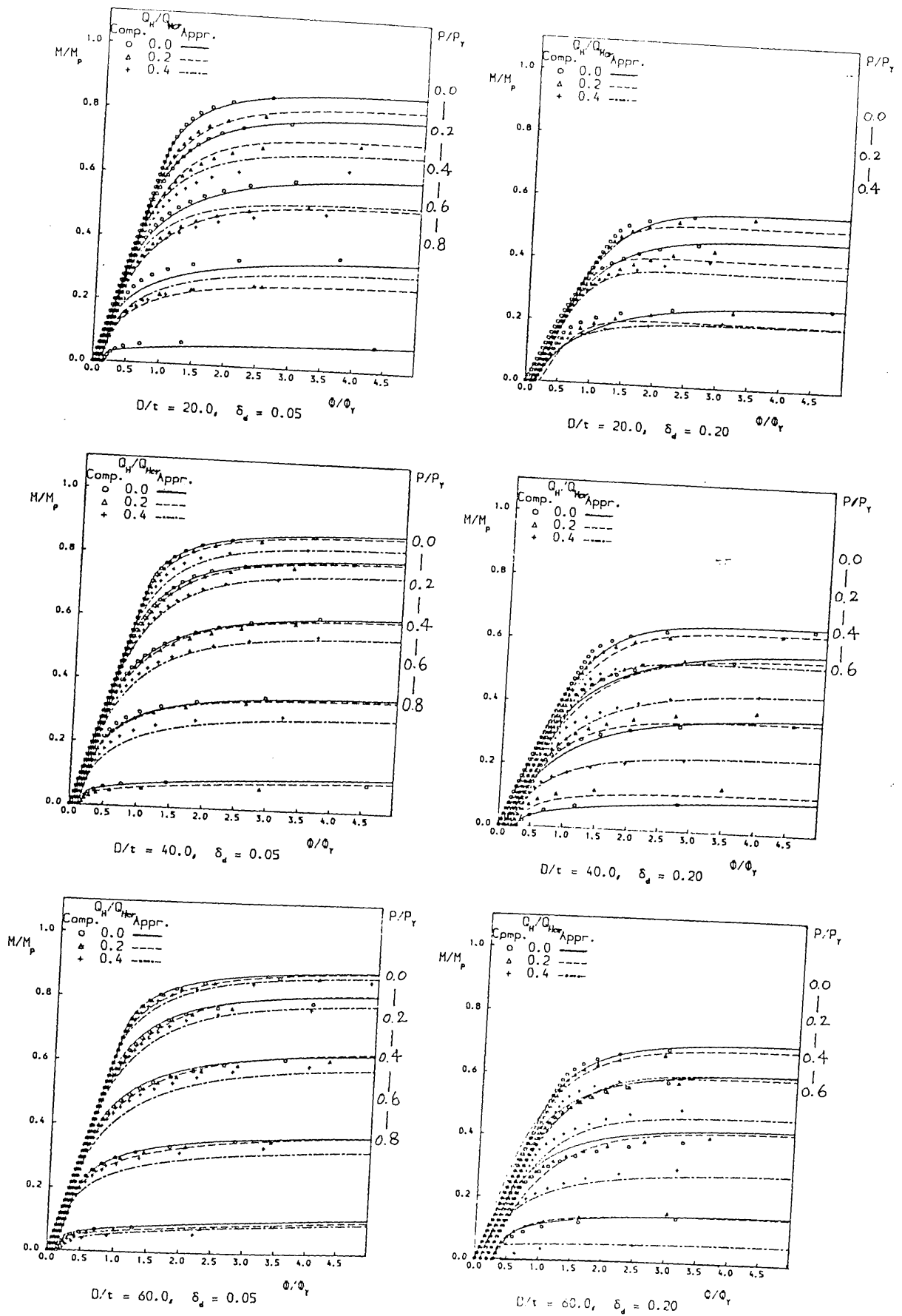


Fig. 5.6 Approximate Equations for  $M - P_{ext} - Q_H - \Phi$  Relationships  
of Damaged Tubulars as Derived from Computed Data



The results are illustrated in Fig.5.7 of pure bending tests on damaged tubulars (compression in dent) given in ref.70 where  $M_u$  is the experimental ultimate bending moment and  $M_{pd}$  is the fully plastic bending moment of the dented section obtained using eqn.(A9). As clearly be seen in the figure the fully plastic capacity of damaged tubulars under pure bending can be reduced further for the thinner and more deeply dented ones. This is probably due to the local shell deformation at damaged part, which can be exhibited through the growth of dent depth. Therefore, a modification must be made of the moment-curvature relationships derived neglecting the change of the cross-section in order to account for such a deteriorating effect.

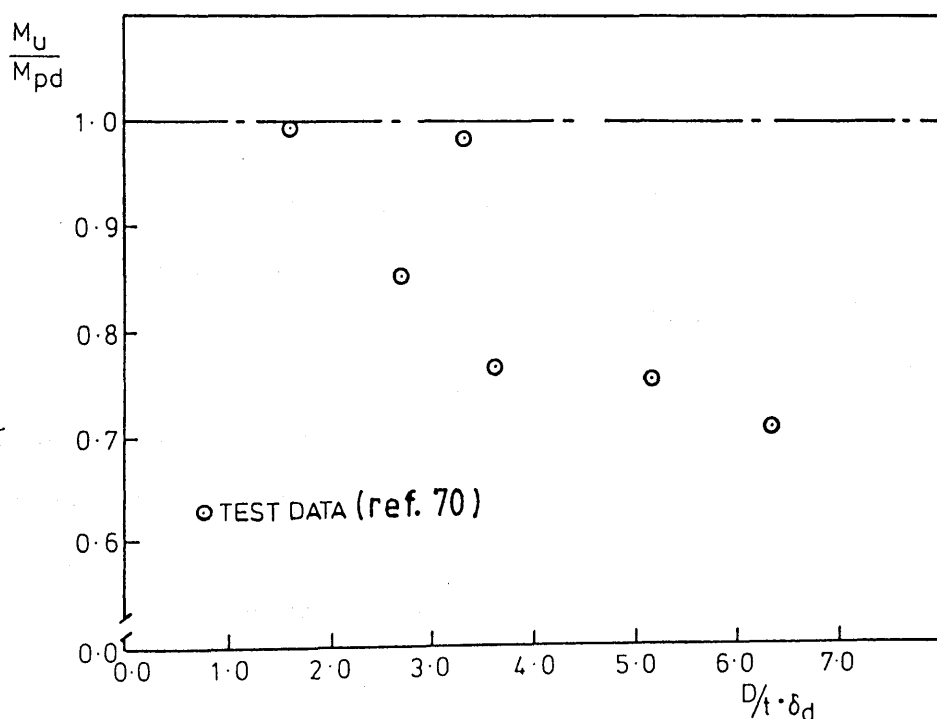


Fig. 5.7 Dependence of Ultimate Strength of Damaged Tubulars under Bending Moment (Compression in Dent) on Diameter to Thickness Ratio ( $D/t$ ) and Depth of Dent ( $\delta_d$ )

Based on the test data given in ref.70 a correction factor ( $C_s$ ), eqn.(5.32), has been derived for the ultimate strength of damaged tubulars under pure bending moment (compression in dent) to take into consideration the local shell deformation at damaged part.

$$C_s = \begin{cases} \exp (0.44 - 0.011 D/t - 1.6 \delta_d) & C_s < 1 \\ 1 & C_s \geq 1 \end{cases} \quad (5.32)$$

As a by-product the ultimate bending strength of damaged tubulars can be estimated from eqn.(5.33) which was obtained by multiplying eqn.(5.32) by eqn.(A9).

$$M_u/M_p = C_s \{1 - 0.23 \delta_d^{0.3} \exp (4.4 \delta_d)\} \quad (5.33)$$

where  $M_u$  : ultimate strength of a damaged tubular under bending moment

Finally, in order to take into account the deteriorating effect of local deformation in beam-column analysis of damaged tubulars, the moment-curvature relationships, which were derived using the tangent stiffness method and then approximated by regression, have been modified. By multiplying the correction factor  $C_s$  by  $m_1$  and  $m_{pc}$ , i.e. reducing both the linear limit moment and the non-linear part by  $C_s$ , the modified moment-curvature relationships have been obtained and which are shown graphically in Fig.5.8.

### 5.3.2 Newmark's Integration Method

Having obtained the modified  $M - P_{ext} - Q_H - \Phi$  relationships for dented tubular sections, the residual strength of damaged tubulars can be determined by using the Newmark's integration method[101,108,109] or the finite segment approach[106,73]. In this study, however, the Newmark's integration method has been adopted, which was initially proposed particularly for the determination of buckling loads of bars of variable cross-section and which has recently been employed successfully for the ultimate strength analysis of fabricated tubular columns[114,115].

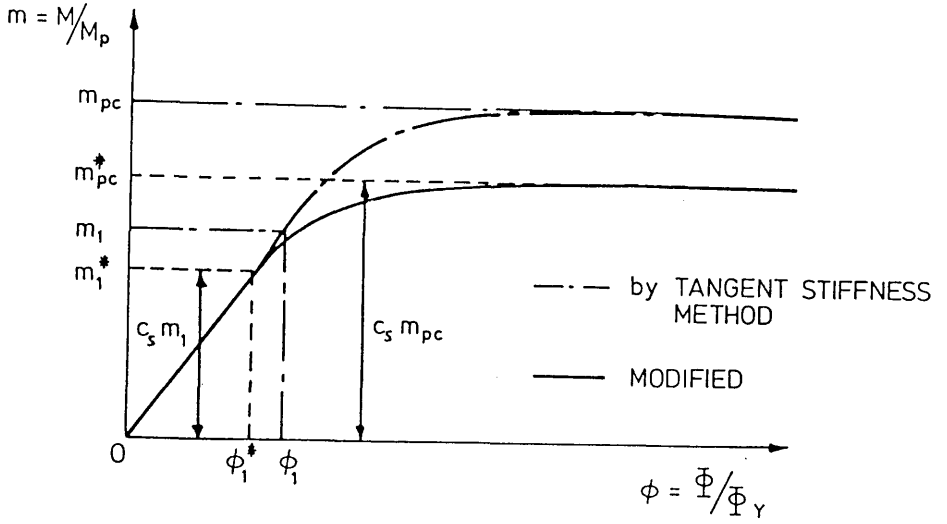


Fig. 5.8 Modified Moment - Curvature Relationship for Damaged Tubulars Considering Shell Effects

The calculation steps of the Newmark's numerical procedure are described in the following to determine the residual strength of a damaged tubular having simply supported boundaries.

• Procedure of Calculation :

1) Divide the upper undamaged part, damaged part and lower undamaged part into  $N_1$ ,  $N_D$  and  $N_2$  segments respectively. The nodal points are called stations (the number of the total stations  $N_s$  is  $N_1 + N_D + N_2 + 1$ ). Describe the initial out-of-straightness  $w_i$  at all stations in the member and the depth of dent at all stations in damaged part.

2) Assume an additional deflection  $w_a$  at every station (for the first iteration of the first load increment  $w_a$  can be assumed to be zero).

3) Compute bending moment  $M_z$  about z-axis (see Fig.5.9) at all stations due to the given axial load  $P$  by

$$M_z = P_{ext} w = P_{ext} (w_i + w_a) \quad (5.34)$$

where  $M_z$  : internal moment due to deflection  $w_a$   
 $w$  : total deflection  
 $w_i$  : initial defection, i.e. initial out-of-straightness  
 $w_a$  : deflection amplified by externally applied axial force

4) Compute curvatures at all stations from the  $M - P_{ext} - \Phi$  relationships of the section (from eqn.5.31). Negative sign must be taken for curvatures in order to hold the sign convention in Fig.5.9.

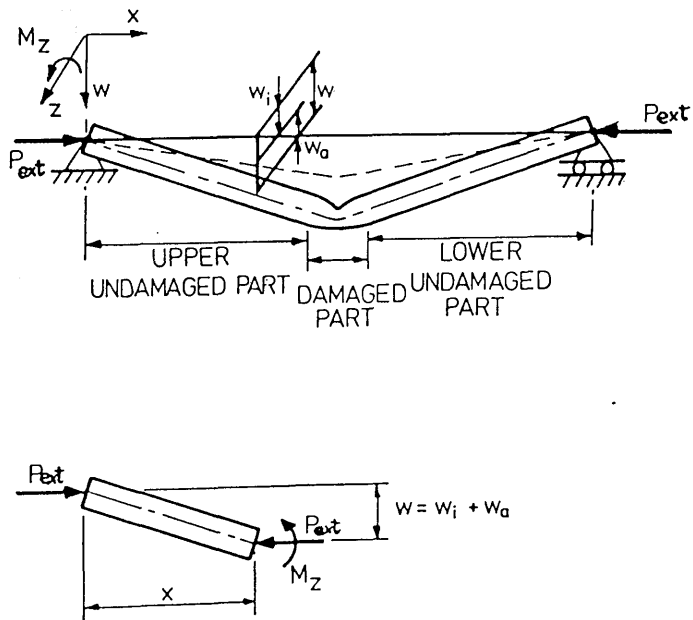


Fig. 5.9 Simply Supported Damaged Tubulars

5) Determine the deflection at all stations using the Newmark's integration method:

(i) Assume the distribution of curvature between two stations to be quadratic and compute the contribution of the curvature to the slope at adjacent stations by

$$\bar{\alpha}_i = \frac{l_i}{12(l_i + l_{i+1})} \{ 3 l_i (\Phi_i + \Phi_{i+1}) + 2 l_{i+1} (2\Phi_i + \Phi_{i+1}) + \frac{l_i^2}{l_{i+1}} (\Phi_{i+1} - \Phi_{i+2}) \} \quad ; i = 1$$

$$\bar{\alpha}_i = \frac{(l_{i-1} + l_i)}{12} (\Phi_{i-1} + 4\Phi_i + \Phi_{i+1}) + \frac{l_i^2}{12 l_{i-1}} (\Phi_i - \Phi_{i-1}) + \frac{l_{i-1}^2}{12 l_i} (\Phi_i - \Phi_{i+1}) \quad ; 2 \leq i \leq N_s - 1 \quad (5.35)$$

$$\bar{\alpha}_i = \frac{l_i}{12(l_i + l_{i-1})} \{ 3 l_i (\Phi_i + \Phi_{i-1}) + 2 l_{i-1} (2\Phi_i + \Phi_{i-1}) + \frac{l_i^2}{l_{i-1}} (\Phi_{i-1} - \Phi_{i-2}) \} \quad ; i = N_s$$

where  $\bar{\alpha}_i$  : equivalent concentrated curvature at the  $i$  th station

$l_i$  : length of the  $i$  th segment, i.e. of the segment between the  $i$  th and  $i+1$ th stations

$\Phi_i$  : curvature at the  $i$  th station

(ii) Compute relative average slopes for all stations by

$$\left( \frac{dw'}{dx} \right)_j^* = \sum_{k=1}^i \bar{\alpha}_k \quad (5.36)$$

where

$(\frac{dw'_a}{dx})_j^*$  : relative average slope of the j th segment to that of the 1st station.

(iii) Determine the slope at the 1st station from the condition that the deflection at the last station is zero.

$$(\frac{dw'_a}{dx})_{x=0} = -\frac{1}{L} \sum_{k=1}^{N_s-1} (\frac{dw'_a}{dx})_k^* l_k \quad (5.37)$$

where

$(\frac{dw'_a}{dx})_{x=0}$  : slope at the 1st station

(iv) Compute average slopes for all segments by

$$(\frac{dw'_a}{dx})_j = (\frac{dw'_a}{dx})_{x=0} + (\frac{dw'_a}{dx})_j^* \quad (5.38)$$

where

$(\frac{dw'_a}{dx})_j$  : average slope of the j th segment

(v) Compute deflections at all stations by

$$(w'_a)_i = \begin{cases} \sum_{k=1}^{i-1} (\frac{dw'_a}{dx})_k l_k & ; 2 \leq i \leq N_s + 1 \\ 0 & ; i = 1, N_s \end{cases} \quad (5.39)$$

where  $(w'_a)_i$  : new deflection at the i th station

6) Compare the new deflections  $w'_a$  with the assumed additional deflections  $w_a$  (check convergence). If they show an acceptable agreement,  $w_a$  is the correct

additional deflection of the member for the given load. If not, repeat steps 2-5 until the deflected shape converges into a prescribed error bound. For that case the new deflections  $w'_a$  can be a new assumed additional deflections.

7) Increase the axial load and repeat steps 2-6 until the resultant deflections  $w_i + w_a$  diverge, at which the axial load exceeds the ultimate strength of the member.

## 5.4 Correlation Study and Discussion

Based on the analysis procedure described above a computer program was written for determining the residual strength of a damaged tubulars subjected to axial compression and hydrostatic pressure. Using the program a correlation study has been performed with available test data in order to validate the proposed method. In the correlation study the member was divided into thirty segments (ten segments per each undamaged part and another ten in damaged part).

### 5.4.1 Available Test Data

A total of fifty seven test data is available for axial compression or combined axial compression and hydrostatic pressure loading from refs.65, 66, 67 and 69 and the tests conducted as part of this study. All of them were conducted on heat-treated cold-drawn seamless tubes with the exception of models E2 and F2 in ref.67 which were obtained from a removed North Sea platform following completion of service. For all test models denting was imposed using a "sharp" indenter having a knife edge with a round tip except models R1B, R1C and R2A of ref.69. For models R1B and R1C "square" and "round" indentors were used respectively while for model R2A an "extended" dent was produced by five sequential applications of the square indenter. Another fifty eight tests (forty eight tests with simply supported boundaries and ten with clamped ones) are reported in refs.71 and 72 but unfortunately their results are not available.

Table 5.1 Results of Correlation Study

**A. Axial Compression Tests**

Model	ref.	D/t	$E/\sigma_Y$	$\bar{\lambda}$	$\delta_d$	$\delta_o$	$x_d/L$	$\sigma_u/\sigma_Y$		$\sigma_u$ act. $\sigma_u$ pred.
								Exp.	Theory	
A3	[65]	29.2	867	1.06	0.048	0.0055	0.5	0.48	0.43	1.12
A4	ditto	29.0	839	1.09	0.001	0.0050	0.5	0.50	0.47	1.07
B3	ditto	45.2	1081	0.76	0.082	0.0050	0.5	0.52	0.50	1.04
B4	ditto	45.8	975	0.80	0.011	0.0050	0.5	0.61	0.58	1.06
C3	ditto	58.1	845	0.67	0.034	0.0004	0.5	0.76	0.83	0.92
C4	ditto	57.8	821	0.68	0.016	0.0005	0.5	0.84	0.86	0.98
D3	ditto	86.3	495	0.98	0.037	0.0003	0.5	0.53	0.67	0.79
D4	ditto	84.8	463	1.01	0.022	0.0010	0.5	0.64	0.60	1.06
IAI	[66]	61.3	922	0.84	0.051	0.00074	0.375	0.67	0.72	0.93
IAII	ditto	61.3	929	0.84	0.102	0.00183	0.375	0.52	0.57	0.91
IBI	ditto	50.1	844	0.88	0.051	0.00054	0.375	0.64	0.74	0.87
IBII	ditto	49.9	861	0.88	0.102	0.00151	0.375	0.53	0.60	0.89
ICI	ditto	40.8	693	0.98	0.051	0.00057	0.375	0.66	0.71	0.93
ICII	ditto	40.4	604	1.05	0.100	0.00206	0.375	0.51	0.52	0.98
IIAI	ditto	63.4	570	0.84	0.051	0.00023	0.375	0.68	0.76	0.89
IIAII	ditto	63.6	501	0.89	0.102	0.00166	0.375	0.44	0.58	0.76
IIAIII	ditto	63.4	595	0.82	0.020	0.00106	0.375	0.70	0.76	0.92
IIBI	ditto	52.3	572	0.84	0.050	0.00120	0.375	0.53	0.72	0.74
IIBII	ditto	52.1	870	0.68	0.102	0.00194	0.375	0.58	0.64	0.91
IIBIII	ditto	52.2	752	0.73	0.020	0.00051	0.375	0.80	0.85	0.94
IICI	ditto	39.4	417	0.99	0.055	0.00091	0.375	0.61	0.68	0.90
IICII	ditto	39.1	440	0.96	0.103	0.00217	0.375	0.48	0.55	0.87
IICIII	ditto	39.3	500	0.90	0.020	0.00077	0.375	0.79	0.78	1.01
IIIAI	ditto	59.2	396	0.64	0.051	0.00060	0.375	0.58	0.78	0.74
IIIAII	ditto	58.6	402	0.64	0.104	0.00100	0.375	0.46	0.68	0.68
IIIBI	ditto	48.1	426	0.62	0.055	0.00010	0.375	0.71	0.82	0.87
IIIBII	ditto	48.0	455	0.60	0.106	0.00200	0.375	0.53	0.66	0.80
IIICI	ditto	41.6	419	0.63	0.052	0.00087	0.375	0.73	0.78	0.94
IIICII	ditto	41.7	434	0.62	0.102	0.00183	0.375	0.56	0.67	0.83
E2S	[67]	30.1	726	0.82	0.003	0.0034	0.5	0.63	0.68	0.93
F2S	ditto	40.9	755	0.67	0.127	0.0050	0.5	0.46	0.51	0.90
E2	ditto	31.5	712	0.83	0.018	0.0032	0.5	0.73	0.66	1.10
F2	ditto	40.0	730	0.65	0.128	0.0018	0.5	0.57	0.61	0.94

(cont'd)



Table 5.1 Results of Correlation Study (cont'd)

**A. Axial Compression Tests (cont'd)**

Model	ref.	D/t	$E/\sigma_Y$	$\bar{\lambda}$	$\delta_d$	$\delta_o$	$x_d/L$	$\sigma_u/\sigma_Y$		$\sigma_u$ act. $\sigma_u$ pred.
								Exp.	Theory	
P1A	[69]	45.4	585	0.92	0.096	0.00195	0.5	0.61	0.57	1.07
P1B	ditto	45.9	585	0.92	0.092	0.00195	0.25	0.56	0.60	0.93
P2A	ditto	45.9	620	0.89	0.094	0.0005	0.125	0.67	0.73	0.92
P2B	ditto	45.4	620	0.89	0.181	0.00102	0.125	0.50	0.57	0.88
R1A	ditto	25.8	432	0.91	0.147	0.00278	0.5	0.46	0.47	0.97
R1B	ditto	25.8	432	0.91	0.138	0.00144	0.5	0.49	0.52	0.95
R1C	ditto	25.7	432	0.91	0.142	0.00089	0.5	0.56	0.54	1.04
R2A	ditto	26.9	436	0.91	0.143	0.0021	0.5	0.52	0.46	1.12
R2B	ditto	26.9	436	1.09	0.107	0.0011	0.25	0.60	0.57	1.06
P1C	ditto	46.4	585	0.92	0.181	0.00371	0.5	0.38	0.40	0.94
P2C	ditto	45.4	620	0.45	0.094	0.00130	0.5	0.72	0.73	0.99
P2D	ditto	45.4	620	0.45	0.122	0.00204	0.25	0.64	0.68	0.94
B1	present study	41.4	411	1.25	0.062	0.0023	0.5	0.45	0.46	0.97
C2	ditto	40.7	459	0.85	0.209	0.0149	0.5	0.26	0.26	0.99
D2	ditto	41.1	421	0.88	0.125	0.0058	0.49	0.46	0.46	1.00
D3	ditto	41.1	417	1.24	0.107	0.0055	0.49	0.38	0.37	1.04
F1P	ditto	24.1	475	1.18	0.016	0.0006	0.5	0.61	0.62	0.98
F2	ditto	24.1	475	0.85	0.043	0.0014	0.51	0.78	0.72	1.09
G1	ditto	24.0	471	0.85	0.035	0.0016	0.49	0.82	0.72	1.14
H1	ditto	24.0	468	1.19	0.006	0.0005	0.49	0.67	0.63	1.06

**B. Combined Axial Compression and Hydrostatic Pressure Tests**

Model	ref.	D/t	$E/\sigma_Y$	$\bar{\lambda}$	$\delta_d$	$\delta_o$	$x_d/L$	$Q_H/Q_{Hcr}$	$(\sigma_{x\ ext})_u/\sigma_Y$		$(\sigma_{x\ ext})_u$ act. $(\sigma_{x\ ext})_u$ pred.
									Exp.	Theory	
C4	present study	40.7	458	1.19	0.137	0.0087	0.5	0.143	0.27	0.31	0.88
D4	ditto	41.1	417	1.24	0.183	0.0147	0.5	0.287	0.18	0.19	0.93
G2	ditto	23.8	471	1.19	0.037	0.0024	0.5	0.057	0.54	0.51	1.05
D4	ditto	24.2	480	1.18	0.065	0.0054	0.5	0.092	0.39	0.41	0.95

Table 5.2 Summary of Correlation Study

ref.	Loading Type	Number of Tests	Actual to Predicted Strength Ratio	
			Mean	COV
[65]	Axial Comp.	8	1.005	10.6 %
[66]	ditto	21	0.872	9.8 %
[67]	ditto	4	0.968	9.3 %
[69]	ditto	12	0.984	7.4 %
present study	ditto	8	1.034	5.8 %
<u>sub total (Axial Comp.)</u>		<u>53</u>	<u>0.949</u>	<u>10.9 %</u>
present study	Axial Comp.+ Hydro. Press.	4	0.953	7.5 %
<u>Total (including all data)</u>		<u>57</u>	<u>0.950</u>	<u>10.6 %</u>
(excluding the data in ref.66)		<u>36</u>	<u>0.994</u>	<u>8.1 %</u>

5.4.2 Results of Correlation Study

The correlation study results are given in Table 5.1 which include non-dimensionalised geometric and material properties and extents and locations of damage as well as actual and predicted ultimate residual strengths and their ratios. A summary for the actual to predicted strength ratios using the proposed method is made in Table 5.2 and a plot of the ratios against the reduced column slenderness ratio  $\bar{\lambda}$  is provided in Fig.5.10. The actual to predicted ratios for the total of fifty seven test data give a 10.6 % COV together with a 0.950 mean. However, twenty one Trondheim test data give a much smaller mean than those of other sources, which is probably because the dent depth was measured relative to the upper generatrices of the undamaged part of the tube wall in which the measured value easily can be too small<sup>[71]</sup>. When excluding these data the COV and mean are improved to 8.1 % and 0.994 respectively.

Comparing these values with a 8.2 % COV and 0.992 mean obtained by analytical predictions<sup>[71]</sup> of forty four Trondheim test data (clamped tubes and tubes with D/t ratios above 80 were omitted) and an 11 % COV and 1.01 mean obtained using a nonlinear finite beam-column element computer program<sup>[116]</sup> for fifty seven test data in refs.65, 66, 67 and 69 (models with D/t ratios above 65 were excluded but undamaged models were included), it seems that the proposed theoretical method provides reasonably reliable and at the same time accurate estimates of residual strength for damaged tubulars. According to the COV and mean excluding the Trondheim test data, only one data , model D3 in ref.65, is on the unsafe side of the characteristic strength defined as mean minus 2 standard deviation, i.e.  $0.832 = 0.994 - 2 \times 0.081$  (see Fig.5.10).

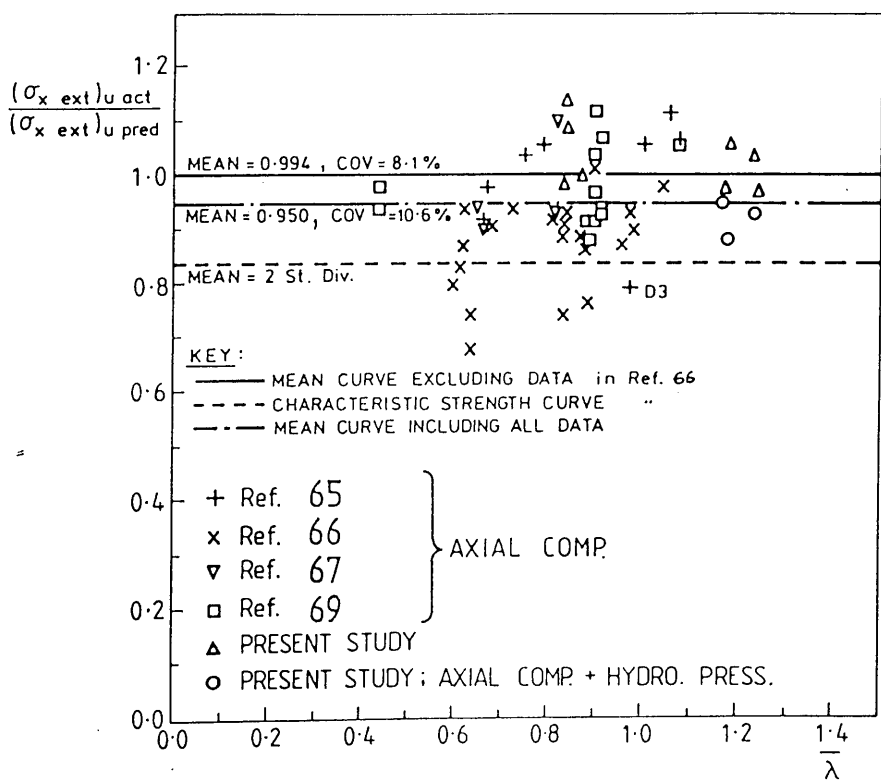


Fig. 5.10 Comparison of Actual to Predicted Strength Using Proposed Theoretical Method for Damaged Tubulars under Combined Axial Compression and Hydrostatic Pressure

5.4.3 Effect of Local Shell Deformation

The predictions considering the local shell deformation using eqn.(5.32) are compared with those obtained neglecting the local shell deformation and both are illustrated in Fig.5.11. As be seen in the figure when considering that effect in the analysis more accurate and reliable estimations have been achieved. Therefore, for thinner and deeply dented tubulars it seems necessary to consider the local shell deformation, which can be exhibited through growth of dent, in the analysis in order to safely estimate the residual strength of damaged tubulars.

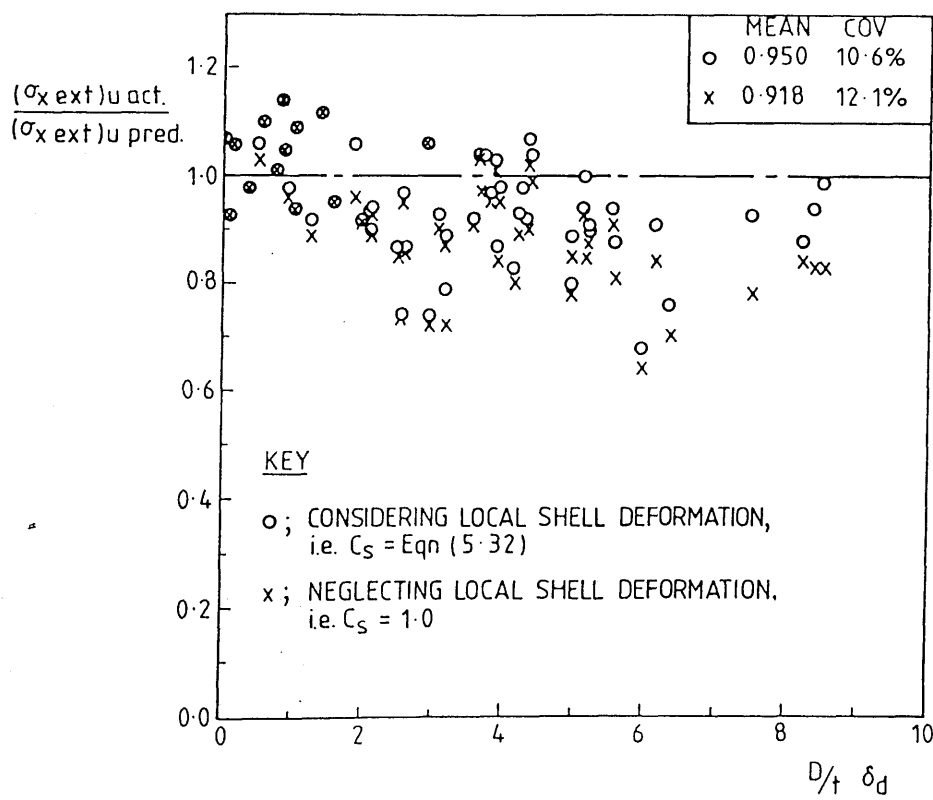


Fig. 5.11 Effect of Local Shell Deformation on Residual Strength of Damaged Tubulars under Combined Axial Compression and Hydrostatic Pressure

The proposed method may be applied to study the effects of various parameters affecting the residual strength of damaged tubular members. In this chapter, however, the results are included only of the parametric studies to investigate the effects of axial location of damage and of dent shape on the residual strength of damaged tubulars under combined axial compression and hydrostatic pressure. The results for other parameters are provided in chapter 6. Typical tubes of  $D/t = 40$ ,  $E/\sigma_Y = 600$ ,  $\lambda = 1.0$ ,  $\delta_d = 0.1$ ,  $\delta_o = 0.005$  were adopted and the ranges  $Q_H/Q_{Hcr} = 0.0-0.4$ ,  $x_d/L = 0.1-0.5$  and  $B/D = 0.0-2.0$  were chosen where  $x_d$  is the axial location of the dent centre (see Fig.5.12) and  $B$  is the length of the flattened part (see Fig.5.13). For the case of damage location  $B/D$  was assumed to be zero, i.e. sharp dent while for the effect of dent shape the damage location  $x_d/L$  to be 0.5, i.e. at midspan.

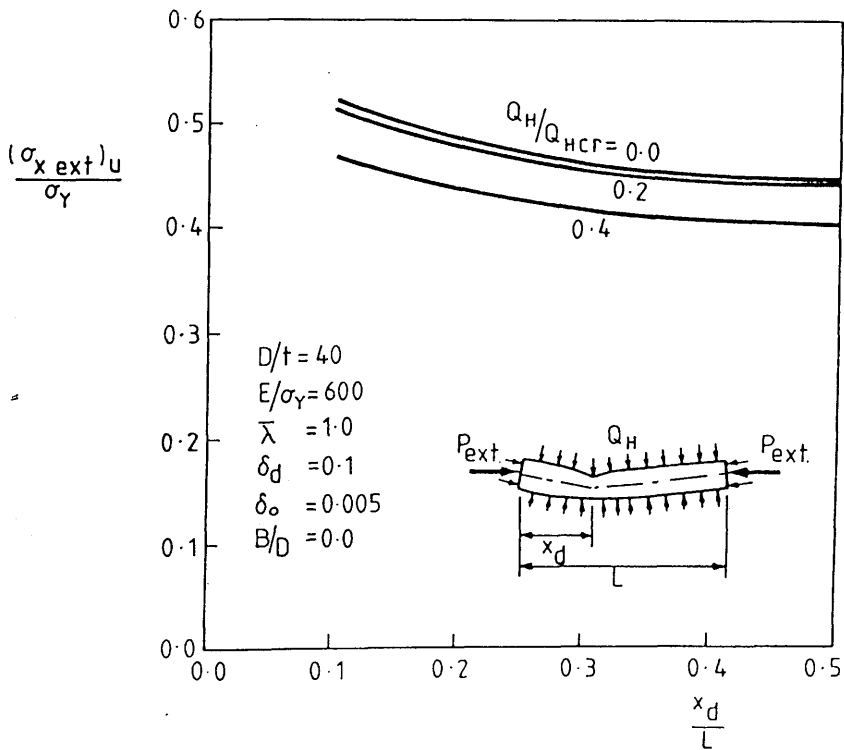


Fig. 5.12 Effect of Damage Location on Residual Strength of Damaged Tubulars under Combined Axial Compression and Hydrostatic Pressure

5.4.4 Effect of Damage Location

The results are illustrated in Fig.5.12 which shows the residual strength can be increased by some 8 % and 16 % when the damage location changes from  $x_d/L=0.5$ , midspan, to  $x_d/L=0.2$  and  $0.1$  respectively with negligible differences depending on hydrostatic pressure. These results are similar to those of the experimental findings in ref.69, that the increase in residual strength of damaged tubulars under axial compression can be expected to be about 8 % by moving the damage location from  $x_d/L=0.5$  to  $x_d/L=0.125$ . The figure also shows that the difference in the residual strength is insignificant if the centre of damage is in the middle half of the tube.

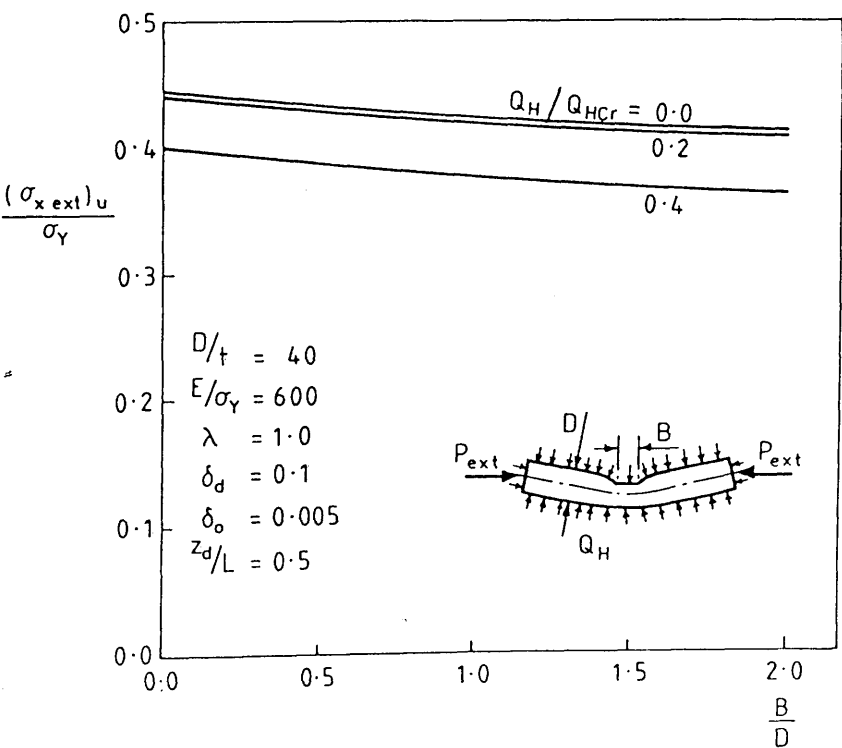


Fig. 5.13 Effect of Dent Shape on Residual Strength of Damaged Tubulars under Combined Axial Compression and Hydrostatic Pressure

#### 5.4.4.5 Effect of Dent Shape

For the parametric study to investigate the effect of dent shape on the residual strength of damaged tubulars subjected to combined axial compression and hydrostatic pressure the damaged part was divided into twenty segments and the results are shown in Fig.5.13. According to the figure when the length of flattened part B is twice of the diameter the reduction of strength upon that of sharp dent can be about 8 % for  $Q_H/Q_{Hcr} = 0.0$  and 0.2 and about 11 % for  $Q_H/Q_{Hcr} = 0.4$ . Unlike the case for damage location a little bit further decrease can be expected for higher hydrostatic pressure. For the case of  $Q_H/Q_{Hcr} = 0.0$ , i.e. under pure axial compression, the results confirm the conclusion in ref. 69 based on the comparison of the collapse strengths for R1A, R1B, R1C and R2A having different shapes of dent but dents of approximately equal depth, that the strength of these tubes differ by no more than 10%.

The strength reduction curves were derived by using the Perry-Robertson imperfection parameter  $A_{PR}$ . Even though it is not clear how to be achieved by either methods, more preference is given to the latter as it has more physical meaning and that the Perry factor  $Q$  (eqn(1)) was obtained by substituting as the value of failure and by considering the buckling stress as the value of the deflection [23]. The lower reduction factor is based on the latter stress.

$$Q = 1 + \frac{1}{2} \left( \frac{\sigma_{cr} - \sigma_y}{\sigma_y} \right)^2 \frac{A_{PR}}{V_{cr}}$$

where  $\sigma_y$  = yield stress

## Chapter 6

### DERIVATION OF DESIGN FORMULAE

#### 6.1 Introduction

Any Design formula can be developed analytically, empirically or numerically. The inherent weaknesses of all three methods were critically reviewed by Faulkner et.al.[117] A problem arising in experimental and numerical modellings is how to formulate the results obtained. However, the column formulas has been taken as the line of best fit to the scatter band of test results. For the SSRC[118] / API[75] / AISC[119] / BS 6235[78] column curves, this was achieved by a direct curve fit to the test data with the reduced column slenderness ratio  $\bar{\lambda}$  as a dependent variable whereas the ECCS[120] / DnV- OS[86] curves were derived by curve fitting the secondary term, i.e. the Perry-Robertson imperfection parameter  $\lambda_{PR}$ . Even though reasonably accurate estimations may be achieved by either methods, more preference can be given to the latter which expresses the physical meaning and thus may be called semi-empirical formula. The Perry formula, eqn.(6.1), was obtained by defining the first yield load as that of the failure and by considering the buckling strength of the column in determination of the deflection[121]. The lower root of the quadratic equation can be taken as the failure stress.

$$(\sigma_Y - \sigma_u) (\sigma_{cr} - \sigma_u) = \lambda_{PR} \sigma_{cr} \sigma_u \quad (6.1)$$

where  $\sigma_u$  : failure stress  
 $\sigma_{cr}$  : Euler column buckling strength  
 $\lambda_{PR}$  : Perry - Robertson 'imperfection' parameter



Another well-known semi-empirical column formula was proposed by Rankine[122] and for a particular case of the Rankine formula the failure load can be estimated using eqn.(6.2), a linear interaction between yielding and elastic buckling[123].

$$\frac{\sigma_u}{\sigma_Y} + \frac{\sigma_u}{\sigma_{cr}} = 1 \quad (6.2)$$

Generalised versions of the particular case of the Rankine formula, eqn.(6.2), have been proposed in aiming to improve its prediction accuracy and to broaden its applicability by including other failure mode of the column and by extending to other types of structures. Initially generalisation of eqn.(6.2) was proposed by Merchant[124] and its more versatile version, eqn.(6.3), was given by Allen[125] to consider the interaction between overall and local buckling.

$$\left(\frac{\sigma_u}{\sigma_Y}\right)^n + \left(\frac{\sigma_u}{\sigma_{cr}}\right)^n + \left(\frac{\sigma_u}{\sigma_{crL}}\right)^n = 1 \quad (6.3)$$

where,     n   : imperfection index  
                $\sigma_{crL}$  : local elastic buckling stress

Odland and Faulkner[126] generalised eqn.(6.2) to take into account multiple loads for thin shell structures by assuming a linear interaction between each elastic buckling mode and a quadratic interaction between yielding and elastic buckling. For the case of two dimensional biaxial stress the generalised interaction equation is given as

$$\left(\frac{\sigma_{x0}}{\rho_x \sigma_{xcr}} + \frac{\sigma_{\theta 0}}{\rho_\theta \sigma_{\theta cr}}\right)^2 + \left(\frac{\sigma_e}{\sigma_Y}\right)^2 = 1 \quad (6.4)$$

where

$$\begin{aligned}\sigma_{x0} &= -\sigma_x && ; \sigma_x < 0 \\ &= 0 && ; \sigma_x \geq 0 \\ \sigma_{\theta 0} &= -\sigma_\theta && ; \sigma_\theta < 0 \\ &= 0 && ; \sigma_\theta \geq 0 \\ \sigma_e &: \text{von Mises equivalent stress, } \sqrt{\sigma_x^2 - \sigma_x \sigma_\theta + \sigma_\theta^2} \\ \rho_x, \rho_\theta &: \text{knockdown factors}\end{aligned}$$

It must be noted that in eqn.(6.4) the elastic buckling strengths for actual structure are introduced by multiplying the knockdown factors to the elastic buckling strengths of ideal structure and tensile stresses which are not destabilising are included by assuming any non-compressive direct stress to be zero when it appeared in the buckling interaction part of the formulation. An application of eqn.(6.4) to shell interframe collapse in ring-stiffened cylinders was made and reported in refs. 127 and 128 and its extract is given in Appendix 3.

However, in the direct interpretation of column test results, the inevitable experimental errors due to unavoidable eccentricity of applied load and end frictional resistance of the normally employed spherical end blocks can be transferred in the column formula. This shortcoming can be eliminated for the cases of analytical or numerical models. Therefore, in this study a rigorous parametric study was first carried out using the proposed theoretical method to estimate the residual strength of damaged tubulars under combined axial compression and radial pressure, which was validated with the available test data. And then a design formula was derived based on the parametric study results where the Perry formula was adopted as a basis of the formulation. While for the design equations to predict the possible extent of damage of unstiffened tubulars subjected to lateral impacts, a direct fit was attempted to the parametric study results obtained using the numerical procedure described in chapter 3.

## 6.2 Extent of Damage due to Lateral Impact

### 6.2.1 Parametric Study

Following the step by step procedure described in section 3.4 to trace the dynamic behaviour of unstiffened tubulars having simply supported roller conditions subjected to lateral impacts from a rigid striker having a knife edge, parametric studies were conducted. Computations were performed for the following values of geometric and material property parameters and speed and mass of the striker.

$$D/t = 20, 40, 60$$

$$L/D = 15, 25$$

$$E/\sigma_Y = 600$$

$$V_i = 0.5, 1.0, 1.5, 2.0 \text{ m/s}$$

$$M_s = 25, 50, 75, 100 \text{ Kg}$$

The ranges of the non-dimensional basic parameters resulted from the values given above are

$$R_k = 2.73 - 30.44$$

$$R_E = 0.045 - 8.62$$

$$R_v = 0.0026 - 0.0465$$

$$R_m = 13.1 - 261.2$$

For a total of ninety six cases, local denting damage ( $\delta_{df}$ ), overall bending damage ( $\delta_{of}$ ), maximum spring forces ( $F_{sdm}$  and  $F_{sbm}$ ) and plastically dissipated energy ( $E_D$ ) and its components ( $E_{Dd}$  and  $E_{Db}$ ) were obtained as the results of the parametric studies.

### 6.2.2 Design Equations

Plastically Dissipated Energy ( $E_D$ ) : After surveying the trends of the basic parameter  $R_k$ ,  $R_E$ ,  $R_v$  and  $R_m$  with  $E_D/E_k$ , and examining the variability of the parametric study results for  $E_D/E_k$  using various combinations of the basic parameters as variables the most suitable variable ( $X_{E_D}$ ) was selected and the corresponding

coefficient was then obtained by best fitting to the parametric study results. The equation finally obtained is

$$E_D/E_k = \begin{cases} 0 & ; X_{ED} \leq 0.34 \\ 4.91 (\log X_{ED} + 0.469)^2 & ; 0.34 < X_{ED} < 0.96 \\ 1 & ; X_{ED} \geq 0.96 \end{cases} \tag{6.5}$$

where  $X_{ED} = R_k^{-0.07} R_E^{0.02} R_V^{0.3} R_m^{0.35}$

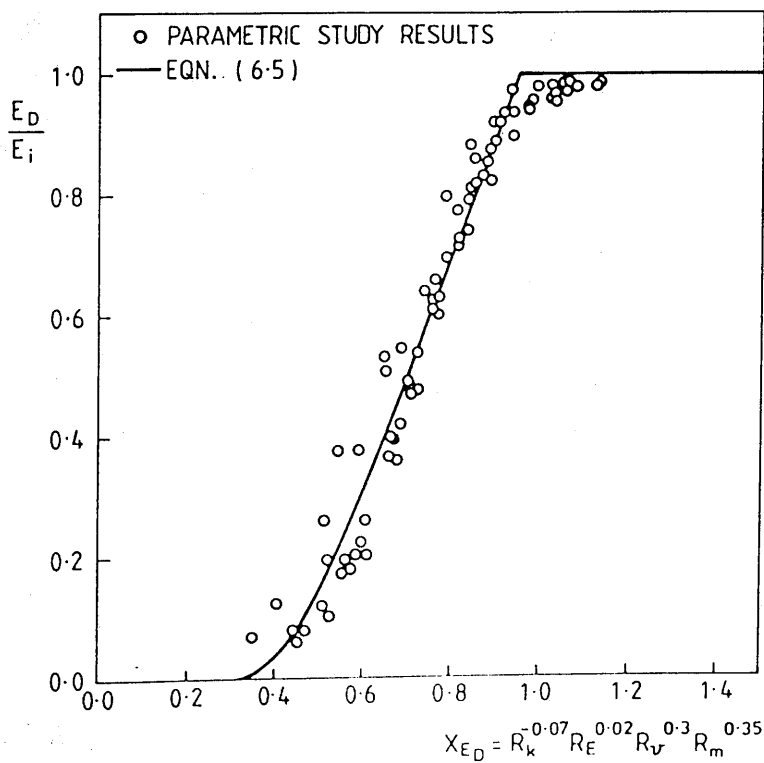


Fig. 6.1 Equation for  $E_D$  as Derived from Parametric Study Results

In Fig.6.1 eqn.(6.5) is illustrated together with the parametric study results. As can be seen in the figure a reasonably accurate estimation of the plastically dissipated energy can be obtained using eqn.(6.5). The rebound velocity of the striker can approximately be estimated from eqn.(6.6).

$$V_r = \sqrt{2(E_k - E_D)/M_s} \quad (6.6)$$

· Maximum Lateral Load ( $F_{sm}$ ) : The maximum lateral load arising during the impact was defined the average of  $F_{sdm}$  and  $F_{sbm}$ . Following the same procedure for the case of  $E_D/E_k$  the equation obtained for  $F_{sm}$  is

$$F_{sm}/(4 M_p/L) = 0.26 R_k^{0.5} R_E^{0.5} R_V^{-0.1} \quad (6.7)$$

· Local Denting Damage ( $\delta_{df}$ ) : Having determined the maximum lateral load  $F_{max}$ , the local denting damage can be calculated using eqns.(3.25a) and (3.25b). The energy dissipated due to local denting damage  $E_{Dd}$  can also be obtained by integrating these equations. The equations obtained for  $\delta_{df}$  and  $E_{Dd}$  are as follows.

$$\delta_{df} = 0.16 \frac{F_{sm}}{m_p (E/\sigma_Y)} \left\{ \frac{F_{sm}}{m_p (D/t)^{0.4}} - 1.25 \right\} \quad (6.8)$$

$$E_{Dd} = 0.107 \frac{F_{sm}^2 D}{m_p (E/\sigma_Y)} \left\{ \frac{F_{sm}}{m_p (D/t)^{0.4}} - 0.563 \right\} \quad (6.9)$$

· Overall Bending Damage ( $\delta_{df}$ ) : The energy dissipated due to overall bending damage  $E_{Db}$  can be determined from eqn.(6.10) and then the overall bending damage  $\delta_{of}$  can be calculated using eqn.(6.11) which relationship was obtained by curve fitting the parametric study results.

$$E_{D_b} = E_D - E_{D_d} \quad (6.10)$$

$$\delta_{of} = \frac{1}{4} \frac{E_{D_b}}{M_p} R_k^{-0.1} R_E^{-0.7} R_v^{0.5} R_m^{0.6} \quad (6.11)$$

### 6.3 Residual Strength of Damaged Tubulars

#### 6.3.1 Parametric Study

Using the developed method described in section 5.3 a rigorous parametric study has been performed to calculate the residual strengths of the damaged tubulars under pure axial compression and under combined axial compression and hydrostatic pressure for the following values of parameters. In the calculation  $E/\sigma_Y$  was assumed to be 600.

- for pure axial compression loading;

$$D/t = 20, 40, 60$$

$$\bar{\lambda} = 0.25, 0.50, 0.75, 1.00, 1.25, 1.50$$

$$\delta_d = 0.0, 0.01, 0.05, 0.10, 0.15$$

$$\delta_o = 0.0005, 0.001, 0.005, 0.01, 0.02$$

- for combined axial compression and hydrostatic pressure loading;

$$D/t = 20, 40, 60$$

$$\bar{\lambda} = 0.50, 0.75, 1.00, 1.25$$

$$\delta_d = 0.0, 0.01, 0.05, 0.10, 0.15$$

$$\delta_o = 0.0005, 0.001, 0.005, 0.01, 0.02$$

$$Q_H/Q_{Hcr} = 0.1, 0.2, 0.3$$

#### 6.3.2 Design Formula

The Perry formula, eqn.(6.1), is adopted as the basis of the proposed design equation to predict the residual strength of damaged tubulars under combined axial compression and hydrostatic pressure. Using the parametric study results for a total of 1350 cases, among them 450 cases were under axial compression and 900 cases were under combined axial compression and hydrostatic pressure, the Perry - Robertson

'imperfection' parameter  $\lambda_{PR}$  were evaluated by rearranging eqn.(6.1) as follows

$$\lambda_{PR} = \frac{(\sigma_Y - \sigma_u)(\sigma_{cr} - \sigma_u)}{\sigma_{cr} \sigma_u} \quad (6.12)$$

For the cases of combined loading  $(\sigma_{x \text{ ext}})_u$  were used for  $\sigma_u$ . Before deriving an expression for  $\lambda_{PR}$ , it was assumed that  $\lambda_{PR}$  consists of three parts namely

$$\lambda_{PR} = \lambda_{PRO} \lambda_{PRL} \lambda_{PRH} \quad (6.13)$$

where  $\lambda_{PRO}$  : overall straightness imperfection parameter  
 $\lambda_{PRL}$  : equivalent imperfection parameter for local denting  
 $\lambda_{PRH}$  : equivalent imperfection parameter for hydrostatic pressure

Using the values of  $\lambda_{PR}$  calculated from the parametric study results for pure axial compression, the expressions for  $\lambda_{PRO}$  and  $\lambda_{PRL}$  were determined and then the results of combined loading were used for the case of  $\lambda_{PRH}$ . The equations finally derived are as follows

$$\lambda_{PRO} = 22.2 (\delta_o \bar{\lambda})^{0.7} \quad (6.14)$$

$$\lambda_{PRL} = 1.0 + 1.26 \delta_d^{1.3} (D/t)^{0.6} \quad (6.15)$$

$$\lambda_{PRH} = \exp[0.025 (Q_H/Q_{Hcr})^2 \bar{\lambda}^{0.5} (D/t)^{-0.5} \delta_o^{-1}] \quad (6.16)$$

Having derived the expression for  $\lambda_{PR}$ , eqn.(6.13) together with eqns.(6.14), (6.15) and (6.16), the residual strength of damaged tubulars under combined axial compression and hydrostatic pressure can be estimated using eqn.(6.17) which is the lower root of eqn.(6.1).

$$\sigma_u = \frac{\sigma_Y + (1 + \lambda_{PR}) \sigma_{cr}}{2} - \sqrt{\left\{ \frac{\sigma_Y + (1 + \lambda_{PR}) \sigma_{cr}}{2} \right\}^2 - \sigma_{cr} \sigma_Y} \quad (6.17)$$

## 6.4 Discussion

### 6.4.1 Extent of Damage

#### 6.4.1.1 Proposed Equations

Using the parametric study results the simple equations, eqns.(6.8) and (6.11) have been derived to predict the local denting and overall bending damage to unstiffened tubulars having simply supported boundaries subjected to lateral impacts from rigid strikers having knife edge. The equations are also provided to estimate the maximum lateral load arising during impact as well as the energy dissipated plastically and its components, i.e. the energy dissipated due to local denting and overall bending damage. The predictions using the proposed equations, eqns.(6.8) and (6.11), for the fourteen cases of the lateral impact tests, whose extents of damage exceeded the tolerance specifications given in ref.86, provide a 27.0 % COV with a mean of 1.15 and a 30.9 % COV with a mean of 1.11 for local denting and overall bending damage respectively. These COVs are a bit higher than those of the theory i.e. 20.9 % and 25.3 % for local denting and overall bending damage respectively(see section 3.5). However, comparing with the predictions by the existing formulae (see Fig.2.12) it seem that the equations can provide useful estimations for plastically dissipated energy, maximum lateral load and extent of damage.

#### 6.4.1.2 Boundary Conditions

The end conditions for the unstiffened members of offshore structures are, of course, different from the simply supported roller end conditions which were simulated in the tests and assumed in the theoretical computations. In offshore structures, there rotational and axial restraints which are likely to generate damage at the ends in the form of yielding, fracture and possible local buckling.

Furthermore, for the case of fixed platforms the effect of the lateral deflection of the whole structures, probably elastic, on the dynamic response may be significant and for the case of floating platforms the lateral movement of the structure can increase the impact duration and consequently the lateral force during impact may be reduced. Naturally, interaction with the surrounding water will also alter the dynamic response



and therefore the pattern of energy absorption and type of damage generated. Also, the rigid knife edge of the striker may generate more detrimental types of damage in the models than might occur in the case of an encounter by an attendant vessel.

#### 6.4.1.3 Size Effect

In addition to end conditions discussed above, the size of the model may be another factor to alter the dynamic response and therefore the extent of damage. If a structural member of a full scale offshore installation and a scaled down model whose scale factor is  $\lambda$  (which is greater than unity) are made from the same material, for this case mild steel, it is recommended in ref. 27 and 129 to conduct model tests at the same characteristic velocity (e.g. speed of the striker) in order to hold the non-dimensionalised parameter  $V_i/c$  same for both the full scale structure and a model, where  $c$  is the wave propagation speed  $\sqrt{E/\rho}$ . Then a characteristic, non-dimensionalised strain rate in the model is  $\lambda$  times larger than the corresponding value in the full scale structure[27] and consequently the extent of damage to the full scale structure may be larger than that to the scaled down model[130]. Therefore, for a strain rate sensitive material, strict geometric scaling and equality of the characteristic velocity makes it impossible to properly scale strain rate effects.

#### 6.4.1.4 Application Limit

As discussed above, strictly speaking, the proposed equations can provide results reliable only for the cases whose boundaries are simply supported and roller ended and whose size is the same as the test models. The ranges of mass ratio  $R_m$  considered in this study are much smaller than those of actual collisions between supply vessels and offshore installations. According to an offshore collision case study[12], the elastic strain energy stored in the whole platform is greater than that absorbed by the struck elements. However, the extents of damage generated in the lateral impact tests and in the parametric study are in the range of those relevant to offshore collisions. Therefore, it seem possible to draw a conclusion that the mass of striker cannot be increased beyond the range considered in this study, which virtually leads to the collapse of the model, without proper simulation of the lateral movement restraints at

both ends. In other words, the mass ratio  $R_m$  in the tests on an isolated member having simply supported or fixed boundaries cannot be the same of the case of a structural member of the structural system in order to generate same level of extent of damage.

Therefore, it is premature to expect the results of the present study to be directly applicable to the design of offshore structures. However, by modification of the proposed equations to take account of the differences attributable to the end conditions, the size effect, the shape of the impactor and fluid-interaction, the above could form the basis of a procedure for the economic design of offshore structure members against impacts and collisions.

## 6.4.2 Residual Strength

### 6.4.2.1 Proposed Formula

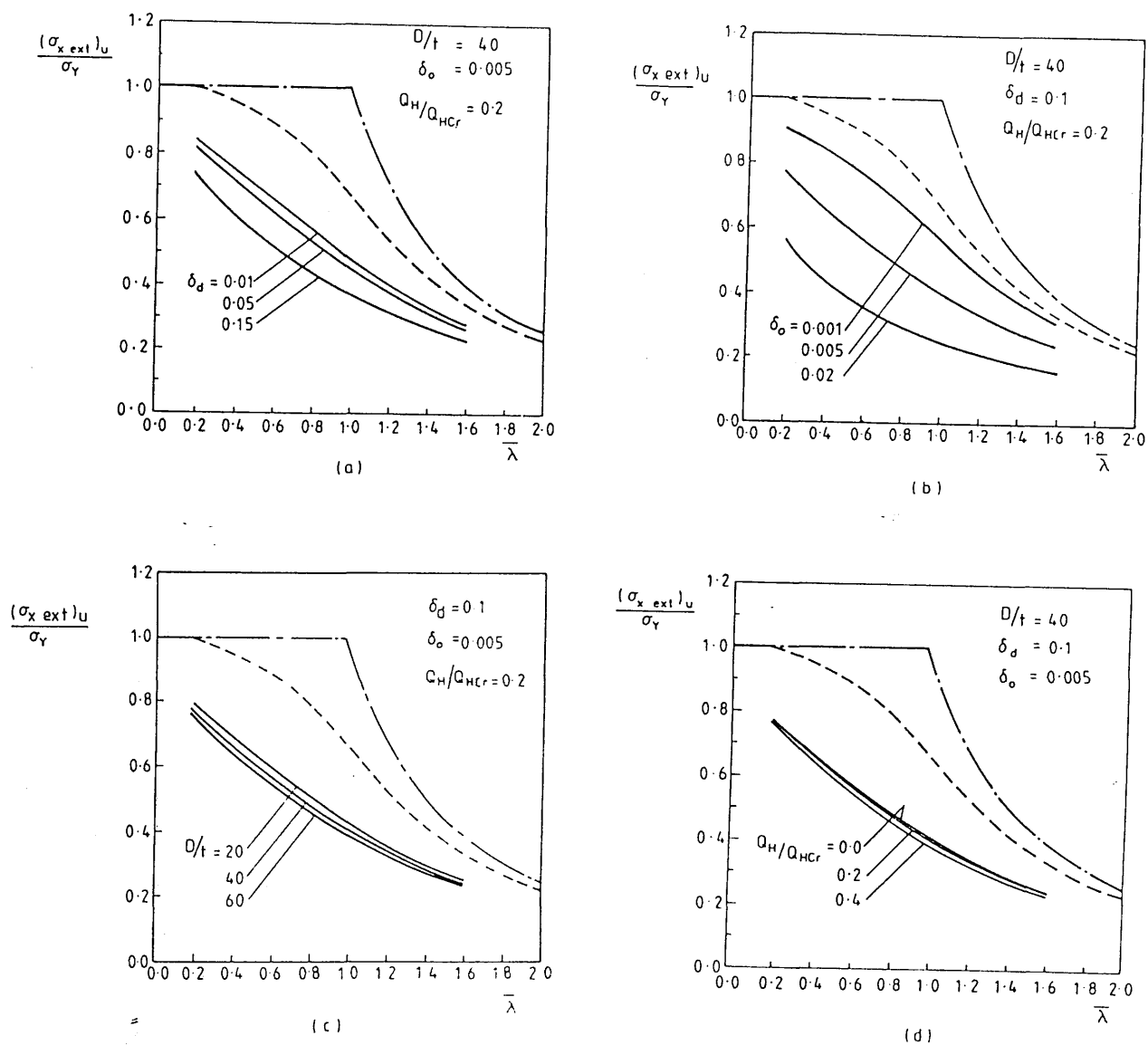
Adopting the Perry formula as the basis and deriving the Perry-Robertson 'imperfection' parameter  $\lambda_{PR}$  from a best-fit to the parametric study results the simple design formula, eqn.(6.17) together with eqns.(6.13)-(6.16), has been obtained to predict the residual strength of simply supported damaged tubulars having a sharp dent at mid-length under combined axial compression and hydrostatic pressure. It must be noted here that the non-dimensionalised out-of-straightness  $\delta_0$  in the formula is that of the plastic neutral axis. Therefore if the measured  $\delta_0$  is that of the generatrix opposite to dent a correction must be made to the  $\delta_0$  especially for the cases of deep dent, where eqn.(2.8) can be used. The correlation of the available test results with predictions using the proposed formula is summarised in Table 6.1. In comparison with the prediction accuracy of the theory, i.e. 10.6 % COV for all of the available test results and 8.1 % excluding the results given in ref.66 (see Table 5.2), the accuracy of the predictions using the proposed formula is found to be a little bit worse. Despite the fact that the location of damage and shape of dent were not considered in the calculation, the accuracy of the predictions, however, is in the range accepted as a well formulated one for static structural problems, say less than 13 % [117].

Table 6.1 Correlation of Test Results with Predictions

Using Proposed Formula

ref.	Loading Type	Number of Tests	Actual to Predicted Strength Ratio	
			Mean	COV
[65]	Axial Comp.	8	0.994	13.5 %
[66]	ditto	21	0.891	11.6 %
[67]	ditto	4	1.016	13.0 %
[69]	ditto	12	1.010	7.7 %
present study	ditto	8	1.129	4.8 %
sub total (Axial Comp.)		53	0.978	13.0 %
present study	Axial Comp.+ Hydro. Press.	4	1.055	8.0 %
Total (including all data)		57	0.983	12.8 %
(excluding the data in ref.66)		36	1.037	10.1 %

As mentioned earlier, in the parametric study the dent centre was assumed to be at mid-length of the tube and the shape of dent 'sharp'. Therefore, if the dent centre is off the mid-length and/or the dent shape has a flattened part a correction needs to be made to the predictions using the proposed formula. Even though the effect of those factors on the residual strength is comparatively insignificant (see sections 5.4.3 and 5.4.4), but the effect of dent shape is in unsafe side while the opposite is true for that of dent location.



- Column Strength Curve for 'Perfect' Tube
- .-.-.-.- DnV Column Strength Curve 'a'
- Proposed Formula, eqn.(6.17) together with eqns.(6.13)-(6.16)

**Fig. 6.2 Influences of Parameters on Residual Strength of Damaged Tubulars**  
under Combined Axial Compression and Hydrostatic Pressure :  
(a) Depth-of-Dent ( $\delta_d$ ), (b) Out-of-Straightness, (c) Diameter to  
Thickness Ratio ( $D/t$ ), (d) Hydrostatic Pressure ( $Q_H/Q_{HCr}$ )

The influences of extent of damage, depth of dent ( $\delta_d$ ) and out-of-straightness ( $\delta_o$ ), diameter to thickness ratio ( $D/t$ ) and hydrostatic pressure ( $Q_H/Q_{Hcr}$ ) on the residual strength of simply supported damaged tubulars having a 'sharp' dent at mid-length under combined axial compression and hydrostatic pressure are demonstrated in Figs.6.2(a)-(d). The influence of extent of damage on the residual strength is most significant, while that of hydrostatic pressure is negligible when  $Q_H/Q_{Hcr} = 0.2$  (which is corresponding to approximately 150 m water depth) and when  $Q_H/Q_{Hcr} = 0.4$  (which is corresponding to approximately 300 m water depth) the loss of strength due to hydrostatic pressure is at most about 7 % for a damaged tube of  $\delta_d = 0.1$ ,  $\delta_o = 0.005$  and  $D/t = 40$ .

#### 6.4.2.2 End Conditions

The proposed formula is based on the parametric study results of damaged tubulars having simply supported boundaries. Obviously, the end restraint of offshore unstiffened tubulars is different from that of simply supported. However, for undamaged tubular columns the effect of the end conditions is normally accounted for by means of the effective length concept. But direct application of the effective length approach for undamaged tubulars to damaged ones gives conservative results especially for severely damaged cases[72,116]. On top of that in the case of bracing members supported by chords the end restraint may be influenced not only by the flexural rigidities of chord members but also by local flexibility of chord walls[131]. Therefore in order to improve the prediction accuracy it seems necessary to modify the effective length calculated for the corresponding undamaged tubulars in which the local flexibility of chord walls is also considered.

#### 6.4.2.3 Effects of Residual Stresses due to Cold-Rolling and Welding

Offshore tubular members are generally formed by cold-rolling and welding of flat plates and the residual stresses due to the such fabrication can affect their strength, which are not considered in the present study. The effects of these residual stresses on the load carrying capacity of tubulars were theoretically investigated by Smith et. al.[65] and the results show that the loss of column strength due to cold-rolling and

welding residual stresses are less than 10 % each. An experimental study[67] was conducted with two full-scale damaged models (models E2 and F2) obtained from the dismantled BP West Sole Platform and two corresponding small-scale models (models E2S and F2S) prepared from cold-drawn seamless tubes and heat-treated. Despite differences in the manufacturing process and inevitable slight differences in damage conditions, satisfactory correlation was obtained between large and small-scale tests, which may suggest the effects of these residual stresses on the load carrying capacity of damaged tubulars may be insignificant. Therefore, it seems possible to take into account these effect by reducing the yield stress by 5 % [86].

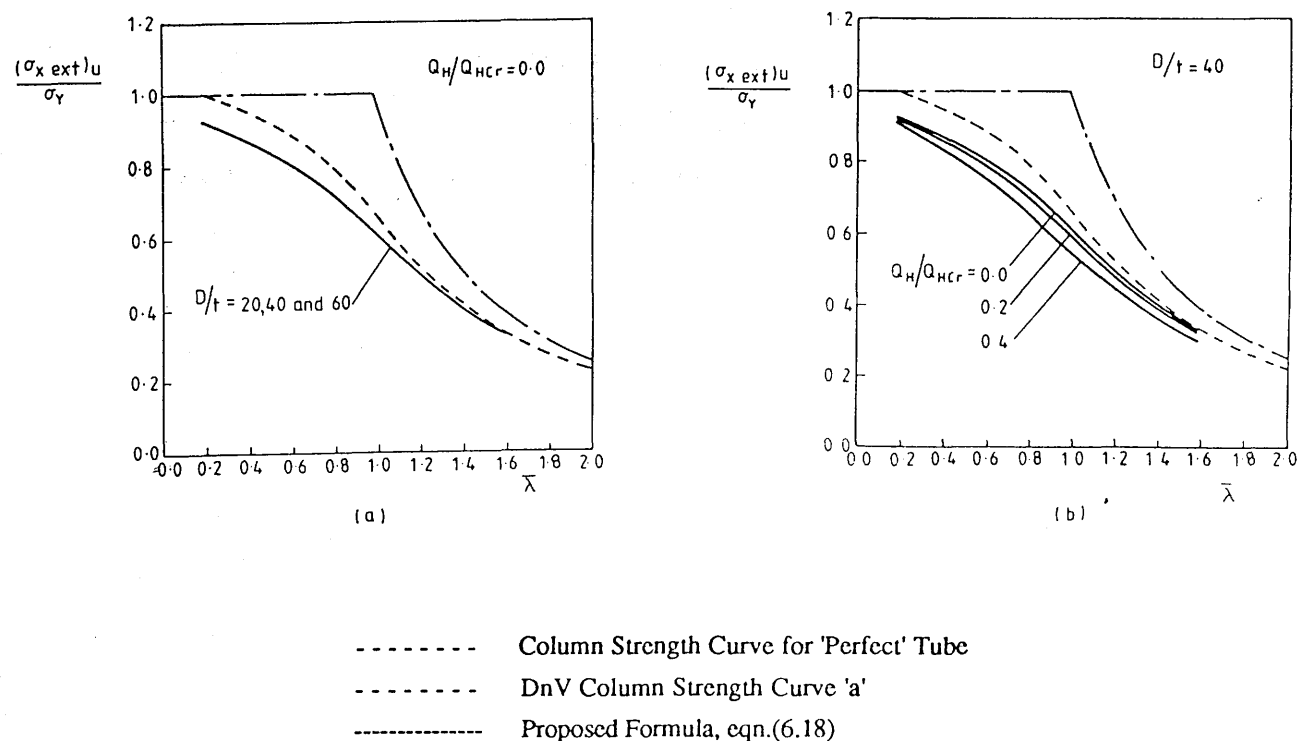


**Fig. 6.3 Influences of Parameters on Residual Strength of Damaged Tubulars,**  
**Having Equivalent Extent of Damage to DnV Shape Imperfection Tolerance**  
**Limit for Undamaged Tubulars, under Combined Axial Compression and**  
**Hydrostatic Pressure :**(a) **Diameter to Thickness Ratio (D/t),**  
(b) **Hydrostatic Pressure ( $Q_H/Q_{Hcr}$ )**

#### 6.4.2.4 Ultimate Strength of Undamaged Tubulars

The shape imperfection, initial out-of-straightness and ovality, of undamaged tubulars is different from that due to damage. However, it might be interesting to consider undamaged tubulars having such shape imperfection as one extreme of damaged ones. In the DnV-OS Rules[86], the initial shape imperfection tolerances are specified as 0.01 and 0.0015 for ovality ( $[D_{\max} - D_{\min}]/D_{\text{mean}}$ ) and out-of-straightness respectively. Using eqn.(2.7), the limit of initial ovality, 0.01, can be interpreted as an equivalent dent depth parameter of 0.008. By substituting  $\delta_d = 0.008$  and  $\delta_o = 0.0015$ , eqn.(6.13) can be rewritten as follow:

$$\lambda_{\text{PR}} = 0.234 \bar{\lambda}^{0.7} \{1.0 + 0.00237(D/t)^{0.6}\} \exp\{16.7(Q_H/Q_{H\text{Cr}})^2 \bar{\lambda}^{0.5} (D/t)^{-0.5}\} \quad (6.18)$$

The ultimate strength of undamaged tubulars can be estimated by substituting eqn.(6.18) into eqn.(6.17). The ultimate strengths obtained using these equations are illustrated in Figs.6.3(a), (b). When  $Q_H/Q_{H\text{Cr}} = 0.0$ , i.e. under pure axial compression, the effect of  $D/t$  ratio is negligible and for stocky and intermediate columns the equations predict much lower strengths than the DnV curve 'a'. It seems further investigation is needed to conclude whether that is simply because of the difference in shape imperfection and of the material strain hardening which is not considered in the derivation of the equations or because of optimism in the relevant rule. The influence of hydrostatic pressure on the ultimate strength of undamaged tubulars, for this case of very slightly damaged tubulars, are a little bit more significant than for severely damaged tubulars (see Fig.6.2d).

## Chapter 7

# CONCLUSIONS AND PROPOSALS FOR FUTURE WORK

### 7.1 Conclusions

Existing models and methods were reviewed for predicting the probability of offshore collisions and consequential probable extents of damage, and for evaluating the residual strength of damaged members. As an outcome of this part of the work the following shortcomings were identified for fuller treatment before more efficient design of offshore structures against collisions can results :

- a) It has been found that the static plastic approach for dealing with collision mechanics, in which the motion and vibration of the impacting bodies and the elastic deformation of the whole structure are commonly neglected, can lead to an excessive conservatism at least for some cases, and that it is necessary to keep collision records as detailed as possible so that any proposed simplified dynamic approach can be validated and the conservatism in the static approach can be assessed ;
- b) no lateral impact tests on tubular members have been reported in the literature so far, with whose results existing theoretical methods to estimate the energy absorption capacity of tubular members can be compared ;
- c) reasonably accurate predictions for the strength of axially compressed damaged tubulars can be obtained using the existing methods. However, no research work on the structural behaviour of damaged tubulars under combined loadings including



hydrostatic pressure have been reported in the literature ; and

- d) no specific guidance is available in the relevant offshore codes on estimating the resistance of offshore structures against impact loads and the consequential damage, and on methods to evaluate the residual strength of damaged members or structures.

#### Dynamic Response of a Tubular Member under Lateral Impact

Twenty four lateral impact tests have successfully been conducted on stress-relieved cold drawn seamless tubes having simply supported roller end conditions. The experience gained from preparing the models and performing the experiments and the results obtained led to the following observations :

- a) In heat-treatments conducted to reduce the yield strength of cold-formed material by removing the work-hardening effect, the warming-up rate is another important factor to achieve the purpose in addition to the heating temperature and holding time ;
- b) from the geometry of the damaged tubes simple empirical equations, eqns.(2.7)-(2.12), have been derived to realistically describe the geometric configuration of damaged tubulars ;
- c) the dynamic response of a tubular member under lateral impact may be divided into three stages, namely,
  - stage 1 ; elastic-plastic deformation
  - stage 2 ; elastic spring-back
  - stage 3 ; free elastic vibrationwhere for the case of very low energy impact the elastic-plastic deformation stage can be replaced by a pure elastic one ;
- d) in the elastic-plastic stage of the impact tests a purely local denting deformation occurred before overall bending together with additional local denting. This is

different from the static deformation history of the tubes, whose length to diameter ratios are in the same range, but rather similar to those of much shorter tubes under static load ;

- e) for the behaviour of tubular members subjected to low velocity impacts considered in this study, the influence of localised bending on the gross structural response may be negligible but the higher mode effect substantiated by the reverse curvature in the vicinity of supports may play a role for the flexural behaviour of the tubular members, especially in the early stage ; and
- f) a comparison between the predicted extents of damage using the existing formulae and the test results showed lack of consistency and excessive pessimism in the existing formulae especially for the small extents of damage where the detrimental effect of damage on the residual strength of the damaged tubes is most sensitive. For the larger extents of damage of interest, however, very rough upper bounds for the extent of damage can be obtained using the existing formulae.

A simple numerical model has been developed to simulate the dynamic response of a tubular member having simply supported roller end conditions. In the model the tubular member is reduced to a spring-mass system with two degrees-of-freedom, one for overall bending deformation and the other for local denting deformation. The characteristics of the impact history curves obtained using the developed model have shown that :

- a) Purely local denting deformation is followed by overall bending together with additional local denting, which is similar to that of the experiments ;
- b) in the purely local denting phase very high acceleration is imposed on the equivalent mass for overall bending,  $m_2$ , probably due to high local denting stiffness, which consequently develops the velocity of  $m_2$  greater than the initial impact velocity ; and

- c) maximum spring force occurring during impact can far surpass the maximum static lateral load,  $4M_p/L$ , and despite the fact that dynamic force equilibrium only is retained in the formulation, energy conservation has been achieved throughout the procedure with a negligible violation in the purely local denting phase.

A comparison between the numerical model and the experimental results showed that :

- a) The predictions for fourteen cases, whose extents of damage exceeded the tolerance specifications given in the DnV-OS Rules[86], provide a 20.9 % COV with a mean of 1.080 and a 25.3 % COV with a mean of 0.993 for local denting damage and overall bending damage respectively, where the COVs are somewhat higher than those of static structural problems. However, considering the complexity of the dynamic problem and the computing efficiency the usefulness of the proposed model can be justified ; and
- b) a shortcoming of the proposed model is the underestimation of both impact durations,  $T_D$ , and peak bending deformations,  $d_{opk}$ , for the higher values of  $R_k$   $R_E$   $R_v$   $R_m$ , which seems to be improved by consideration of overall bending damage in the derivation of the spring coefficient for denting deformation.

#### Residual Strength of Damaged Tubulars under Combined Loading

Four combined axial compression and hydrostatic pressure loading tests have been conducted on damaged tubes. Besides these combined loading tests, pure axial compression tests were also conducted on five undamaged tubes and eight damaged ones. The following conclusions are drawn from the experience obtained in performing the experiments and from the experimental results :

- a) It is necessary to develop a technique to accurately measure the effective length of a tubular column for a meaningful interpretation of its test results ;

- b) the effect of hydrostatic pressure on the behaviour of the damaged models before their ultimate state was not apparent but the parallel shifting (see Figs.4.6 and 4.7) of the axial strain-external axial compression curves ; and
- c) the cross-sectional shape of the collapsed models under pure axial compression showed no recognisable change other than the deepening of dent depth, whereas those under combined loading showed apparent turning of the flattened segments in the dent side into concave ones. This was noticed especially for the thinner models where the whole dented sections can turn into peanut shell-like shapes (see Fig.4.14).

An analytical method has been developed to estimate the residual strength of damaged tubular members under combined axial compression and hydrostatic pressure, in which the damaged tubular member is treated as a beam-column having varying cross-sections and residual stresses. Using the developed method a correlation study with available test data and parametric studies have been performed. With reference to the results obtained from these studies the following conclusions can be made :

- a) The actual to predicted residual strength ratios for a total of fifty seven test data available gives a 10.6 % COV together with a 0.950 mean. When excluding twenty one Trondheim test data the COV and mean are improved to 8.1 % and 0.994 respectively. It seems that the proposed theoretical method provides reasonably reliable and at the same time accurate estimates of residual strength for damaged tubulars ;
- b) for thinner and deeply dented tubulars it is necessary to consider the local shell deformation in the analysis in order to safely estimate the residual strength of damaged tubulars ;
- c) the influence of the extent of damage on the residual strength is most significant, while that of hydrostatic pressure is insignificant. A 7 % reduction in residual

strength can be expected due to hydrostatic pressure of  $Q_H/Q_{HCr} = 0.4$  for a tube, whose  $\delta_d = 0.1$ ,  $\delta_o = 0.005$  and  $D/t = 40$ .

- d) the residual strength of a damaged tubular, whose  $D/t = 40$ ,  $\lambda = 1.0$ ,  $\delta_d = 0.1$  and  $\delta_o = 0.005$ , can be increased by some 8 % and 16 % when the damage location changes from  $x_d/L = 0.5$ , midspan, to  $x_d/L = 0.2$  and  $0.1$  respectively with negligible differences arising from hydrostatic pressure, but the change of the residual strength is insignificant if the centre of damage is in the middle half of the tube ; and
- e) for a damaged tubular, whose  $D/t = 40$ ,  $\lambda = 1.0$ ,  $\delta_d = 0.1$ ,  $\delta_o = 0.005$  and where the length of flattened part B is twice the diameter, the reduction of the residual strength can be about 8 % for  $Q_H/Q_{HCr} = 0.0$  and  $0.2$  and about 11 % for  $Q_H/Q_{HCr} = 0.4$  when compared with that for the sharp dented model. Unlike the case for damage location a little more decrease can be expected for higher hydrostatic pressure.

### Design Formulae

Rigorous parametric studies were first carried out using the proposed methods, and then a direct fit was attempted to the parametric study results for deriving design equations to predict the possible extent of damage of unstiffened tubulars subjected to lateral impacts. The following conclusions are drawn :

- a) Plastically dissipated energy,  $E_D$ , maximum lateral load,  $F_{sm}$ , local denting damage,  $\delta_d$ , and overall bending damage,  $\delta_o$ , can be estimated using eqns.(6.5), (6.7), (6.8) and (6.11) respectively ;
- b) the predictions using the proposed equations, eqns.(6.8) and (6.11), for the fourteen cases of the lateral impact tests, whose extents of damage exceeded the tolerance specifications given in DnV-OS Rules<sup>[86]</sup>, provide a 27.0 % COV with a mean of 1.15 and a 30.9 % COV with a mean of 1.11 for local denting and overall bending damage respectively. These COVs are a bit higher than those of the

theory. However, comparing with the predictions by the existing formulae it seem that the equations can provide useful estimations for plastically dissipated energy, maximum lateral load and extent of damage of an isolated member due to impact ; and

- c) it is premature to expect the results of the present study to be directly applicable to the design of offshore structures, but by modification of the proposed equations to take account of the differences attributable to the end conditions, the size effect, the shape of the impactor and fluid-interaction, the above could form the basis of a procedure for more efficient design of offshore structure members against impacts and collisions.

For a design formula to estimate the residual strength of damaged tubulars under combined axial compression and radial pressure, the Perry formula was adopted as the basis of the formulation and then an expression for the Perry-Robertson 'imperfection' parameter was obtained based on the parametric study results. The following are the findings :

- a) Eqn.(6.17) together with eqns.(6.13)-(6.16) can be used to predict the residual strength of simply supported damaged tubulars having a sharp dent at mid-length under combined axial compression and hydrostatic pressure ;
- b) the correlation of the available test results with predictions using the proposed formula gives a 12.8 % COV together with a mean of 0.983. The accuracy of the predictions using the proposed formula is a little bit worse than those of the theory. But the accuracy of the predictions, however, is still in the range accepted as a well formulated one for static structural problems ;
- c) for undamaged tubulars which have initial shape imperfection equal to the DnV tolerance limits<sup>[86]</sup> their ultimate strength can be estimated by substituting eqn.(6.18) into eqn.(6.17); and

- d) according to the predictions using eqns.(6.17) and (6.18) the influence of hydrostatic pressure on the ultimate strength of tubulars having very small damage is rather more significant than for severely damaged tubulars.

## 7.2 Proposals for Future Work

It is comparatively recently that impact due to ship collisions has been considered in the structural design of offshore structures. Existing design methods generally have assumptions which are too pessimistic. This is not only because of the uncertain nature of the collision itself but because research in this field is still progressing. The work reported in this thesis provides some experimental and theoretical information which can be a stepping stone towards more economical and at the same time safer designs of offshore structures against collisions. Extensions of the present work which are considered to be worth undertaking are :

- a) In order to improve the prediction accuracy of the proposed model for estimating the extent of damage of a tubular member due to impact, the influence of overall bending deformation on local denting resistance should be considered in the derivation of the spring coefficient for local denting. Of course, a finite element shell analysis may be employed for this calculation, but the use of a conventional finite element analysis is unacceptably expensive. Therefore analytical or simplified numerical methods should be developed ;
- b) providing design formulae which are directly available for predicting the extent of damage of impacted members of the platform can be achieved by simulating the actual boundary conditions of impacted members and realistic behaviour of the ship structure in the analysis. This requires the inclusion of more degrees-of-freedom in the proposed model. The spring coefficients for these degrees-of-freedom can be approximated from the static force-deformation relationships obtained by using existing analytical or numerical methods. However, for the validation of such a simple approach and any other rigorous methods, it is necessary to conduct more

impact tests in which adjacent members to the impacted tubular are included and the striker has a deformable bow. From these tests information can also be obtained on the failure of tubular joints under impact, whose occurrence can make the impacted member totally ineffective in contributing to the residual strength of the structure ; and

- c) the proposed analytical method for evaluating the residual strength of damaged tubulars under combined load can be extended to trace the strength of an isolated damaged member beyond the ultimate state preferably using the assumed deflection method or a finite segment method. But for the assessment of the residual strength of the whole structure more efficient methods than those existing are required. The substructuring method based on finite element space frame analysis can be a solution for this purpose, in which it is not necessary to compute the stiffness matrix of the substructures in elastic range at every load increment.



## References

1. Graff, W.J. 'Introduction to Offshore Structures : Design, Fabrication and Installation', chapter 2, Gulf Publishing Company, Houston, 1981.
2. Miller, N.S. and Faulkner, D. 'The Development of the Offshore Engineering Industry in UK and Europe', in European Shipbuilding One Hundred Years of Change', eds. Walker, F.M. and Slaven, A., Marine Publications International Ltd., London, pp 140-152, 1983.
3. Faulkner, D. 'Design and Construction Concepts for Compliant Production Platforms in Exposed Deep Water Sites', WEMT '84, West European Conf. on Marine Technology, 'Optimising Maritime Operations', ATMA, Paris, July 1984.
4. Caldwell, J.B. Report to Committee 10 on 'Design Philosophy and Procedure', Proc. 3rd Intl. Ship Structures Congress (ISSC), Oslo, 1967.
5. Mansour, A.E. 'Probabilistic Design Concept in Ship Structural Safety and Reliability', Trans. SNAME, vol. 80, pp 64-97, 1972.
6. Faulkner, D. and Sadden, J. 'Towards a Unified Approach to Ship Structural Safety', Trans. RINA, vol. 121, pp 1-28, 1979
7. Cloughley, T.M.G. 'Problems with Offshore Structures still Being Faces by Oil Companies', Proc. Oceanology International '78, pp 75-78, London, 1978.
8. Donegan, E. 'New Platform Designs Minimize Ship Collision Damage', Petroleum Engineering International, pp 76, Feb. 1982.
9. Lewison, G.R.G. 'The Risk of Collision between Ships and Offshore Structures', Jour. Society for Underwater Technology, vol. 6, no. 2, pp 16-22, June 1980.

10. Laheld, P. 'Statistics on Collision Accidents Involving Offshore Structures', Introductory Report of IABSE Colloquium on Ship Collision with Bridges and Offshore Structures (IABSE Report vol. 41), pp 27-45, Copenhagen, 1983.
11. Standing, R.G. and Brending, W. 'Collisions of Attendant Vessels with Offshore Installations : Part 1 - General Description and Principal Results', Dept of Energy(UK) Offshore Technology Report OTH84208, HMSO, London, 1985.
12. Nataraja, R. and Pemsing, K. 'Impact Energy due to Supply Vessel Collision: Case Studies', Proc. 3rd Intl Symp. on Integrity of Offshore Structures (IOS'87), Glasgow Univ., pp 441-463, Sep. 1987.
13. Harding, J.E., Onoufriou, A. and Tsang, S.K. 'Collisions - What is the Danger to Offshore Rigs ?', Jour. of Constructional Steel Research, vol. 3, no. 2, 1983.
14. Mavrikios, Y. and de Oliveira, J.G. 'Design Against Collision for Offshore Structures', MIT Sea Grant Report MITSG 83-7, Massachusetts Institute of Technology, Apr. 1983.
15. Ellinas, C.P. and Valsgard, S. 'Collisions and Damage of Offshore Structures : A State-of-the Art', Jour. of Energy Resources Technology, ASME, vol. 107, pp 297-314, Sep. 1985.
16. Furnes, O. and Kohler, P.E. 'Safety of Offshore Platforms - Classification Rules and Lessons Learned', in Marine and Offshore Safety, eds. Frieze, P.A., McGregor, R.C. and Winkle, I.E., Elsevier Science Publishers, Amsterdam, pp 53-70, 1984.
17. Lloyds Register of Shipping 'Boat Impact Study', Dept of Energy (UK) Offshore Technology Report OTH 85224, HMSO, London, 1985.
18. Technica 'The Risk of Ship/Platform Collisions in the Area of the United Kingdom Continental Shelf', Dept of Energy (UK) Offshore Technology Report

OTH 86217, HMSO, London, 1986.

- 19 Furnes, O. and Amdahl, J. 'Computer Simulation Study of Offshore Collisions and Analysis of Ship-Platform Impacts', *Applied Ocean Research*, vol. 2, no. 3, pp 119-127, 1980.
- 20 Pettersen, E. and Johnsen, K.R. 'New Non-Linear Methods for Estimation of Collision Resistance of Mobile Offshore Units', *Proc. 13th Offshore Technology Conf.* paper OTC 4135, pp 173-186, Houston, May 1981.
- 21 Foss, G. and Edvardsen, G. 'Energy Absorption During Ship Impact on Offshore Steel Structures', *Proc. 14th Offshore Technology Conf.*, paper OTC 4217, pp 625-634, Houston, May 1982.
- 22 Soreide, T.H. and Amdahl, J. 'Deformation Characteristics of Tubular Members with Reference to Impact Loads from Collision and Dropped Objects', *Norwegian Maritime Research*, no. 2, pp 3-12, 1982.
- 23 Soreide, T.H., Moan, T., Amdahl, J. and Taby, J. 'Analysis of Ship/Platform Impacts', *Proc. 3rd Intl Conf. on Behaviour of Offshore Structures (BOSS'82)*, eds. Chrysosostomidis, C. and Connor, J.J., vol. 2, pp 257-278, Boston, Aug. 1982.
- 24 Fjeld, S. 'Design Assumptions and Influence on Design of Offshore Structures', *Introductory Report of IABSE Colloquium on Ship Collision with Bridges and Offshore Structures (IABSE Report vol. 41)*, pp 213-232, Copenhagen, 1983.
- 25 Minorsky, N.U. 'An Analysis of Ship Collision with Reference to Protection of Nuclear Ships', *Jour.of Ship Research*, vol. 3, pp 1-4, 1959.
- 26 Jones, N. 'A literature Survey on the Collision and Grounding Protection of Ships', *Ship Structure Committee Report SSC-283*, 1979.
- 27 Jones, N. 'Structural Aspects of Ship Collisions', in Structural Crashworthi-

- ness, chapter 11, eds. Jones, N. and Wierzbicki, T, Butterworths, London, 1983.
- 28 Van Mater, P.R.Jr. and Giannotti, J.G. 'Critical Evaluation of Low Energy Ship Collision - Damage Theories and Design Methodologies - vol. II - Literature Search and Review', Ship Structure Committee Report SSC-285, 1979.
  - 29 Samuelides, E. 'Structural Dynamic and Rigid Body Response Coupling in Ship Collisions', PhD Thesis, Glasgow Univ., 1984.
  - 30 Arochiasamy, M., Swamidas, A.S.J. and El-Tahan, H. 'Response of Offshore Structures to Bergy-Bit and Iceberg Impacts', in Behaviour of Offshore Structures (Proc. BOSS '85) ed. Battjes, J.A., Elsevier Science Publishers, Amsterdam, pp 951-961, 1985.
  - 31 Petersen, M.J. and Pedersen, P.T. 'Collisions between Ships and Offshore Platforms', Proc. 13th Offshore Technology Conf., paper OTC 4134, pp 163-171, Houston, May 1981.
  - 32 Davies, I.L. and Mavrides, A. 'Assessment of the Damage Arising from Collisions between Ships and Offshore Structures', in Integrity of Offshore Structures (Proc. IOS'81), eds. Faulkner, D. et.al., Applied Science Publishers, London, pp 363-380, 1981.
  - 33 Ueda, Y., Murakawa, H., Hsu, C.Z. and Ohno, K. 'Fundamental Study on Elastic Response of Offshore Structures under Collision', Jour. Society of Naval Architects of Japan, vol. 160, pp 275-285, Dec. 1986 (in Japanese).
  - 34 Hodgkinson, E. 'On the Collision of Imperfectly Elastic Bodies', Report of the British Association for the Advancement of Science, 4th Report, pp 534-543, 1834.
  - 35 Hodgkinson, E 'Impact upon Beams', Report of the British Association for the

Advancement of Science, 5th Report, pp 93-116, 1835.

- 36 Timoshenko, S. 'History of Strength of Materials', McGraw-Hill, New York, 1953.
- 37 Rawlings, B 'The Present State of Knowledge of the Behaviour of Steel Structures under the Action of Impulsive Loads', Civil Engineering Trans. Institution of Engineers, Australia, CE5, no. 2, pp 89-103, Sep. 1963.
- 38 Rawlings, B 'Recent Progress in the Study of Steel Structures Subjected to Impulsive Overload', in Dynamic Waves in Civil Engineering, eds. Howells, D.A., Haigh, I.P. and Taylor, C., Wiley Interscience, New York, pp 543-565, 1971.
- 39 Jones, N. 'A Literature Review of the Dynamic Plastic Response of Structures', Shock and Vibration Digest, vol. 7, no. 8, pp 89-105, Aug. 1975.
- 40 Jones, N. 'Response of Structures to Dynamic Loading', Inst. Phys. Conf. Ser. no. 47, chapter 3, the Institute of Physics, 1979.
- 41 Cox, H. 'On Impact on Elastic Beams', Trans. of the Cambridge Philosophical Society, vol. 9, pp 73-78, 1856.
- 42 Lee, E.H. 'The Impact of a Mass Striking a Beam', Jour. of Applied Mechanics, ASME, vol. 7, no. 4, pp A129-A138, Dec. 1940.
- 43 Mason, H.L. 'Impact on Beams', Jour. of Applied Mechanics, ASME, vol. 3 no. 2, pp A55-A61, June 1936.
- 44 Barnhart, K.E.Jr. and Goldsmith, W. 'Stresses in Beams During Transverse Impact', Jour. of Applied Mechanics, ASME, vol. 24, no. 3, pp 440-446, Sep. 1957.
- 45 Hoppmann, W.H.2nd 'Impact of a Mass on a Damped Elastically Supported

- Beam', Jour. of Applied Mechanics, ASME, vol. 15, no. 2, pp 125-136, June 1948.
- 46 Duwez, P.E., Clark, D.S. and Bohnenblust, H.F. 'The Behavior of Long Beams under Impact Loading', Jour. of Applied Mechanics, ASME, vol. 17, no. 1, pp 27-34, March 1950.
- 47 Conroy, M.F. 'Plastic-Rigid Analysis of Long Beams under Transverse Impact Loading', Jour. of Applied Mechanics, ASME, vol. 19, no. 4, pp 465-470, Dec. 1952.
- 48 Lee, E.H. and Symonds, P.S. 'Large Plastic Deformations of Beams under Transverse Impact', Jour. of Applied Mechanics, ASME, vol. 19, no. 3, pp 308-314, Sep. 1952.
- 49 Parkes, E.W. 'Some Simple Experiments on the Dynamic Plastic Behaviour of Mild-Steel Beams', British Welding Jour., vol. 3, pp 362-366, Aug. 1956.
- 50 de Oliveira, J.G. 'Simple Methods of Estimating the Energy Absorption Capacity of Steel Tubular Members Used in Offshore Structures', Division of Marine Structures Report no.SK/R50, Norwegian Institute of Technology, Trondheim, 1979.
- 51 de Oliveira, J.G. 'The Behavior of Steel Offshore Structures under Accidental Collisions', Proc. 13th Offshore Technology Conf., Houston, Paper OTC 4136, pp 187-198, May 1981.
- 52 Furnes, O. and Amdahl, J. 'Ship Collision with Offshore Platforms', Intermaritec '80 Symp., Hamburg, Sep. 1980.
- 53 Soreide, T.H. 'Ultimate Load Analysis of Marine Structure', chapter 4, Tapir Publishing Company, Trondheim, 1981.
- 54 Ellinas, C.P. and Walker, A.C. 'Effects of Damage on Offshore Tubular Bracing

Members', Proc. IABSE Colloquim on Ship Collision with Bridges and Offshore Structures, Copenhagen, pp 253-261, May 1983.

- 55 Wierzbicki, T. and Suh, M.S. 'Denting Analysis of Tubes under Combined Loading', MIT Sea Grant Report MITSG 86-5, Massachusetts Institute of Technology, Mar. 1986.
- 56 Thomas, S.G., Reid, S.R. and Johnson, W. 'Large Deformations of Thin-Walled Circular Tubes under Transverse Loading-I', Int. Jour. of Mechanical Sciences, vol. 18, pp 325-333, 1976.
- 57 Frieze, P.A. and Sachinis, A. 'Compressive Strength of Stress-Relieved Ring-Stiffened Cylinders Including Local Damage', in Marine and Offshore Safety, eds. Frieze, P.A., McGregor, R.C. and Winkle, I.E., Elsevier Science Publishers, Amsterdam, pp 341-362, 1984.
- 58 Onoufriou, A., Elnashai, A.S., Harding, J.E. and Dowling, P.J. 'Numerical Modelling of Damage to Ring Stiffened Cylinders', Proc. 6th Intl. Symp. on Offshore Mechanics and Arctic Engineering(OMAE), ASME, eds. Chung, J.S. et al., vol. I, pp 281-289, Houston, 1986.
- 59 Kwok, M.K. and Walker, A.C. 'Process of Damage in Thin-Walled Cylindrical Shells', in Advances in Marine Structure, eds. Smith, C.S. and Clarke, J.D., Elsevier Applied Science Publishers, London, pp 111-135, 1987.
- 60 Walker, A.C., McCall, S. and Kwok, M.K. 'Strength of Damaged Ring Stiffened Cylinders Subjected to Simultaneous External Pressure and Axial Compressive Loading', Proc. Structural Stability Research Council (SSRC) Annual Technical Session, Houston, pp 275-286, March 1987.
- 61 Smith, C.S. and Creswell, D.J. 'Effects of Damage on the Strength of Ring-Stiffened Cylinders under External Pressure', Proc. 3rd Intl Symp. on Practical Design of Ships and Mobile Units(PRADS '87), Trondheim, pp 1004-1015,

June 1987.

- 62 Ronalds, B.F. and Dowling, P.J. 'Finite Deformations of Stringer Stiffened Plates and Shells under Knife Edge Loading', Proc. 5th Intl. Symp. on Offshore Mechanics and Arctic Engineering(OMAE), ASME, eds. Chung, J.S. et al., vol. III, pp 323, Tokyo, 1986.
- 63 Dowling, P.J. and Ronalds, B.F. 'On the Behaviour of Damaged and Intact Stiffened Cylindrical Shells', Proc. Structural Stability Research Council (SSRC) Annual Technical Session, Houston, pp 265-274, March 1987.
- 64 Dowling, P.J., Ronald, B.F. and Onoufriou, A. 'Resistance of Buoyancy Columns to Vessel Impact', Proc. 3rd Intl Symp. on Practical Design of Ships and Mobile Units(PRADS '87), Trondheim, pp 1034-1042, June 1987.
- 65 Smith, C.S., Kirkwood, W. and Swan, J. W. 'Buckling Strength and Post-Collapse Behaviour of Tubular Bracing Members Including Damage Effects', Proc. 2nd Intl Conf. on Behaviour of Offshore Structures(BOSS '79), BHRA Fluid Engg, Cranfield, pp 303-326, Aug. 1979.
- 66 Taby, J., Moan, T. and Rashed, S.M.H. 'Theoretical and Experimental Study of the Behaviour of Damaged Tubular Members in Offshore Structures', Norwegian Maritime Research, vol. 9, no. 2, pp 26-33, 1981.
- 67 Smith, C.S., Somerville, W.L. and Swan, J.W. 'Residual Strength and Stiffness of Damaged Steel Bracing Members', Proc. 13th Offshore Technology Conf., Houston, Paper OTC 3981, pp 273-282, May 1981.
- 68 Ellinas, C.P. 'Ultimate Strength of Damaged Tubular Bracing Members', Jour. of Structural Engg, ASCE, vol. 110, no. 2, pp 245-259, Feb. 1983.
- 69 Smith, C.S. 'Assessment of Damage in Offshore Steel Platforms', in Marine and Offshore Safety, eds. Frieze, P.A., McGregor, R.C. and Winkle, I.E., Elsevier Science Publishers, Amsterdam, pp 279-307, 1984.



- 70 Ueda, Y. and Rashed, S.M.H. 'Behaviour of Damaged Tubular Structural Members', Jour. of Energy Resources Technology, ASME, vol. 107, pp 342-349, Sep. 1985.
- 71 Taby, J. and Moan, T. 'Collapse and Residual Strength of Damaged Tubular Members', in Behaviour of Offshore Structures (Proc. BOSS'85), ed. Battjes, J.A., Elsevier Science Publishers, Amsterdam, pp 395-408, 1985.
- 72 Taby, J. and Moan, T. 'Ultimate Behaviour of Circular Tubular Members with Large Initial Imperfections', Proc. Structural Stability Research Council (SSRC) Annual Technical Session, Houston, pp 79-104, March 1987.
- 73 Richards, D.M. and Andronicou, A. 'Residual Strength of Dented Tubulars: Impact Energy Correlation', Jour. of Energy Resources Technology, ASME, vol. 107, pp 485-492, Dec. 1985.
- 74 Yao, T., Fujikubo, M., Bai, Y. and Nakagawa, S. 'Load Carrying Capacity of Damaged Tubular Members', Trans. West Japan Society of Naval Architects, no. 73, pp 136-150, March 1987(in Japanese).
- 75 American Petroleum Institute 'Recommended Practice for Planning, Designing and Constructing Fixed Offshore Platforms', API RP2A, 13th ed., Washington, D.C., 1982.
- 76 American Petroleum Institute 'Recommended Practice for Planning, Designing and Constructing Tension Leg Platforms', API RP2T, 1st ed., Washington, D.C., 1987.
- 77 Department of Energy (UK) 'Offshore Installations : Guidance on Design and Construction', HMSO, London, 1984.
- 78 British Standard Institution 'Code of Practice for Fixed Offshore Structures', BS6235, London, 1984.

- 79 Det Norske Veritas 'Design Against Accidental Loads : Fixed Offshore Installations', Technical Note TNA 101, Oslo, 1981.
- 80 Det Norske Veritas 'Impact Loads from Boats : Fixed Offshore Installations', Technical Note TNA 102, Oslo, 1981.
- 81 Det Norske Veritas 'Rules for Classification of Mobile Offshore Units', Part 3, Oslo, 1984.
- 82 Cho, S.-R. and Frieze, P.A. 'Lateral Impact Tests on Unstiffened Cylinders ; Final Report', Dept of Naval Architecture and Ocean Engineering Report NAOE-85-56, Glasgow Univ., 1986 (see volume II of this thesis).
- 83 Frieze, P.A. and Sands, G. 'Conoco/ABS Ring Stiffened Cylinder Tests : Final Report', Dept of Naval Architecture and Ocean Engineering, Glasgow Univ., Feb. 1984.
- 84 British Standards Institution 'Methods for Testing of Metals : Part 2, Steel (General)', BS18 : Part 2, London, 1971.
- 85 Transport & Road Research Laboratory 'Recommended Standard Practices for Structural Testing of Steel Models', Supplementary Report 254, 1977.
- 86 Det norske Veritas 'Rules for the Design, Construction and Inspection of Offshore Structures, 1977, Appendix C : Steel Structures', Oslo, with corrections, 1982.
- 87 Watson, A.R., Reid, S.R., Johnson, W. and Thomas, S.G. 'Large Deformation of Thin-Walled Circular Tubes under Transverse Loading-II', Int. Jour. of Mechanical Sciences, vol. 18, pp 387-397, 1976.
- 88 Johnson, W. 'Impact Strength of Material', Edward Arnold, London, 1972, with corrections, 1983.

- 89 de Oliveira, J.G. 'Design of Steel Offshore Structures against Impact Loads due to Dropped Objects', Proc. 3rd Intl Symp. on Offshore Engineering Structures, eds. Carneiro, F.L.L.B. et al, Rio de Janeiro, pp 466-483, 1981.
- 90 Ellinas, C.P., Supple, W.J. and Walker, A.C. 'Buckling of Offshore Structures : A State-of-the-Art Review', Granada, London, 1984.
- 91 Cho, S.-R. and Frieze, P.A. 'Axial Compression Tests on Damaged and Undamaged Tubulars ; Final Report', Dept of Naval Architecture and Ocean Engineering Report NAOE-86-40, Glasgow Univ., 1986.
- 92 Sorensen, K.A. 'Behaviour of Reinforced and Prestressed Concrete Tubes under Static and Impact Loading', Proc. 1st Intl Conf. on Behaviour of Offshore Structures (BOSS '76), Norwegian Institute of Technology, Trondheim, pp 798-813, Aug. 1976.
- 93 Miller, B.L. 'Wave Slamming on Offshore Structures', National Maritime Institute Report no. NMI R81(OT-R-8041), pp 15, Mar. 1980.
- 94 Moan, T. 'Loads and Load Effect Analysis for Offshore Steel Structures', Second WEGEMT, Trondheim, 1979.
- 95 Seiler, J.A., Cotter, B.A. and Symonds, P.S. 'Impulsive Loading of Elastic-Plastic Beams', Jour. of Applied Mechanics, ASME, vol. 23, no. 4, pp 515-521, Dec. 1956.
- 96 Bodner, S.R. and Symonds, P.S. 'Experimental and Theoretical Investigation of the Plastic Deformation of Cantilever Beams Subjected to Impulsive Loading', Jour. of Applied Mechanics, ASME, vol. 29, no. 4, pp 719-728, Dec. 1962.
- 97 Cho, K.N. 'Practical Collision Analysis of a Semi-Submersible', Proc. 3rd Intl Symp. on Practical Design of Ships and Mobile Units (PRADS '87), Trondheim, pp 1024-1033, June 1987.

- 98 Paz, M. 'Structural Dynamics : Theory & Computation', 2nd ed., Van Nostrand Reinhold, New York, 1985.
- 99 Newmark, N.M. 'A Method of Computation for Structural Dynamics', Jour. of Engineering Mechanics Div., ASCE, vol. 85, no. EM3, pp 67-94, July 1959.
- 100 Timoshenko, S. Young, D.H. and Weaver, w. Jr. 'Vibration Problems in Engineering', 4th ed., John Wiley & Sons, New York, 1974.
- 101 Newmark, N.M. 'Numerical Procedure for Computing Deflections, Moments and Buckling Loads', Trans. of ASCE, vol. 108, pp 1161-1234, 1943.
- 102 Chen, W.F. and Ross, D.A. 'Tests of Fabricated Tubular Columns', Jour. of Struc. Div., ASCE, vol. 103, no. ST3, pp 619-634, Mar. 1977.
- 103 Toma, S., Chen, W.F. and Finn, L.D. 'External Pressure and Sectional Behavior of Fabricated Tubes', Jour. of Struc. Div., ASCE, vol. 108, no. ST1, pp 177-194, Jan. 1982.
- 104 Stuiver, W. and Tomalin, P.F. 'The Failure of Tubes under Combined External Pressure and Axial Load', Proc. Society for Experimental Stress Analysis, vol. 16, no. 2, pp 39-48, 1959.
- 105 Smith, D., Csenki, A. and Ellinas, C.P. 'Ultimate Limit State Analysis of Unstiffened and Stiffened Structural Components', Proc. 3rd Intl Symp. on Integrity of Offshore Structures (IOS'87), Glasgow Univ., pp 145-167, Sep. 1987.
- 106 Chen, W.F. and Atsuta, T. 'Theory of Beam-Columns : volume 2 - Space Behavior and Design', McGraw-Hill, New York, 1977.
- 107 Santathadaporn, S. and Chen, W.F. 'Tangent Stiffness Method for Biaxial Bending', Jour. of Struc. Div., ASCE, vol. 98, no. ST1, pp 153-163, Jan. 1972.

- 108 Chen, W.F. and Atsuta, T. 'Theory of Beam-Columns : volume 1 - In-Plane Behavior and Design', McGraw-Hill, New York, 1976.
- 109 Chen, W.F. and Han, D.J. 'Tubular Members in Offshore Structures', Pitman, Boston, 1985.
- 110 Breckenridge, R.A. and Haynes, H.H. 'Behavior of Structural Elements in the Deep Ocean', Proc. Conf. on Civil Engineering in the Oceans, ASCE, San Francisco, pp 147-178, 1967.
- 111 Wagner, A.L., Mueller, W.H. and Erzurumlu, H. 'Ultimate Strength of Tubular Beam-Columns', Jour of Struc. Div., ASCE, vol. 103, no. ST1, pp 9-22, Jan. 1977.
- 112 Sherman, D.R., Erzurumlu, H. and Mueller, W.H. 'Behavioral Study of Circular Tubular Beam-Columns', Jour of Struc. Div., ASCE, vol. 105, no. ST6, pp 1055- 1068, June 1979.
- 113 Sohal, I.S. and Chen, W.F. 'Moment-Curvature Expressions for Fabricated Tubes', Jour of Struc. Engg., ASCE, vol. 111, no. 11, pp 2738-2757, Nov. 1984.
- 114 Toma, S. and Chen, W.F. 'Analysis of Fabricated Tubular Columns', Jour of Struc. Div., ASCE, vol. 105, no. ST11, pp 2343-2366, Nov. 1979.
- 115 Toma, S. and Chen, W.F. 'Design of Vertical Chords in Deepwater Platform', Jour of Struc. Engg., ASCE, vol. 109, no. 11, pp 2733-2746, Nov. 1984.
- 116 Smith, C.S. 'Imperfections and Damage Effects in Offshore Tubulars', Proc. Steel Construction Offshore/Onshore Conf., Imperial College, London, April 1987.
- 117 Faulkner, D., Guedes Soares, C. and Warwick, D.M. 'Modelling Requirements for Structural Design and Assessment', Proc. 3rd Intl Symp. on Integrity of

Offshore Structures (IOS'87), Glasgow Univ., pp 25-54, Sep. 1987.

- 118 Johnston, B.G. 'Third SSRC Guide with Column Design Applications', Jour. of Struc. Div., ASCE, vol. 103, no. ST11, pp 2243-2257, Nov. 1976.
- 119 American Institute of Steel Construction (AISC) 'AISC Specification for the Design, Fabrication and Erection of Structural Steel for Buildings', 8th ed., 1980.
- 120 European Convention for Constructional Steelwork (ECCS) 'European Recommendations for Steel Construction', Construction Press, London, 1981.
- 121 Ayrton, W.E. and Perry, J. 'On Struts', The Engineer, vol. 62, pp 464-465, Dec. 1886.
- 122 Rankine, W.J.M. 'Useful Rules and Tables Relating to Mensuration, Engineering, Structures and Machines', pp 210-211, Charles Griffin and Company, London, 1866.
- 123 Horne, M.R. and Merchant, W. 'The Stability of Frames', pp 35, Pergamon Press, London, 1965.
- 124 Merchant, W. 'The Failure Load of Rigid Jointed Frameworks as Influenced by Stability', Structural Engineer, Jour. Inst. of Str. Engg. vol. 32, no. 7, pp 185-190, July 1954.
- 125 Allen, D. 'Merchant-Rankine Approach to Member Stability', Jour. of Struc. Div., ASCE, vol. 104, no. ST12, Dec. 1978.
- 126 Odland, J. and Faulkner, D. 'Buckling of Curved Steel Structures - Design Formulations', in Integrity of Offshore Structures, ed. Faulkner, D. et.al., pp 419-443, Applied Science Publishers, London, 1981.

- 127 Frieze, P.A., Cho, S.-R. and Faulkner, D. 'Strength of Ring Stiffened Cylinders under Combined Loads', Proc. 16th Annual Offshore Technology Conf., Houston, paper OTC 4714, May 1984.
- 128 Cho, S.-R. and Frieze, P.A. 'Strength Formulation for Ring-Stiffened Cylinders under Combined Axial Loading and Radial Pressure', Jour. of Constructional Steel Research, 1987 (Submitted for publication).
- 129 Woisin, G. 'Design Against Collision', Proc. Intl Symp. on Advances in Marine Technology, Trondheim, June, 1979.
- 130 Jones, N. 'Influence of Strain Hardening and Strain-Rate Sensitivity on the Permanent Deformation of Impulsively Loaded Rigid-Plastic Beam', Int. Jour. of Mechanical Sciences, vol. 9, pp 777-796, 1967.
- 131 Fessler, H. and Spooner, H. 'Experimental Determination of Stiffness of Tubular Joints', in Integrity of Offshore Structures (Proc. IOS'81), eds. Faulkner, D. et.al., Applied Science Publishers, London, pp 493-511, 1981.
- 132 Windenburg, D.F. and Trilling, G. 'Collapse by Instability of Thin Cylindrical Shells under External Pressure', Experimental Model Basin (EMB), Ref. no. 385, July 1934 (also Trans. of ASME, vol. 56, no. 11, Nov. 1934).
- 133 Cho, S.-R., Frieze, P.A. 'Derivation of a Strength Formulation for Ring-Stiffened Cylindrical Shells Subjected to Combined Axial Loading and Radial Pressure', Dept. of Naval Architecture and Ocean Engineering, Report NAOE-86-23, Glasgow Univ., Feb. 1986.
- 134 Tennyson, R.C. et al. 'Buckling of Short Cylinders under Combined Loading', Jour. of Applied Mechanics, ASME, vol. 45, pp 574-579, 1978.
- 135 Galletly, G.D. and Pemsing, K. 'On Design Procedures for the buckling of Cylinders under Combined Axial Compression and External Pressure', 4th Nat. Congress of Pressure Vessels and Piping Technology, ASME, Portland, 1983.

136 Timoshenko, S.P. and Gere, J.M. 'Theory of Elastic Stability', chapter 11, 2nd ed., McGraw-Hill, New York, 1963.

137 British Standard Institute 'Specification for Unfired Fusion Welded Pressure Vessels': BS 5500', London, with modifications, 1976.



## Appendix 1

### Approximate Equations for Bending Moment - Axial Compression - Hydrostatic Pressure - Curvature Relationships of Damaged Tubulars

$$m = \begin{cases} 0 & (\phi \leq \phi_0) \\ a (\phi - \phi_0) & (\phi_0 < \phi \leq \phi_1) \\ m_{pc} - (m_{pc} - m_1) \exp\{f(\phi)\} & (\phi_1 < \phi) \end{cases} \quad (A1)$$

where

$$f(\phi) = -c_1 (\phi - \phi_1)^{c_2} \quad (A2)$$

$$\phi_1 = m_1/a + \phi_0 \quad (A3)$$

$$a = \pi/4 \{1 - 0.466 \delta_d^{0.4} \exp(2.25 \delta_d)\} \quad (A4)$$

$$\phi_0 = \exp(p_0) - 1 \quad (A5)$$

where

$$p_0 = 0.653 \delta_d^{0.5} p + 1.15 \delta_d p^2 + 1.64 \delta_d q^2 (1 - 16.1 p^5) - 15.8 \delta_d^2 q^4 (1 - 2030 p^{10}) + (1 - 0.025 D/t) \{0.537 \delta_d^{0.5} q - 0.0946 \delta_d p^{1.5} - 47.6 \delta_d q^2 p^5\} + (1 - 0.025 D/t)^2 \{3.43 \delta_d q^2 + 4.47 \delta_d^{1.5} q^{0.5} - 2.27 \delta_d^2 p^3 (1 + 45800 q^4 p^7)\} - 369 \delta_d^3 q (1 - 0.025 D/t)^4$$

$$c_1 = \exp(c_{1p}) \quad (A6)$$

where

$$c_{1p} = 0.436 + 0.606 p^{0.1} - 0.633 p^{0.2} - 1.51 p^2 (1 - 1.25 p^2) + 0.0907 q^{0.1} (1.48 p^{0.1} - p^2) + 0.139 q^{0.2} (8.78 p^{10} - 1.13 p^{0.2} + p^4) + 0.434 q^{0.3} p^{10} - 1.60 p^{20} (2.69 q^{0.4} + q^{0.6}) + 0.273 q (3.43 q - 4.29 q p^{0.5} + 2.73 q p^4 - p^2) - 2.51 q^4 (1 - 1.95 p) + 15.8 q^{10} p^{0.5} - 3420 q^{20} p + 0.152 \delta_d^{0.1} \{1 + 1.22 q^{0.1} + 2.82 p^4 - 13.7 p^{10} (1 + 4.07 q^{0.1}) + 0.253 \delta_d \{-0.794 + 353 q^9 - q^{0.2} + 108 p^{20} (1 + 2.68 q^{0.2}) + 21.0 p^5 - 10.2 p^8\} + 0.269 \delta_d^{0.3} (q - 4.66 p) - 58.8 \delta_d^{0.4} (p^{10} + 265 q^{18}) + 1.23$$

$$\begin{aligned}
& \delta_d^{0.5} p^5 - 1.21 \delta_d^{0.6} (q^2 - 4.02 p^2) + 57.0 \delta_d^{0.7} q^{1.2} p^3 - 0.793 \delta_d \{1 - 8.06 p^{4.5} - 2.75 \\
& p^4 (1 - 31.5 q^2) + 21.2 p^8 (p^2 - 189 q^5)\} - 5310 \delta_d^{1.4} q^{2.4} p^6 - 8.53 \delta_d^{1.5} q^{1.5} (q - \\
& 11.6 p^4) + 4.38 \delta_d^2 \{1 - 13.4 q - 21.6 p^8 (1 + 3.67 p + 65.9 q^4 + 36500 q^{10} p^8) + 4.38 \\
& q^5 p^{0.6} + 216 \delta_d^{0.5} p^5\} + 30.4 \delta_d^3 \{[1.25 - q^{0.3} + 10.5 q^3 (q + 1.33 q^2 - 8.77 q^2 p - \\
& 504 p^8) - 1.60 q^{0.1} p^{0.3}] + 17.0 \delta_d \{4.61 q^2 + 919 q^{10} p^{1.2} + q^{0.1} p (1 + 2.21 p^2)\} - \\
& 21.0 \delta_d^2 \{1420 p^{10} + 1.66 p^{0.1} (1 - 1.62 q^{0.5}) - p\} - 6410 \delta_d^6 \{[1 - 1.07 q^{0.6} + 57.1 \\
& q^8 (1 - 25.3 q^2 p^2) - 1.83 q^{0.2} p^{0.6}] - 70.8 \delta_d^2 \{q^{0.2} p^2 (18.6 p^4 - 1) + 3.24 \delta_d^2 p^{0.2} \\
& (1 - 4.88 q) - 16.0 \delta_d^2 p^2\} + (1 - 0.025 D/t) [0.0569 p^3 - 0.0250 q^{0.1} (1 - 18.6 p^{0.5} - \\
& 8.60 p) + 0.730 q^{0.5} + 0.102 q - 22.5 q^{1.5} p^{10} - 76.3 q^5 (p^3 + 1.78 q^4 p + 14.8 q^{10}) + \\
& 0.184 \delta_d^{0.1} - 1.31 \delta_d^{0.5} (q^{0.1} + 2.66 p^{1.5}) - 0.968 \delta_d^{0.7} q^{0.1} - 1890 \delta_d^2 q^3 p - 7.75 \\
& \delta_d^{2.5} - 43.6 \delta_d^3 \{1 - 19.7 q^5 p^{0.1} - 6.67 q^{0.1} p^2 (1 + 3.13 p^2)\} + 1670 \delta_d^5 (7.90 q^{2.5} \\
& + 1.90 q^{0.1} + p^{0.2})] + (1 - 0.025 D/t)^2 [0.492 p^{0.1} + 0.312 p^6 - 0.0490 q^{0.2} (1 - 15.3 \\
& p - 7.94 p^2) - 5.05 p^{10} (q^{0.7} + 7.23 q^{1.5}) - 1.47 q - 0.263 q^2 + 10.6 q^{2.5} p^{0.1} - 20.8 \\
& q^3 p^{10} (12.8 p^{10} - 1) - 3630 q^{10} p^6 - 40300 q^{18} p^2 + 1540000 q^{30} - 2.76 \delta_d^{0.1} (7.79 \\
& q^4 - q^{0.2}) + 0.0207 \delta_d^{0.2} - 112 \delta_d^{0.5} q p^3 + 2.12 \delta_d (1 + 1.51 q^{0.2} - 7.12 q^{0.1} - 8.44 \\
& p^3) + 2.09 \delta_d^{1.4} q^{0.2} - 404 \delta_d^2 p^3 (1 + 4.78 p^5 - 1.12 q^{1.5}) - 1790 \delta_d^{2.5} q p^2 - 17.7 \\
& \delta_d^4 [87.0 p^{0.1} (1 - 1.60 q^{0.1}) + 89600 q^6 p^2 - \delta_d - 56.5 \delta_d q^{0.1} + 86.4 \delta_d^2 \{1 + 19.8 \\
& q^{0.2} p^4 (1 - 48.9 p^4) - 4740 q^{10} p^{0.2}\} - 127000 \delta_d^6 (19.8 q^5 - q^{0.2} + 6.21 p^{0.2})] + (1 \\
& - 0.025 D/t)^4 [-2.19 p^{0.2} + 21.7 q^2 - 256 q^5 p^{0.2} + 257 p^{20} (q^{1.4} + 4.40 q^3 - 4.86 q^6) \\
& + 17.5 \delta_d^{0.2} (35.6 q^8 - q^{0.4}) - 47.1 \delta_d (\delta_d - 8.68 \delta_d q^{0.2} - 427 q^2 p^6) + 313000 \delta_d^4 [p^4 \\
& \{p^2 (1 + 1.68 q^3) + 22.2 p^{12} + 13.1 \delta_d q^2\} - 9.04 \delta_d^4 \{\delta_d^2 q^{0.2} - 1.63 p^{0.2} (1 - 1.86 \\
& q^{0.2})\}]]],
\end{aligned}$$

$$c_2 = \exp(c_{2p}) \quad (A7)$$

where

$$\begin{aligned}
c_{2p} = & -0.288 - 0.743 p (1.82 p - 1) + 0.703 q p^3 (3.78 q p^3 - 1) - 0.178 q^{0.5} \\
& p^{0.1} (1.66 q^{0.5} p^{0.1} - 1) - 3.25 \delta_d^{0.5} (\delta_d^{0.8} - 2.18 q^2) + 6.99 \delta_d \{-5.78 q^4 + 1.27 p^{0.2} \\
& (\delta_d^{0.5} - 7.13 q^3) + q^2 p^2 + 7.18 \delta_d^2 (7.94 \delta_d^{0.6} + q^{0.1} - 30.5 \delta_d p^{0.4} + 55.8 \delta_d^{0.5} p^5 \\
& + 287 q^6 p^{0.4} - 2.52 q^{0.1} p^{0.1} - 468 q^4 p^4) - 219 \delta_d^4 \{q^{0.2} (1 - 3.50 p^{0.2}) + 1580 \delta_d \\
& p^{10}\} + (1 - 0.025 D/t) [0.131 q^{0.1} (q^{0.4} + 2.34 p - 35.9 q^5 p (p + 4.37 q^5) + 0.223 \\
& \delta_d^{0.1} (p - 30.3 \delta_d^{0.4} q^2 - 2.91 \delta_d^{0.2} p^{0.5}) - 1.91 \delta_d \{\delta_d q^{0.1} - 1.08 - 285 \delta_d (1.13 \delta_d q^5 -
\end{aligned}$$

$$1.57 \delta_d^2 p^2 - q^3 p + 3.27 \delta_d^3 q^{0.1} p)]] + (1 - 0.025 D/t)^2 [-0.531 q (1 - 4.82 p^{0.1}) + 0.562 q^{0.2} p^2 (1 - 5.27 q^{0.3} p) - 1340 q^{10} p^2 (p^2 + 54.1 q^{10}) + 0.110 \delta_d^{0.2} p^2 - 3.59 \delta_d^{0.5} \{2.25 q^3 (3.53 + q^2) + \delta_d^{0.1} p + 2.17 p^4\} + 0.547 \delta_d \{\delta_d + 46.4 \delta_d^{0.5} - 106 q^4 - 148 \delta_d p^{0.1} - 55.0 q^{0.1} p^4\} + 436 \delta_d^4 \{q^{0.2} (1 - 23400 \delta_d^6 p^2) + 998 q^6 (\delta_d^2 q^4 - 1.28 p^2) - 2410 \delta_d^4 p^4\}] + (1 - 0.025 D/t)^4 [5.31 q (q - 3.99 q p^{0.2} + 7.14 p^6) + 473 \delta_d \{-2.77 \delta_d^2 (1 - 9.39 p^{0.2}) + 1.36 q^6 (2.38 - q^4) + p^8 (1 + 24.7 \delta_d q^{0.2})\}],$$

$$m_1 = p/4(1 - p)\{1 - 0.217 d_d^{0.13} \exp(10.0 d_d)\} \exp(b_{m1}) \quad (A8)$$

where

$$b_{m1} = -0.232 q^2 (1 - 1.97 q^2) + 0.00202 q^{0.5} p^{0.7} \{56.9 + q p^{0.3} - 1.72 q^{0.5} p^{0.7} (113 - q^2 p^{0.6})\} - 106 \delta_d^3 \{\delta_d (1 - 30.9 q^{0.4} - 48.0 \delta_d^{0.2} p) + 203 q^{3.2} - 659 \delta_d^5 (1 - 247 q^{0.8} - 1110 \delta_d^{0.4} p^2)\} + 0.639 \delta_d^{0.5} \{\delta_d^{0.9} - 10.4 \delta_d^{2.3} - 36.5 \delta_d^{0.5} p^{4.2} - 9.37 p^{2.1} - 80.3 \delta_d^{0.8} q^{1.6} (\delta_d^{0.2} + 12300 \delta_d^{1.3} q^{7.4} - 7.19 q^{2.9})\} + 1.27 \delta_d^{0.1} q p^{0.3} (1 - 5.59 \delta_d^{0.1} q p^{0.3}) + 3.10 \delta_d q^{0.1} p^{0.1} \{p^{0.9} (1 + 14.7 q^{1.4} - 4.06 q^{0.2}) - 82.0 \delta_d^2 q^{0.1} p^{0.2} \{p^{0.8} (1.29 + q^{0.1} p + 165 q^{2.9} p) - 3.32 q^{0.5} + 17.1 \delta_d q^{0.1} p^{0.6} (q^{0.8} - 21.9 \delta_d p^{1.2} - 5170 \delta_d^3 q^{1.8} p^{0.8})\} + (1 - 0.025 D/t) [0.0536 q^{0.1} p^{0.3} (1.11 + q^{0.1} p^{0.1} - 32.5 q^{0.8} p^{0.9} - 2160 q^{9.9} p^{0.7}) - 1.19 q^2 + 0.225 \delta_d^{0.1} q (q - 22.2 p^{1.7}) + 3.50 \delta_d \{q^{0.2} p^{0.2} + 20.7 q^5 - 6.14 p^{4.3} - 4.03 \delta_d (1 + 8.78 \delta_d^{0.7} + 350 q^{2.8} + 9.16 \delta_d p^{0.3} - 476 \delta_d q p + 45.2 q^{2.5} p^{0.1} - 171 \delta_d q^{1.5} p^{0.3})\}]\} + (1 - 0.025 D/t)^2 [0.0689 q^{0.2} p^{0.6} (1 - 6.10 q^{0.3} p^{1.4} + 1.18 q^{0.2} p^{0.2}) - 0.505 q \{1 + 14.0 q^3 + 17.8 q^{0.8} p^{2.4} + 9.31 q p (1 + 11800 q^{18} p + 8.66 q^6 p)\} - 2.25 \delta_d^{0.1} q^2 \{4.62 p^{0.5} + \delta_d^{0.1} (q^2 + 30.4 p^{3.4})\} + 71.9 \delta_d [q p^{0.1} - 4.16 \delta_d q^{0.9} - 2.63 q^{1.5} p^{1.5} - 1.56 \delta_d \{p^{8.6} + 1.21 \delta_d^{0.4} + 14.3 q^{2.4} - 1480 q^{10} + 18.2 \delta_d p^{0.9} - 1.14 q^{0.4} p^{0.4} - 2.26 q^{0.1} p + 10.3 \delta_d^2 (1 + 1.92 \delta_d^{1.4} + 5790 q^{5.6} - 66.6 \delta_d^2 p^{0.6} + 27500 \delta_d^2 q^2 p^2 + 2390 q^5 p^{0.2} - 18200 \delta_d^2 q^3 p^{0.6})\}]] + (1 - 0.025 D/t)^4 [3.67 q \{q + 1.85 p^4 + 26.5 q^3 p (p + 197 q^{12} p^3 + 3.12 \delta_d^{0.2})\} - 10700 \delta_d^2 \{q^2 (p^{0.2} - 30.7 q p^3) - 2.53 \delta_d (\delta_d^{1.8} + 40.3 \delta_d^5 + 4.55 \delta_d^{0.23} q^{1.8} + 288 \delta_d q^{4.8} + 300 \delta_d^3 p^{1.8} - 6.48 \delta_d q^{0.2} p^2)\}]],$$

$$m_{pc} = \sin\{p/2(1 - p)\}\{1 - 0.23 d_d^{0.3} \exp(4.4 d_d)\} \exp(b_{mpc}) \quad (A9)$$

where

$$\begin{aligned}
b_{\text{mpc}} = & -0.0125 q^{0.8} (1 + 1.48 q^{0.8}) - 0.242 q^{1.5} p^3 (1 + 5.45 q^{1.5} p^3) - 0.155 \\
& \delta_d^{0.2} p^{0.5} \{1 + 11.9 \delta_d^{0.3} p^{1.2} - 2.30 \delta_d^{0.2} p^{0.5} (1 + 1.87 \delta_d^{0.1} q^{1.7} - 59.1 \delta_d^{0.6} p^{2.4})\} - \\
& 27.2 \delta_d q^3 (\delta_d^{0.2} + 6.62 q^{0.4} p^2 - 24.6 \delta_d^{1.4} q^3) + (1 - 0.025 D/t) [-1.08 q^{0.8} (q^{1.2} + \\
& 1.71 p^{1.4}) - 2.63 \delta_d^{0.5} (\delta_d + 2.95 q^4 + 267 \delta_d^{2.2} p^4) + 0.532 \delta_d^{0.1} q^{0.1} p^{0.2} \{\delta_d^{0.3} p^{0.6} \\
& - 141 \delta_d^{0.7} q^{6.5} - 10.5 q^{1.1} p^{0.5} (\delta_d^{0.6} + 7.86 q^{4.5} p^{2.7} + 173 \delta_d q^{3.1} p^{1.8})\}] + (1 - \\
& 0.025 D/t)^2 [-1.12 q^{1.6} \{7.0 p^{2.8} + q^{0.4} (1 + 5.87 q^2 + 8.33 q^{0.2} p^{1.7})\} - 0.348 \delta_d^{0.2} \\
& \{q^{1.5} - 1.77 \delta_d^{0.8} p^{0.1} (1.8 + \delta_d^5 q^{0.2} p^{1.5})\} - 116 \delta_d (\delta_d^2 + 1.90 q^8 + 5990 \delta_d^{4.4} p^8) + \\
& 20.6 \delta_d^{0.2} q^{0.1} p^{0.4} \{3.13 \delta_d^{0.9} q^{1.2} p^{0.6} (1 - 12200 \delta_d^{1.1} q^{7.3} p^4 - 32.3 \delta_d^{0.1} q^{0.9} p^{0.2} \\
& + 67.4 \delta_d^{0.3} q^{1.1} p^{0.4}) - 395 q^{11.3} (p^{6.4} + 2.89 \delta_d^{1.4} q^{1.8}) + \delta_d^{2.8} (p^{0.4} + 56.8 \delta_d^{1.2} \\
& q^{0.5})\}] + (1 - 0.025 D/t)^4 [14.0 q^4 (1 + 15.3 q^{0.4} p^{3.4}) + 4.22 \delta_d^{0.4} \{q^3 - 8.51 \delta_d^{1.6} \\
& (p^{0.2} - 1290 \delta_d^4)\} - 36600 \delta_d^{2.2} q^{0.2} p^{0.8} \{q^{2.4} (p^{1.2} - 2.04 \delta_d^{0.2} q^{1.8} p^{1.6}) - 2.43 \delta_d^{3.8} \\
& (p^{0.8} - 112 \delta_d^{2.4} q)\}]
\end{aligned}$$

$\alpha$  = volume fraction of the shell

$R$  = mean radius of the shell

$r$  = radius of the shell

$\nu$  = Poisson's ratio of the material

$$a_1 = \alpha(1 - \nu)/(1 + \nu)$$

$$a_2 = \alpha(1 + \nu)/(1 - \nu)$$

$$a_3 = \alpha(1 + \nu) \cdot a^2 \{ \nu(1 + 2\nu) + (1 - \nu)(1 - \alpha\nu)(1 + \nu) \}$$

$$a_4 = \frac{1}{(1 + \nu)(1 + \alpha\nu)}$$

## Appendix 2

### Approximate Formula for Elastic Buckling Pressure of Circular Cylinder under Radial Pressure alone

For perfect, elastic and simply supported cylindrical shells under radial pressure alone, the buckling formula, eqn.(A10), was obtained by von Mises in corrected form[132].

$$p_{rm} = \frac{E (t/R)^3}{12 (1 - \nu^2)} \left( n^2 - 1 + \frac{\lambda_1 n^4 - \lambda_2 n^2 + \lambda_3}{n^2 - 1} \right) + E (t/R) \frac{1}{(n^2 - 1) \{n^2 (L/\pi R)^2 + 1\}^2} \quad (A10)$$

where  $p_{rm}$  = shell buckling pressure under radial pressure alone

$L$  = unsupported span of the shell

$R$  = mean radius of the shell

$t$  = thickness of the shell

$n$  = number of lobes in circumferential direction

$$\lambda_1 = \alpha (2 - \alpha)/(1 - \alpha)^2$$

$$\lambda_2 = \alpha \{3 + \nu + (1 - \nu^2) \alpha\}$$

$$\lambda_3 = \alpha (1 + \nu) - \alpha^2 \{ \nu (1 + 2\nu) + (1 - \nu^2) (1 - \alpha \nu) (1 + \frac{1 + \nu}{1 - \nu} \alpha) \}$$

$$\alpha = \frac{1}{\{n^2 (L/\pi R)^2 + 1\}}$$

#### 1. Cylinders Longer than Critical Length

Any cylinder longer than the critical length (determined later) can be considered as a cylinder of infinite length since its collapse pressure is independent of a further increase in length. Hence, by neglecting the terms containing the square of  $L/R$  in the denominator in eqn.(A10), eqn.(A11) can be obtained.

$$p_{rm} = \frac{E (t/R)^3}{12 (1 - \nu^2)} (n^2 - 1) \quad (A11)$$

For  $n = 2$ , eqn.(A11) gives a minimum value.

$$p_{rm} = \frac{E (t/R)^3}{4 (1 - \nu^2)} \quad (A12)$$

## 2. Cylinder Shorter than Critical Length

Eqn.(A13) can be obtained by rearranging eqn.(A10).

$$p_{rm} = \frac{E (t/R)^3}{12 (1 - \nu^2)} \{ (1 + \lambda_1) (n^2 - 1) + (2 \lambda_1 - \lambda_2) + \frac{-3 \lambda_1 + \lambda_2 + \lambda_3}{n^2 - 1} \} + \frac{E (t/R) \alpha^2}{n^2 - 1} \quad (A13)$$

The third term in the curly bracket of eqn.(A13) can be neglected in comparison with the first term since for practical geometries, with  $L/R = 0.1 - 8.0$  and  $R/t = 10 - 500$  the values of  $\alpha$  lie between 0.006 and 0.507, where small values of  $\alpha$  correspond to small  $n$  and large values to large  $n$ .  $\alpha$  can be represented by eqn.(A14), which is a function of  $Z$  only, unless  $Z$  is very small or very large ( $Z$  is the Batdorf slenderness parameter,  $\sqrt{1 - \nu^2} L^2/Rt$ ).

$$\alpha \approx \alpha^* = \frac{1}{\sqrt{Z}} \left(1 - \frac{0.4}{\sqrt{Z}}\right) \quad (\text{A14})$$

Substituting eqn.(A14) into eqn.(A13) and neglecting higher order terms of  $\alpha^*$  ( $t/R$ )

$$p_{rm} \approx \frac{E (t/R)^3}{12 (1 - v^2)} \left[ \frac{1}{1 - 2 \alpha^*} (n^2 - 1) + \frac{\alpha^*}{1 - 2 \alpha^*} \{(1 - v) + (3 + 2v + v^2) \alpha^*\} \right] + E (t/R) \frac{(\alpha^*)^2}{n^2 - 1} \quad (\text{A15})$$

Differentiating eqn.(A15) with respect to  $n$  and equating the result to zero,

$$\frac{\partial p_{rm}}{\partial n} = \frac{E (t/R)^3}{12 (1 - v^2)} \frac{2n}{1 - 2 \alpha^*} - E (t/R) \frac{2n (\alpha^*)^2}{(n^2 - 1)^2} = 0 \quad (\text{A16})$$

The solution of eqn.(A16) for  $n$  gives the value which will make  $p_{rm}$  a minimum. Although the value of  $n$  will not in general be integer, it could be an approximation to the correct value of  $n$ . By factoring out common terms and making further approximations, eqn.(A17) can be obtained from eqn.(A16).

$$n^2 - 1 \approx \frac{2 \sqrt{3 (1 - v^2)}}{t/R} \alpha^* (1 - \alpha^*) \quad (\text{A17})$$

Substituting eqn.(A17) into eqn.(A15) and rearranging,

$$p_{rm} = \frac{E (t/R)^2}{2\sqrt{3(1-v^2)}} \frac{\alpha^*}{1-2\alpha^*} \left[ 1 - \alpha^* + \frac{1-2\alpha^*}{1-\alpha^*} + \frac{t/R}{2\sqrt{3(1-v^2)}} \{ 1 - v + (3 + 2v + v^2) \alpha^* \} \right] \quad (A18)$$

For practical geometries, the third term in the square brackets of eqn.(A18) is much smaller than the others. By neglecting that term and making further approximations, eqn.(A19) can be obtained.

$$p_{rm} = \frac{E (t/R)^2}{\sqrt{3(1-v^2)}} \alpha^* (1 + 2\alpha^*) (1 - \alpha^*) \quad (A19)$$

Substituting eqn.(A14) into eqn.(A19),

$$\begin{aligned} p_{rm} &= \frac{1.4 E}{\sqrt{3(1-v^2)}} \frac{(t/R)^2}{\sqrt{Z}} \left( 1 + \frac{0.7}{\sqrt{Z}} - \frac{2}{Z} + \frac{1}{Z\sqrt{Z}} \right) \\ &\approx \frac{1.4 E}{\sqrt{3(1-v^2)}} \frac{(t/R)^2}{\sqrt{Z}} \left( 1 + \frac{0.7}{\sqrt{Z}} \right) \end{aligned} \quad (A20a)$$

For  $v = 0.3$ ,

$$= \frac{0.85 E (t/R)^2}{\sqrt{Z}} \left( 1 + \frac{0.7}{\sqrt{Z}} \right) \quad (A20b)$$

For practical geometries, with  $L/R = 0.1 - 8.0$ ,  $R/t = 10 - 500$ , the ratios of eqn.(A20) to eqn.(A10) are very small, especially for small  $Z$ . In order to improve the accuracy and the applicable range of the approximate formula, a reapproximation of



eqn.(A19) is needed. By using eqn.(A21) instead of eqn.(A19) and making further approximations, a more accurate formula, eqn.(A22), can be obtained.

$$P_{rm} \approx \frac{E (t/R)^2}{\sqrt{3 (1 - v^2)}} \alpha^* (1 + 2 \alpha^*) \quad (A21)$$

$$= \frac{1.4 E}{\sqrt{3 (1 - v^2)}} \frac{(t/R)^2}{\sqrt{Z}} \left(1 + \frac{2.1}{\sqrt{Z}}\right) \quad (A22a)$$

For  $v = 0.3$ ,

$$= \frac{0.85 E (t/R)^2}{\sqrt{Z}} \left(1 + \frac{2.1}{\sqrt{Z}}\right) \quad (A22b)$$

For large  $Z$ , eqns.(A20a) and (A22a) can be reduced to eqn.(A23a).

$$P_{rm} \approx \frac{1.4 E}{\sqrt{3 (1 - v^2)}} \frac{(t/R)^2}{\sqrt{Z}} \quad (A23a)$$

For  $v = 0.3$ ,

$$= \frac{0.85 E (t/R)^2}{\sqrt{Z}} \quad (A23b)$$

The ratios of eqns.(A22b) and (A23b) and DnV Rules<sup>[86]</sup> formula to eqn.(A10) for practical geometries ( $L/R = 0.1 - 8.0$ ,  $R/t = 10 - 500$ ,  $Z = 1 - 20000$ ) are illustrated in Fig. A1. The discontinuous nature of the ratios is result of using finite values of  $n$  in eqn.(A10). It can be seen that eqn.(A22b) generally provides a better estimate to eqn.(A10) than the DnV equation over the range  $2 < \sqrt{Z} < 20$  while outside this range the reverse, in general, true. Eqn.(A23b) only appears to be reasonable for  $\sqrt{Z} > 60$ .

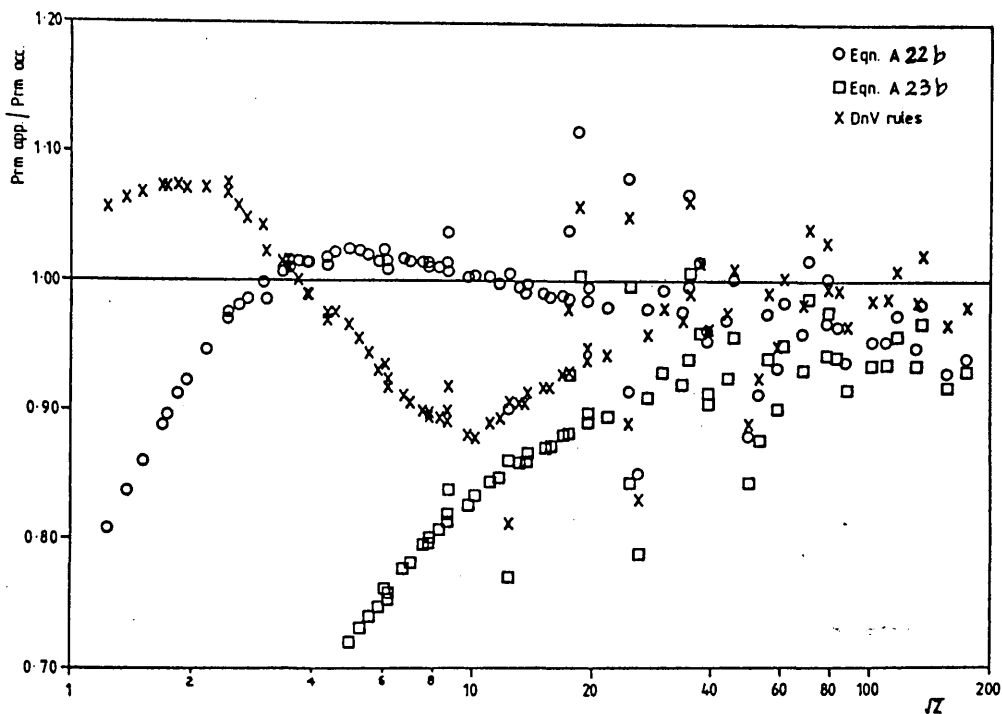


**Fig. A1 Comparison of Approximate Formulae for  $p_{rm}$  with Accurate Equation (eqn.A10)**

### 3. Critical Length

The critical length, eqn.(A24), can be obtained by equating eqns.(A12) and (A23a).

$$Z = 10.5 (1 - \nu^2) (R/t)^2 \quad (A24a)$$

For  $\nu = 0.3$ ,

$$Z = 9.6 (R/t)^2 \quad (A24b)$$

Since ring-stiffened cylinders in most marine structures are shorter than the critical length, i.e.  $Z < 10 (R/t)^2$ , eqns.(A22a) and (A23a) can be used as approximate formulae.

## Appendix 3

### Derivation of a Strength Formulation for Ring-Stiffened Cylindrical Shells Subjected to Combined Axial Loading and Radial Pressure

The quadratic Merchant - Rankine formula in generalised form as suggested by Odland and Faulkner<sup>[126]</sup>, eqn.(6.4), is adopted as the basis of a new formulation for predicting the ultimate strength of ring-stiffened cylindrical shell subjected to combined axial loading and radial pressure. a brief description of the derivation procedure is given herein. The details of the procedure can be found elsewhere<sup>[128,133]</sup>.

#### 1. Elastic Buckling Interaction

As indicated above, it is intended to use eqn.(6.4) as the basis of a new formulation with  $\rho_x$  and  $\rho_\theta$  derived from an empirical fit to test data. At the stocky end of geometries, the Mises-Hencky criterion will be eminently suitable for predicting the failure strength. At the slender end eqn.(6.4) adopts a linear interaction between each elastic buckling. It is worth while examining the suitability of this in the present application.

For perfect, elastic and simply supported cylindrical shells, the calculation of the interactive buckling stress using shell buckling computer codes has been carried out by other investigators<sup>[134,135]</sup>. According to these results, for larger values of  $Z$ , the interaction is linear while for smaller values of  $Z$ , the linear relation is sometimes conservative but in other cases non-conservative. However, for ideal cylindrical shells under hydrostatic pressure loading, the linear relation can be shown to be suitable as follows. Assume  $p = p_m$ , where  $p_m$  is the shell buckling pressure under hydrostatic pressure, then

$$\frac{\sigma_x}{\sigma_{xcr}} = \frac{p_m R/2t}{0.605 E t/R} \quad (A25)$$

$$\frac{\sigma_\theta}{\sigma_{\theta cr}} \approx \frac{p_m}{p_{rm}} \quad (A26)$$

$$p_m \approx \frac{0.92 E (t/R)^2}{1.024 \sqrt{Z} - 0.636} \quad (A27)$$

where the equation for  $\sigma_{xcr}$  is the elastic critical buckling strength of 'long' cylinders[136], while the expression for  $p_m$  is an approximate formula given in ref.132.

By substituting eqns.(A22b) and (A27) into eqns.(A25) and (A26), the sum of the latter can be written, after rearrangement, as

$$\frac{\sigma_x}{\sigma_{xcr}} + \frac{\sigma_\theta}{\sigma_{\theta cr}} = 1.057 \left\{ 1 + \frac{-0.777\sqrt{Z} + 2.778}{Z + 1.479\sqrt{Z} - 1.304} \right\} \quad (A28)$$

which for large  $Z$  tends to 1.057. Even for  $Z = 10$ , eqn.(A28) gives 1.082 confirming that for the hydrostatic combination of axial compression and radial pressure at least, the linear sum of elastic buckling stress ratios provides a suitable basis for estimating the combined buckling stress.

## 2. Inelastic Buckling

The quadratic interaction between yielding and buckling demonstrated by eqn.(6.4) accounts directly for the effect of plasticity in reducing the buckling stress below its theoretical value. The influence of initial distortions, probably the most

important 'imperfection' is reflected in the correction factors. A separate factor could be introduced to account for residual stresses from either welding or rolling but this will be shown to be unnecessary thus justifying the selection of elasto-plastic knockdown factors.

Theoretically boundary conditions can influence the results significantly. In practice, however, the end conditions are frequently of less importance in ring-stiffened cylinders unless they relate to single bay length cylinders. Appreciating boundary conditions are dependent on the ring frame torsional and extensional stiffnesses, on the length of the adjacent bays and the loading, it seems preferable to avoid the need to make what are often subjective decisions on whether the boundary is rotationally, tangentially or extensionally restrained, or free, and just assume the simplest arrangement.

### 3. Evaluation of Elasto-Plastic Knockdown Factors

Prior to evaluating  $\rho_x$  and  $\rho_\theta$ , it is instructive to examine the DnV Rules[86] predictions and compare them with the available test data. This has been done for the cases of axial compression and hydrostatic pressure, the latter requiring interaction between axial compression and external radial pressure be considered. The results are presented in Table A1 in terms of means and COVs of the ratios of actual to predicted strength, where  $p_c$  is the collapse hydrostatic pressure. The effect of ignoring the (elastic) knockdown factors, i. e.  $\rho_x = \rho_\theta = 1$  is also examined in the table.

The knockdown factors used in the DnV Rules ostensibly correspond to lower bound estimates on elastic buckling. The strength predictions, however, are purported to correspond to a 5 % probability of failure which, for a normally distributed population, correspond to the mean minus 1.645 x standard deviation or, more simply,  $m(1 - 1.645 \text{ COV})$  where  $m$  is the mean value. These 'characteristic' values are also listed in Table A1.

From the table it can be seen that the DnV Rules formulations represent neither the mean nor the purported characteristic strength of the available test data particularly with respect to axial compression. More importantly, however, factors, while not necessarily improving the mean predictions, has reduced the degree of scatter as measured by COV. Interestingly, the COV in relation to hydrostatic loading shows a significant improvement on the BS 5500 value[133].

It can be concluded from this small investigation that it is at least possible to improve upon the DnV formulation for axial compression and the BS 5500 formulation[137] for hydrostatic loading can be bettered.

Table A1 Means and COVs of Ratios of Actual Strength to DnV Rules Predicted Strength for Axial Compression and Hydrostatic Pressure

Loading	Elastic Buckling Strength	$\sigma_x(\text{act.})/\sigma_x(\text{pred.})$ or $p_c(\text{act.})/p_c(\text{pred.})$		
		Mean	COV	5% Char.
Axial Compression	$\rho_x \sigma_{xcr}$	1.44	26.2 %	0.82
	$1 \sigma_{xcr}$	0.83	15.1 %	0.62
Hydrostatic Pressure	$\rho_x \sigma_{xcr}, \rho_\theta \sigma_{\theta cr}$	1.05	8.0 %	0.91
	$1 \sigma_{xcr}$	0.90	7.0 %	0.80

notes :  $\sigma_{xcr}$ ,  $\sigma_{\theta cr}$ ,  $\rho_x$  and  $\rho_\theta$  are eqns C3-5, C3-8, Figures C3-4 and C3-7 of Ref. 86 respectively.









3.1 Axial Compression Elasto-Plastic Knockdown Factor,  $\rho_x$

Using axial compression test data,  $\rho_x$  can be evaluated by rearranging the appropriate one-dimension version of eqn.(6.4) as follows:

$$\rho_x = \frac{\sigma_x \sigma_Y}{\sigma_{xcr} \sqrt{\sigma_Y^2 - \sigma_x^2}} \tag{A29}$$

The shortcoming of eqn.(A29) is that the test data whose collapse stresses,  $\sigma_x$ , approach or are greater than the material yield stress,  $\sigma_Y$ , cannot be taken into account in the evaluation of  $\rho_x$ . Fortunately, however, the collapse stresses of all the available axial compression test data are well below  $\sigma_Y$ [133]. However, for other loading cases to be considered, some test data have equivalent stresses,  $\sigma_e$ , greater than  $\sigma_Y$ . An attempt to overcome this and so consider test data in the yielding regime will be made later.

Table A2 Dependence of  $\rho_x$  on Non-Dimensional Geometry and Material Parameter

Parameter	$\rho_x$	Degree of Dependency
L/R 		Strong
R/t 		Medium
L/t 		Medium
E/ $\sigma_Y$ 		Weak

To find a suitable dependent parameter on which to derive  $\rho_x$ , first the relations between  $\rho_x$  and various appropriate non-dimensional geometric and material property parameters ( $L/R$ ,  $R/t$  and  $L/t$  as geometric parameters,  $E/\sigma_Y$  as material property parameter) were considered. The results are presented in detail in ref.133 while the trends are summarised in Table A2.  $L/R$  is seen to be the dominant parameter with, somewhat surprisingly,  $E/\sigma_Y$  having the smallest influence.

Traditionally, Batdorf parameter,  $Z (= \sqrt{1-v^2} L^2/Rt)$ , has been used as the slenderness parameter for specifying knockdown and buckling coefficient parameters for ring-stiffened cylinders. This can be considered as a combination, apart from a multiplying constant, of  $(L/R)^2 R/t$  or  $L/R L/t$  both of which include the dominant parameter  $L/R$  and one parameter of secondary influence. Despite the apparent lack of importance of material properties, it was considered desirable not to ignore  $E/\sigma_Y$  when evaluating various combinations of the basic variables to find the one giving the least scatter of the ratio of actual to predicted strength.

Table A3 Equations for  $\rho_x$  and Their Resulting Accuracy

Variable (X)	Mean Curve of $\rho_x$ $\rho_x = A + B X^{-C}$	COV of $\rho_x$	COV of $(\sigma_x)_{act.}/(\sigma_x)_{pred.}$
Z	A=0.034, B= 0.871, C=0.151	21.3 %	13.8 %
$\sqrt{Z} \cdot E/\sigma_Y$	A=0.278, B=18.9, C=0.516	20.7 %	11.3 %
$\sqrt{Lt}/R \cdot E/\sigma_Y$	A=0.034, B= 4.82, C=1.140	15.9 %	10.1 %

The combinations of variable examined are listed in Table A3 together with the equations for  $\rho_x$ , their COVs and the COVs of the ratio of actual strength to predicted



one. It can be seen that the best results are obtained by using

$$\rho_x = 0.398 + 4.82 (\sqrt{Lt}/R \cdot E/\sigma_Y) - 1.14 \quad (13)$$

Somewhat surprisingly, the degree of uncertainty found in  $\rho_x$  is not transferred in full to the ratio of actual to predicted strength.

### 3.2 Radial pressure Elasto-Plastic Knockdown Factor, $\rho_\theta$

Unfortunately it is necessary to use combined loading test data for the evaluation of  $\rho_\theta$  since there few experiments reported in the open literature on fabricated steel models subjected to radial pressure alone. Using the test data for hydrostatic pressure and combined axial loading and the equations for  $\rho_x$  given in Table A3, the procedures followed in the derivation of  $\rho_x$  have been carried out in relation to  $\rho_\theta$ .

An expression for  $\rho_\theta$  is found by rearranging eqn (6.4) : it is as given by the following:

$$\rho_\theta = \frac{\sigma_\theta / \sigma_{\theta cr}}{\sqrt{1 - \frac{\sigma_x^2 - \sigma_x \sigma_\theta + \sigma_\theta^2}{\sigma_Y^2}} - \frac{\sigma_{xo}}{\rho_x \sigma_{xcr}}} \quad (A31)$$

where

$$\sigma_x = \frac{p_x R}{2 t} \quad (A32a)$$

$$\sigma_\theta = \frac{p_r R}{t} (1 - \gamma' G) \quad (A32b)$$

$$\sigma_{\theta cr} = \frac{p_{rm} R}{t} (1 - \gamma'' G) \quad (A32c)$$

$$p_x = F_x / R^2$$

$$G = 2 (\sinh \alpha L/2 \cos \alpha L/2 + \cosh \alpha L/2 \sin \alpha L/2) / (\sinh \alpha L/2 + \sin \alpha L/2)$$

$$\alpha L = 1.285 L/\sqrt{Rt}$$

$$\gamma = \frac{A (1 - mv/2)}{(A + b t) (1 + B)} \quad (A33a)$$

$$\gamma'' = \frac{A}{(A + b t) (1 + B)} \quad (A33b)$$

$$m = p_x / p_r$$

$$A = A_s (R/R_s)^2$$

$$A_s = \text{cross-sectional area of ring-frame}$$

$$R_s = \text{radius of centroid of ring-frame}$$

$$B = 2 t N/\alpha (A + b t)$$









$$N = (\cosh \alpha L - \cos \alpha L) / (\sinh \alpha L + \sin \alpha L)$$

$$b = \text{width of ring-frame in contact with shell : } t_w \text{ for toe welded frame}$$

Eqns.(A33a) and (A33b) were derived from the BS 5500 formulation[137]. The dependence of  $\rho_\theta$  on the different geometry and material property parameters is presented in detail in ref.133 and summarised in Table A4

The trends and degree of dependency are similar to those exhibited by  $\rho_x$  except  $L/R$  is now less influential. As in the case of  $\rho_x$ , various combinations of parameters were investigated to identify the most suitable one on which to base  $\rho_\theta$ ; the results are shown in Table 6. Unexpectedly, the influences on  $\rho_\theta$  of the different variable show almost the opposite trends to those on  $\rho_x$ . The variable  $\sqrt{Lt/R} E/\sigma_Y$ , which provides the best basis for  $\rho_x$ , gives the worst means and COVs for all cases. It is found to give  $\rho_\theta \approx 1.00$  irrespective of the variables of  $\rho_\theta$  with the worst final results.

Table A4 Dependence of  $\rho_\theta$  on Non-Dimensional Geometry  
and Material Parameter

Parameter	$\rho_x$	Degree of Dependency
$L/R$ 		Medium
$R/t$ 		Medium
$L/t$ 		Medium
$E/\sigma_Y$ 		Weak

Furthermore, the COVs of  $\rho_\theta$  are much larger than those of  $\rho_x$  in spite of greater imperfection sensitivity of cylinders under axial compression loading. However, the means of the ratios of actual to predicted strength are acceptable for design purposes and the COVs are less than those for axial compression loading. The large uncertainty associated with  $\rho_\theta$  as demonstrated in Table 6 is not a true reflection of this parameter because the factor was evaluated indirectly using eqn.(A31) together with combined loading test data so that all of the uncertainties in  $\rho_x$ , the linear summation of elastic buckling stress ratio, and the quadratic interaction of yield and elastic buckling are concentrated into  $\rho_\theta$ . Even if the best results for all combined loading data are obtained by using eqn.(A34), it would be better to examine the mean and COV of each loading separately.

$$\rho_\theta = 1.01 + (L/R \cdot \sqrt{L/t}) - 1.41 \quad (A34)$$

Table A5 Equation for  $\rho_\theta$  and Their Resulting Accuracy

$\rho_x$		$\rho_\theta$				$(\sigma_x)_{act.}/(\sigma_x)_{act.} \text{ or } (\sigma_x)_{act.}/(\sigma_x)_{act}$	
A + B X <sup>-C</sup>		A + B X <sup>-C</sup>			COV	Mean	COV
A = 0.034	X = L/R·√L/t	A = 1.01	B = 1.00	C = 1.41	31.5 %	0.976	8.8 %
B = 0.871	X = Z	A = 0.999	B = 3.74	C = 0.871	31.5 %	0.978	9.0 %
C = 0.151	X = √Z E/σ <sub>Y</sub>	A = 1.01	B = 82300	C = 1.58	31.7 %	0.978	9.2 %
X = Z	X = √Lt/R·E/σ <sub>Y</sub>	A = 1.58	B = -0.00058	C = -1.17	40.2 %	0.941	13.2 %
A = 0.278	X = L/R·√L/t	A = 1.01	B = 0.940	C = 1.33	31.6 %	0.976	9.0 %
B = 18.9	X = Z	A = 1.01	B = 3.51	C = 0.871	31.5 %	0.978	9.2 %
C = 0.516	X = √Z E/σ <sub>Y</sub>	A = 0.956	B = 2390	C = 1.10	32.1 %	0.976	9.4 %
X = √Z E/σ <sub>Y</sub>	X = √Lt/R·E/σ <sub>Y</sub>	A = 1.62	B = -0.0040	C = -0.861	37.9 %	0.944	13.0 %
A = 0.398							
B = 18.9		$\rho_\theta = 1.00$				1.095	12.9 %
C = 1.14							
X = √Lt/R·E/σ <sub>Y</sub>							

### 3.3 Final Selection of Factors

The means and COVs of the ratios of actual to predicted strength for the complete range of combinations of axial and radial pressure loadings were then calculated using all combinations of the best two equations for  $\rho_x$  from Table A3 and the best three equations for  $\rho_\theta$  from Table A5. The results for each set of evaluations are presented in Table A6. It can be seen that the equations for  $\rho_x$  and  $\rho_\theta$  whose variables are  $\sqrt{Lt}/R \cdot E/\sigma_Y$  and  $L/R \cdot \sqrt{L}/t$  respectively give the best results. However, for the convenience of designers, it would be preferable to use a common variable for both  $\rho_x$  and  $\rho_\theta$  unless the penalty is a significant decrease in accuracy. Hence eqns (A35a) and (A35b) were determined.

$$\rho_x = 0.278 + 18.9 X^{-0.516} \quad (A35a)$$

$$\rho_\theta = 0.956 + 2390 X^{-1.10} \quad (A35b)$$

Where  $X = \sqrt{Z} E / \sigma_Y$

**Table A6 Comparison of Means and COVs for all combinations of Axial and Radial Pressure Loading with Various Combinations of  $\rho_x$  and  $\rho_\theta$  Equations**

$\rho_x$ (=A+BX <sup>-C</sup> )	$\rho_\theta$ (=A+BX <sup>-C</sup> )	Axial Comp.		Hydrostatic		Axial Comp.+ Radial Pres.		Axial Tens.+ Radial Pres.	
				Pres.					
		Mean	COV	Mean	COV	Mean	COV	Mean	COV
A=0.278  B=18.9  C=0.516	A=1.01 ,B=1.00, C=1.41, X=L/R·√L/t			0.962	8.2%	0.973	8.7%	1.112	8.8%
	A=0.999,B=3.74, C=1.10, X=Z	0.993	11.3%	0.956	8.2%	0.987	9.2%	1.113	8.8%
	A=0.956,B=1.00, C=1.10, X=√Z·E/σ <sub>Y</sub>			0.963	8.5%	0.977	9.2%	1.116	9.0%
A=0.398  B=4.82  C=1.14	A=1.01 ,B=1.00, C=1.10, X=L/R·√L/t			1.004	9.4%	0.950	8.0%	1.112	8.8%
	A=0.999,B=3.74, C=1.10, X=Z	0.991	10.1%	1.001	9.5%	0.965	8.5%	1.113	8.8%
	A=0.956,B=1.00, C=1.10, X=√Z·E/σ <sub>Y</sub>			1.006	9.8%	0.955	8.5%	1.116	9.0%

In order to overcome the shortcoming of eqns.(A29) and (A31) and take account of the test data in the yielding regime, the coefficients in eqns.(A35a) and (A35b) were re-examined using the entire database. The results were the following

$$\rho_x = 0.281 + 19.2 X^{-0.518} \quad (A36a)$$

$$\rho_\theta = 0.833 + 3510. X^{-1.13} \quad (A36b)$$

Where  $X = \sqrt{Z} E / \sigma_Y$

As expected there are negligible changes in eqns.(A36a) compared with eqn (A35a) because all the axial compression collapse stresses are well below their yield stresses,  $\sigma_Y$ . However, for the radial pressure knockdown factor there are some notable alterations compared with eqn (A35b) which improve the accuracy of the strength predictions for hydrostatic pressure and for combined axial compression and radial pressure loadings.



**DESIGN APPROXIMATIONS FOR  
OFFSHORE TUBULARS AGAINST COLLISIONS**

**volume II**

by

Sang - Rai Cho  
B.Sc., M.Sc., C. Eng., MRINA

A Thesis Submitted for the Degree of  
Doctor of Philosophy  
in the Faculty of Engineering in Glasgow University

December, 1987

# Department of Naval Architecture & Ocean Engineering University of Glasgow

## REPORT CONTROL SHEET

Report Status :		Authorisation :	Date :
CONFIDENTIAL		Author	21/1/86
INTERNAL Restricted		S.-R. Cho	
INTERNAL Open		Supervisor	3/2/86
INTERNAL Restricted		P.A. Frieze	
INTERNAL Open	***	Head of Department Professor D. Faulkner	5/2/86
PUBLICATION		Date, Place & Name of Publication/Conference	
CONFERENCE PAPER			

<b>Title :</b>  <div style="text-align: center;"> <b>LATERAL IMPACT TESTS ON UNSTIFFENED CYLINDERS</b> </div>	<b>Date :</b>  January 1986 <b>Pages</b> total : Vol. I : 45 Vol. II : 257
---	--

**Report no. :** NAOE-85-56

**Authors :** Sang-Rai Cho and Paul A. Frieze

**Sponsor, Grant, Contract, Project no. :**

**Project NA3A :** SERC GR/C/7139.2, Research Student (Korea), NAOE Department.

**Abstract**

This report describes the detailed testing procedures and results of twenty lateral impact tests conducted on small scale unstiffened tubulars undertaken in effort to develop data for the design of offshore structures against collision.

Simple empirical formulae to predict the possible extent of damage to stiffened circular cylinders suffering from impacts are provided in explicit form along with the results of the tests. Comparisons between the proposed and other available formulae with the test results are given.

This report is in two parts. Volume I contains the Main Report with descriptions of the test procedures and summaries of the test results, development of empirical formulae and the correlations. Volume II, which is presented as an appendix, contains details of the test records.

**Keywords :**

Lateral Impact Tests, Damaged Tubulars, Offshore Structure, Empirical Formula

**Address of Origination :**

James Watt Building, University of Glasgow, Glasgow, G12 8QQ.

**Control/Printing/Stock contact :** Dr. P. Mayo, Department of Naval Architecture and Ocean Engineering, University of Glasgow, Glasgow, G12 8QQ.

**Computer text file :**  
YES/NOX

**File name :** Cho, Cho2



**LATERAL IMPACT TESTS ON UNSTIFFENED CYLINDERS**

**FINAL REPORT**

**VOLUME I - MAIN REPORT**

**Sang-Rai CHO**

**Paul A. FRIEZE**

**Department of Naval Architecture and Ocean Engineering,  
University of Glasgow.**

## ABSTRACT

This report describes the detailed testing procedures and results of twenty four lateral impact tests conducted on small scale unstiffened tubulars undertaken in an effort to develop data for the design of offshore structures against collision.

Simple empirical formulae to predict the possible extent of damage to unstiffened circular cylinders suffering from impacts are provided in explicit form using the results of the tests. Comparisons between the proposed and other available formulae with the test results also given.

This report is in two parts. Volume I contains the Main Report with descriptions of the test procedures, and summaries of the test results, development of the empirical formulae and the correlations. Volume II, which is presented as an Appendix, contains details of the test records.

---

## CONTENTS

	<u>Page</u>
Abstract	(i)
Nomenclature	(iii)
1. INTRODUCTION	1
2. TEST MODELS AND RIG	2
2.1 Choice of Model Parameters	3
2.2 Heat-Treatment	3
2.3 Test Rig	4
3. TEST PROCEDURE	5
3.1 Pre-Test Measurements	5
3.2 Impact Tests	7
4. RESULTS	9
4.1 Pre-Test Measurements	9
4.2 Impact Tests	10
5. DAMAGE PREDICTION	13
5.1 Existing Formulae	13
5.2 Derivation of Proposed Formulae	15
5.3 Discussion of the Proposed Formulae	17
6. CONCLUSION	18
Acknowledgements	19
References	20
Tables 1-5	
Figures 1-11b	
Appendix (Volume II)	
APPENDIX A. PRELIMINARY HEAT-TREATMENT RESULTS	
APPENDIX B. PRE-TEST MEASUREMENTS	
APPENDIX C. DETAILED TEST RESULTS	

Nomenclature

$D$	Diameter to mid-thickness of the model
$D_o$	Outside diameter of the model
$E$	Young's Modulus
$E_d$	Energy absorbed during the formation of a local dent
$E_k$	$1/2 MV_o^2$ , initial kinetic energy of the striker
$E_o$	Energy absorbed during overall bending
$L$	Length of the actual model
$L_i$	$L - 50$ mm. Length of the model for impact test
$M_p$	$D^2 t \sigma_Y$ , plastic moment capacity of an undamaged tubular's cross section
$N_o$	$\pi D t \sigma_Y$ , fully plastic axial force
$P$	Ultimate lateral load
$T_D$	Impact duration
$T_E$	Period of the natural vibration
$V_o$	Speed of the striker immediately before impact
$V_r$	Rebound speed of the striker immediately after impact
$d_d$	Depth of dent
$d_o$	Out-of-straightness
$d_{oi}$	Initial out-of-straightness
$f$	Natural frequency
$k$	Constant, defined in text
$m$	Mass of the model
$m_p$	$1/4 \sigma_Y t^2$ , plastic moment resultant of a tube wall
$t$	Thickness of the model
$\delta_d$	$d_d/D$ , non-dimensionalised depth of dent
$\delta_o$	$d_o/L$ , non-dimensionalised out-of-straightness
$\lambda_E$	$N_o L_i t / E_k D$ , energy parameter
$\rho$	Material density
$\sigma_Y$	Static tensile yield strength

## 1. INTRODUCTION

Unstiffened circular cylinders are widely used as chord or bracing members of fixed and floating offshore platforms. In the offshore environment these structures may be exposed to impact loadings from collisions by attendant vessels, floating ice, or dropped objects. Even though such impacts are random events of low probability, they can demand costly repairs or, in extreme cases, claim the loss of the structure. Therefore, it is appropriate to consider this form of loading at the design stage of an offshore structure. For these purposes, prediction of the possibility of a collision or other form of damage, the probable extent of damage, and a method for the evaluation of the deterioration in the load carrying capacity of the structure are needed. Of course this is not to say that there is no need for the collision resistant-type structure as often adopted in the construction of Nuclear or LNG carriers or, alternatively, fendering. However, from the viewpoint of economic design, energy absorbing type structures are generally to be preferred, while it is unlikely the fenders can give significant protection without appreciable increases in the wave forces on platforms<sup>[1]</sup>.

For predicting the possibility of impact damage, some surveys of incidents involving offshore structures in the North Sea are available<sup>[2,3]</sup>. The survey given in Ref. 2 shows that a total number of 107 incidents with UK North Sea sector installations were reported from 1976 to 1982, that is, 15 incidents per annum.

The damage to unstiffened tubulars resulting from impacts can be divided into two modes. These are, local denting of the cylinder wall and overall bending of the member as a beam. Some combination of these two modes is the most likely outcome for the range of structures which are considered here. Some analytical or semi-analytical formulations have been suggested to predict the extent of these two modes of damage. However, most of these seem to have adopted unrealistic or too conservative assumptions as far as the unstiffened cylindrical members of offshore structures are concerned, or are given in implicit form thereby ignoring the extent of contribution of the two modes. Some of these formulations are reviewed later in this report. Also, it is difficult for the designer to use such formulations with confidence because none has been substantiated by any actual lateral impact test which realistically simulates collisions offshore.

The deteriorating effect of damage on the load carrying capacity of unstiffened circular cylinders subjected to axial compression has been investigated theoretically and experimentally<sup>[4-10]</sup>. References 4, 5 and 9 describe tests on 24 damaged tubulars which were subsequently used to establish the effective stiffnesses and strengths of damaged cylinders as a function of the extent of damage. Taby, Moan and Rashed<sup>[6]</sup> presented a method of analysis to evaluate the ultimate strength and post ultimate strength behaviour of damaged tubular members and also reported results of tests on 21 damaged tubulars. Other analytical methods were suggested in Refs 7 and 8.

This report describes 24 lateral impact tests on 23 unstiffened tubulars covering the choice of geometric and material parameters, the preparation of the models, and the test equipment and procedure. Finally, a simple and reliable empirical formulation is proposed to predict explicitly the extent of damage of unstiffened circular cylinders suffering lateral impact loading.

This report consists of two volumes, Volume I - Main Report, and Volume II - Appendix. Details of the pre-test measurements and the test results are contained in Volume II.

The second phase of this study to assess experimentally the ultimate strength of the damaged cylinders when subjected to combined axial compression and radial pressure loading are to be conducted in the near future.

## 2. TEST MODELS AND RIG

Ideally the model parameters chosen for a test series should cover what is considered to be the practical range of geometries, material properties and fabrication sequences of actual unstiffened cylindrical members of offshore structures. Also the real damage situations and the boundary conditions should be simulated in the test set-up. However, because of testing facility limitations and budget constraints, it was decided to perform dry tests on small scale tubes.

Fabricated tubes, which are generally formed by cold-rolling and welding of flat plates, are used for the unstiffened cylindrical members of offshore platforms. It is virtually impossible to simulate correctly scaled distortions and residual stresses on small scale tubes. Therefore, it was

decided to use CDS-24 cold-drawn seamless tube from which to form the specimens.

## 2.1 Choice of Model Parameters

Characteristic cross-sectional dimensions of bracing elements in the water-plane of jackets and semi-submersibles are given in Ref. 7 as follows:

$$20 < D/t < 100$$

$$10 < L/D < 30$$

However, the structural framework of most offshore platforms is formed by long unstiffened tubular members whose diameter/thickness ratio ( $D/t$ ) is usually chosen to be less than 50-60 in order to avoid unfavourable local buckling of the tube walls<sup>[5]</sup>. Hence, 50.80 mm x 1.22 mm (nominal outside diameter x thickness) and 50.80 mm x 2.03 mm tubes whose nominal diameter/thickness ratios ( $D/t$ ) are 40.6 and 20.0 respectively were chosen for the models. For the length ( $L$ ) of the models, 1.0, 1.4 and 1.8 m, whose approximate nominal length/diameter ratios ( $L/D$ ) are 20.3, 28.5 and 36.6 respectively, were selected, dictated primarily by the available test facilities.

The yield stress of normally fabricated offshore structure tubulars is in the range 250 - 400 N/mm<sup>2</sup>. However, the tube material procured for the present test series was found to be variable and to have a much higher yield stress of 500-600 N/mm<sup>2</sup> (see Tables A1-A4). In order to achieve yield strengths in the practical range and to remove unknown residual stresses caused by cold-drawing, it was decided that the tubes should be subject to heat-treatment.

## 2.2 Heat-Treatment

The factors which can influence the yield strength of heat-treated material are the heating temperature, the warming-up time (heating rate), the holding time, and the cooling-down time (cooling-rate) of the heat-treatment and the original yield stress. Some heat-treatments, whose aims were to eliminate the residual stresses associated with fabrication or cold-drawing procedures and/or to reduce the yield strength of cold-formed material by removing the work-hardening effect, were reported in Refs. 4,5,6,9 and 11.

However, it proved impossible to derive any relationship between the aforementioned factors and the final yield strength from the data given in these references because the heat-treatment procedures were not fully described

except in Ref. 11. The heating temperatures ranged from 550°C to 800°C while very slow cooling was common. Hence a series of systematic preliminary heat-treatments was proposed to select the appropriate procedure for the current models. Firstly, six 300 mm length tensile specimens were cut from each parent tube and flattened (the effect of flattening on the static tensile yield strength is discussed later). Secondly, the specimens were heat-treated in a sand box inside the University's Hedlin Electric Furnace whose chamber volume is 43,000 cm<sup>3</sup> to various heating temperatures in the range 350°C to 750°C with various holding times between 0 and 3 hours. Finally, the furnace was allowed to cool overnight to ambient conditions.

Results of the preliminary heat-treatment are presented in Appendix A. In Figs. A1 and A2, the variation of yield stress with heating temperature and holding time are plotted. From these results, a temperature of 550°C and two hours of holding time were selected for the first main heat-treatment, while 550°C and three hours of holding time were selected for the second, the aim being to reduce the yield stress to some 250 N/mm<sup>2</sup> while also avoiding the development of thick scale.

The two main heat-treatments were conducted by an independent firm. However, the results of these showed the yield stress to be higher than expected, by some 200 N/mm<sup>2</sup>. The much shorter warming-up time (see Fig. A3) which could not be simulated in the preliminary heat-treatments seemed to be the main cause of the difference. The scale effect arising from the difference in furnace sizes may also have been a contributing factor. It is suggested that warming-up time is an important factor in determining heat-treatment effects.

## 2.3 Test Rig

2.3.1 **Striker and Runway:** In order to bring a rigid striker, having a pre-determined amount of kinetic energy, into violent contact with a deformable model, it was decided to use an existing runway and striker (see Fig. 1). The striker consisted of a box mounted on four wheels having a vertical aluminium wedge, whose angle was 45° and tip was sharp, mounted on the front of the box. The light weight of the striker was 18.8 kg which could be increased to 50.0 kg by the addition of weights in the box. The runway was constructed from a pair of angled rails mounted on a frame. It consisted of a straight path inclined at 30° which was joined to a horizontal one by a curved



segment. By releasing the striker from different heights on the inclined section of the runway, the speed of the striker could be varied up to approximately  $3.0 \text{ ms}^{-1}$ . Further details of both are given in Ref. 12.

2.3.2 Test Rig: In order to avoid the possibility of fracture of the tension side and local crippling of the compression side of the model ends, it was decided to adopt simply supported roller support conditions. This would allow free rotational and axial movement of the ends of the specimens but no lateral movement. This configuration was achieved with a test rig which consisted of a pair of rigid frames bolted to the laboratory floor and a pair of model holders. Each model holder was doubly-hinged, created by two carefully machined pins, and was mounted on the rear face of the front member of the rigid frame (see Fig. 2). The width of the model holders was 50 mm and their insides were lined with rubber in order to prevent unfavourable scratching of the model surface during installation and testing.

### 3. TEST PROCEDURE

The procured tubes were cut in accordance with the schedule shown in Fig. 3. Both ends of each model were machined flat. Models B1, B3, D4, E3 and H1 were sent off for the first main heat-treatment and the others for the second one. The detailed procedure of both main heat-treatments is described in Section 2.2. Following heat-treatment all models were marked with a grid using a steel pin. The grid was to assist in the measurements described below.

#### 3.1 Pre-Test Measurements

After grid-marking, the thickness, circularity and straightness of each tube was surveyed. Also their static tensile yield stress and Young's modulus were measured.

Thickness was measured at 60 points along each tube using a KrautKramer-Branson CL204 ultrasonic thickness probe with a grease couplant. Records were taken at the ends, the quarter points and the mid-length of each model every  $30^\circ$  around the circumference. The measurements were checked against micrometer readings taken at the tube ends. Outside diameter was measured at these same positions using a vernier calliper.

Five LVDTs were used for the measurement of initial out-of-straightness. Their output was logged using a Solatron 3510 Integrated Measuring System in conjunction with an Apple micro-computer. Prior to the model measurements, the LVDT gauge factors were checked with slip gauges and the reference points for the LVDTs were determined using a solid, straight and round datum bar whose straightness had been checked with a straight edge and circularity with a vernier caliper.

The datum bar, whose measured mean diameter was 50.55 mm, was positioned in a lathe. Five LVDTs were placed at positions selected according to tube length and the bar position (Fig. 4). The datum bar was then rotated every 90° and its position recorded each time. The reference point of each LVDT, which was distant 25.27 mm from the centre of the lathe, was then found by taking the mean of the corresponding results.

With the reference points established, the datum bar was replaced by a model. The distances between the reference points and the corresponding points on the model were then recorded every 30° around the circumference. The initial out-of-straightness was then found by calculating the deviations at mid-length and quarter points from the straight line joining the end points. The average initial out-of-straightness was determined by taking the mean of the two deviations in the same plane.

Material properties were determined from at least six tensile tests from each parent tube. Test specimens were prepared in accordance with Ref. 13 and tests were conducted more or less according to the procedure recommended in Ref. 14. Tests were performed in a Tinius-Olsen 0-20,000 lb testing machine (Fig. 5). The speed of crosshead separation is recommended to provide a rate of strain in the specimen of 300 micro-strain per minute in the plastic range of the test. For the purpose of these tests, however, the specimens were loaded steadily at a rate of strain such that it took about five minutes to pass the yield point and at a strain of 5000 micro-strain the crossheads were stopped for two minutes. The minimum value recorded during this period was taken as the corresponding static tensile yield stress. Young's modulus was obtained from the initial slope of the stress-strain curve.

### 3.2 Impact Tests

3.2.1 *Light Emitting Diode and Detector:* In order to record the displacement history of the striker and the overall bending deformation history of the struck model, a light emitting diode (LED 1) was attached to the top of the front wall of the striker and to the mid- and quarter-points of the model (LED 2 and 3 respectively). For recording, a light detector was attached to a beam of the laboratory ceiling. The principle on which the system is based is that when infra-red light from an LED is focussed onto the detector surface, a photocurrent divided among 4 electrodes occurs which is then used to obtain 2 signals linearly related to the coordinates of the LED on a plane parallel to the detector surface. The velocities of the striker immediately before and after impact were obtained from the slopes of the displacement curve of the LED on the striker.

3.2.2 *Infra-Red Switches:* Two infra-red switches were placed 110 mm apart near the bottom end of the runway to confirm the striker velocity obtained from the LED on the striker (Fig. 6). The first one was set to start a timer and the second to stop it as the striker passed in front of each. The impact speed was estimated as the ratio of the distance between the two infra-red switches to the time recorded.

3.2.2 *Mass of Striker:* The mass of the striker including the vertical wedge and any added lead weight was measured using a weight scale.

3.2.4 *Strain-Gauging:* All the models were gauged with nine or ten quarter bridge strain gauges to record the strain histories during and after impact and their residual strains (Fig. C1).

3.2.5 *High Speed Tape Recorder:* In order to store the output from the 3 LED's and 4 strain gauges during the impact tests a seven channel high speed tape recorder was used in conjunction with four strain amplifiers. The tape speed was set to 60 inches per second for recording and to 15/16 inches per second for realisation of the recorded data using a four channel pen-recorder.

3.2.6 *Model Installation:* The model was carefully positioned in the test rig such that first contact by the striker would occur at mid-length and at the 180° position on the circumference. Both ends of the model were then gripped firmly in the model holders.

After installation of the model, wiring of the strain gauges and fixing of the LEDs, the striker with added weights if necessary was released at particular heights on the runway to acquire the required speed.

A preliminary test on a dummy model was made to measure the deceleration of the striker during impact using an accelerometer attached to the dummy in order to establish the history of the interactive force between the striker and the model. However, from the recorded results it was not possible to separate the rigid body acceleration of the striker from the vibrations of the member on which the instrument was mounted. Hence, the accelerometer was not used any more in the main tests. A video tape recording was made of the first three tests in the hope of developing a better understanding of the sequence of local denting and overall bending damage which occurred during the impact. However, it was not used further because the recording speed of 25 frames per second was not fast enough for this purpose.

**3.2.7 Extent of Damage Measurements:** The same technique which was established for the initial out-of-straightness measurements (see section 3.1) was employed to measure the overall bending damage on the struck model (Fig.7). The deviations from the straight line joining the two end points were measured on the opposite side to that of the dent at the mid- and quarter-length positions. Measurement was also made at the dent centre when the dent centre was off mid-length. The overall bending damage of the opposite side to that of the dent was determined by subtracting the initial out-of-straightness values. The overall bending damage of the specimen centroid was then calculated by adding the change of the distance between the specimen centroid and the opposite side to that of the dent<sup>[20]</sup>.

For the local denting damage measurements, the outside diameter of the struck model was measured using a vernier calliper. Measurements were performed in the axial plane coinciding with the position of maximum indentation along the longitudinal centre line of the dent every 5 mm up to points 50 mm away from the transverse centre line and every 10 mm beyond these points. The dent depths were estimated by subtracting these values from the initial outside diameter measurements of the model.

## 4. RESULTS

### 4.1 Pre-test Measurements

Detailed results of all the pre-test measurements are presented in Appendix B. They include the thickness, outside diameter and initial out-of-straightness measurements including initial out-of-straightness plots, yield strength, and Young's Modulus values, with at least one typical stress-strain curve per each parent tube.

**4.1.1 Initial Out-of-Roundness:** In Table B1, the initial out-of-roundness in the form of initial ovality ( $\frac{D_{\max} - D_{\min}}{D_{\text{mean}}} \times 10^2$ ) is presented. For most of the models the initial ovality at both ends is much higher than in the middle. Also the ovality of some thinner models (nominal thickness = 1.22 mm) is higher than that of the remaining specimens. The initial ovality of models A4, B4 and C4 is higher than the limit of 1.00 specified in the DnV-OS Rules<sup>[15]</sup>.

In Table 1, a summary of mean model geometry and material properties is given including some corresponding cov's and geometric parameters.

**4.1.2 Initial out-of-straightness:** Initial out-of-straightness was determined by averaging the values in each plane, i.e. 0°-180° and so on, of the model. The initial out-of-straightness of models C3, F3 and H2 is higher than the limit ( $\frac{doi}{L} \times 10^3 = 1.5$ ) specified in Ref. 15.

**4.1.3 Yield Strength and Young's Modulus:** Most of the tensile test specimens were cut from 300 mm long heat-treated stubs and then flattened and machined. Initially, the influence of flattening on the yield strength was investigated by comparing the mean yield strength of flattened specimens with that of curved specimens. The results are given in Table 2. From the table, it seems likely that the values of yield strength obtained from the flattened specimens can be used as a measure of the yield stress in the corresponding model because the changes due to flattening are within the variation expected of a variable having a cov of 5-6%. The tests on the curved specimens demonstrated typical elastic-rigid-plastic stress-strain responses, while those on the flattened specimens demonstrated a 'rounded' response which confirmed the unknown residual stresses due to cold forming had been removed by the heat treatment.

Most of the specimens demonstrated a 1-4% cov in yield strength (Table 1) while the mean yield strength of the thinner models (nominal thickness = 1.22mm) was greater than that of thicker specimens (nominal thickness = 2.03mm) by some 40 N/mm<sup>2</sup>.

Of the total number of 82 specimens, a mean of  $2.12 \times 10^5$  N/mm<sup>2</sup> together with an 8.8% COV was obtained for Young's modulus. The dubious accuracy of drawing tangential lines to rounded stress-strain curves contributes to the scatter found for this material constant.

#### 4.2 Impact Tests

From recordings made during the impact tests, the following tables and figures have been prepared and are presented for each model in turn in Appendix C:

- . the mass and impact speed of the striker and the residual strains in the struck model;
- . the dynamic recording of the LEDs and the strain gauges;
- . measurements of the extent of damage; and
- . plots of the extent of damage.

A summary of the test results is given in Table 3. They include the striker's mass and the velocities immediately before and after impact, the extent of damage of the struck model together with their non-dimensionalised values, impact duration and the period of elastic vibration after impacts.

Model F1 was tested again with a different mass and velocity for the striker because only negligible residual strains were generated by the original test: the second test has been designated FIP. During the test on model B4 the high speed tape recorder was not operated properly so that its dynamic recording results were lost. Its results were not used in the prediction formulae derivation and the following comparisons. For the test on model H1 the wire connecting LED1, which was fixed to the striker, was cut due to its significant lateral movement.

4.2.1 LED Results: The velocities of the striker immediately before and after impact were measured from the slopes of displacement history of LED1. The result was then compared with the value measured using the infra-red switches. All the velocities measured using LED1 were smaller than those found from the infra-red switches, except that of model F2. The difference between the result of the two methods is probably due to the deceleration of the striker during its passage over the distance of some 300 mm between the infra-red switches and the model.

The outputs from LED2 and 3, attached at the mid- and quarter-lengths of the model respectively, were found to be very useful in understanding the overall bending behaviour of the model during and after impact. Some delay in their movement after the beginning of contact between the striker and the model indicated that most of the purely local denting occurred before overall bending together with some additional local denting deformation similar to that observed in static tests of simply supported tubes subjected to lateral knife edge loads<sup>[16]</sup>. Most of the output from LED2 and 3 showed that elastic overall bending vibrations occurred after impact, but some of these were more clearly demonstrated by the strain gauges.

4.2.2 Strain Gauge Results: Most of the strain history curves obtained from the output of the four strain gauges monitored during each test initially have sharp knees which can be used to indicate the beginning of contact between the striker and the model and then very apparent elastic vibrations following impact. They proved to be very useful in the determination of both the impact duration and the period of elastic vibration after impact. Impact duration was determined by measuring the time from the beginning of contact to the start of elastic vibration.

There is some disagreement between the results for residual strain found by using the strain meter and from the strain amplifier, especially for the first three tests on models A3, B1 and C3, in which proper strain gauge wire terminals were not used.

4.2.3 End Boundary Conditions: From the periods of elastic vibration after impact and the strain history of Strain-Gauge 10, which was located at a point 100 mm distant from the bottom end and at 180° on the circumference (see Fig. C1), it is possible to make some judgements concerning the end conditions realised during the tests.

The period of natural vibration,  $T_E$ , of a thin-walled circular section is given in Ref. 17 as follows:

$$T_E = \frac{1}{f} = \frac{1}{k} \sqrt{\frac{8\rho}{E}} \cdot \frac{L_1^2}{D} \quad (1)$$

where  $f$  = natural frequency

$E$  = Young's Modulus ( $2.12 \times 10^5$  N/mm<sup>2</sup>, mean of the tensile test results)

$\rho$  = material density ( $7.8 \times 10^{-6}$  kg/mm<sup>3</sup> for steel)

$k$  = constant depending upon the mode of vibration and the end constraints for the fundamental mode;

$k = 1.57$  , simply supported end conditions

$k = 3.57$  , built-in end conditions

In Table 4, the natural periods of elastic vibration (fundamental mode) of the undamaged models as calculated from the above for both the simply supported and built-in end conditions are given. In most of the tests the fundamental mode dominated and the periods were greater than the values corresponding to the simply supported end conditions. For all of the tests the strain history during impact of Strain-Gauge 10 exhibited a much smaller amplitude than that of the other strain gauges (Strain-Gauges 1, 3, 4, 7 or 8), except the test on model C2 which was larger. From the results it seems likely that the end conditions realised were much closer to those of the simple support than to the built-in one, although the effect of damage on the free vibration of the models has not been examined.

4.2.4 Extent of Damage: The locations of the centre of impact are given in Appendix B. In some tests the striker unexpectedly impacted off centre both longitudinally and circumferentially due to its lateral movement and bounce. The depth of dent and out-of-straightness plots show a corresponding



asymmetry. Interestingly, the tests on models C3 and G3 showed a negative out-of-straightness, i.e. towards the striker. The reason for this is not obvious. The depth of dent and out-of-straightness non-dimensionalised with respect to model diameter and length respectively are given in Table 3.

## 5. DAMAGE PREDICTION

### 5.1 Existing Formulae

Even though a number of studies on the plastic dynamic behaviour of structures have been reported, only a few are available to predict the extent of damage of unstiffened tubulars suffering from impacts. Those available are briefly reviewed here, together with their assumptions.

In Ref. 8, Ellinas and Walker proposed a semi-analytic method to predict both the local denting and overall bending damage of fully flexurally restrained tubes. The non-dimensionalised depth of dent is obtained by solving eqns. (2) and (3) simultaneously.

$$P = 150 m_p \delta_d^{1/2} \quad (2)$$

$$P = \frac{4M_p}{L_i} (1 + \cos\beta - \beta) \quad (3)$$

where  $P$  = ultimate lateral load at which the overall bending deformation starts

$$m_p = \frac{1}{4} \sigma_Y t^2 \quad , \text{ plastic moment resultant of the tube wall}$$

$$\delta_d = \frac{d_d}{D} \quad , \text{ non-dimensionalised dent depth}$$

$$M_p = D^2 t \sigma_Y \quad , \text{ plastic moment capacity of the undamaged tube cross-section}$$

$$\beta = \left(1 - \frac{\sigma_{pd}}{\sigma_Y}\right) \delta_d^{1/2}$$

$$\sigma_{pd} = \sigma_Y \frac{D}{t} \left[ \left(\frac{4}{3} \delta_d\right)^2 + \left(\frac{t}{D}\right)^2 \right]^{1/2} - \frac{4}{3} \sigma_d$$

For overall bending damage, eqn (4) was derived by assuming that all the kinetic energy of the striker,  $E_k$ , was absorbed by the tube developing deformations in both the local denting and overall bending modes.

$$\delta_o = \frac{E_k - E_d}{4 M_p (1 + \cos \beta - \beta)} \quad (4)$$

where  $\delta_o = \frac{d_o}{L}$ , non-dimensionalised out-of-straightness

$E_k = \frac{1}{2} M V_o^2$ , initial kinetic energy of the striker

$M$  = mass of the striker

$V_o$  = speed of the striker immediately before impact

$E_d = 100 m_p D \delta_d^{3/2}$ , energy absorbed during the formation of the local dent

For overall bending damage only, de Oliveira derived eqn (5) using a mode approximation technique based on the assumptions of a rigid-plastic hollow circular section member which is perfectly clamped and fully restrained axially at both ends, and that geometry changes are disregarded<sup>[18]</sup>:

$$\delta_o = \frac{1}{2} \frac{E_k}{N_o D} \left( \frac{1}{1 + \frac{m}{3M}} \right) \quad (5)$$

where  $N_o = \pi D t \sigma_y$  fully plastic axial force

$m$  = mass of the tube model

Ellinas et al suggested another very simple formula, eqn (6), for the local denting damage prediction in Ref. 19. The tube was assumed to be sufficiently stiff in bending that all the impact energy was absorbed by the local denting mode.

$$\delta_d = \left( \frac{0.051 E_k}{D t^2 \sigma_y} \right)^{2/3} \quad (6)$$

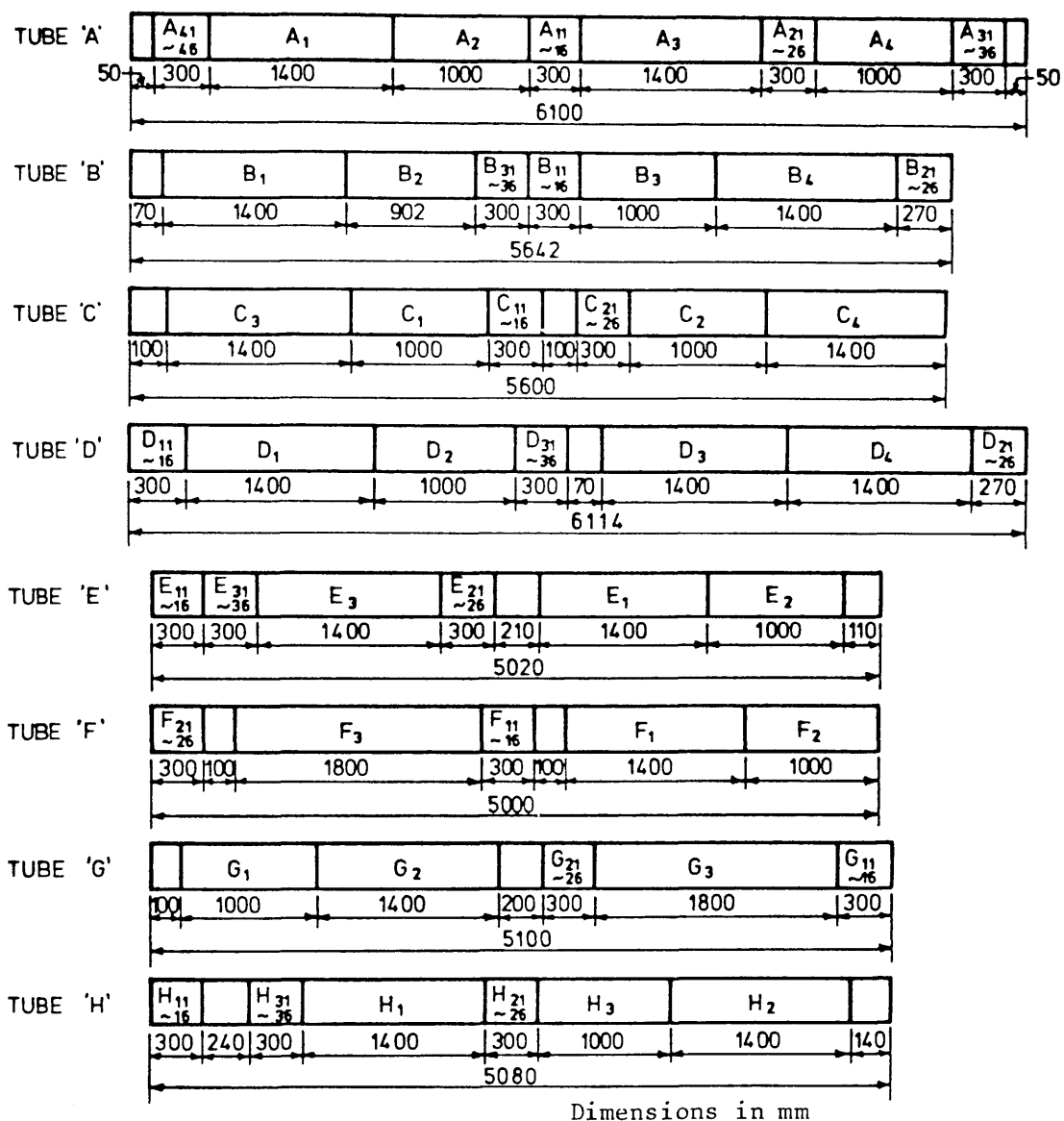


**Fig. 3 TUBE CUTTING PLAN**

## 5.2 Derivation of Proposed Formulae

As can be seen from the test results in Table 3, all the initial kinetic energy of the striker,  $E_k$ , is not absorbed as damage by the struck model. Also, in most cases both modes of local denting and overall bending damage co-exist. Accordingly, the existing formulae, which were briefly reviewed above, are either conservative or not strictly applicable. Of course, it is not easy to analytically solve the detailed dynamic elastic-plastic behaviour of even a simple structure like the unstiffened tubular which is considered here. Therefore, exploitation of the present results is probably most usefully done through the derivation of an empirical formula based on the results.

A simple relationship, eqn. (7), between the energy,  $E_d$ , absorbed during the formation of a local dent, and the non-dimensionalised dent depth, was suggested by Ellinas and Walker in Ref. 8 as follows:

$$E_d = 100 m_p D \delta_d^{3/2} \quad (7)$$

According to rigid plastic theory the energy,  $E_o$ , absorbed by a simply supported beam which collapses by the formation of a centre hinge is given by:

$$E_o = 4 M_p \delta_o \quad (8)$$

Equations (7) and (8) have been selected as the basis of the present derivation not necessarily because they can predict the actual absorbed energies accurately, but because of their simplicity.

After surveying the trends of the basic parameters,  $N_o L/t/E_k D$  was selected as a common variable for the ratios of the absorbed energies to the initial kinetic energy of the striker. Using eqns (7) and (8) and the test results, equations for the means and upper bounds of the two ratios,  $E_d/E_k$  and  $E_o/E_k$  were obtained as follows:

Mean: /

Mean:

$$\begin{aligned} E_d/E_k &= 0.377 (2.54 - \log \lambda_E)^2 & ; \log \lambda_E < 2.54 \\ 0 & & ; \log \lambda_E \geq 2.54 \end{aligned} \quad (9a)$$

$$\begin{aligned} E_o/E_k &= 0.345 (2.62 - \log \lambda_E)^2 & ; \log \lambda_E < 2.62 \\ 0 & & ; \log \lambda_E \geq 2.62 \end{aligned} \quad (10a)$$

Upper Bound:

$$\begin{aligned} E_d/E_k &= 0.377 (2.77 - \log \lambda_E)^2 & ; \log \lambda_E < 2.77 \\ 0 & & ; \log \lambda_E \geq 2.77 \end{aligned} \quad (9b)$$

$$\begin{aligned} E_o/E_k &= 0.345 (2.77 - \log \lambda_E)^2 & ; \log \lambda_E < 2.77 \\ 0 & & ; \log \lambda_E \geq 2.77 \end{aligned} \quad (10b)$$

where  $\lambda_E = \frac{N_o L_i t}{E_k D}$ , is the energy parameter

The mean and upper bound equations, eqns (9a,9b) and (10a,10b) with the corresponding test data are illustrated in Figs 8a and 8b respectively.

Finally, substituting eqns (9a,9b) and (10a,10b) into eqns (7) and (8) respectively, expressions for predicting the means and upper bounds for the local denting and overall bending damage of the unstiffened tubular resulting from an impact are found to be:

Mean:

$$\begin{aligned} \delta_d &= 0.131 (2.54 - \log \lambda_E)^{4/3} \left( \frac{E_k}{N_o t} \right)^{2/3} & ; \log \lambda_E < 2.54 \\ 0 & & ; \log \lambda_E \geq 2.54 \end{aligned} \quad (11a)$$

$$\begin{aligned} \delta_o &= 0.271 (2.62 - \log \lambda_E)^2 \frac{E_k}{N_o D} & ; \log \lambda_E < 2.62 \\ 0 & & ; \log \lambda_E \geq 2.62 \end{aligned} \quad (12a)$$

Upper Bound:

$$\begin{aligned} \delta_d &= 0.131 (2.77 - \log \lambda_E)^{4/3} \left( \frac{E_k}{N_o t} \right)^{2/3} & ; \log \lambda_E < 2.77 \\ 0 & & ; \log \lambda_E \geq 2.77 \end{aligned} \quad (11b)$$

$$\begin{aligned} \delta_o &= 0.271 (2.62 - \log \lambda_E)^2 \frac{E_k}{N_o D} & ; \log \lambda_E < 2.77 \\ 0 & & ; \log \lambda_E \geq 2.77 \end{aligned} \quad (12b)$$

### 5.3 Discussions of the Proposed Formulae

Comparisons between predictions by the proposed and the existing formulae with the present test results are presented in Table 5. These are also illustrated in Figs. 9a and 10a for the proposed, and Figs. 9b and 10b for the existing formulae respectively. The accuracy of a prediction can be measured by its COV of the ratios of predicted to actual values. However, it is not possible to obtain a meaningful COV when actual values approach zero. Therefore COVs were calculated for the test data whose extents of damage exceeded the tolerance specifications given in Ref. 15, i.e.  $\delta_0 \text{ act.} \geq 0.01$  for the local denting damage, and  $\delta_0 \text{ act.} \geq 0.0015$  for overall bending damage. In Figs. 11a and 11b, the ratios of the predicted values using these formulae to the test results are presented together with their means and COVs. From the figures, the improved accuracy and consistency of the proposed formulae compared with that of the others can be seen.

Interestingly, according to the proposed upper bound equations, eqns (11b) and (12b), no damage in either the local denting or overall bending modes is to be expected when the energy parameter,  $\lambda_E = N_0 L_{it} / E_k D$ , is greater than about 600. This critical value would appear to provide some guidance for the impact resistance design of tubulars.

The method suggested in Ref. 8 to predict both modes of damage appears to suffer from the following shortcomings:

- for the local denting damage, the predicted values are constant in relation to the geometry and the material properties of the struck models irrespective of the striker's mass and speed because eqns (2) and (3) contain no terms to represent the kinetic energy of the striker; and
- for the overall bending damage, the lack of consistency shown in Figs. 10b and 11b is due to the too conservative estimate of the extent of local denting.

The formulae suggested in Refs. 19 and 18, although they overpredict the experimental results, especially in the ranges  $\delta_d$  of 0.01–0.05 and  $\delta_0$  of

0.0015-0.002 where the detrimental effect of damage on the ultimate strength of the damaged tubes is most sensitive<sup>[8,9]</sup>, can be seen in Figs. 10b and 9b to demonstrate some consistency with the measured values.

Of course, the end conditions of the unstiffened tubular members of offshore structures are different from the simply supported roller end conditions which were simulated approximately in the present tests. In offshore structures, there are flexural and axial restraints which are likely to generate damage at the ends in the form of yielding, fracture and possibly local buckling. Should the overall bow become significant, some energy absorption will occur through membrane action should the axial restraints be adequate. Also, the rigid knife edge of the striker may generate more detrimental types of damage in the models than might occur in the case of an encounter by an attendant vessel. Naturally, interaction with the surrounding water will also alter the dynamic response and therefore the pattern of energy absorption and type of damage generated.

Therefore, it is premature to expect the results of the present tests to be directly applicable to the design of offshore structures. However, by modification of the proposed empirical formulae to take account of the differences attributable to the end conditions, the shape of the impactor, and fluid-interaction, the above could form the basis of a procedure for the economic design of offshore structure members against impacts and collisions.

## 6. CONCLUSION

Twenty four lateral impact tests on heat-treated seamless cold drawn tubes have been successfully completed. Notable findings observed in the present experiments are:

- both local denting and overall bending modes of damage were produced during all tests;
- most of the purely local denting phase occurred before overall bending was initiated and then accompanied by some additional local denting; and

- in the most cases, elastic flexural vibrations of the struck models were clearly apparent after impact.

Very simple mean and upper bound empirical formulae in explicit form have been proposed using the present test results to predict the possible extent of damage to unstiffened tubular members suffering from impacts. According to the upper bound equations, no damage in the form of either local denting or overall bending is likely when the energy parameter,  $\lambda_E = N_0 L_1 t / E_k D$ , is greater than some 600.

In order that the results of this study can be made relevant to the design of offshore structures against collisions or other impacts, further experimental and/or theoretical work is necessary, especially to examine the influence of the end conditions upon the extent of damage.

## ACKNOWLEDGEMENTS

Acknowledgements are due to many of the technical staff of Glasgow University, in particular Messrs. C. Miller, R.B. Christison, J. Fulton and R. McLetchie, for their assistance in carrying out the experiments.

The financial support of the SERC Marine Technology Directorate for some of the earlier phases of this work is also acknowledged.

## REFERENCES/



## REFERENCES

1. Donegan, E.: 'New Platform Designs Minimize Ship Collision Damage', *Petroleum Engineer International*, p. 76, Feb. 1982.
2. Standing, R.G. and Brendling, W.: 'Collision of Attendant Vessels with Offshore Installations: Part 1 - General Description and Principal Results', UK Dept. of Energy, Offshore Technology Report OTH 84208, 1984.
3. Furnes, O. and Kohler, P.E.: 'Safety of Offshore Platforms - Classification Rules and Lessons Learned', in *Marine and Offshore Safety*, eds. Frieze, P.A., McGregor, R.C. and Winkle, I.E., Elsevier Science Publishers, Amsterdam, pp 53-170, 1984.
4. Smith, C.S., Kirkwood, W. and Swan, J.W.: 'Buckling Strength and Post-Collapse Behaviour of Tubular Bracing Members Including Damage Effects', *Proc. of Second Intl Conf. on Behaviour of Offshore Structures (BOSS 79)*, BHRA Fluid Engg, Cranfield, pp 303-326, Aug. 1979.
5. Smith, C.S., Somerville, W.L. and Swan J.W.: 'Residual Strength and Stiffness of Damaged Steel Bracing Members', *Proc. of the Thirteenth Annual Offshore Technology Conference*, Houston, Paper OTC 3981, pp 273-282, May 1981.
6. Taby, J., Moan, T. and Rashed, S.M.H.: 'Theoretical and Experimental Study of the Behaviour of Damaged Tubular Members in Offshore Structures', *Norwegian Maritime Research*, vol. 9, no. 2, pp 26-33, 1981.
7. Valsgård, S. and Foss, G.: 'Buckling Research in Det norske Veritas', in *Buckling of Shells in Offshore Structures*, eds. Harding, H.E. et al., Granada, London, pp 491-548, 1982.
8. Ellinas, C.P. and Walker, A.C.: 'Effects of Damage on Offshore Tubular Bracing Members', *Proc. of IABSE Colloquium on Ship Collision with Bridges and Offshore Structures*, Copenhagen, pp 253-261, May 1983.
9. Smith, C.S.: 'Assessment of Damage in Offshore Steel Platforms', in *Marine and Offshore Safety*, eds. Frieze, P.A., McGregor, R.C. and Winkle, I.E., Elsevier Science Publishers, Amsterdam, pp 279-307, 1984.
10. Ellinas, C.P.: 'Ultimate Strength of Damaged Tubular Bracing Members', *Proc. ASCE, Jnl of Structural Engg*, vol. 110, no. 2, pp 245-259, Feb. 1984.
11. Frieze, P.A. and Sands, G.: 'Conoco/ABS Ring Stiffened Cylinder Tests: Final Report', Dept. of Naval Architecture and Ocean Engineering, University of Glasgow, Feb. 1984.
12. Samuelides, E.: 'Structural Dynamic and Rigid Body Response Coupling in Ship Collisions', PhD Thesis, University of Glasgow, 1984.
13. 'Methods for Tensile Testing of Metals: Part 2. Steel (General)', BS18: Part 2, British Standards Institution, London, 1971.

## REFERENCES (Cont'd)

14. 'Recommended Standard Practices for Structural Testing of Steel Models', Transport & Road Research Laboratory, Supplementary Report 254, 1977.
  15. DnV 'Rules for the Design, Construction and Inspection of Offshore Structures, 1977, Appendix C: Steel Structures', Det norske Veritas, Oslo, with corrections, 1982.
  16. Thomas, S.G., Reid, S.R. and Johnson, W.: 'Large Deformations of Thin-Walled Circular Tubes under Transverse Loading - I', Int. J. Mechanical Sciences, vol. 18, pp 325-333, 1976.
  17. Miller, B.L.: 'Wave Slaming on Offshore Structures', National Maritime Institute, Report No. NMI R81 (OT-R-8041), p 15, Mar. 1980.
  18. de Oliveira, J.G.: 'Design of Steel Offshore Structures against Impact Loads due to Dropped Objects', Proc. of the Third Intl Symp. on Offshore Engineering Structures, pp 466-483, edited by F.L.L.B. Carneiro et al, Rio de Janeiro, 1981.
  19. Ellinas, C.P., Supple, W.J. and Walker, A.C.: 'Buckling of Offshore Structures: A State-of-the-art Review', Granada, London, 1984.
  20. Cho, S-R and Frieze, P.A.: 'Axial Compression Tests on Undamaged and Damaged Tubulars: Final Report', University of Glasgow, Dept. of Naval Architecture and Ocean Engineering Report (in preparation).
-

Model No.	Length (mm)		Outside Diameter $D_o$		Diameter to mid-thickness $D$ (mm)	Thickness $t$		Maximum Initial out-of-straightness $d_{oi}$ (mm)	Heat Treatment	Static Tensile Yield Strength $\sigma_y$		Young's Modulus $E$		$D/t$	$L_i/D$	$d_{oi} \times 10^3 \over L$
	Actual $L$	for impact test $L_i$	Mean (mm)	COV (%)		Mean (mm)	COV (%)			Mean $\sigma_y$ (N/mm <sup>2</sup> )	COV (%)	Mean $E$ (N/mm <sup>2</sup> $\times 10^5$ )	COV (%)			
E3	1400	1350	50.91	0.11	48.86	2.05	3.17	0.15	1st	467	1.26	2.21	4.56	23.8	27.6	0.11
F1	1400	1350	50.91	0.09	48.88	2.03	1.48	0.49	2nd	425	1.40	2.22	7.92	24.1	27.6	0.35
F2	1000	950	50.90	0.12	48.87	2.03	1.97	0.71	2nd	425	1.40	2.22	7.92	24.1	19.4	0.71
F3	1800	1750	50.86	0.12	48.84	2.02	1.28	2.83	2nd	425	1.40	2.22	7.92	24.2	35.8	1.57
G1	1000	950	50.95	0.14	48.91	2.04	1.37	0.17	2nd	429	1.96	2.00	2.56	24.0	19.4	0.17
G2	1400	1350	50.92	0.05	48.87	2.05	1.24	0.12	2nd	429	1.96	2.00	2.56	23.8	27.6	0.09
G3	1800	1750	50.93	0.14	48.89	2.04	1.43	0.16	2nd	429	1.96	2.00	2.56	24.0	35.8	0.09
H1	1400	1350	50.90	0.07	48.86	2.04	1.44	0.49	1st	431	3.01	2.16	8.80	24.0	27.6	0.35
H2	1400	1350	50.92	0.16	48.90	2.02	3.06	3.48	2nd	421	3.29	2.12	11.2	24.2	27.6	2.49
H3	1000	950	50.94	0.19	48.91	2.03	2.23	0.19	2nd	421	3.29	2.12	11.2	24.1	19.4	0.19

Notes:

The nominal outside diameter of all models is 50.80 mm, and the nominal thicknesses are 1.22 mm (A3 to D4) and 2.03 mm (E3 to H3).

The geometry and material properties of model F1p are the same as model F1.

Details of 1st and 2nd heat-treatment are given in the main report, section 2.2.

Table 1 : Measured Model Geometry and Material Properties

Model No.	Length (mm)		Outside Diameter $D_o$		Diameter to mid-thickness $D$ (mm)	Thickness $t$		Maximum Initial out-of-straightness $d_{oi}$ (mm)	Heat Treatment	Static Tensile Yield Strength $\sigma_y$		Young's Modulus $E$		$D/t$	$L_i/D$	$d_{oi} \times 10^3 \frac{L}{D}$
	Actual $L$	for impact test $L_i$	Mean (mm)	COV (%)		Mean (mm)	COV (%)			Mean $2$ (N/mm $^2$ )	COV (%)	Mean $2$ (N/mm $^2 \times 10^5$ )	COV (%)			
A3	1400	1350	50.88	0.12	49.65	1.23	1.46	0.37	2nd	472	4.25	2.00	4.73	40.4	27.2	0.26
A4	1000	950	50.89	0.35	49.69	1.20	1.41	0.28	2nd	472	4.25	2.00	4.73	41.4	19.1	0.28
B1	1400	1350	50.86	0.15	49.66	1.20	2.18	0.72	1st	491	2.52	2.05	8.20	41.4	27.2	0.51
B3	1000	950	50.92	0.11	49.72	1.20	0.70	0.50	2nd	482	2.36	2.04	9.99	41.4	19.1	0.50
B4	1400	1350	50.86	0.22	49.66	1.20	1.03	0.28	2nd	482	2.36	2.04	9.99	41.4	27.2	0.20
C1	1000	950	50.97	0.21	49.76	1.21	1.59	0.91	2nd	441	3.00	2.32	12.5	41.1	19.1	0.91
C2	1000	950	50.91	0.18	49.69	1.22	1.81	0.31	2nd	441	3.00	2.32	12.5	40.7	19.1	0.31
C3	1400	1350	50.86	0.14	49.64	1.22	1.79	3.68	2nd	441	3.00	2.32	12.5	40.7	27.2	2.63
C4	1400	1350	50.85	0.24	49.63	1.22	1.71	0.25	2nd	441	3.00	2.32	12.5	40.7	27.2	0.18
D1	1400	1350	50.91	0.09	49.71	1.20	1.71	0.43	2nd	480	2.56	2.11	6.77	41.4	27.2	0.31
D2	1000	950	50.98	0.10	49.77	1.21	1.18	0.14	2nd	480	2.56	2.11	6.77	41.1	19.1	0.14
D3	1400	1350	50.91	0.08	49.70	1.21	1.57	0.64	1st	485	3.07	2.10	7.83	41.1	27.2	0.46
D4	1400	1350	50.90	0.14	49.69	1.21	1.70	0.28	1st	485	3.07	2.10	7.83	41.1	27.2	0.20

Table 1 : Measured Model Geometry and Material Properties(contd.)

Nominal Thickness (mm)	Curved		Flattened		
	Specimen No.	Mean Yield Strength (N/mm <sup>2</sup> )	Specimen No.	Mean Yield Strength (N/mm <sup>2</sup> )	Change
1.22	A21,A23,A25	498	A23,A24,A26	465	-7%
	B34,B35,B36	497	B31,B32,B33	485	-2%
2.03	G21,G23,G25	422	G22,G24,G26	436	+3%
	H34,H35,H36	425	H31,H32,H33	438	+3%

Table 2 : Effect of Flattening of Tensile Specimen on Yield Strength

Nominal Dimensions DxtxLi (mm)	Corresponding Model No.	Natural Period (ms)		
		Measured (Damaged)	Simply Supported End Conditions	Built-in End Conditions
49.58x1.22x 950	A4,B3,C1,C2,D2	9.2-13.3	6.3	2.8
49.58x1.22x1350	A3,B1,B4,C3 C4,D1,D3,D4	15.5-19.5	12.7	5.6
48.77x2.03x 950	F2,G1,H3	5.9-10.2	6.4	2.8
48.77x2.03x1350	E3,F1,F1p, G2,H1,H2	14.1-16.1	12.9	5.7
48.77x2.03x1750	F3,G3	23.9-24.1	21.7	9.5

Table 4: Natural Period of Elastic Vibration (Fundamental Mode) of Undamaged Models

Model No.	Mass of Striker M (KG)	Initial Velocity of Striker $V_o$ (m/s)	Rebound Velocity of Striker $V_r$ (m/s)	Extent of Damage		$d_d/D$	$d_o/L$	Impact Duration $T_D$ (ms)	Period of Elastic Vibration after Impact $T_E$ (ms)
				Depth of Dent $d_d$ (mm)	Out-of-straightness $d_o$ (mm)				
A3	18.8	2.34 (2.42)	0.94	3.5	4.12	0.071	0.003	33.6	18.0
A4	18.8	2.43 (2.77)	1.16	4.6	3.51	0.093	0.004	25.0	12.7
B1	23.5	2.52 (2.63)	1.47	3.1	3.90	0.062	0.003	37.8	17.5
B3	28.3	1.57 (1.75)	0.89	2.8	1.69	0.056	0.002	28.0	12.8
B4	28.3	- (2.27)	-	2.2	2.37	0.044	0.002	-	-
C1	41.1	1.18 (1.26)	0.53	2.0	1.13	0.040	0.001	31.3	13.1
C2	41.1	2.32 (2.64)	0.84	10.4	14.96	0.209	0.015	51.4	13.3
C3	41.1	0.92 (1.07)	0.69	0.5	0.17	0.010	0.000	45.6	15.5
C4	41.1	2.06 (2.15)	1.04	6.8	12.03	0.137	0.009	61.7	15.5
D1	28.3	1.16 (1.15)	1.04	0.2	0.52	0.004	0.000	37.8	17.2
D2	28.3	2.52 (2.83)	1.12	6.2	5.87	0.125	0.006	30.5	9.2
D3	28.3	2.55 (2.84)	1.24	5.3	7.78	0.107	0.006	41.9	17.3
D4	41.1	2.59 ( - )	1.09	9.1	20.70	0.183	0.015	69.7	19.5

Note: Initial velocities in parenthesis were measured using Infra-red Switches

Table 3 :    Test Results (contd.)

Model No.	Mass of Striker M(KG)	Initial Velocity of Striker $V_o$ (m/s)	Rebound Velocity of Striker $V_r$ (m/s)	Extent of Damage		$d_d/D$	$d_o/L$	Impact Duration $T_D$ (ms)	Period of Elastic Vibration after Impact $T_E$ (ms)
				Depth of Dent $d_d$ (mm)	Out-of-straightness $d_o$ (mm)				
E3	28.3	2.49 (2.66)	2.14	0.4	0.51	0.008	0.000	30.5	15.9
F1	50.0	0.55 (0.82)	0.31	0.0	0.00	0.000	0.000	39.8	14.1
F1p	41.1	1.91 (1.97)	1.13	0.8	1.13	0.016	0.001	36.1	15.9
F2	41.1	1.78 (1.65)	1.45	2.1	1.99	0.043	0.002	23.4	6.1
F3	28.3	2.53 (2.99)	1.70	1.2	2.76	0.025	0.002	42.2	23.9
G1	28.3	2.24 (2.73)	1.34	1.7	1.73	0.035	0.002	11.4	5.9
G2	28.3	2.59 (2.81)	1.84	1.8	3.40	0.037	0.002	32.0	15.9
G3	41.1	1.69 (1.86)	1.41	0.2	-0.54	0.004	0.000	52.2	24.1
H1	18.8	2.90 (2.96)	-	0.3	0.40	0.006	0.000	25.3	16.1
H2	41.1	2.55 (2.55)	1.39	3.2	6.06	0.065	0.004	39.1	15.9
H3	41.1	1.08 (1.16)	0.64	0.0	0.01	0.000	0.000	23.1	10.2

Notes:

Initial velocities in parentheses were measured using Infra-Red Switches.

Minus sign of out-of-straightness denotes opposite direction.

Table 3 :

Test Results

Model No.	Local Denting Damage ( $\delta_d$ )					Overall Bending Damage ( $\delta_o$ )				
	Test	Proposed		Ellinas & Walker Ref. 8	Ellinas Supple & Walker Ref. 19	Test	Proposed		Ellinas & Walker Ref. 8	Oliveira Ref. 18
		Mean	Upper Bound				Mean	Upper Bound		
A3	0.070	0.059	0.083	0.079	0.182	0.003	0.002	0.003	0.006	0.005
A4	0.093	0.082	0.109	0.137	0.192	0.004	0.004	0.005	0.002	0.006
B1	0.062	0.092	0.124	0.079	0.227	0.003	0.005	0.006	0.009	0.008
B3	0.056	0.043	0.061	0.137	0.139	0.002	0.002	0.002	-0.002	0.004
C1	0.040	0.036	0.052	0.135	0.127	0.001	0.001	0.002	-0.002	0.003
C2	0.209	0.194	0.241	0.133	0.310	0.015	0.013	0.017	0.013	0.013
C3	0.010	0.009	0.019	0.077	0.090	0.000	0.000	0.000	0.000	0.002
C4	0.137	0.123	0.161	0.076	0.265	0.009	0.007	0.009	0.013	0.010
D1	0.004	0.010	0.020	0.079	0.093	0.000	0.000	0.000	0.000	0.002
D2	0.125	0.142	0.180	0.136	0.258	0.006	0.008	0.011	0.008	0.010
D3	0.107	0.120	0.157	0.078	0.261	0.006	0.007	0.009	0.013	0.009
D4	0.183	0.193	0.244	0.078	0.341	0.015	0.013	0.017	0.020	0.014
E3	0.008	0.027	0.042	0.031	0.130	0.000	0.001	0.002	0.008	0.006
F1	0.000	0.000	0.000	0.031	0.027	0.000	0.000	0.000	0.000	0.001
F1p	0.016	0.025	0.040	0.031	0.126	0.001	0.001	0.002	0.008	0.005
F2	0.043	0.029	0.043	0.057	0.116	0.002	0.001	0.002	0.005	0.005
F3	0.025	0.027	0.043	0.020	0.144	0.002	0.001	0.002	0.010	0.006
G1	0.035	0.031	0.046	0.057	0.120	0.002	0.002	0.002	0.005	0.005
G2	0.037	0.035	0.053	0.031	0.145	0.002	0.002	0.003	0.010	0.007
G3	0.004	0.010	0.021	0.020	0.105	0.000	0.000	0.001	0.006	0.004
H1	0.006	0.026	0.041	0.031	0.128	0.000	0.001	0.002	0.008	0.005
H2	0.065	0.062	0.087	0.032	0.187	0.004	0.004	0.006	0.015	0.010
H3	0.000	0.003	0.009	0.058	0.059	0.000	0.000	0.000	-0.001	0.002

Table 5 : Comparison of Prediction with Test results



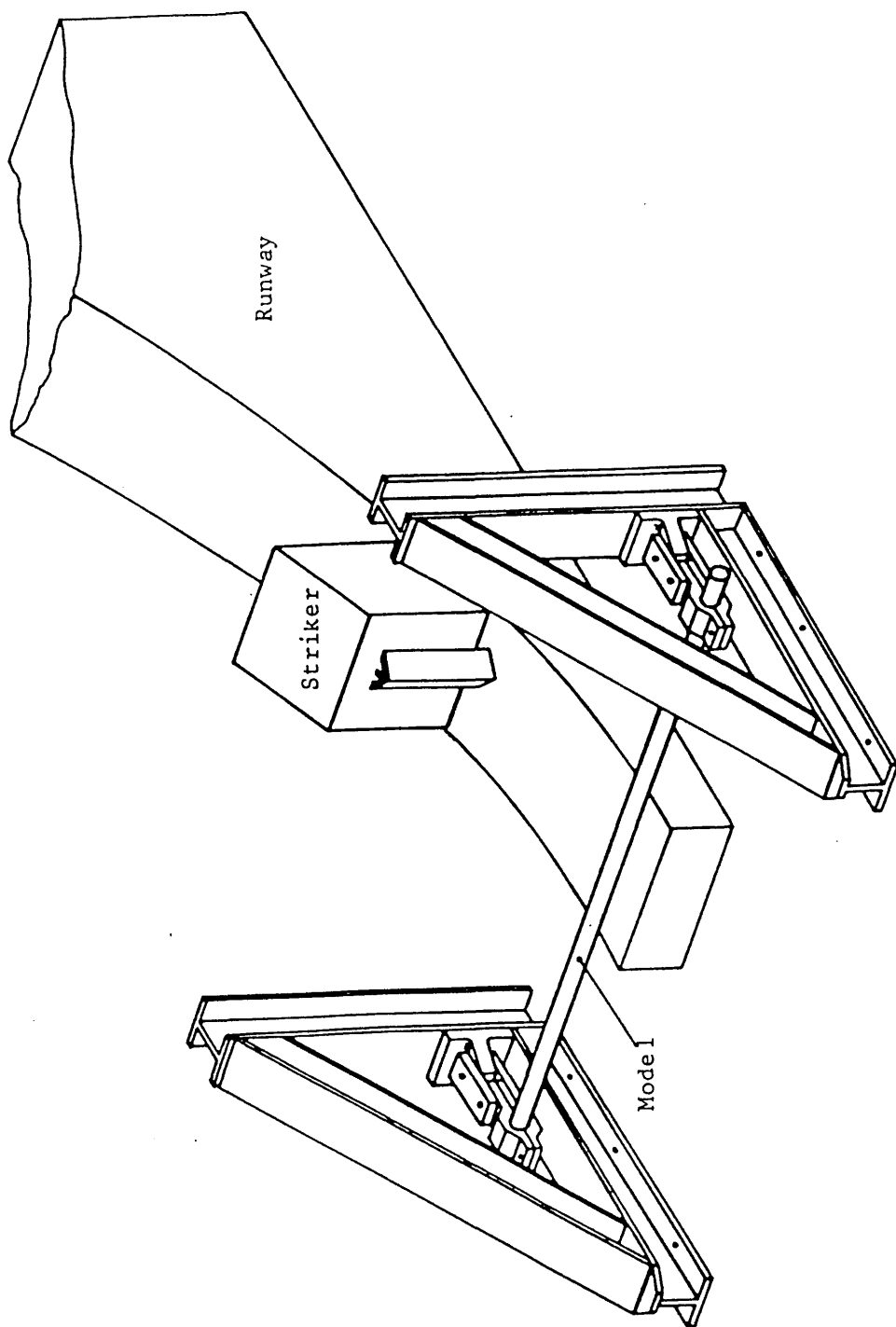


FIG. 1. ARRANGEMENT OF RUNWAY AND TEST RIG  
FOR LATERAL IMPACT TEST

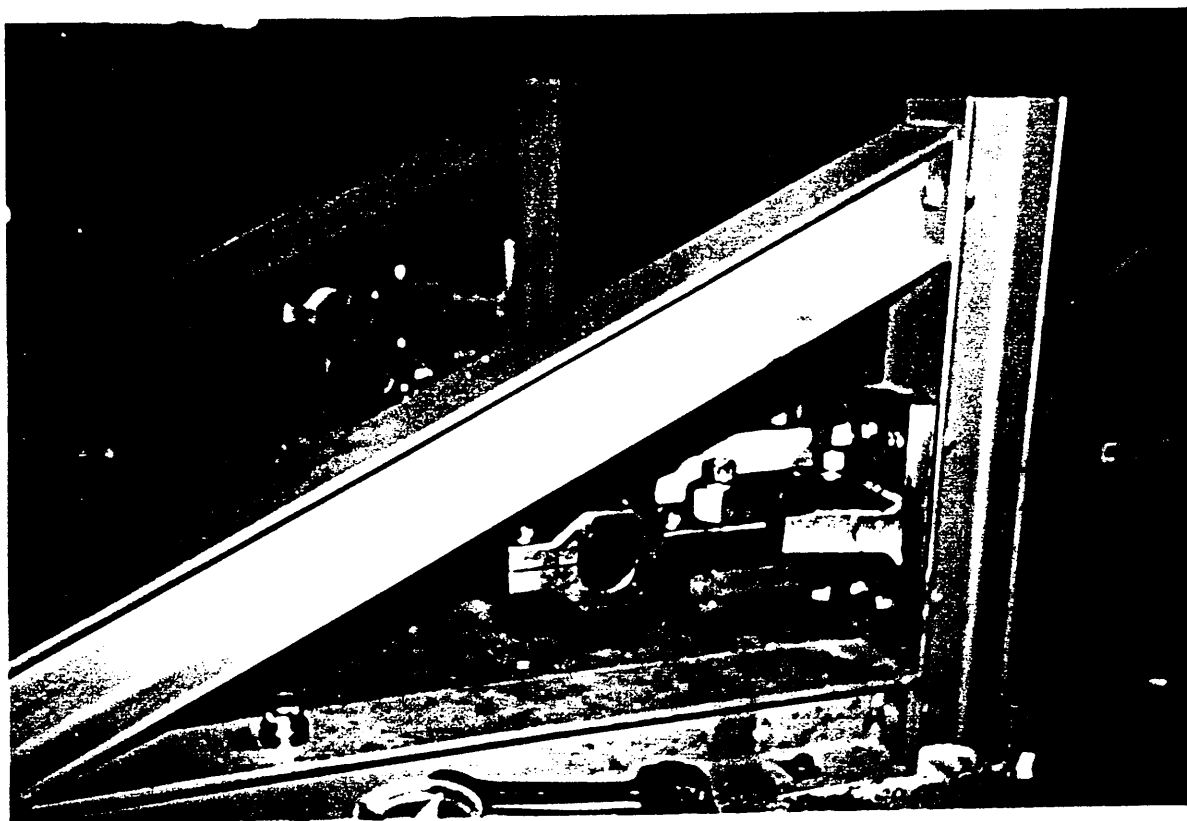


FIG. 2. CLOSE-UP OF TEST RIG

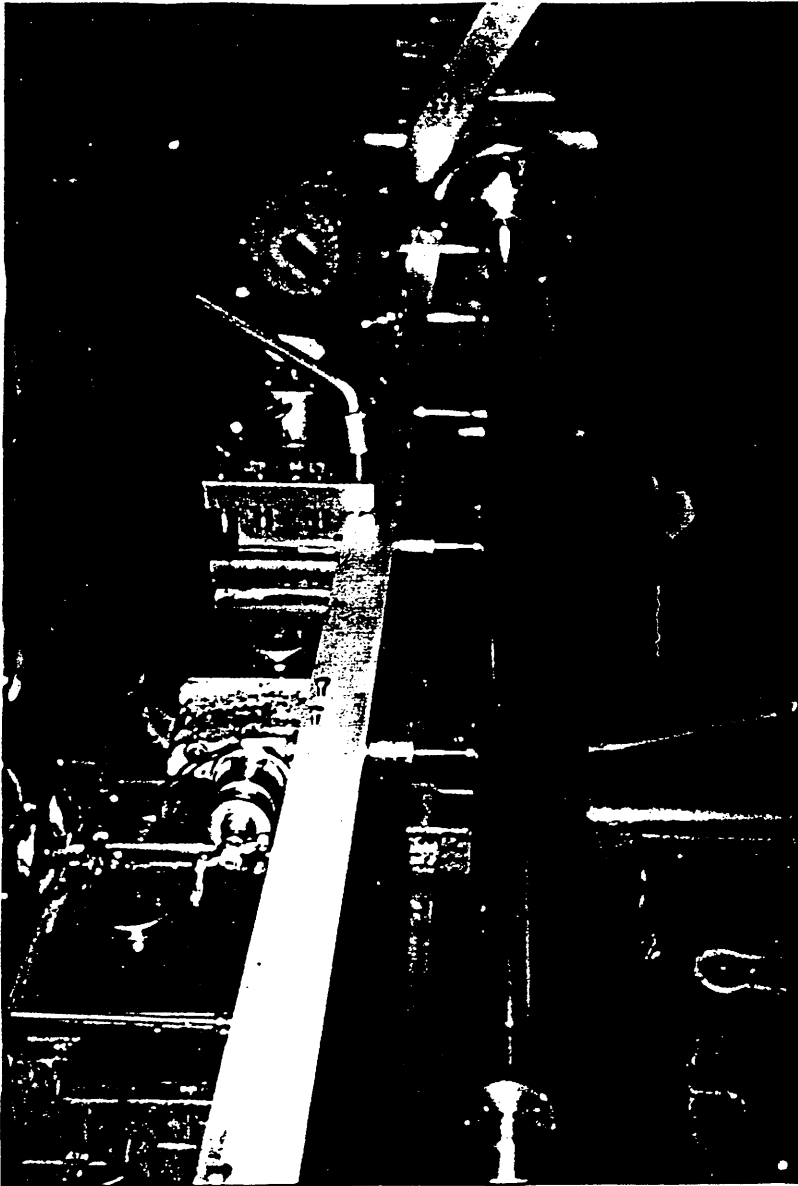


FIG. 4. DATUM BAR IN LATHE

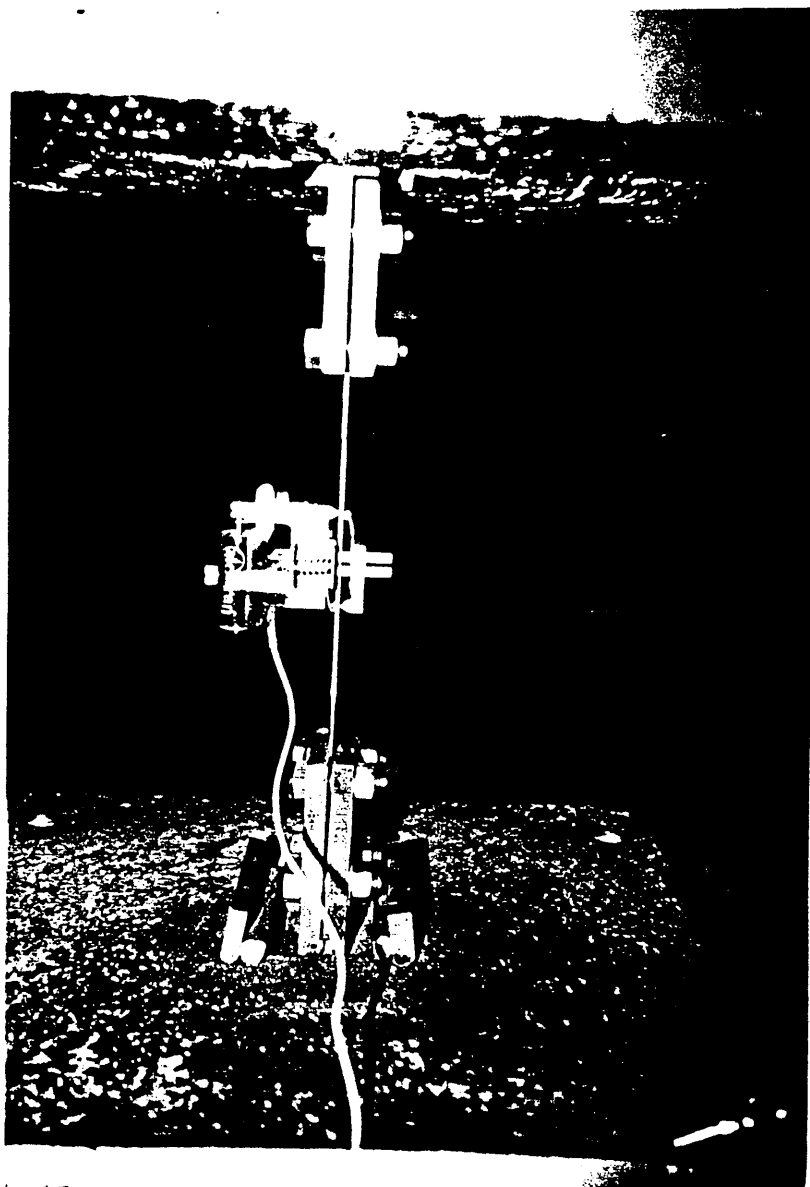


FIG. 5. TENSILE TEST SPECIMEN SET-UP IN JAWS  
OF TESTING MACHINE

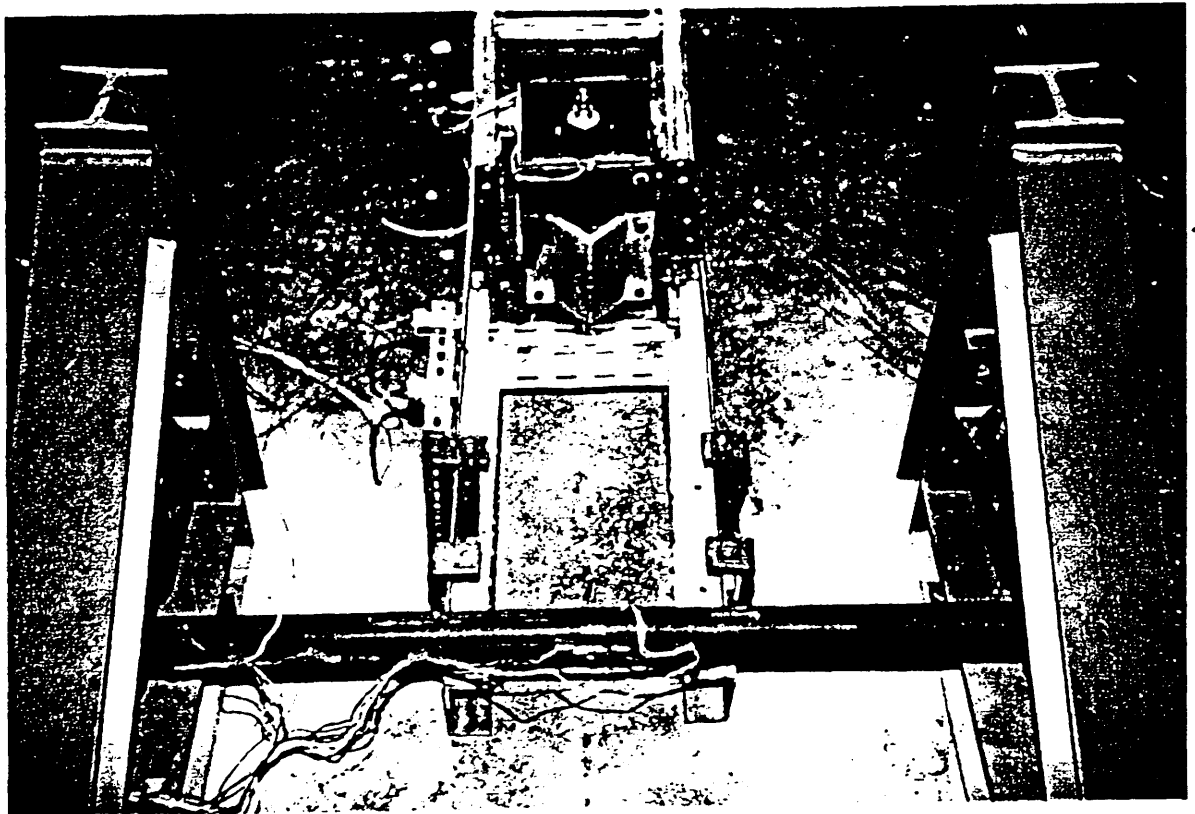


FIG. 6. STRIKER, INFRA-RED SWITCHES AND STRAIN-GAUGING  
MODEL IN TEST RIG PRIOR TO TEST

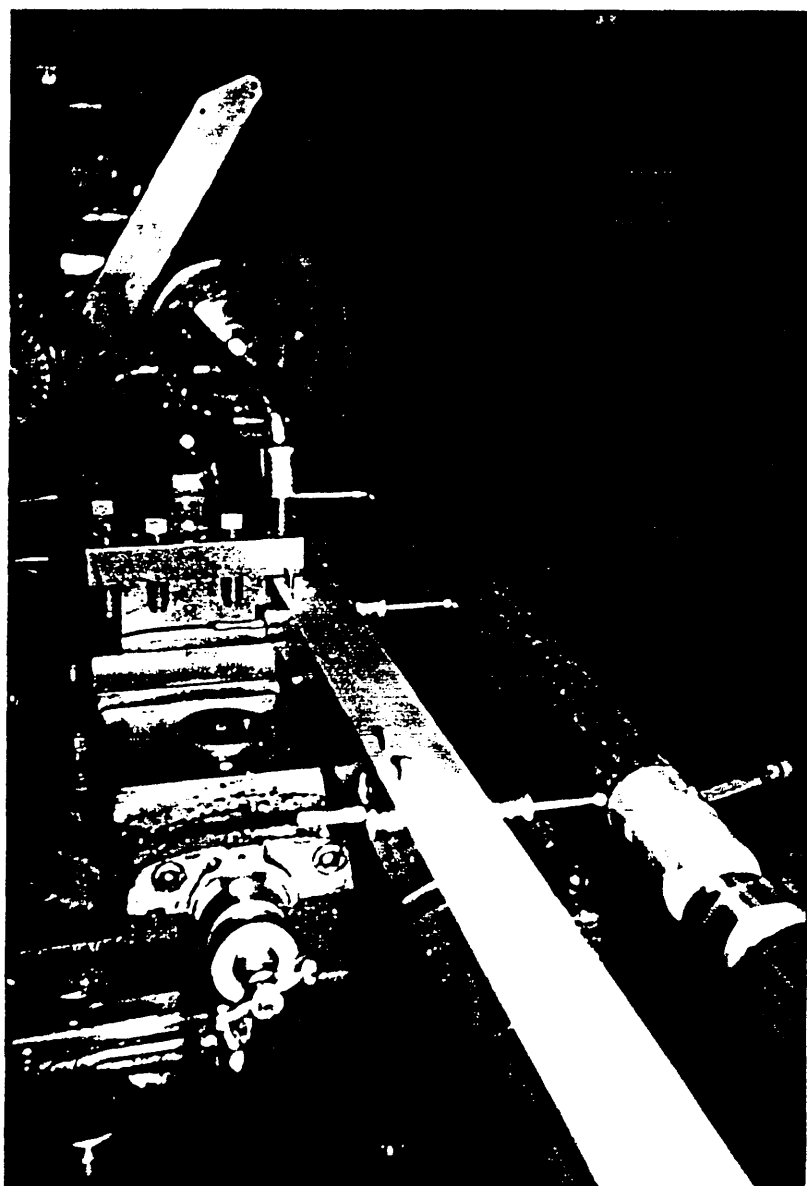


FIG. 7. OUT-OF-STRAIGHTNESS MEASUREMENT OF  
DAMAGED TUBE

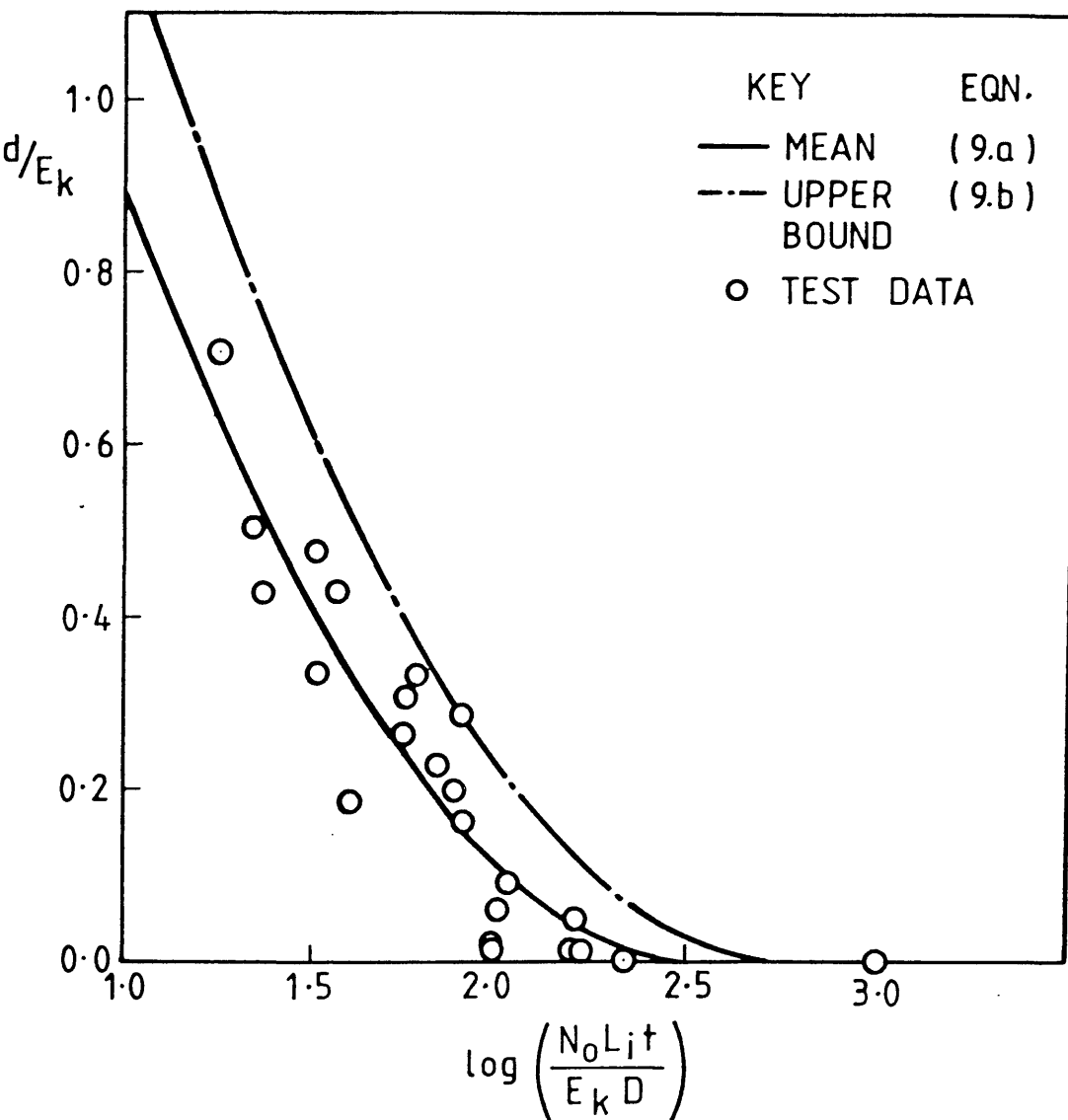


Fig. 8 a. MEAN AND UPPER BOUND CURVES  
FOR  $E_d/E_k$  WITH TEST DATA

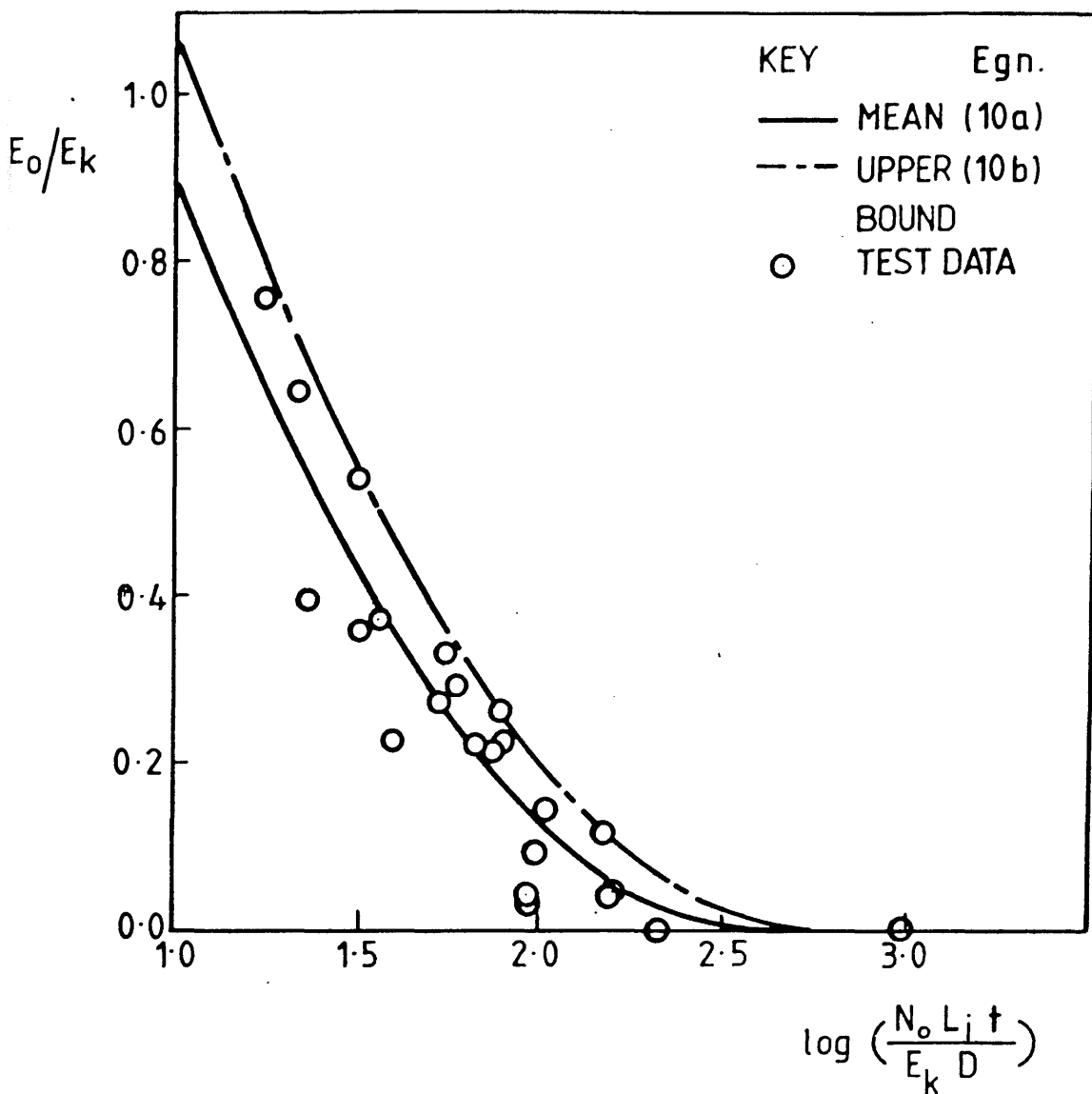


Fig 8b MEAN and UPPER BOUND CURVES  
for  $E_o/E_k$  with TEST DATA



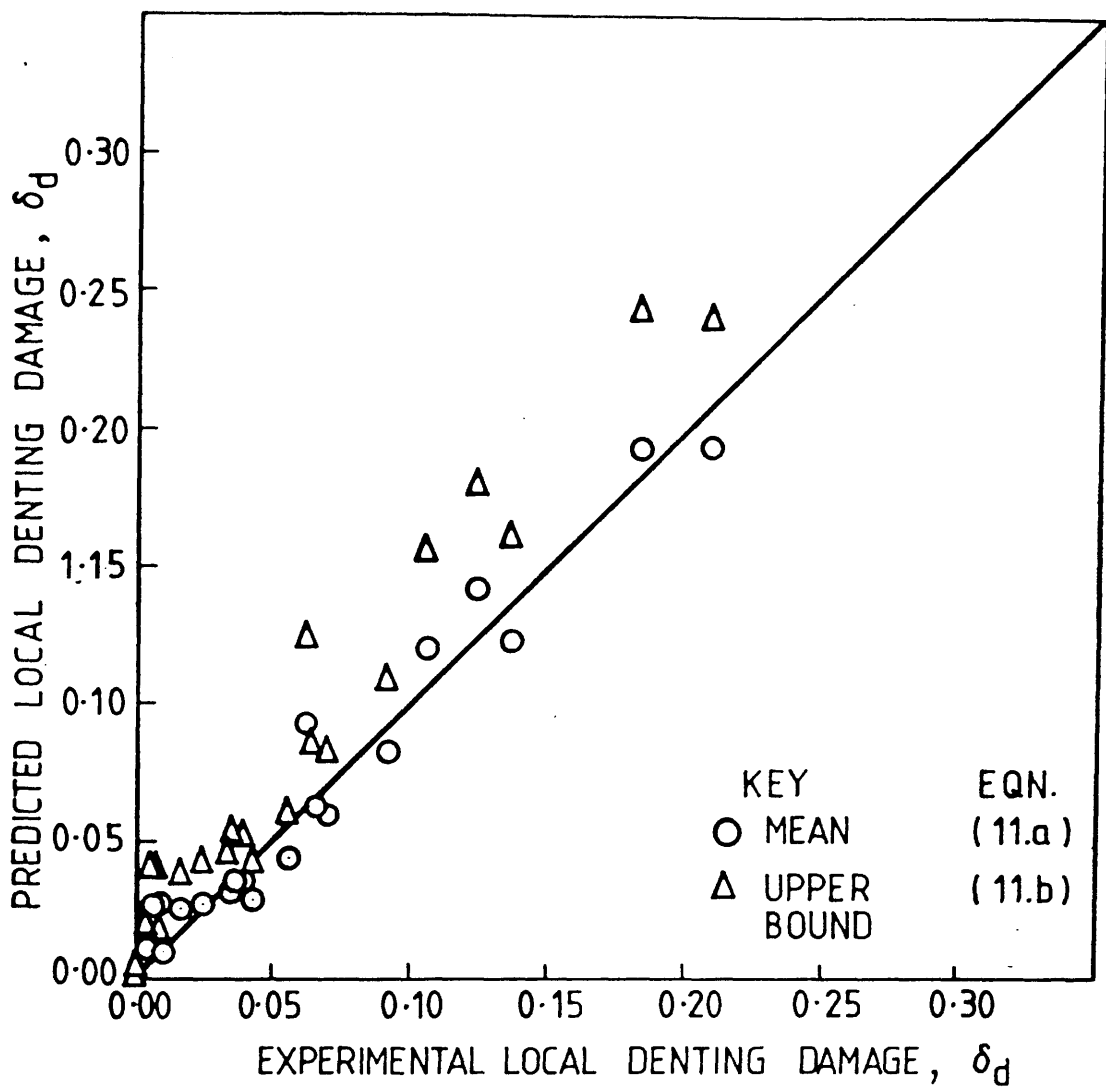


Fig.9a. COMPARISONS BETWEEN PREDICTIONS OF PROPOSED FORMULAE AND TEST RESULTS FOR LOCAL DENTING DAMAGE

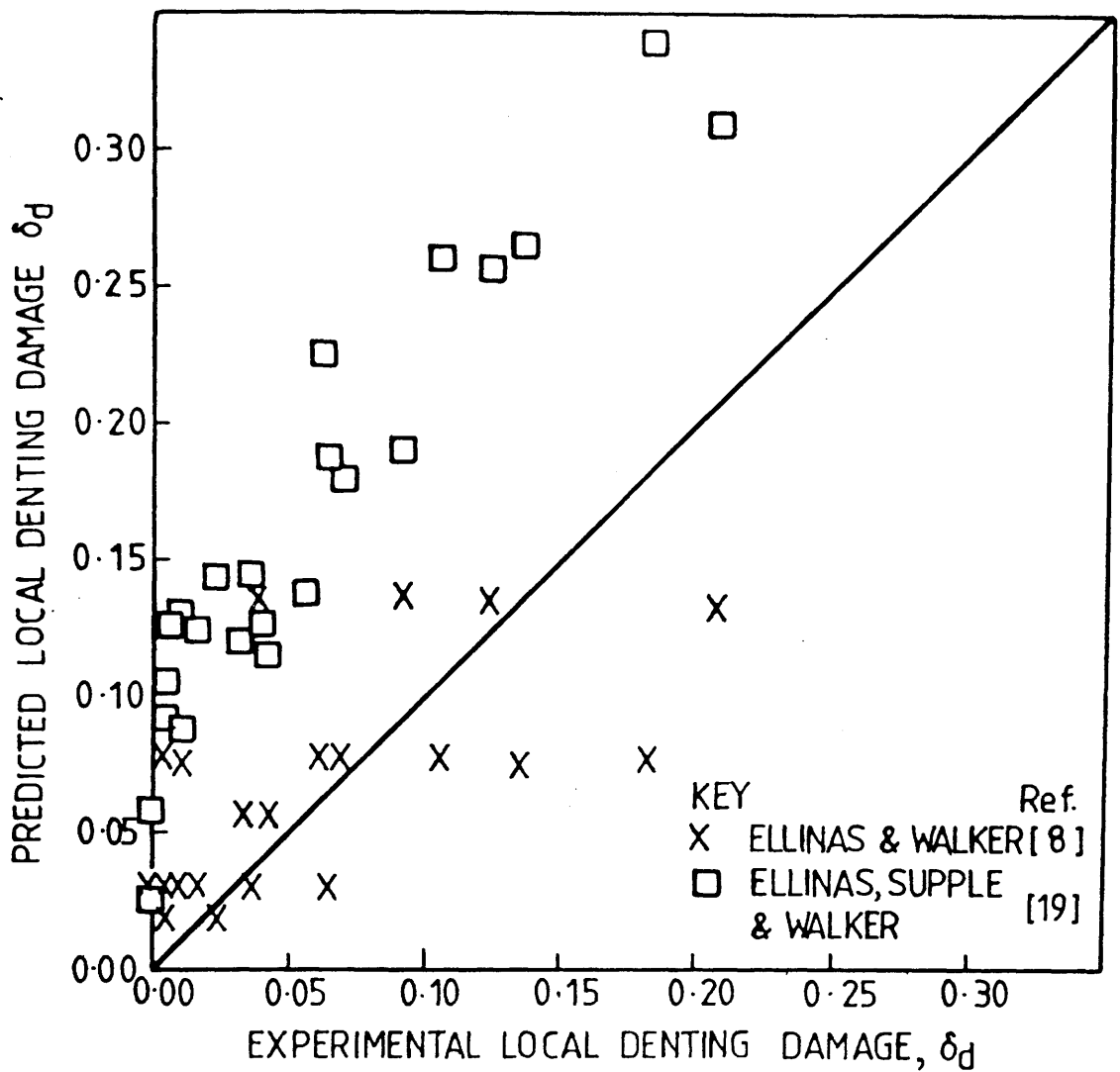


Fig. 9b. COMPARISONS BETWEEN PREDICTIONS of EXISTING FORMULAE and TEST RESULTS for LOCAL DENTING DAMAGE.

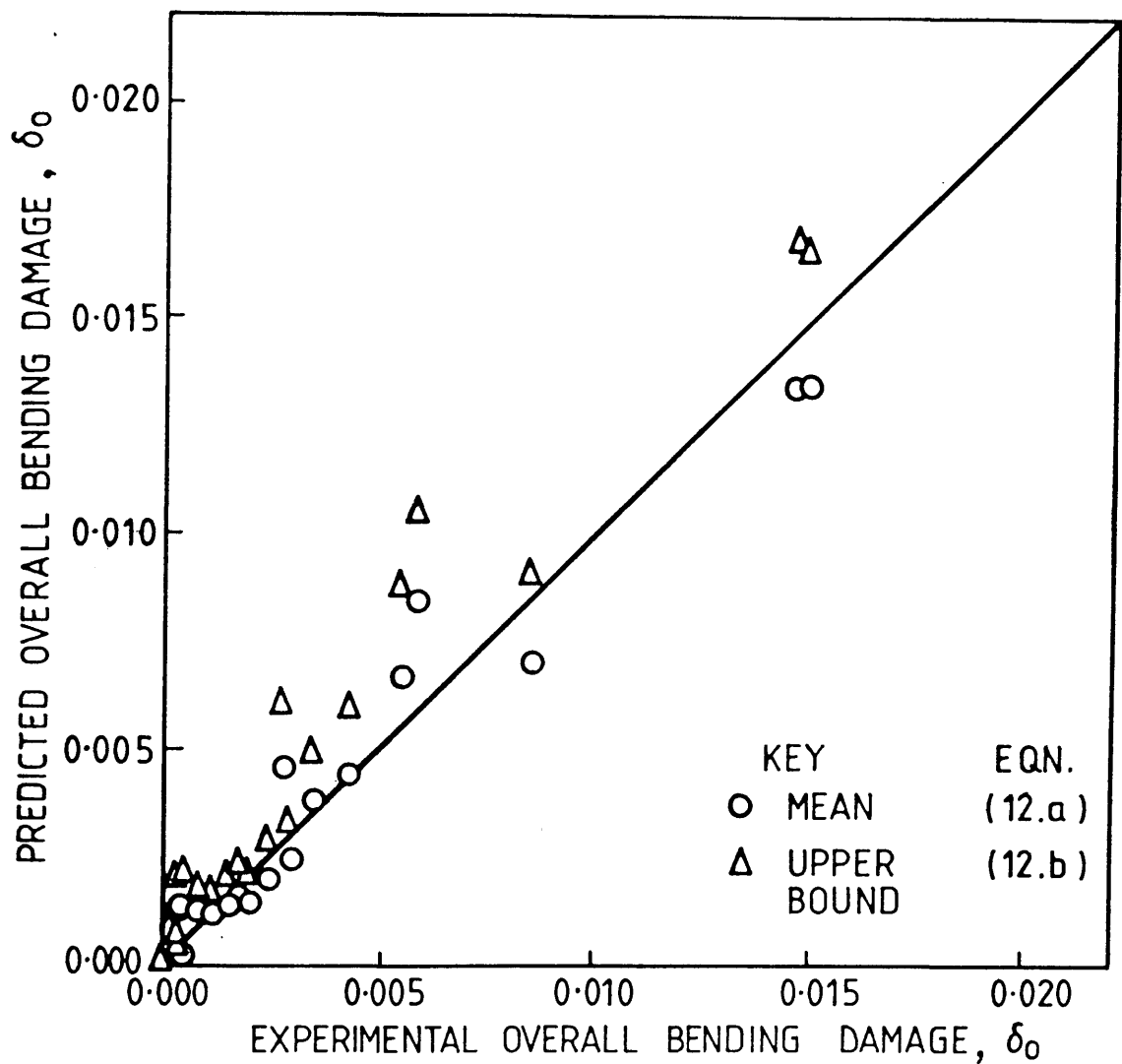


Fig. 10a. COMPARISONS BETWEEN PREDICTIONS OF PROPOSED FORMULAE AND TEST RESULTS FOR OVERALL DENTING DAMAGE

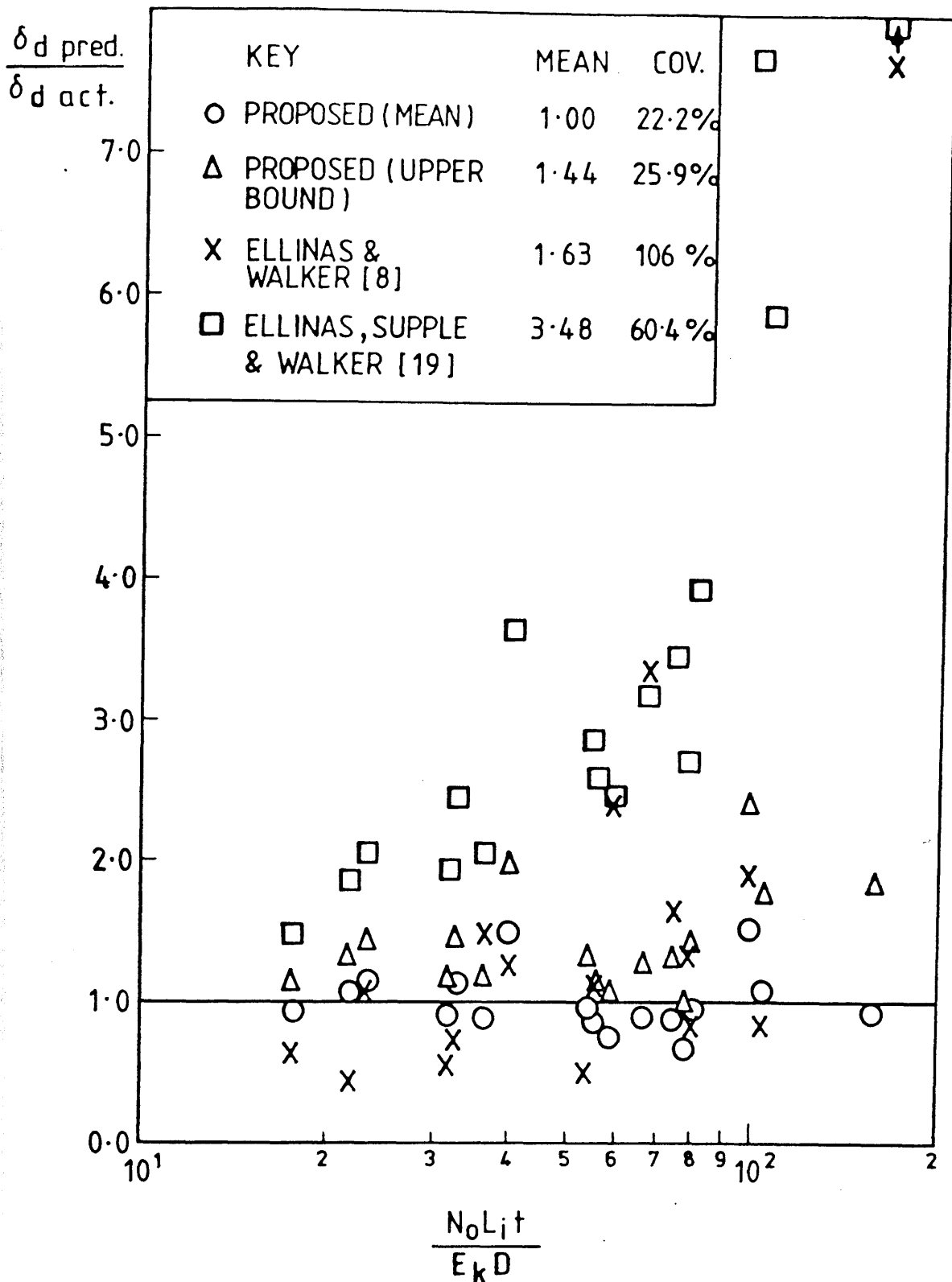


Fig.11a. COMPARISONS BETWEEN PREDICTIONS OF PROPOSED AND EXISTING FORMULAE AND TEST RESULTS FOR LOCAL DENTING DAMAGE (WHEN  $\delta_d \text{ act.} \geq 0.01$ )

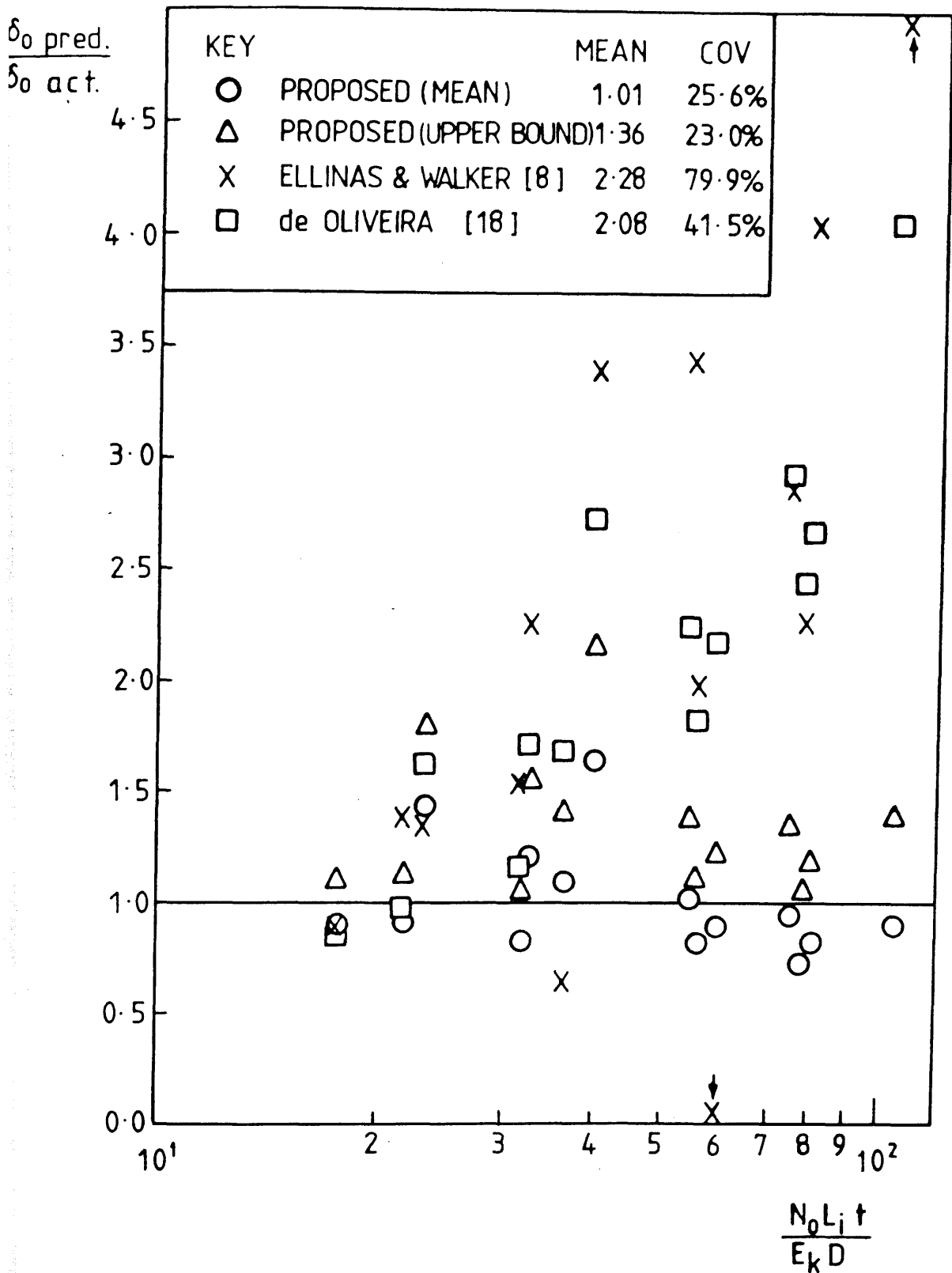


Fig. 11b. COMPARISONS BETWEEN PREDICTIONS of PROPOSED and EXISTING FORMULAE and TEST RESULTS for OVERALL BENDING DAMAGE (WHEN  $\delta_0 \text{ ACT.} \geq 0.0015$ )

**LATERAL IMPACT TESTS ON UNSTIFFENED CYLINDERS**

**FINAL REPORT**

**Volume II - Appendix**

**Sang-Rai CHO**

**Paul A. FRIEZE**

**Department of Naval Architecture and Ocean Engineering,  
University of Glasgow.**

## CONTENTS

	<u>Page</u>
INTRODUCTION	1
APPENDIX A. PRELIMINARY HEAT-TREATMENT RESULTS	2
APPENDIX B. PRE-TEST MEASUREMENTS	10
B. I          Thickness Measurements	11
B. II        Initial Shape Measurements	40
B. II. 1    Outside Diameter Measurements	42
B. II. 2    Initial Out-of-Straightness Measurements Table	56
B. II. 3    Initial Out-of-Straightness Plots	84
B. III        Tensile Test Results	112
B. III. 1    Typical Stress Strain Curves	113
B. III. 2    Tensile Test Results Table	131
APPENDIX C. DETAILED TEST RESULTS	138
C. I          Mass and Initial Velocity of Striker and Residual Strain Measurements	139
C. II        Dynamic Recording Results	153
C. III        Extent of Damage Measurements	209
C. III. 1    Extent of Damage Measurements Table	210
C. III. 2    Extent of Damage Plots	234

## INTRODUCTION

Twenty four lateral impact tests were conducted on twenty three unstiffened cylinders at the Department of Naval Architecture and Ocean Engineering, University of Glasgow. These tests and their results are documented in the report "Lateral Impact Tests on Unstiffened Cylinders". This report is contained in two volumes, Volume I - Main Report, and Volume II - Appendix.

Volume I describes the test programme and includes the derivation of formulae with which the extent of damage suffered in the collision of unstiffened cylindrical members of offshore structures with supply vessels or other objects can be predicted explicitly.

Volume II - Appendix contains the detailed information on which Volume I was based. The detailed preliminary heat-treatment, pre-test measurement and test results are contained in Volume II - Appendix.



## APPENDIX A.

### PRELIMINARY HEAT-TREATMENT RESULTS

Specimen No.	Breadth (mm)	Thickness (mm)	Static Yield Load (N)	Static Tensile Yield Strength (N/mm <sup>2</sup> )	Heat - Treatment		
					Heating Temperature (°C)	Warming-Up Time (Hr)	Holding Time (Hr)
A11	20.4	1.20	14000	571 (2.14)	-	-	-
A12	20.3	1.06	3860	180	750	2.9	2.5
A13	20.8	1.22	4710	186	550	1.7	2.5
A14	20.7	1.21	13400	544	350	0.8	2.8
A15	20.3	1.21	5320	216	550	1.7	2.0
A16	20.4	1.21	12000	487	450	1.2	2.5
B11	20.1	1.20	14500	602 (2.19)	-	-	-
B12	20.9	1.13	4110	174	750	2.9	3.0
B13	19.8	1.13	4210	188	650	2.3	2.5
B14	21.0	1.22	4140	162	750	2.9	0.0
B15	20.8	1.12	3770	162	750	2.9	1.0
B16*	20.6	1.22	12300	488	550	0.5	1.9

Notes: The figures in parentheses are the corresponding Young's Moduli in 10<sup>5</sup> x N/mm<sup>2</sup>  
 \*Specimen B16 was sent for the first main heat-treatment

TABLE A1: Results of Preliminary Heat-Treatment (I)

Specimen No.	Breadth (mm)	Thickness (mm)	Static Yield Load (N)	Static Tensile Yield Strength (N/mm <sup>2</sup> )	Heat - Treatment		
					Heating Temperature (°C)	Warming-Up Time (Hr)	Holding Time (Hr)
C11	19.7	1.21	12400	521 (2.34)	-	-	-
C12	18.7	1.22	6510	286	550	1.7	1.0
C13	18.3	1.22	4330	194	550	1.7	3.0
C14	20.4	1.22	6050	243	550	1.7	1.5
C15	21.1	1.18	10600	427	550	1.7	0.0
C16*	19.7	1.20	9210	390	550	0.5	2.9
D11	19.7	1.21	14100	592 (2.01)	-	-	-
D12	21.0	1.16	4510	185	750	2.9	3.0
D13	20.9	1.14	4450	187	650	2.3	2.5
D14	21.1	1.20	12000	473	560	1.7	0.0
D15	20.6	1.22	13500	540	350	0.8	1.0
D16	21.1	1.21	14600	572	350	0.8	0.2

Notes: The figures in parentheses are the corresponding Young's Moduli in  $10^5 \times \text{N/mm}^2$   
 \*Specimen C16 was sent for the second main heat-treatment

TABLE A2: Results of Preliminary Heat-Treatment (II)

Specimen No.	Breadth (mm)	Thickness (mm)	Static Yield Load (N)	Static Tensile Yield Strength (N/mm <sup>2</sup> )	Heat - Treatment		
					Heating Temperature (°C)	Warming-Up Time (Hr)	Holding Time (Hr)
E11	20.4	2.00	8230	202	550	1.7	2.0
E12	21.2	1.97	8320	199	650	2.3	2.5
E13	21.4	1.96	8230	196	750	2.9	0.0
E14	20.3	2.10	21500	505 (2.15)	-	-	-
E15	20.8	2.07	23600	548	350	0.8	0.2
E16*	20.3	2.03	17200	418	550	0.5	2.9
F11	20.1	2.05	22000	534 (2.15)	-	-	-
F12	20.3	1.93	7430	189	750	2.9	2.5
F13	18.9	1.97	7270	195	550	1.7	2.5
F14	20.3	2.03	18400	446	350	0.8	2.8
F15	20.6	1.99	21000	511	350	0.8	0.2
F16*	20.1	1.98	15900	400	550	0.5	1.9

Notes: The figures in parentheses are the corresponding Young's Moduli in 10<sup>5</sup> x N/mm<sup>2</sup>  
 \*Specimens F16 and E16 were sent for the first and second main heat-treatment respectively

TABLE A3: Results of Preliminary Heat-Treatment (III)

Specimen No.	Breadth (mm)	Thickness (mm)	Static Yield Load (N)	Static Tensile Yield Strength (N/mm <sup>2</sup> )	Heat - Treatment		
					Heating Temperature (°C)	Warming-Up Time (Hr)	Holding Time (Hr)
G11	20.7	1.97	21800	534 (2.23)	-	-	-
G12	21.1	1.98	17600	421	550	1.7	0.0
G13	20.9	2.04	21400	503	350	0.8	1.0
G14	20.2	2.00	7030	174	750	2.9	1.0
G15	19.6	2.06	8050	199	550	1.7	2.0
G16	18.3	2.01	7160	195	550	1.7	1.5
H11	20.3	2.00	21000	517 (1.82)	-	-	-
H12	21.1	2.01	8760	207	550	1.7	2
H13	19.9	1.97	7010	179	650	2.3	2.5
H14	19.8	1.99	11300	288	550	1.7	1.0
H15	19.8	2.01	8410	211	550	1.7	3.0
H16	19.8	2.01	15200	382	560	1.7	0.0

Note: The figures in parentheses are the corresponding Young's Moduli in  $10^5 \times \text{N/mm}^2$

TABLE A4: Results of Preliminary Heat-Treatment (IV)

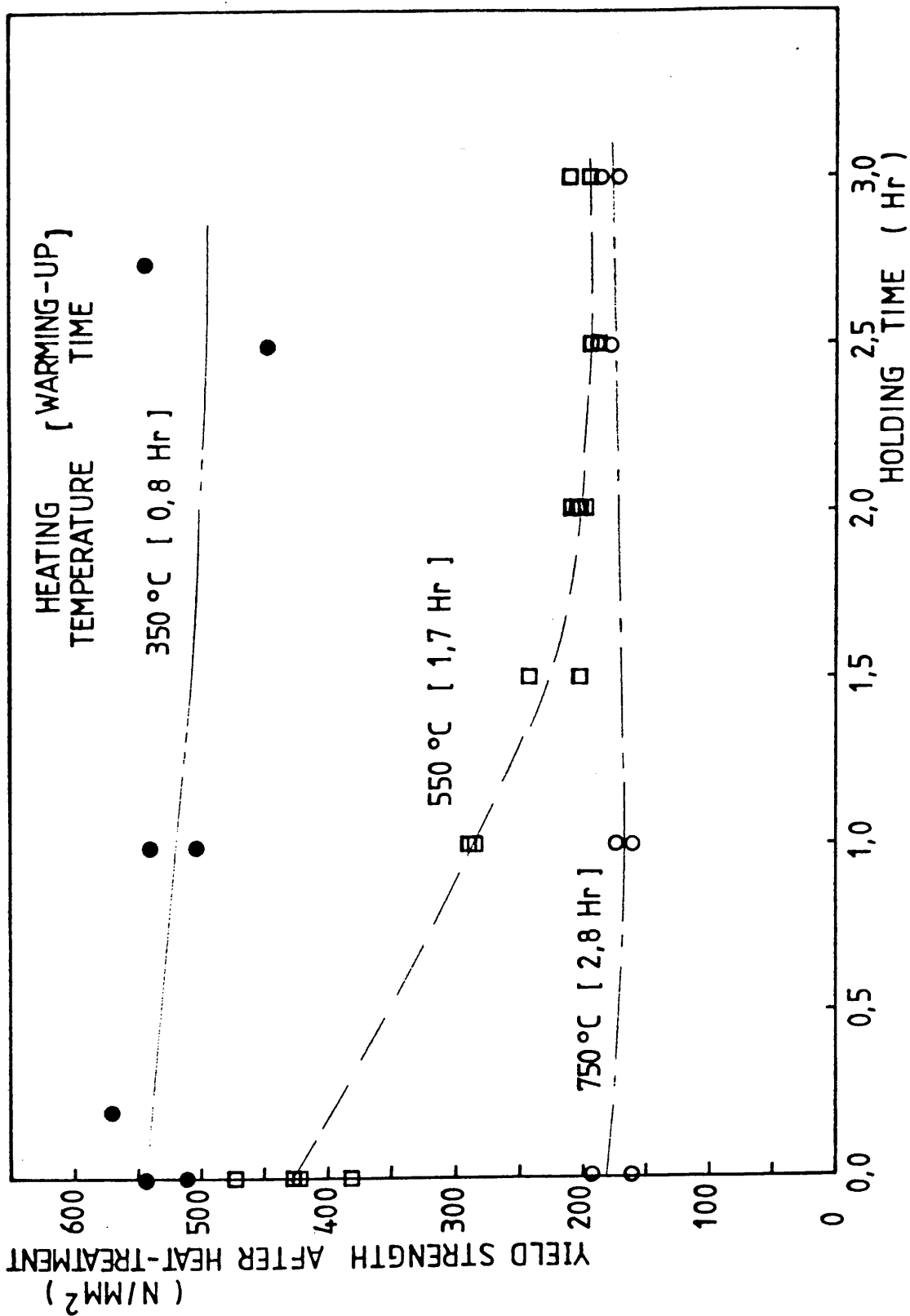


Fig.A1 Effect of Holding Time on Yield Strength of Cold Drawn Seamless Tube

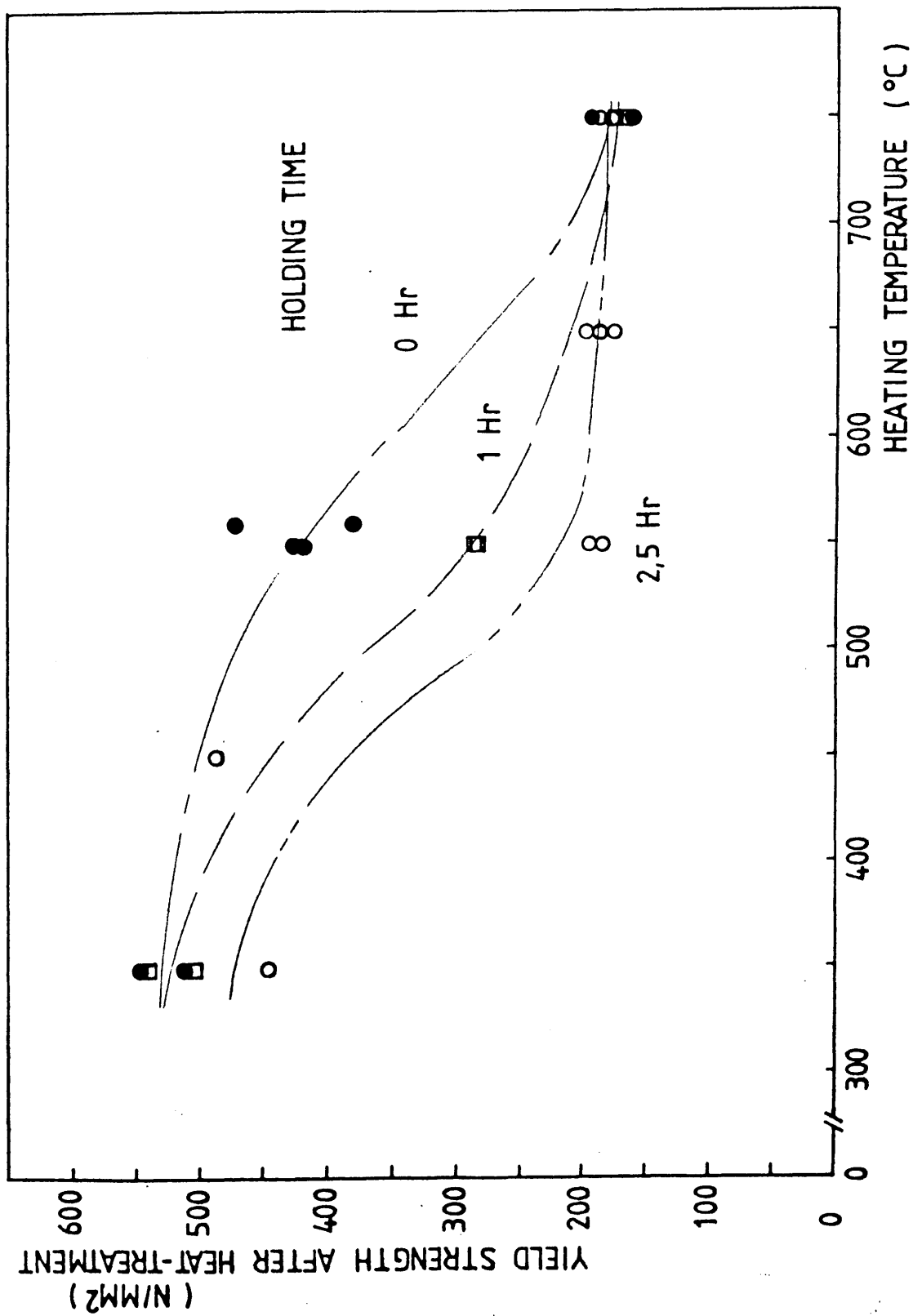


Fig.A2 Effect of Heating Temperature on Yield Strength of Cold Drawn Seamless Tube

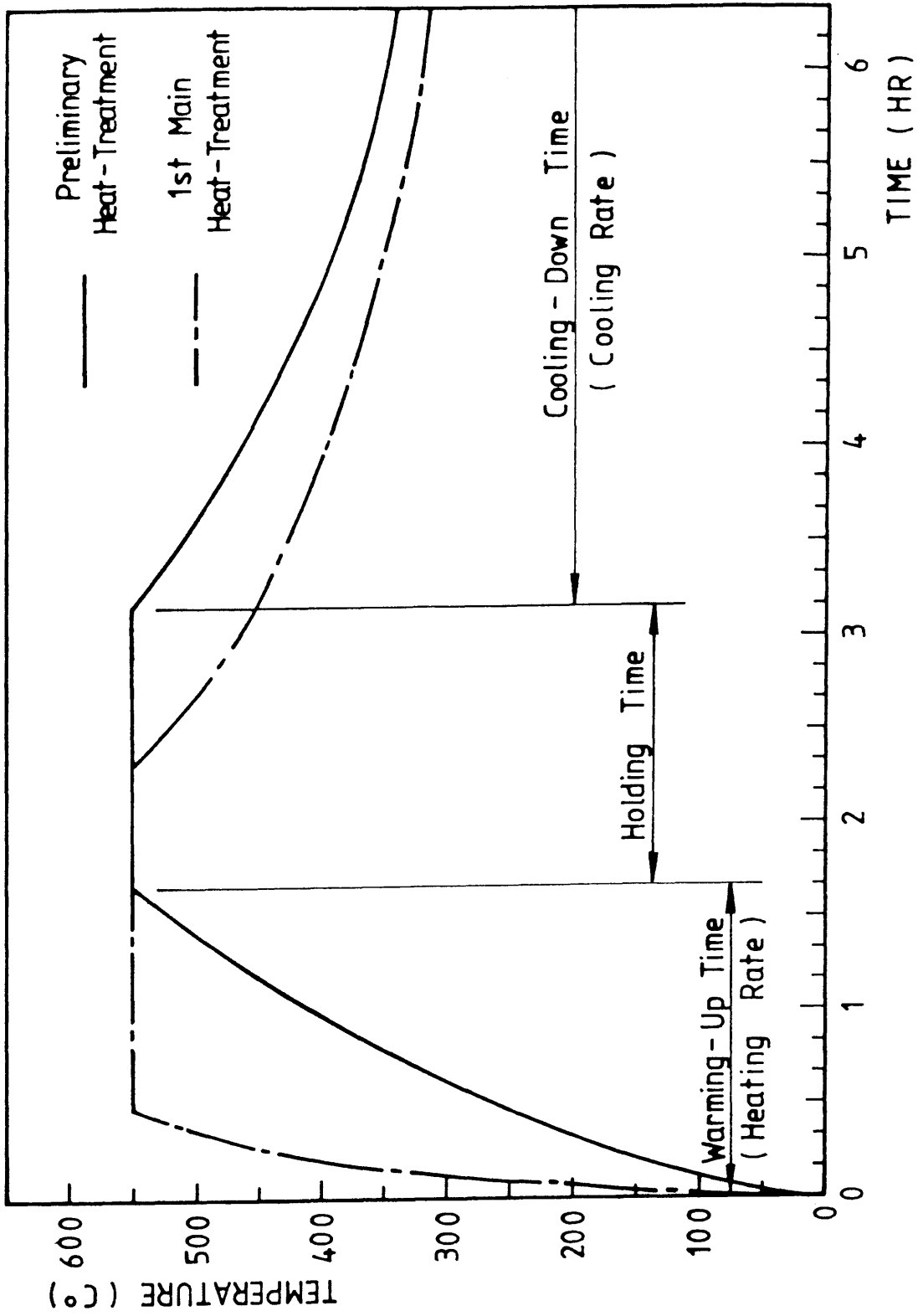


Fig. A3 Typical Temperature History of Heat-Treatment



## **APPENDIX B.**

### **PRE-TEST MEASUREMENTS**

#### **B. I            Thickness Measurements**

#### **B. II            Initial Shape Measurements**

##### **B. II. 1        Outside Diameter Measurements**

##### **B. II. 2        Initial Out-of-Straightness Measurements Table**

##### **B. II. 3        Initial Out-of-Straightness Plots**

#### **B. III          Tensile Test Results**

##### **B. III. 1       Typical Stress Strain Curves**

##### **B. III. 2       Tensile Test Results Table**

## **B.1      Thickness   Measurements**

# MEASUREMENTS OF THICKNESS

MODEL : A1  
 LENGTH(L) : 1400 MM  
 UNIT : MM

LOCATION	I	TOP				BOTTOM	I	AVE.
	I	0.30L	0.25L	0.50L	0.75L	1.00L	I	
0 DEG.	I	1.21	1.20	1.21	1.20	1.17	I	1.20
30 DEG.	I	1.21	1.20	1.21	1.19	1.17	I	1.20
60 DEG.	I	1.19	1.19	1.19	1.19	1.17	I	1.19
90 DEG.	I	1.19	1.19	1.19	1.18	1.19	I	1.19
120 DEG.	I	1.19	1.20	1.19	1.19	1.20	I	1.19
150 DEG.	I	1.18	1.19	1.18	1.18	1.20	I	1.19
180 DEG.	I	1.18	1.19	1.19	1.20	1.22	I	1.20
210 DEG.	I	1.19	1.20	1.20	1.20	1.23	I	1.20
240 DEG.	I	1.21	1.22	1.22	1.23	1.24	I	1.22
270 DEG.	I	1.21	1.21	1.22	1.23	1.23	I	1.22
300 DEG.	I	1.23	1.22	1.21	1.22	1.21	I	1.22
330 DEG.	I	1.23	1.23	1.23	1.22	1.21	I	1.23
AVE.	I	1.20	1.20	1.20	1.20	1.20	I	

TOTAL AVERAGE = 1.20 MM  
 C. O. V. = 1.46 %

# MEASUREMENTS OF THICKNESS

MODEL : A2  
 LENGTH(L) : 1000 MM  
 UNIT : MM

LOCATION	I	TOP				BOTTOM	I	AVE.
	I	0.00L	0.25L	0.50L	0.75L	1.00L	I	
0 DEG.	I	1.18	1.18	1.17	1.17	1.18	I	1.18
30 DEG.	I	1.20	1.19	1.19	1.20	1.21	I	1.20
60 DEG.	I	1.20	1.19	1.20	1.21	1.21	I	1.20
90 DEG.	I	1.20	1.21	1.20	1.21	1.22	I	1.21
120 DEG.	I	1.22	1.22	1.22	1.24	1.23	I	1.23
150 DEG.	I	1.21	1.23	1.22	1.23	1.23	I	1.22
180 DEG.	I	1.22	1.23	1.22	1.23	1.22	I	1.23
210 DEG.	I	1.22	1.22	1.21	1.21	1.20	I	1.21
240 DEG.	I	1.22	1.22	1.21	1.20	1.19	I	1.21
270 DEG.	I	1.20	1.21	1.20	1.19	1.19	I	1.20
300 DEG.	I	1.20	1.18	1.18	1.19	1.19	I	1.19
330 DEG.	I	1.19	1.18	1.18	1.18	1.18	I	1.18
AVE.	I	1.21	1.21	1.20	1.21	1.20	I	

TOTAL AVERAGE = 1.20 MM  
 C. O. V. = 1.45 %

# MEASUREMENTS OF THICKNESS

MODEL : A3  
 LENGTH(L) : 1400 MM  
 UNIT : MM

LOCATION	I	TOP				BOTTOM	I	AVE.
	I	0.00L	0.25L	0.50L	0.75L	1.00L	I	
<hr/>								
0 DEG.	I	1.22	1.19	1.19	1.19	1.17	I	1.19
	I	(1.20)				(1.18)	I	
30 DEG.	I	1.22	1.21	1.20	1.20	1.18	I	1.20
	I	(1.22)				(1.18)	I	
60 DEG.	I	1.23	1.21	1.20	1.19	1.20	I	1.21
	I	(1.22)				(1.19)	I	
90 DEG.	I	1.21	1.21	1.20	1.19	1.22	I	1.20
	I	(1.21)				(1.21)	I	
120 DEG.	I	1.20	1.21	1.20	1.20	1.22	I	1.21
	I	(1.20)				(1.21)	I	
150 DEG.	I	1.21	1.22	1.21	1.22	1.23	I	1.22
	I	(1.20)				(1.23)	I	
180 DEG.	I	1.20	1.20	1.20	1.21	1.23	I	1.21
	I	(1.19)				(1.23)	I	
210 DEG.	I	1.18	1.18	1.22	1.23	1.23	I	1.21
	I	(1.18)				(1.22)	I	
240 DEG.	I	1.17	1.19	1.19	1.22	1.20	I	1.19
	I	(1.18)				(1.21)	I	
270 DEG.	I	1.19	1.18	1.21	1.21	1.20	I	1.20
	I	(1.18)				(1.20)	I	
300 DEG.	I	1.19	1.21	1.20	1.19	1.19	I	1.20
	I	(1.19)				(1.19)	I	
330 DEG.	I	1.20	1.20	1.19	1.19	1.17	I	1.19
	I	(1.20)				(1.18)	I	
<hr/>								
AVE.	I	1.20	1.20	1.20	1.20	1.20	I	
	I	(1.20)				(1.20)	I	
<hr/>								

\* THE THICKNESSES IN PARENTHESES WERE  
 MEASURED WITH A MICROMETER

TOTAL AVERAGE = 1.20 MM  
 C. O. V. = 1.23 %

MEASUREMENTS OF THICKNESS

-----

MODEL : A4  
 LENGTH(L) : 1000 MM  
 UNIT : MM

LOCATION	I	TOP				BOTTOM	I	AVE.
	I	0.00L	0.25L	0.50L	0.75L	1.00L	I	
-----								
	I						I	
0 DEG.	I	1.23	1.18	1.18	1.18	1.19	I	1.19
	I						I	
30 DEG.	I	1.23	1.18	1.18	1.19	1.18	I	1.19
	I						I	
60 DEG.	I	1.21	1.19	1.19	1.19	1.19	I	1.20
	I						I	
90 DEG.	I	1.20	1.20	1.20	1.19	1.20	I	1.20
	I						I	
120 DEG.	I	1.18	1.21	1.20	1.20	1.20	I	1.20
	I						I	
150 DEG.	I	1.18	1.20	1.23	1.21	1.22	I	1.21
	I						I	
180 DEG.	I	1.17	1.22	1.23	1.23	1.22	I	1.21
	I						I	
210 DEG.	I	1.18	1.22	1.22	1.21	1.22	I	1.21
	I						I	
240 DEG.	I	1.18	1.21	1.21	1.20	1.21	I	1.20
	I						I	
270 DEG.	I	1.21	1.22	1.20	1.21	1.21	I	1.21
	I						I	
300 DEG.	I	1.22	1.21	1.19	1.20	1.19	I	1.20
	I						I	
330 DEG.	I	1.23	1.19	1.18	1.17	1.18	I	1.19
-----								
AVE.	I	1.20	1.20	1.20	1.20	1.20	I	
-----								

TOTAL AVERAGE = 1.20 MM  
 C. O. V. = 1.41 %

# MEASUREMENTS OF THICKNESS

MODEL : B1  
 LENGTH(L) : 1400 MM  
 UNIT : MM

LOCATION	I	TOP				BOTTOM	I	AVE.
	I	0.00L	0.25L	0.50L	0.75L	1.00L	I	
0 DEG.	I	1.14	1.18	1.17	1.20	1.21	I	1.18
	I	(1.14)				(1.20)	I	
30 DEG.	I	1.13	1.19	1.16	1.21	1.20	I	1.18
	I	(1.13)				(1.21)	I	
60 DEG.	I	1.12	1.18	1.17	1.20	1.20	I	1.17
	I	(1.13)				(1.19)	I	
90 DEG.	I	1.18	1.20	1.18	1.22	1.19	I	1.19
	I	(1.16)				(1.19)	I	
120 DEG.	I	1.23	1.21	1.20	1.21	1.20	I	1.21
	I	(1.22)				(1.19)	I	
150 DEG.	I	1.23	1.19	1.21	1.19	1.17	I	1.20
	I	(1.24)				(1.18)	I	
180 DEG.	I	1.25	1.19	1.21	1.19	1.18	I	1.21
	I	(1.26)				(1.18)	I	
210 DEG.	I	1.25	1.20	1.22	1.20	1.20	I	1.21
	I	(1.26)				(1.19)	I	
240 DEG.	I	1.26	1.22	1.24	1.20	1.21	I	1.23
	I	(1.26)				(1.21)	I	
270 DEG.	I	1.25	1.21	1.20	1.19	1.22	I	1.21
	I	(1.24)				(1.22)	I	
300 DEG.	I	1.20	1.20	1.21	1.19	1.20	I	1.20
	I	(1.20)				(1.21)	I	
330 DEG.	I	1.18	1.20	1.19	1.20	1.22	I	1.20
	I	(1.17)				(1.21)	I	
AVE.	I	1.20	1.20	1.20	1.20	1.20	I	
	I	(1.20)				(1.20)	I	

\* THE THICKNESSES IN PARENTHESES WERE  
 MEASURED WITH A MICROMETER

TOTAL AVERAGE = 1.20 MM  
 C. O. V. = 2.18 %

# MEASUREMENTS OF THICKNESS

MODEL : B2  
 LENGTH(L) : 9020 MM  
 UNIT : MM

LOCATION	I	TOP				BOTTOM	I	AVE.
	I	0.00L	0.25L	0.50L	0.75L	1.00L	I	
0 DEG.	I	1.19	1.19	1.19	1.20	1.19	I	1.19
30 DEG.	I	1.19	1.19	1.19	1.20	1.20	I	1.19
60 DEG.	I	1.19	1.19	1.20	1.20	1.20	I	1.20
90 DEG.	I	1.18	1.19	1.20	1.19	1.20	I	1.19
120 DEG.	I	1.18	1.18	1.20	1.20	1.20	I	1.19
150 DEG.	I	1.20	1.21	1.20	1.21	1.22	I	1.21
180 DEG.	I	1.21	1.22	1.21	1.20	1.23	I	1.21
210 DEG.	I	1.21	1.20	1.20	1.20	1.20	I	1.20
240 DEG.	I	1.21	1.20	1.20	1.20	1.21	I	1.20
270 DEG.	I	1.21	1.20	1.21	1.20	1.20	I	1.20
300 DEG.	I	1.21	1.20	1.19	1.19	1.19	I	1.19
330 DEG.	I	1.20	1.20	1.18	1.20	1.17	I	1.19
AVE.	I	1.20	1.20	1.20	1.20	1.20	I	

TOTAL AVERAGE = 1.20 MM  
 C. O. V. = 0.84 %



# MEASUREMENTS OF THICKNESS

MODEL : B3  
 LENGTH(L) : 1000 MM  
 UNIT : MM

LOCATION	I	TOP				BOTTOM	I	AVE.
	I	0.00L	0.25L	0.50L	0.75L	1.00L	I	
0 DEG.	I	1.21	1.20	1.19	1.20	1.19	I	1.20
30 DEG.	I	1.21	1.21	1.20	1.20	1.19	I	1.20
60 DEG.	I	1.20	1.21	1.21	1.21	1.19	I	1.21
90 DEG.	I	1.21	1.21	1.21	1.21	1.20	I	1.21
120 DEG.	I	1.20	1.21	1.21	1.21	1.21	I	1.21
150 DEG.	I	1.19	1.22	1.21	1.20	1.20	I	1.20
180 DEG.	I	1.19	1.20	1.21	1.22	1.22	I	1.21
210 DEG.	I	1.18	1.20	1.20	1.20	1.22	I	1.20
240 DEG.	I	1.19	1.20	1.20	1.20	1.21	I	1.20
270 DEG.	I	1.20	1.20	1.20	1.21	1.22	I	1.21
300 DEG.	I	1.21	1.21	1.20	1.21	1.20	I	1.20
330 DEG.	I	1.21	1.21	1.20	1.20	1.20	I	1.21
AVE.	I	1.20	1.21	1.20	1.21	1.20	I	

TOTAL AVERAGE = 1.20 MM  
 C. O. V. = 0.70 %

# MEASUREMENTS OF THICKNESS

MODEL : B4  
 LENGTH(L) : 1400 MM  
 UNIT : MM

LOCATION	I	TOP				BOTTOM	I	AVE.
	I	0.00L	0.25L	0.50L	0.75L	1.00L	I	
0 DEG.	I	1.21	1.21	1.21	1.20	1.21	I	1.21
30 DEG.	I	1.21	1.20	1.21	1.23	1.22	I	1.21
60 DEG.	I	1.18	1.18	1.18	1.20	1.21	I	1.19
90 DEG.	I	1.19	1.18	1.20	1.20	1.21	I	1.20
120 DEG.	I	1.19	1.18	1.21	1.21	1.21	I	1.20
150 DEG.	I	1.21	1.20	1.22	1.21	1.22	I	1.21
180 DEG.	I	1.21	1.21	1.21	1.21	1.20	I	1.21
210 DEG.	I	1.20	1.21	1.20	1.18	1.17	I	1.19
240 DEG.	I	1.20	1.20	1.20	1.19	1.19	I	1.20
270 DEG.	I	1.20	1.21	1.20	1.19	1.18	I	1.19
300 DEG.	I	1.20	1.22	1.20	1.19	1.19	I	1.20
330 DEG.	I	1.21	1.20	1.19	1.19	1.19	I	1.19
AVE.	I	1.20	1.20	1.20	1.20	1.20	I	

TOTAL AVERAGE = 1.20 MM  
 C. O. V. = 1.03 %

MEASUREMENTS OF THICKNESS

---

MODEL : C1  
 LENGTH(L) : 1000 MM  
 UNIT : MM

LOCATION	I	TOP				BOTTOM	I	AVE.
	I	0.00L	0.25L	0.50L	0.75L	1.00L	I	
<hr style="border-top: 1px dashed black;"/>								
0 DEG.	I	1.19	1.18	1.17	1.21	1.18	I	1.19
	I						I	
30 DEG.	I	1.19	1.20	1.19	1.20	1.19	I	1.19
	I						I	
60 DEG.	I	1.20	1.19	1.19	1.20	1.20	I	1.19
	I						I	
90 DEG.	I	1.23	1.21	1.21	1.22	1.22	I	1.22
	I						I	
120 DEG.	I	1.23	1.22	1.23	1.22	1.23	I	1.23
	I						I	
150 DEG.	I	1.23	1.22	1.23	1.22	1.23	I	1.23
	I						I	
180 DEG.	I	1.24	1.23	1.24	1.24	1.25	I	1.24
	I						I	
210 DEG.	I	1.22	1.23	1.24	1.23	1.25	I	1.23
	I						I	
240 DEG.	I	1.21	1.22	1.24	1.23	1.24	I	1.23
	I						I	
270 DEG.	I	1.20	1.20	1.22	1.21	1.21	I	1.21
	I						I	
300 DEG.	I	1.19	1.20	1.21	1.20	1.21	I	1.20
	I						I	
330 DEG.	I	1.19	1.20	1.20	1.22	1.20	I	1.20
<hr style="border-top: 1px dashed black;"/>								
AVE.	I	1.21	1.21	1.21	1.22	1.22	I	
<hr style="border-top: 1px dashed black;"/>								

TOTAL AVERAGE = 1.21 MM  
 C. O. V. = 1.59 %

# MEASUREMENTS OF THICKNESS

MODEL : C2  
 LENGTH(L) : 1000 MM  
 UNIT : MM

LOCATION	I	TOP				BOTTOM	I	AVE.
	I	0.00L	0.25L	0.50L	0.75L	1.00L	I	
0 DEG.	I	1.23	1.23	1.24	1.23	1.22	I	1.23
30 DEG.	I	1.22	1.21	1.21	1.22	1.20	I	1.21
60 DEG.	I	1.19	1.19	1.19	1.21	1.19	I	1.20
90 DEG.	I	1.20	1.20	1.20	1.20	1.20	I	1.20
120 DEG.	I	1.20	1.19	1.20	1.20	1.19	I	1.19
150 DEG.	I	1.19	1.19	1.19	1.19	1.18	I	1.19
180 DEG.	I	1.20	1.21	1.20	1.20	1.19	I	1.20
210 DEG.	I	1.22	1.22	1.22	1.22	1.22	I	1.22
240 DEG.	I	1.24	1.24	1.23	1.24	1.24	I	1.24
270 DEG.	I	1.26	1.24	1.24	1.24	1.24	I	1.24
300 DEG.	I	1.24	1.25	1.25	1.24	1.24	I	1.25
330 DEG.	I	1.24	1.25	1.24	1.25	1.24	I	1.24
AVE.	I	1.22	1.22	1.22	1.22	1.21	I	

TOTAL AVERAGE = 1.22 MM  
 C. O. V. = 1.81 %

# MEASUREMENTS OF THICKNESS

MODEL : C3  
 LENGTH(L) : 1400 MM  
 UNIT : MM

LOCATION	I	TOP				BOTTOM	I	AVE.
	I	0.00L	0.25L	0.50L	0.75L	1.00L	I	
0 DEG.	I	1.25	1.23	1.23	1.23	1.23	I	1.23
30 DEG.	I	1.24	1.23	1.22	1.23	1.22	I	1.23
60 DEG.	I	1.23	1.21	1.22	1.23	1.21	I	1.22
90 DEG.	I	1.21	1.22	1.21	1.18	1.19	I	1.20
120 DEG.	I	1.19	1.20	1.21	1.19	1.19	I	1.19
150 DEG.	I	1.17	1.20	1.19	1.18	1.18	I	1.18
180 DEG.	I	1.18	1.23	1.20	1.20	1.20	I	1.20
210 DEG.	I	1.19	1.21	1.22	1.20	1.20	I	1.20
240 DEG.	I	1.21	1.21	1.20	1.23	1.20	I	1.21
270 DEG.	I	1.22	1.20	1.23	1.22	1.22	I	1.22
300 DEG.	I	1.26	1.24	1.22	1.24	1.24	I	1.24
330 DEG.	I	1.26	1.24	1.23	1.26	1.24	I	1.25
AVE.	I	1.22	1.22	1.22	1.22	1.21	I	

TOTAL AVERAGE = 1.22 MM  
 C. O. V. = 1.79 %

MEASUREMENTS OF THICKNESS

---

MODEL : C4  
 LENGTH(L) : 1400 MM  
 UNIT : MM

LOCATION	I	TOP				BOTTOM	I	AVE.
	I	0.00L	0.25L	0.50L	0.75L	1.00L	I	
<hr style="border-top: 1px dashed black;"/>								
0 DEG.	I	1.23	1.24	1.24	1.24	1.24	I	1.24
	I	(1.24)				(1.24)	I	
30 DEG.	I	1.24	1.24	1.24	1.24	1.26	I	1.24
	I	(1.24)				(1.24)	I	
60 DEG.	I	1.24	1.24	1.25	1.25	1.25	I	1.25
	I	(1.24)				(1.23)	I	
90 DEG.	I	1.22	1.23	1.23	1.23	1.24	I	1.23
	I	(1.22)				(1.24)	I	
120 DEG.	I	1.20	1.20	1.21	1.22	1.21	I	1.21
	I	(1.20)				(1.21)	I	
150 DEG.	I	1.19	1.19	1.19	1.20	1.19	I	1.19
	I	(1.19)				(1.19)	I	
180 DEG.	I	1.20	1.19	1.20	1.20	1.21	I	1.20
	I	(1.18)				(1.19)	I	
210 DEG.	I	1.19	1.19	1.20	1.21	1.20	I	1.20
	I	(1.18)				(1.19)	I	
240 DEG.	I	1.19	1.19	1.20	1.21	1.21	I	1.20
	I	(1.18)				(1.19)	I	
270 DEG.	I	1.20	1.20	1.21	1.20	1.23	I	1.21
	I	(1.19)				(1.19)	I	
300 DEG.	I	1.22	1.21	1.23	1.23	1.23	I	1.22
	I	(1.20)				(1.21)	I	
330 DEG.	I	1.24	1.24	1.25	1.25	1.25	I	1.25
	I	(1.22)				(1.24)	I	
<hr style="border-top: 1px dashed black;"/>								
AVE.	I	1.21	1.21	1.22	1.22	1.23	I	
	I	(1.21)				(1.21)	I	
<hr style="border-top: 1px dashed black;"/>								

\* THE THICKNESSES IN PARENTHESES WERE  
 MEASURED WITH A MICROMETER

TOTAL AVERAGE = 1.22 MM  
 C. O. V. = 1.71 %

# MEASUREMENTS OF THICKNESS

MODEL : D1  
 LENGTH(L) : 1400 MM  
 UNIT : MM

LOCATION	I	TOP				BOTTOM	I	AVE.
	I	0.00L	0.25L	0.50L	0.75L	1.00L	I	
0 DEG.	I	1.19	1.19	1.21	1.18	1.18	I	1.19
30 DEG.	I	1.18	1.19	1.19	1.16	1.17	I	1.18
60 DEG.	I	1.20	1.20	1.19	1.18	1.20	I	1.19
90 DEG.	I	1.20	1.19	1.19	1.20	1.21	I	1.20
120 DEG.	I	1.18	1.17	1.18	1.19	1.20	I	1.19
150 DEG.	I	1.21	1.21	1.19	1.22	1.23	I	1.21
180 DEG.	I	1.21	1.21	1.21	1.22	1.22	I	1.21
210 DEG.	I	1.24	1.23	1.24	1.24	1.24	I	1.24
240 DEG.	I	1.23	1.22	1.23	1.24	1.24	I	1.23
270 DEG.	I	1.21	1.21	1.22	1.21	1.21	I	1.21
300 DEG.	I	1.22	1.22	1.22	1.21	1.21	I	1.22
330 DEG.	I	1.19	1.20	1.21	1.18	1.17	I	1.19
AVE.	I	1.21	1.20	1.21	1.20	1.21	I	

TOTAL AVERAGE = 1.20 MM  
 C. O. V. = 1.71 %

# MEASUREMENTS OF THICKNESS

MODEL : D2  
 LENGTH(L) : 1000 MM  
 UNIT : MM

LOCATION	I	TOP				BOTTOM	I	AVE.
	I	0.00L	0.25L	0.50L	0.75L	1.00L	I	
0 DEG.	I	1.21	1.20	1.20	1.20	1.21	I	1.20
30 DEG.	I	1.19	1.18	1.19	1.19	1.21	I	1.19
60 DEG.	I	1.19	1.19	1.19	1.21	1.22	I	1.20
90 DEG.	I	1.18	1.19	1.18	1.20	1.21	I	1.19
120 DEG.	I	1.19	1.20	1.21	1.20	1.22	I	1.20
150 DEG.	I	1.21	1.22	1.21	1.21	1.21	I	1.21
180 DEG.	I	1.20	1.21	1.20	1.20	1.20	I	1.20
210 DEG.	I	1.21	1.22	1.21	1.20	1.20	I	1.21
240 DEG.	I	1.22	1.23	1.21	1.20	1.19	I	1.21
270 DEG.	I	1.24	1.24	1.23	1.21	1.21	I	1.23
300 DEG.	I	1.24	1.23	1.23	1.22	1.21	I	1.23
330 DEG.	I	1.21	1.20	1.22	1.21	1.20	I	1.21
AVE.	I	1.21	1.21	1.21	1.20	1.21	I	

TOTAL AVERAGE = 1.21 MM  
 C. O. V. = 1.18 %



MEASUREMENTS OF THICKNESS  
-----

MODEL : D3  
LENGTH(L) : 1400 MM  
UNIT : MM

LOCATION	I	TOP				BOTTOM	I	AVE.
	I	0.00L	0.25L	0.50L	0.75L	1.00L	I	
-----								
0 DEG.	I	1.19	1.18	1.18	1.17	1.18	I	1.18
30 DEG.	I	1.20	1.18	1.20	1.18	1.17	I	1.19
60 DEG.	I	1.22	1.21	1.21	1.21	1.20	I	1.21
90 DEG.	I	1.23	1.21	1.21	1.20	1.20	I	1.21
120 DEG.	I	1.23	1.23	1.23	1.23	1.21	I	1.23
150 DEG.	I	1.22	1.23	1.22	1.24	1.22	I	1.23
180 DEG.	I	1.21	1.22	1.22	1.23	1.23	I	1.22
210 DEG.	I	1.21	1.22	1.23	1.24	1.23	I	1.23
240 DEG.	I	1.21	1.22	1.22	1.21	1.23	I	1.22
270 DEG.	I	1.21	1.22	1.22	1.22	1.23	I	1.22
300 DEG.	I	1.19	1.20	1.19	1.20	1.22	I	1.20
330 DEG.	I	1.19	1.18	1.19	1.17	1.19	I	1.18
-----								
AVE.	I	1.21	1.21	1.21	1.21	1.21	I	
-----								

TOTAL AVERAGE = 1.21 MM  
C. O. V. = 1.57 %

# MEASUREMENTS OF THICKNESS

---

MODEL : D4  
 LENGTH(L) : 1400 MM  
 UNIT : MM

LOCATION	I	TOP				BOTTOM	I	AVE.
	I	0.00L	0.25L	0.50L	0.75L	1.00L	I	
<hr/>								
0 DEG.	I	1.18	1.18	1.18	1.19	1.18	I	1.18
	I	(1.17)				(1.19)	I	
30 DEG.	I	1.22	1.22	1.21	1.22	1.21	I	1.21
	I	(1.20)				(1.20)	I	
60 DEG.	I	1.22	1.22	1.21	1.22	1.21	I	1.22
	I	(1.22)				(1.21)	I	
90 DEG.	I	1.23	1.23	1.23	1.22	1.22	I	1.23
	I	(1.22)				(1.21)	I	
120 DEG.	I	1.23	1.23	1.24	1.22	1.22	I	1.23
	I	(1.22)				(1.22)	I	
150 DEG.	I	1.23	1.23	1.24	1.22	1.22	I	1.23
	I	(1.23)				(1.22)	I	
180 DEG.	I	1.24	1.23	1.22	1.22	1.23	I	1.23
	I	(1.23)				(1.22)	I	
210 DEG.	I	1.21	1.21	1.21	1.22	1.21	I	1.21
	I	(1.22)				(1.20)	I	
240 DEG.	I	1.20	1.20	1.20	1.20	1.20	I	1.20
	I	(1.20)				(1.20)	I	
270 DEG.	I	1.19	1.19	1.19	1.20	1.20	I	1.19
	I	(1.19)				(1.19)	I	
300 DEG.	I	1.18	1.18	1.17	1.17	1.18	I	1.17
	I	(1.17)				(1.17)	I	
330 DEG.	I	1.17	1.18	1.17	1.20	1.18	I	1.18
	I	(1.17)				(1.17)	I	
<hr/>								
AVE.	I	1.21	1.21	1.21	1.21	1.20	I	
	I	(1.20)				(1.20)	I	
<hr/>								

\* THE THICKNESSES IN PARENTHESES WERE  
 MEASURED WITH A MICROMETER

TOTAL AVERAGE = 1.21 MM  
 C. O. V. = 1.70 %

# MEASUREMENTS OF THICKNESS

MODEL : E1  
 LENGTH(L) : 1400 MM  
 UNIT : MM

LOCATION	I	TOP				BOTTOM	I	AVE.
	I	0.00L	0.25L	0.50L	0.75L	1.00L	I	
0 DEG.	I	2.04	2.03	2.02	2.01	2.00	I	2.02
30 DEG.	I	2.00	1.99	1.98	1.96	1.99	I	1.98
60 DEG.	I	1.97	1.95	1.97	1.95	1.95	I	1.96
90 DEG.	I	1.97	1.97	1.98	1.97	1.98	I	1.97
120 DEG.	I	1.98	1.97	1.99	1.99	1.99	I	1.98
150 DEG.	I	2.02	2.02	2.04	2.05	2.05	I	2.04
180 DEG.	I	2.07	2.08	2.10	2.10	2.10	I	2.09
210 DEG.	I	2.09	2.11	2.12	2.12	2.12	I	2.11
240 DEG.	I	2.12	2.14	2.13	2.15	2.15	I	2.14
270 DEG.	I	2.12	2.14	2.12	2.13	2.14	I	2.13
300 DEG.	I	2.11	2.12	2.12	2.11	2.11	I	2.11
330 DEG.	I	2.08	2.08	2.06	2.06	2.05	I	2.06
AVE.	I	2.05	2.05	2.05	2.05	2.05	I	

TOTAL AVERAGE = 2.05 MM  
 C. O. V. = 3.17 %

# MEASUREMENTS OF THICKNESS

MODEL : E2  
 LENGTH(L) : 1000 MM  
 UNIT : MM

LOCATION	I	TOP				BOTTOM	I	AVE.
	I	0.00L	0.25L	0.50L	0.75L	1.00L	I	
0 DEG.	I	1.98	2.00	2.00	2.02	2.02	I	2.00
	I	(1.97)				(2.02)	I	
30 DEG.	I	2.01	2.04	2.04	2.07	2.06	I	2.04
	I	(2.02)				(2.06)	I	
60 DEG.	I	2.06	2.07	2.08	2.09	2.09	I	2.08
	I	(2.04)				(2.09)	I	
90 DEG.	I	2.10	2.11	2.11	2.12	2.11	I	2.11
	I	(2.11)				(2.11)	I	
120 DEG.	I	2.12	2.12	2.12	2.11	2.11	I	2.12
	I	(2.12)				(2.11)	I	
150 DEG.	I	2.12	2.11	2.13	2.09	2.10	I	2.11
	I	(2.13)				(2.09)	I	
180 DEG.	I	2.10	2.10	2.09	2.07	2.07	I	2.09
	I	(2.10)				(2.06)	I	
210 DEG.	I	2.07	2.06	2.06	2.03	2.03	I	2.05
	I	(2.08)				(2.03)	I	
240 DEG.	I	2.01	2.02	2.00	1.98	1.99	I	2.00
	I	(2.02)				(1.99)	I	
270 DEG.	I	1.97	1.99	1.97	1.96	1.97	I	1.97
	I	(1.97)				(1.96)	I	
300 DEG.	I	1.96	1.98	1.96	1.97	1.97	I	1.97
	I	(1.96)				(1.97)	I	
330 DEG.	I	1.95	1.98	1.95	1.97	1.98	I	1.97
	I	(1.94)				(1.98)	I	
AVE.	I	2.04	2.05	2.04	2.04	2.04	I	
	I	(2.04)				(2.04)	I	

\* THE THICKNESSES IN PARENTHESES WERE  
 MEASURED WITH A MICROMETER

TOTAL AVERAGE = 2.04 MM  
 C. O. V. = 2.81 %

# MEASUREMENTS OF THICKNESS

MODEL : E3  
 LENGTH(L) : 1400 MM  
 UNIT : MM

LOCATION	I	TOP				BOTTOM	I	AVE.
	I	0.00L	0.25L	0.50L	0.75L	1.00L	I	
0 DEG.	I	2.04	2.05	2.03	2.01	1.99	I	2.02
30 DEG.	I	2.02	2.03	2.01	1.99	1.97	I	2.00
60 DEG.	I	1.98	1.98	1.96	1.96	1.95	I	1.97
90 DEG.	I	1.99	1.97	1.96	1.97	1.97	I	1.97
120 DEG.	I	1.99	1.98	1.98	2.00	2.00	I	1.99
150 DEG.	I	2.02	2.01	2.02	2.05	2.05	I	2.03
180 DEG.	I	2.07	2.06	2.08	2.10	2.10	I	2.08
210 DEG.	I	2.09	2.08	2.10	2.12	2.12	I	2.10
240 DEG.	I	2.11	2.11	2.14	2.14	2.14	I	2.13
270 DEG.	I	2.11	2.11	2.13	2.12	2.12	I	2.12
300 DEG.	I	2.11	2.12	2.12	2.10	2.10	I	2.11
330 DEG.	I	2.08	2.10	2.08	2.06	2.05	I	2.07
AVE.	I	2.05	2.05	2.05	2.05	2.05	I	

TOTAL AVERAGE = 2.05 MM  
 C. O. V. = 2.86 %

# MEASUREMENTS OF THICKNESS

MODEL : F1  
 LENGTH(L) : 1400 MM  
 UNIT : MM

LOCATION	I	TOP				BOTTOM	I	AVE.
	I	0.00L	0.25L	0.50L	0.75L	1.00L	I	
0 DEG.	I	1.98	2.00	1.99	2.00	1.98	I	1.99
30 DEG.	I	2.00	2.00	2.00	2.01	1.99	I	2.00
60 DEG.	I	2.01	2.01	2.02	2.01	2.03	I	2.01
90 DEG.	I	2.04	2.03	2.05	2.02	2.05	I	2.04
120 DEG.	I	2.06	2.05	2.05	2.04	2.07	I	2.05
150 DEG.	I	2.08	2.07	2.07	2.05	2.07	I	2.07
180 DEG.	I	2.09	2.08	2.08	2.06	2.07	I	2.08
210 DEG.	I	2.08	2.07	2.04	2.04	2.05	I	2.06
240 DEG.	I	2.07	2.07	2.04	2.05	2.05	I	2.06
270 DEG.	I	2.03	2.03	2.01	2.03	2.02	I	2.02
300 DEG.	I	2.01	2.02	2.00	2.01	1.99	I	2.01
330 DEG.	I	2.00	2.01	2.00	2.00	1.99	I	2.00
AVE.	I	2.04	2.04	2.03	2.03	2.03	I	

TOTAL AVERAGE = 2.03 MM  
 C. O. V. = 1.48 %

# MEASUREMENTS OF THICKNESS

MODEL : F2  
 LENGTH(L) : 1000 MM  
 UNIT : MM

LOCATION	I	TOP				BOTTOM	I	AVE.
	I	0.00L	0.25L	0.50L	0.75L	1.00L	I	
<hr/>								
0 DEG.	I	2.01	2.02	2.00	2.02	1.99	I	2.01
	I	(2.02)				(1.99)	I	
30 DEG.	I	1.98	1.99	1.99	2.00	1.99	I	1.99
	I	(1.98)				(1.98)	I	
60 DEG.	I	1.95	1.97	1.98	2.00	1.98	I	1.97
	I	(1.96)				(1.98)	I	
90 DEG.	I	1.95	1.97	1.98	2.00	1.99	I	1.98
	I	(1.95)				(1.99)	I	
120 DEG.	I	1.96	1.97	1.98	2.00	2.00	I	1.98
	I	(1.96)				(2.00)	I	
150 DEG.	I	2.00	2.00	2.02	2.02	2.05	I	2.02
	I	(1.97)				(2.03)	I	
180 DEG.	I	2.03	2.03	2.04	2.04	2.04	I	2.04
	I	(2.01)				(2.05)	I	
210 DEG.	I	2.06	2.05	2.06	2.06	2.07	I	2.06
	I	(2.05)				(2.08)	I	
240 DEG.	I	2.09	2.08	2.09	2.07	2.07	I	2.08
	I	(2.08)				(2.08)	I	
270 DEG.	I	2.09	2.08	2.08	2.06	2.05	I	2.07
	I	(2.09)				(2.06)	I	
300 DEG.	I	2.10	2.08	2.08	2.06	2.05	I	2.07
	I	(2.10)				(2.04)	I	
330 DEG.	I	2.06	2.03	2.03	2.03	2.02	I	2.04
	I	(2.06)				(2.02)	I	
<hr/>								
AVE.	I	2.02	2.02	2.03	2.03	2.03	I	
	I	(2.02)				(2.02)	I	
<hr/>								

\* THE THICKNESSES IN PARENTHESES WERE  
 MEASURED WITH A MICROMETER

TOTAL AVERAGE = 2.03 MM  
 C. O. V. = 1.97 %

MEASUREMENTS OF THICKNESS

-----

MODEL : F3  
 LENGTH(L) : 1800 MM  
 UNIT : MM

LOCATION	I	TOP				BOTTOM	I	AVE.
	I	0.00L	0.25L	0.50L	0.75L	1.00L	I	
-----								
0 DEG.	I	2.06	2.05	2.07	2.02	2.00	I	2.04
	I	(2.07)				(2.01)	I	
30 DEG.	I	2.05	2.04	2.05	2.02	1.99	I	2.03
	I	(2.07)				(2.01)	I	
60 DEG.	I	2.03	2.03	2.04	2.02	2.01	I	2.03
	I	(2.04)				(2.02)	I	
90 DEG.	I	1.99	2.00	2.01	2.01	2.01	I	2.00
	I	(2.00)				(2.01)	I	
120 DEG.	I	1.98	2.00	1.99	2.01	2.00	I	2.00
	I	(1.99)				(2.02)	I	
150 DEG.	I	1.97	1.99	1.98	2.03	2.01	I	1.99
	I	(1.98)				(2.02)	I	
180 DEG.	I	1.97	1.99	1.99	2.04	2.02	I	2.00
	I	(1.98)				(2.03)	I	
210 DEG.	I	1.98	2.00	2.01	2.04	2.03	I	2.01
	I	(2.00)				(2.03)	I	
240 DEG.	I	2.01	2.02	2.02	2.05	2.02	I	2.02
	I	(2.02)				(2.03)	I	
270 DEG.	I	2.03	2.04	2.05	2.05	2.02	I	2.04
	I	(2.05)				(2.03)	I	
300 DEG.	I	2.05	2.06	2.06	2.04	2.03	I	2.05
	I	(2.05)				(2.03)	I	
330 DEG.	I	2.05	2.05	2.06	2.03	2.00	I	2.04
	I	(2.07)				(2.01)	I	
-----								
AVE.	I	2.02	2.02	2.03	2.03	2.01	I	
	I	(2.03)				(2.02)	I	
-----								

\* THE THICKNESSES IN PARENTHESES WERE  
 MEASURED WITH A MICROMETER

TOTAL AVERAGE = 2.02 MM  
 C. O. V. = 1.28 %



# MEASUREMENTS OF THICKNESS

MODEL : G1  
 LENGTH(L) : 1000 MM  
 UNIT : MM

LOCATION	I	TOP				BOTTOM	I	AVE.
	I	0.00L	0.25L	0.50L	0.75L	1.00L	I	
0 DEG.	I	2.00	2.00	2.01	2.01	2.02	I	2.01
	I	(2.00)				(2.02)	I	
30 DEG.	I	2.00	2.01	2.02	2.02	2.04	I	2.02
	I	(2.00)				(2.03)	I	
60 DEG.	I	2.01	2.02	2.04	2.04	2.07	I	2.04
	I	(2.00)				(2.05)	I	
90 DEG.	I	2.03	2.04	2.05	2.06	2.09	I	2.06
	I	(2.02)				(2.08)	I	
120 DEG.	I	2.04	2.06	2.07	2.07	2.08	I	2.07
	I	(2.03)				(2.08)	I	
150 DEG.	I	2.06	2.08	2.08	2.08	2.08	I	2.07
	I	(2.06)				(2.08)	I	
180 DEG.	I	2.08	2.08	2.08	2.07	2.07	I	2.08
	I	(2.08)				(2.08)	I	
210 DEG.	I	2.08	2.07	2.08	2.06	2.05	I	2.07
	I	(2.08)				(2.04)	I	
240 DEG.	I	2.08	2.06	2.05	2.04	2.03	I	2.05
	I	(2.08)				(2.03)	I	
270 DEG.	I	2.07	2.05	2.04	2.03	2.01	I	2.04
	I	(2.06)				(2.01)	I	
300 DEG.	I	2.04	2.03	2.01	2.02	2.00	I	2.02
	I	(2.04)				(2.00)	I	
330 DEG.	I	2.01	2.02	2.00	2.01	2.00	I	2.01
	I	(2.01)				(2.00)	I	
AVE.	I	2.04	2.04	2.04	2.04	2.05	I	
	I	(2.04)				(2.04)	I	

\* THE THICKNESSES IN PARENTHESES WERE  
 MEASURED WITH A MICROMETER

TOTAL AVERAGE = 2.04 MM  
 C. O. V. = 1.37 %

# MEASUREMENTS OF THICKNESS

MODEL : G2  
 LENGTH(L) : 1400 MM  
 UNIT : MM

LOCATION	I	TOP				BOTTOM	I	AVE.
	I	0.00L	0.25L	0.50L	0.75L	1.00L	I	
0 DEG.	I	2.02	2.02	2.01	2.04	2.04	I	2.03
30 DEG.	I	2.01	2.01	2.00	2.03	2.04	I	2.02
60 DEG.	I	2.00	2.01	2.01	2.03	2.04	I	2.02
90 DEG.	I	2.02	2.03	2.04	2.04	2.05	I	2.03
120 DEG.	I	2.03	2.04	2.06	2.04	2.06	I	2.05
150 DEG.	I	2.05	2.06	2.07	2.06	2.07	I	2.06
180 DEG.	I	2.08	2.08	2.09	2.07	2.07	I	2.08
210 DEG.	I	2.10	2.09	2.09	2.07	2.08	I	2.08
240 DEG.	I	2.09	2.09	2.08	2.07	2.06	I	2.08
270 DEG.	I	2.09	2.07	2.07	2.06	2.05	I	2.07
300 DEG.	I	2.06	2.05	2.05	2.04	2.04	I	2.05
330 DEG.	I	2.03	2.03	2.02	2.03	2.03	I	2.03
AVE.	I	2.05	2.05	2.05	2.05	2.05	I	

TOTAL AVERAGE = 2.05 MM  
 C. O. V. = 1.24 %

# MEASUREMENTS OF THICKNESS

MODEL : G3  
 LENGTH(L) : 1800 MM  
 UNIT : MM

LOCATION	I	TOP				BOTTOM	I	AVE.
	I	0.00L	0.25L	0.50L	0.75L	1.00L	I	
0 DEG.	I	2.02	2.04	2.07	2.09	2.08	I	2.06
	I	(2.03)				(2.09)	I	
30 DEG.	I	2.03	2.05	2.08	2.09	2.09	I	2.07
	I	(2.04)				(2.10)	I	
60 DEG.	I	2.05	2.07	2.08	2.09	2.09	I	2.08
	I	(2.06)				(2.10)	I	
90 DEG.	I	2.06	2.07	2.06	2.08	2.08	I	2.07
	I	(2.07)				(2.08)	I	
120 DEG.	I	2.08	2.06	2.05	2.05	2.08	I	2.06
	I	(2.08)				(2.06)	I	
150 DEG.	I	2.06	2.05	2.03	2.03	2.06	I	2.05
	I	(2.08)				(2.03)	I	
180 DEG.	I	2.04	2.05	2.02	2.00	2.03	I	2.03
	I	(2.06)				(2.00)	I	
210 DEG.	I	2.04	2.03	2.00	1.99	2.00	I	2.01
	I	(2.04)				(2.00)	I	
240 DEG.	I	2.02	2.02	2.01	2.01	1.98	I	2.01
	I	(2.03)				(1.99)	I	
270 DEG.	I	2.01	2.02	2.02	2.01	1.99	I	2.01
	I	(2.02)				(2.01)	I	
300 DEG.	I	2.00	2.03	2.04	2.05	2.02	I	2.03
	I	(2.02)				(2.04)	I	
330 DEG.	I	2.01	2.03	2.07	2.07	2.06	I	2.05
	I	(2.02)				(2.08)	I	
AVE.	I	2.04	2.04	2.04	2.05	2.05	I	
	I	(2.05)				(2.05)	I	

\* THE THICKNESSES IN PARENTHESES WERE  
 MEASURED WITH A MICROMETER

TOTAL AVERAGE = 2.04 MM  
 C. O. V. = 1.43 %

# MEASUREMENTS OF THICKNESS

---

MODEL : H1  
 LENGTH(L) : 1400 MM  
 UNIT : MM

LOCATION	I	TOP				BOTTOM	I	AVE.
	I	0.00L	0.25L	0.50L	0.75L	1.00L	I	
0 DEG.	I	2.09	2.08	2.07	2.07	2.04	I	2.07
30 DEG.	I	2.06	2.08	2.08	2.07	2.04	I	2.07
60 DEG.	I	2.05	2.06	2.08	2.07	2.06	I	2.06
90 DEG.	I	2.00	2.02	2.04	2.05	2.05	I	2.03
120 DEG.	I	1.99	2.01	2.03	2.04	2.04	I	2.02
150 DEG.	I	1.98	1.99	2.00	2.02	2.03	I	2.00
180 DEG.	I	1.98	1.99	1.99	2.00	2.02	I	2.00
210 DEG.	I	2.00	2.00	2.01	2.00	2.02	I	2.01
240 DEG.	I	2.02	2.02	2.00	2.01	2.03	I	2.02
270 DEG.	I	2.07	2.05	2.04	2.03	2.04	I	2.05
300 DEG.	I	2.09	2.06	2.04	2.03	2.04	I	2.05
330 DEG.	I	2.09	2.07	2.05	2.05	2.03	I	2.06
AVE.	I	2.03	2.04	2.04	2.04	2.04	I	

TOTAL AVERAGE = 2.04 MM  
 C. O. V. = 1.44 %

# MEASUREMENTS OF THICKNESS

MODEL : H2  
 LENGTH(L) : 1400 MM  
 UNIT : MM

LOCATION	I	TOP				BOTTOM	I	AVE.
	I	0.00L	0.25L	0.50L	0.75L	1.00L	I	
0 DEG.	I	2.09	2.10	2.12	2.11	2.13	I	2.11
30 DEG.	I	2.09	2.10	2.11	2.11	2.13	I	2.11
60 DEG.	I	2.07	2.06	2.09	2.09	2.10	I	2.08
90 DEG.	I	2.06	2.06	2.07	2.07	2.06	I	2.07
120 DEG.	I	2.02	2.00	2.01	2.00	1.99	I	2.00
150 DEG.	I	1.98	1.97	1.98	1.98	1.96	I	1.97
180 DEG.	I	1.95	1.96	1.94	1.95	1.92	I	1.94
210 DEG.	I	1.96	1.97	1.95	1.93	1.92	I	1.94
240 DEG.	I	1.98	1.98	1.96	1.96	1.94	I	1.96
270 DEG.	I	1.99	2.01	1.99	1.99	1.98	I	1.99
300 DEG.	I	2.03	2.06	2.03	2.04	2.04	I	2.04
330 DEG.	I	2.06	2.09	2.09	2.07	2.09	I	2.08
AVE.	I	2.02	2.03	2.03	2.02	2.02	I	

TOTAL AVERAGE = 2.02 MM  
 C. O. V. = 3.06 %

# MEASUREMENTS OF THICKNESS

MODEL : H3  
 LENGTH(L) : 1000 MM  
 UNIT : MM

LOCATION	I	TOP				BOTTOM	I	AVE.
	I	0.00L	0.25L	0.50L	0.75L	1.00L	I	
<hr/>								
0 DEG.	I	2.08	2.09	2.08	2.08	2.07	I	2.08
	I	(2.07)				(2.07)	I	
30 DEG.	I	2.10	2.09	2.09	2.08	2.07	I	2.08
	I	(2.09)				(2.07)	I	
60 DEG.	I	2.09	2.09	2.08	2.08	2.08	I	2.08
	I	(2.08)				(2.07)	I	
90 DEG.	I	2.07	2.05	2.05	2.06	2.05	I	2.06
	I	(2.06)				(2.04)	I	
120 DEG.	I	2.03	2.04	2.02	2.03	2.02	I	2.03
	I	(2.03)				(2.02)	I	
150 DEG.	I	2.00	1.99	2.00	1.99	1.98	I	1.99
	I	(1.99)				(1.98)	I	
180 DEG.	I	1.97	1.97	1.99	1.97	1.98	I	1.98
	I	(1.96)				(1.97)	I	
210 DEG.	I	1.96	1.96	1.98	1.98	1.96	I	1.96
	I	(1.95)				(1.99)	I	
240 DEG.	I	1.96	1.96	1.98	1.97	1.98	I	1.97
	I	(1.95)				(1.97)	I	
270 DEG.	I	1.99	1.99	2.02	2.00	2.00	I	2.00
	I	(1.98)				(2.00)	I	
300 DEG.	I	2.02	2.03	2.04	2.03	2.03	I	2.03
	I	(2.01)				(2.01)	I	
330 DEG.	I	2.07	2.08	2.08	2.07	2.07	I	2.08
	I	(2.05)				(2.06)	I	
<hr/>								
AVE.	I	2.03	2.03	2.03	2.03	2.03	I	
	I	(2.02)				(2.02)	I	
<hr/>								

\* THE THICKNESSES IN PARENTHESES WERE  
 MEASURED WITH A MICROMETER

TOTAL AVERAGE = 2.03 MM  
 C. O. V. = 2.23 %

## **B. II            Initial Shape Measurements**

### **B. II. 1            Outside Diameter Measurements**

### **B. II. 2            Initial Out-of-Straightness Measurements Table**

### **B. II. 3            Initial Out-of-Straightness Plots**

Model No.	D <sub>max</sub> - D <sub>min</sub> (mm)					Max. $\frac{D_{\max} - D_{\min}}{D_{\text{mean}}} \times 10^2$
	TOP	0.25L	0.5L	0.75L	BOTTOM	
A1	0.20	0.10	0.10	0.10	0.10	0.39
A2	0.20	0.05	0.05	0.10	0.15	0.39
A3	0.15	0.10	0.15	0.10	0.15	0.29
A4	0.80	0.30	0.30	0.10	0.55	1.57
B1	0.30	0.10	0.10	0.10	0.25	0.59
B2	0.20	0.05	0.10	0.10	0.35	0.69
B3	0.15	0.10	0.05	0.05	0.20	0.39
B4	0.55	0.10	0.10	0.20	0.20	1.08
C1	0.50	0.10	0.10	0.30	0.05	0.98
C2	0.20	0.10	0.10	0.15	0.45	0.88
C3	0.20	0.10	0.05	0.10	0.30	0.39
C4	0.10	0.10	0.10	0.10	0.70	1.38
D1	0.20	0.05	0.05	0.10	0.10	0.39
D2	0.10	0.10	0.15	0.10	0.10	0.29
D3	0.05	0.10	0.05	0.10	0.15	0.29
D4	0.15	0.10	0.15	0.10	0.25	0.49
E1	0.10	0.05	0.10	0.10	0.10	0.20
E2	0.15	0.10	0.10	0.10	0.10	0.29
E3	0.10	0.05	0.10	0.10	0.15	0.29
F1	0.10	0.05	0.10	0.10	0.05	0.20
F2	0.15	0.20	0.10	0.10	0/.05	0.39
F3	0.10	0.15	0.00	0.18	0.16	0.35
G1	0.25	0.10	0.20	0.10	0.10	0.49
G2	0.05	0.05	0.00	0.05	0.05	0.10
G3	0.10	0.20	0.15	0.10	0.05	0.39
H1	0.05	0.10	0.10	0.15	0.05	0.29
H2	0.30	0.25	0.20	0.10	0.10	0.59
H3	0.20	0.25	0.30	0.10	0.05	0.49

TABLE B1: Initial Ovality (Out-of-Roundness)



## MEASUREMENTS OF OUTSIDE DIAMETER

MODEL : A1  
 LENGTH(L) : 1400 MM  
 UNIT : MM

LOCATION	I	TOP				BOTTOM	I	AVE.
	I	0.00L	0.25L	0.50L	0.75L	1.00L	I	
0-180 DEG.	I	50.90	50.85	50.90	51.00	50.85	I	50.90
30-210 DEG.	I	50.85	50.85	50.90	50.90	50.80	I	50.86
60-240 DEG.	I	50.75	50.85	50.90	50.95	50.80	I	50.85
90-270 DEG.	I	50.75	50.85	51.00	50.95	50.85	I	50.88
120-300 DEG.	I	50.90	50.90	50.90	50.95	50.90	I	50.91
150-330 DEG.	I	50.95	50.95	50.95	50.95	50.90	I	50.94
AVE.	I	50.85	50.87	50.92	50.95	50.85	I	

TOTAL AVERAGE = 50.89 MM

C. O. V. = 0.12 %

## MEASUREMENTS OF OUTSIDE DIAMETER

MODEL : A2  
 LENGTH(L) : 1000 MM  
 UNIT : MM

LOCATION	I	TOP				BOTTOM	I	AVE.
	I	0.00L	0.25L	0.50L	0.75L	1.00L	I	
0-180 DEG.	I	50.80	50.90	50.90	50.90	50.95	I	50.89
30-210 DEG.	I	50.80	50.95	50.90	50.90	50.90	I	50.89
60-240 DEG.	I	50.90	50.95	50.95	51.00	50.80	I	50.92
90-270 DEG.	I	50.90	50.90	50.90	51.00	50.85	I	50.91
120-300 DEG.	I	51.00	50.90	50.90	50.95	50.90	I	50.93
150-330 DEG.	I	50.90	50.90	50.90	50.90	50.95	I	50.91
AVE.	I	50.88	50.92	50.91	50.94	50.89	I	

TOTAL AVERAGE = 50.91 MM

C. O. V. = 0.10 %

## MEASUREMENTS OF OUTSIDE DIAMETER

MODEL : A3  
 LENGTH(L) : 1400 MM  
 UNIT : MM

LOCATION	I	TOP				BOTTOM	I	AVE.
	I	0.00L	0.25L	0.50L	0.75L	1.00L	I	
0-180 DEG.	I	50.90	50.90	50.85	50.85	50.90	I	50.88
30-210 DEG.	I	50.75	50.90	50.85	50.90	50.80	I	50.84
60-240 DEG.	I	50.75	50.80	50.90	50.90	50.95	I	50.86
90-270 DEG.	I	50.90	50.90	50.95	50.90	50.90	I	50.91
120-300 DEG.	I	50.90	50.80	51.00	50.90	50.95	I	50.91
150-330 DEG.	I	50.90	50.85	50.85	50.80	50.95	I	50.87
AVE.	I	50.85	50.86	50.90	50.87	50.91	I	

TOTAL AVERAGE = 50.88 MM  
 C. O. V. = 0.12 %

## MEASUREMENTS OF OUTSIDE DIAMETER

MODEL : A4  
 LENGTH(L) : 1000 MM  
 UNIT : MM

LOCATION	I	TOP				BOTTOM	I	AVE.
	I	0.00L	0.25L	0.50L	0.75L	1.00L	I	
0-180 DEG.	I	51.30	51.10	50.85	50.95	51.10	I	51.06
30-210 DEG.	I	51.10	50.80	50.80	50.90	51.15	I	50.95
60-240 DEG.	I	50.60	50.85	50.85	50.95	50.90	I	50.83
90-270 DEG.	I	50.50	50.95	50.90	50.85	50.60	I	50.76
120-300 DEG.	I	50.70	51.00	51.00	50.85	50.60	I	50.83
150-330 DEG.	I	51.10	51.00	50.90	50.85	50.85	I	50.94
AVE.	I	50.88	50.95	50.88	50.89	50.87	I	

TOTAL AVERAGE = 50.89 MM  
 C. O. V. = 0.35 %

## MEASUREMENTS OF OUTSIDE DIAMETER

MODEL : B1  
 LENGTH(L) : 1400 MM  
 UNIT : MM

LOCATION	I	TOP				BOTTOM	I	AVE.
	I	0.00L	0.25L	0.50L	0.75L	1.00L	I	
0-180 DEG.	I	50.95	50.90	50.80	50.85	50.80	I	50.86
30-210 DEG.	I	50.75	50.80	50.85	50.80	50.70	I	50.78
60-240 DEG.	I	50.70	50.85	50.90	50.80	50.80	I	50.81
90-270 DEG.	I	50.80	50.85	50.90	50.85	50.90	I	50.86
120-300 DEG.	I	51.00	50.90	50.85	50.90	50.95	I	50.92
150-330 DEG.	I	51.00	50.90	50.90	50.90	50.90	I	50.92
AVE.	I	50.87	50.87	50.87	50.85	50.84	I	

TOTAL AVERAGE = 50.86 MM

C. O. V. = 0.15 %

## MEASUREMENTS OF OUTSIDE DIAMETER

MODEL : B2  
 LENGTH(L) : 902 MM  
 UNIT : MM

LOCATION	I	TOP				BOTTOM	I	AVE.
	I	0.00L	0.25L	0.50L	0.75L	1.00L	I	
0-180 DEG.	I	50.95	51.00	51.00	50.95	50.80	I	50.94
30-210 DEG.	I	50.95	50.95	51.00	51.00	51.05	I	50.99
60-240 DEG.	I	51.00	51.00	51.00	51.00	51.10	I	51.02
90-270 DEG.	I	50.90	51.00	50.90	50.90	50.95	I	50.93
120-300 DEG.	I	50.80	51.00	50.95	50.95	50.80	I	50.90
150-330 DEG.	I	50.90	51.00	50.90	50.90	50.75	I	50.89
AVE.	I	50.92	50.99	50.96	50.95	50.91	I	

TOTAL AVERAGE = 50.94 MM

C. O. V. = 0.16 %

## MEASUREMENTS OF OUTSIDE DIAMETER

MODEL : B3  
 LENGTH(L) : 1000 MM  
 UNIT : MM

LOCATION	I	TOP				BOTTOM	I	AVE.
	I	0.00L	0.25L	0.50L	0.75L	1.00L	I	
0-180 DEG.	I	50.80	50.90	50.90	50.90	50.95	I	50.89
30-210 DEG.	I	50.90	50.90	50.90	50.95	51.00	I	50.93
60-240 DEG.	I	50.95	51.00	50.90	50.95	50.90	I	50.94
90-270 DEG.	I	50.95	50.90	50.95	50.95	50.80	I	50.91
120-300 DEG.	I	50.95	51.00	50.95	50.90	50.80	I	50.92
150-330 DEG.	I	50.90	51.00	50.95	50.95	50.80	I	50.92
AVE.	I	50.91	50.95	50.92	50.93	50.87	I	

TOTAL AVERAGE = 50.92 MM  
 C. O. V. = 0.11 %

## MEASUREMENTS OF OUTSIDE DIAMETER

MODEL : B4  
 LENGTH(L) : 1400 MM  
 UNIT : MM

LOCATION	I	TOP				BOTTOM	I	AVE.
	I	0.00L	0.25L	0.50L	0.75L	1.00L	I	
0-180 DEG.	I	50.60	50.90	50.85	51.00	50.85	I	50.84
30-210 DEG.	I	50.75	50.85	50.90	50.85	50.80	I	50.83
60-240 DEG.	I	51.00	50.80	50.90	50.80	50.75	I	50.85
90-270 DEG.	I	51.15	50.95	50.85	50.90	50.80	I	50.93
120-300 DEG.	I	50.85	50.90	50.80	50.90	50.90	I	50.87
150-330 DEG.	I	50.60	50.95	50.80	50.95	51.00	I	50.86
AVE.	I	50.82	50.89	50.85	50.90	50.85	I	

TOTAL AVERAGE = 50.86 MM  
 C. O. V. = 0.22 %

## MEASUREMENTS OF OUTSIDE DIAMETER

MODEL : C1  
 LENGTH(L) : 1000 MM  
 UNIT : MM

LOCATION	I	TOP				BOTTOM	I	AVE.
	I	0.00L	0.25L	0.50L	0.75L	1.00L	I	
0-180 DEG.	I	51.20	50.90	51.00	50.80	50.90	I	50.96
30-210 DEG.	I	51.20	50.95	51.00	50.95	50.95	I	51.01
60-240 DEG.	I	51.20	50.95	50.90	51.10	50.95	I	51.02
90-270 DEG.	I	51.00	51.00	51.00	51.00	50.95	I	50.99
120-300 DEG.	I	50.70	51.00	51.00	51.00	50.95	I	50.93
150-330 DEG.	I	50.80	51.00	50.95	50.90	50.90	I	50.91
AVE.	I	51.02	50.97	50.97	50.96	50.93	I	

TOTAL AVERAGE = 50.97 MM

C. O. V. = 0.21 %

## MEASUREMENTS OF OUTSIDE DIAMETER

MODEL : C2  
 LENGTH(L) : 1000 MM  
 UNIT : MM

LOCATION	I	TOP				BOTTOM	I	AVE.
	I	0.00L	0.25L	0.50L	0.75L	1.00L	I	
0-180 DEG.	I	50.75	50.90	50.90	51.00	50.65	I	50.84
30-210 DEG.	I	50.90	50.90	50.90	51.00	50.70	I	50.88
60-240 DEG.	I	50.95	50.90	51.00	51.00	50.90	I	50.95
90-270 DEG.	I	50.95	50.95	50.90	50.90	51.10	I	50.96
120-300 DEG.	I	50.90	50.90	50.90	50.85	51.00	I	50.91
150-330 DEG.	I	50.90	50.85	50.95	50.95	50.85	I	50.90
AVE.	I	50.89	50.90	50.92	50.95	50.87	I	

TOTAL AVERAGE = 50.91 MM

C. O. V. = 0.18 %

## MEASUREMENTS OF OUTSIDE DIAMETER

MODEL : C3  
 LENGTH(L) : 1400 MM  
 UNIT : MM

LOCATION	I	TOP				BOTTOM	I	AVE.
	I	0.00L	0.25L	0.50L	0.75L	1.00L	I	
0-180 DEG.	I	50.80	50.85	50.95	50.80	50.70	I	50.82
30-210 DEG.	I	50.70	50.90	50.95	50.90	50.80	I	50.85
60-240 DEG.	I	50.75	50.95	50.90	50.80	50.80	I	50.84
90-270 DEG.	I	50.95	50.90	50.90	50.90	50.90	I	50.91
120-300 DEG.	I	50.90	50.85	50.90	50.90	50.85	I	50.88
150-330 DEG.	I	50.90	50.90	50.95	50.80	50.90	I	50.89
AVE.	I	50.83	50.89	50.92	50.85	50.82	I	

TOTAL AVERAGE = 50.86 MM  
 C. O. V. = 0.14 %

## MEASUREMENTS OF OUTSIDE DIAMETER

MODEL : C4  
 LENGTH(L) : 1400 MM  
 UNIT : MM

LOCATION	I	TOP				BOTTOM	I	AVE.
	I	0.00L	0.25L	0.50L	0.75L	1.00L	I	
0-180 DEG.	I	50.85	50.90	50.85	50.90	50.50	I	50.80
30-210 DEG.	I	50.90	50.90	50.80	50.80	50.60	I	50.80
60-240 DEG.	I	50.85	50.80	50.80	50.80	50.95	I	50.84
90-270 DEG.	I	50.80	50.80	50.90	50.90	51.20	I	50.92
120-300 DEG.	I	50.80	50.80	50.90	50.90	51.00	I	50.88
150-330 DEG.	I	50.80	50.90	50.90	50.90	50.70	I	50.84
AVE.	I	50.83	50.85	50.86	50.87	50.82	I	

TOTAL AVERAGE = 50.85 MM  
 C. O. V. = 0.24 %

MEASUREMENTS OF OUTSIDE DIAMETER

MODEL : D1  
 LENGTH(L) : 1400 MM  
 UNIT : MM

LOCATION	I	TOP				BOTTOM	I	AVE.
	I	0.00L	0.25L	0.50L	0.75L	1.00L	I	
0-180 DEG.	I	50.80	50.90	50.90	50.95	50.90	I	50.89
30-210 DEG.	I	50.80	50.90	50.90	50.95	50.90	I	50.89
60-240 DEG.	I	50.90	50.95	50.90	50.95	50.80	I	50.90
90-270 DEG.	I	50.95	50.90	50.90	50.90	50.90	I	50.91
120-300 DEG.	I	51.00	50.95	50.90	51.00	50.90	I	50.95
150-330 DEG.	I	50.90	50.90	50.95	50.90	50.90	I	50.91
AVE.	I	50.89	50.92	50.91	50.94	50.88	I	

TOTAL AVERAGE = 50.91 MM  
 C. O. V. = 0.09 %

MEASUREMENTS OF OUTSIDE DIAMETER

MODEL : D2  
 LENGTH(L) : 1000 MM  
 UNIT : MM

LOCATION	I	TOP				BOTTOM	I	AVE.
	I	0.00L	0.25L	0.50L	0.75L	1.00L	I	
0-180 DEG.	I	51.00	51.00	50.95	51.05	50.90	I	50.98
30-210 DEG.	I	51.00	51.00	50.95	50.95	51.00	I	50.98
60-240 DEG.	I	51.00	51.00	50.95	50.95	51.00	I	50.98
90-270 DEG.	I	51.10	50.90	51.10	51.00	50.90	I	51.00
120-300 DEG.	I	51.00	50.95	51.00	50.95	50.90	I	50.96
150-330 DEG.	I	51.00	50.90	51.00	50.95	50.95	I	50.96
AVE.	I	51.02	50.96	50.99	50.97	50.94	I	

TOTAL AVERAGE = 50.98 MM  
 C. O. V. = 0.10 %

## MEASUREMENTS OF OUTSIDE DIAMETER

MODEL : D3  
 LENGTH(L) : 1400 MM  
 UNIT : MM

LOCATION	I	TOP				BOTTOM	I	AVE.
	I	0.00L	0.25L	0.50L	0.75L	1.00L	I	
0-180 DEG.	I	50.90	50.95	50.90	50.95	50.90	I	50.92
30-210 DEG.	I	50.90	50.90	50.90	50.95	50.90	I	50.91
60-240 DEG.	I	50.90	50.90	50.90	50.90	51.05	I	50.93
90-270 DEG.	I	50.85	50.90	50.90	50.90	50.95	I	50.90
120-300 DEG.	I	50.85	50.90	50.95	50.85	50.90	I	50.89
150-330 DEG.	I	50.90	51.00	50.90	50.90	50.90	I	50.92
AVE.	I	50.88	50.92	50.91	50.91	50.93	I	

TOTAL AVERAGE = 50.91 MM

C. O. V. = 0.08 %

## MEASUREMENTS OF OUTSIDE DIAMETER

MODEL : D4  
 LENGTH(L) : 1400 MM  
 UNIT : MM

LOCATION	I	TOP				BOTTOM	I	AVE.
	I	0.00L	0.25L	0.50L	0.75L	1.00L	I	
0-180 DEG.	I	50.90	50.90	50.90	50.85	51.00	I	50.91
30-210 DEG.	I	50.80	51.00	50.90	50.90	50.80	I	50.88
60-240 DEG.	I	50.90	50.95	50.85	50.90	50.70	I	50.86
90-270 DEG.	I	50.90	50.95	51.00	50.90	50.75	I	50.90
120-300 DEG.	I	50.95	50.95	50.90	50.90	50.90	I	50.92
150-330 DEG.	I	50.90	51.00	50.90	50.80	51.00	I	50.92
AVE.	I	50.89	50.96	50.91	50.87	50.86	I	

TOTAL AVERAGE = 50.90 MM

C. O. V. = 0.14 %



# MEASUREMENTS OF OUTSIDE DIAMETER

MODEL : E1  
 LENGTH(L) : 1400 MM  
 UNIT : MM

LOCATION	I	TOP				BOTTOM	I	AVE.
	I	0.00L	0.25L	0.50L	0.75L	1.00L	I	
0-180 DEG.	I	50.85	50.90	51.00	50.95	50.90	I	50.92
30-210 DEG.	I	50.85	50.90	50.95	50.95	50.90	I	50.91
60-240 DEG.	I	50.85	50.95	50.90	50.90	50.90	I	50.90
90-270 DEG.	I	50.90	50.90	50.90	50.90	50.90	I	50.90
120-300 DEG.	I	50.95	50.90	50.95	51.00	50.95	I	50.95
150-330 DEG.	I	50.95	50.90	51.00	50.95	51.00	I	50.96
AVE.	I	50.89	50.91	50.95	50.94	50.92	I	

TOTAL AVERAGE = 50.92 MM  
 C. O. V. = 0.08 %

# MEASUREMENTS OF OUTSIDE DIAMETER

MODEL : E2  
 LENGTH(L) : 1000 MM  
 UNIT : MM

LOCATION	I	TOP				BOTTOM	I	AVE.
	I	0.00L	0.25L	0.50L	0.75L	1.00L	I	
0-180 DEG.	I	50.85	50.95	50.90	51.00	50.95	I	50.93
30-210 DEG.	I	50.80	50.90	51.00	50.95	50.90	I	50.91
60-240 DEG.	I	50.80	50.90	51.00	50.95	50.85	I	50.90
90-270 DEG.	I	50.90	50.85	51.00	50.90	50.90	I	50.91
120-300 DEG.	I	50.90	50.95	50.95	51.00	50.85	I	50.93
150-330 DEG.	I	50.95	50.95	50.95	51.00	50.90	I	50.95
AVE.	I	50.87	50.92	50.97	50.97	50.89	I	

TOTAL AVERAGE = 50.92 MM  
 C. O. V. = 0.11 %

## MEASUREMENTS OF OUTSIDE DIAMETER

MODEL : E3  
 LENGTH(L) : 1400 MM  
 UNIT : MM

LOCATION	I	TOP				BOTTOM	I	AVE.
	I	0.00L	0.25L	0.50L	0.75L	1.00L	I	
0-180 DEG.	I	50.90	50.95	50.80	50.90	50.95	I	50.90
30-210 DEG.	I	51.00	50.95	50.85	50.90	51.00	I	50.94
60-240 DEG.	I	50.90	50.95	50.80	50.95	50.85	I	50.89
90-270 DEG.	I	50.95	50.95	50.90	50.85	50.85	I	50.90
120-300 DEG.	I	50.90	50.90	50.80	50.90	50.95	I	50.89
150-330 DEG.	I	50.95	50.90	50.85	50.90	51.00	I	50.92
AVE.	I	50.93	50.93	50.83	50.90	50.93	I	

TOTAL AVERAGE = 50.91 MM  
 C. O. V. = 0.11 %

## MEASUREMENTS OF OUTSIDE DIAMETER

MODEL : F1  
 LENGTH(L) : 1400 MM  
 UNIT : MM

LOCATION	I	TOP				BOTTOM	I	AVE.
	I	0.00L	0.25L	0.50L	0.75L	1.00L	I	
0-180 DEG.	I	50.90	50.90	50.90	50.90	50.85	I	50.89
30-210 DEG.	I	50.85	50.95	50.90	50.95	50.90	I	50.91
60-240 DEG.	I	50.90	50.95	50.95	50.90	50.85	I	50.91
90-270 DEG.	I	50.80	50.90	51.00	51.00	50.85	I	50.91
120-300 DEG.	I	50.90	50.95	50.90	50.95	50.90	I	50.92
150-330 DEG.	I	50.95	50.90	50.90	50.90	50.90	I	50.91
AVE.	I	50.88	50.92	50.92	50.93	50.87	I	

TOTAL AVERAGE = 50.91 MM  
 C. O. V. = 0.09 %

## MEASUREMENTS OF OUTSIDE DIAMETER

MODEL : F2  
 LENGTH(L) : 1000 MM  
 UNIT : MM

LOCATION	I	TOP				BOTTOM	I	AVE.
	I	0.00L	0.25L	0.50L	0.75L	1.00L	I	
0-180 DEG.	I	50.95	51.10	50.95	50.90	50.90	I	50.96
30-210 DEG.	I	50.95	50.90	51.00	50.85	50.90	I	50.92
60-240 DEG.	I	50.85	50.90	50.95	50.95	50.90	I	50.91
90-270 DEG.	I	50.80	50.90	50.90	50.90	50.85	I	50.87
120-300 DEG.	I	50.80	50.95	50.95	50.90	50.85	I	50.89
150-330 DEG.	I	50.80	50.90	50.90	50.95	50.85	I	50.88
AVE.	I	50.86	50.94	50.94	50.91	50.87	I	

TOTAL AVERAGE = 50.90 MM  
 C. O. V. = 0.12 %

## MEASUREMENTS OF OUTSIDE DIAMETER

MODEL : F3  
 LENGTH(L) : 1800 MM  
 UNIT : MM

LOCATION	I	TOP				BOTTOM	I	AVE.
	I	0.00L	0.25L	0.50L	0.75L	1.00L	I	
0-180 DEG.	I	50.80	50.90	50.90	50.88	50.78	I	50.85
30-210 DEG.	I	50.85	50.90	50.90	50.82	50.80	I	50.85
60-240 DEG.	I	50.90	50.95	50.90	50.82	50.82	I	50.88
90-270 DEG.	I	50.80	50.95	50.90	51.00	50.88	I	50.91
120-300 DEG.	I	50.80	50.90	50.90	50.84	50.78	I	50.84
150-330 DEG.	I	50.80	50.80	50.90	50.84	50.72	I	50.81
AVE.	I	50.82	50.90	50.90	50.87	50.80	I	

TOTAL AVERAGE = 50.86 MM  
 C. O. V. = 0.12 %

## MEASUREMENTS OF OUTSIDE DIAMETER

MODEL : G1  
 LENGTH(L) : 1000 MM  
 UNIT : MM

LOCATION	I	TOP				BOTTOM	I	AVE.
	I	0.00L	0.25L	0.50L	0.75L	1.00L	I	
0-180 DEG.	I	51.00	50.95	50.95	50.90	50.90	I	50.94
30-210 DEG.	I	50.95	50.95	51.00	50.90	50.85	I	50.93
60-240 DEG.	I	50.95	51.00	50.90	50.95	50.90	I	50.94
90-270 DEG.	I	50.95	51.00	50.95	50.90	50.90	I	50.94
120-300 DEG.	I	51.20	51.00	51.10	51.00	50.90	I	51.04
150-330 DEG.	I	51.00	50.90	50.90	50.90	50.95	I	50.93
AVE.	I	51.01	50.97	50.97	50.92	50.90	I	

TOTAL AVERAGE = 50.95 MM  
 C. O. V. = 0.14 %

## MEASUREMENTS OF OUTSIDE DIAMETER

MODEL : G2  
 LENGTH(L) : 1400 MM  
 UNIT : MM

LOCATION	I	TOP				BOTTOM	I	AVE.
	I	0.00L	0.25L	0.50L	0.75L	1.00L	I	
0-180 DEG.	I	50.90	50.95	50.90	50.95	50.90	I	50.92
30-210 DEG.	I	50.95	50.90	50.90	50.90	50.95	I	50.92
60-240 DEG.	I	50.90	50.90	50.90	50.90	50.95	I	50.91
90-270 DEG.	I	50.90	50.95	50.90	50.95	50.95	I	50.93
120-300 DEG.	I	50.95	50.95	50.90	50.95	50.95	I	50.94
150-330 DEG.	I	50.95	50.95	50.90	50.90	50.90	I	50.92
AVE.	I	50.92	50.93	50.90	50.92	50.93	I	

TOTAL AVERAGE = 50.92 MM  
 C. O. V. = 0.05 %

## MEASUREMENTS OF OUTSIDE DIAMETER

MODEL : G3  
 LENGTH(L) : 1800 MM  
 UNIT : MM

LOCATION	I	TOP				BOTTOM	I	AVE.
	I	0.00L	0.25L	0.50L	0.75L	1.00L	I	
0-180 DEG.	I	50.85	50.90	51.00	50.90	50.90	I	50.91
30-210 DEG.	I	50.90	50.95	50.95	50.95	50.85	I	50.92
60-240 DEG.	I	50.90	50.90	51.00	51.00	50.90	I	50.94
90-270 DEG.	I	50.90	51.00	50.95	51.00	50.90	I	50.95
120-300 DEG.	I	50.85	51.10	51.10	51.00	50.90	I	50.99
150-330 DEG.	I	50.80	51.00	50.95	50.90	50.85	I	50.90
AVE.	I	50.87	50.97	50.99	50.96	50.88	I	

TOTAL AVERAGE = 50.93 MM

C. O. V. = 0.14 %

## MEASUREMENTS OF OUTSIDE DIAMETER

MODEL : H1  
 LENGTH(L) : 1400 MM  
 UNIT : MM

LOCATION	I	TOP				BOTTOM	I	AVE.
	I	0.00L	0.25L	0.50L	0.75L	1.00L	I	
0-180 DEG.	I	50.90	50.95	50.90	51.00	50.90	I	50.93
30-210 DEG.	I	50.90	50.90	50.90	50.90	50.95	I	50.91
60-240 DEG.	I	50.90	50.90	50.90	50.85	50.90	I	50.89
90-270 DEG.	I	50.90	50.85	50.90	50.85	50.95	I	50.89
120-300 DEG.	I	50.85	50.90	51.00	50.90	50.90	I	50.91
150-330 DEG.	I	50.90	50.90	50.90	50.90	50.90	I	50.90
AVE.	I	50.89	50.90	50.92	50.90	50.92	I	

TOTAL AVERAGE = 50.90 MM

C. O. V. = 0.07 %

MEASUREMENTS OF OUTSIDE DIAMETER

MODEL : H2  
 LENGTH(L) : 1400 MM  
 UNIT : MM

LOCATION	I	TOP				BOTTOM	I	AVE.
	I	0.00L	0.25L	0.50L	0.75L	1.00L	I	
0-180 DEG.	I	50.85	50.95	50.90	50.90	50.80	I	50.88
30-210 DEG.	I	51.10	50.85	50.95	51.00	50.90	I	50.96
60-240 DEG.	I	50.90	50.90	51.00	50.90	50.85	I	50.91
90-270 DEG.	I	50.80	51.10	51.10	50.95	50.90	I	50.97
120-300 DEG.	I	50.90	50.90	51.00	50.95	50.80	I	50.91
150-330 DEG.	I	50.85	50.95	50.95	51.00	50.85	I	50.92
AVE.	I	50.90	50.94	50.98	50.95	50.85	I	

TOTAL AVERAGE = 50.92 MM  
 C. O. V. = 0.16 %

MEASUREMENTS OF OUTSIDE DIAMETER

MODEL : H3  
 LENGTH(L) : 1000 MM  
 UNIT : MM

LOCATION	I	TOP				BOTTOM	I	AVE.
	I	0.00L	0.25L	0.50L	0.75L	1.00L	I	
0-180 DEG.	I	51.00	51.00	51.00	50.95	50.90	I	50.97
30-210 DEG.	I	50.90	50.90	50.90	51.00	50.90	I	50.92
60-240 DEG.	I	50.80	50.95	51.00	50.95	50.85	I	50.91
90-270 DEG.	I	50.80	50.90	51.20	50.90	50.80	I	50.92
120-300 DEG.	I	50.90	50.95	51.15	50.90	50.85	I	50.95
150-330 DEG.	I	51.00	51.15	51.00	50.95	50.90	I	51.00
AVE.	I	50.90	50.97	51.04	50.94	50.87	I	

TOTAL AVERAGE = 50.94 MM  
 C. O. V. = 0.19 %



### INITIAL CUT-OFF STRAIGHTNESS

```

MODEL      : A2
LENGTH(L)  : 1000 MM
OUTSIDE DIA.: 50.91MM
THICKNESS  : 1.20 MM
UNIT       : MM

```

LOCATION	I	TOP				BOTTOM	
		I	0.00L	0.25L	0.50L	0.75L	1.00L
-----							
	I						
0 DEG.	I	0.000	-0.050	-0.117	-0.097	0.000	
	I						
30 DEG.	I	0.000	-0.107	-0.175	-0.234	0.000	
	I						
60 DEG.	I	0.000	-0.128	-0.203	-0.243	0.000	
	I						
90 DEG.	I	0.000	-0.105	-0.153	-0.189	0.000	
	I						
120 DEG.	I	0.000	-0.044	-0.053	-0.093	0.000	
	I						
150 DEG.	I	0.000	-0.006	-0.025	-0.113	0.000	
	I						
180 DEG.	I	0.000	0.085	0.126	0.024	0.000	
	I						
210 DEG.	I	0.000	0.150	0.203	0.148	0.000	
	I						
240 DEG.	I	0.000	0.151	0.175	0.204	0.000	
	I						
270 DEG.	I	0.000	0.116	0.115	0.211	0.000	
	I						
300 DEG.	I	0.000	0.072	0.058	0.156	0.000	
	I						
330 DEG.	I	0.000	0.018	-0.019	0.048	0.000	

## (AVERAGE OF INITIAL OUT-OF-STRAIGHTNESS)

	I								
0-180 DEG.	I	0.000	-0.068	-0.121	-0.060	0.000			
	I								
30-210 DEG.	I	0.000	-0.128	-0.189	-0.191	0.000			
	I								
60-240 DEG.	I	0.000	-0.140	-0.189	-0.224	0.000			
	I								
90-270 DEG.	I	0.000	-0.110	-0.134	-0.200	0.000			
	I								
120-300 DEG.	I	0.000	-0.058	-0.055	-0.125	0.000			
	I								
150-330 DEG.	I	0.000	-0.012	-0.003	-0.081	0.000			



# INITIAL OUT-OF-STRAIGHTNESS

MODEL : A3  
 LENGTH(L) : 1400 MM  
 OUTSIDE DIA.: 50.88MM  
 THICKNESS : 1.20 MM  
 UNIT : MM

LOCATION	I	TOP				BOTTOM
	I	0.00L	0.25L	0.50L	0.75L	1.00L
0 DEG.	I	0.000	0.003	-0.082	-0.101	0.000
30 DEG.	I	0.000	0.148	0.155	0.101	0.000
60 DEG.	I	0.000	0.192	0.301	0.247	0.000
90 DEG.	I	0.000	0.172	0.347	0.291	0.000
120 DEG.	I	0.000	0.141	0.367	0.355	0.000
150 DEG.	I	0.000	0.017	0.166	0.206	0.000
180 DEG.	I	0.000	-0.093	-0.022	0.094	0.000
210 DEG.	I	0.000	-0.170	-0.218	-0.040	0.000
240 DEG.	I	0.000	-0.246	-0.371	-0.210	0.000
270 DEG.	I	0.000	-0.248	-0.389	-0.287	0.000
300 DEG.	I	-0.000	-0.176	-0.330	-0.285	0.000
330 DEG.	I	0.000	-0.123	-0.234	-0.221	0.000
(AVERAGE OF INITIAL OUT-OF-STRAIGHTNESS)						
0-180 DEG.	I	0.000	0.048	-0.030	-0.097	0.000
30-210 DEG.	I	0.000	0.159	0.186	0.070	0.000
60-240 DEG.	I	0.000	0.219	0.336	0.228	0.000
90-270 DEG.	I	0.000	0.210	0.368	0.289	0.000
120-300 DEG.	I	0.000	0.159	0.349	0.320	0.000
150-330 DEG.	I	0.000	0.070	0.200	0.213	0.000











### INITIAL CUT-OFF STRAIGHTNESS

```

MODEL      : C1
LENGTH(L) : 1000 MM
OUTSIDE DIA.: 50.97MM
THICKNESS  : 1.21 MM
UNIT       : MM

```

LOCATION	I	TOP				BOTTOM
		0.00L	0.25L	0.50L	0.75L	
	I					
0 DEG.	I	0.000	-0.196	-0.292	-0.505	0.000
	I					
30 DEG.	I	0.000	-0.451	-0.728	-0.859	0.000
	I					
60 DEG.	I	0.000	-0.610	-0.969	-1.019	0.000
	I					
90 DEG.	I	0.000	-0.606	-0.965	-0.930	0.000
	I					
120 DEG.	I	0.000	-0.436	-0.733	-0.684	0.000
	I					
150 DEG.	I	0.000	-0.187	-0.359	-0.300	0.000
	I					
180 DEG.	I	0.000	0.106	0.106	0.182	0.000
	I					
210 DEG.	I	0.000	0.373	0.543	0.645	0.000
	I					
240 DEG.	I	0.000	0.549	0.805	0.858	0.000
	I					
270 DEG.	I	0.000	0.566	0.856	0.822	0.000
	I					
300 DEG.	I	0.000	0.394	0.628	0.509	0.000
	I					
330 DEG.	I	0.000	0.105	0.198	0.009	0.000
-----						
(AVERAGE OF INITIAL OUT-OF-STRAIGHTNESS)						
-----						
	I					
0-180 DEG.	I	0.000	-0.151	-0.199	-0.344	0.000
	I					
30-210 DEG.	I	0.000	-0.412	-0.636	-0.752	0.000
	I					
60-240 DEG.	I	0.000	-0.580	-0.887	-0.938	0.000
	I					
90-270 DEG.	I	0.000	-0.586	-0.910	-0.876	0.000
	I					
120-300 DEG.	I	0.000	-0.415	-0.680	-0.596	0.000
	I					
150-330 DEG.	I	0.000	-0.146	-0.279	-0.155	0.000







# INITIAL OUT-OF-STRAIGHTNESS

MODEL : C4  
 LENGTH(L) : 1400 MM  
 OUTSIDE DIA.: 50.85MM  
 THICKNESS : 1.22 MM  
 UNIT : MM

LOCATION	I	TOP				BOTTOM
	I	0.00L	0.25L	0.50L	0.75L	1.00L
0 DEG.	I	0.000	0.099	0.109	0.137	0.000
30 DEG.	I	0.000	-0.023	-0.044	0.100	0.000
60 DEG.	I	0.000	-0.189	-0.198	-0.014	0.000
90 DEG.	I	0.000	-0.282	-0.286	-0.174	0.000
120 DEG.	I	0.000	-0.284	-0.281	-0.213	0.000
150 DEG.	I	0.000	-0.207	-0.235	-0.153	0.000
180 DEG.	I	0.000	-0.145	-0.232	-0.198	0.000
210 DEG.	I	0.000	-0.100	-0.153	-0.226	0.000
240 DEG.	I	0.000	0.048	0.071	-0.036	0.000
270 DEG.	I	0.000	0.138	0.203	0.152	0.000
300 DEG.	I	0.000	0.157	0.207	0.151	0.000
330 DEG.	I	0.000	0.166	0.203	0.123	0.000
(AVERAGE OF INITIAL OUT-OF-STRAIGHTNESS)						
0-180 DEG.	I	0.000	0.122	0.170	0.168	0.000
30-210 DEG.	I	0.000	0.038	0.055	0.163	0.000
60-240 DEG.	I	0.000	-0.118	-0.135	0.011	0.000
90-270 DEG.	I	0.000	-0.210	-0.245	-0.163	0.000
120-300 DEG.	I	0.000	-0.220	-0.244	-0.182	0.000
150-330 DEG.	I	0.000	-0.187	-0.219	-0.138	0.000











# INITIAL OUT-OF-STRAIGHTNESS

MODEL : E2  
 LENGTH(L) : 1000 MM  
 OUTSIDE DIA.: 50.92MM  
 THICKNESS : 2.04 MM  
 UNIT : MM

LOCATION	I	TOP					BOTTOM
	I	0.00L	0.25L	0.50L	0.75L	1.00L	
0 DEG.	I	0.000	-0.120	-0.215	-0.062	0.000	
30 DEG.	I	0.000	-0.081	-0.124	0.098	0.000	
60 DEG.	I	0.000	-0.092	-0.015	0.212	0.000	
90 DEG.	I	0.000	-0.011	0.126	0.263	0.000	
120 DEG.	I	0.000	0.172	0.311	0.358	0.000	
150 DEG.	I	0.000	0.216	0.327	0.288	0.000	
180 DEG.	I	0.000	0.259	0.301	0.179	0.000	
210 DEG.	I	0.000	0.235	0.181	-0.024	0.000	
240 DEG.	I	0.000	0.137	0.003	-0.176	0.000	
270 DEG.	I	0.000	0.002	-0.159	-0.251	0.000	
300 DEG.	I	0.000	-0.073	-0.233	-0.215	0.000	
330 DEG.	I	0.000	-0.098	-0.255	-0.136	0.000	

## (AVERAGE OF INITIAL OUT-OF-STRAIGHTNESS)

0-180 DEG.	I	0.000	-0.190	-0.258	-0.121	0.000
30-210 DEG.	I	0.000	-0.158	-0.153	0.061	0.000
60-240 DEG.	I	0.000	-0.115	-0.009	0.194	0.000
90-270 DEG.	I	0.000	-0.006	0.142	0.257	0.000
120-300 DEG.	I	0.000	0.123	0.272	0.286	0.000
150-330 DEG.	I	0.000	0.157	0.291	0.212	0.000





# INITIAL CUT-OF STRAIGHTNESS

MODEL : F1  
 LENGTH(L) : 1400 MM  
 OUTSIDE DIA.: 50.91MM  
 THICKNESS : 2.03 MM  
 UNIT : MM

LOCATION	I	TOP					BOTTOM
	I	0.00L	0.25L	0.50L	0.75L	1.00L	
0 DEG.	I	0.000	-0.304	-0.181	-0.272	0.000	
30 DEG.	I	0.000	-0.102	0.058	-0.046	0.000	
60 DEG.	I	0.000	0.134	0.272	0.173	0.000	
90 DEG.	I	0.000	0.378	0.409	0.325	0.000	
120 DEG.	I	0.000	0.454	0.389	0.337	0.000	
150 DEG.	I	0.000	0.376	0.233	0.254	0.000	
180 DEG.	I	0.000	0.165	-0.008	0.092	0.000	
210 DEG.	I	0.000	-0.009	-0.196	-0.059	0.000	
240 DEG.	I	0.000	-0.270	-0.422	-0.263	0.000	
270 DEG.	I	0.000	-0.379	-0.471	-0.376	0.000	
300 DEG.	I	0.000	-0.516	-0.462	-0.459	0.000	
330 DEG.	I	0.000	-0.485	-0.371	-0.409	0.000	
(AVERAGE OF INITIAL CUT-OF-STRAIGHTNESS)							
0-180 DEG.	I	0.000	-0.235	-0.086	-0.182	0.000	
30-210 DEG.	I	0.000	-0.047	0.127	0.006	0.000	
60-240 DEG.	I	0.000	0.202	0.347	0.218	0.000	
90-270 DEG.	I	0.000	0.378	0.440	0.351	0.000	
120-300 DEG.	I	0.000	0.485	0.425	0.398	0.000	
150-330 DEG.	I	0.000	0.431	0.302	0.332	0.000	

# INITIAL OUT-OF-STRAIGHTNESS

MODEL : F2  
 LENGTH(L) : 1000 MM  
 OUTSIDE DIA.: 50.90MM  
 THICKNESS : 2.03 MM  
 UNIT : MM

LOCATION	I	TOP					BOTTOM
	I	0.00L	0.25L	0.50L	0.75L	1.00L	
0 DEG.	I	0.000	0.372	-0.678	-0.305	0.000	
30 DEG.	I	0.000	0.434	-0.402	-0.174	0.000	
60 DEG.	I	0.000	0.389	-0.077	0.021	0.000	
90 DEG.	I	0.000	0.224	0.285	0.204	0.000	
120 DEG.	I	0.000	0.018	0.557	0.354	0.000	
150 DEG.	I	0.000	-0.158	0.676	0.396	0.000	
180 DEG.	I	0.000	-0.264	0.729	0.385	0.000	
210 DEG.	I	0.000	-0.342	0.591	0.273	0.000	
240 DEG.	I	0.000	-0.339	0.141	0.025	0.000	
270 DEG.	I	0.000	-0.237	-0.178	-0.141	0.000	
300 DEG.	I	0.000	-0.014	-0.546	-0.251	0.000	
330 DEG.	I	0.000	0.204	-0.747	-0.327	0.000	
(AVERAGE OF INITIAL OUT-OF-STRAIGHTNESS)							
0-180 DEG.	I	0.000	0.318	-0.704	-0.345	0.000	
30-210 DEG.	I	0.000	0.388	-0.497	-0.223	0.000	
60-240 DEG.	I	0.000	0.364	-0.109	-0.002	0.000	
90-270 DEG.	I	0.000	0.230	0.231	0.172	0.000	
120-300 DEG.	I	0.000	0.016	0.551	0.302	0.000	
150-330 DEG.	I	0.000	-0.181	0.711	0.362	0.000	

### INITIAL OUT-OF STRAIGHTNESS

```

MODEL      : F3
LENGTH(L) : 1800 MM
OUTSIDE DIA.: 50.86MM
THICKNESS  : 2.02 MM
UNIT       : MM

```

LOCATION	TOP					BOTTOM
	I	0.00L	0.25L	0.50L	0.75L	
	I					
0 DEG.	I	0.000	-1.050	-0.944	-0.471	0.000
	I					
30 DEG.	I	0.000	0.283	-0.081	-0.069	0.000
	I					
60 DEG.	I	0.000	1.653	0.829	0.337	0.000
	I					
90 DEG.	I	0.000	2.613	1.505	0.687	0.000
	I					
120 DEG.	I	0.000	2.813	1.768	0.764	0.000
	I					
150 DEG.	I	0.000	2.217	1.542	0.761	0.000
	I					
180 DEG.	I	0.000	0.813	0.770	0.374	0.000
	I					
210 DEG.	I	0.000	-0.658	-0.126	-0.027	0.000
	I					
240 DEG.	I	0.000	-1.984	-1.036	-0.429	0.000
	I					
270 DEG.	I	0.000	-2.715	-1.588	-0.689	0.000
	I					
300 DEG.	I	0.000	-2.843	-1.847	-0.823	0.000
	I					
330 DEG.	I	0.000	-2.189	-1.563	-0.713	0.000
-----						
(AVERAGE OF INITIAL OUT-OF-STRAIGHTNESS)						
-----						
	I					
0-180 DEG.	I	0.000	-0.931	-0.857	-0.423	0.000
	I					
30-210 DEG.	I	0.000	0.470	0.022	-0.021	0.000
	I					
60-240 DEG.	I	0.000	1.819	0.932	0.383	0.000
	I					
90-270 DEG.	I	0.000	2.664	1.547	0.688	0.000
	I					
120-300 DEG.	I	0.000	2.828	1.808	0.793	0.000
	I					
150-330 DEG.	I	0.000	2.203	1.552	0.737	0.000

# INITIAL CUT-OFF STRAIGHTNESS

MODEL : G1  
 LENGTH(L) : 1000 MM  
 OUTSIDE DIA.: 50.95MM  
 THICKNESS : 2.04 MM  
 UNIT : MM

LOCATION	I	TOP				BOTTOM
		0.00L	0.25L	0.50L	0.75L	1.00L
	I					
0 DEG.	I	0.000	-0.143	-0.107	-0.066	0.000
	I					
30 DEG.	I	0.000	-0.095	-0.117	-0.082	0.000
	I					
60 DEG.	I	0.000	-0.052	-0.093	-0.056	0.000
	I					
90 DEG.	I	0.000	0.067	0.012	0.014	0.000
	I					
120 DEG.	I	0.000	0.087	0.067	0.044	0.000
	I					
150 DEG.	I	0.000	0.171	0.150	0.070	0.000
	I					
180 DEG.	I	0.000	0.193	0.158	0.057	0.000
	I					
210 DEG.	I	0.000	0.136	0.120	0.061	0.000
	I					
240 DEG.	I	0.000	0.102	0.110	0.093	0.000
	I					
270 DEG.	I	0.000	0.042	0.077	0.076	0.000
	I					
300 DEG.	I	0.000	-0.094	-0.028	0.009	0.000
	I					
330 DEG.	I	0.000	-0.122	-0.064	-0.031	0.000
	I					
(AVERAGE OF INITIAL CUT-OFF-STRAIGHTNESS)						
	I					
0-180 DEG.	I	0.000	-0.168	-0.133	-0.061	0.000
	I					
30-210 DEG.	I	0.000	-0.115	-0.118	-0.072	0.000
	I					
60-240 DEG.	I	0.000	-0.077	-0.101	-0.074	0.000
	I					
90-270 DEG.	I	0.000	0.013	-0.032	-0.031	0.000
	I					
120-300 DEG.	I	0.000	0.091	0.047	0.018	0.000
	I					
150-330 DEG.	I	0.000	0.146	0.107	0.050	0.000





# INITIAL OUT-OF STRAIGHTNESS

MODEL : H1  
 LENGTH(L) : 1400 MM  
 OUTSIDE DIA.: 50.90MM  
 THICKNESS : 2.04 MM  
 UNIT : MM

LOCATION	I	TOP				BOTTOM
	I	0.00L	0.25L	0.50L	0.75L	1.00L
0 DEG.	I	0.000	0.233	0.290	0.206	0.000
30 DEG.	I	0.000	0.061	0.020	-0.098	0.000
60 DEG.	I	0.000	-0.140	-0.243	-0.361	0.000
90 DEG.	I	0.000	-0.269	-0.403	-0.466	0.000
120 DEG.	I	0.000	-0.397	-0.557	-0.531	0.000
150 DEG.	I	0.000	-0.356	-0.519	-0.436	0.000
180 DEG.	I	0.000	-0.244	-0.298	-0.164	0.000
210 DEG.	I	0.000	-0.148	-0.109	0.004	0.000
240 DEG.	I	0.000	0.010	0.135	0.229	0.000
270 DEG.	I	0.000	0.185	0.343	0.434	0.000
300 DEG.	I	0.000	0.292	0.425	0.453	0.000
330 DEG.	I	0.000	0.308	0.410	0.388	0.000
(AVERAGE OF INITIAL OUT-OF-STRAIGHTNESS)						
0-180 DEG.	I	0.000	0.239	0.294	0.185	0.000
30-210 DEG.	I	0.000	0.105	0.064	-0.051	0.000
60-240 DEG.	I	0.000	-0.075	-0.189	-0.295	0.000
90-270 DEG.	I	0.000	-0.227	-0.373	-0.450	0.000
120-300 DEG.	I	0.000	-0.344	-0.491	-0.492	0.000
150-330 DEG.	I	0.000	-0.332	-0.464	-0.412	0.000



# INITIAL OUT-OF-STRAIGHTNESS

MODEL : H2  
 LENGTH(L) : 1400 MM  
 OUTSIDE DIA. : 50.92MM  
 THICKNESS : 2.02 MM  
 UNIT : MM

LOCATION	I	TOP				BOTTOM
		0.00L	0.25L	0.50L	0.75L	1.00L
0 DEG.	I	0.000	0.771	1.431	0.936	0.000
30 DEG.	I	0.000	1.325	2.544	1.606	0.000
60 DEG.	I	0.000	1.831	3.489	2.251	0.000
90 DEG.	I	0.000	1.751	3.337	2.145	0.000
120 DEG.	I	0.000	1.197	2.241	1.409	0.000
150 DEG.	I	0.000	0.327	0.569	0.347	0.000
180 DEG.	I	0.000	-0.915	-1.718	-1.099	0.000
210 DEG.	I	0.000	-1.620	-3.036	-1.997	0.000
240 DEG.	I	0.000	-1.845	-3.467	-2.249	0.000
270 DEG.	I	0.000	-1.863	-3.500	-2.314	0.000
300 DEG.	I	0.000	-1.282	-2.434	-1.610	0.000
330 DEG.	I	0.000	-0.511	-1.028	-0.659	0.000
(AVERAGE OF INITIAL OUT-OF-STRAIGHTNESS)						
0-180 DEG.	I	0.000	0.843	1.574	1.017	0.000
30-210 DEG.	I	0.000	1.473	2.790	1.802	0.000
60-240 DEG.	I	0.000	1.838	3.478	2.250	0.000
90-270 DEG.	I	0.000	1.807	3.418	2.229	0.000
120-300 DEG.	I	0.000	1.239	2.338	1.510	0.000
150-330 DEG.	I	0.000	0.419	0.798	0.503	0.000

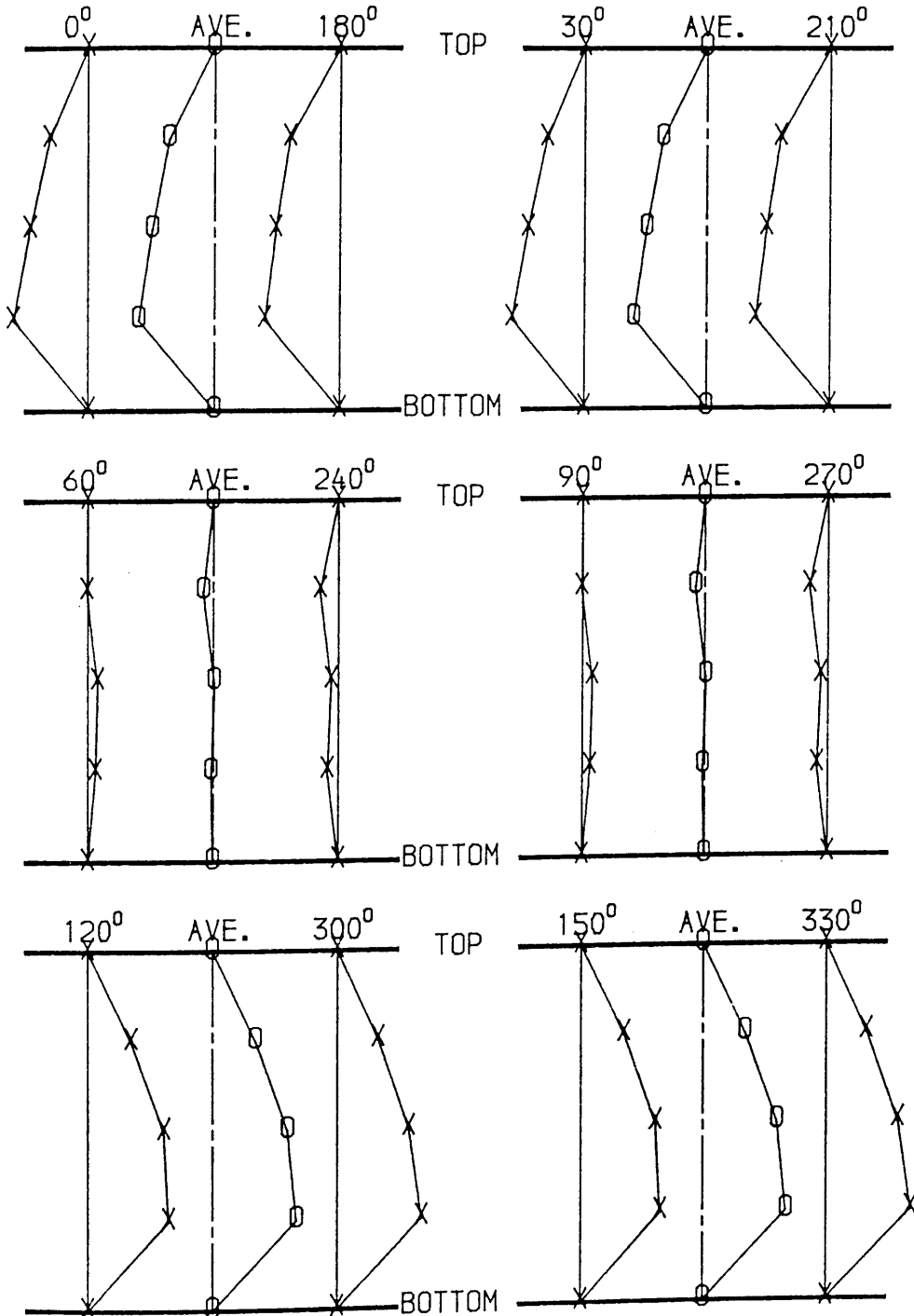
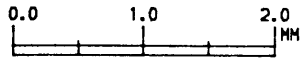
# INITIAL OUT-OF-STRAIGHTNESS

MODEL : H3  
 LENGTH(L) : 1000 MM  
 OUTSIDE DIA. : 50.94MM  
 THICKNESS : 2.03 MM  
 UNIT : MM

LOCATION	I	TOP				BOTTOM
	I	0.00L	0.25L	0.50L	0.75L	1.00L
0 DEG.	I	0.000	0.128	0.209	0.220	0.000
30 DEG.	I	0.000	0.147	0.189	0.184	0.000
60 DEG.	I	0.000	0.063	0.095	0.078	0.000
90 DEG.	I	0.000	0.045	0.032	0.015	0.000
120 DEG.	I	0.000	0.054	-0.020	-0.040	0.000
150 DEG.	I	0.000	0.044	-0.060	-0.109	0.000
180 DEG.	I	0.000	-0.022	-0.107	-0.158	0.000
210 DEG.	I	0.000	-0.005	-0.092	-0.112	0.000
240 DEG.	I	0.000	-0.034	-0.081	-0.063	0.000
270 DEG.	I	0.000	-0.049	0.017	0.037	0.000
300 DEG.	I	0.000	0.005	0.110	0.108	0.000
330 DEG.	I	0.000	0.076	0.186	0.185	0.000
(AVERAGE OF INITIAL OUT-OF-STRAIGHTNESS)						
0-180 DEG.	I	0.000	0.075	0.158	0.189	0.000
30-210 DEG.	I	0.000	0.076	0.141	0.148	0.000
60-240 DEG.	I	0.000	0.049	0.088	0.071	0.000
90-270 DEG.	I	0.000	0.047	0.007	-0.011	0.000
120-300 DEG.	I	0.000	0.025	-0.065	-0.074	0.000
150-330 DEG.	I	0.000	-0.016	-0.123	-0.147	0.000

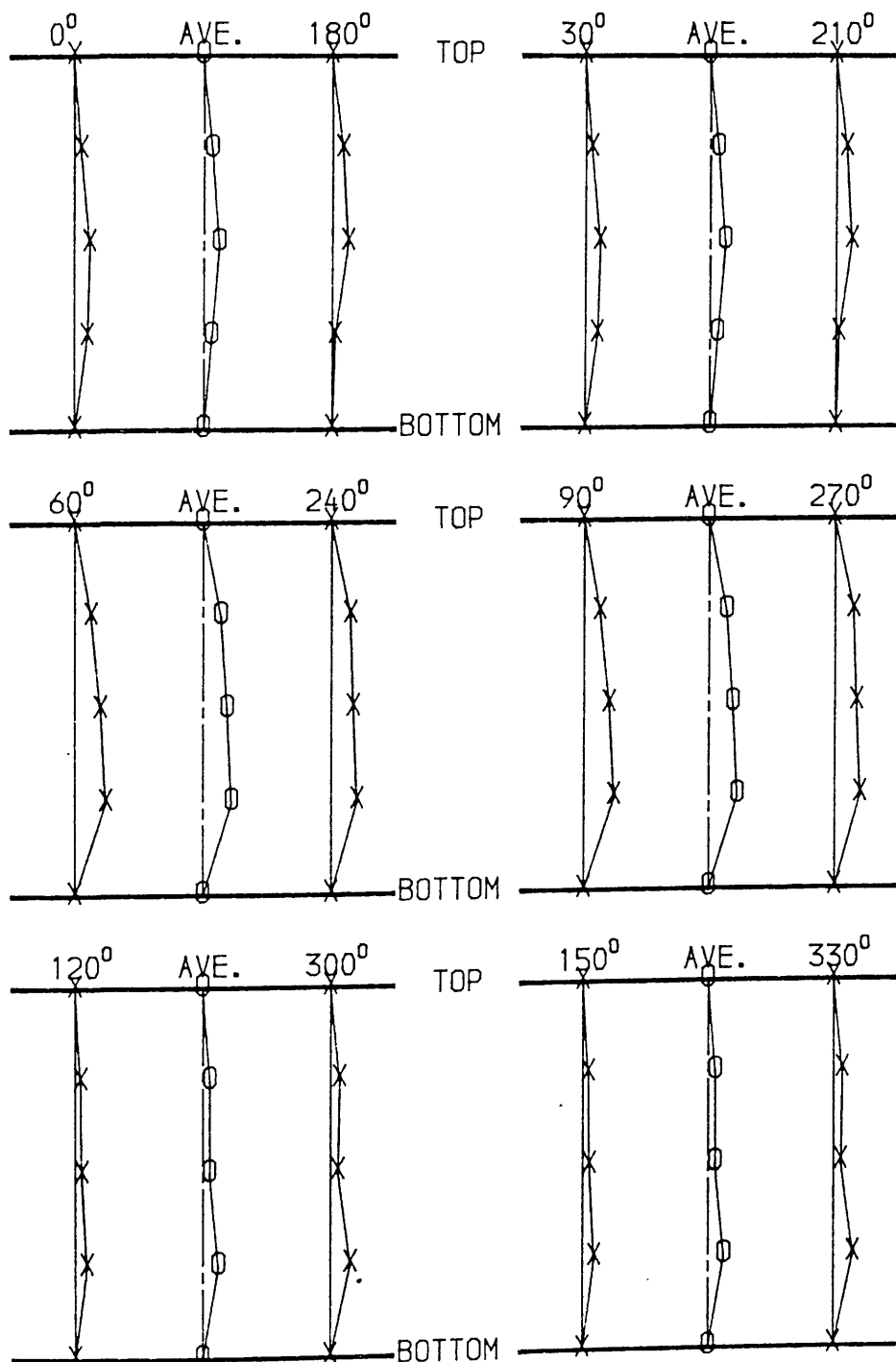
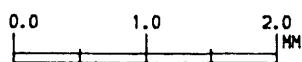
## INITIAL OUT-OF-STRAIGHTNESS

MODEL : A1  
 LENGTH (L) : 1400 MM  
 OUTSIDE DIA. : 50.89MM  
 THICKNESS : 1.20 MM



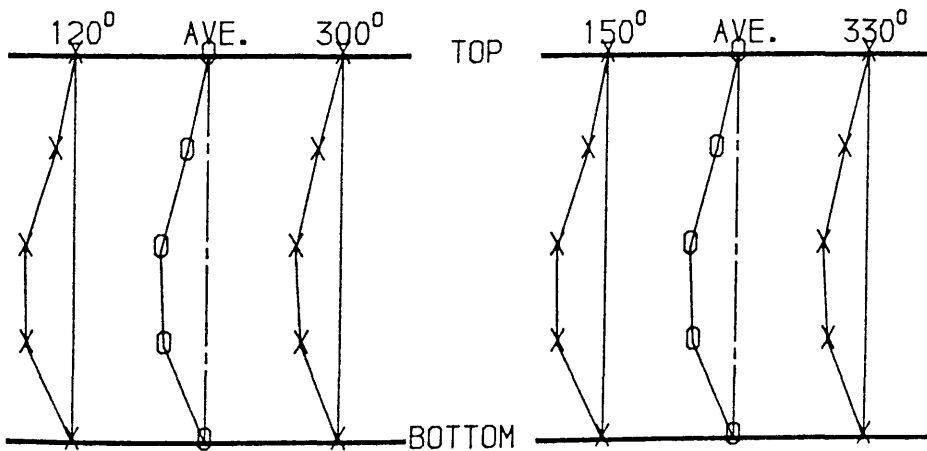
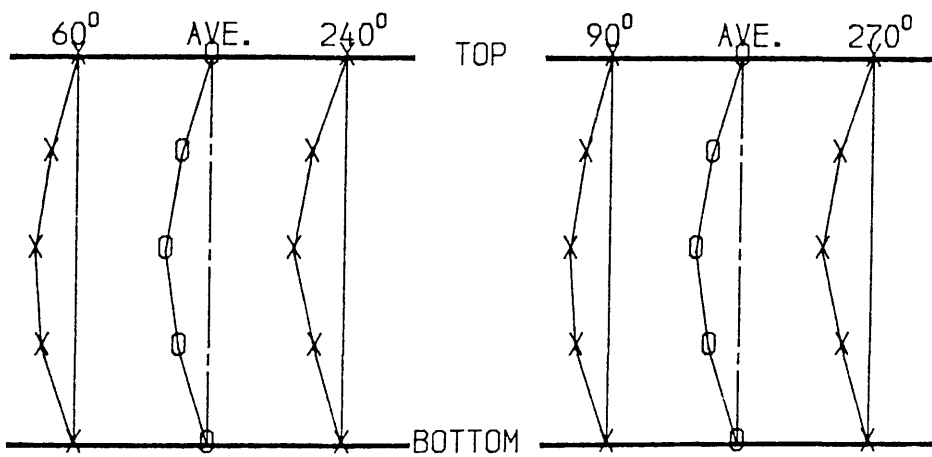
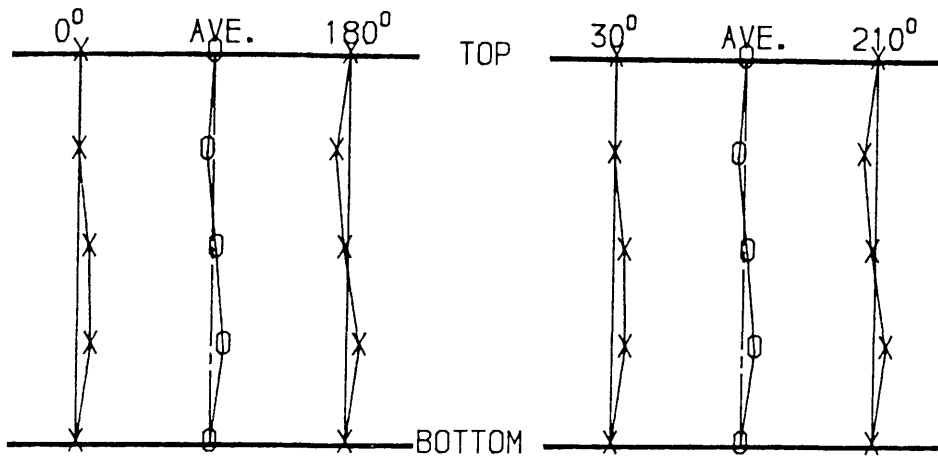
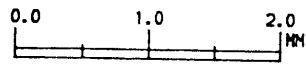
## INITIAL OUT-OF-STRAIGHTNESS

MODEL : A2  
 LENGTH (L) : 1000 MM  
 OUTSIDE DIA. : 50.91MM  
 THICKNESS : 1.20 MM



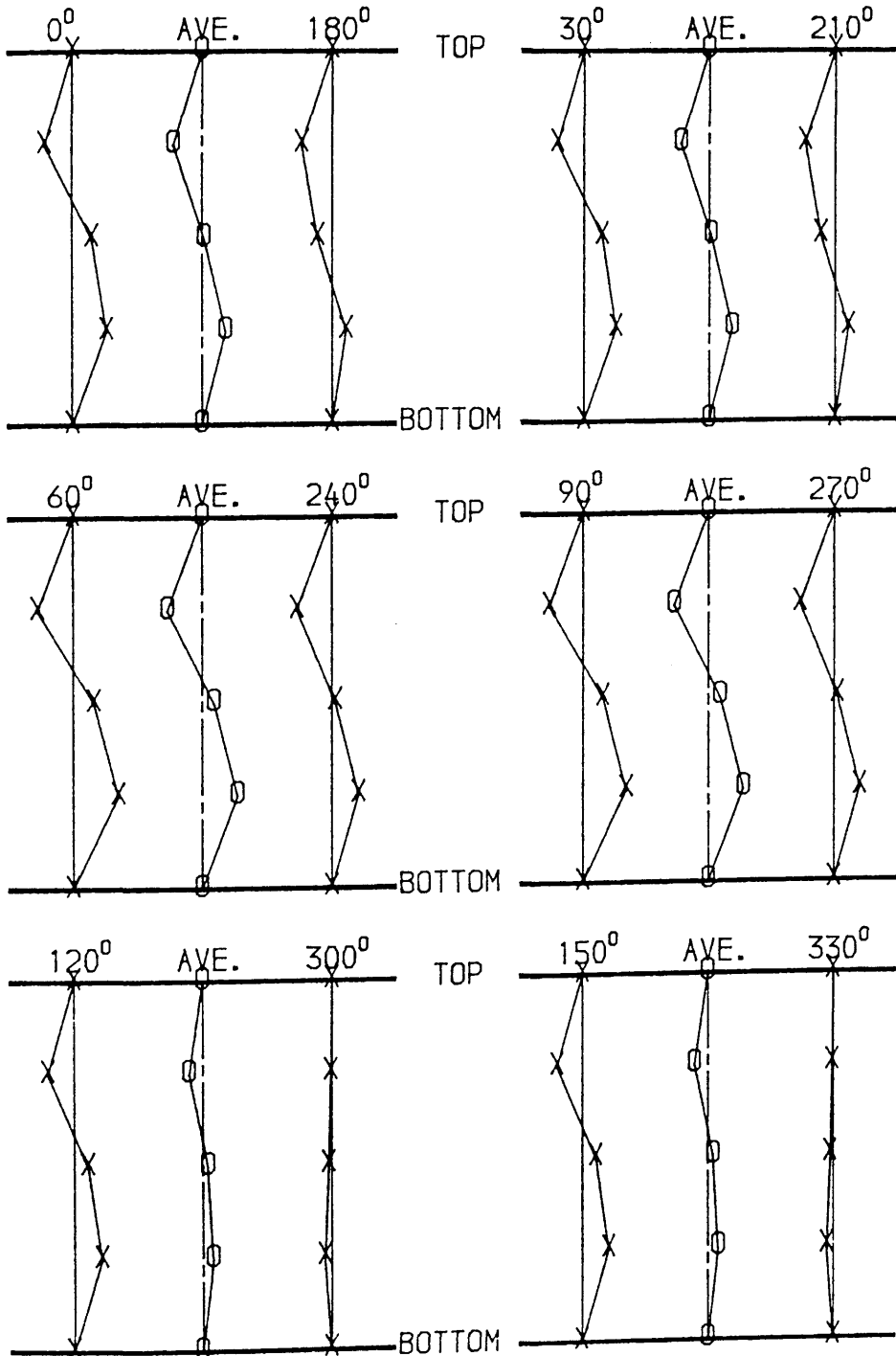
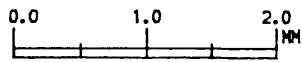
## INITIAL OUT-OF-STRAIGHTNESS

MODEL : A3  
 LENGTH (L) : 1400 MM  
 OUTSIDE DIA. : 50.8MM  
 THICKNESS : 1.20 MM



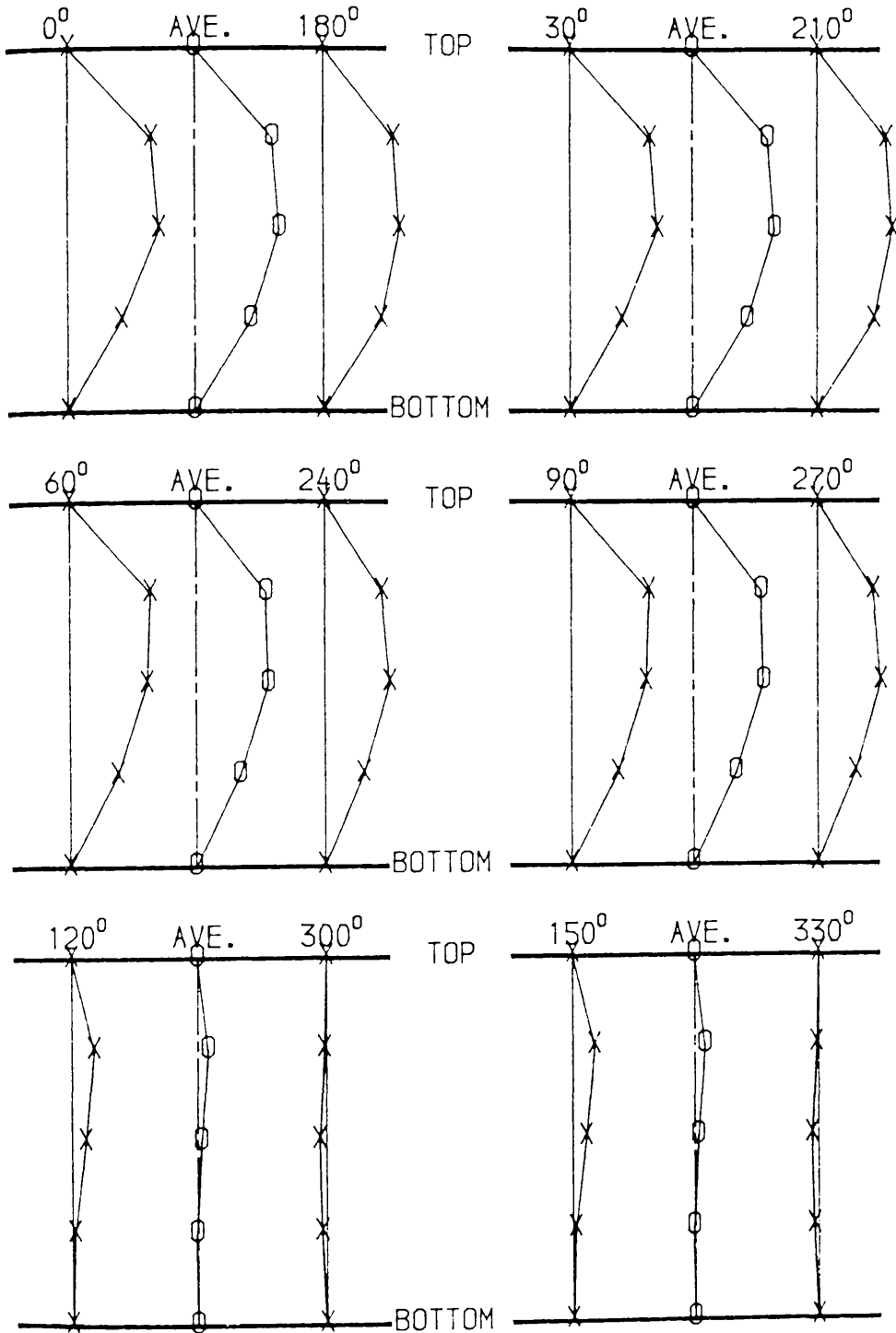
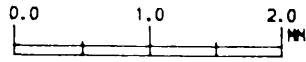
## INITIAL OUT-OF-STRAIGHTNESS

MODEL : A4  
 LENGTH (L) : 1400 MM  
 OUTSIDE DIA. : 50.89MM  
 THICKNESS : 1.20 MM



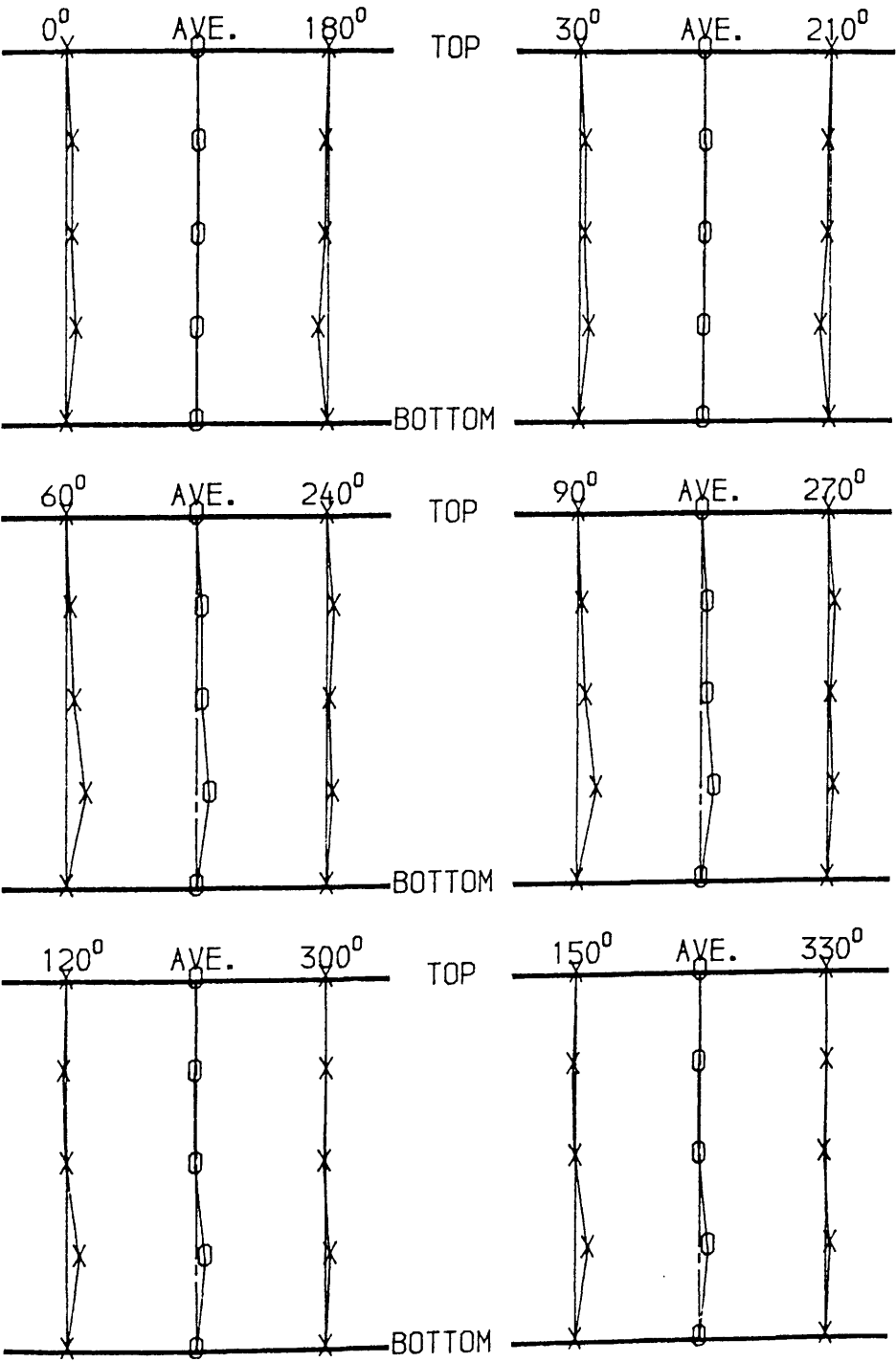
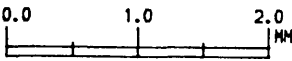
## INITIAL OUT-OF-STRAIGHTNESS

MODEL : B1  
 LENGTH (L) : 1400 MM  
 OUTSIDE DIA. : 50.86MM  
 THICKNESS : 1.20 MM



INITIAL OUT-OF-STRAIGHTNESS

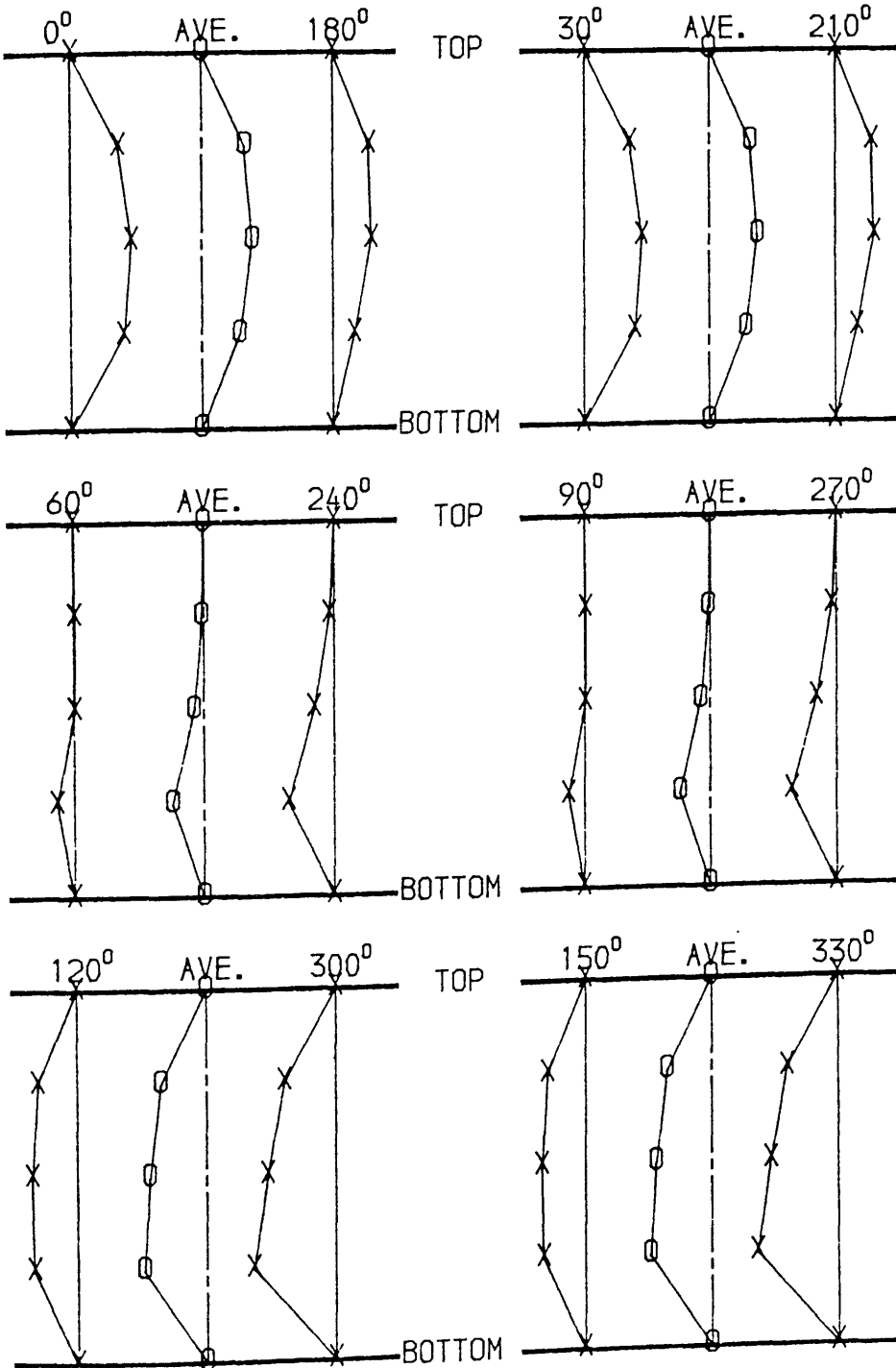
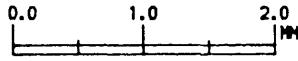
MODEL , B2  
LENGTH (L) , 902 MM  
OUTSIDE DIA. , 50.94MM  
THICKNESS , 1.20 MM





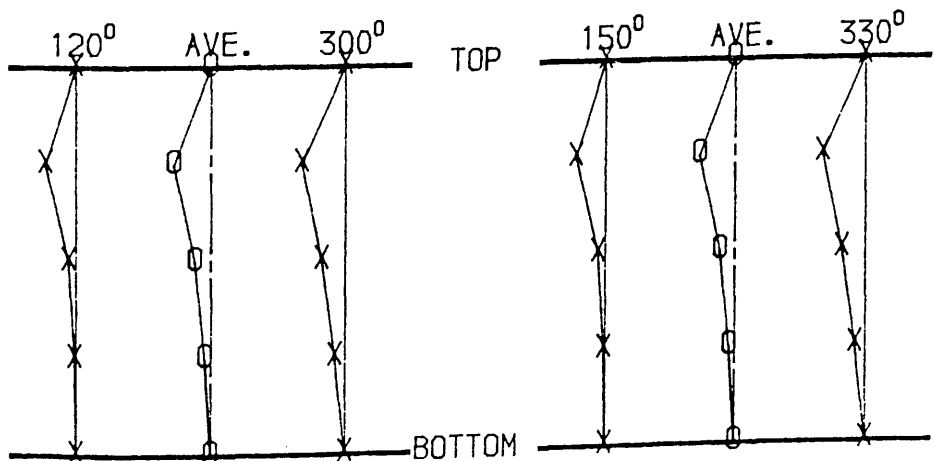
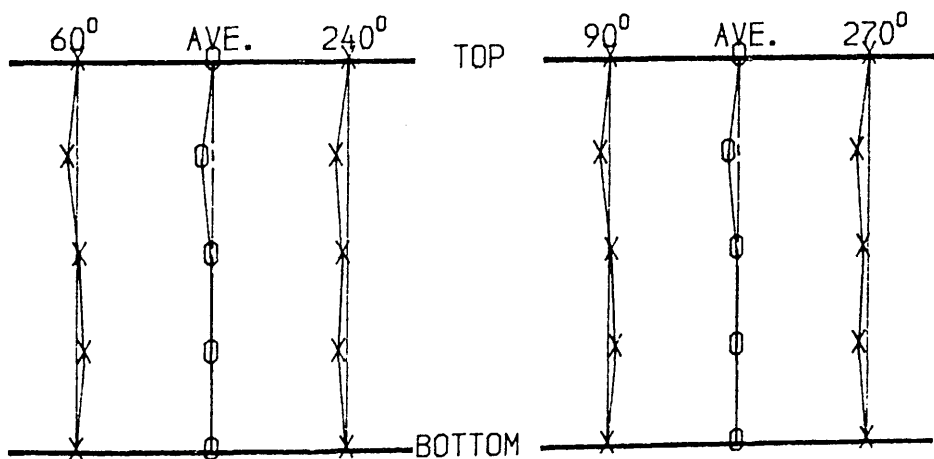
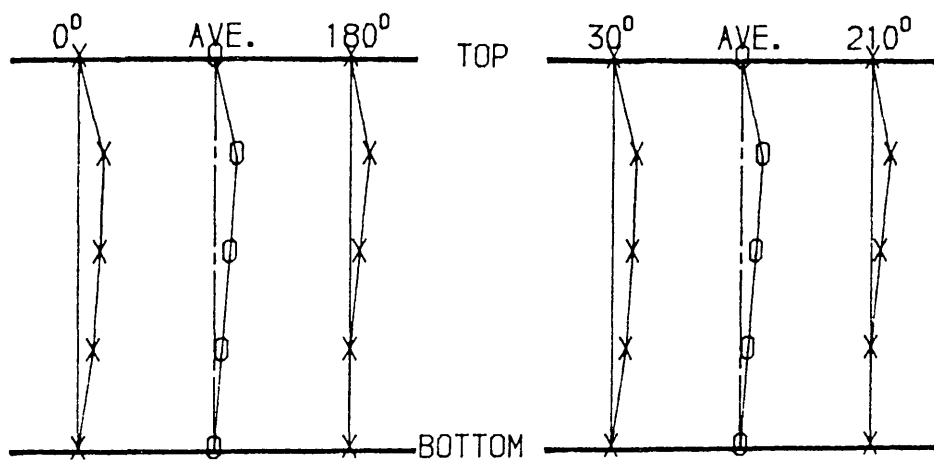
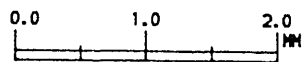
## INITIAL OUT-OF-STRAIGHTNESS

MODEL : B3  
 LENGTH (L) : 1000 MM  
 OUTSIDE DIA. : 50.92MM  
 THICKNESS : 1.20 MM



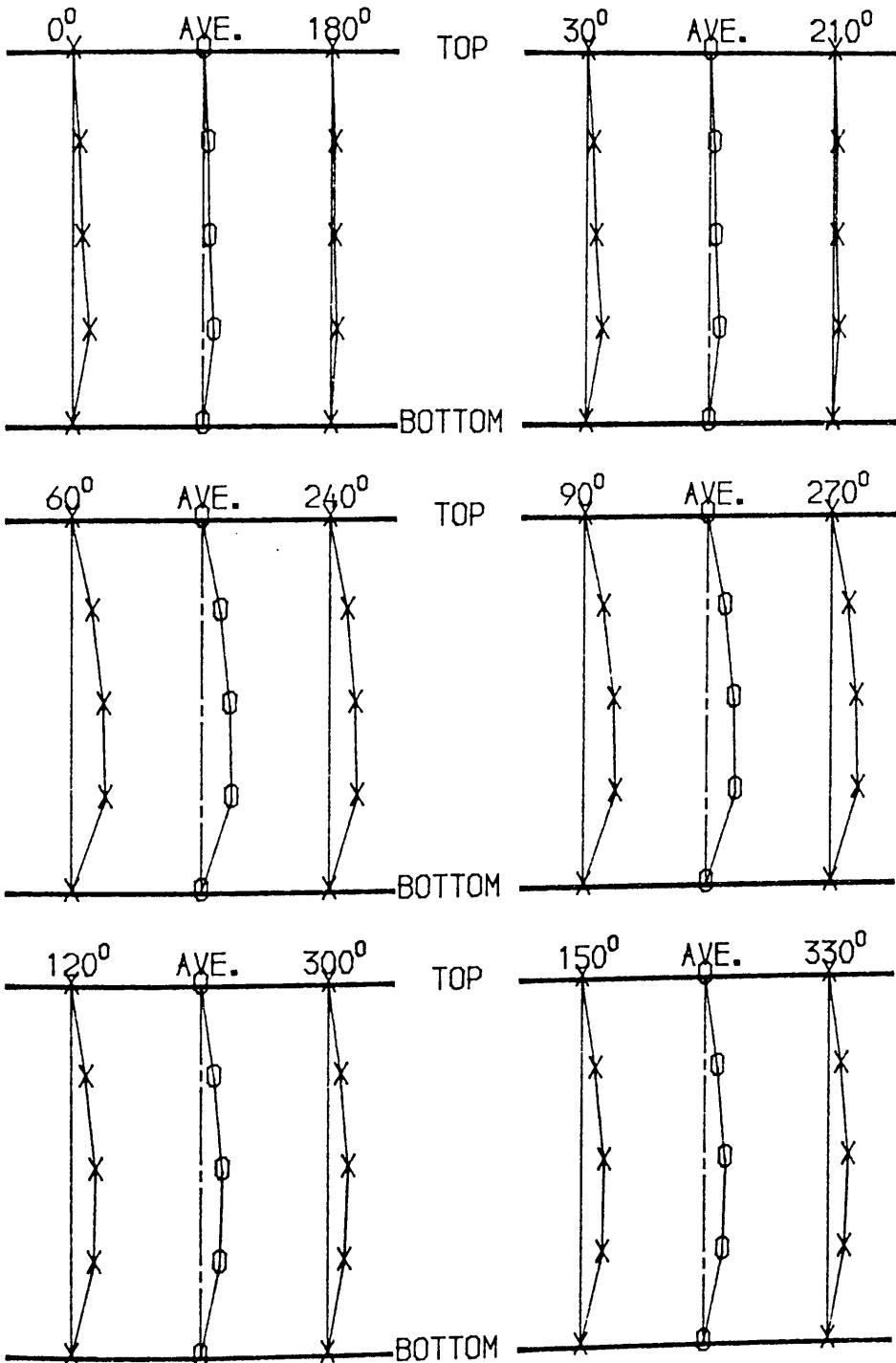
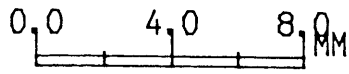
## INITIAL OUT-OF-STRAIGHTNESS

MODEL , B4  
 LENGTH (L) , 1400 MM  
 OUTSIDE DIA. , 50.86MM  
 THICKNESS , 1.20 MM



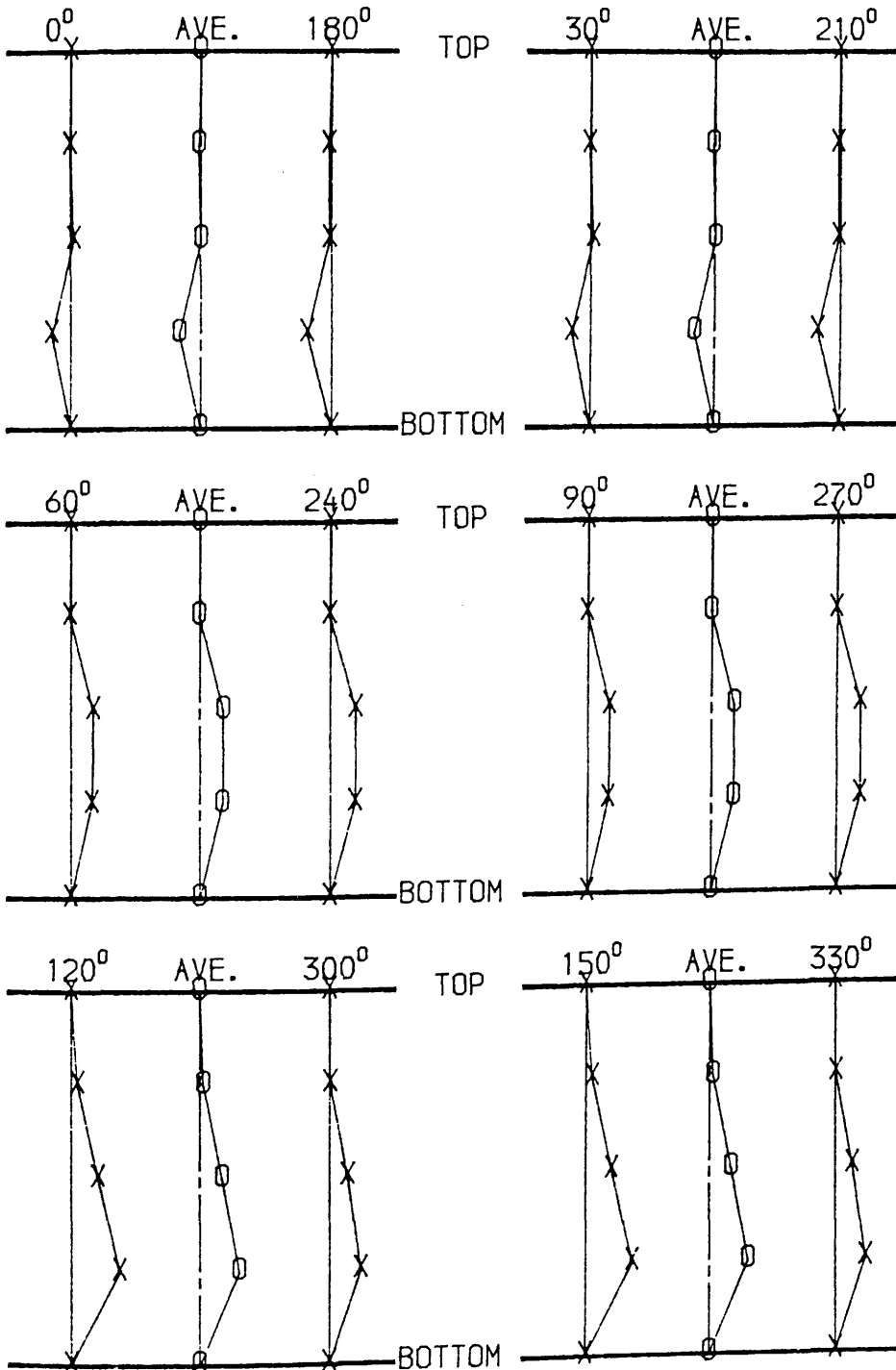
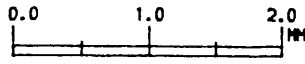
## INITIAL OUT-OF-STRAIGHTNESS

MODEL . C1  
 LENGTH (L) . 1000 MM  
 OUTSIDE DIA. . 50.97MM  
 THICKNESS . 1.21 MM



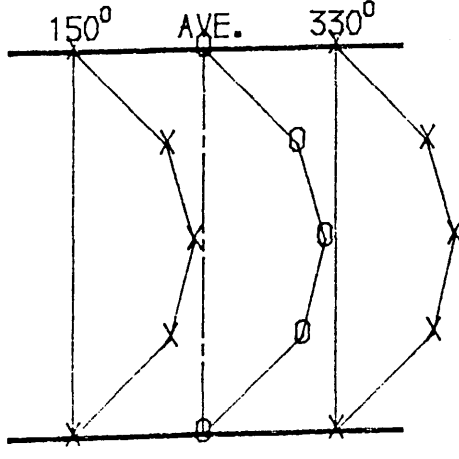
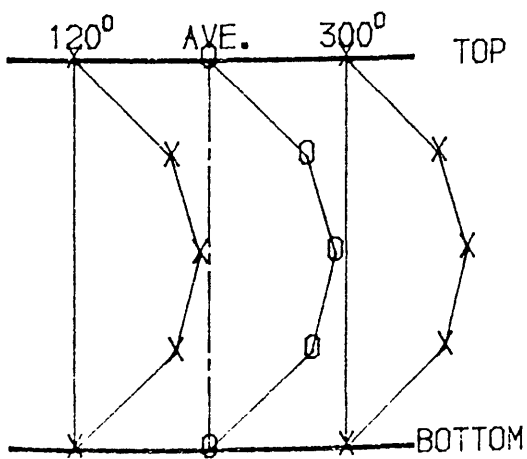
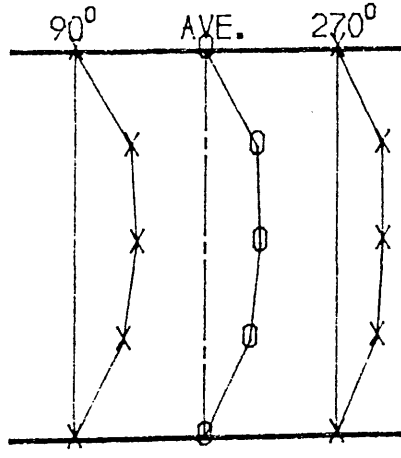
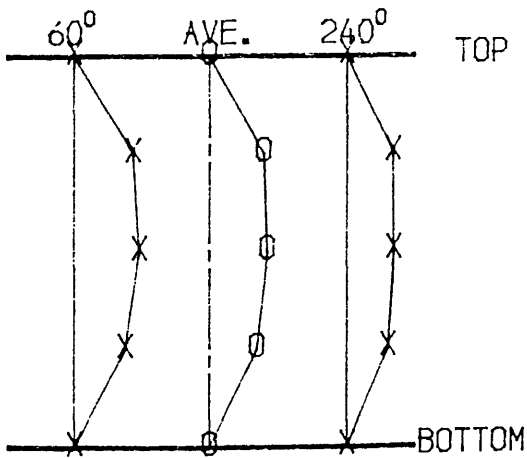
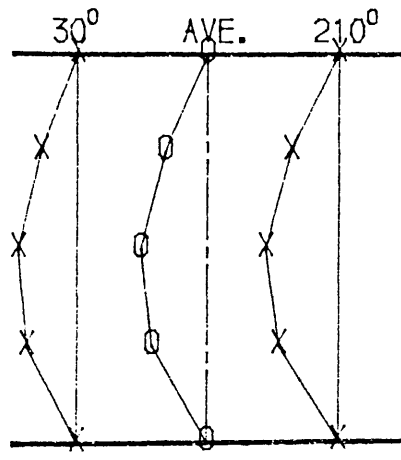
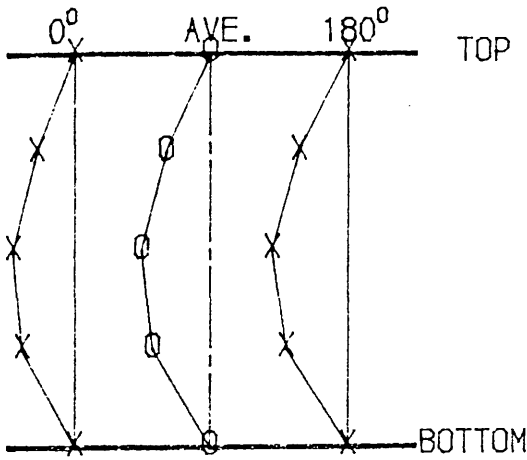
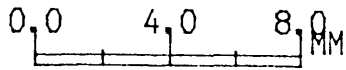
## INITIAL OUT-OF-STRAIGHTNESS

MODEL , C2  
 LENGTH (L) , 1000 MM  
 OUTSIDE DIA. , 50.91MM  
 THICKNESS , 1.22 MM



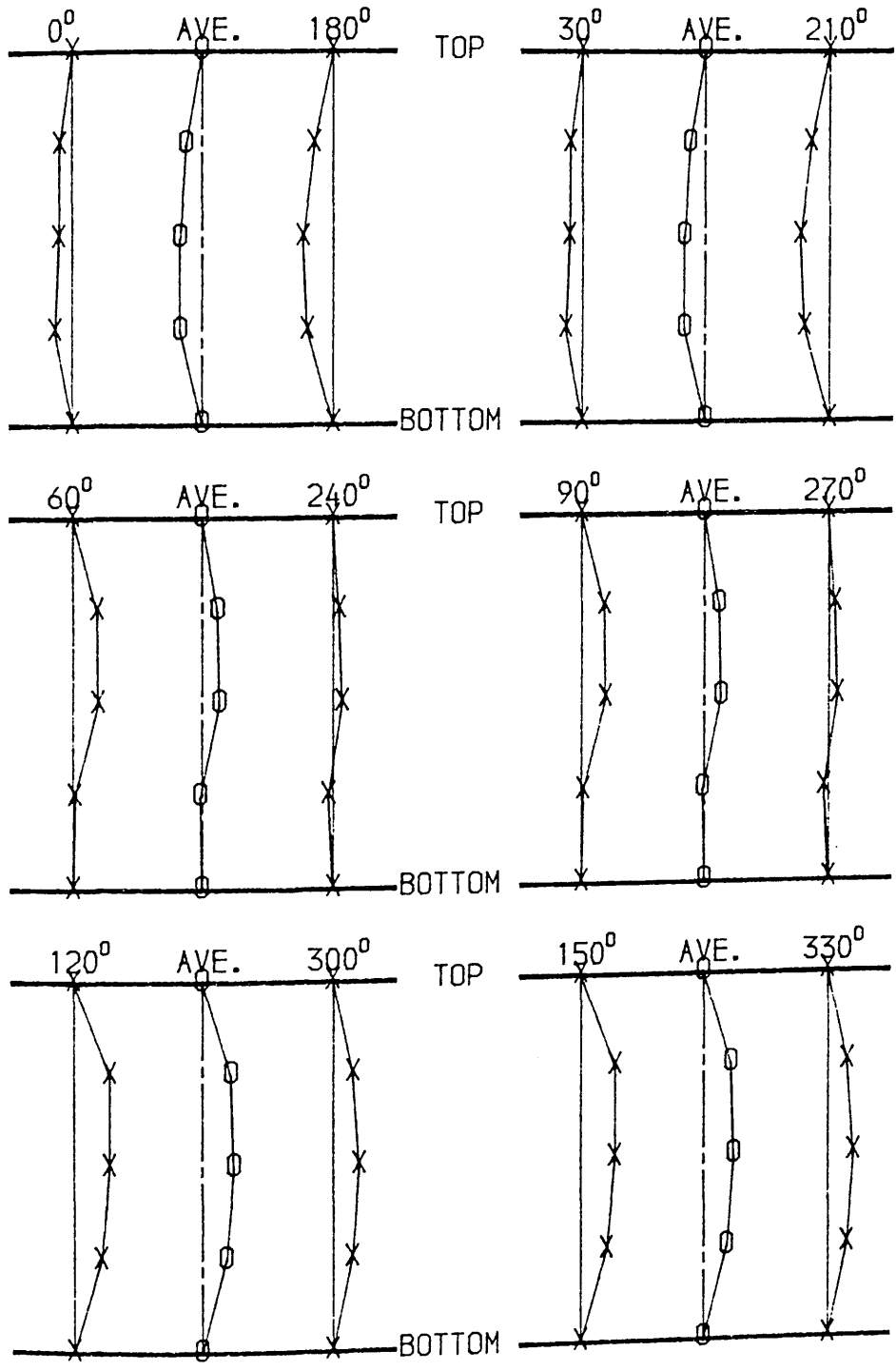
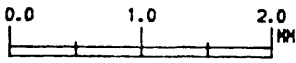
## INITIAL OUT-OF-STRAIGHTNESS

MODEL . C3  
 LENGTH (L) . 1400 MM  
 OUTSIDE DIA. . 50.86MM  
 THICKNESS . 1.22 MM



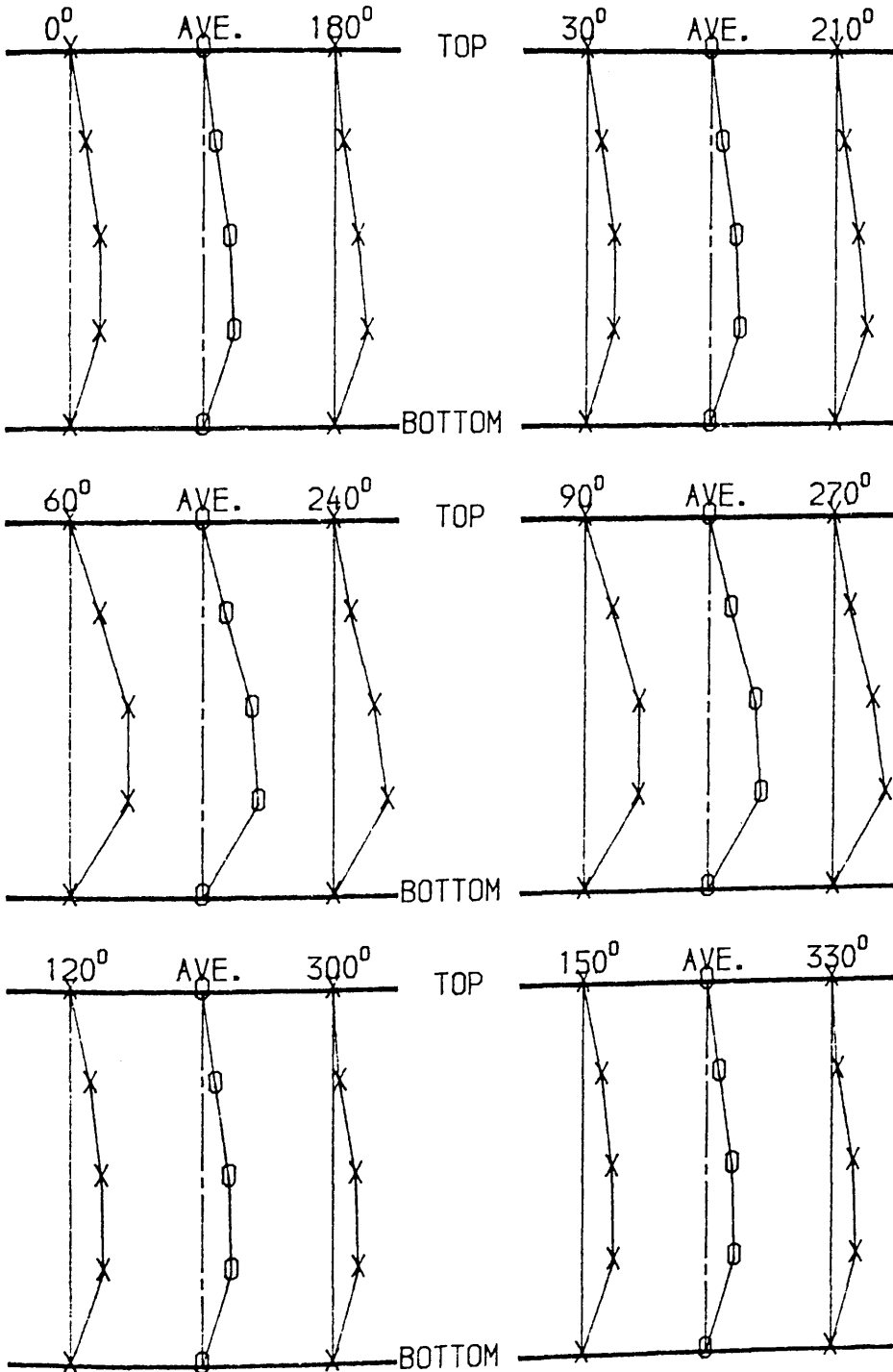
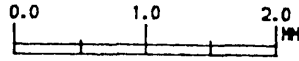
INITIAL OUT-OF-STRAIGHTNESS

MODEL , C4  
LENGTH (L) , 1400 MM  
OUTSIDE DIA. , 50.85MM  
THICKNESS , 1.22 MM



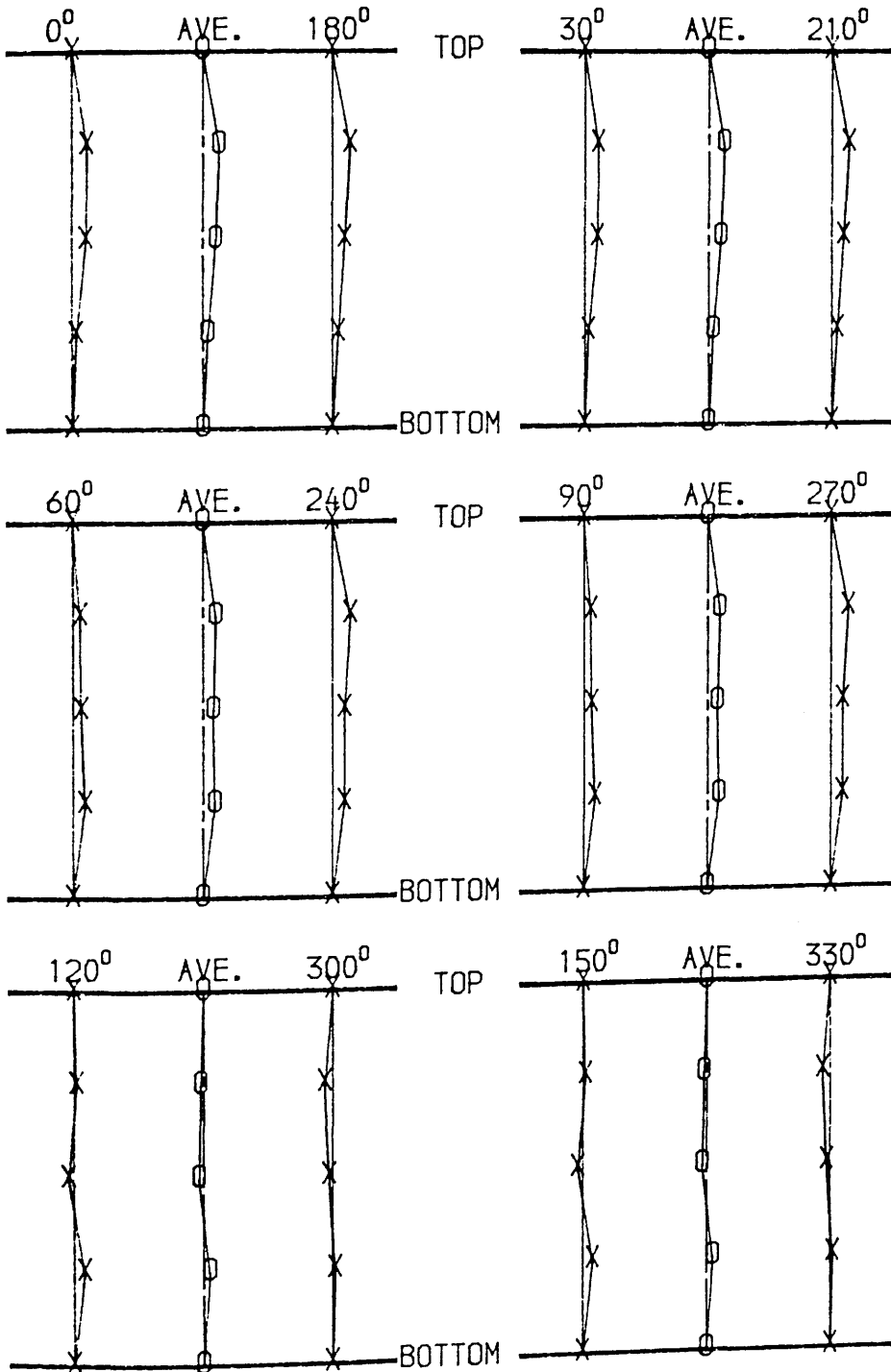
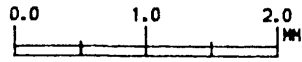
## INITIAL OUT-OF-STRAIGHTNESS

MODEL : D1  
 LENGTH (L) : 1400 MM  
 OUTSIDE DIA. : 50.91MM  
 THICKNESS : 1.20 MM



## INITIAL OUT-OF-STRAIGHTNESS

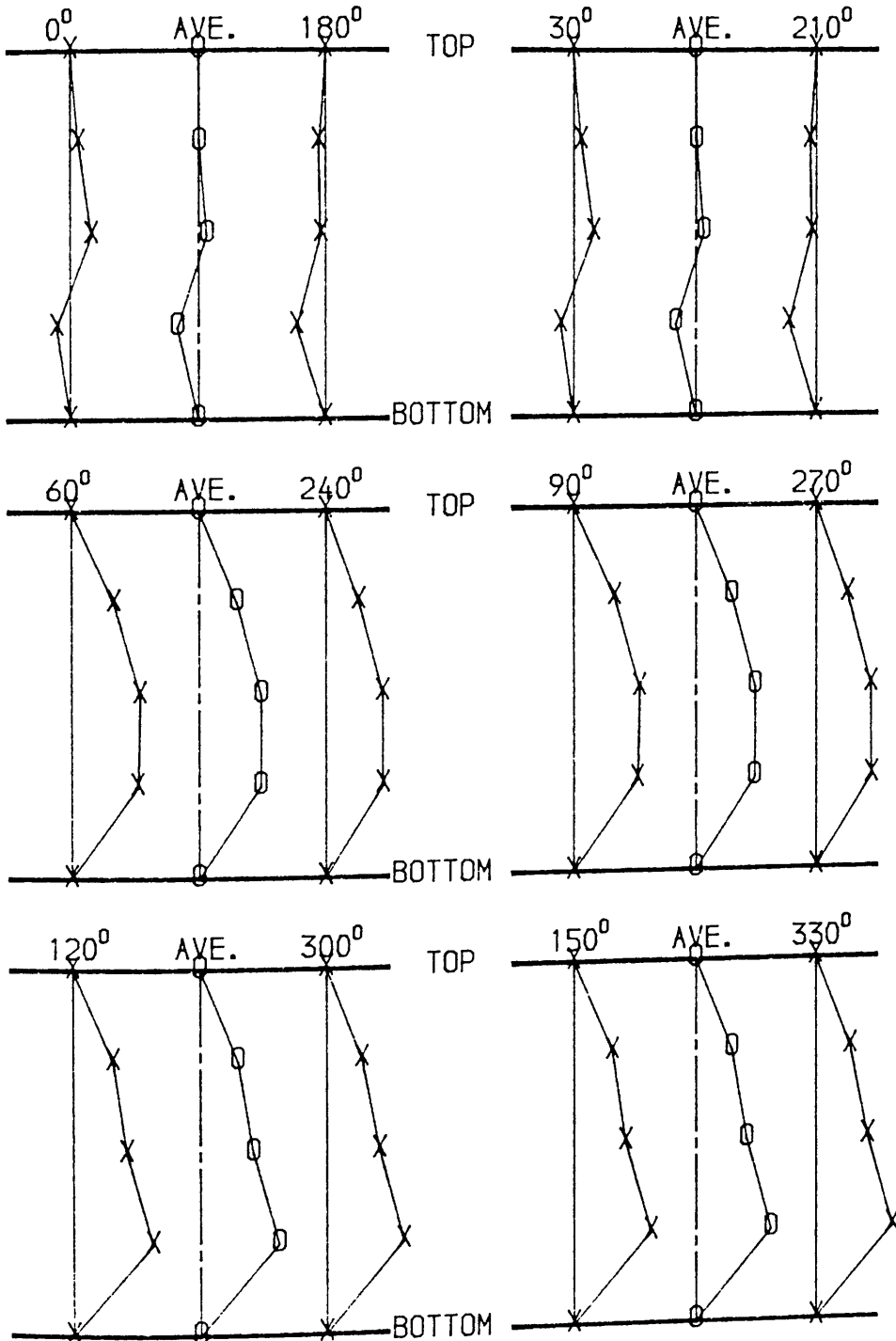
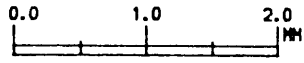
MODEL : D2  
 LENGTH (L) : 1000 MM  
 OUTSIDE DIA. : 50.98MM  
 THICKNESS : 1.21 MM





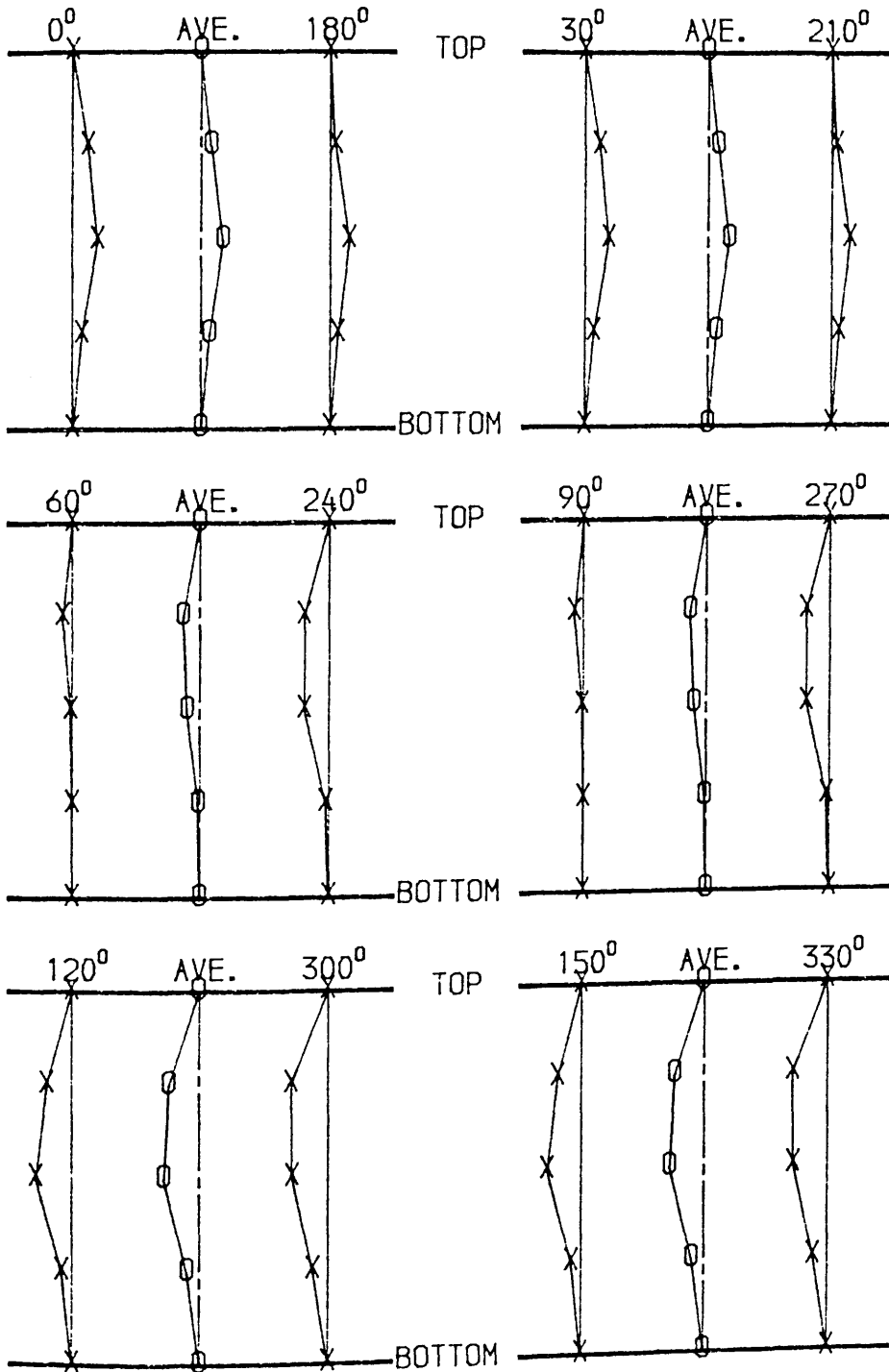
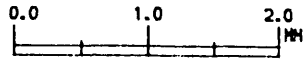
## INITIAL OUT-OF-STRAIGHTNESS

MODEL : D3  
 LENGTH (L) : 1400 MM  
 OUTSIDE DIA. : 50.91MM  
 THICKNESS : 1.21 MM



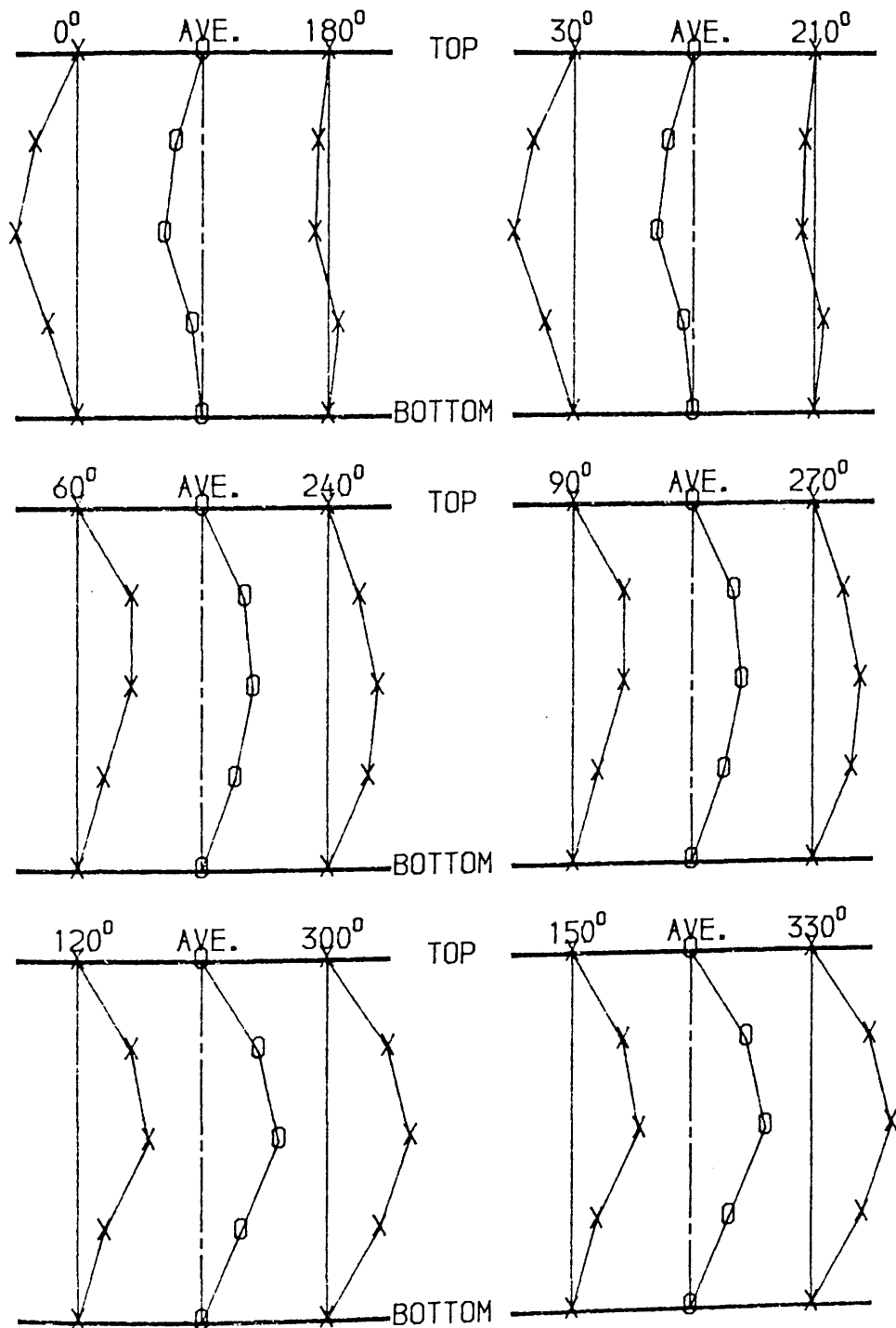
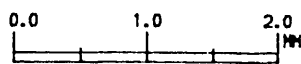
## INITIAL OUT-OF-STRAIGHTNESS

MODEL : D4  
 LENGTH (L) : 1400 MM  
 OUTSIDE DIA. : 50.90MM  
 THICKNESS : 1.21 MM



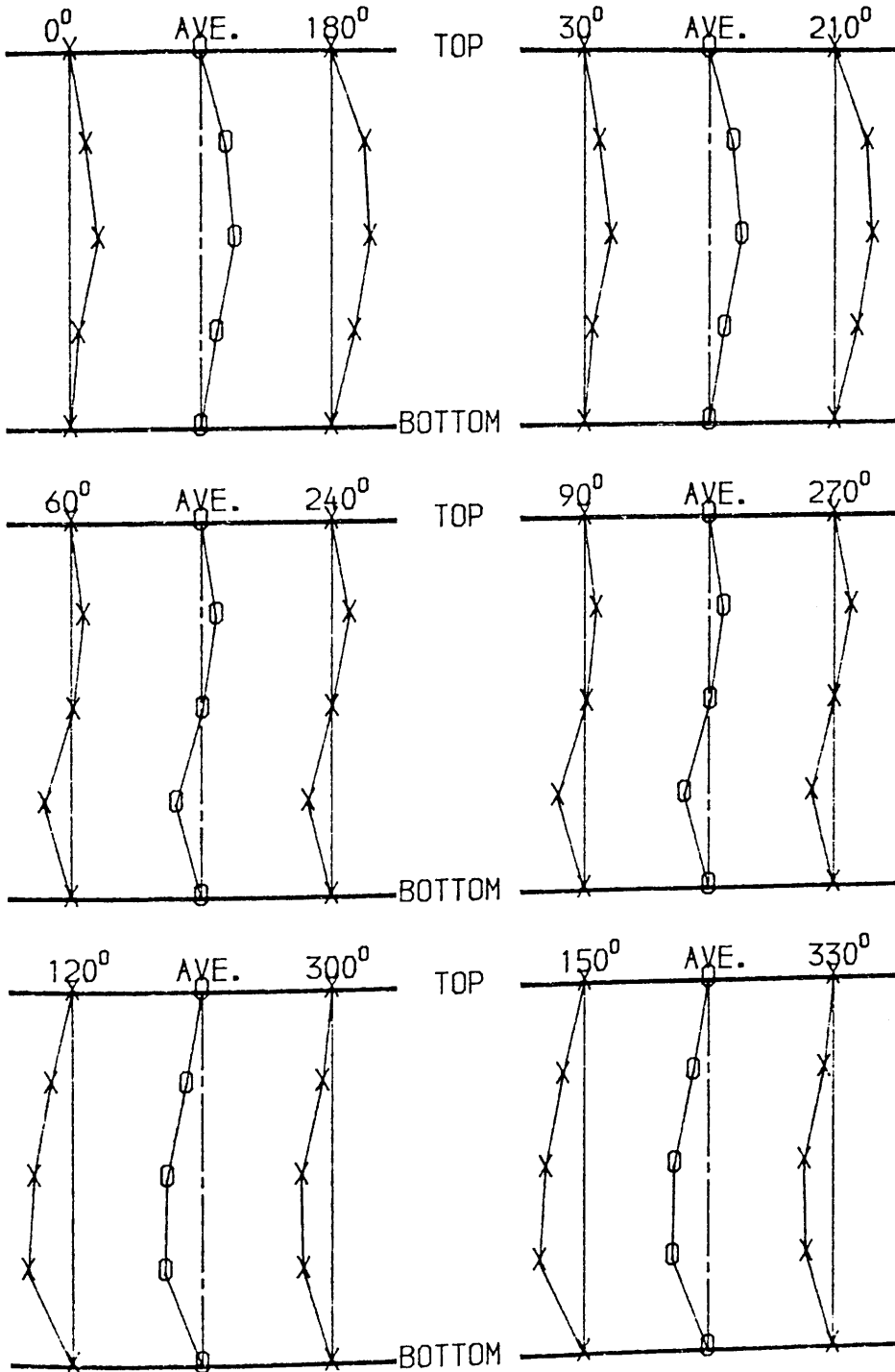
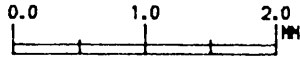
## INITIAL OUT-OF-STRAIGHTNESS

MODEL : E1  
 LENGTH (L) : 1400 MM  
 OUTSIDE DIA. : 50.92MM  
 THICKNESS : 2.05 MM



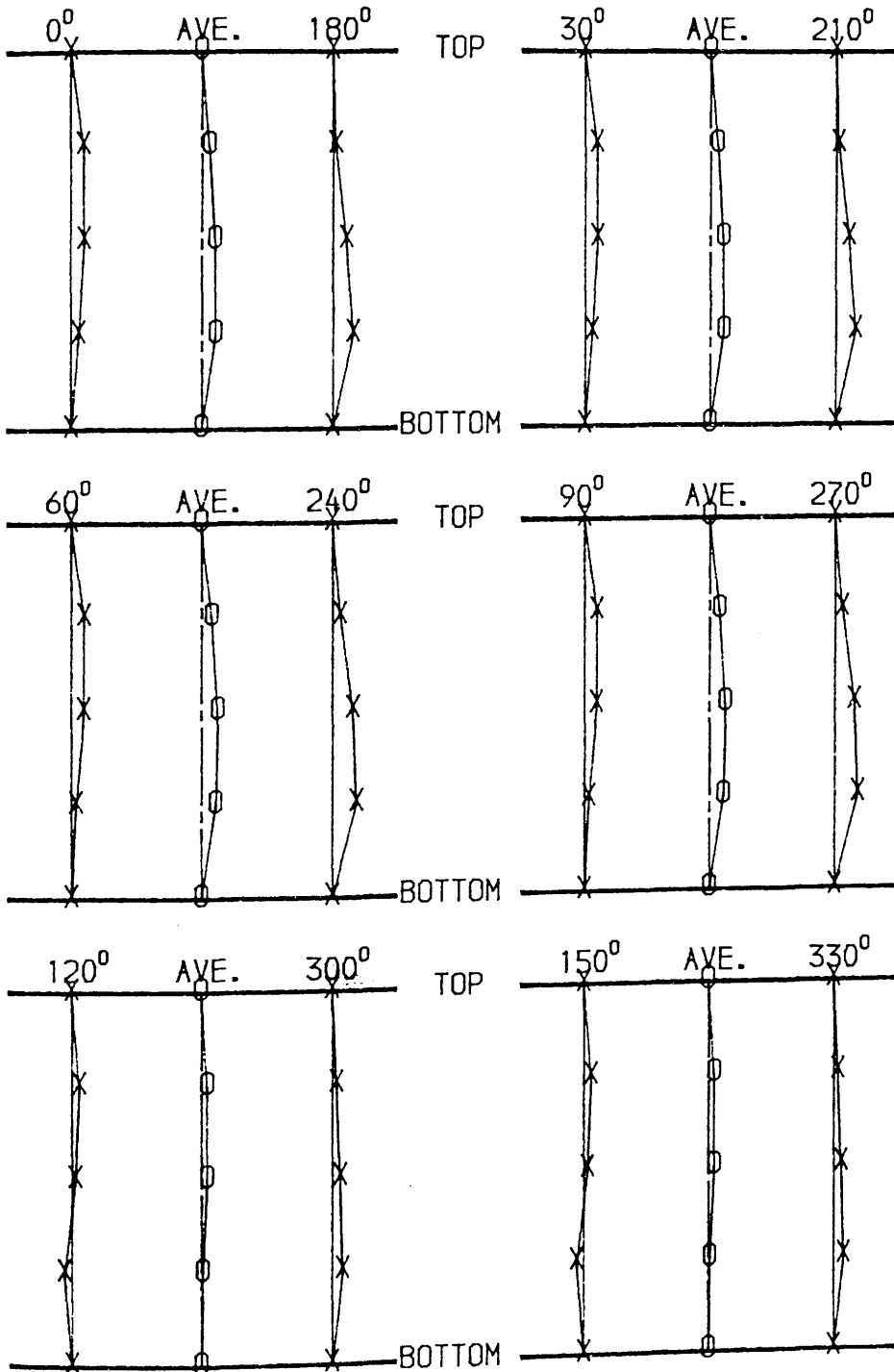
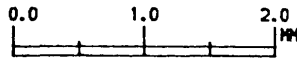
## INITIAL OUT-OF-STRAIGHTNESS

MODEL . E2  
 LENGTH (L) . 1000 MM  
 OUTSIDE DIA. . 50.92MM  
 THICKNESS . 2.04 MM



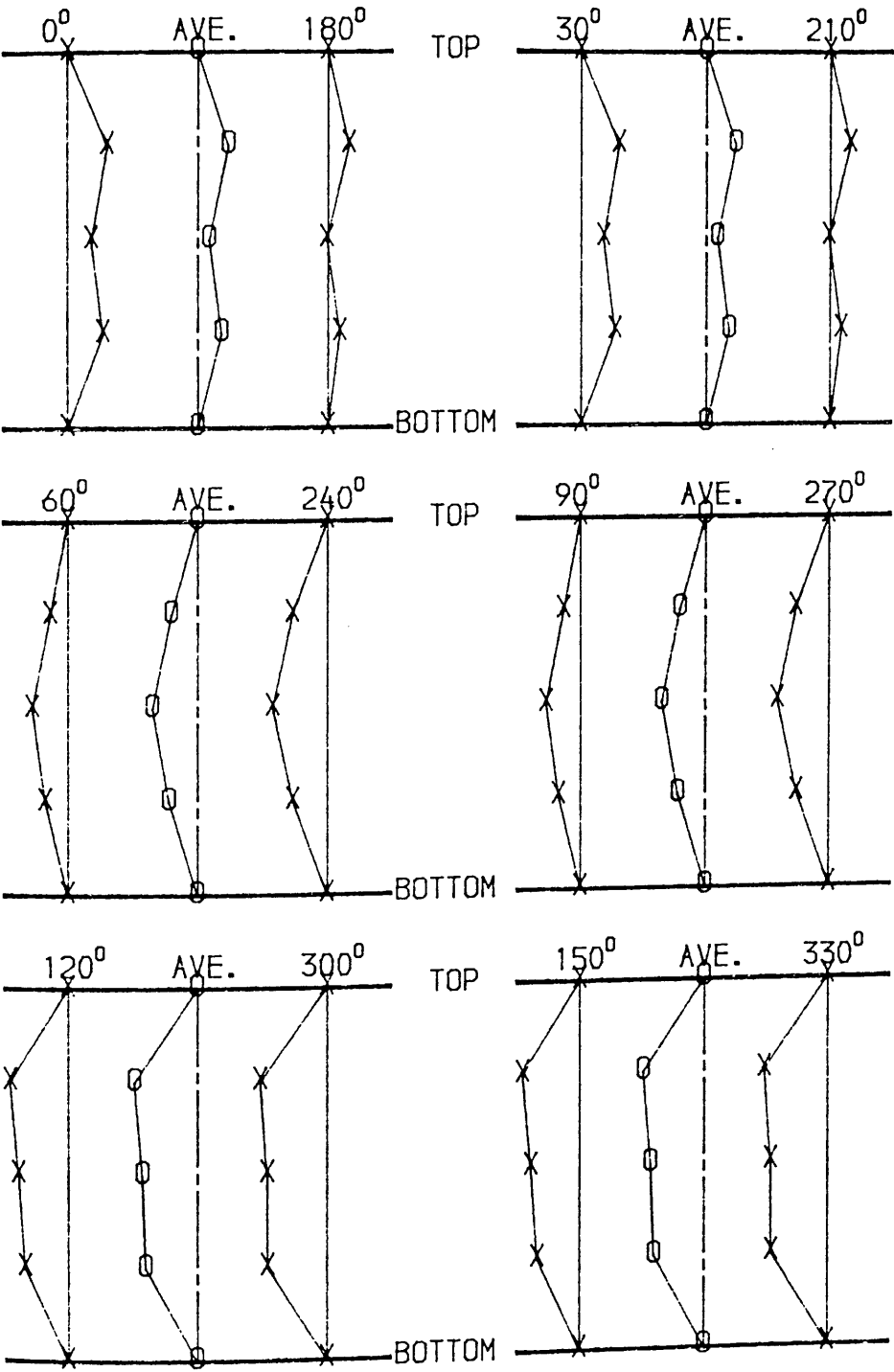
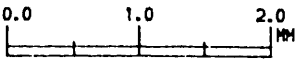
## INITIAL OUT-OF-STRAIGHTNESS

MODEL , E3  
 LENGTH (L) : 1400 MM  
 OUTSIDE DIA. : 50.91MM  
 THICKNESS : 2.05 MM



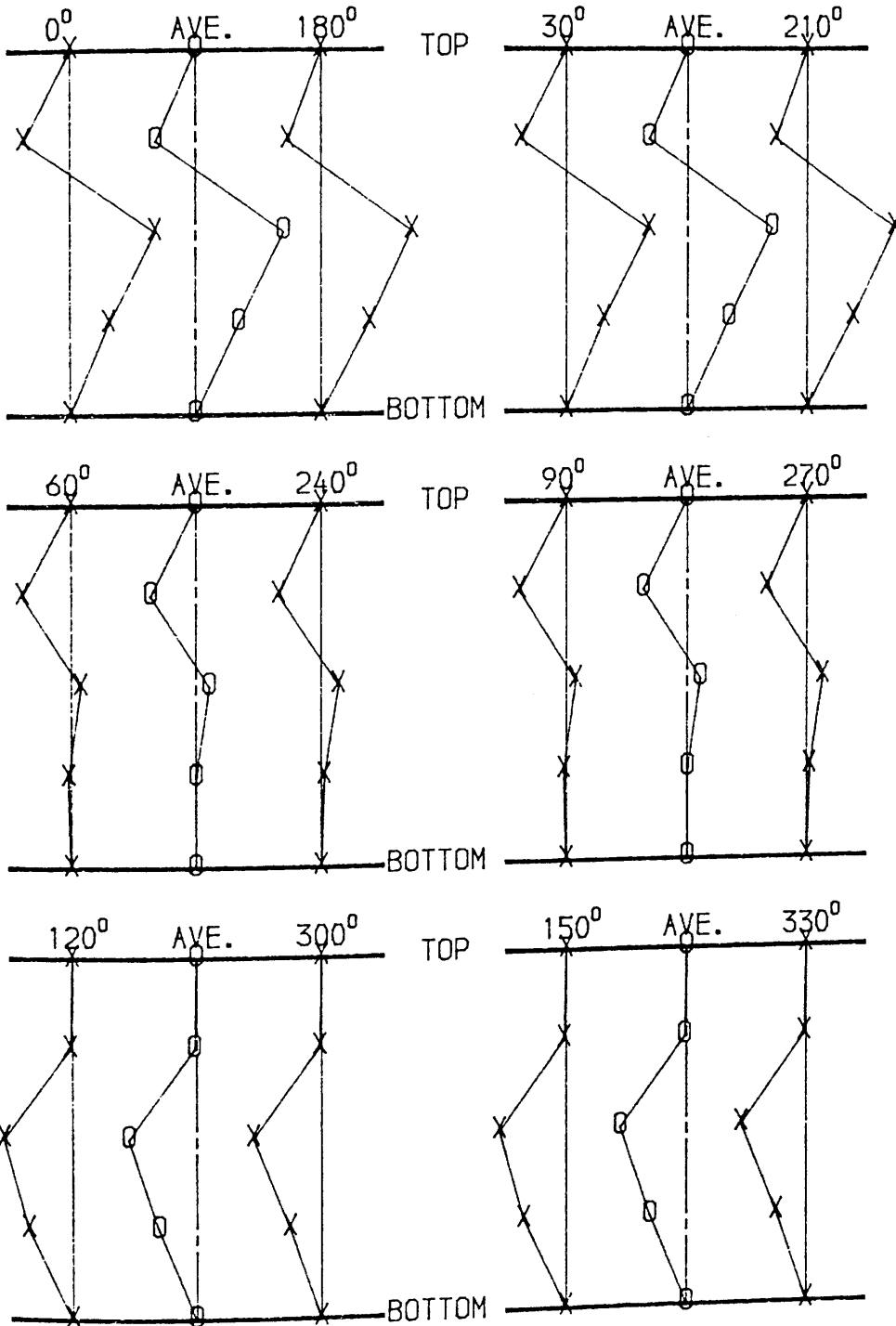
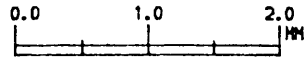
INITIAL OUT-OF-STRAIGHTNESS

MODEL , F1  
LENGTH (L) , 1400 MM  
OUTSIDE DIA. , 50.91MM  
THICKNESS , 2.03 MM



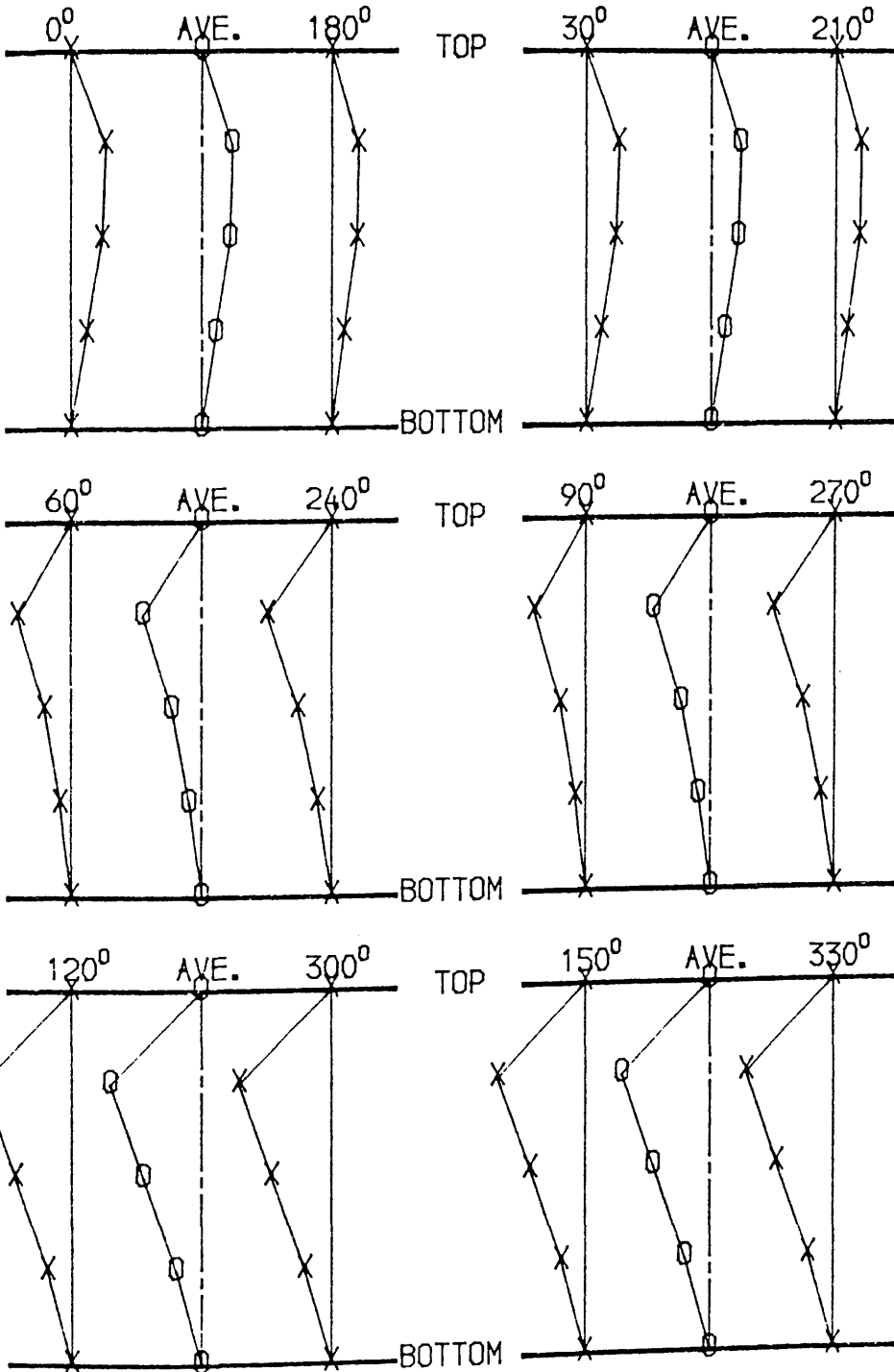
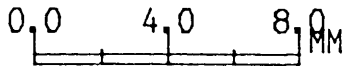
## INITIAL OUT-OF-STRAIGHTNESS

MODEL : F2  
 LENGTH (L) : 1000 MM  
 OUTSIDE DIA. : 50.90MM  
 THICKNESS : 2.03 MM



## INITIAL OUT-OF-STRAIGHTNESS

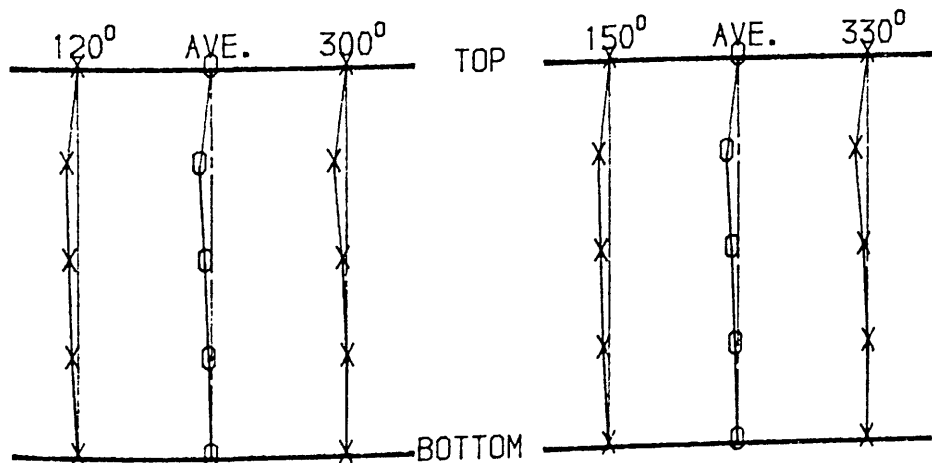
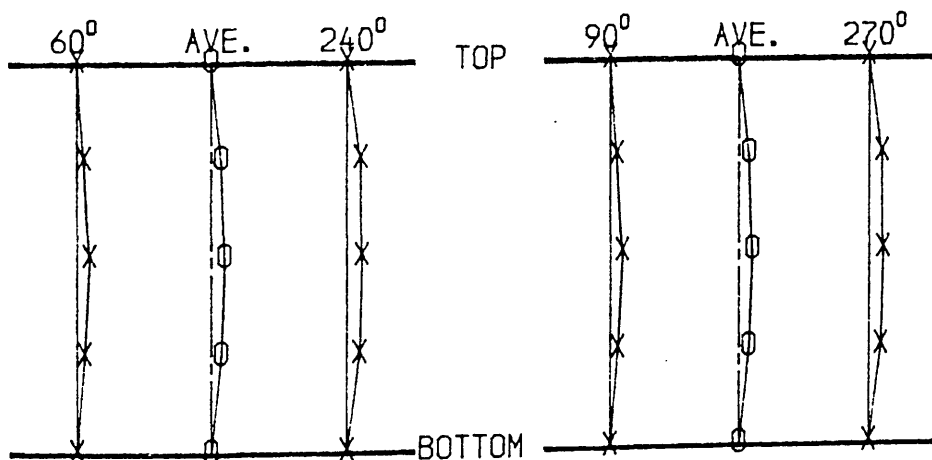
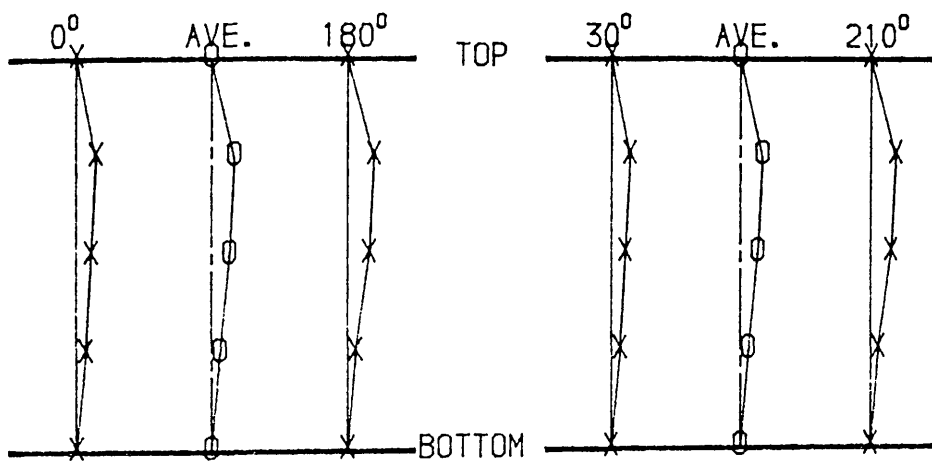
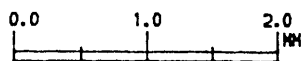
MODEL : F3  
 LENGTH (L) : 1800 MM  
 OUTSIDE DIA. : 50.86MM  
 THICKNESS : 2.02 MM





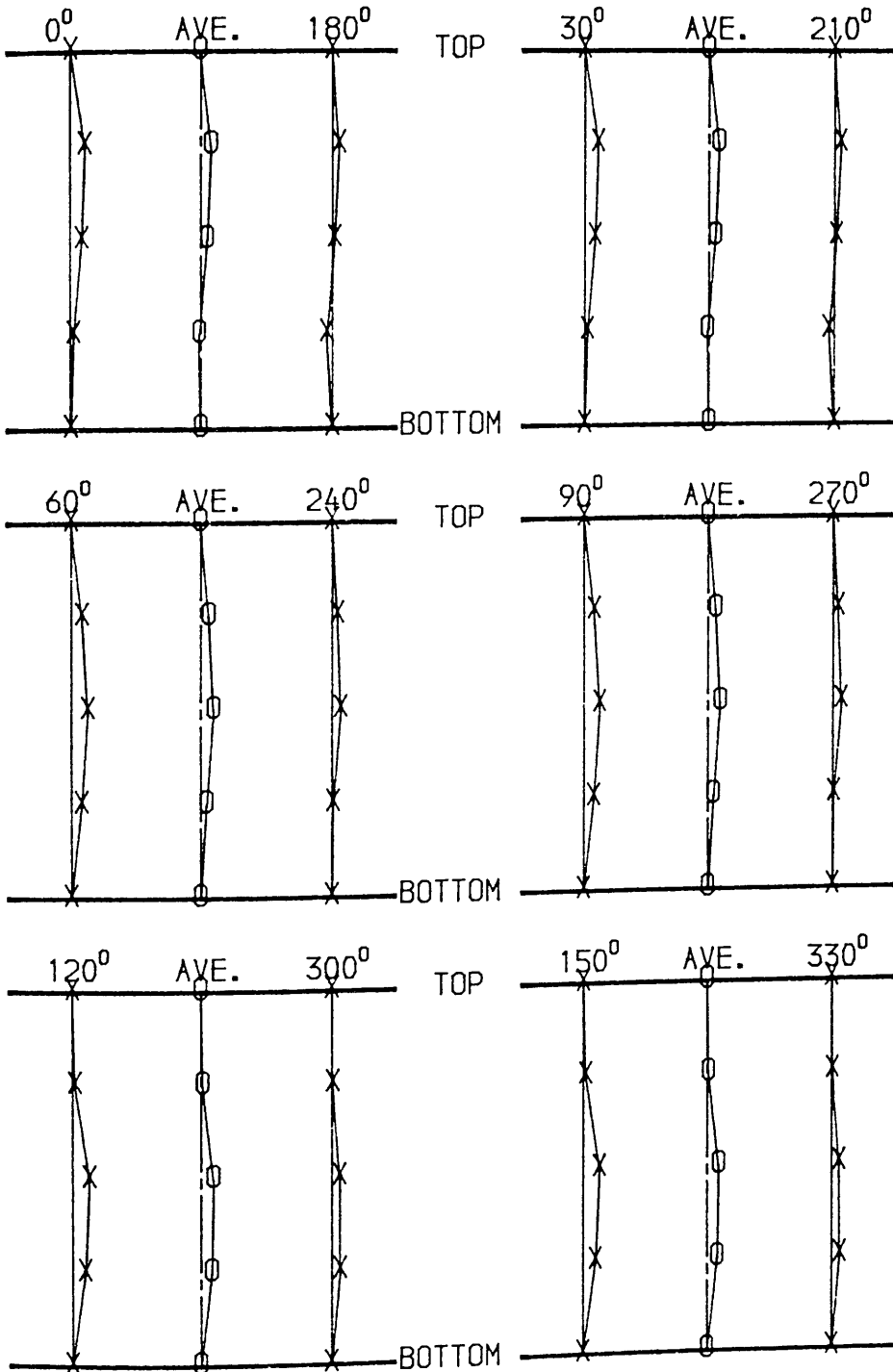
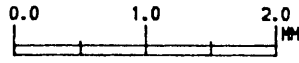
## INITIAL OUT-OF-STRAIGHTNESS

MODEL . G1  
 LENGTH (L) . 1000 MM  
 OUTSIDE DIA. . 50.95MM  
 THICKNESS . 2.04 MM



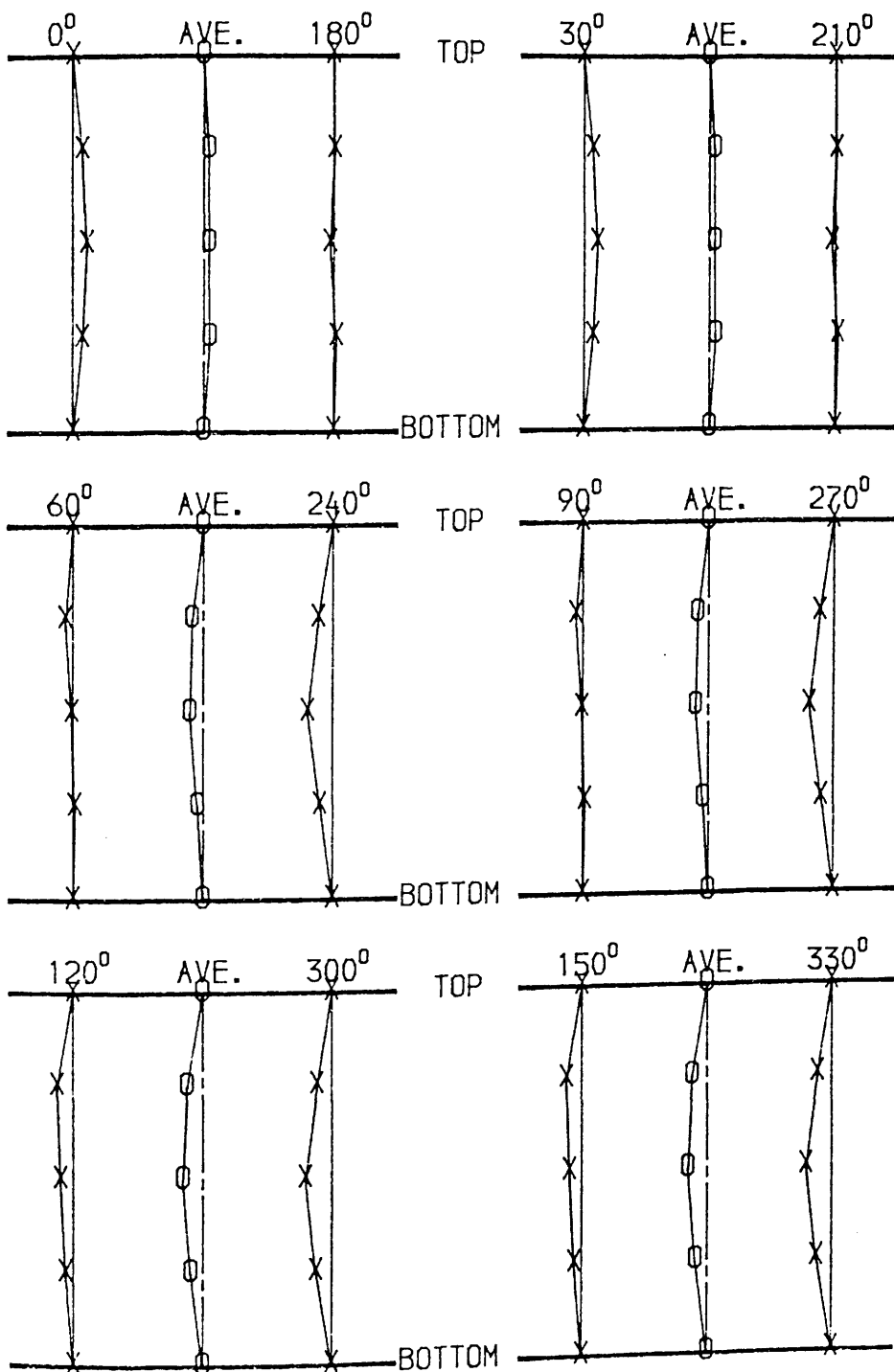
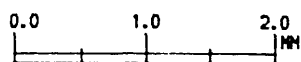
## INITIAL OUT-OF-STRAIGHTNESS

MODEL , G2  
 LENGTH (L) , 1400 MM  
 OUTSIDE DIA. , 50.92MM  
 THICKNESS , 2.05 MM



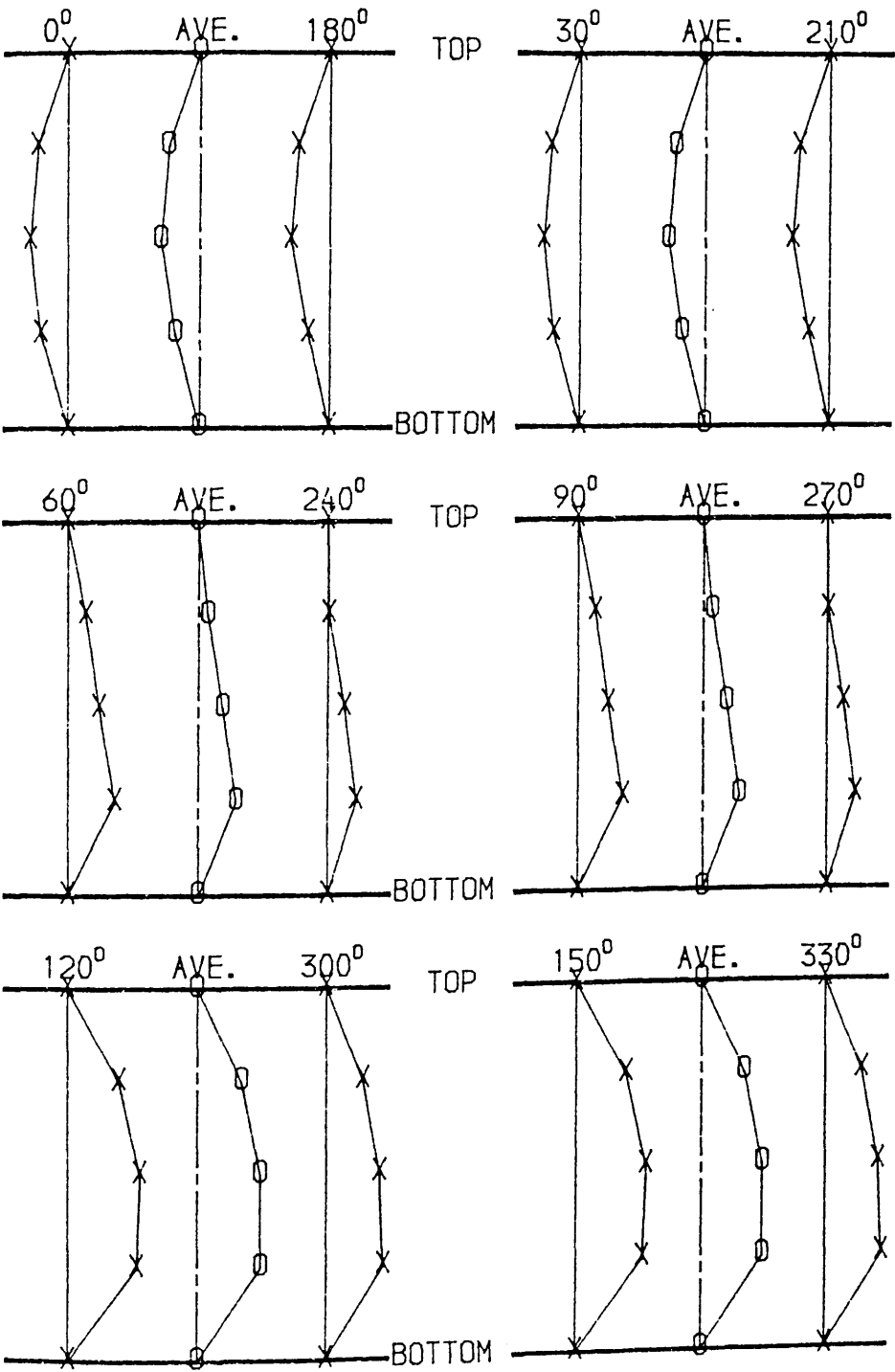
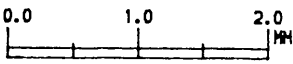
## INITIAL OUT-OF-STRAIGHTNESS

MODEL . G3  
 LENGTH (L) . 1800 MM  
 OUTSIDE DIA. . 50.93MM  
 THICKNESS . 2.04 MM



INITIAL OUT-OF-STRAIGHTNESS

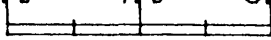
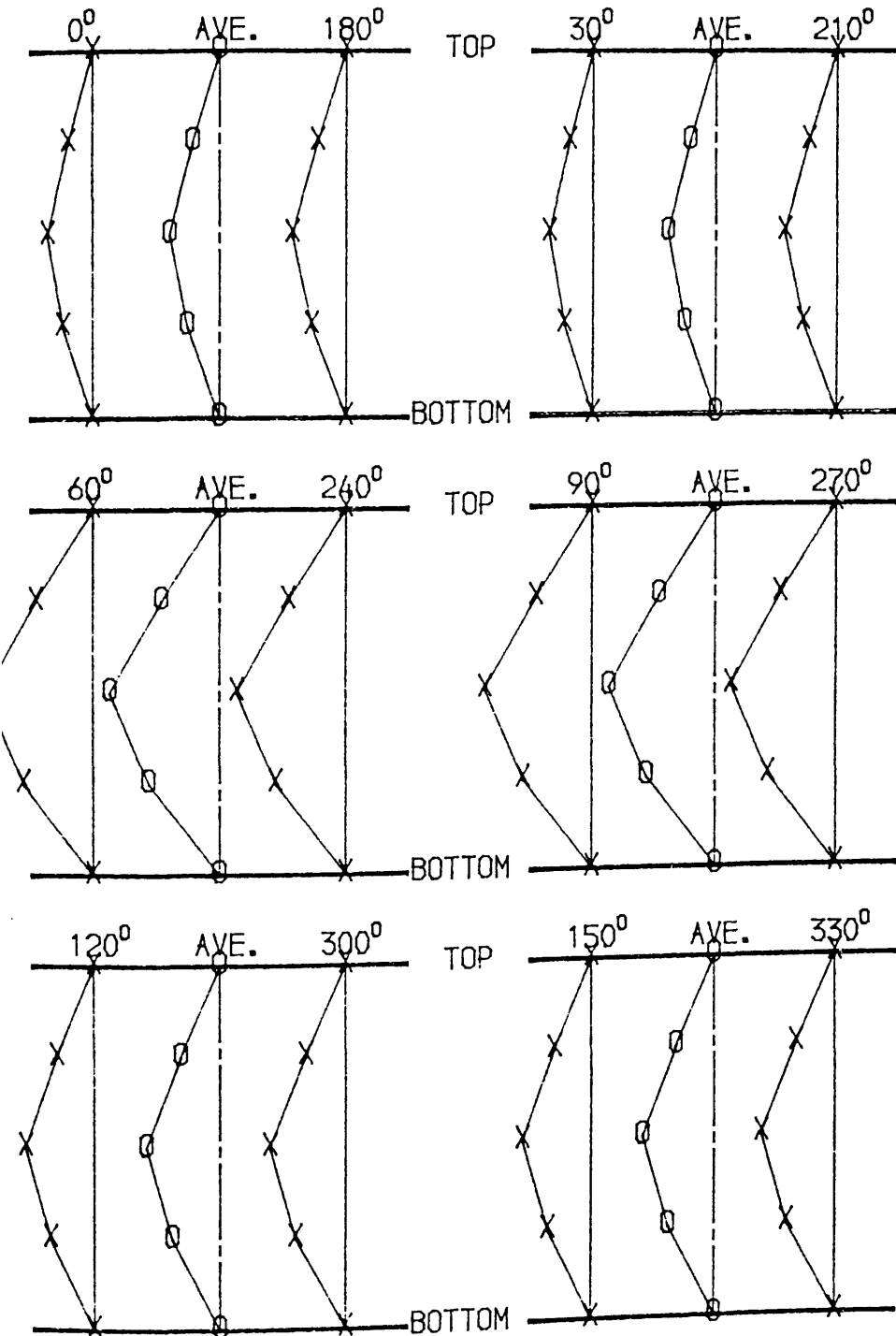
MODEL , H1  
LENGTH (L) : 1400 MM  
OUTSIDE DIA. : 50.90MM  
THICKNESS : 2.04 MM



## INITIAL OUT-OF-STRAIGHTNESS

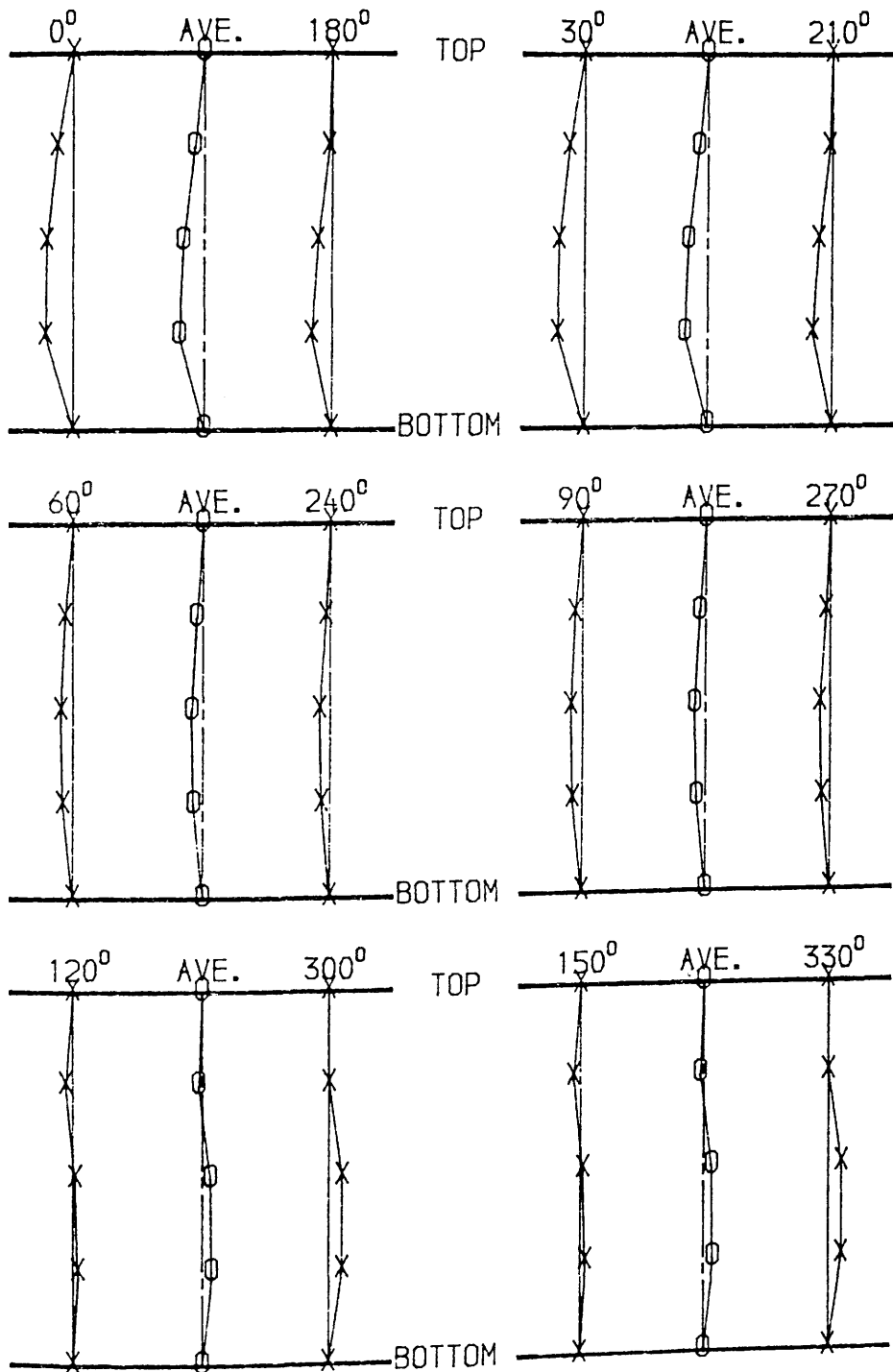
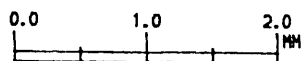
MODEL . H2  
 LENGTH (L) . 1400 MM  
 OUTSIDE DIA. . 50.92MM  
 THICKNESS . 2.02 MM

0.0 4.0 8.0 MM

## INITIAL OUT-OF-STRAIGHTNESS

MODEL : H3  
 LENGTH (L) : 1000 MM  
 OUTSIDE DIA. : 50.94MM  
 THICKNESS : 2.03 MM



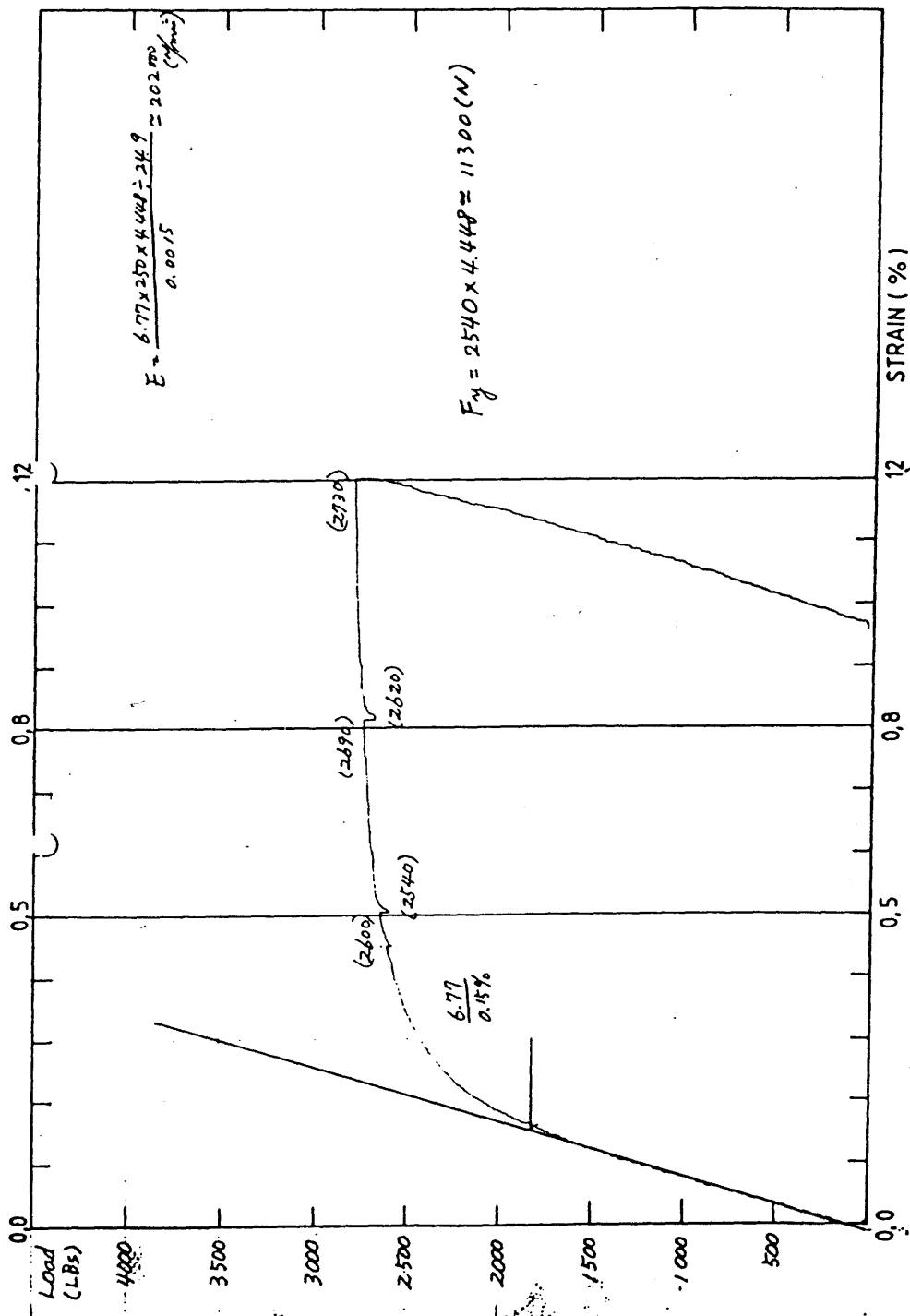
**B. III Tensile Test Results**

**B. III. 1      Typical Stress Strain Curves**

**B. III. 2      Tensile Test Results Table**

## STRESS-STRAIN CURVE

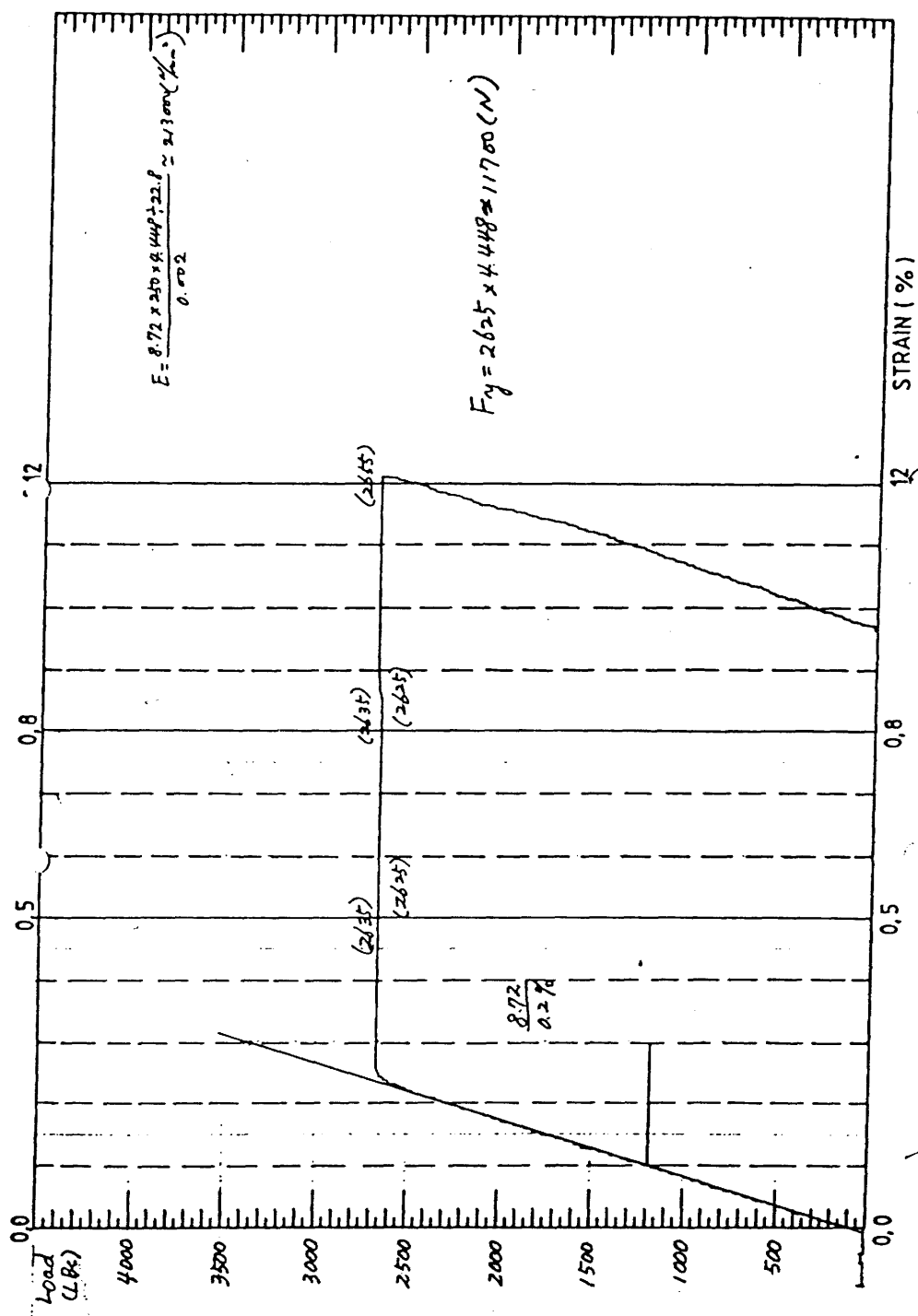
Specimen : A<sub>24</sub>      Size (W x T) : 20.3 x 1.23 (MM)  
 The figures in parentheses are tensile forces in pounds





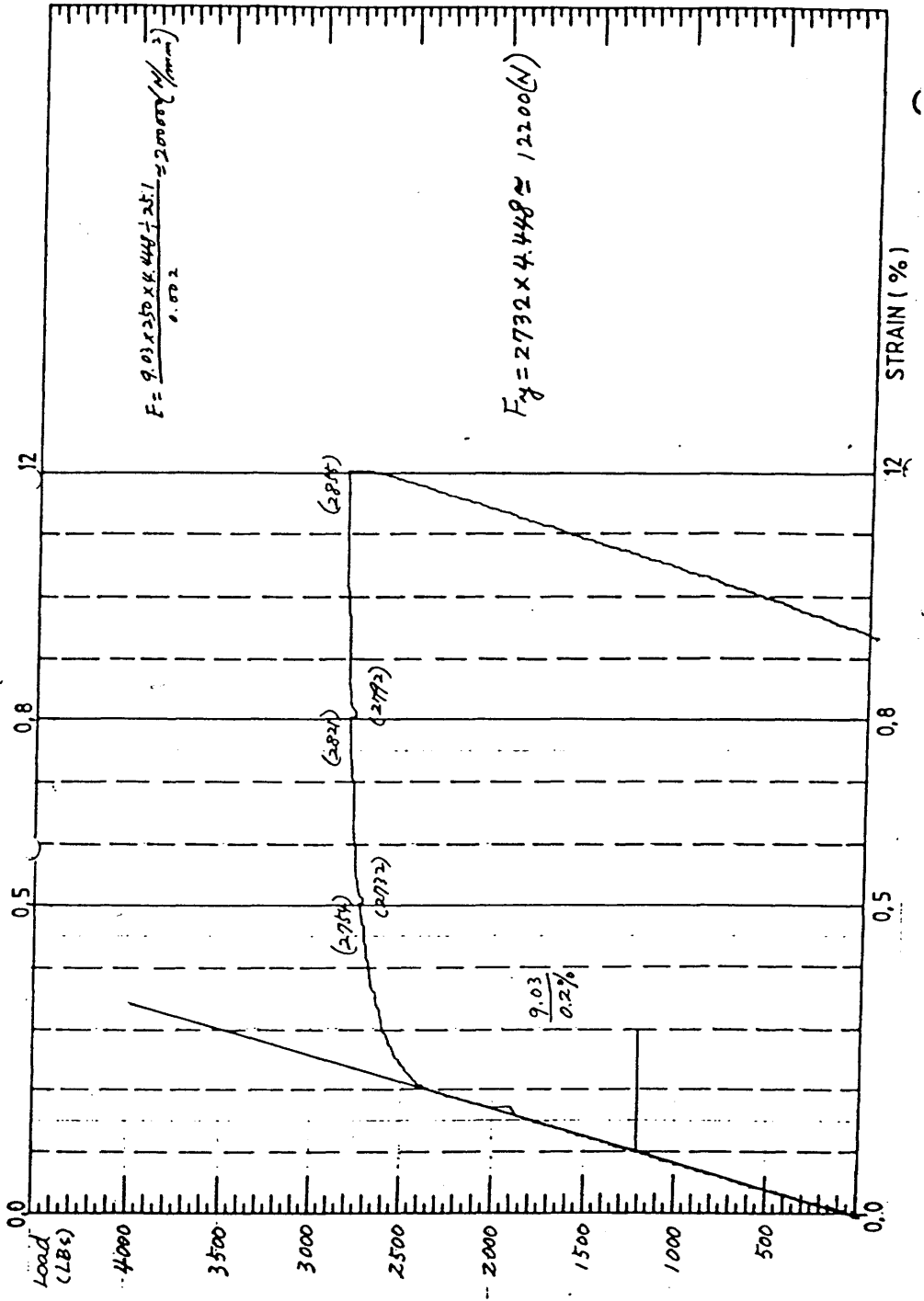
## STRESS-STRAIN CURVE

Specimen : Az5 (Curved)      Size (W x T) : 18.9 x 1.21 (MM)  
 The figures in parentheses are tensile forces in pounds



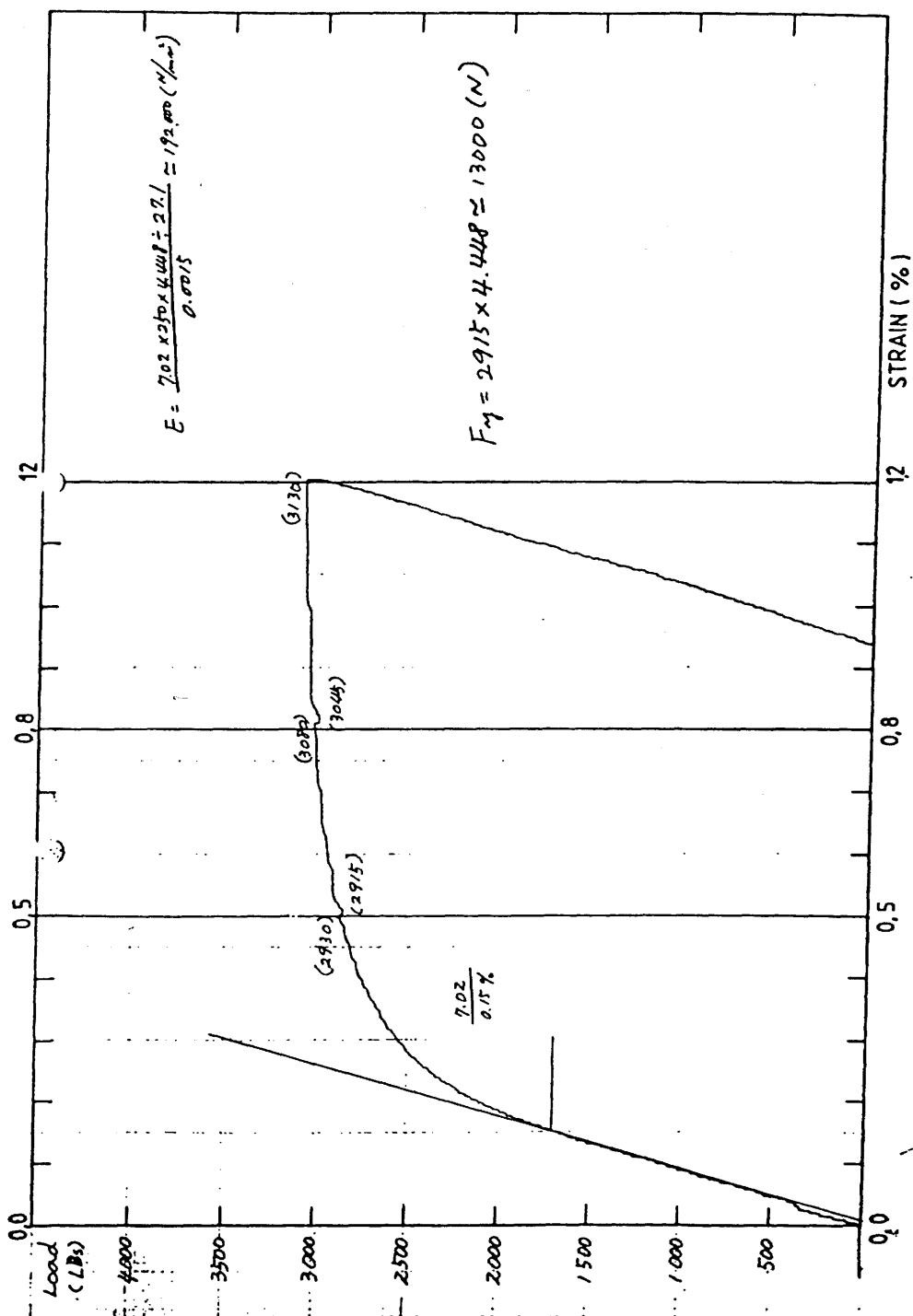
STRESS-STRAIN CURVE

Specimen : A<sub>31</sub>  
 Size (W x T) : 20.6 x 1.22 (MM)  
 The figures in parentheses are tensile forces in pounds



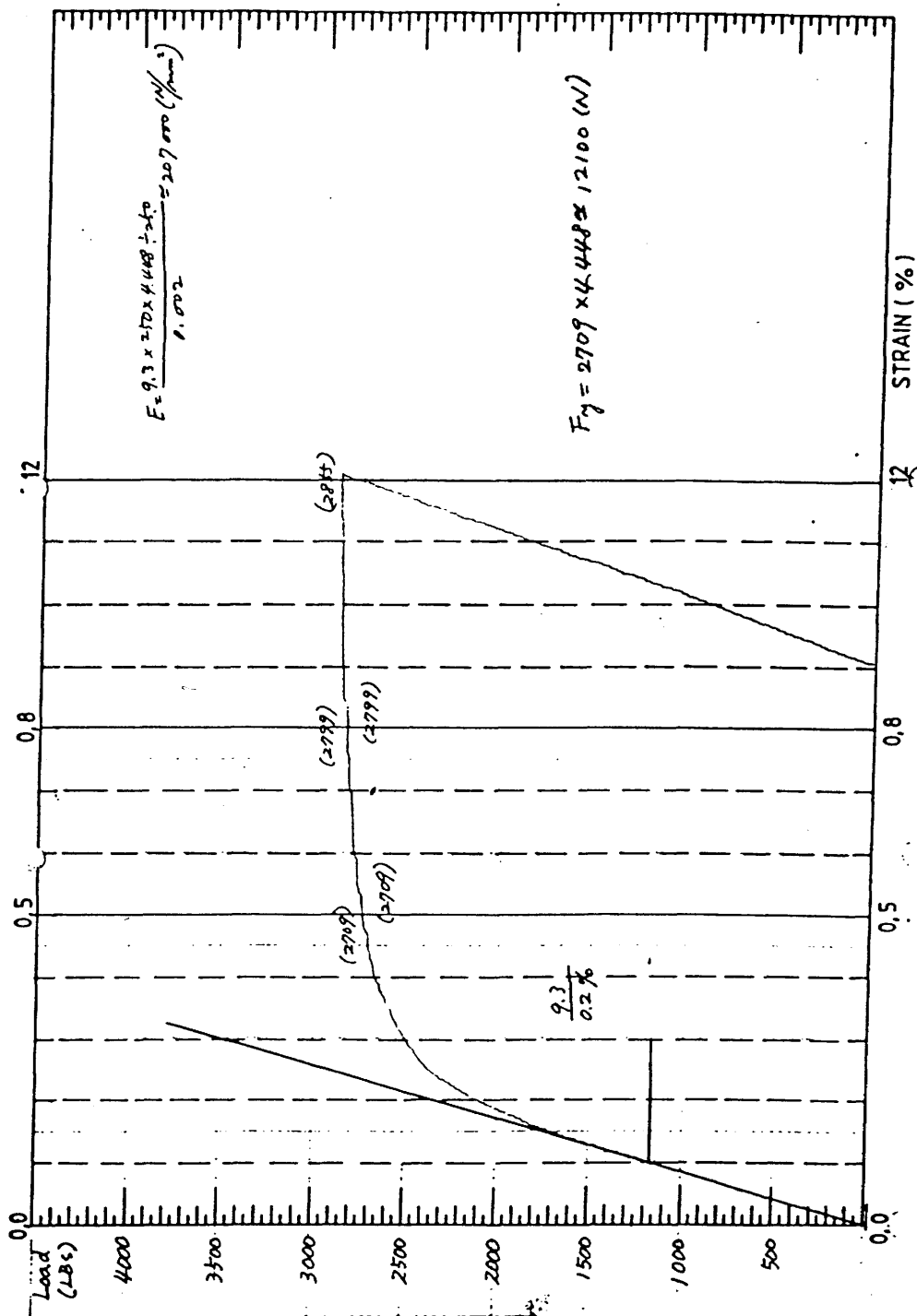
## STRESS-STRAIN CURVE

Specimen : A41  
 Size (W x T) : 22.4 x 1.21 (MM)  
 The figures in parentheses are tensile forces in pounds



## STRESS-STRAIN CURVE

Specimen : B<sub>21</sub>  
 Size (W x T) : 20.8 x 1.20 (MM)  
 The figures in parentheses are tensile forces in pounds

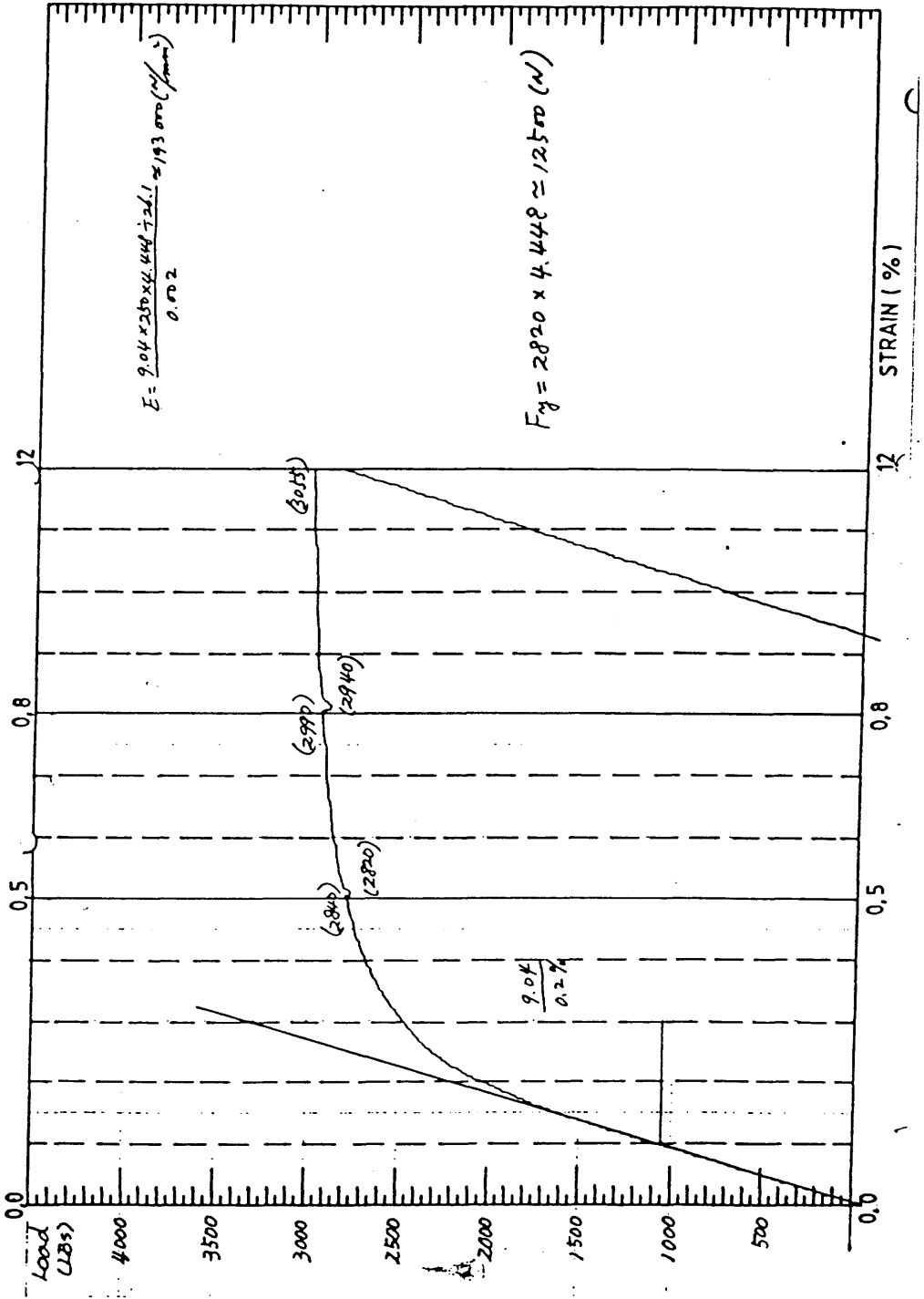


STRESS-STRAIN CURVE

Specimen : B<sub>32</sub>

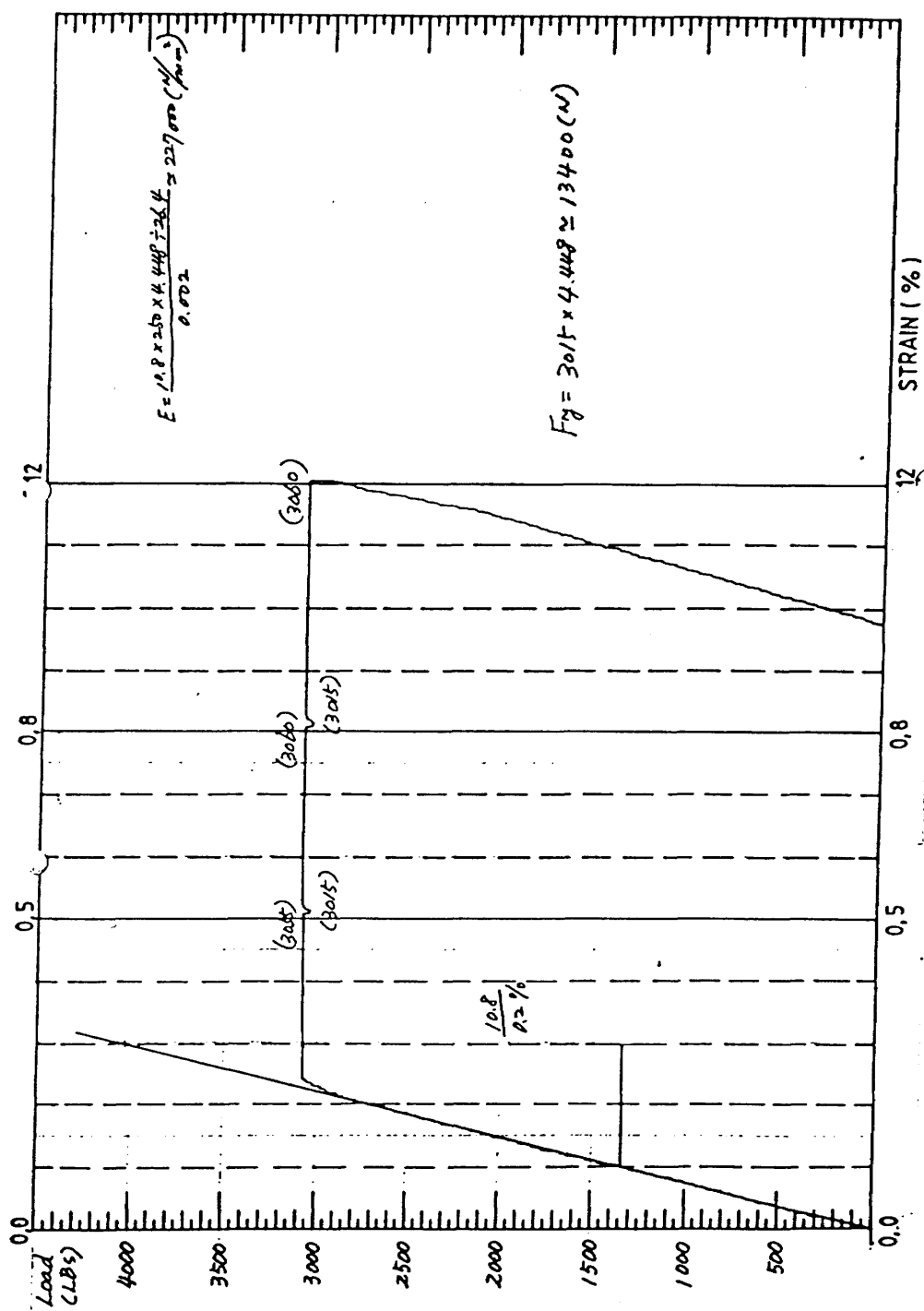
Size (W x T) : 2.16 x 1.21 (MM)

The figures in parentheses are tensile forces in pounds



## STRESS-STRAIN CURVE

Specimen : B<sub>35</sub> (Curved)      Size (W x T) : 22.4 x 1.18 (MM)  
 The figures in parentheses are tensile forces in pounds

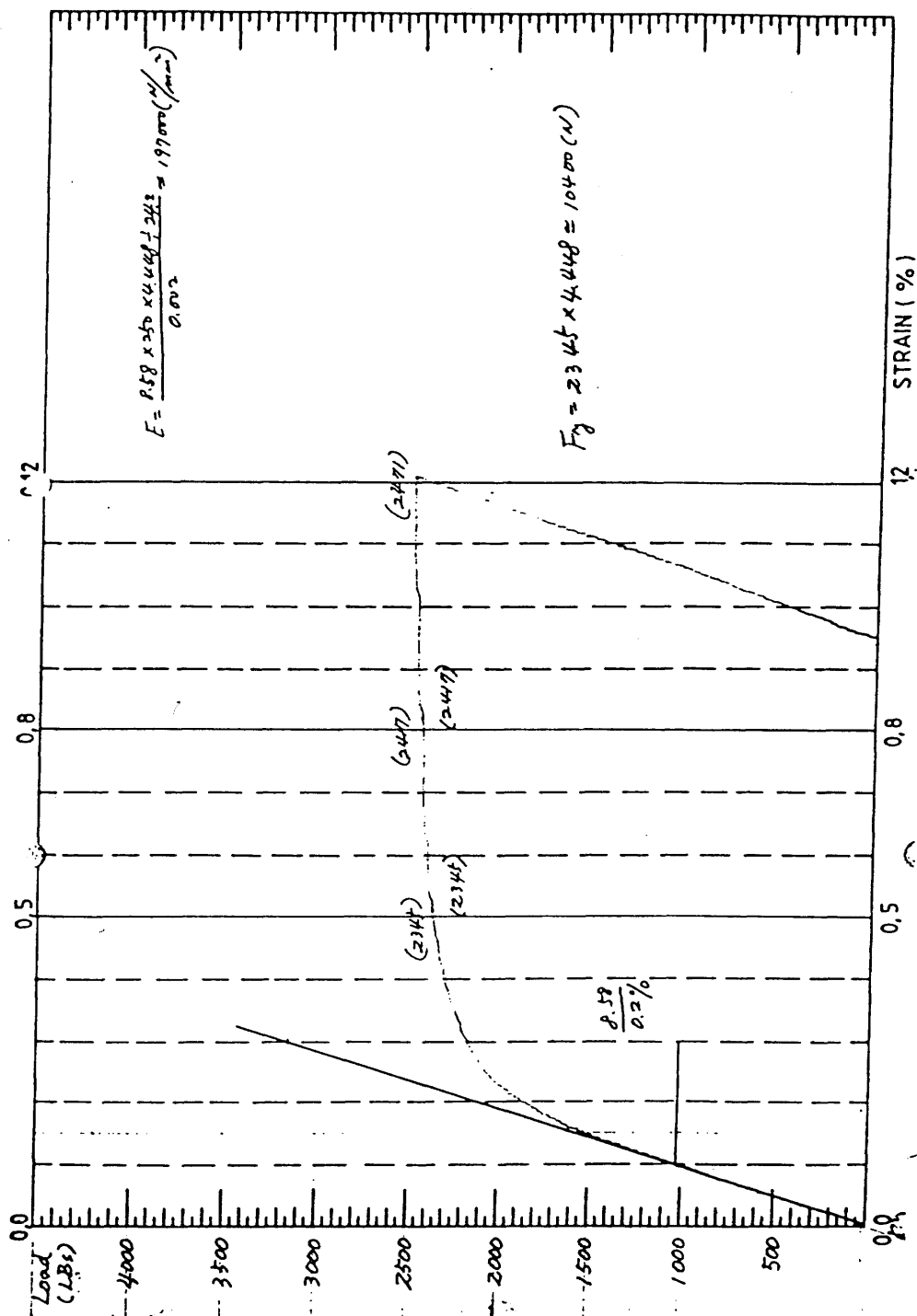


## STRESS-STRAIN CURVE

Specimen : C22

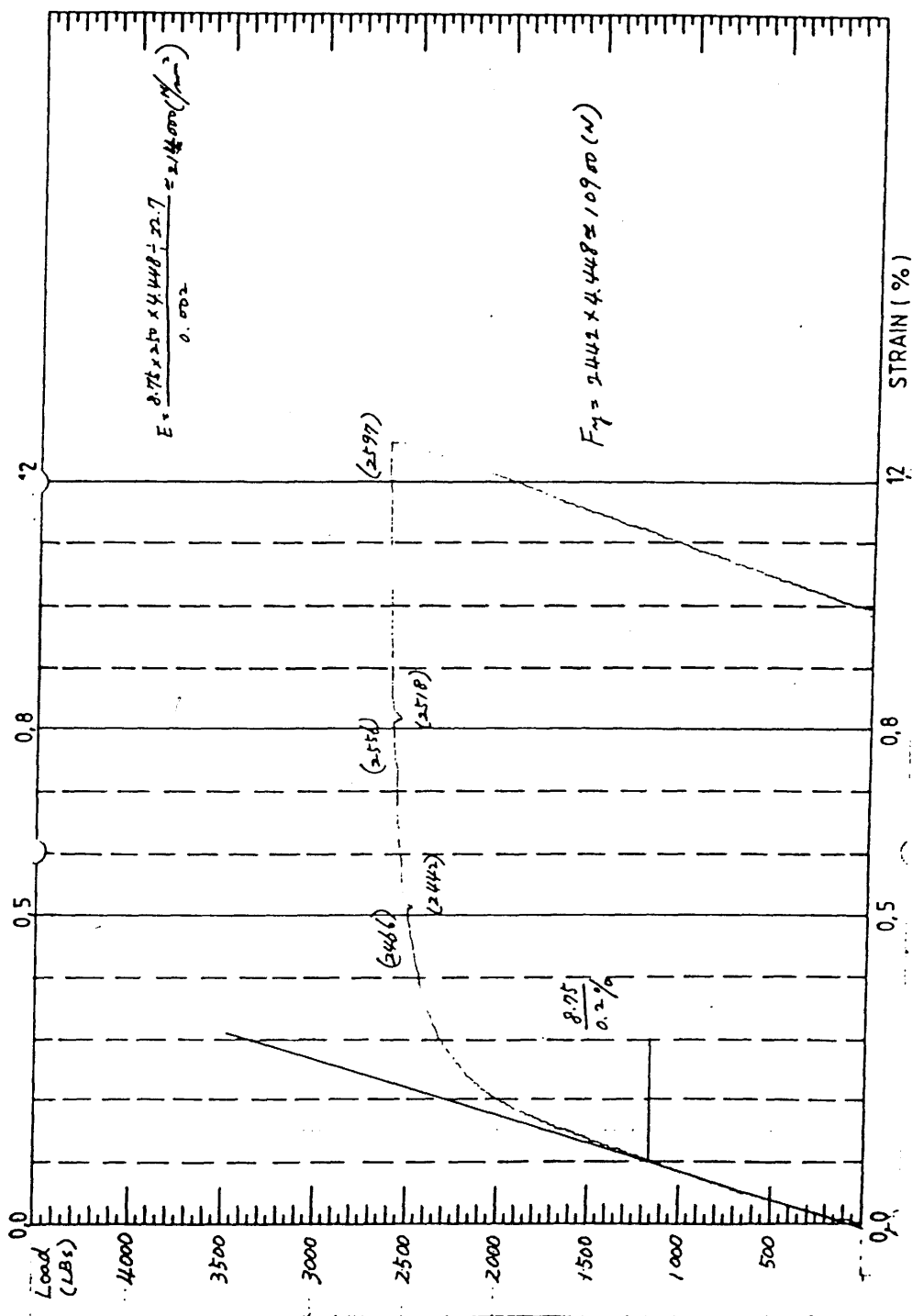
Size (W x T) : 20.5 x 1.18 (MM)

The figures in parentheses are tensile forces in pounds



## STRESS-STRAIN CURVE

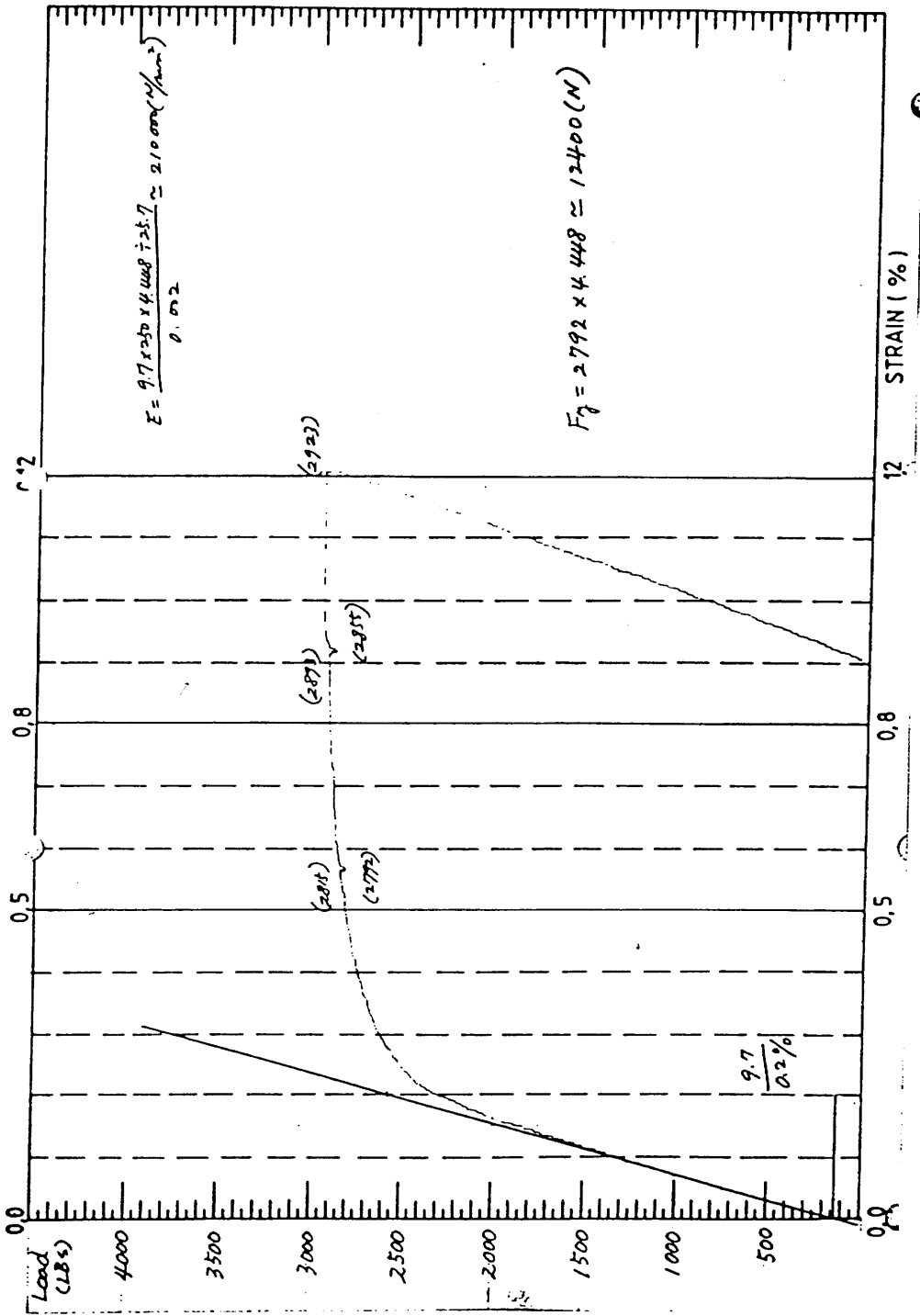
Specimen : D21      Size (W x T) : 1/8" x 1.21" (MM)  
 The figures in parentheses are tensile forces in pounds





## STRESS-STRAIN CURVE

Specimen : D34      Size (W x T) : 21.6 x 1.19 (MM)  
 The figures in parentheses are tensile forces in pounds

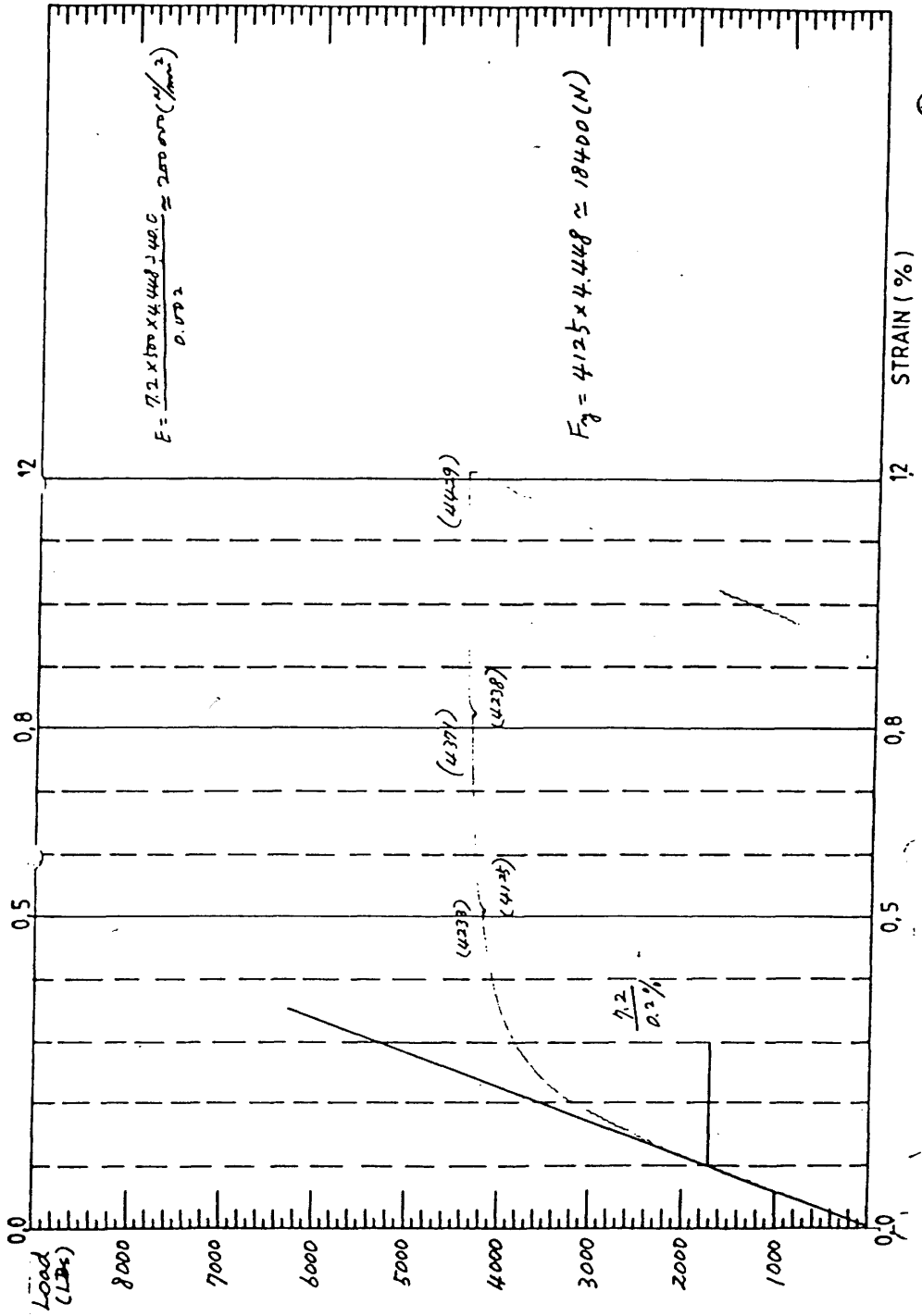


## STRESS-STRAIN CURVE

Specimen : E<sub>25</sub>

Size (W x T) : 20.6 x 1.94 (MM)

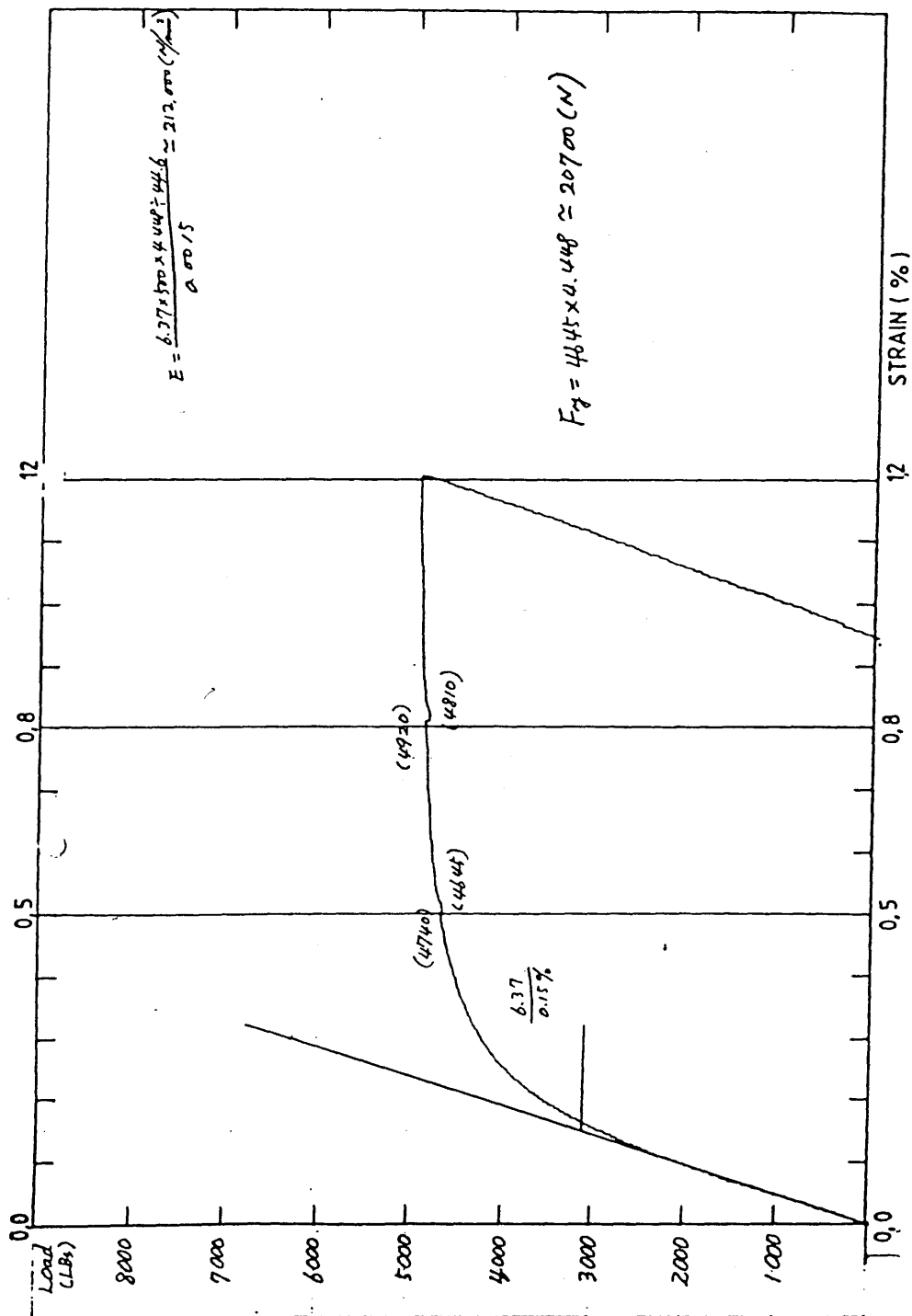
The figures in parentheses are tensile forces in pounds



## STRESS-STRAIN CURVE

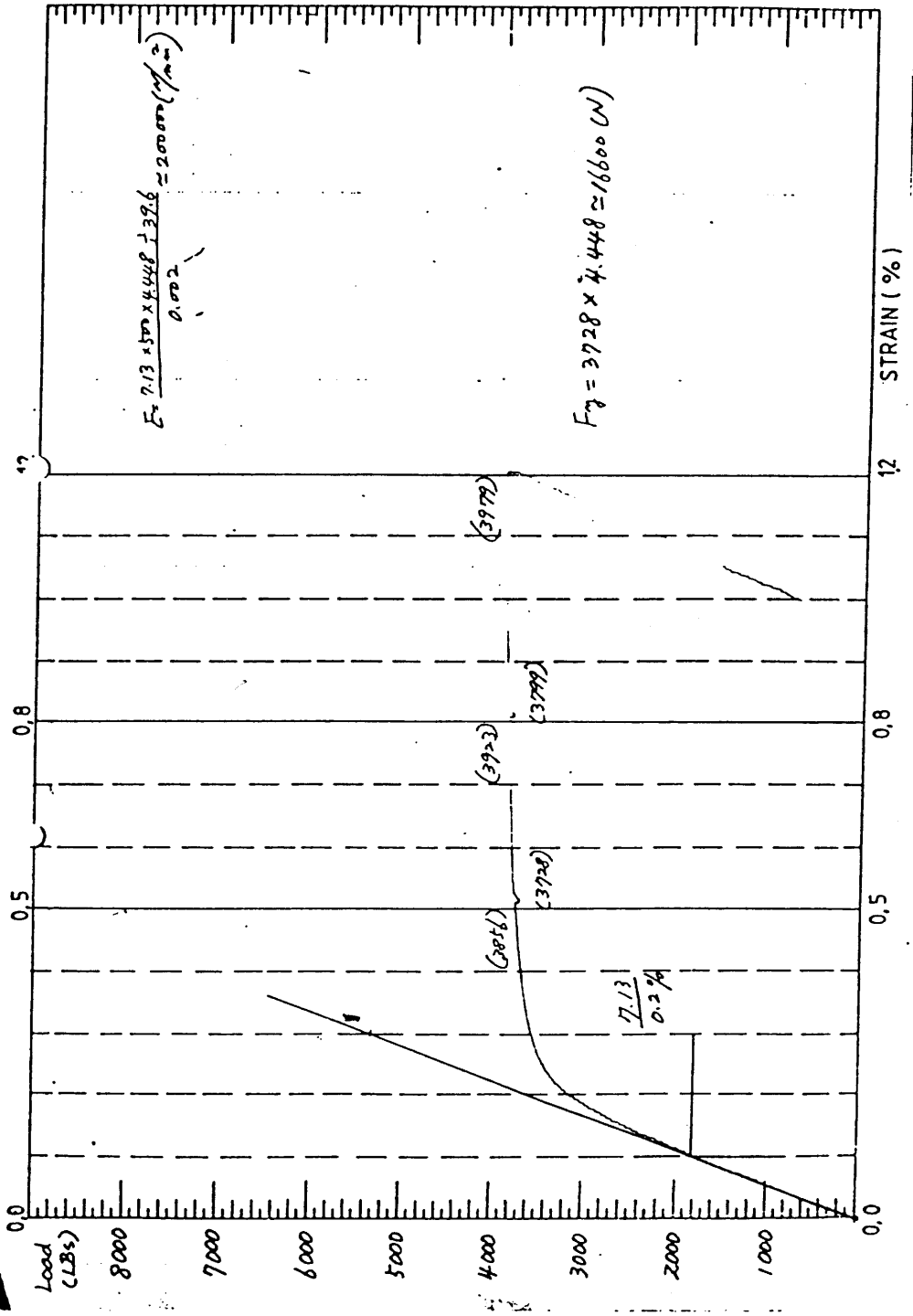
Specimen :  $E_{32}$  Size (W x T) : 22.4 x 1.99 (MM)

The figures in parentheses are tensile forces in pounds



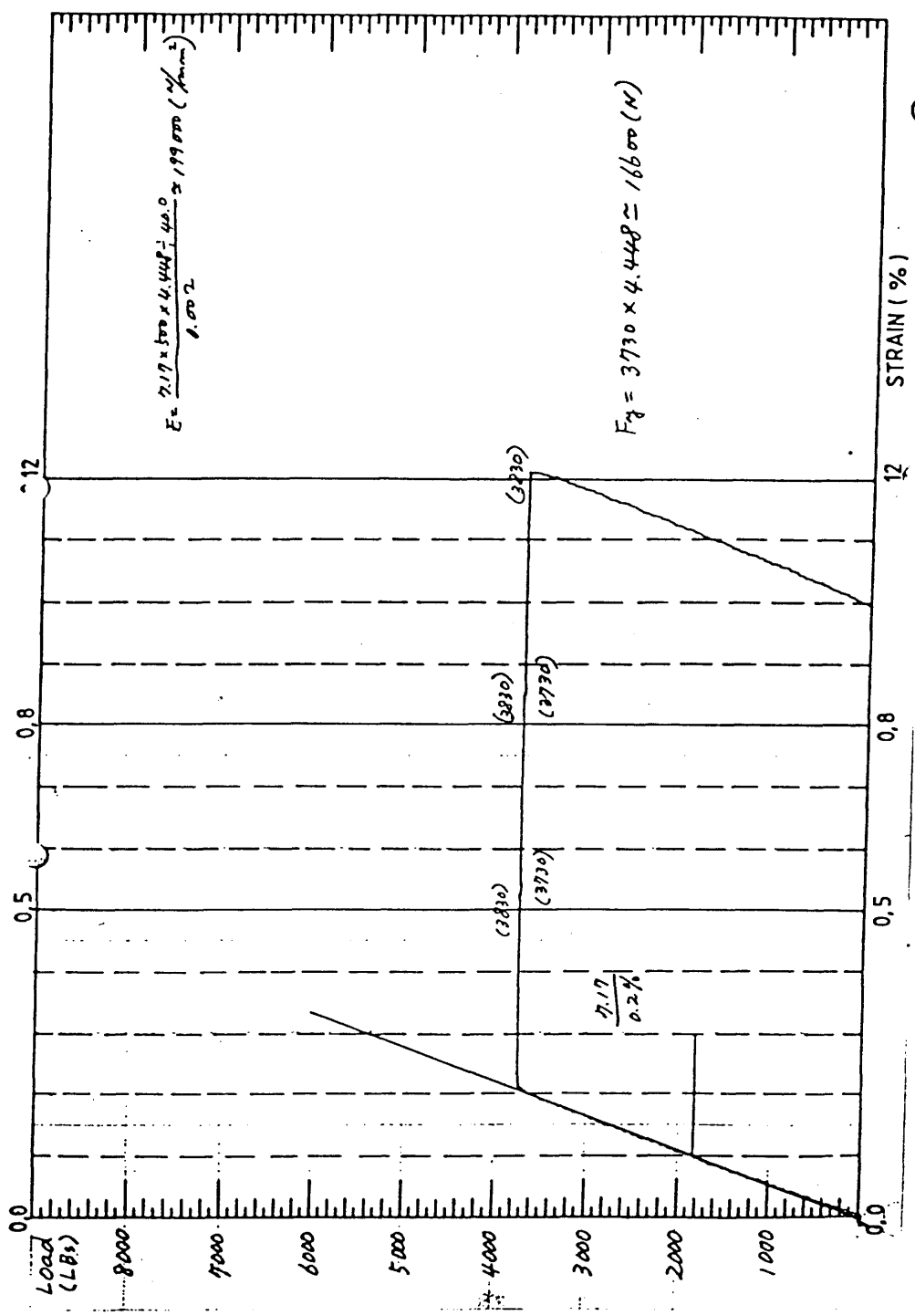
STRESS-STRAIN CURVE

Specimen : F24 Size (W x T) : 19.6 x 2.02 (MM)  
 The figures in parentheses are tensile forces in pounds



STRESS-STRAIN CURVE

Specimen : G<sub>25</sub> (Curved)      Size (W x T) : 19.4 x 2.06 (MM)  
The figures in parentheses are tensile forces in pounds

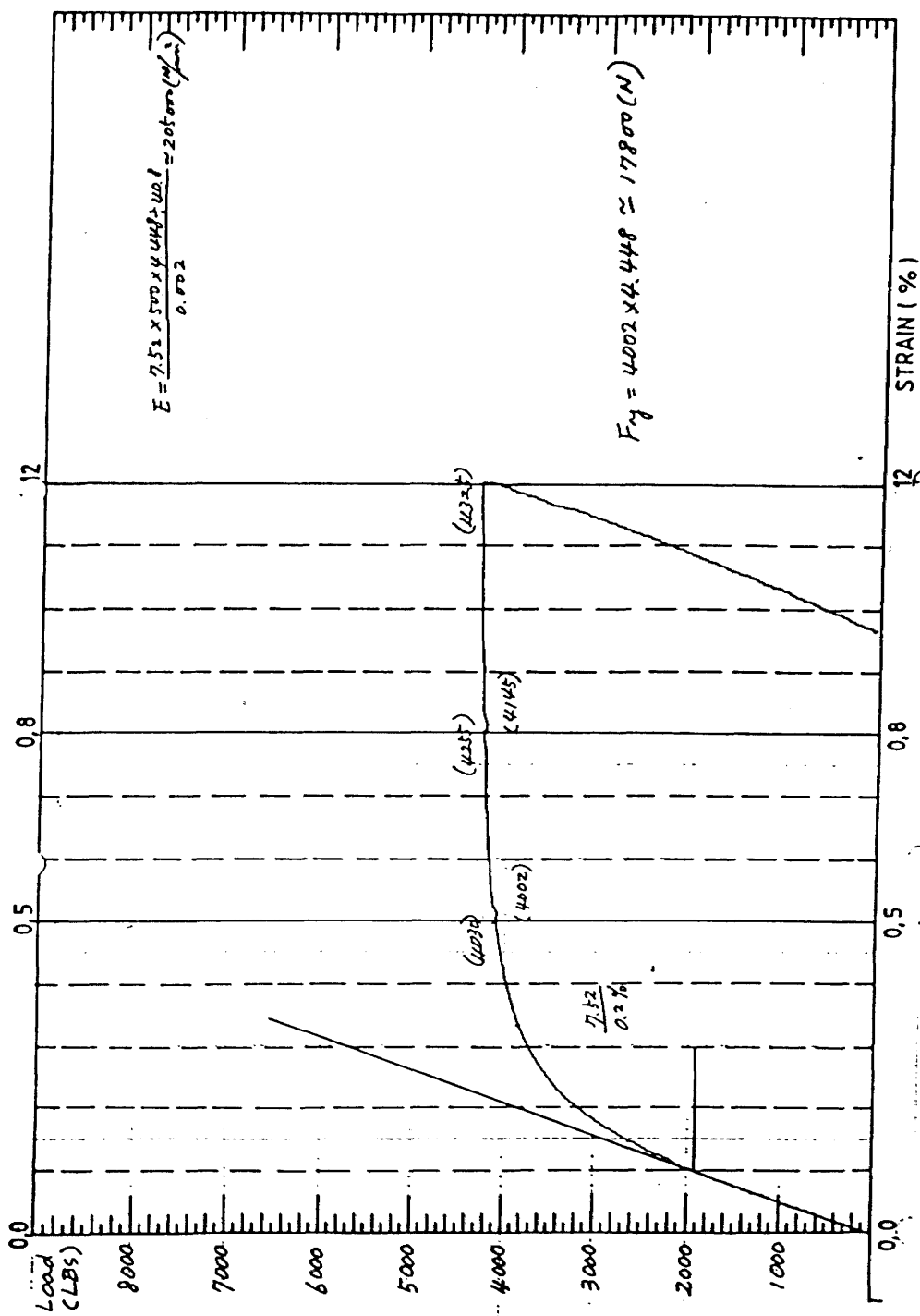


## STRESS-STRAIN CURVE

Specimen : G<sub>2.6</sub>

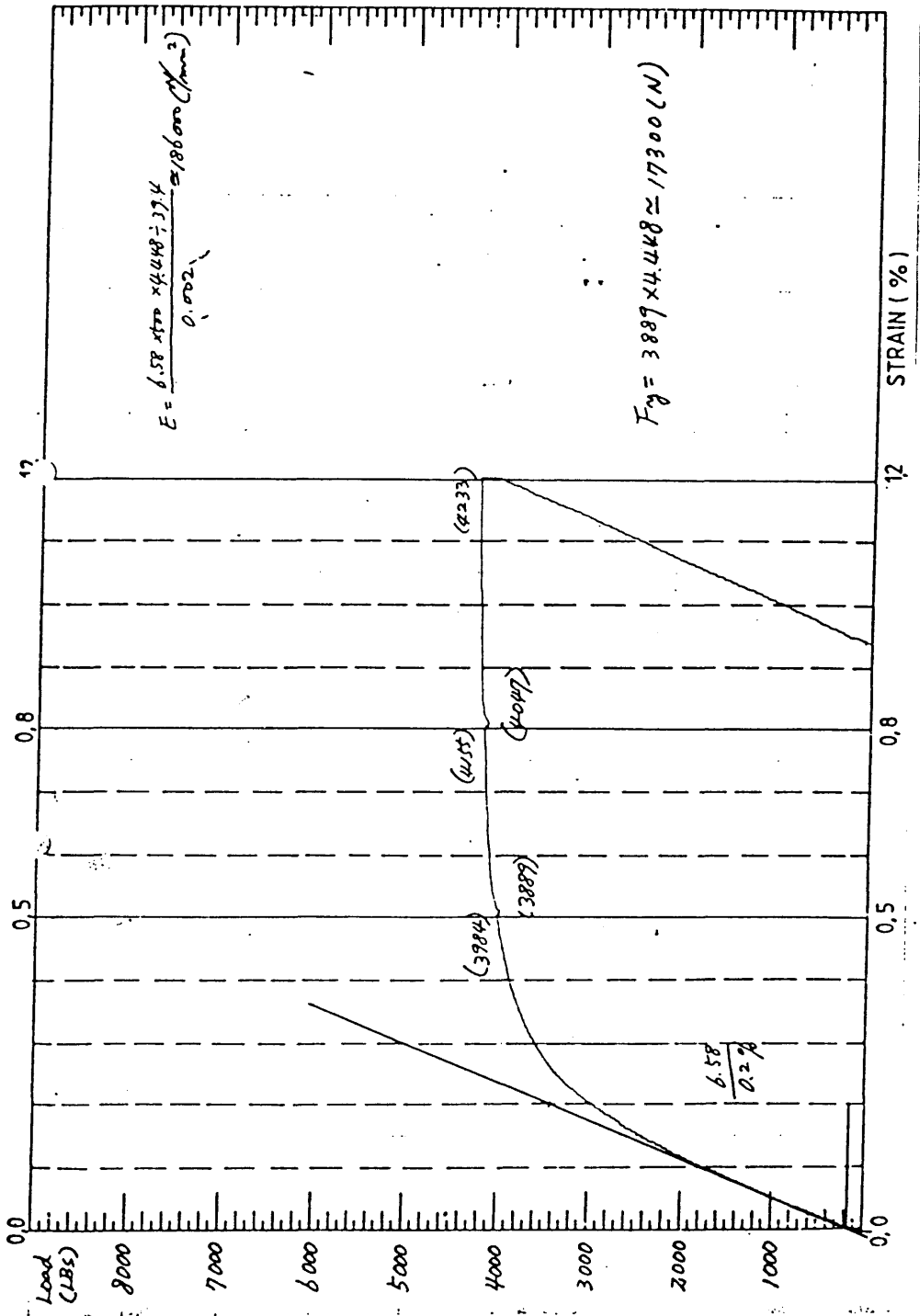
Size (W x T) : 19.8 x 2.06 (MM)

The figures in parentheses are tensile forces in pounds



## STRESS-STRAIN CURVE

Specimen: 1422      Size (W x T): 20.1 x 1.96 (mm)  
 The figures in parentheses are tensile forces in pounds

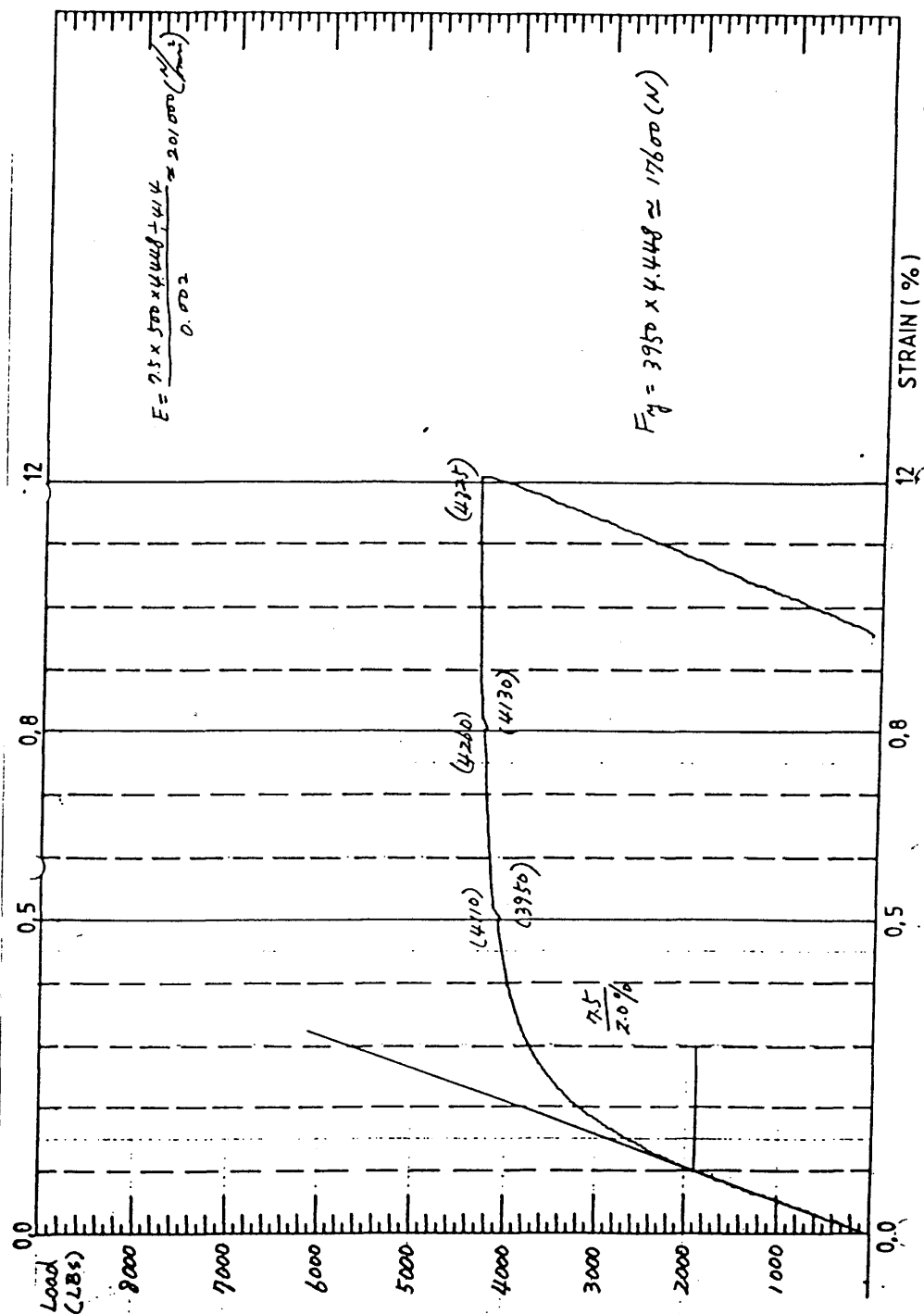


## STRESS STRAIN CURVE

Specimen : H<sub>33</sub>

Size (W x T) : 20.6 x 2.01 (MM)

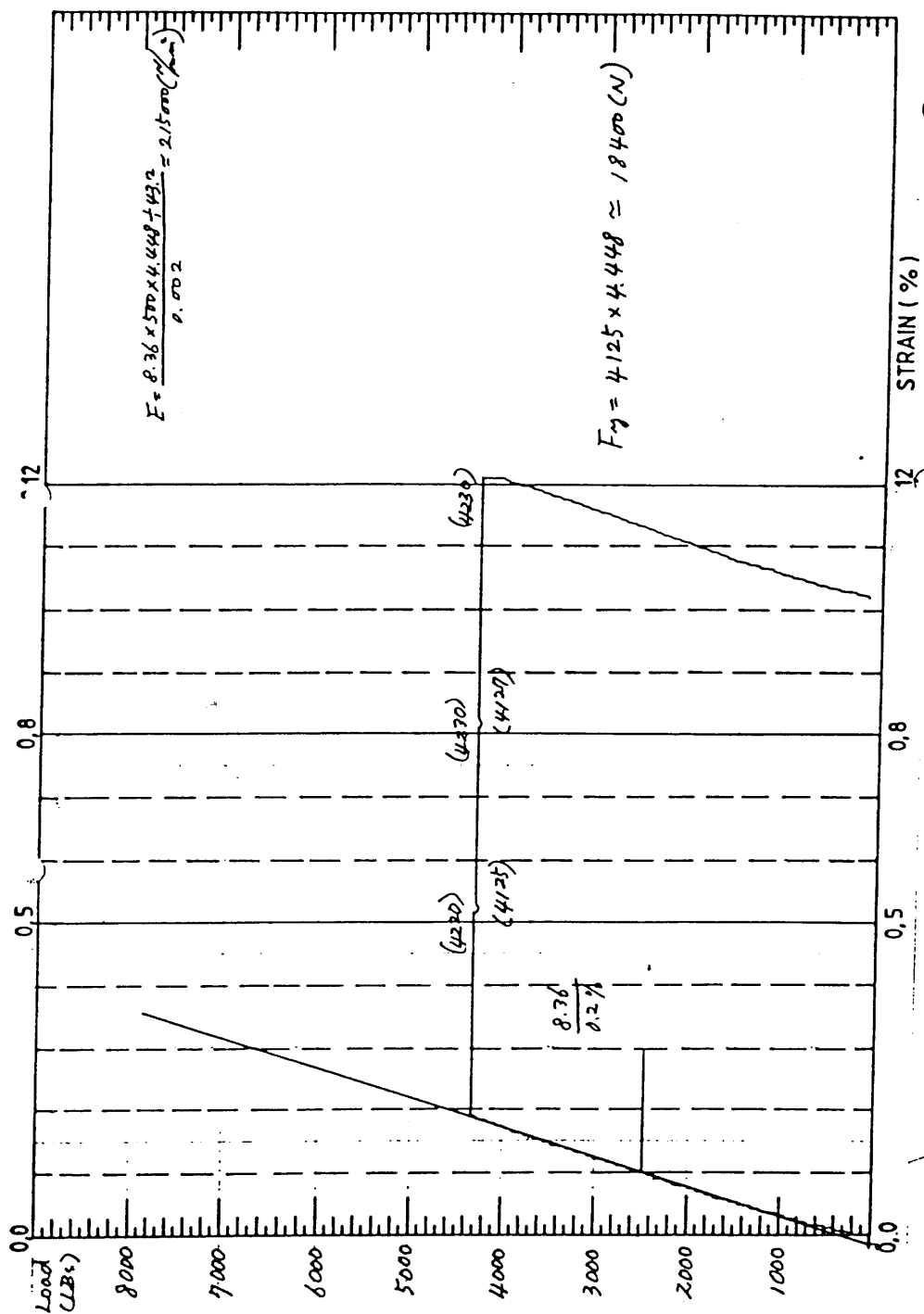
The figures in parentheses are tensile forces in pounds





## STRESS-STRAIN CURVE

Specimen :  $H_{34}$  (Curved) Size (W x T) : 2.6 x 2.00 (MM)  
 The figures in parentheses are tensile forces in pounds



# RESULTS OF TENSILE TESTS

Specimen :  $A_{41} \sim A_{46}$

Corresponding Model :  $A_1, A_2$

Heat-Treatment : 1st

Specimen	Breadth ( MM )	Thickness ( MM )	Static Yield Load ( N )	Static Yield Strength(N/MM <sup>2</sup> )	Young's Mod ( N/MM <sup>2</sup> )
$A_{41}$	22.4	1.21	13000	478	192000
$A_{42}$	22.4	1.24	13400	482	199000
$A_{43}$	22.5	1.18	12900	483	184000
$A_{44}$	22.5	1.20	13000	482	207000
$A_{45}^{**}$	22.6	1.21	12800	470	220000
$A_{46}^{**}$	22.4	1.23	12700	461	221000
Mean				476	204000
C.O.V.				1.85%	7.35%

Specimen :  $B_{21} \sim B_{26}$

Corresponding Model :  $B_2, B_3, B_4$

Heat-Treatment : 2nd

Specimen	Breadth ( MM )	Thickness ( MM )	Static Yield Load ( N )	Static Yield Strength(N/MM <sup>2</sup> )	Young's Modu ( N/MM <sup>2</sup> )
$B_{21}$	20.8	1.20	12100	482	207000
$B_{22}$	20.9	1.19	11700	470	192000
$B_{23}$	20.8	1.19	12100	488	192000
$B_{24}$	20.9	1.21	12600	498	198000
$B_{25}$	20.9	1.21	12300	486	244000
$B_{26}$	20.8	1.22	11900	468	192000
Mean				482	204000
C.O.V.				2.36%	9.99%

\*\* denotes the specimens were sent for 2nd H.-T. as well

RESULTS OF TENSILE TESTS

Specimen : $A_{21} \sim A_{26}$					
Corresponding Model : $A_3, A_4$					
Heat-Treatment : 2nd					
Specimen	Breadth ( MM )	Thickness ( MM )	Static Yield Load ( N )	Static Yield Strength(N/MM <sup>2</sup> )	Young's Modulus ( N/MM <sup>2</sup> )
$A_{21}^*$	17.7	1.18	10100	482	-
$A_{22}$	20.4	1.21	11700	475	194000
$A_{23}^*$	19.0	1.21	11600	501	201000
$A_{24}$	20.3	1.23	11300	454	202000
$A_{25}^*$	18.9	1.21	11700	512	213000
$A_{26}$	20.3	1.19	11300	466	202000
Mean				482	202000
C.O.V.				4.50%	3.37%

Specimen : $A_{31} \sim A_{36}$					
Corresponding Model : $A_3, A_4$					
Heat-Treatment : 2nd					
Specimen	Breadth ( MM )	Thickness ( MM )	Static Yield Load ( N )	Static Yield Strength(N/MM <sup>2</sup> )	Young's Modulus ( N/MM <sup>2</sup> )
$A_{31}$	20.6	1.22	12200	484	200000
$A_{32}$	20.5	1.21	11400	461	199000
$A_{33}$	20.5	1.21	11200	452	187000
$A_{34}$	20.6	1.21	11200	451	183000
$A_{35}$	20.5	1.20	11100	452	205000
$A_{36}$	20.3	1.20	11600	474	214000
Mean				462	198000
C.O.V.				2.98%	5.78%

\* denotes curved specimens

RESULTS OF TENSILE TESTS

Specimen : $A_{41} \sim A_{46}$					
Corresponding Model : $A_1, A_2$					
Heat-Treatment : 1st					
Specimen	Breadth ( MM )	Thickness ( MM )	Static Yield Load ( N )	Static Yield Strength(N/MM <sup>2</sup> )	Young's Modulus ( N/MM <sup>2</sup> )
$A_{41}$	22.4	1.21	13000	478	192000
$A_{42}$	22.4	1.24	13400	482	199000
$A_{43}$	22.5	1.18	12900	483	184000
$A_{44}$	22.5	1.20	13000	482	207000
$A_{45}^{**}$	22.6	1.21	12800	470	220000
$A_{46}^{**}$	22.4	1.23	12700	461	221000
Mean				476	204000
C.O.V.				1.85%	7.35%

Specimen : $B_{21} \sim B_{26}$					
Corresponding Model : $B_2, B_3, B_4$					
Heat-Treatment : 2nd					
Specimen	Breadth ( MM )	Thickness ( MM )	Static Yield Load ( N )	Static Yield Strength(N/MM <sup>2</sup> )	Young's Modulus ( N/MM <sup>2</sup> )
$B_{21}$	20.8	1.20	12100	482	207000
$B_{22}$	20.9	1.19	11700	470	192000
$B_{23}$	20.8	1.19	12100	488	192000
$B_{24}$	20.9	1.21	12600	498	198000
$B_{25}$	20.9	1.21	12300	486	244000
$B_{26}$	20.8	1.22	11900	468	192000
Mean				482	204000
C.O.V.				2.36%	9.99%

\*\* denotes the specimens were sent for 2nd H.-T. as well

RESULTS OF TENSILE TESTS

Specimen : $B_{31} \sim B_{36}$					
Corresponding Model : $B_1$					
Heat-Treatment : 1st					
Specimen	Breadth ( MM )	Thickness ( MM )	Static Yield Load ( N )	Static Yield Strength(N/MM <sup>2</sup> )	Young's Modulus ( N/MM <sup>2</sup> )
$B_{31}$	21.7	1.20	12700	490	190000
$B_{32}$	21.6	1.21	12500	481	193000
$B_{33}$	21.6	1.20	12600	485	197000
$B_{34}^*$	21.9	1.19	13200	504	201000
$B_{35}^*$	22.4	1.18	13400	508	227000
$B_{36}^*$	21.2	1.20	12100	478	227000
Mean				491	205000
C.O.V.				2.52%	8.20%

Specimen : $C_{21} \sim C_{26}$					
Corresponding Model : $C_1, C_2, C_3, C_4$					
Heat-Treatment : 2nd					
Specimen	Breadth ( MM )	Thickness ( MM )	Static Yield Load ( N )	Static Yield Strength(N/MM <sup>2</sup> )	Young's Modulus ( N/MM <sup>2</sup> )
$C_{21}$	20.9	1.21	11600	458	223000
$C_{22}$	20.5	1.18	10400	431	197000
$C_{23}$	20.7	1.19	11200	455	278000
$C_{24}$	20.3	1.20	10400	426	224000
$C_{25}$	20.4	1.22	11000	440	253000
$C_{26}$	20.4	1.22	10800	433	215000
Mean				441	232000
C.O.V.				3.00%	12.52%

\* denotes curved specimens

RESULTS OF TENSILE TESTS

Specimen : $D_{21} \sim D_{26}$					
Corresponding Model : $D_3, D_4$					
Heat-Treatment : 1st					
Specimen	Breadth ( MM )	Thickness ( MM )	Static Yield Load ( N )	Static Yield Strength(N/MM <sup>2</sup> )	Young's Modulus ( N/MM <sup>2</sup> )
$D_{21}$	18.8	1.21	10900	478	214000
$D_{22}$	19.0	1.21	11400	497	201000
$D_{23}$	18.8	1.20	11400	503	221000
$D_{24}$	18.5	1.20	11000	495	232000
$D_{25}$	18.4	1.20	10400	472	205000
$D_{26}$	18.8	1.20	10600	467	185000
Mean				485	210000
C.O.V.				3.07%	7.83%

Specimen : $D_{31} \sim D_{36}$					
Corresponding Model : $D_1, D_2$					
Heat-Treatment : 2nd					
Specimen	Breadth ( MM )	Thickness ( MM )	Static Yield Load ( N )	Static Yield Strength(N/MM <sup>2</sup> )	Young's Modulus ( N/MM <sup>2</sup> )
$D_{31}$	21.6	1.21	12600	481	195000
$D_{32}$	21.6	1.21	12800	491	208000
$D_{33}$	21.7	1.21	12000	456	214000
$D_{34}$	21.6	1.19	12400	483	210000
$D_{35}$	21.5	1.20	12400	481	236000
$D_{36}$	21.3	1.21	12600	487	200000
Mean				480	211000
C.O.V.				2.56%	6.77%

RESULTS OF TENSILE TESTS

Specimen : $E_{21} \sim E_{26}$					
Corresponding Model : $E_1, E_2$					
Heat-Treatment : 2nd					
Specimen	Breadth ( MM )	Thickness ( MM )	Static Yield Load ( N )	Static Yield Strength(N/MM <sup>2</sup> )	Young's Modulus ( N/MM <sup>2</sup> )
$E_{21}$	20.3	2.07	19200	457	232000
$E_{22}$	20.3	2.10	18800	441	236000
$E_{23}$	20.2	2.05	19800	478	239000
$E_{24}$	21.4	1.99	19300	453	222000
$E_{25}$	20.6	1.94	18400	459	200000
$E_{26}$	20.8	1.98	19400	476	245000
Mean				461	229000
C.O.V.				3.06%	7.05%

Specimen : $E_{31} \sim E_{36}$					
Corresponding Model : $E_3$					
Heat-Treatment : 1st					
Specimen	Breadth ( MM )	Thickness ( MM )	Static Yield Load ( N )	Static Yield Strength(N/MM <sup>2</sup> )	Young's Modulus ( N/MM <sup>2</sup> )
$E_{31}$	20.9	2.05	20200	471	218000
$E_{32}$	22.4	1.99	20700	463	212000
$E_{33}$	21.8	2.03	21000	473	238000
$E_{34}$	22.6	1.98	20600	461	210000
$E_{35}^{**}$	22.5	2.10	19500	413	223000
$E_{36}^{**}$	21.7	2.09	20000	440	223000
Mean				454	221000
C.O.V.				5.08%	4.56%

\*\* denotes the specimens were sent for 2nd H.-T. as well

RESULTS OF TENSILE TESTS

Specimen : $F_{21} \sim F_{26}$					
Corresponding Model : $F_1, F_2, F_3$					
Heat-Treatment : 2nd					
Specimen	Breadth ( MM )	Thickness ( MM )	Static Yield Load ( N )	Static Yield Strength(N/MM <sup>2</sup> )	Young's Modulus ( N/MM <sup>2</sup> )
$F_{21}$	19.6	2.00	16400	417	224000
$F_{22}$	19.6	2.02	16800	425	250000
$F_{23}$	19.5	2.03	17100	431	206000
$F_{24}$	19.6	2.02	16600	419	200000
$F_{25}$	19.5	1.97	16500	430	226000
$F_{26}$	19.5	1.97	16500	429	224000
Mean				425	222000
C.O.V.				1.40%	7.92%

Specimen : $G_{21} \sim G_{26}$					
Corresponding Model : $G_1, G_2, G_3$					
Heat-Treatment : 2nd					
Specimen	Breadth ( MM )	Thickness ( MM )	Static Yield Load ( N )	Static Yield Strength(N/MM <sup>2</sup> )	Young's Modulus ( N/MM <sup>2</sup> )
$G_{21}^*$	19.3	2.04	168.00	426	195000
$G_{22}$	19.8	2.01	173.00	435	194000
$G_{23}^*$	19.8	2.01	16900	425	203000
$G_{24}$	19.9	2.03	17600	436	206000
$G_{25}^*$	19.4	2.06	16600	415	199000
$G_{26}$	19.8	2.06	17800	436	205000
Mean				429	200000
C.O.V.				1.96%	2.56%

\* denotes curved specimens



# RESULTS OF TENSILE TESTS

Specimen : $H_{21} \sim H_{26}$					
Corresponding Model : $H_2, H_3$					
Heat-Treatment : 2nd					
Specimen	Breadth ( MM )	Thickness ( MM )	Static Yield Load ( N )	Static Yield Strength(N/MM <sup>2</sup> )	Young's Modulus ( N/MM <sup>2</sup> )
$H_{21}$	19.9	1.99	17100	431	242000
$H_{22}$	20.1	1.96	17300	439	186000
$H_{23}$	19.1	1.97	15600	415	234000
$H_{24}$	19.3	2.02	15900	407	189000
$H_{25}$	19.2	2.05	16000	406	200000
$H_{26}$	20.1	2.05	17700	430	221000
Mean				421	212000
C.O.V.				3.29%	11.19%

Specimen : $H_{31} \sim H_{36}$					
Corresponding Model : $H_1$					
Heat-Treatment : 1st					
Specimen	Breadth ( MM )	Thickness ( MM )	Static Yield Load ( N )	Static Yield Strength(N/MM <sup>2</sup> )	Young's Modulus ( N/MM <sup>2</sup> )
$H_{31}$	20.6	2.01	18900	457	-
$H_{32}$	20.3	2.01	17600	432	196000
$H_{33}$	20.6	2.01	17600	424	201000
$H_{34}^*$	21.6	2.00	18400	425	215000
$H_{35}^*$	21.8	2.01	187.00	427	244000
$H_{36}^*$	22.4	1.99	18800	423	222000
Mean				431	216000
C.O.V.				3.01%	8.80%

\* denotes curved specimens

## **APPENDIX C.**

### **DETAILED TEST RESULTS**

- C.I        Mass and Initial Velocity of Striker and  
             Residual Strain Measurements**
- C.II        Dynamic Recording Results**
- C.III        Extent of Damage Measurements**
  - C.III.1     Extent of Damage Measurements Table**
  - C.III.2     Extent of Damage Plots**

**C.1      Mass and Initial Velocity of Striker  
and Residual Strain Measurements**

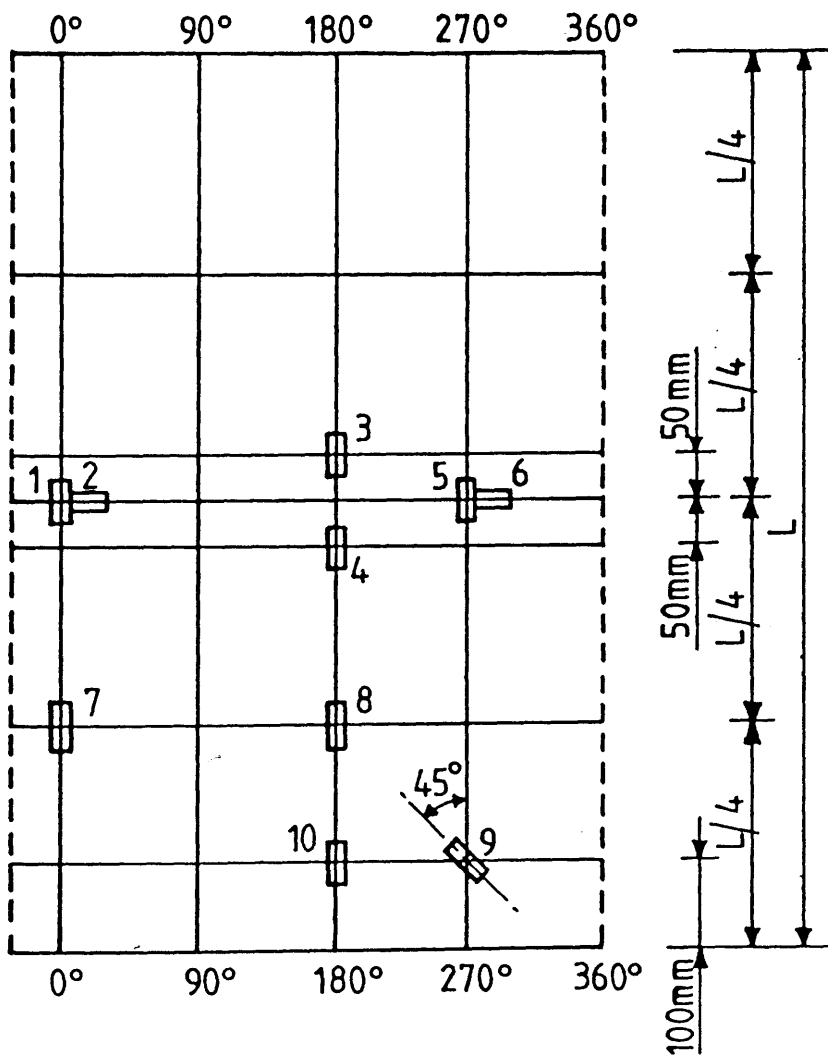


Fig. C1 Strain Gauge Arrangement for Lateral Impact Test

MEASUREMENT OF MASS AND INITIAL VELOCITY  
OF STRIKER AND RESIDUAL STRAINS  
-----

Model : A<sub>3</sub>

- o Mass of striker : 18.8 KG
- o Initial Velocity of Striker ;  
Distance between two  
Infra-red Switches : 110 MM  
Period : 45.5 MS.  
Initial Velocity(Vo) : 2.42 M/S.

o Residual Strains

Strain Gauge Number	Residual Strain ( $\epsilon$ )
1	( 360 ) 345
2	-791
3	1166
4	( 1350 ) 5961
5	91
6	155
7	( -30 ) -50
8	-57
9	( 0 ) 12
10	—

\* The strains in parentheses were measured with strain amplifiers.

Model : A<sub>4</sub>

- o Mass of striker : 18.8 KG
- o Initial Velocity of Striker ;  
Distance between two  
Infra-red Switches : 110 MM  
Period : 39.7 MS.  
Initial Velocity(Vo) : 2.77 M/S.

o Residual Strains

Strain Gauge Number	Residual Strain ( $\epsilon$ )
1	-864
2	528
3	1871
4	( 1420 ) 1424
5	93
6	-294
7	-16
8	( -10 ) -18
9	( 0 ) 20
10	( -10 ) 2

\* The strains in parentheses were measured with strain amplifiers.

MEASUREMENT OF MASS AND INITIAL VELOCITY  
OF STRIKER AND RESIDUAL STRAINS

Model : B<sub>1</sub>

- o Mass of striker : 23.5 KG
- o Initial Velocity of Striker ;  
Distance between two  
Infra-red Switches : 110 MM  
Period : 41.9 MS.  
Initial Velocity(Vo) : 2.63 M/S.
- o Residual Strains

Strain Gauge Number	Residual Strain ( $\epsilon$ )
1	( 300 ) 2972
2	(-1600 ) -486
3	1286
4	( 990 ) 992
5	-57
6	245
7	( -20 ) -2770
8	-12
9	—
10	—

\* The strains in parentheses were measured with strain amplifiers.

Model : B<sub>3</sub>

- o Mass of striker : 28.3 KG
- o Initial Velocity of Striker ;  
Distance between two  
Infra-red Switches : 110 MM  
Period : 62.8 MS.  
Initial Velocity(Vo) : 1.75 M/S.
- o Residual Strains

Strain Gauge Number	Residual Strain ( $\epsilon$ )
1	( -450 ) -450
2	209
3	927
4	( 1010 ) 1034
5	-67
6	-50
7	0
8	( -10 ) -17
9	-5
10	( 0 ) -11

\* The strains in parentheses were measured with strain amplifiers.

MEASUREMENT OF MASS AND INITIAL VELOCITY  
 OF STRIKER AND RESIDUAL STRAINS

Model : B<sub>4</sub>

- o Mass of striker : 28.3 KG
- o Initial Velocity of Striker ;  
 Distance between two  
 Infra-red Switches : 110 MM  
 Period : 48.5 MS.  
 Initial Velocity(Vo) : 2.27 M/S.
- o Residual Strains

Strain Gauge Number	Residual Strain ( $\epsilon$ )
1	—
2	203
3	941
4	714
5	178
6	17
7	( 0 ) -12
8	( -10 ) 26
9	( -30 ) 5
10	( 0 ) -15

\* The strains in parentheses were measured with strain amplifiers.

Model : C<sub>1</sub>

- o Mass of striker : 41.1 KG
- o Initial Velocity of Striker ;  
 Distance between two  
 Infra-red Switches : 110 MM  
 Period : 87.4 MS.  
 Initial Velocity(Vo) : 1.26 M/S.
- o Residual Strains

Strain Gauge Number	Residual Strain ( $\epsilon$ )
1	( -305 ) -252
2	( 110 ) 195
3	668
4	707
5	( -30 ) 366
6	( -40 ) 393
7	23
8	-13
9	-1
10	0

\* The strains in parentheses were measured with strain amplifiers.

MEASUREMENT OF MASS AND INITIAL VELOCITY  
OF STRIKER AND RESIDUAL STRAINS  
-----

Model :  $C_2$

- o Mass of striker : 41.1 KG
- o Initial Velocity of Striker ;  
Distance between two  
Infra-red Switches : 110 MM  
Period : 41.7 MS.  
Initial Velocity( $V_o$ ) : 2.64 M/S.
- o Residual Strains

Strain Gauge Number	Residual Strain ( $\epsilon$ )
1	(-4530 ) -4468
2	3402
3	1566
4	—
5	-627
6	-195
7	47
8	( -20 ) -32
9	-5
10	( 1490 ) 684

\* The strains in parentheses were measured with strain amplifiers.

Model :  $C_3$

- o Mass of striker : 41.1 KG
- o Initial Velocity of Striker ;  
Distance between two  
Infra-red Switches : 110 MM  
Period : 102.8 MS.  
Initial Velocity( $V_o$ ) : 1.07 M/S.
- o Residual Strains

Strain Gauge Number	Residual Strain ( $\epsilon$ )
1	( 20 ) -792
2	( -40 ) 40
3	150
4	( 130 ) -800
5	10
6	-1
7	( 10 ) -976
8	0
9	( 0 ) -1189
10	—

\* The strains in parentheses were measured with strain amplifiers.



MEASUREMENT OF MASS AND INITIAL VELOCITY  
OF STRIKER AND RESIDUAL STRAINS  
-----

Model :  $C_4$

- o Mass of striker : 41.1 KG
- o Initial Velocity of Striker ;  
Distance between two  
Infra-red Switches : 110 MM
- Period : 51.2 MS.
- Initial Velocity( $V_o$ ) : 2.15 M/S.

o Residual Strains

Strain Gauge Number	Residual Strain ( $\epsilon$ )
1	—
2	1302
3	1954
4	1915
5	-208
6	-1227
7	( -10 ) -17
8	( -30 ) -10
9	( 0 ) 16
10	( 0 ) 43

\* The strains in parentheses were measured with strain amplifiers.

Model :  $D_1$

- o Mass of striker : 28.3 KG
- o Initial Velocity of Striker ;  
Distance between two  
Infra-red Switches : 110 MM
- Period : 95.8 MS.
- Initial Velocity( $V_o$ ) : 1.15 M/S.

o Residual Strains

Strain Gauge Number	Residual Strain ( $\epsilon$ )
1	-23
2	2
3	( 40 ) 32
4	( 30 ) 43
5	-5
6	—
7	3
8	—
9	( 10 ) 8
10	( 10 ) 55

\* The strains in parentheses were measured with strain amplifiers.

MEASUREMENT OF MASS AND INITIAL VELOCITY  
OF STRIKER AND RESIDUAL STRAINS  
-----

Model :  $D_2$

- o Mass of striker : 28.3 KG
- o Initial Velocity of Striker ;  
Distance between two  
Infra-red Switches : 110 MM
- Period : 38.9 MS.
- Initial Velocity( $V_o$ ) : 2.83 M/S.
- o Residual Strains

Strain Gauge Number	Residual Strain ( $\epsilon$ )
1	(-1940 ) -1881
2	874
3	2755
4	1684
5	( 1080 ) 1091
6	-580
7	( 10 ) -40
8	( 0 ) -22
9	-28
10	-11

\* The strains in parentheses were measured with strain amplifiers.

Model :  $D_3$

- o Mass of striker : 28.3 KG
- o Initial Velocity of Striker ;  
Distance between two  
Infra-red Switches : 110 MM
- Period : 38.7 MS.
- Initial Velocity( $V_o$ ) : 2.84 M/S.
- o Residual Strains

Strain Gauge Number	Residual Strain ( $\epsilon$ )
1	—
2	—
3	( 2000 ) 2011
4	1223
5	( 680 ) 675
6	129
7	( 0 ) -24
8	-34
9	( -10 ) -17
10	—

\* The strains in parentheses were measured with strain amplifiers.

MEASUREMENT OF MASS AND INITIAL VELOCITY  
OF STRIKER AND RESIDUAL STRAINS  
-----

Model :  $D_4$

- o Mass of striker : 41.1 KG
- o Initial Velocity of Striker ;  
Distance between two  
Infra-red Switches : 110 MM
- Period : — MS.
- Initial Velocity( $V_o$ ) : — M/S.
- o Residual Strains

Strain Gauge Number	Residual Strain ( $\epsilon$ )
1	( -2870 ) -2888
2	3167
3	( 2260 ) 2293
4	( — ) 1892
5	-1015
6	-1180
7	45
8	( -20 ) -33
9	20
10	—

\* The strains in parentheses were measured with strain amplifiers.

Model :  $E_3$

- o Mass of striker : 28.3 KG
- o Initial Velocity of Striker ;  
Distance between two  
Infra-red Switches : 110 MM
- Period : 41.4 MS.
- Initial Velocity( $V_o$ ) : 2.66 M/S.
- o Residual Strains

Strain Gauge Number	Residual Strain ( $\epsilon$ )
1	( 110 ) 99
2	-179
3	552
4	( 215 ) 202
5	188
6	-391
7	5
8	( 0 ) 30
9	—
10	( 20 ) 15

\* The strains in parentheses were measured with strain amplifiers.

MEASUREMENT OF MASS AND INITIAL VELOCITY  
OF STRIKER AND RESIDUAL STRAINS  
-----

Model :  $F_1$

- o Mass of striker : 50.0 KG  
o Initial Velocity of Striker ;  
Distance between two  
Infra-red Switches : 110 MM  
Period : 133.4 MS.  
Initial Velocity( $V_o$ ) : 0.82 M/S.

c Residual Strains

Strain Gauge Number	Residual Strain ( $\epsilon$ )
1	—
2	( 0 ) 0
3	—
4	13
5	( 0 ) 0
6	19
7	( 0 ) 0
8	( 0 ) 0
9	120
10	—

\* The strains in parentheses were measured with strain amplifiers.

Model :  $F_{1p}$

- o Mass of striker : 41.1 KG  
o Initial Velocity of Striker ;  
Distance between two  
Infra-red Switches : 110 MM  
Period : 55.7 MS.  
Initial Velocity( $V_o$ ) : 1.97 M/S.

o Residual Strains

Strain Gauge Number	Residual Strain ( $\epsilon$ )
1	—
2	( 150 ) 118
3	—
4	429
5	( 190 ) 189
6	-352
7	( -20 ) -92
8	( -10 ) -320
9	-12
10	—

\* The strains in parentheses were measured with strain amplifiers.

MEASUREMENT OF MASS AND INITIAL VELOCITY  
OF STRIKER AND RESIDUAL STRAINS  
-----

Model :  $F_2$

- o Mass of striker : 41.1 KG
- o Initial Velocity of Striker ;  
Distance between two  
Infra-red Switches : 110 MM  
Period : 66.6 MS.  
Initial Velocity( $V_o$ ) : 1.65 M/S.
- o Residual Strains

Strain Gauge Number	Residual Strain ( $\epsilon$ )
1	( -740 ) -737
2	( 380 ) 387
3	690
4	—
5	( 60 ) 77
6	( -1550 ) -1542
7	-2
8	-9
9	20
10	10

\* The strains in parentheses were measured with strain amplifiers.

Model :  $F_3$

- o Mass of striker : 28.3 KG
- o Initial Velocity of Striker ;  
Distance between two  
Infra-red Switches : 110 MM  
Period : 36.8 MS.  
Initial Velocity( $V_o$ ) : 2.99 M/S.
- o Residual Strains

Strain Gauge Number	Residual Strain ( $\epsilon$ )
1	( -810 ) -805
2	447
3	( 810 ) 821
4	—
5	206
6	-873
7	7
8	( 0 ) -40
9	( 10 ) 11
10	—

\* The strains in parentheses were measured with strain amplifiers.

**MEASUREMENT OF MASS AND INITIAL VELOCITY  
OF STRIKER AND RESIDUAL STRAINS**

Model :  $G_1$

- o Mass of striker : 28.3 KG
- o Initial Velocity of Striker ;  
Distance between two  
Infra-red Switches : 110 MM
- Period : 40.3 MS.
- Initial Velocity( $V_o$ ) : 2.73 M/S.

o Residual Strains

Strain Gauge Number	Residual Strain ( $\epsilon$ )
1	( -690 ) -704
2	—
3	1167
4	( 670 ) 675
5	( 150 ) 152
6	( -420 ) -411
7	-22
8	-20
9	-10
10	—

\* The strains in parentheses were measured with strain amplifiers.

Model :  $G_2$

- o Mass of striker : 28.3 KG
- o Initial Velocity of Striker ;  
Distance between two  
Infra-red Switches : 110 MM
- Period : 39.1 MS.
- Initial Velocity( $V_o$ ) : 2.81 M/S.

o Residual Strains

Strain Gauge Number	Residual Strain ( $\epsilon$ )
1	( -1010 ) -1024
2	( 650 ) 653
3	( 720 ) 662
4	—
5	( 320 ) 294
6	-980
7	—
8	-3
9	2
10	0

\* The strains in parentheses were measured with strain amplifiers.

**MEASUREMENT OF MASS AND INITIAL VELOCITY  
OF STRIKER AND RESIDUAL STRAINS**

Model :  $G_3$

- o Mass of striker : 41.1 KG
- o Initial Velocity of Striker ;  
Distance between two  
Infra-red Switches : 110 MM
- Period : 59.0 MS.
- Initial Velocity( $V_o$ ) : 1.86 M/S.
- o Residual Strains

Strain Gauge Number	Residual Strain ( $\epsilon$ )
1	( -60 ) -39
2	( 150 ) 183
3	89
4	61
5	1
6	72
7	13
8	( 10 ) -173
9	6
10	( 0 ) 23

\* The strains in parentheses were measured with strain amplifiers.

Model :  $H_1$

- o Mass of striker : 18.8 KG
- o Initial Velocity of Striker ;  
Distance between two  
Infra-red Switches : 110 MM
- Period : 37.2 MS.
- Initial Velocity( $V_o$ ) : 2.96 M/S.
- o Residual Strains

Strain Gauge Number	Residual Strain ( $\epsilon$ )
1	-160
2	—
3	972
4	( 170 ) 163
5	84
6	0
7	45
8	( 0 ) 559
9	( — ) 10
10	( 20 ) -16

\* The strains in parentheses were measured with strain amplifiers.

MEASUREMENT OF MASS AND INITIAL VELOCITY  
OF STRIKER AND RESIDUAL STRAINS

Model :  $H_2$

- o Mass of striker : 41.1 KG
- o Initial Velocity of Striker ;  
Distance between two  
Infra-red Switches : 110 MM
- Period : 43.1 MS.
- Initial Velocity( $V_o$ ) : 2.55 M/S.
- o Residual Strains

Strain Gauge Number	Residual Strain ( $\epsilon$ )
1	-10156
2	—
3	1058
4	1130
5	( 220 ) 248
6	( 975 ) 969
7	( -20 ) 60
8	1
9	18
10	( -30 ) -96

\* The strains in parentheses were measured with strain amplifiers.

Model :  $H_3$

- o Mass of striker : 41.1 KG
- o Initial Velocity of Striker ;  
Distance between two  
Infra-red Switches : 110 MM
- Period : 95.1 MS.
- Initial Velocity( $V_o$ ) : 1.16 M/S.
- o Residual Strains

Strain Gauge Number	Residual Strain ( $\epsilon$ )
1	( -20 ) -26
2	( 0 ) 6
3	42
4	( 40 ) 62
5	( -10 ) -12
6	—
7	9
8	—
9	-1
10	-12

\* The strains in parentheses were measured with strain amplifiers.

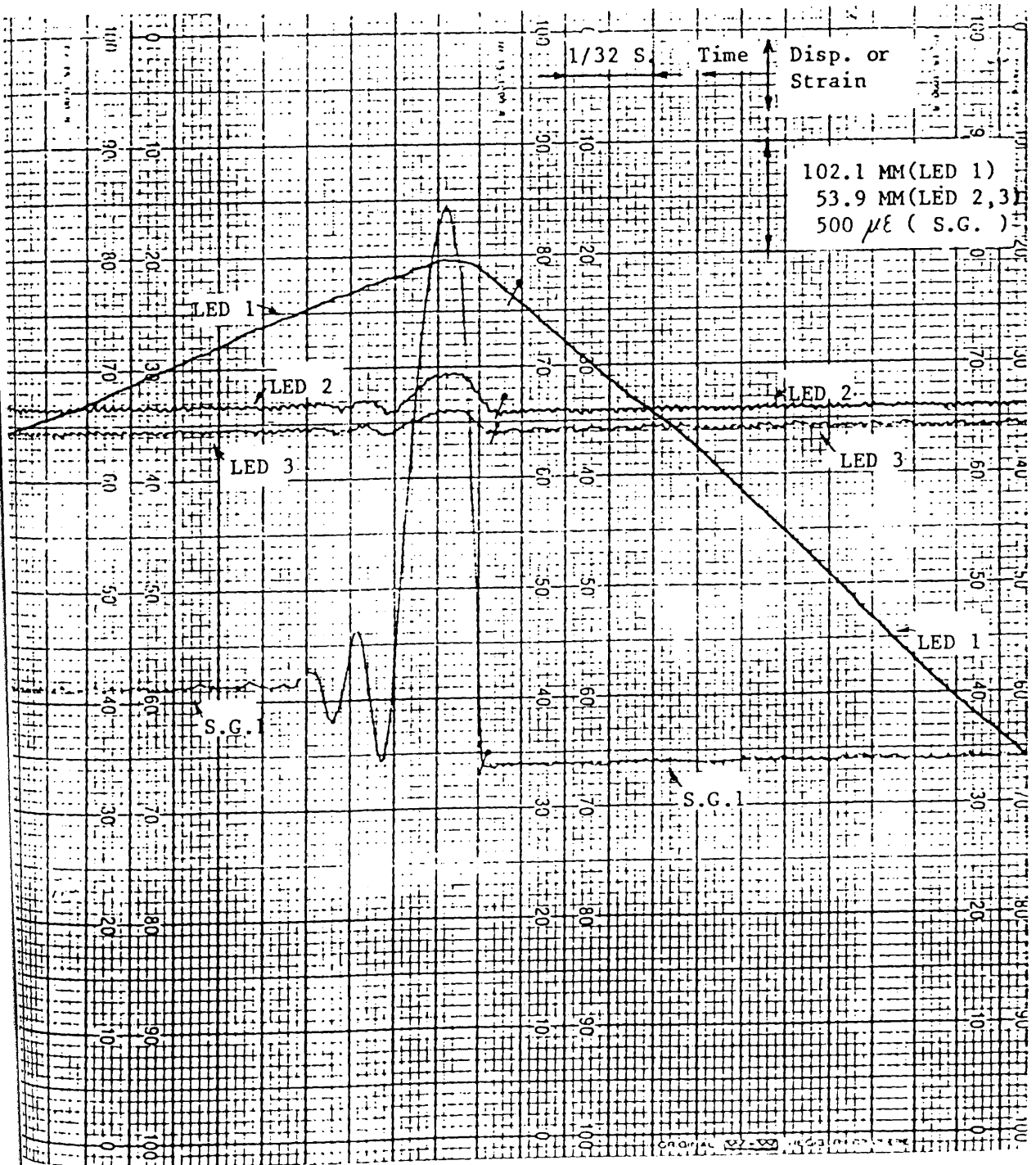


## **C. II    Dynamic Recording Results**

# DYNAMIC RECORDING RESULTS

MODEL :  $A_3$   
 LENGTH(L): 1400 MM  
 LENGTH for IMPACT TEST(Li): 1350 MM  
 OUTSIDE DIA.: 50.88 MM  
 THICKNESS : 1.20 MM

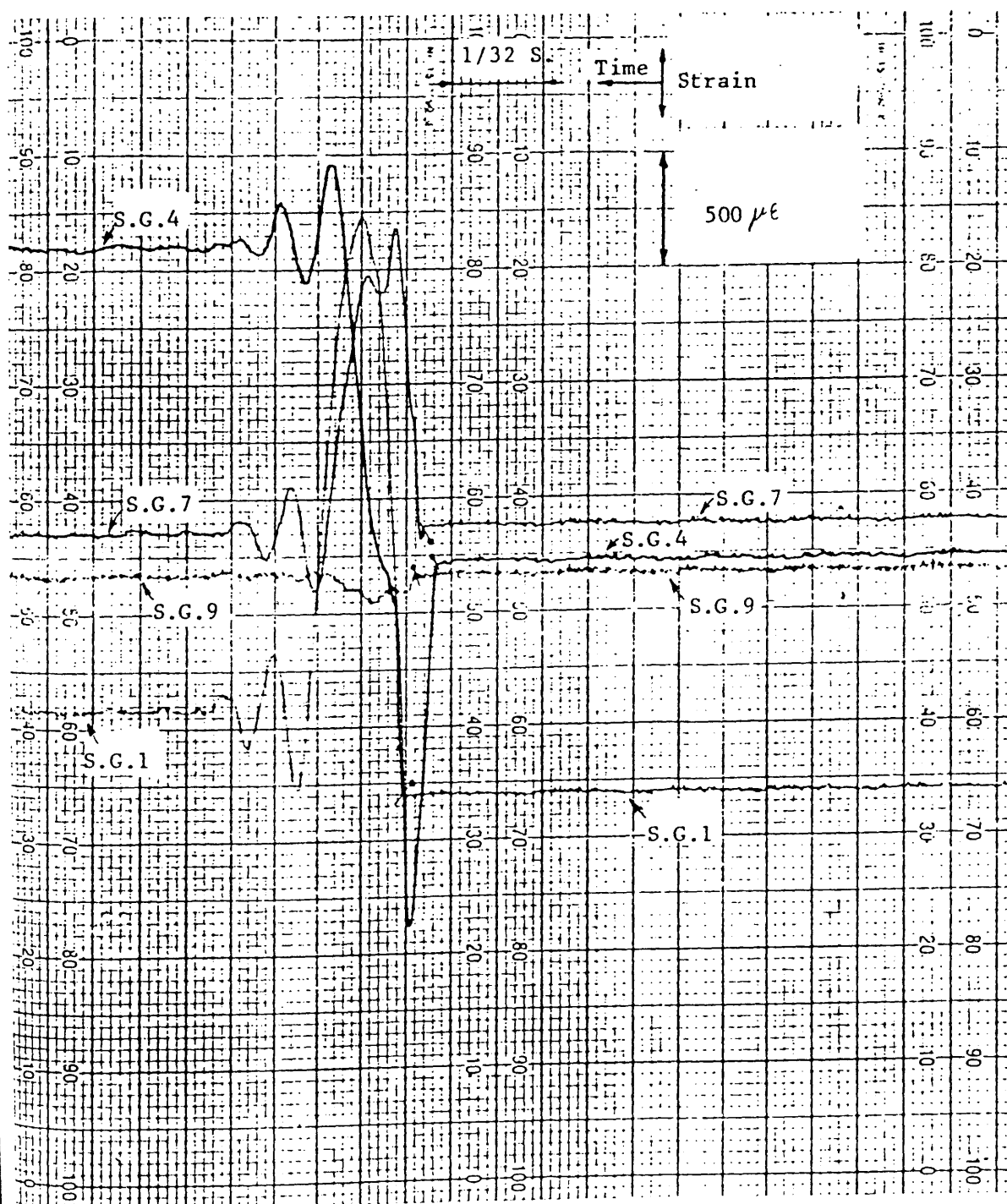
• denotes beginning of contact



DYNAMIC RECORDING RESULTS

MODEL : A<sub>3</sub>  
 LENGTH(L): 1400 MM  
 LENGTH for IMPACT TEST(L<sub>i</sub>): 1350 MM  
 OUTSIDE DIA.: 50.88 MM  
 THICKNESS : 1.20 MM

p denotes beginning of contact



DYNAMIC RECORDING RESULTSMODEL :  $A_4$ 

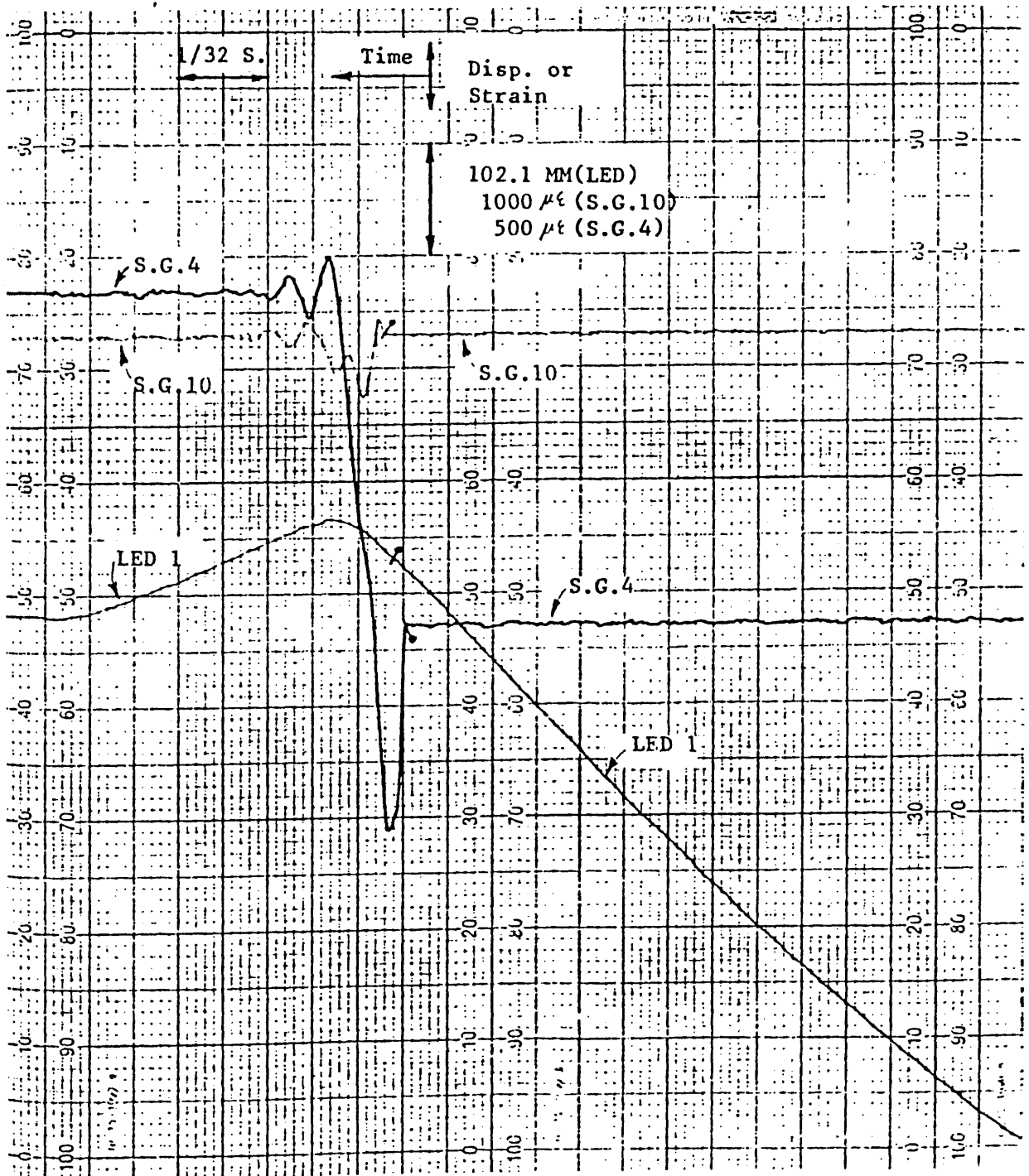
LENGTH(L): 1000 MM

LENGTH for IMPACT TEST(Li): 450 MM

OUTSIDE DIA.: 50.89 MM

THICKNESS : 1.20 MM

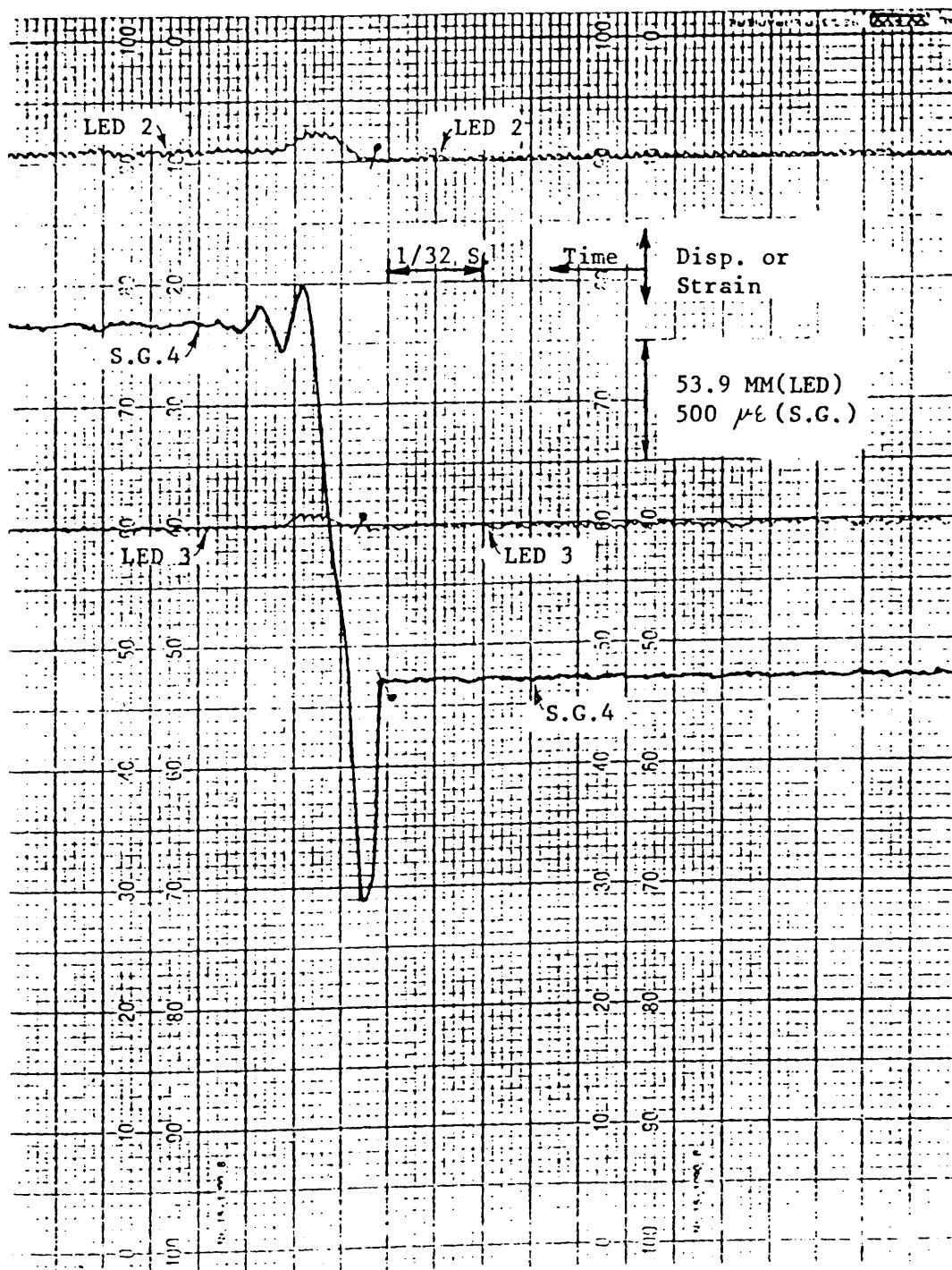
p denotes beginning of contact



DYNAMIC RECORDING RESULTS

MODEL : A<sub>4</sub>  
 LENGTH(L): 1000 MM  
 LENGTH for IMPACT TEST(L<sub>i</sub>): 950 MM  
 OUTSIDE DIA.: 50.89 MM  
 THICKNESS : 1.20 MM

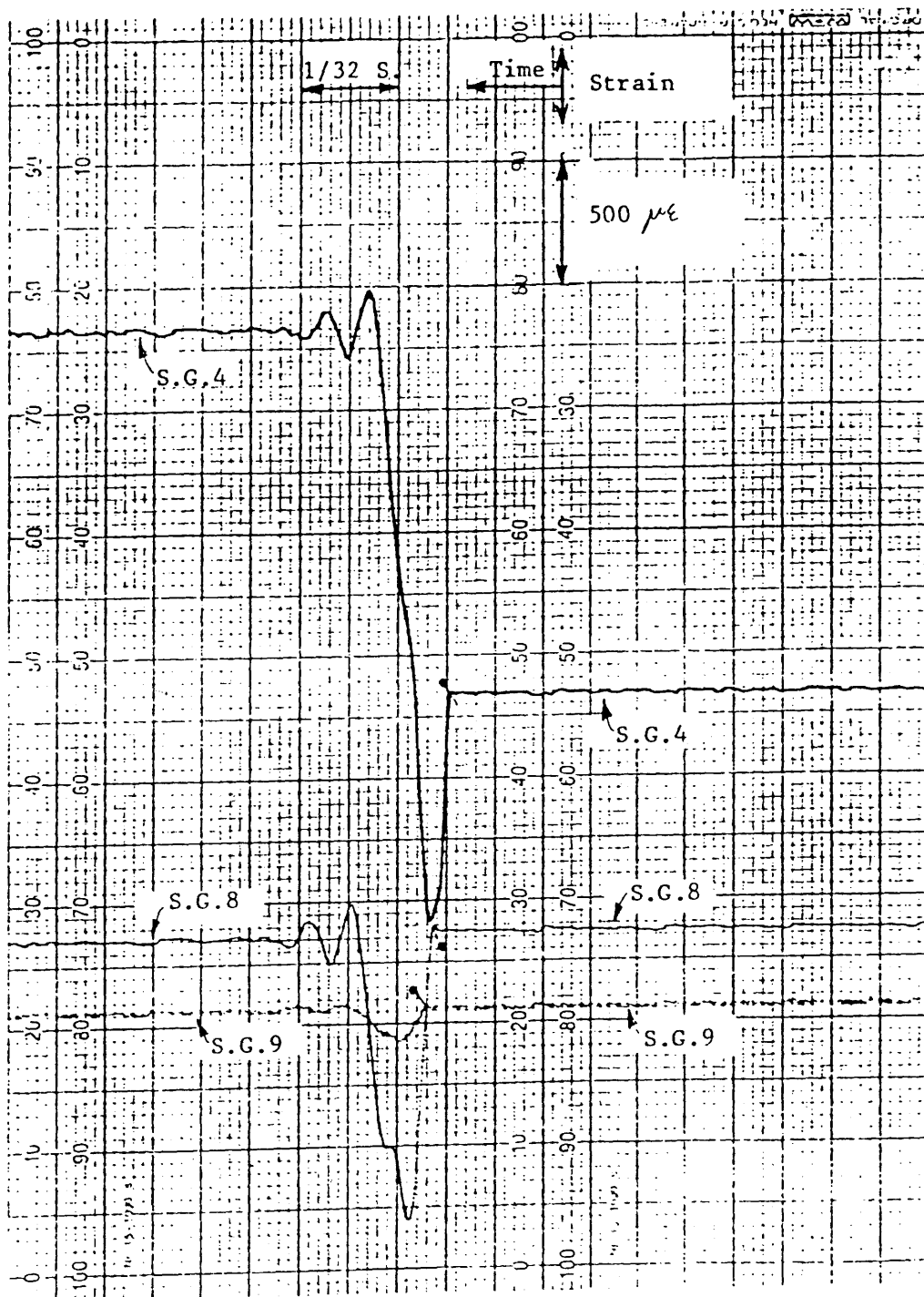
• denotes beginning of contact



DYNAMIC RECORDING RESULTS

MODEL : A4  
 LENGTH(L): 1000 MM  
 LENGTH for IMPACT TEST(Li): 950 MM  
 OUTSIDE DIA.: 50.89 MM  
 THICKNESS : 1.20 MM

• denotes beginning of contact





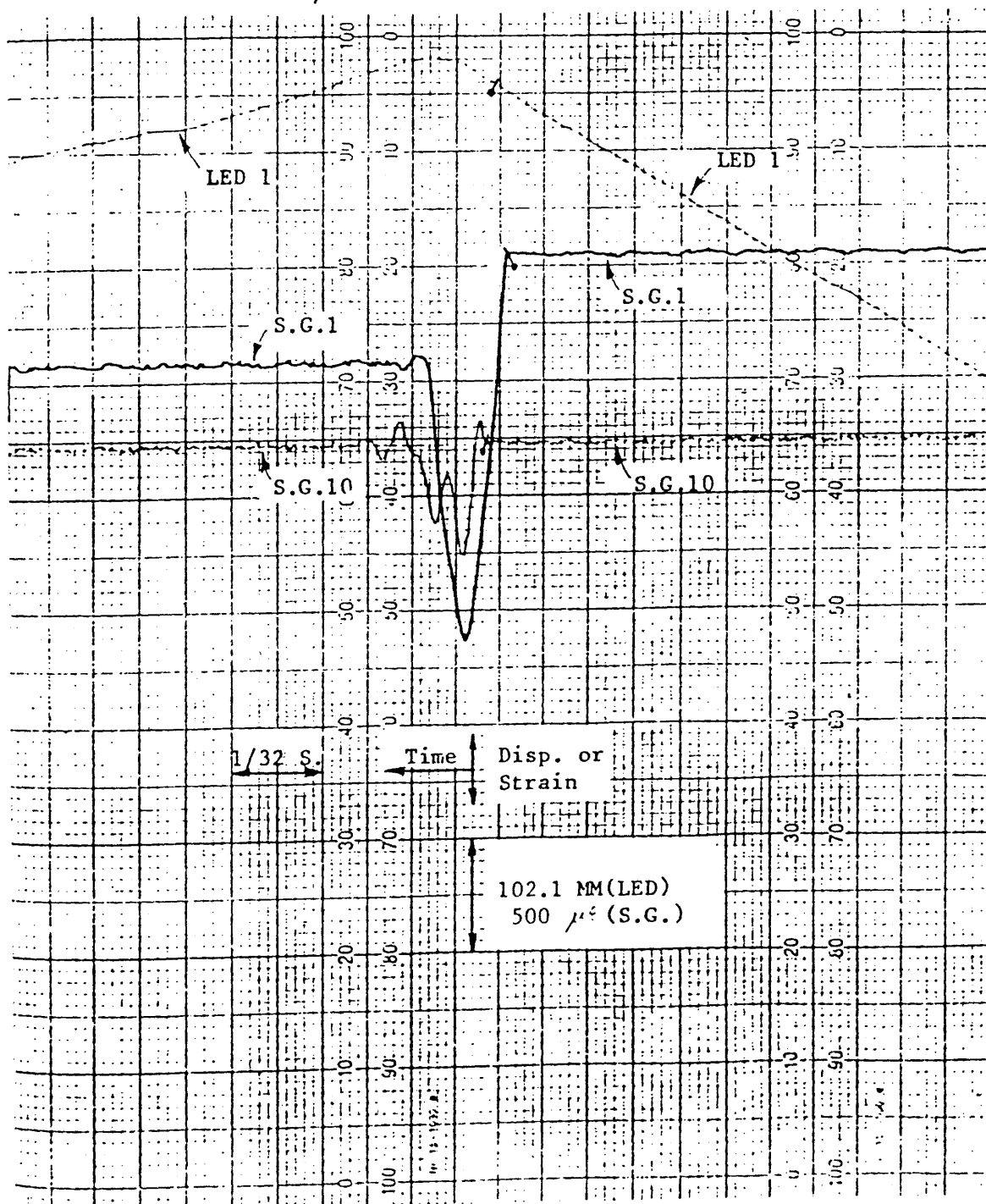




DYNAMIC RECORDING RESULTS

MODEL : B<sub>3</sub>  
 LENGTH(L): 1000 MM  
 LENGTH for IMPACT TEST(L<sub>i</sub>): 950 MM  
 OUTSIDE DIA.: 50.92 MM  
 THICKNESS : 1.20 MM

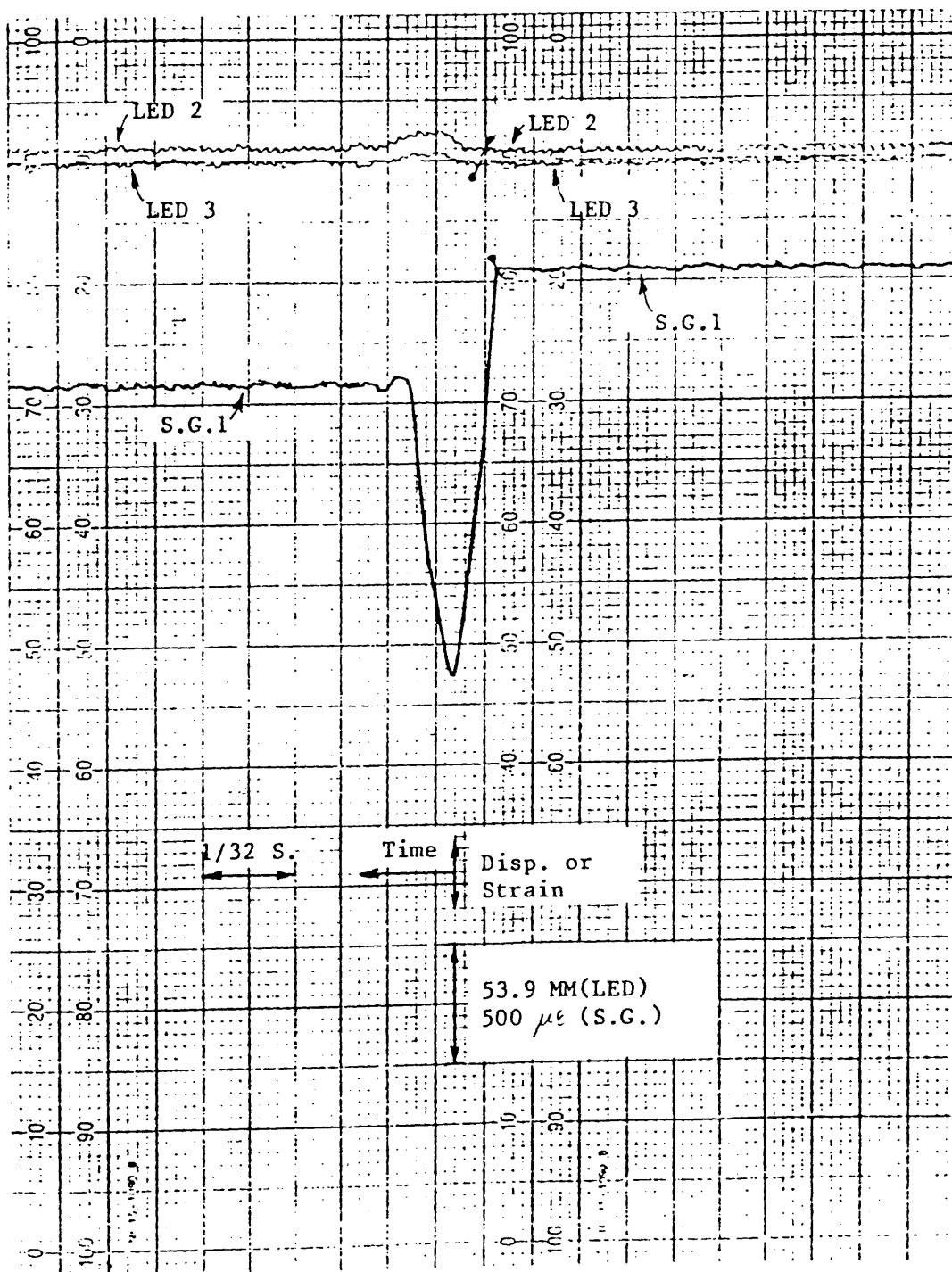
• denotes beginning of contact



DYNAMIC RECORDING RESULTS

MODEL : B<sub>3</sub>  
 LENGTH(L): 1000 MM  
 LENGTH for IMPACT TEST(L<sub>i</sub>): 950 MM  
 OUTSIDE DIA.: 50.92 MM  
 THICKNESS : 1.20 MM

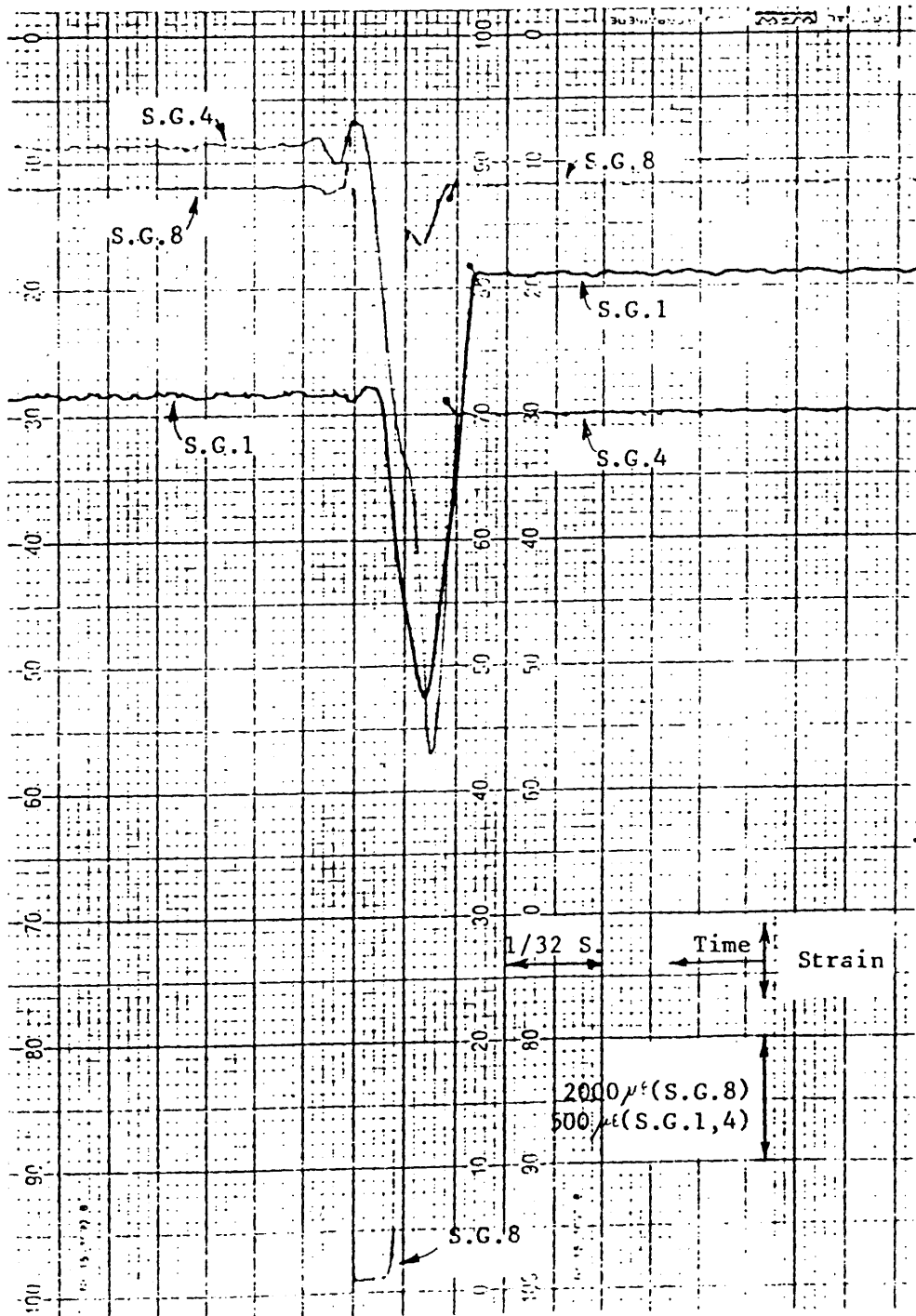
• denotes beginning of contact



DYNAMIC RECORDING RESULTS

MODEL : B<sub>3</sub>  
 LENGTH(L): 1000 MM  
 LENGTH for IMPACT TEST(L<sub>i</sub>): 950 MM  
 OUTSIDE DIA.: 50.92 MM  
 THICKNESS : 1.20 MM

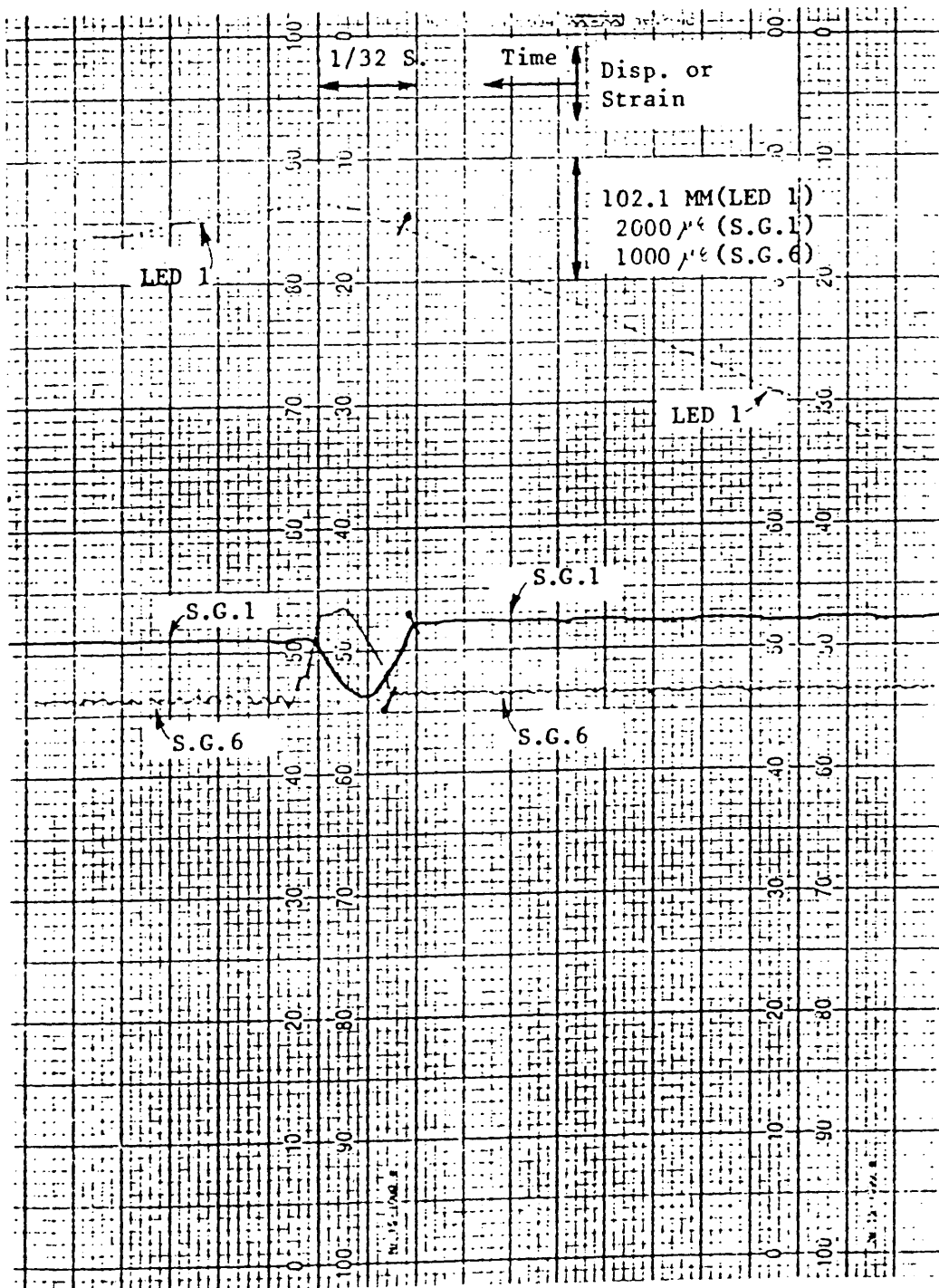
• denotes beginning of contact



DYNAMIC RECORDING RESULTS

MODEL :  $C_1$   
 LENGTH(L): 1000 MM  
 LENGTH for IMPACT TEST(Li): 950 MM  
 OUTSIDE DIA.: 50.97 MM  
 THICKNESS : 1.21 MM

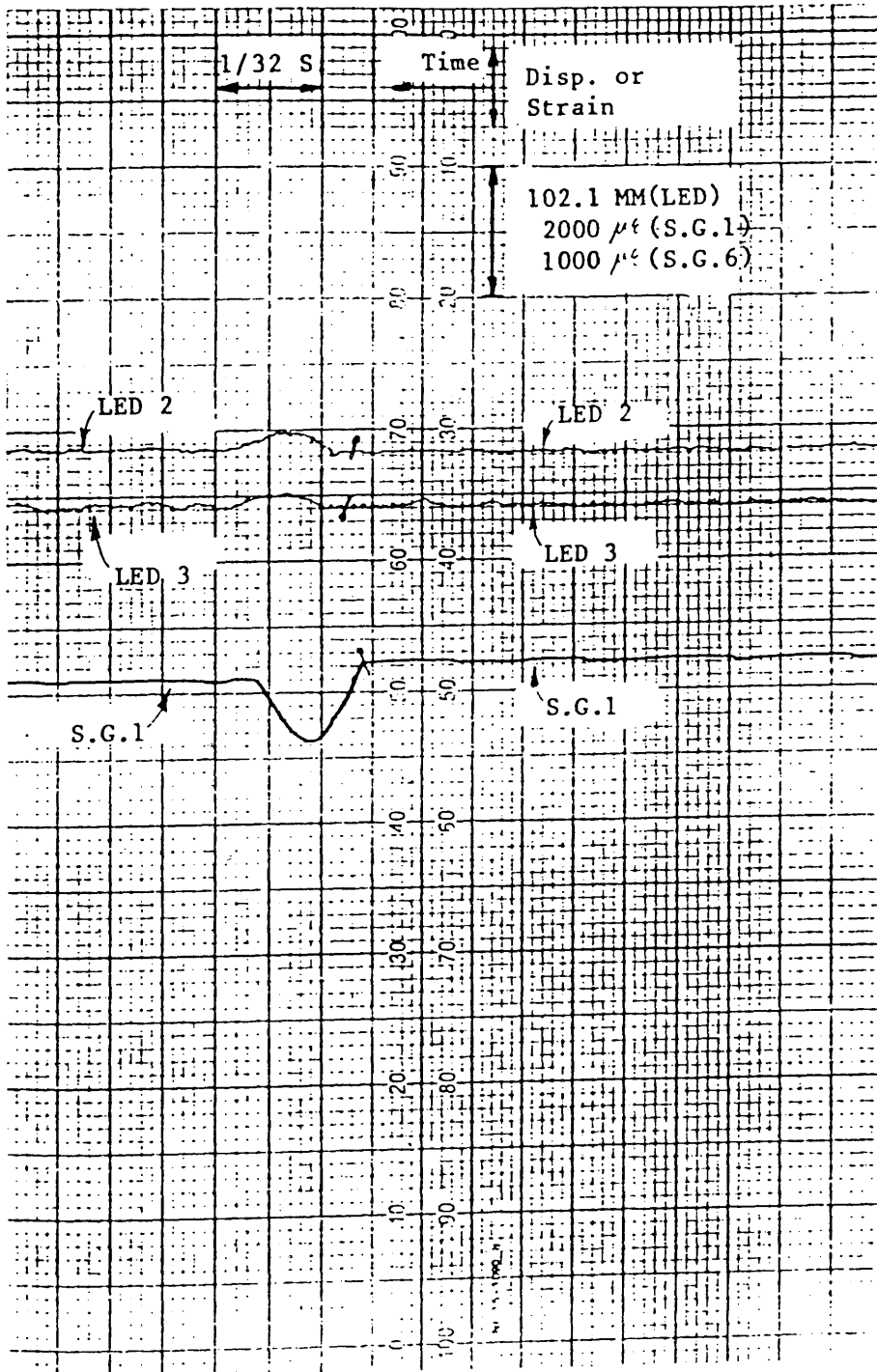
• denotes beginning of contact



DYNAMIC RECORDING RESULTS

MODEL : C<sub>1</sub>  
 LENGTH(L): 1000 MM  
 LENGTH for IMPACT TEST(L<sub>i</sub>): 950 MM  
 OUTSIDE DIA.: 50.97 MM  
 THICKNESS : 1.21 MM

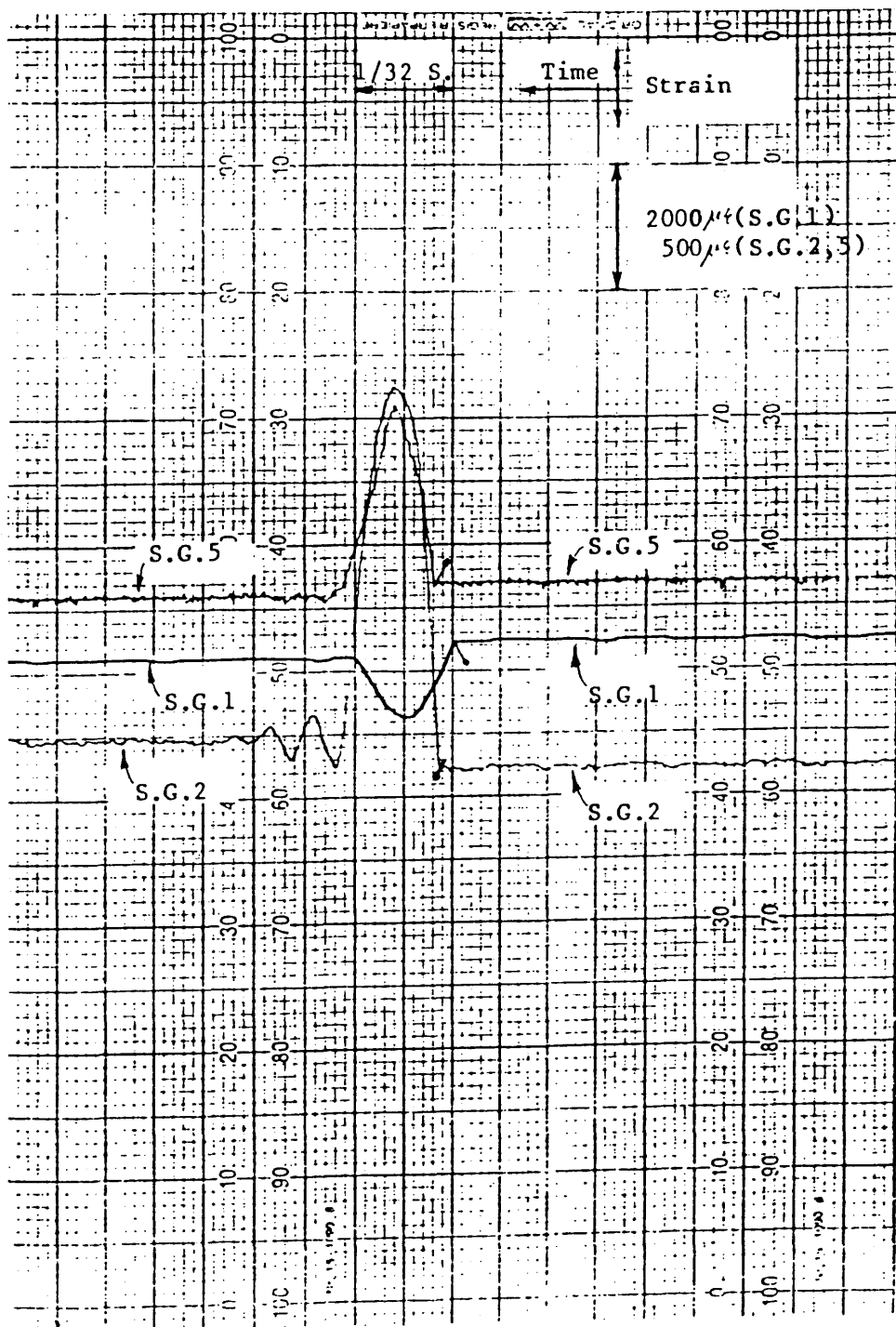
⌋ denotes beginning of contact



# DYNAMIC RECORDING RESULTS

MODEL :  $C_1$   
 LENGTH(L): 1000 MM  
 LENGTH for IMPACT TEST(L<sub>i</sub>): 950 MM  
 OUTSIDE DIA.: 50.97 MM  
 THICKNESS : 1.21 MM

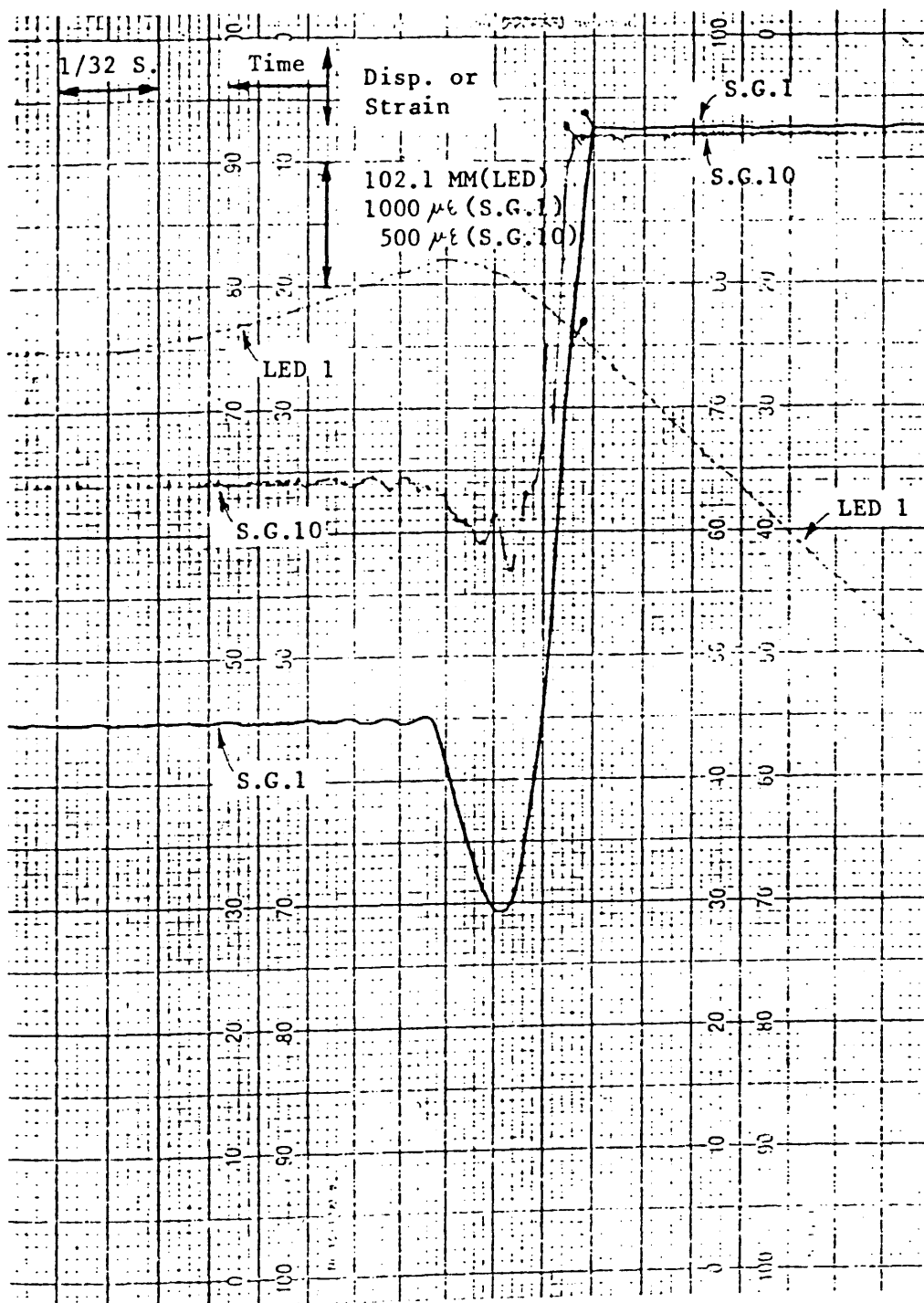
• denotes beginning of contact



DYNAMIC RECORDING RESULTS

MODEL : C2  
 LENGTH(L): 1000 MM  
 LENGTH for IMPACT TEST(Li): 950 MM  
 OUTSIDE DIA.: 50.91 MM  
 THICKNESS : 1.22 MM

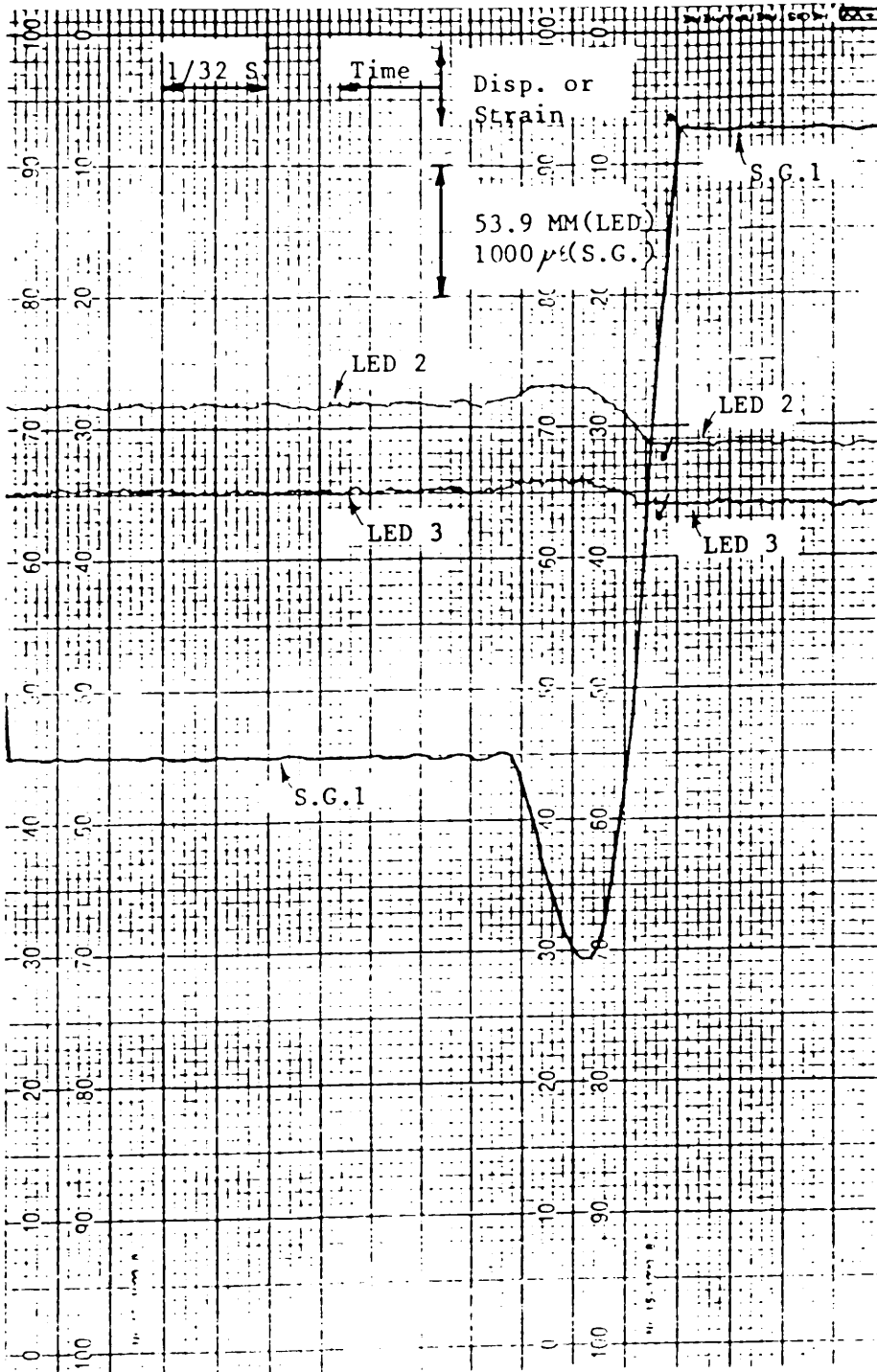
• denotes beginning of contact



# DYNAMIC RECORDING RESULTS

MODEL : C2  
 LENGTH(L): 1000 MM  
 LENGTH for IMPACT TEST(Li): 950 MM  
 OUTSIDE DIA.: 50.91 MM  
 THICKNESS : 1.22 MM

• denotes beginning of contact





DYNAMIC RECORDING RESULTSMODEL : C<sub>2</sub>

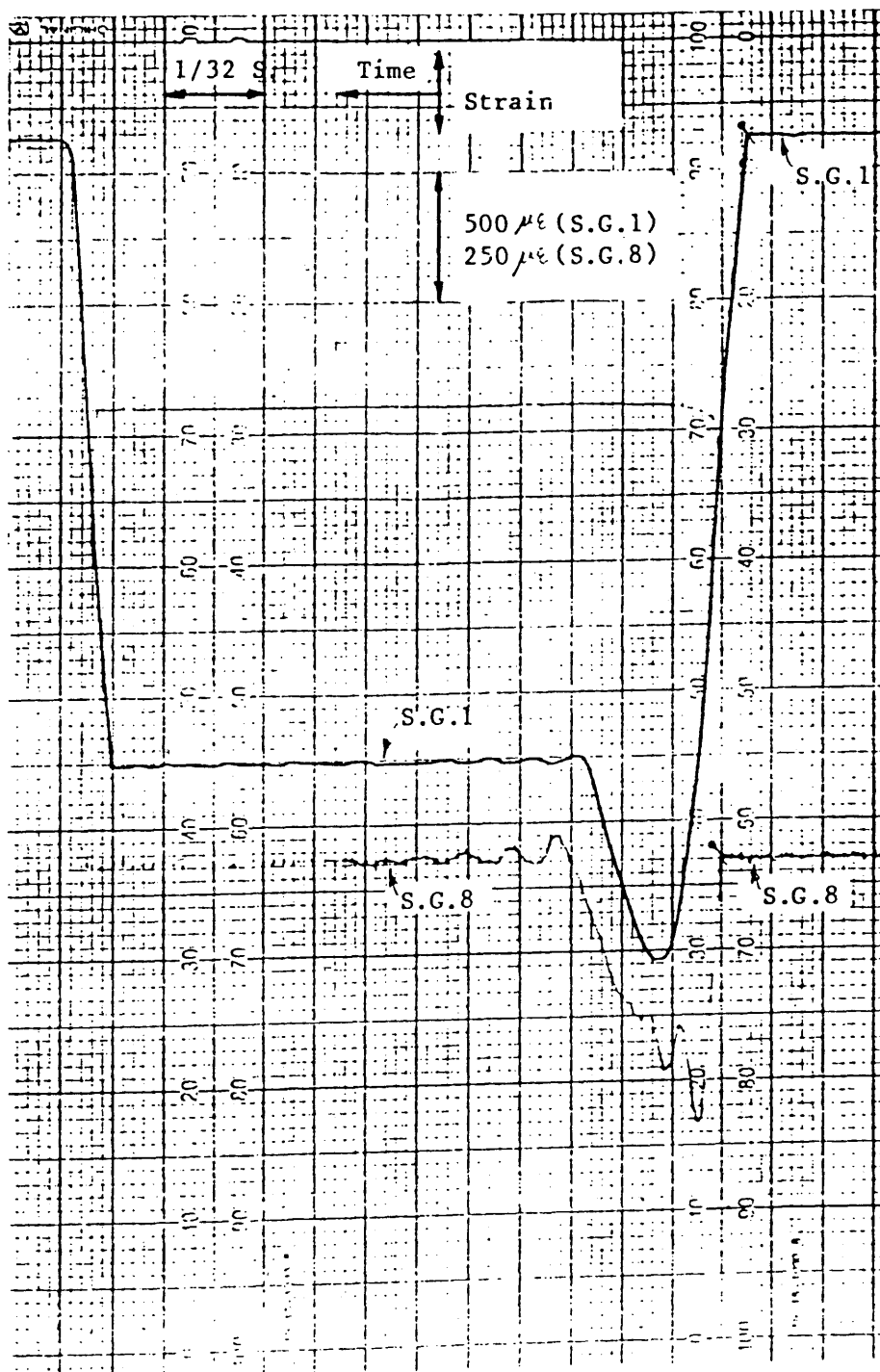
LENGTH(L): 1000 MM

LENGTH for IMPACT TEST(L<sub>i</sub>): 950 MM

OUTSIDE DIA.: 50.91 MM

THICKNESS : 1.22 MM

p denotes beginning of contact



DYNAMIC RECORDING RESULTSMODEL : C<sub>3</sub>

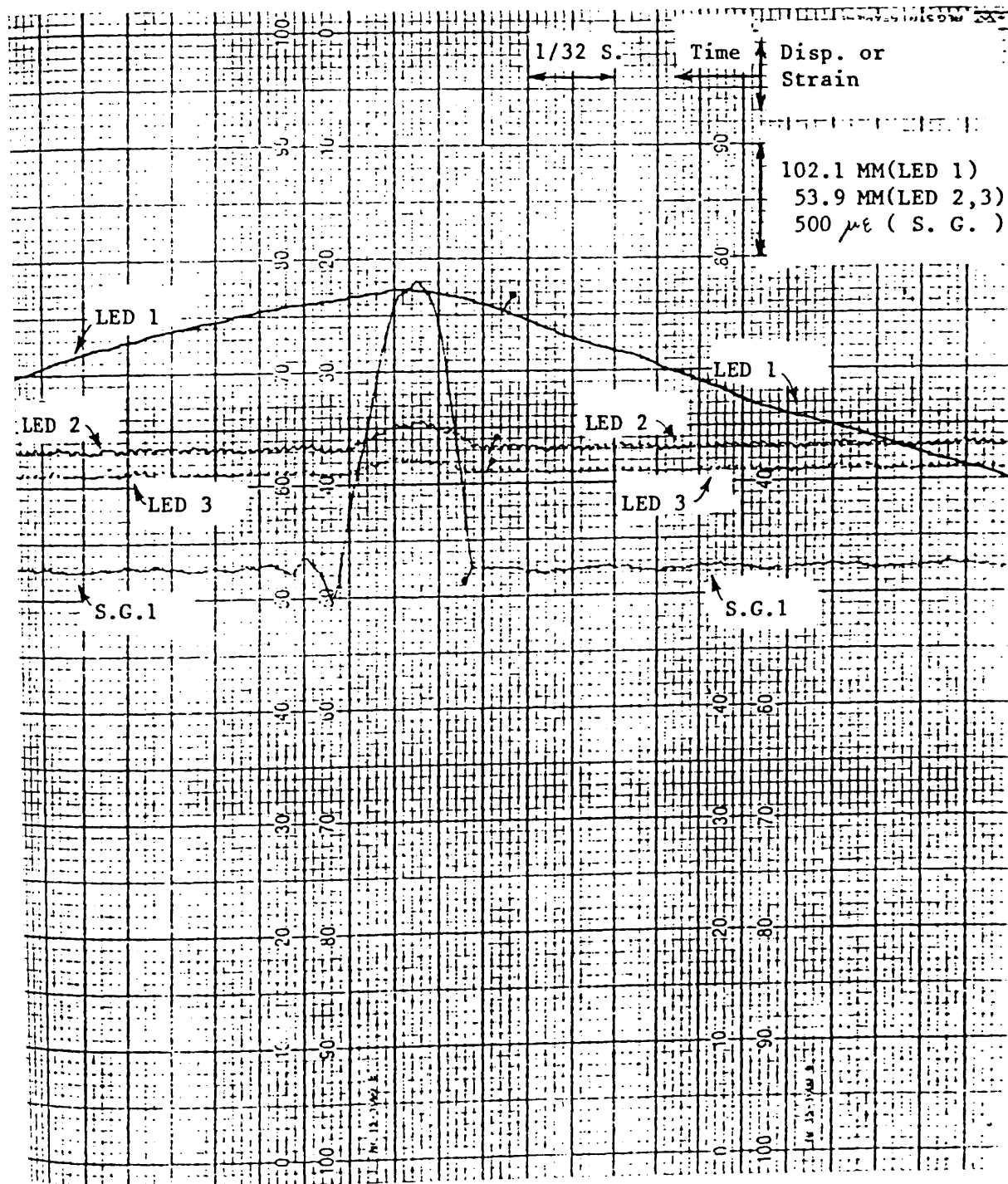
LENGTH(L): 1400 MM

LENGTH for IMPACT TEST(L<sub>i</sub>): 1350 MM

OUTSIDE DIA.: 50.86 MM

THICKNESS : 1.22 MM

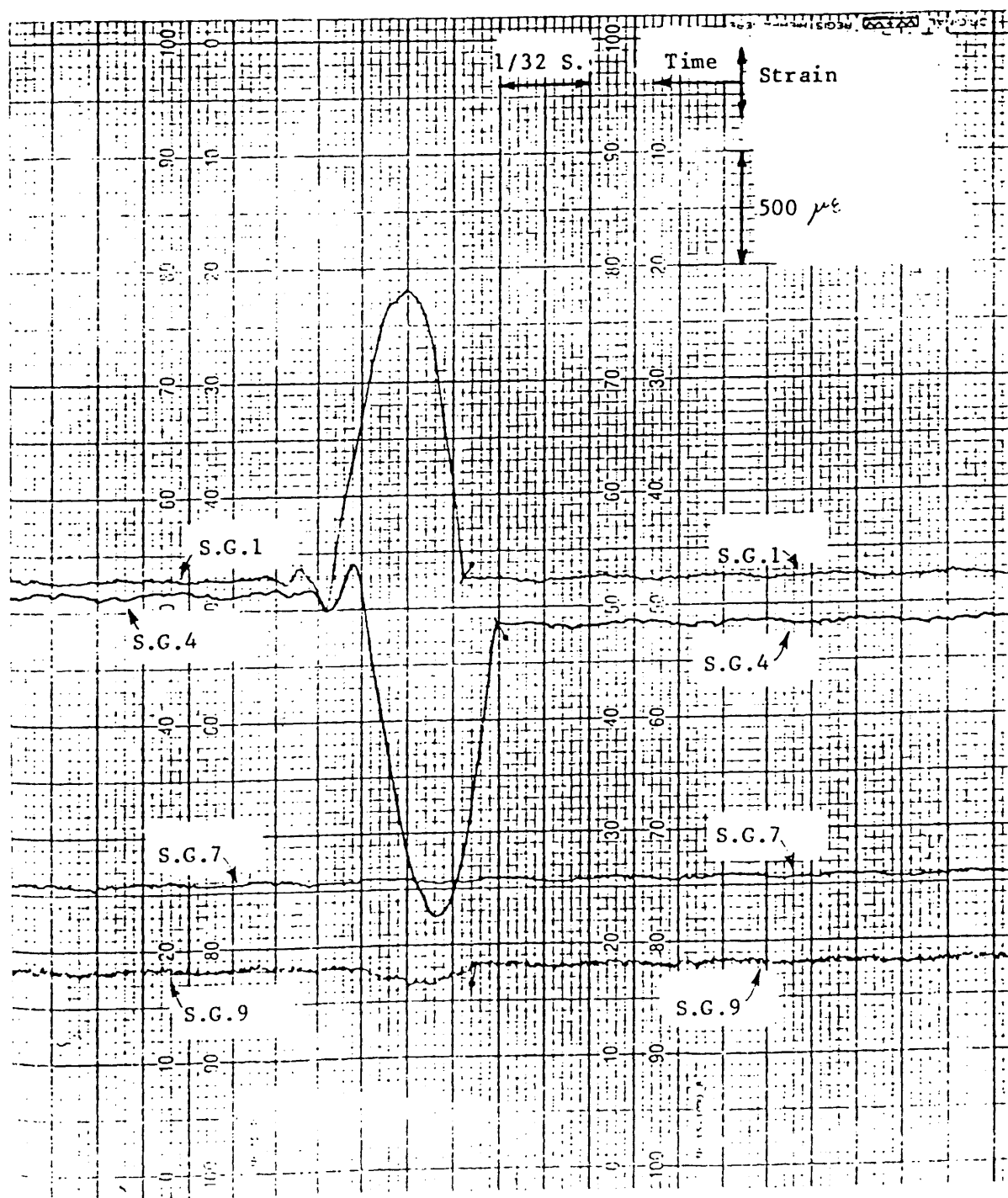
p denotes beginning of contact



DYNAMIC RECORDING RESULTS

MODEL : C<sub>3</sub>  
 LENGTH(L): 1400 MM  
 LENGTH for IMPACT TEST(L<sub>i</sub>): 1350 MM  
 OUTSIDE DIA.: 50.86 MM  
 THICKNESS : 1.22 MM

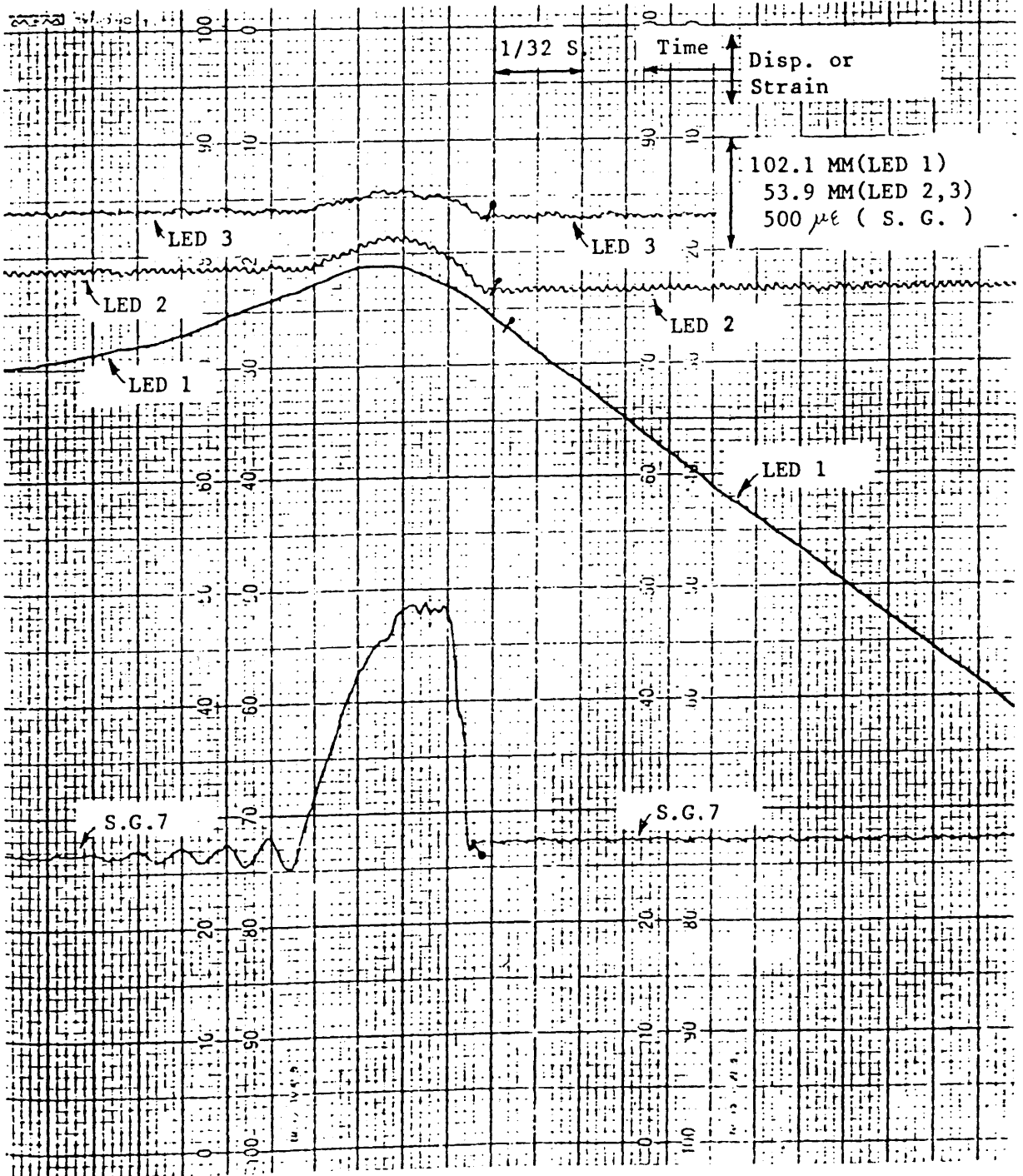
• denotes beginning of contact



DYNAMIC RECORDING RESULTS

MODEL : C4  
 LENGTH(L): 1400 MM  
 LENGTH for IMPACT TEST(Li): 1350 MM  
 OUTSIDE DIA.: 50.85 MM  
 THICKNESS : 1.22 MM

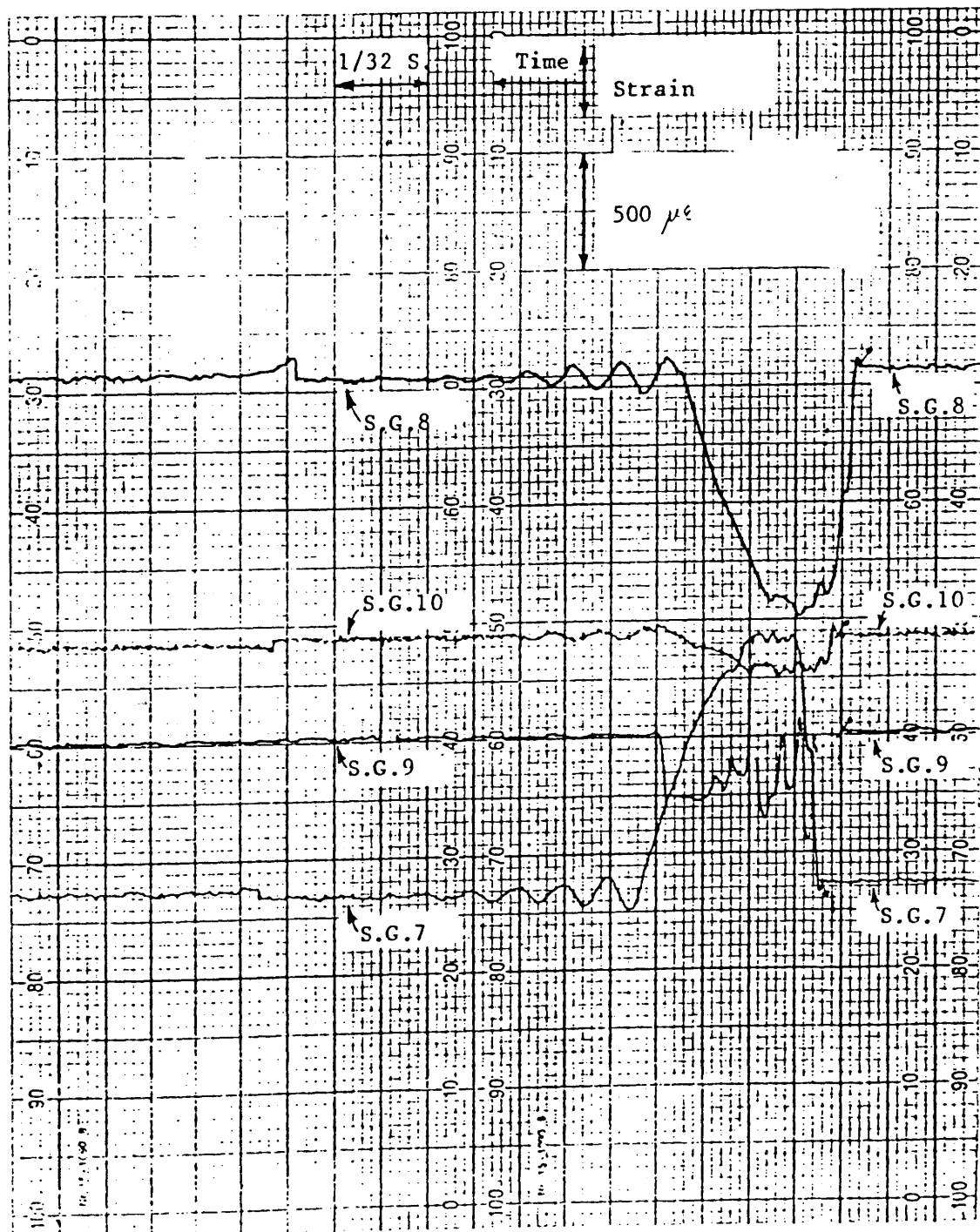
• denotes beginning of contact



DYNAMIC RECORDING RESULTS

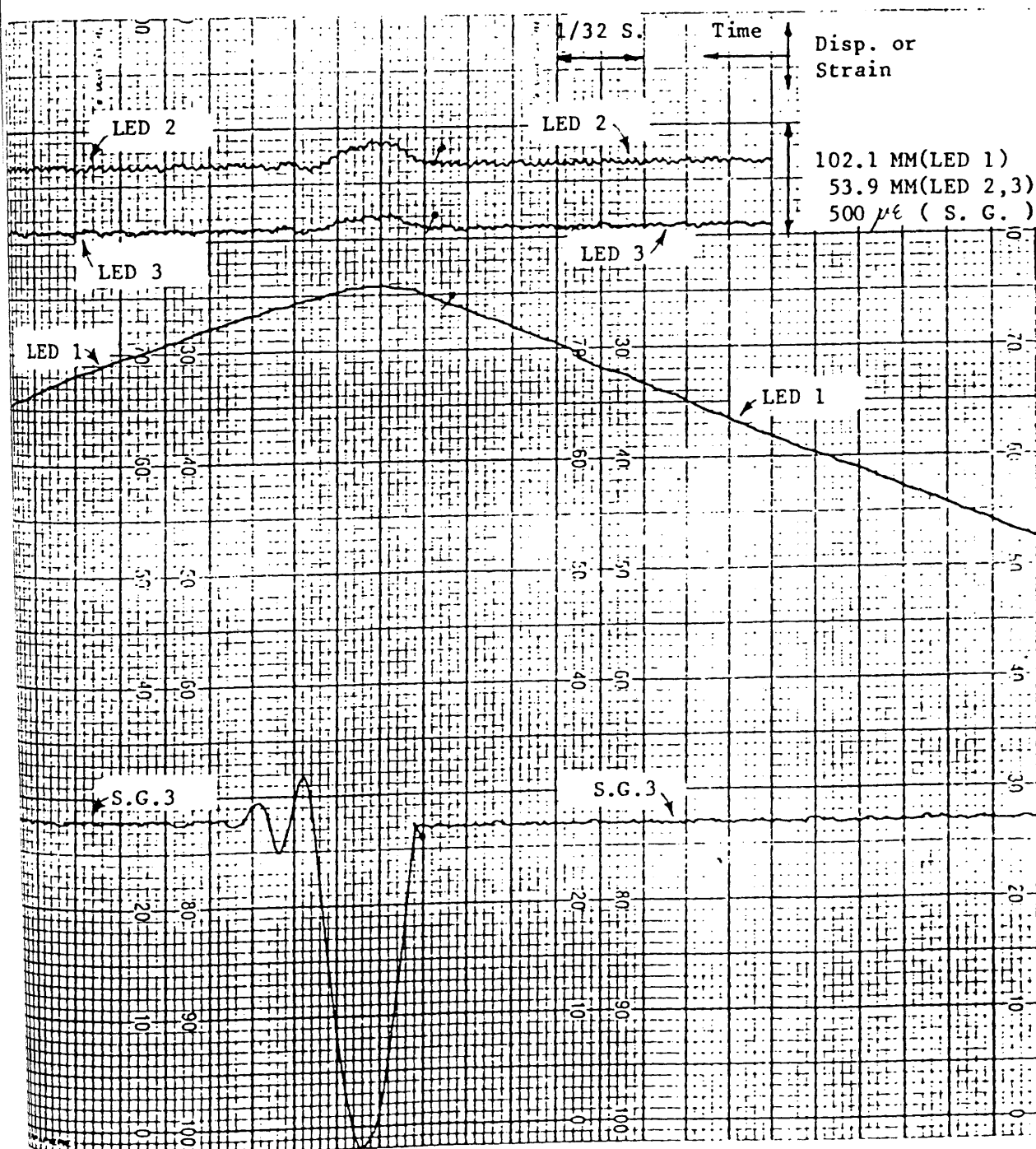
MODEL : C4  
 LENGTH(L): 1400 MM  
 LENGTH for IMPACT TEST(Li): 1350 MM  
 OUTSIDE DIA.: 50.85 MM  
 THICKNESS : 1.22 MM

↗ denotes beginning of contact



DYNAMIC RECORDING RESULTSMODEL : *D1*LENGTH(L): *1400* MMLENGTH for IMPACT TEST(Li): *1350* MMOUTSIDE DIA.: *50.91* MMTHICKNESS : *1.20* MM

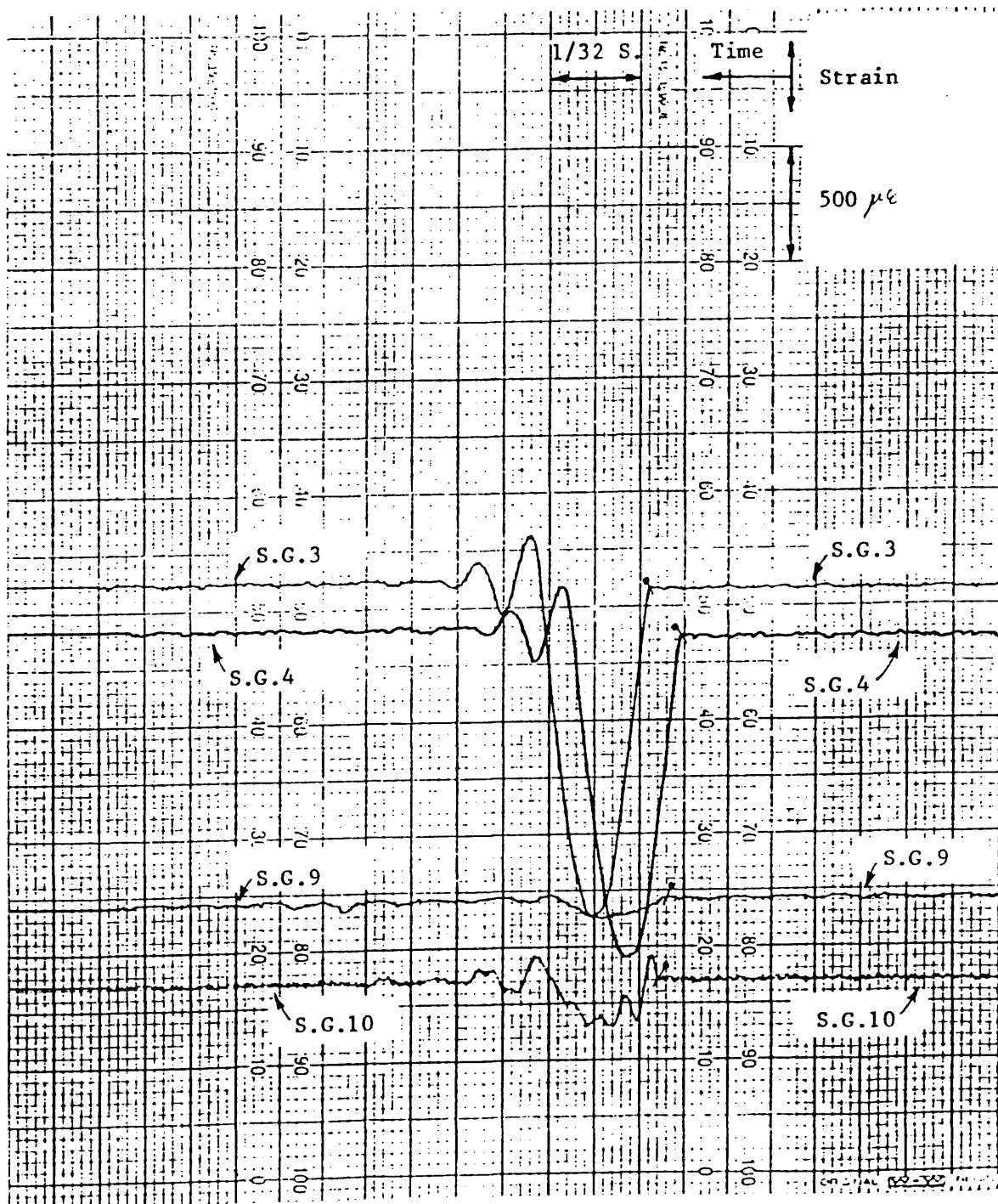
/ denotes beginning of contact



DYNAMIC RECORDING RESULTS

MODEL : *D<sub>1</sub>*  
 LENGTH(L): *1400* MM  
 LENGTH for IMPACT TEST(L<sub>i</sub>): *1350* MM  
 OUTSIDE DIA.: *50.91* MM  
 THICKNESS : *1.20* MM

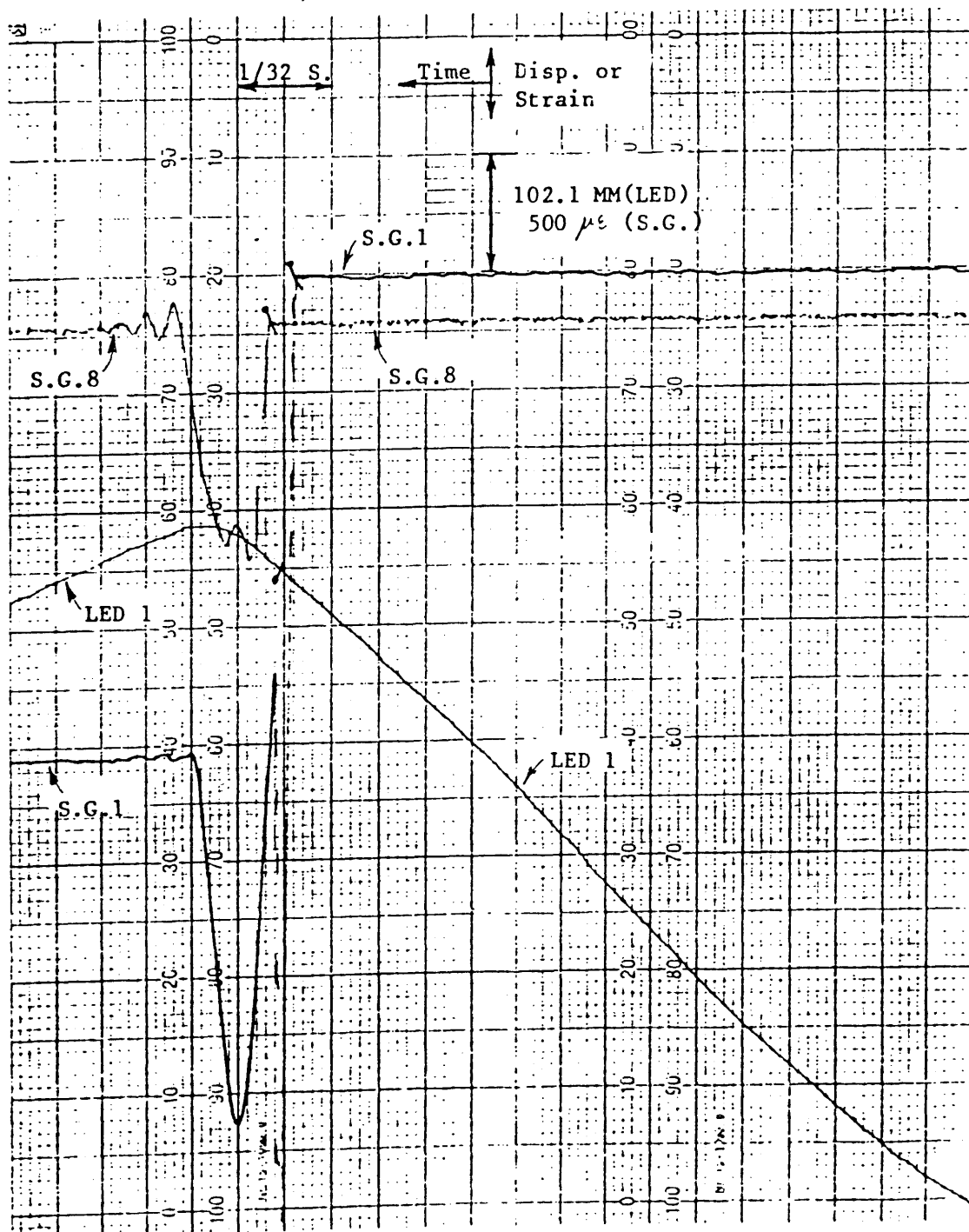
• denotes beginning of contact



DYNAMIC RECORDING RESULTS

MODEL :  $D_2$   
 LENGTH(L): 1000 MM  
 LENGTH for IMPACT TEST(Li): 950 MM  
 OUTSIDE DIA.: 50.98 MM  
 THICKNESS : 1.21 MM

• denotes beginning of contact

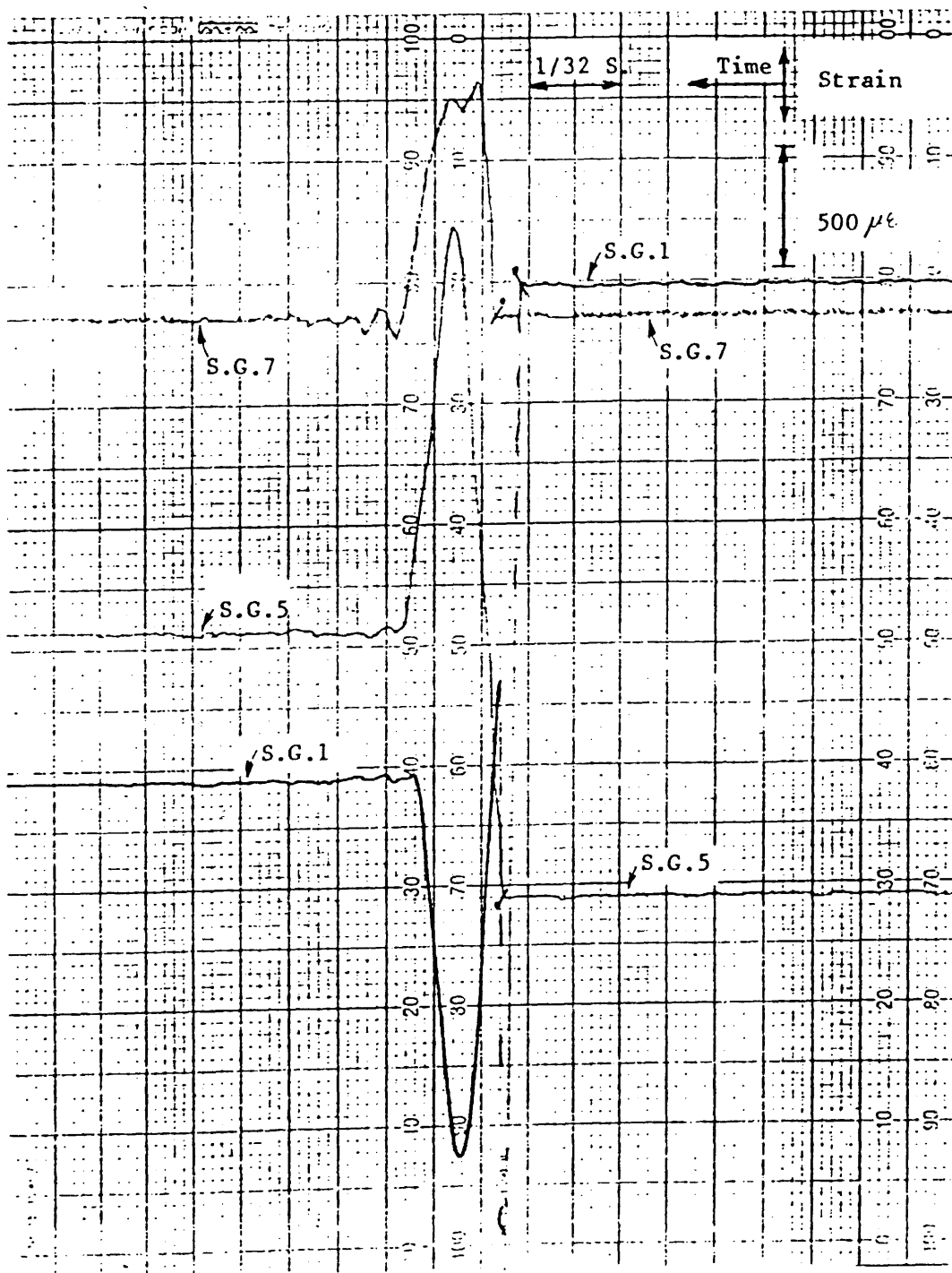




DYNAMIC RECORDING RESULTS

MODEL :  $D_2$   
 LENGTH(L): 1000 MM  
 LENGTH for IMPACT TEST(L<sub>i</sub>): 950 MM  
 OUTSIDE DIA.: 50.98 MM  
 THICKNESS : 1.21 MM

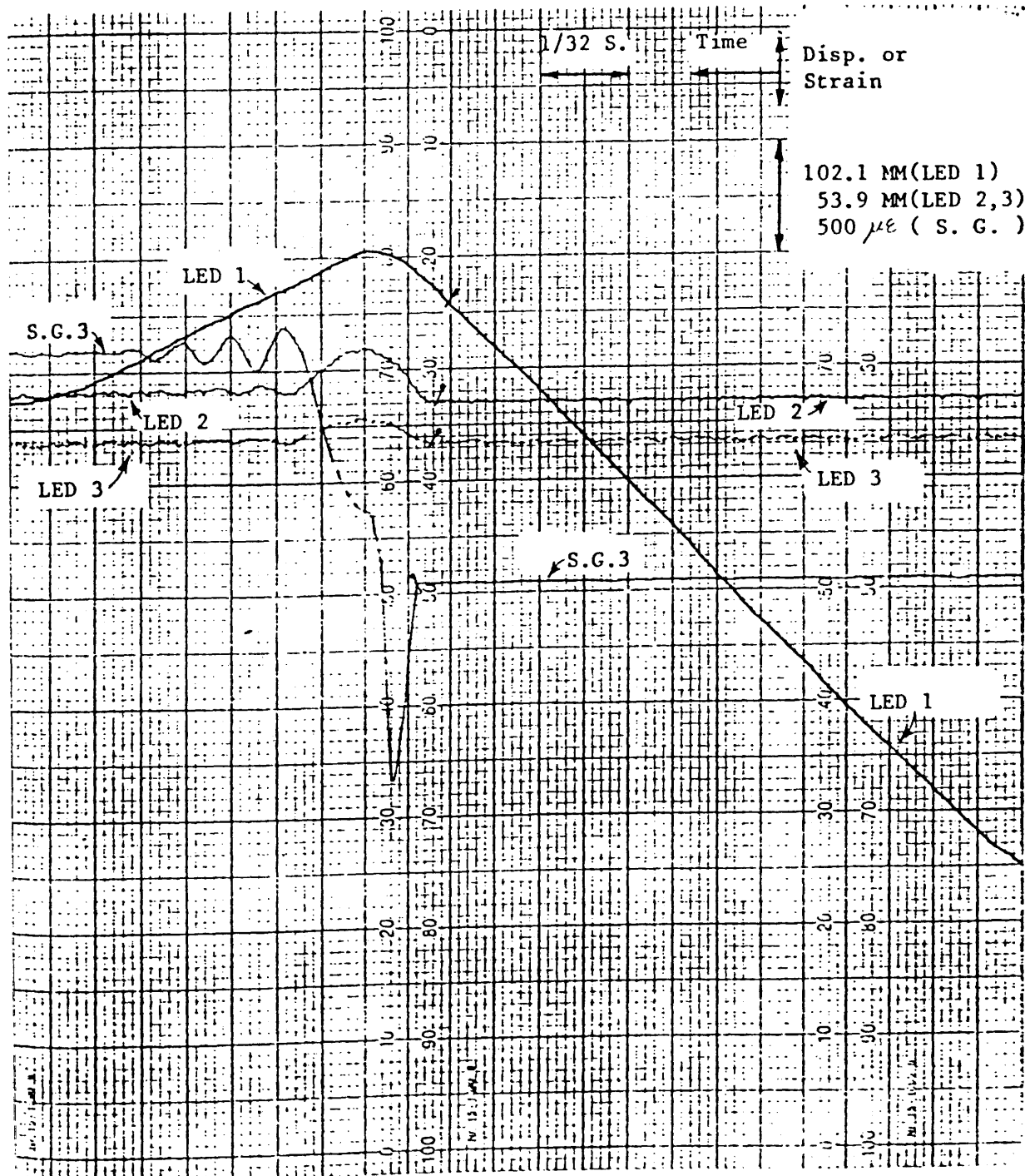
↗ denotes beginning of contact



DYNAMIC RECORDING RESULTS

MODEL :  $D_3$   
 LENGTH(L): 1400 MM  
 LENGTH for IMPACT TEST(L<sub>i</sub>): 1350 MM  
 OUTSIDE DIA.: 50.91 MM  
 THICKNESS : 1.21 MM

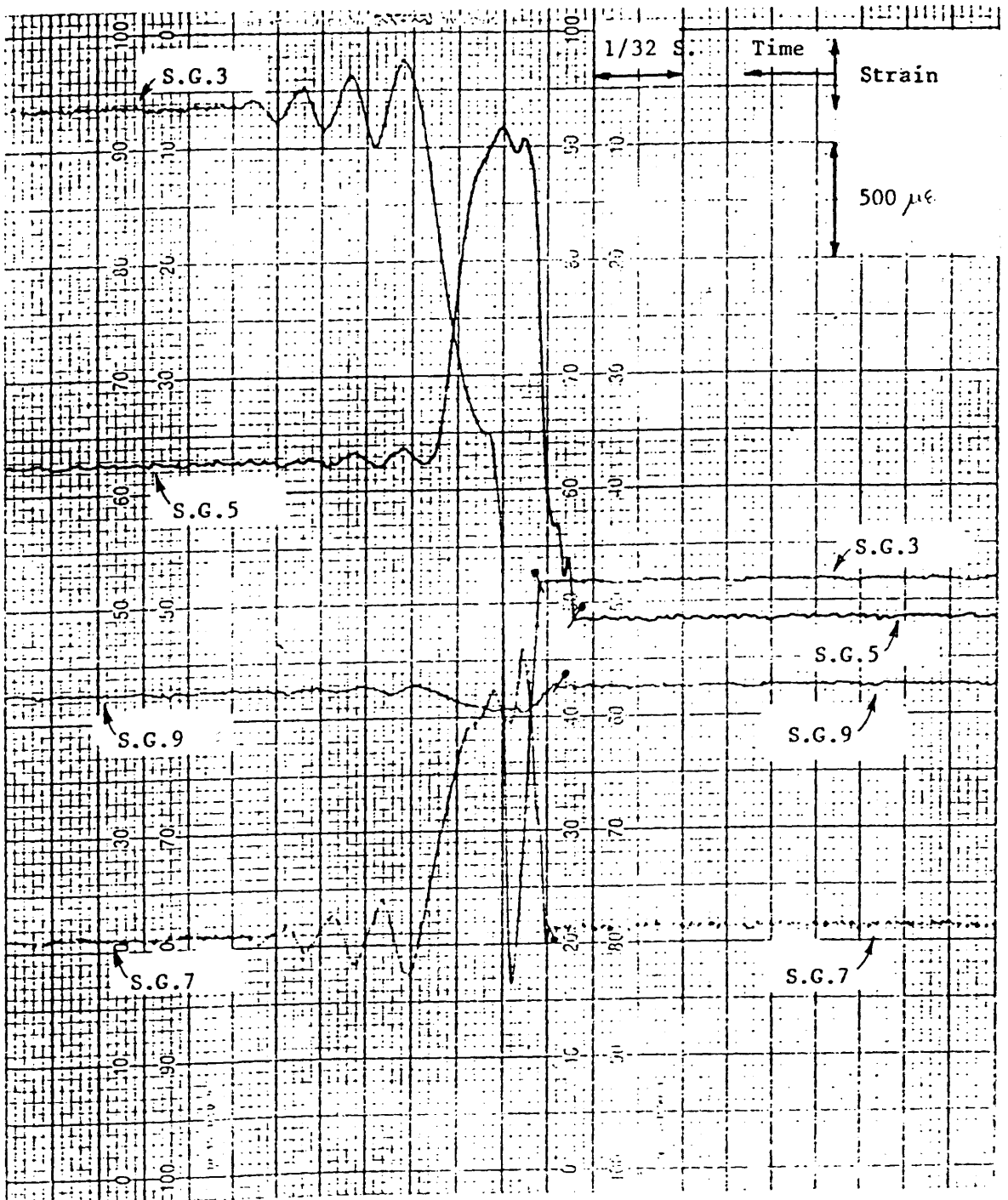
• denotes beginning of contact



DYNAMIC RECORDING RESULTS

MODEL :  $D_3$   
 LENGTH(L): 1400 MM  
 LENGTH for IMPACT TEST(Li): 1350 MM  
 OUTSIDE DIA.: 50.91 MM  
 THICKNESS : 1.21 MM

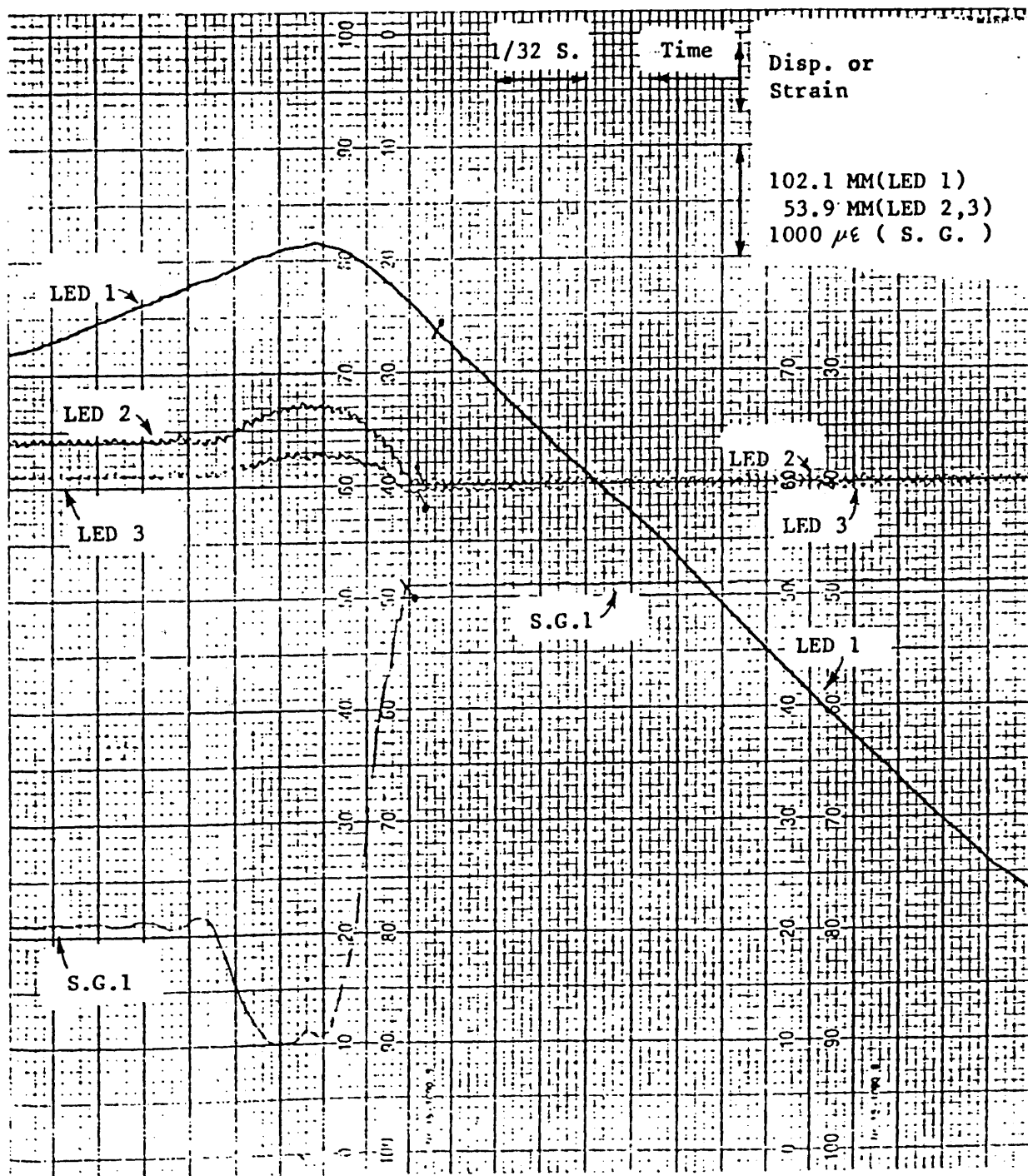
• denotes beginning of contact



DYNAMIC RECORDING RESULTS

MODEL : D4  
 LENGTH(L): 1400 MM  
 LENGTH for IMPACT TEST(Li): 1350 MM  
 OUTSIDE DIA.: 50.90 MM  
 THICKNESS : 1.21 MM

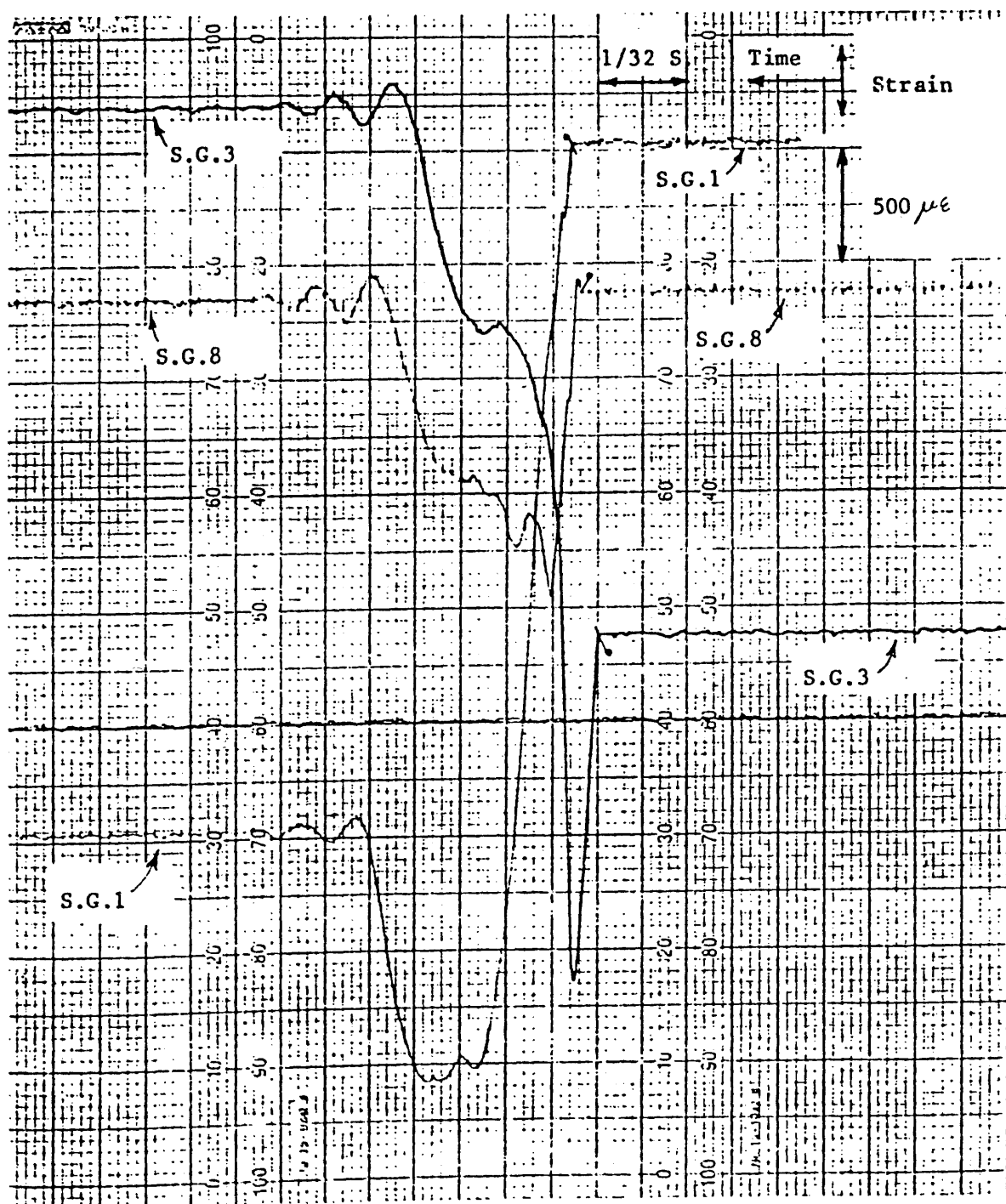
p denotes beginning of contact



DYNAMIC RECORDING RESULTS

MODEL : D4  
 LENGTH(L): 1400 MM  
 LENGTH for IMPACT TEST(Li): 1350 MM  
 OUTSIDE DIA.: 50.90 MM  
 THICKNESS : 1.21 MM

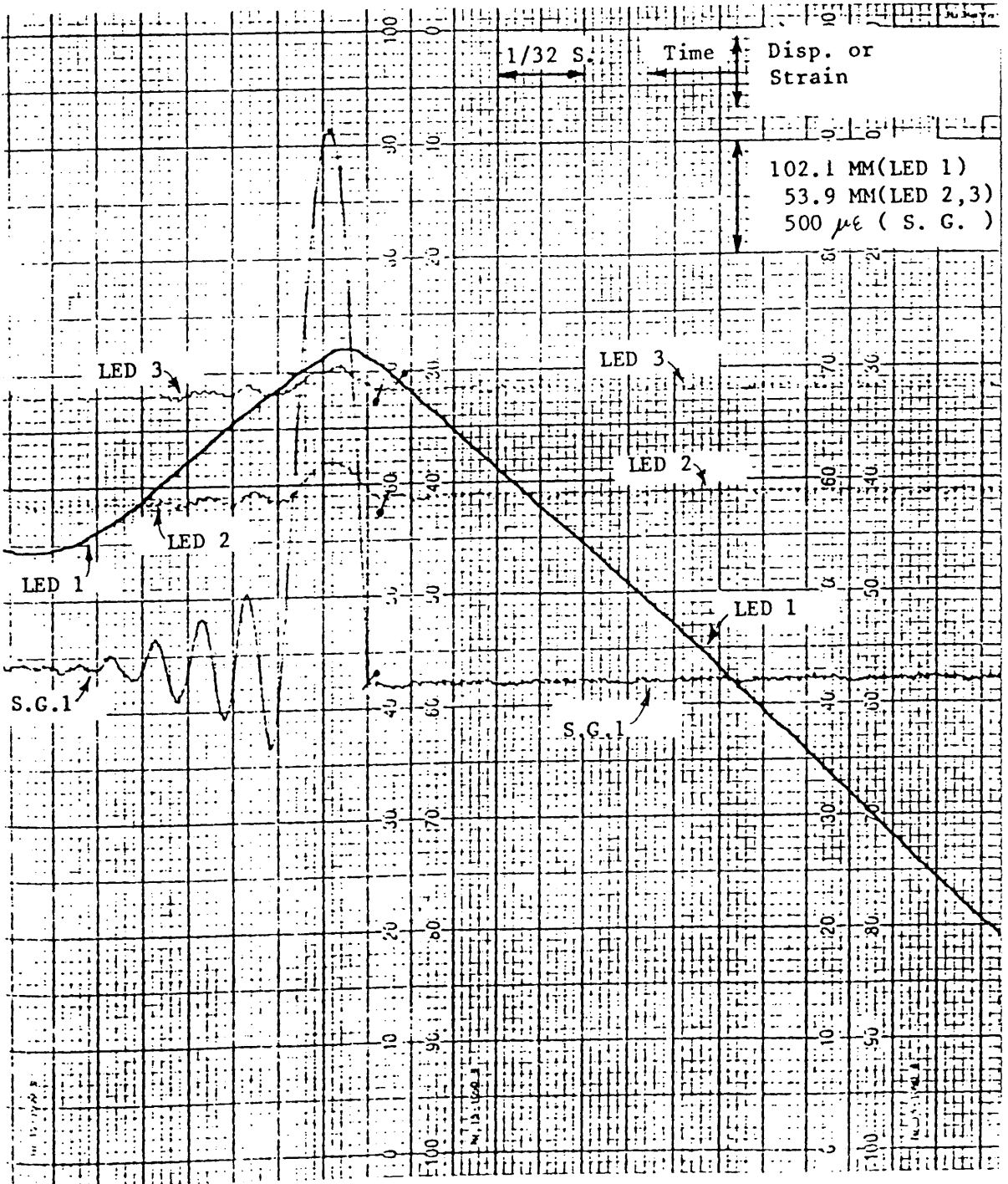
• denotes beginning of contact



# DYNAMIC RECORDING RESULTS

MODEL :  $E_3$   
 LENGTH(L): 1400 MM  
 LENGTH for IMPACT TEST(Li): 1350 MM  
 OUTSIDE DIA.: 50.91 MM  
 THICKNESS : 2.05 MM

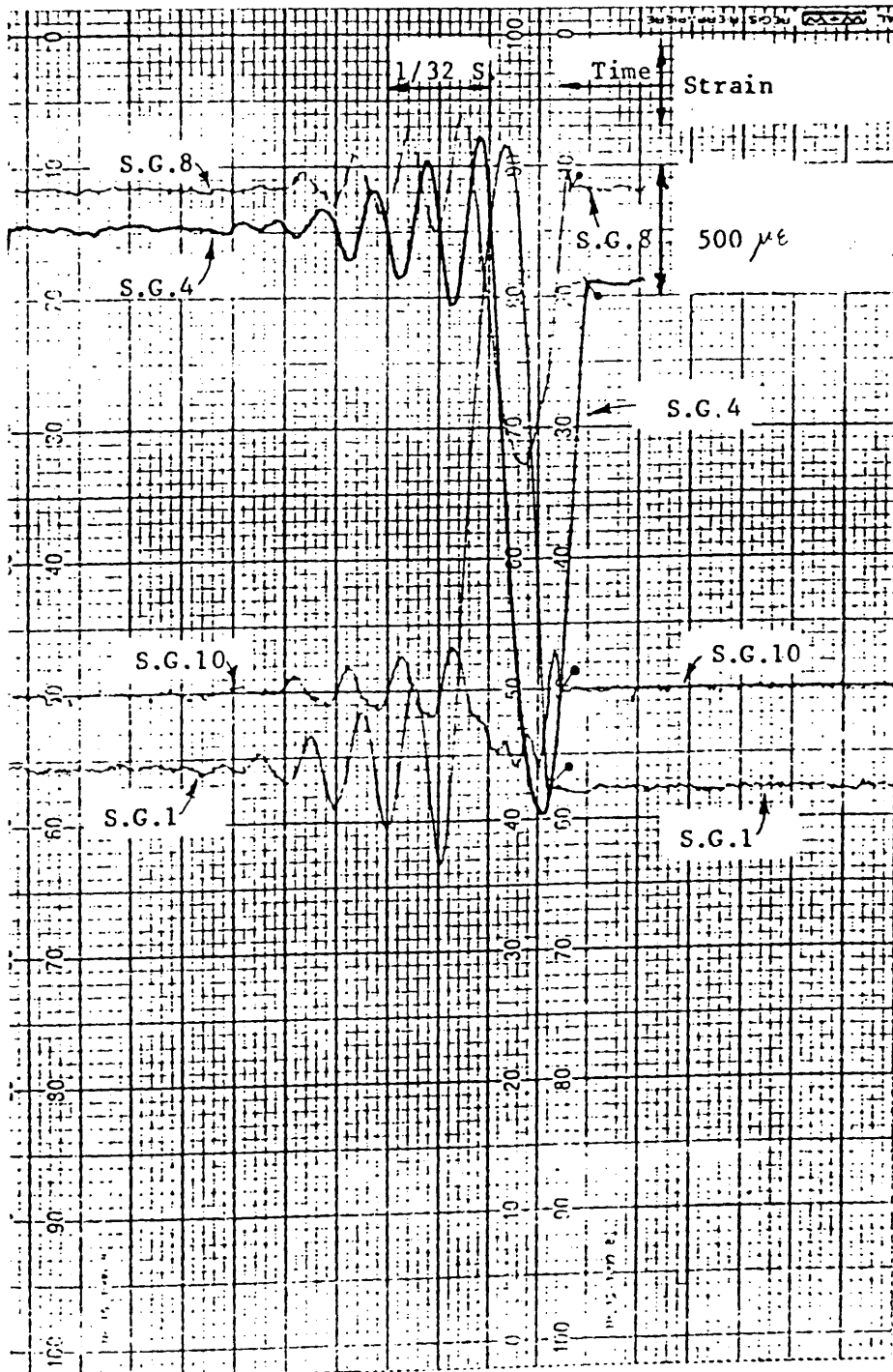
• denotes beginning of contact



DYNAMIC RECORDING RESULTS

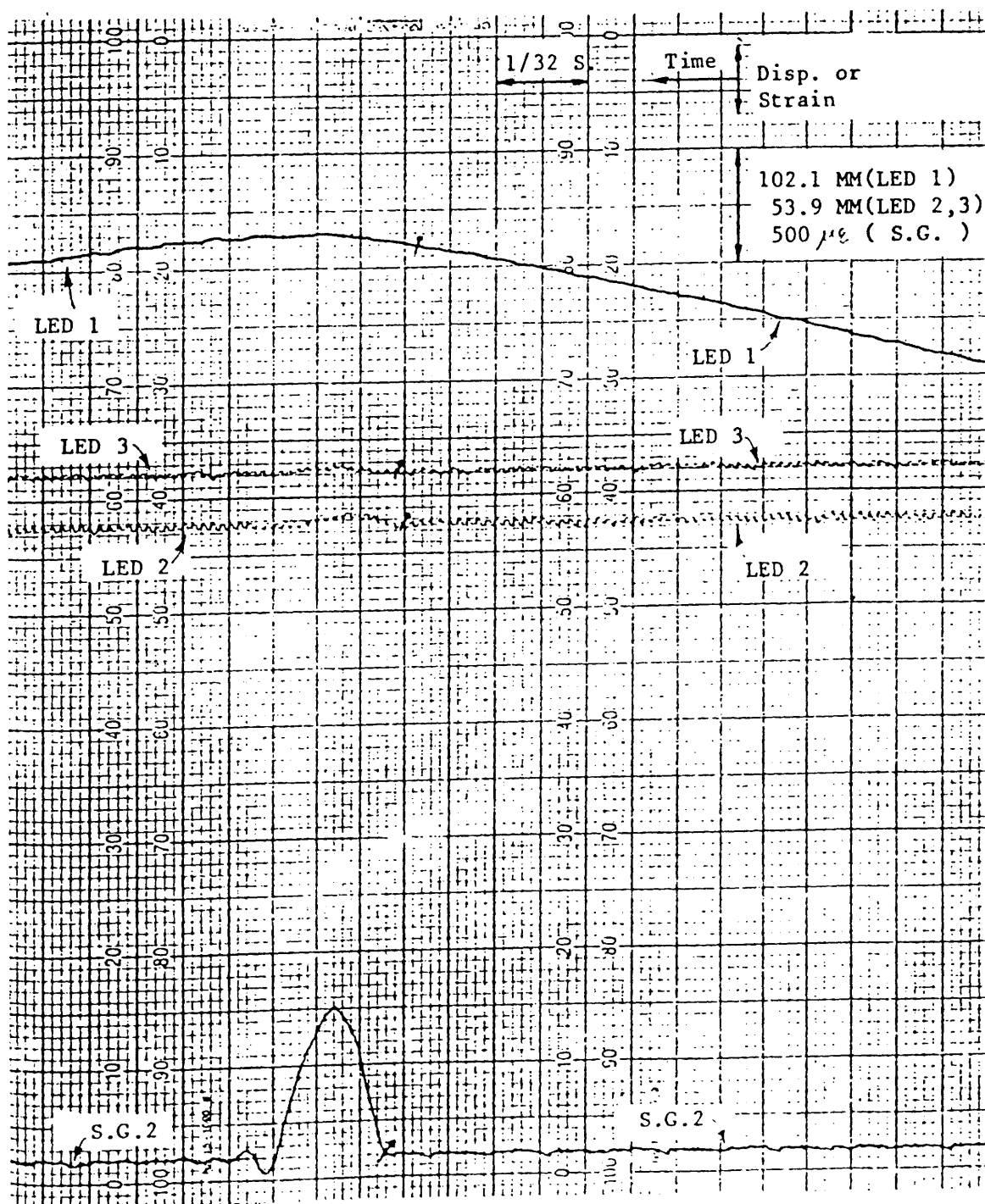
MODEL :  $E_3$   
 LENGTH(L): 1400 MM  
 LENGTH for IMPACT TEST(Li): 1350 MM  
 OUTSIDE DIA.: 50.91 MM  
 THICKNESS : 2.05 MM

• denotes beginning of contact



DYNAMIC RECORDING RESULTSMODEL : *F<sub>1</sub>*LENGTH(L): *1400* MMLENGTH for IMPACT TEST(L<sub>i</sub>): *1350* MMOUTSIDE DIA.: *50.91* MMTHICKNESS : *2.03* MM

p denotes beginning of contact

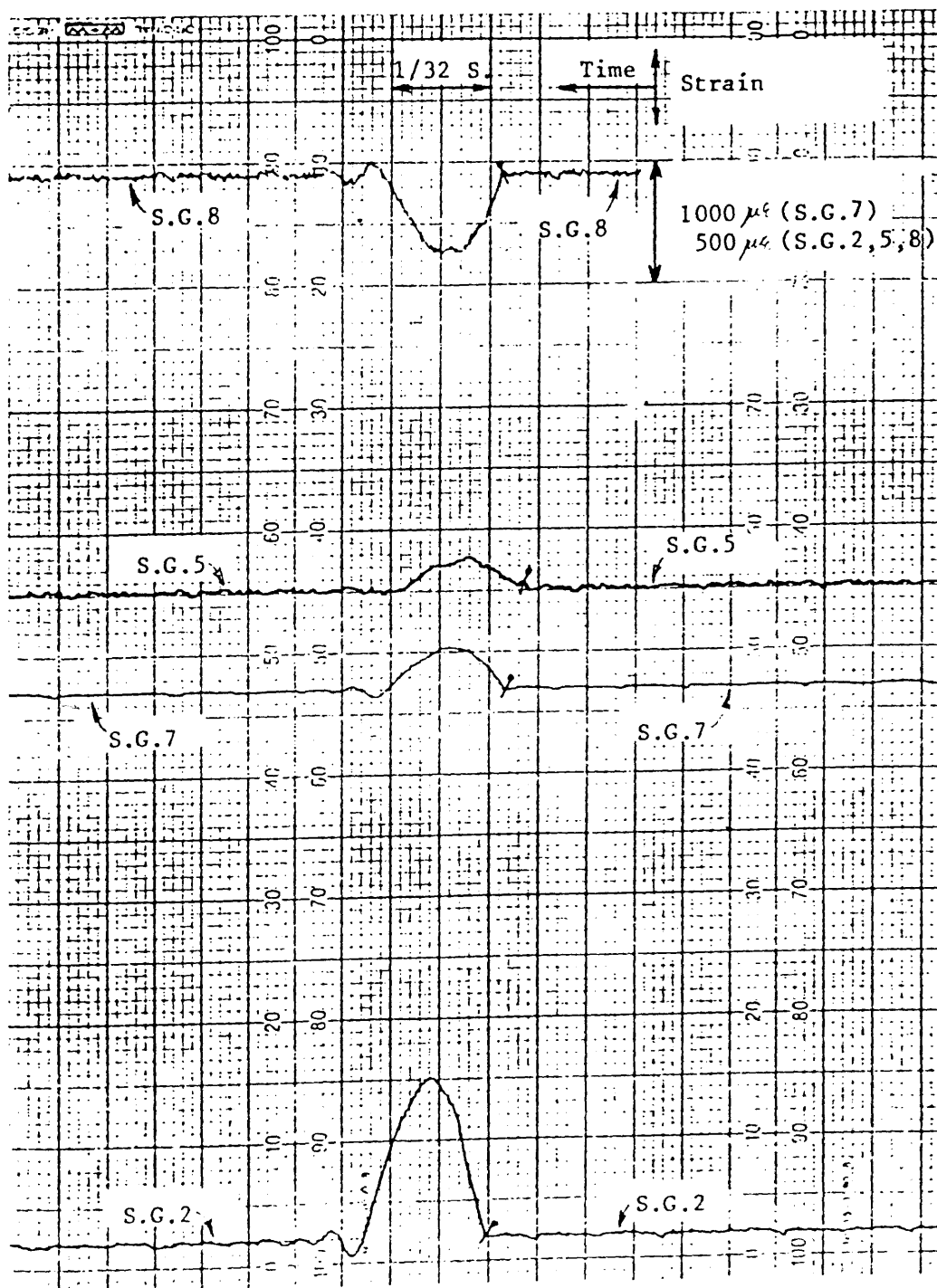




DYNAMIC RECORDING RESULTS

MODEL :  $F_1$   
 LENGTH(L): 1400 MM  
 LENGTH for IMPACT TEST(Li): 1350 MM  
 OUTSIDE DIA.: 50.91 MM  
 THICKNESS : 2.03 MM

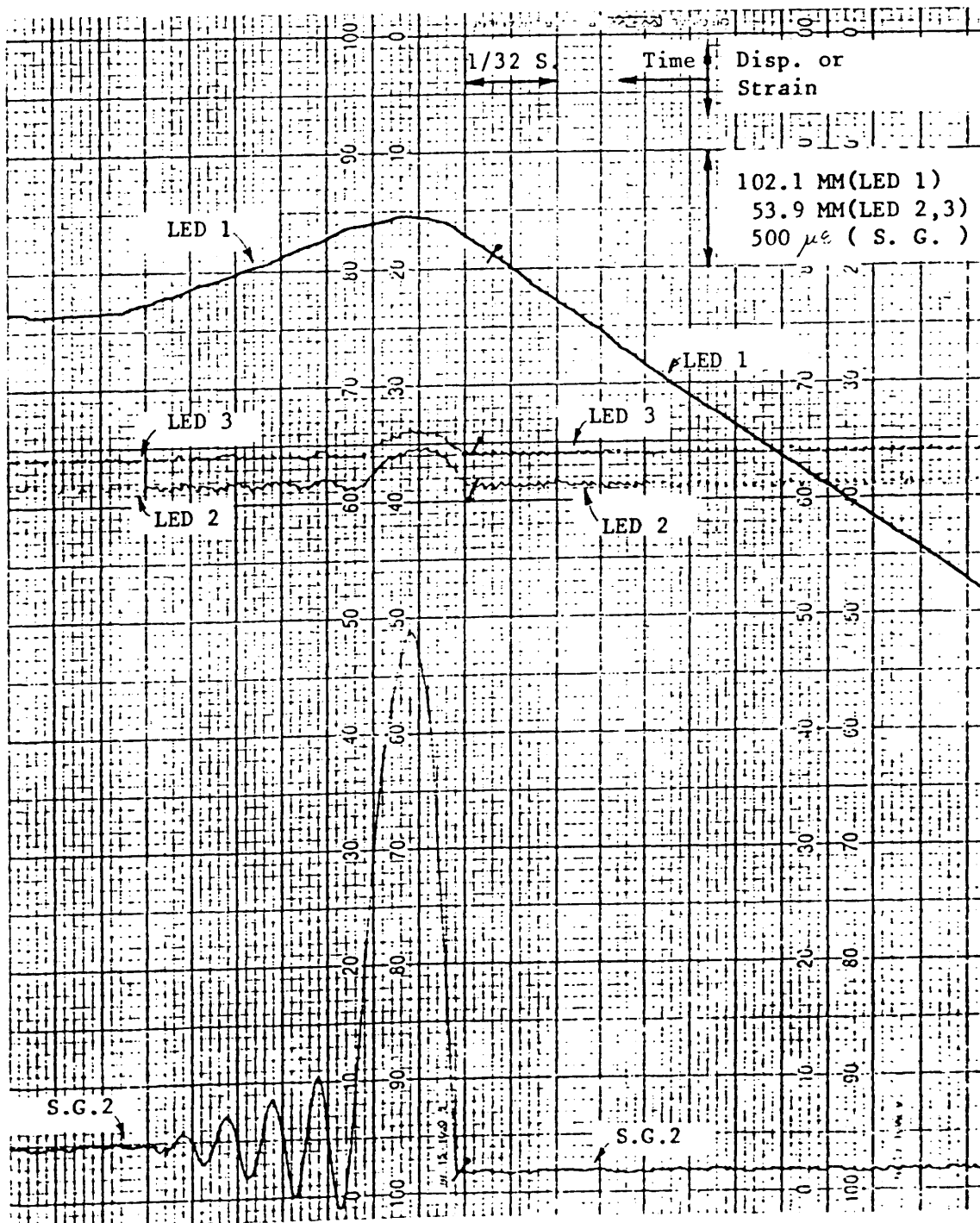
• denotes beginning of contact



DYNAMIC RECORDING RESULTS

MODEL : *Fip*  
 LENGTH(L): *1400* MM  
 LENGTH for IMPACT TEST(Li): *1350* MM  
 OUTSIDE DIA.: *50.91* MM  
 THICKNESS : *2.03* MM

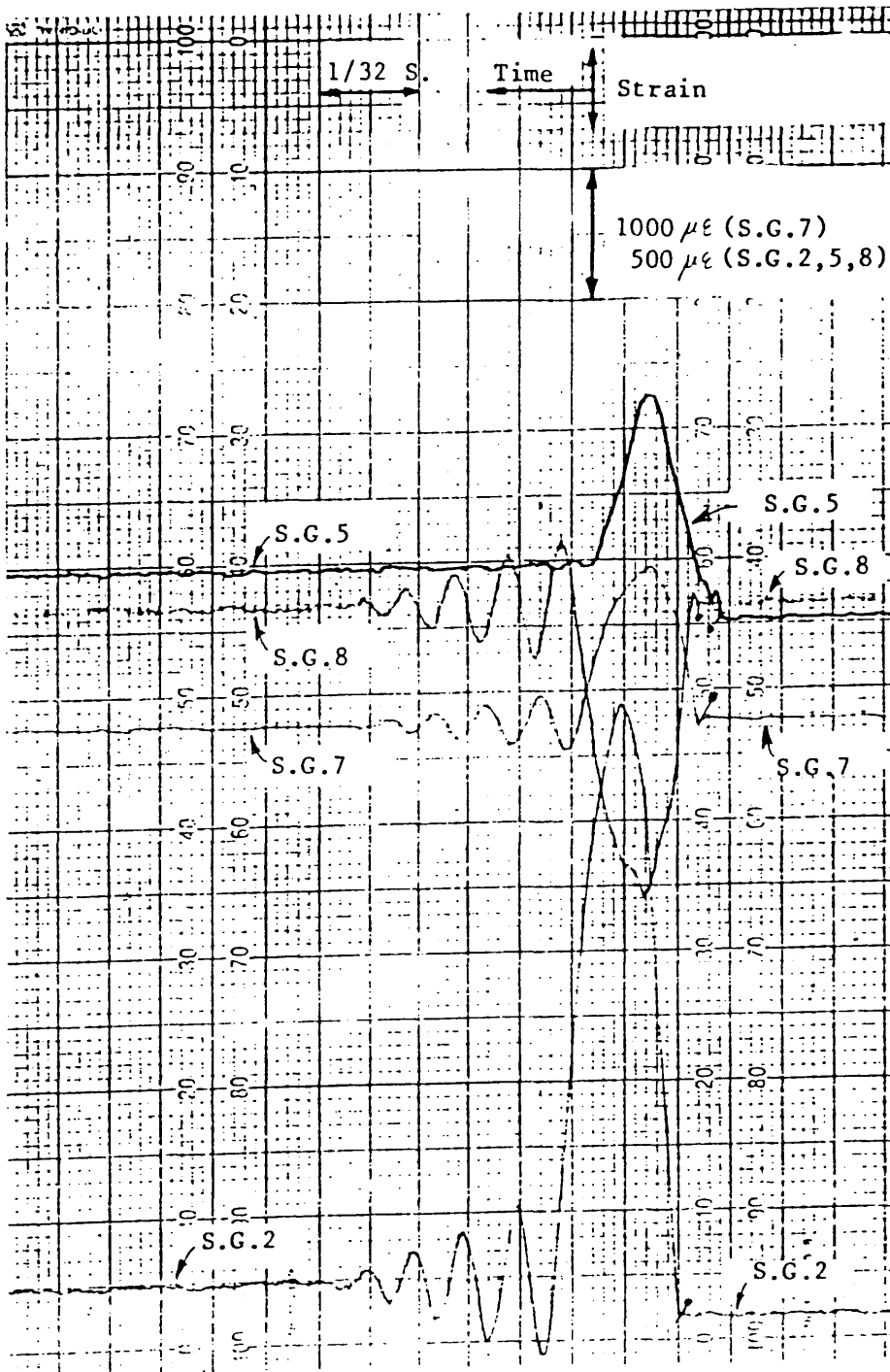
• denotes beginning of contact



DYNAMIC RECORDING RESULTS

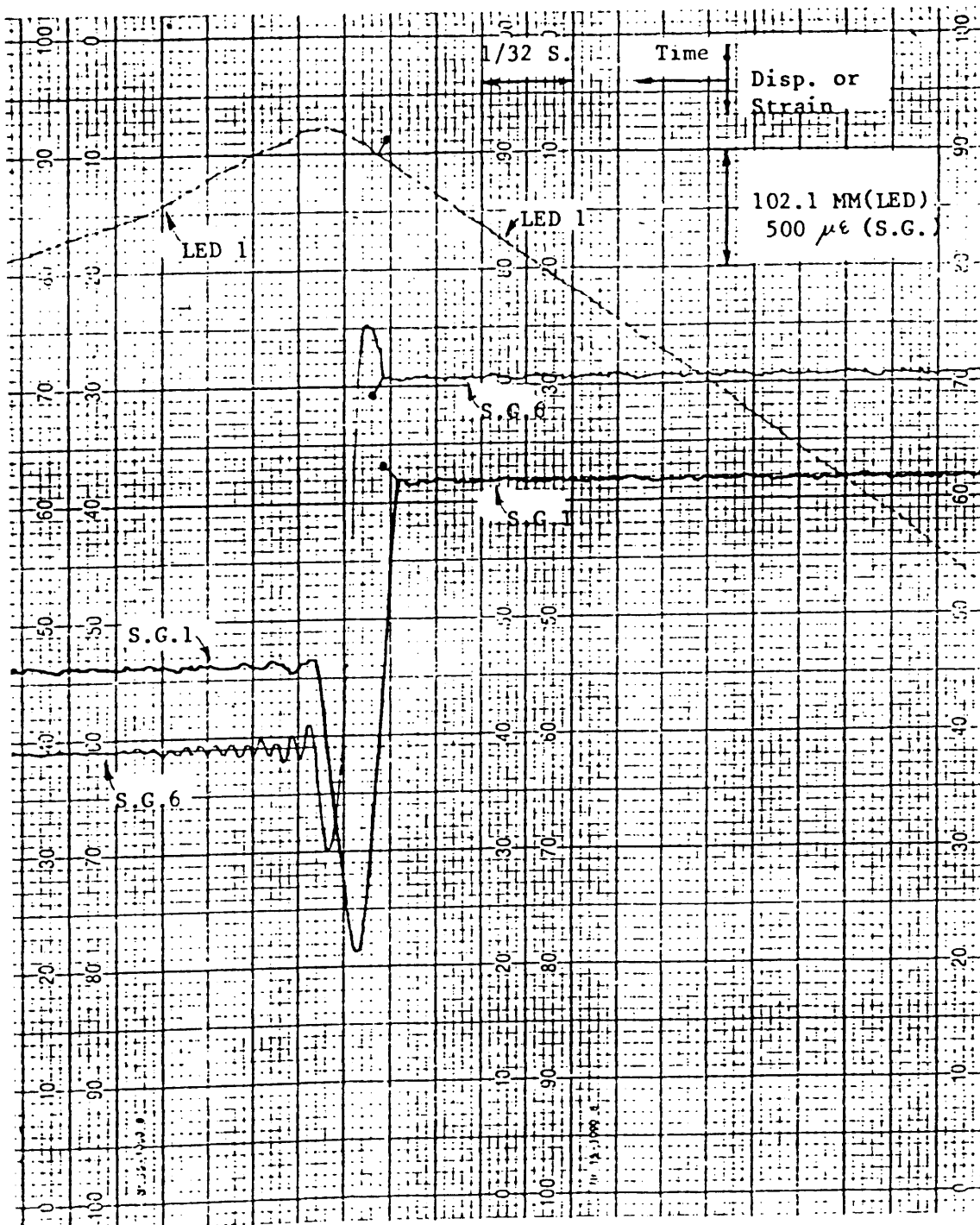
MODEL : *Fip*  
 LENGTH(L): 1400 MM  
 LENGTH for IMPACT TEST(Li): 1350 MM  
 OUTSIDE DIA.: 50.91 MM  
 THICKNESS : 2.03 MM

↗ denotes beginning of contact



DYNAMIC RECORDING RESULTSMODEL : *F2*LENGTH(L): *1000* MMLENGTH for IMPACT TEST(Li): *950* MMOUTSIDE DIA.: *50.90* MMTHICKNESS : *2.03* MM

• denotes beginning of contact



DYNAMIC RECORDING RESULTS

MODEL : F2

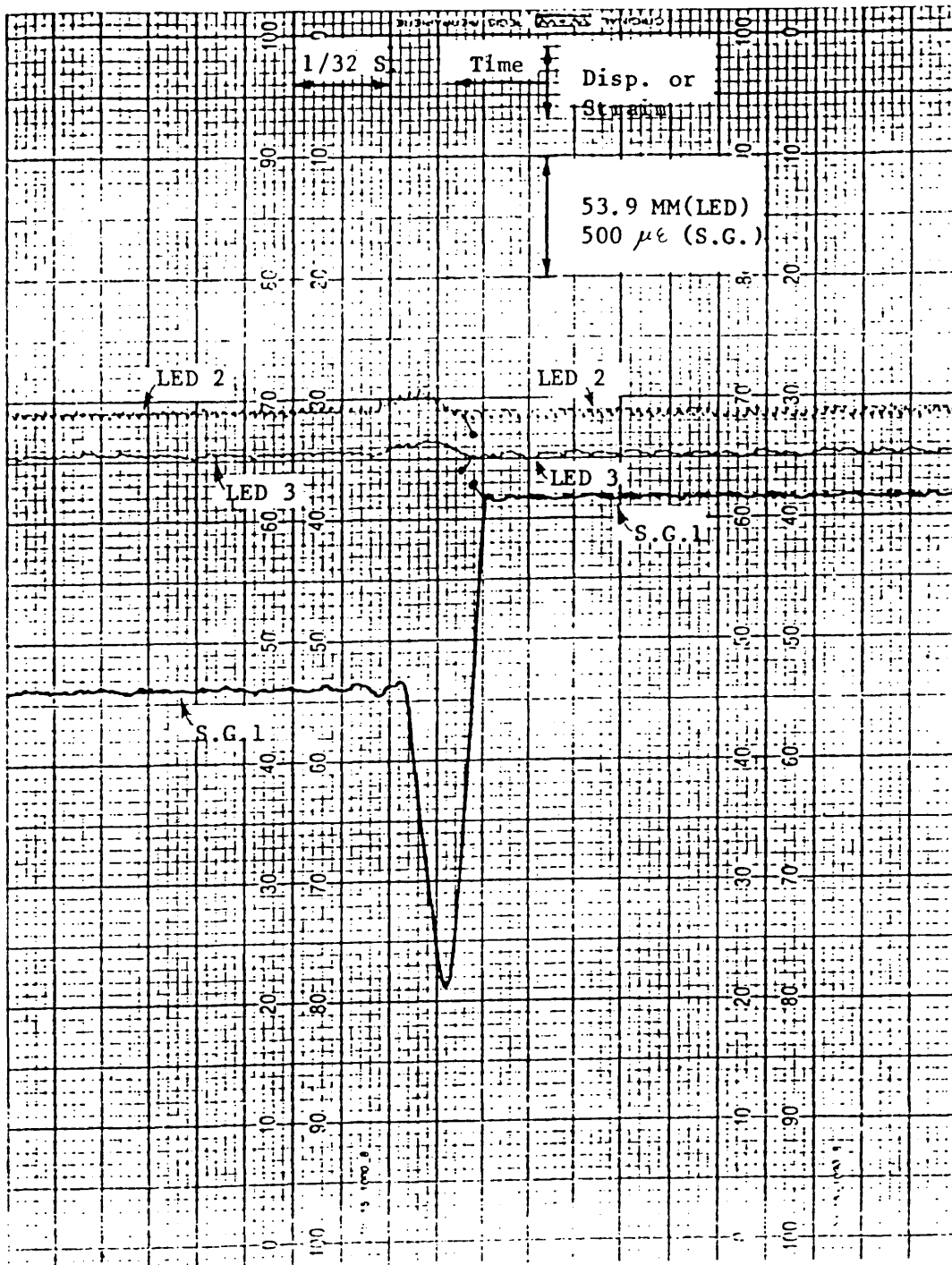
LENGTH(L): 1000 MM

LENGTH for IMPACT TEST(Li): 950 MM

OUTSIDE DIA.: 50.90 MM

THICKNESS : 2.03 MM

• denotes beginning of contact



DYNAMIC RECORDING RESULTSMODEL :  $F_2$ 

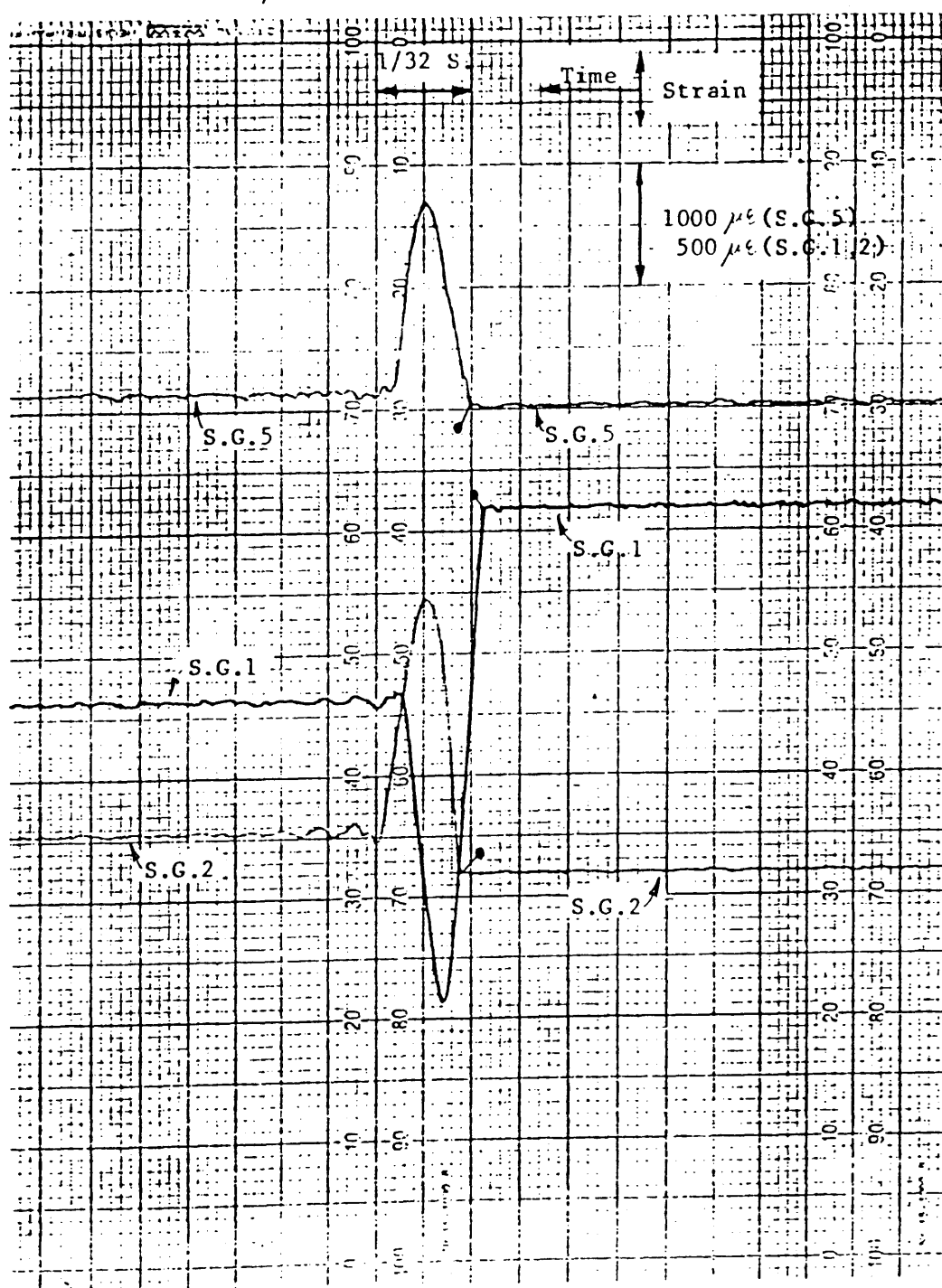
LENGTH(L): 1000 MM

LENGTH for IMPACT TEST(Li): 950 MM

OUTSIDE DIA.: 50.90 MM

THICKNESS : 2.03 MM

• denotes beginning of contact



DYNAMIC RECORDING RESULTSMODEL :  $F_3$ 

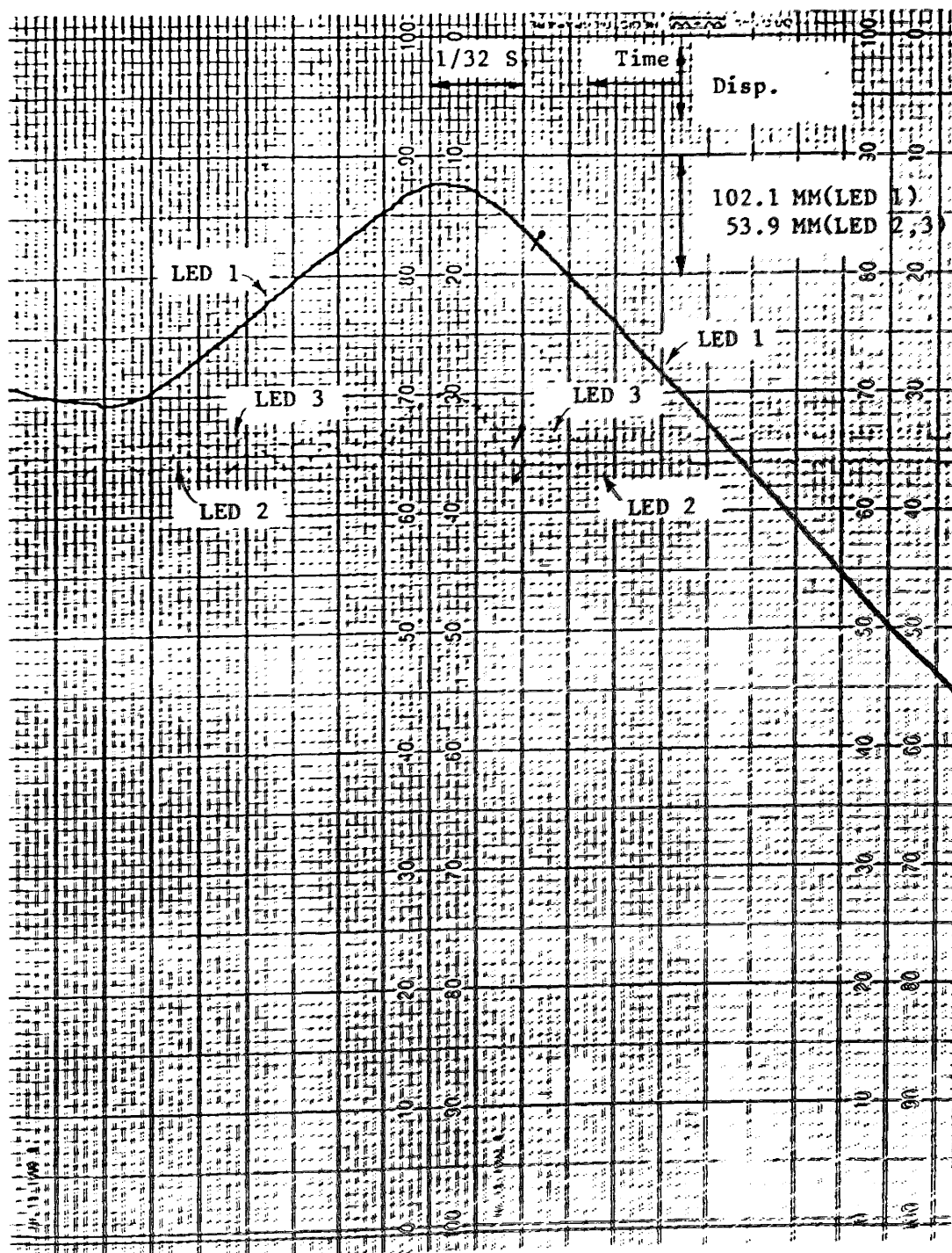
LENGTH(L): 1800 MM

LENGTH for IMPACT TEST(Li): 1750 MM

OUTSIDE DIA.: 50.86 MM

THICKNESS : 2.02 MM

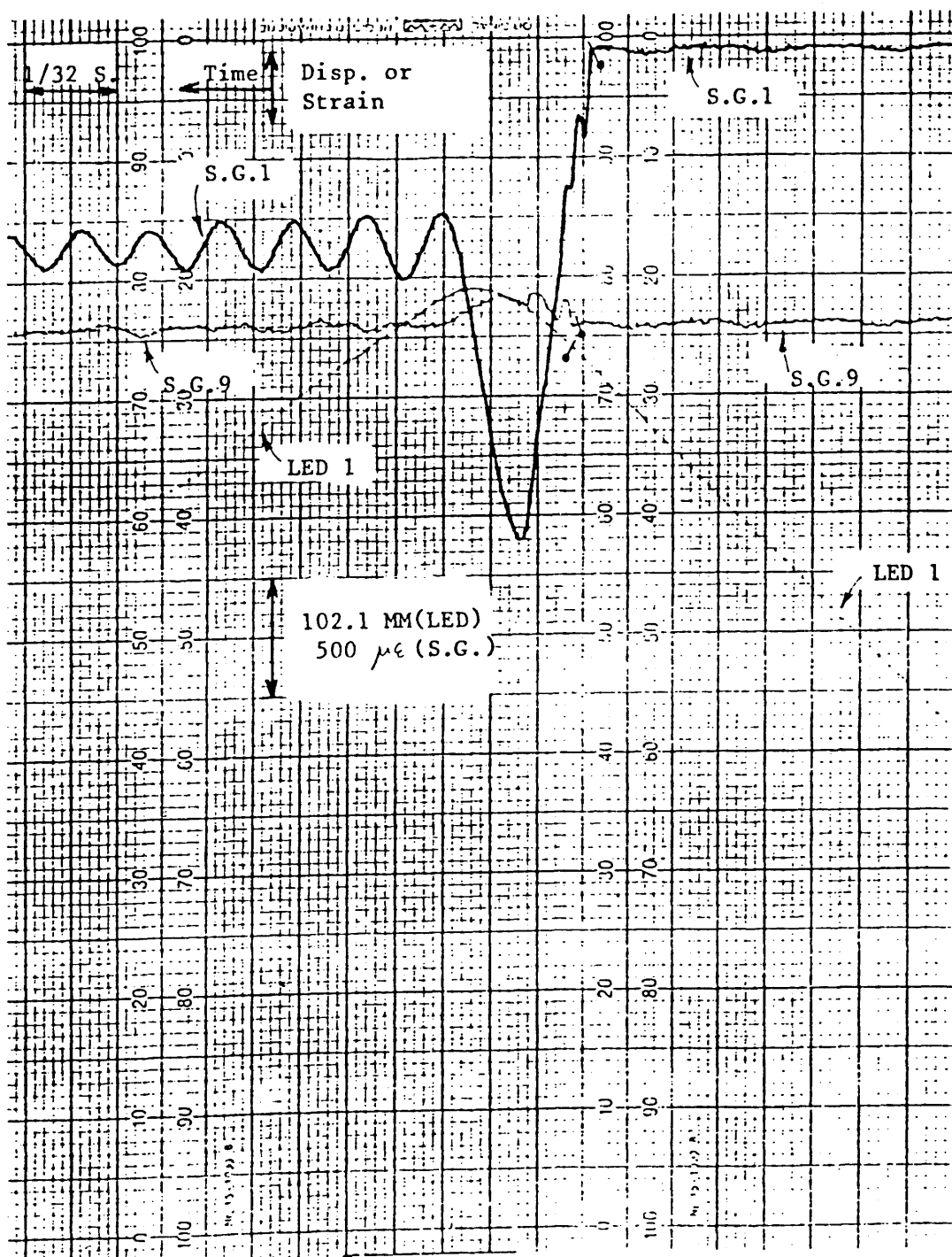
• denotes beginning of contact



DYNAMIC RECORDING RESULTS

MODEL :  $F_3$   
 LENGTH(L): 1800 MM  
 LENGTH for IMPACT TEST(Li): 1750 MM  
 OUTSIDE DIA.: 50.86 MM  
 THICKNESS : 2.02 MM

• denotes beginning of contact

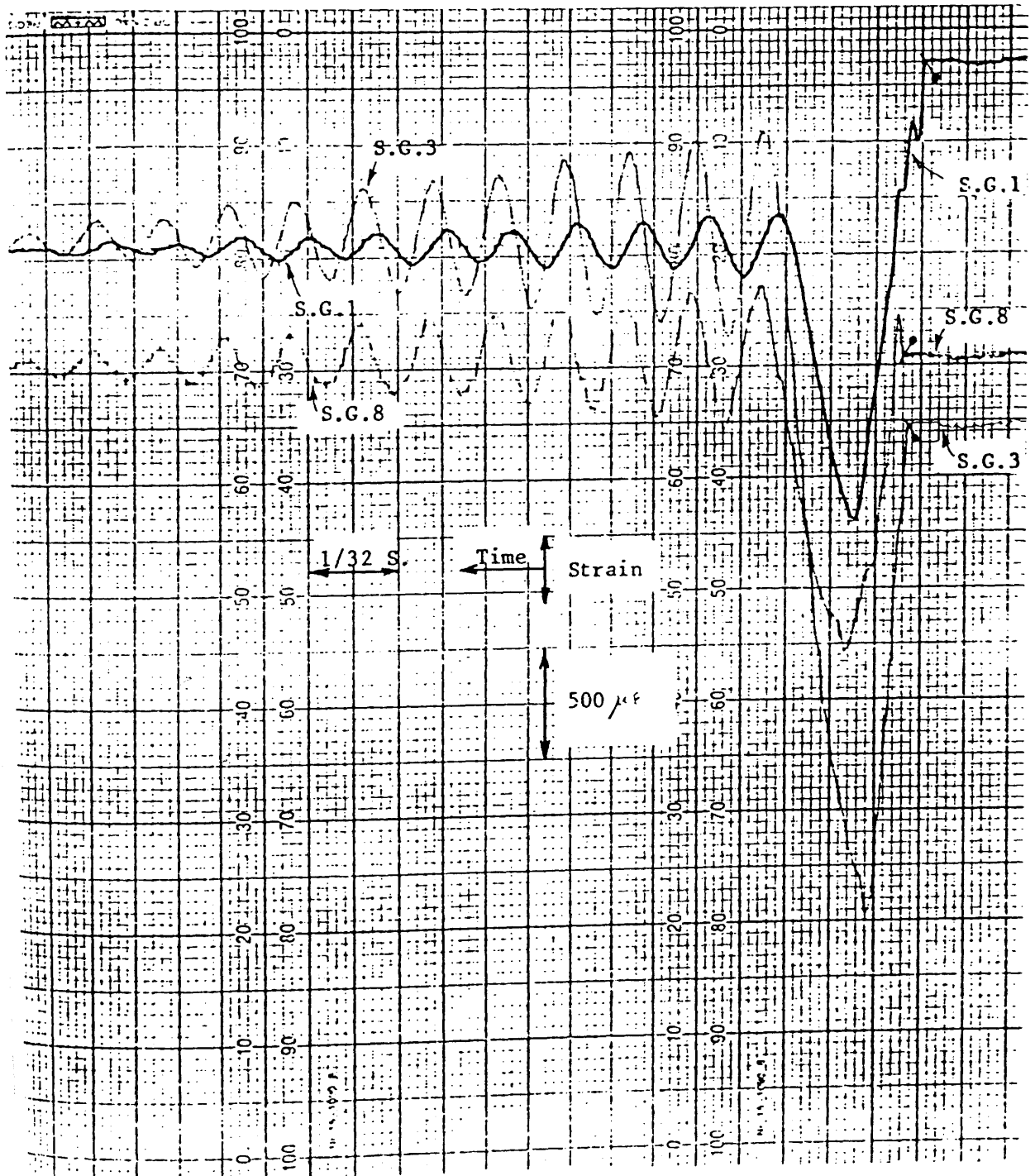




DYNAMIC RECORDING RESULTS

MODEL :  $F_3$   
 LENGTH(L): 1800 MM  
 LENGTH for IMPACT TEST(Li): 1750 MM  
 OUTSIDE DIA.: 50.86 MM  
 THICKNESS : 2.02 MM

• denotes beginning of contact



DYNAMIC RECORDING RESULTSMODEL : *G1*

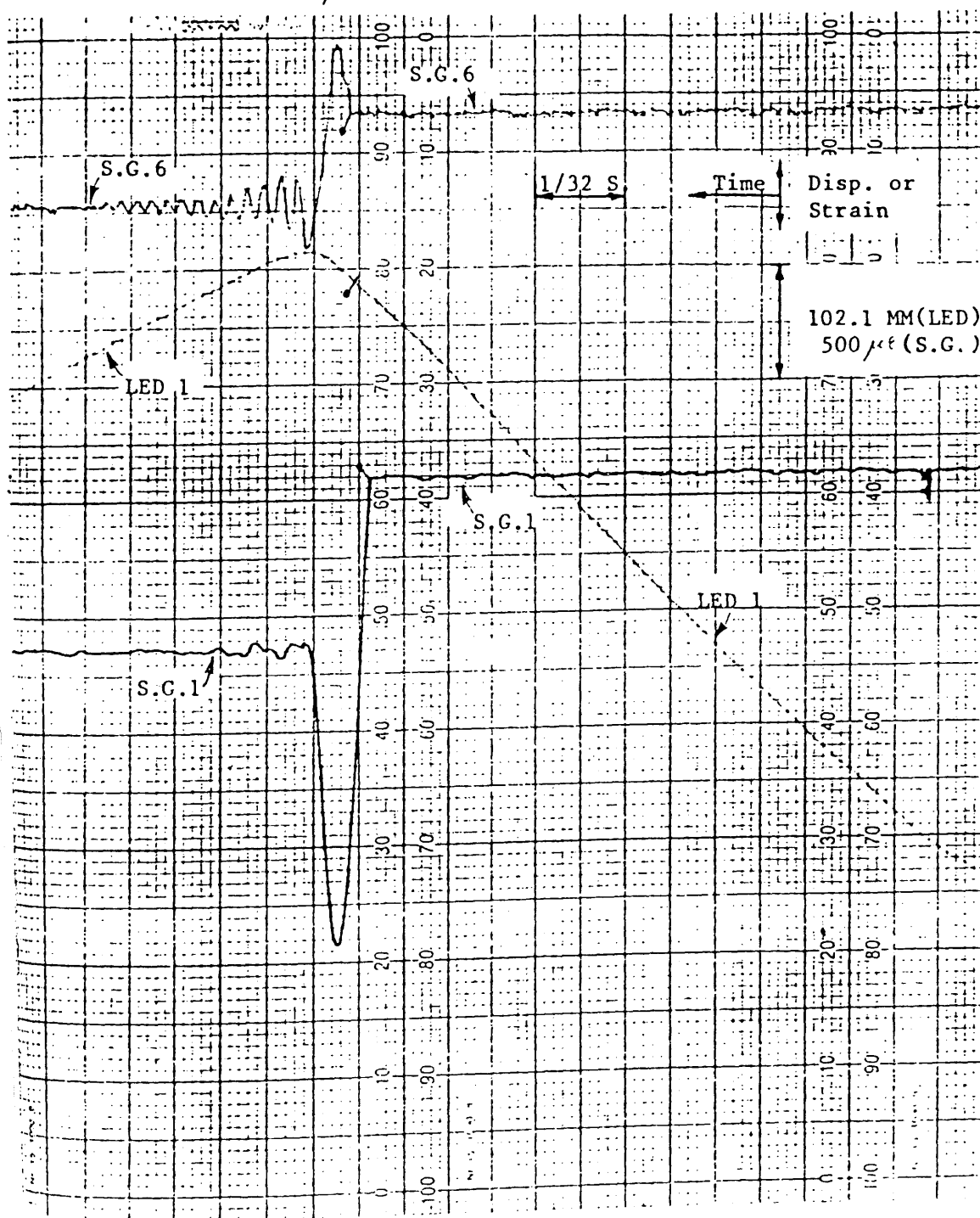
LENGTH(L): 1000 MM

LENGTH for IMPACT TEST(Li): 950 MM

OUTSIDE DIA.: 50.95 MM

THICKNESS : 2.04 MM

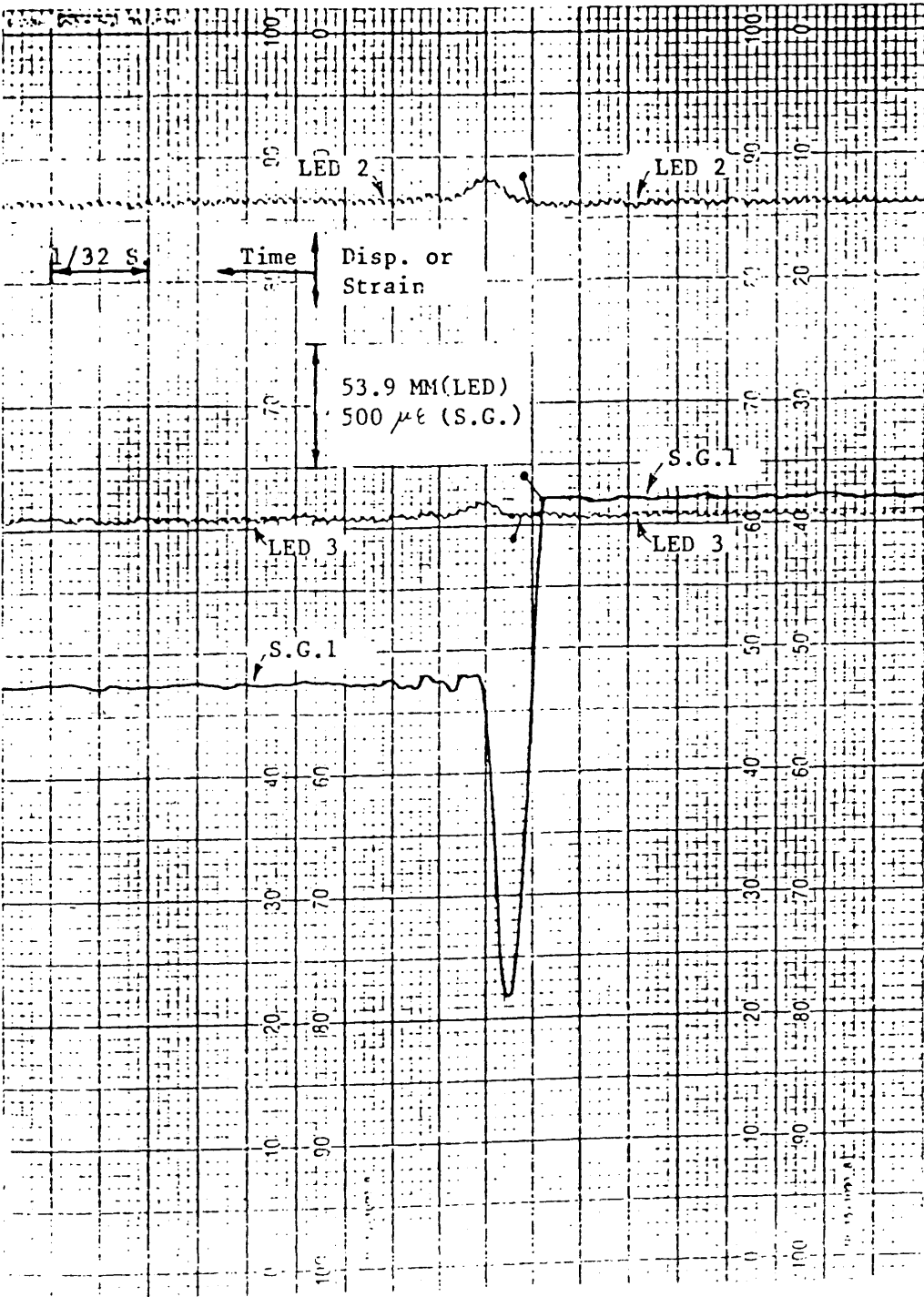
p denotes beginning of contact



DYNAMIC RECORDING RESULTS

MODEL : *G1*  
LENGTH(L): 1000 MM  
LENGTH for IMPACT TEST(Li): 950 MM  
OUTSIDE DIA.: 50.95 MM  
THICKNESS : 2.04 MM

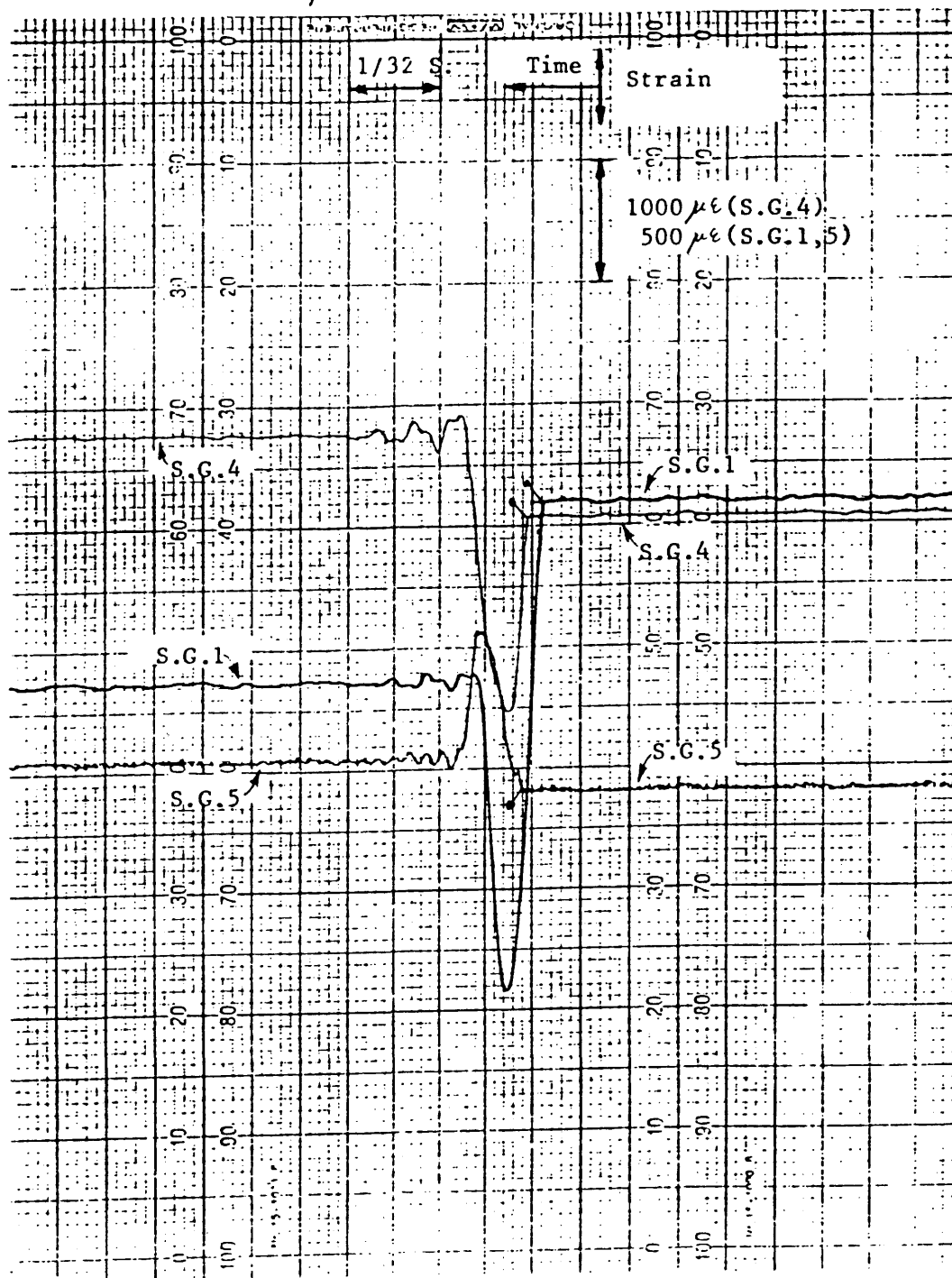
*p* denotes beginning of contact



DYNAMIC RECORDING RESULTS

MODEL : G1  
 LENGTH(L): 1000 MM  
 LENGTH for IMPACT TEST(Li): 950 MM  
 OUTSIDE DIA.: 50.95 MM  
 THICKNESS : 2.04 MM

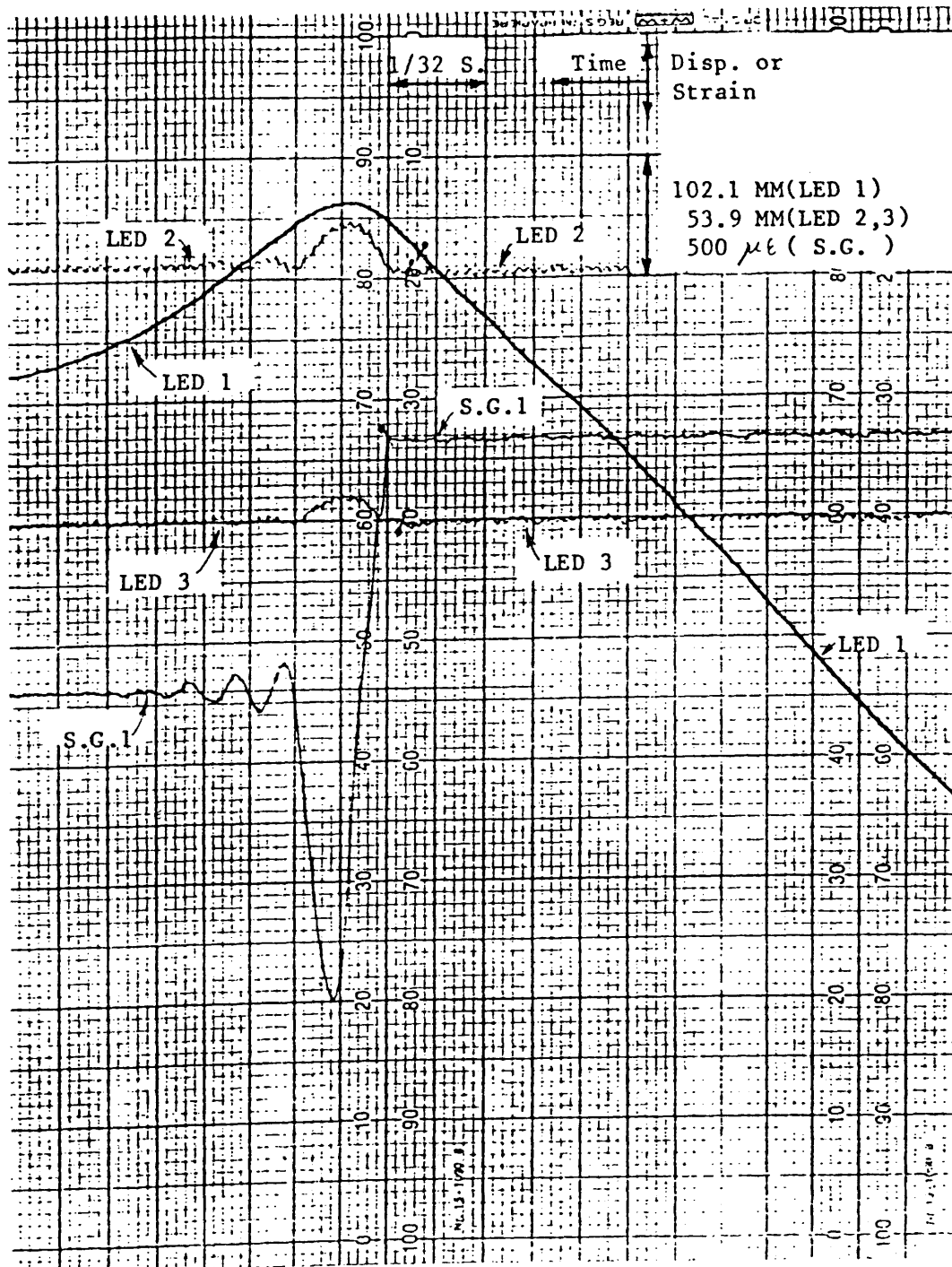
• denotes beginning of contact



DYNAMIC RECORDING RESULTS

MODEL : G<sub>2</sub>  
 LENGTH(L): 1400 MM  
 LENGTH for IMPACT TEST(L<sub>i</sub>): 1350 MM  
 OUTSIDE DIA.: 50.92 MM  
 THICKNESS : 2.05 MM

• denotes beginning of contact



DYNAMIC RECORDING RESULTS

MODEL : G2

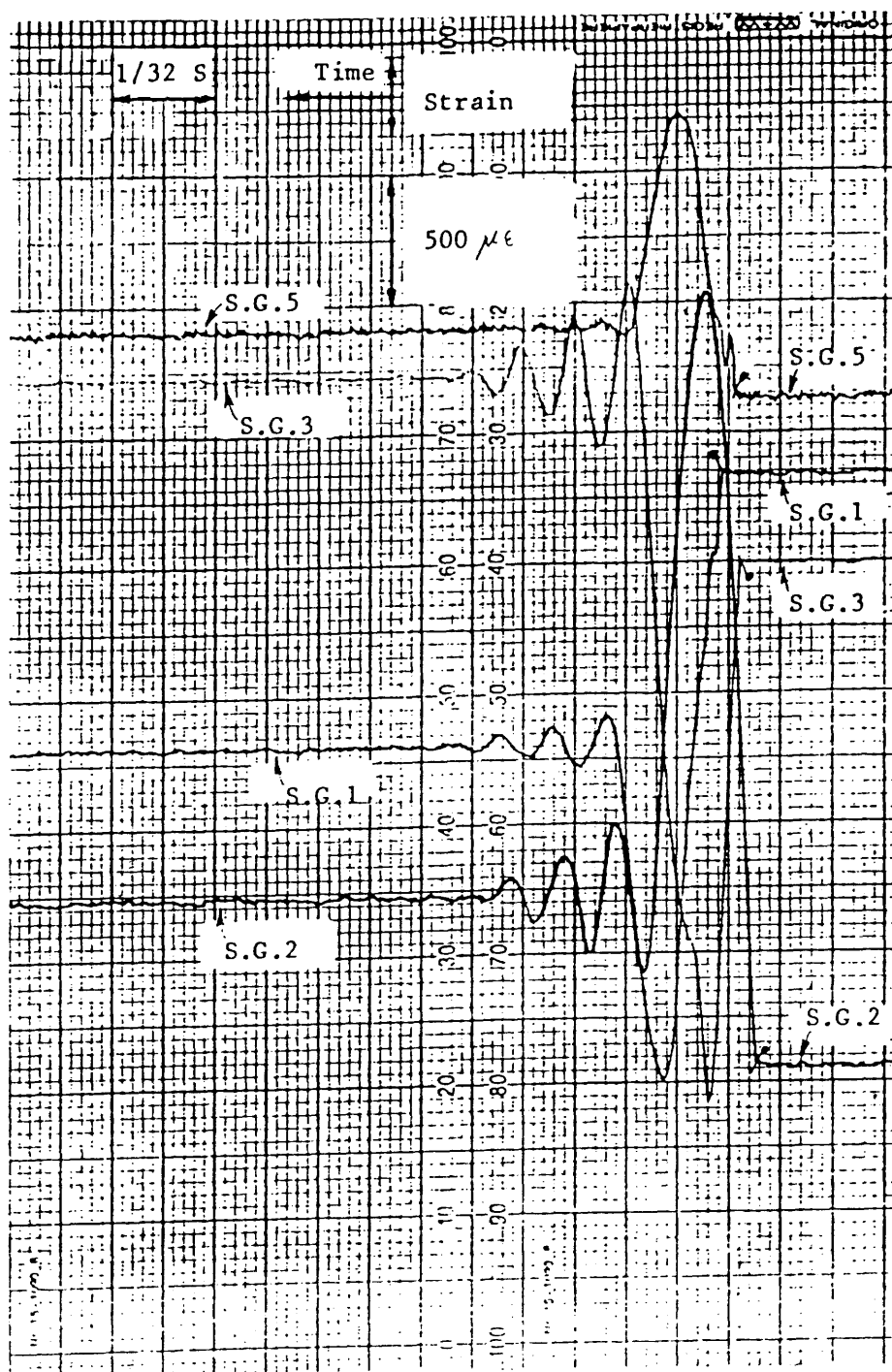
LENGTH(L): 1400 MM

LENGTH for IMPACT TEST(Li): 1350 MM

OUTSIDE DIA.: 50.92 MM

THICKNESS : 2.05 MM

• denotes beginning of contact



DYNAMIC RECORDING RESULTS

MODEL : G3

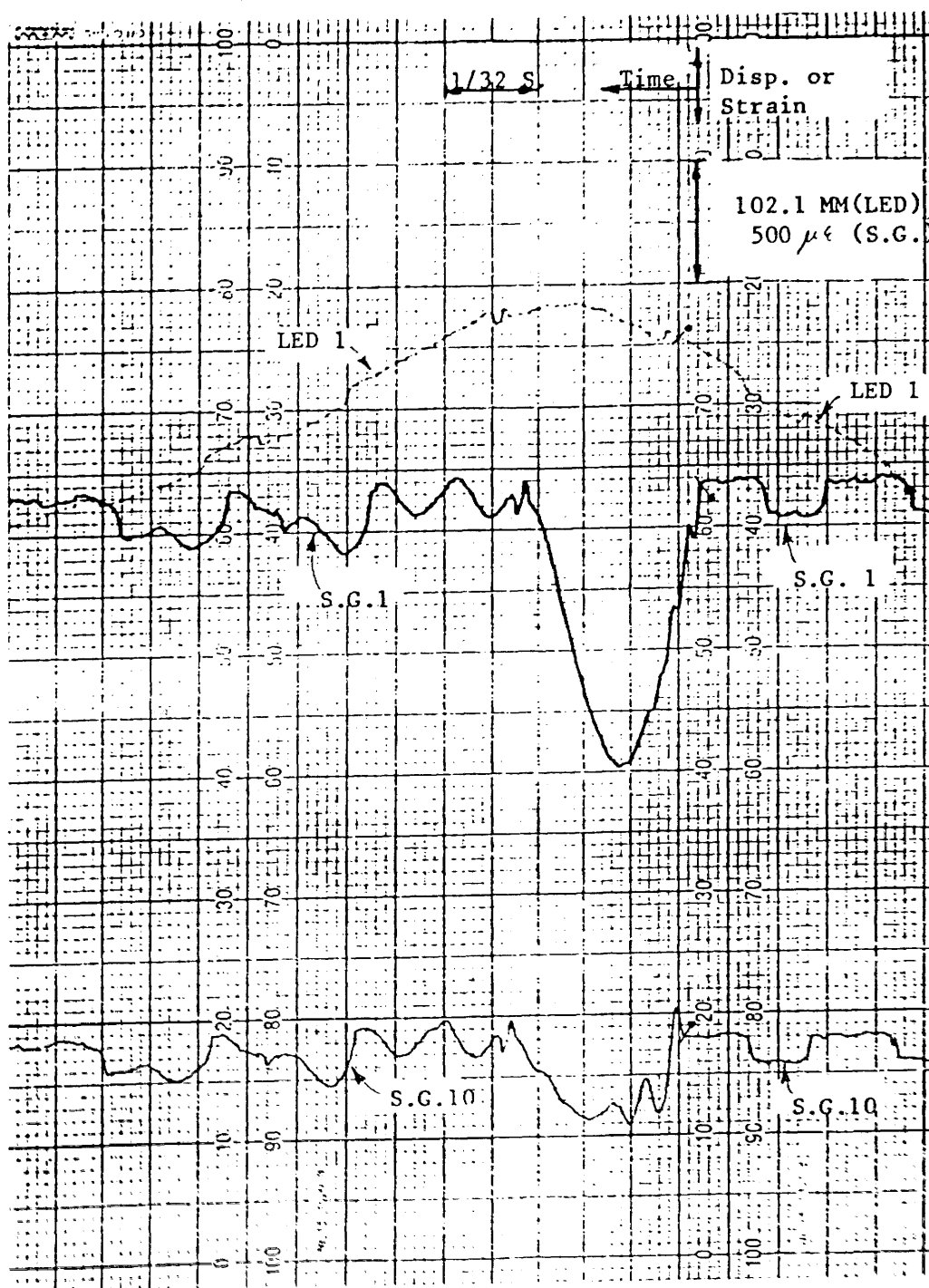
LENGTH(L): 1800 MM

LENGTH for IMPACT TEST(Li): 1750 MM

OUTSIDE DIA.: 50.93 MM

THICKNESS : 2.04 MM

• denotes beginning of contact







DYNAMIC RECORDING RESULTS

MODEL : G3

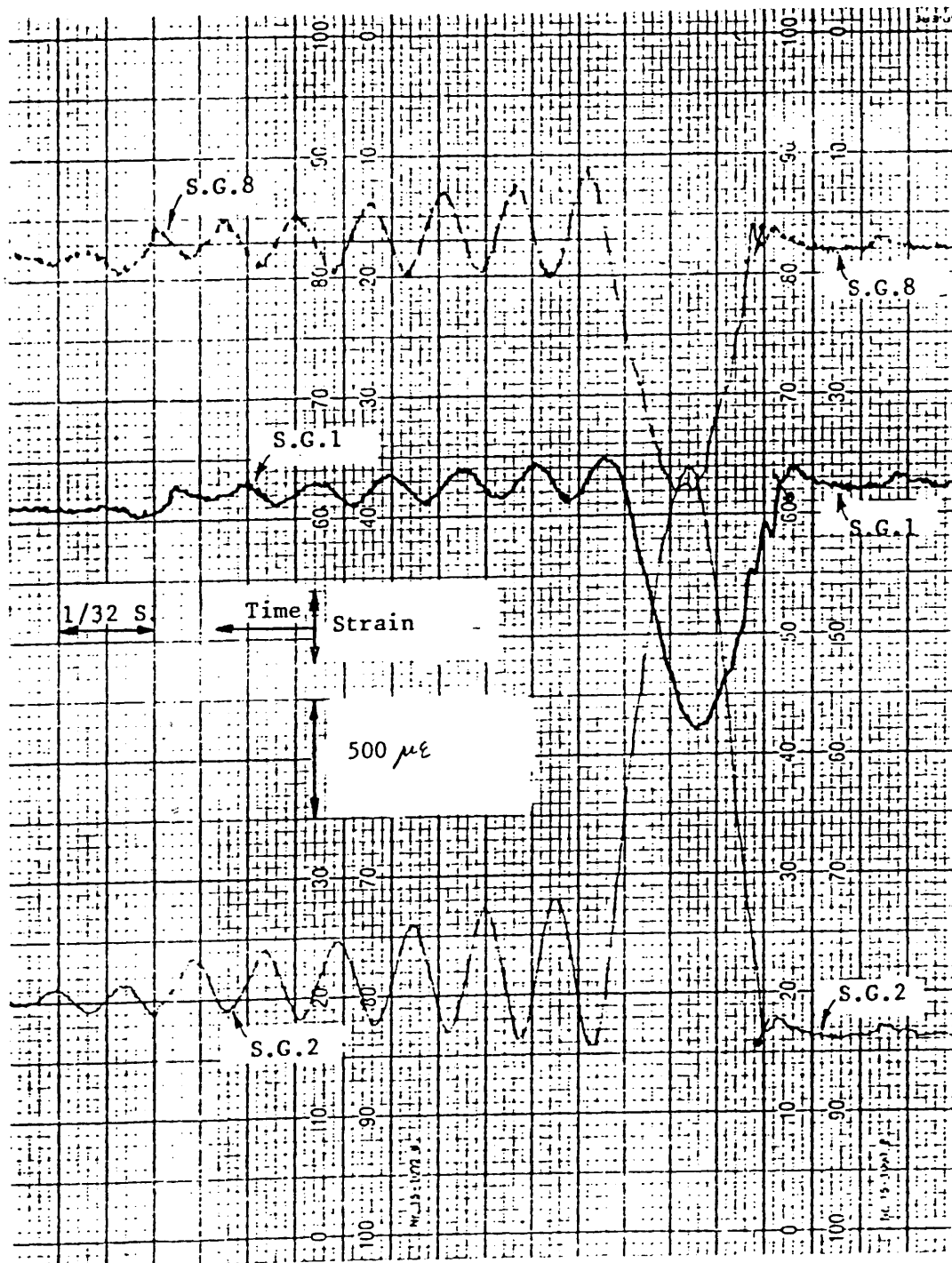
LENGTH(L): 1800 MM

LENGTH for IMPACT TEST(Li): 1750 MM

OUTSIDE DIA.: 50.93 MM

THICKNESS : 2.04 MM

p denotes beginning of contact



DYNAMIC RECORDING RESULTSMODEL : *H<sub>1</sub>*

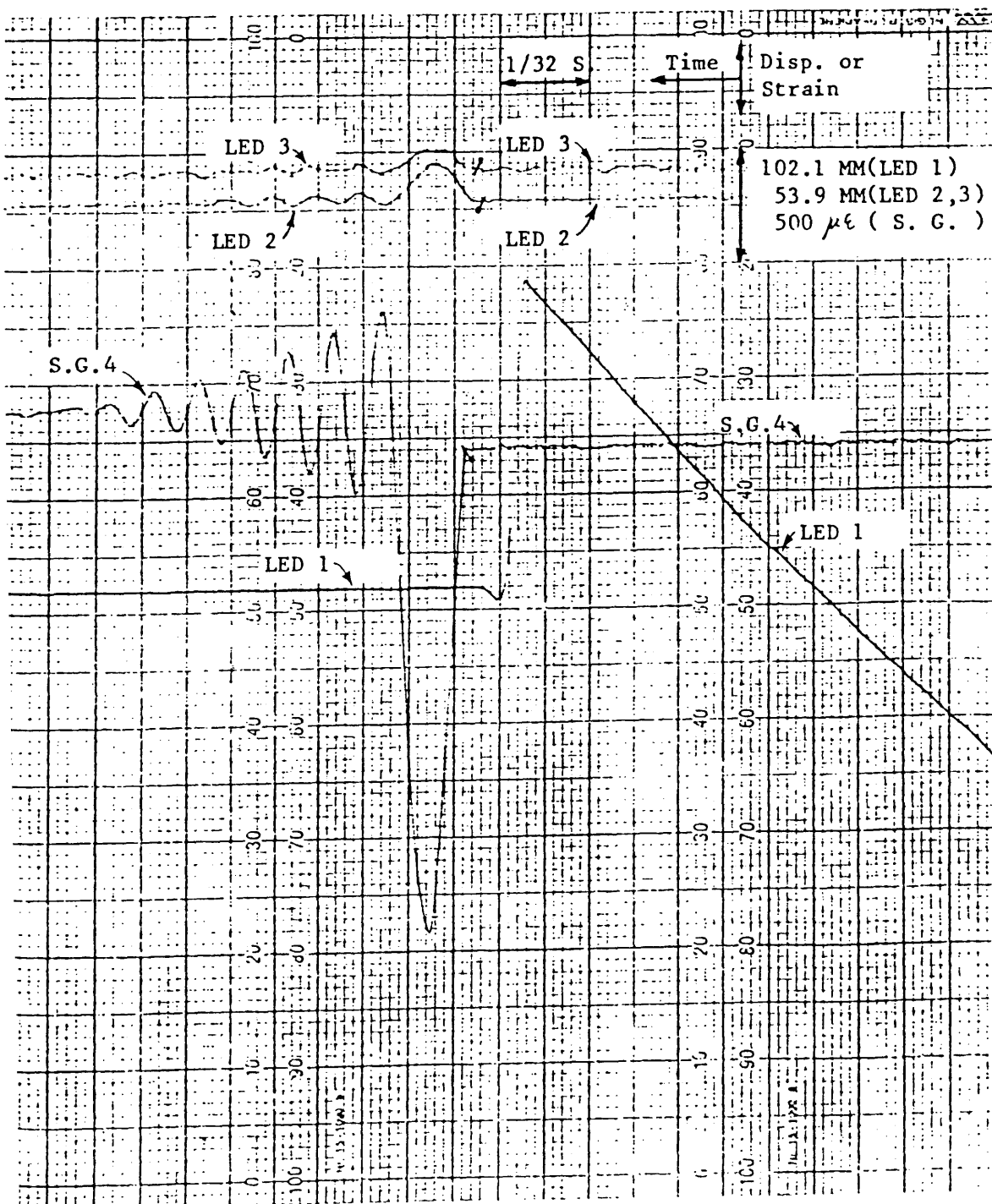
LENGTH(L): 1400 MM

LENGTH for IMPACT TEST(L<sub>i</sub>): 1350 MM

OUTSIDE DIA.: 50.90 MM

THICKNESS : 2.04 MM

• denotes beginning of contact



DYNAMIC RECORDING RESULTSMODEL : *H<sub>1</sub>*

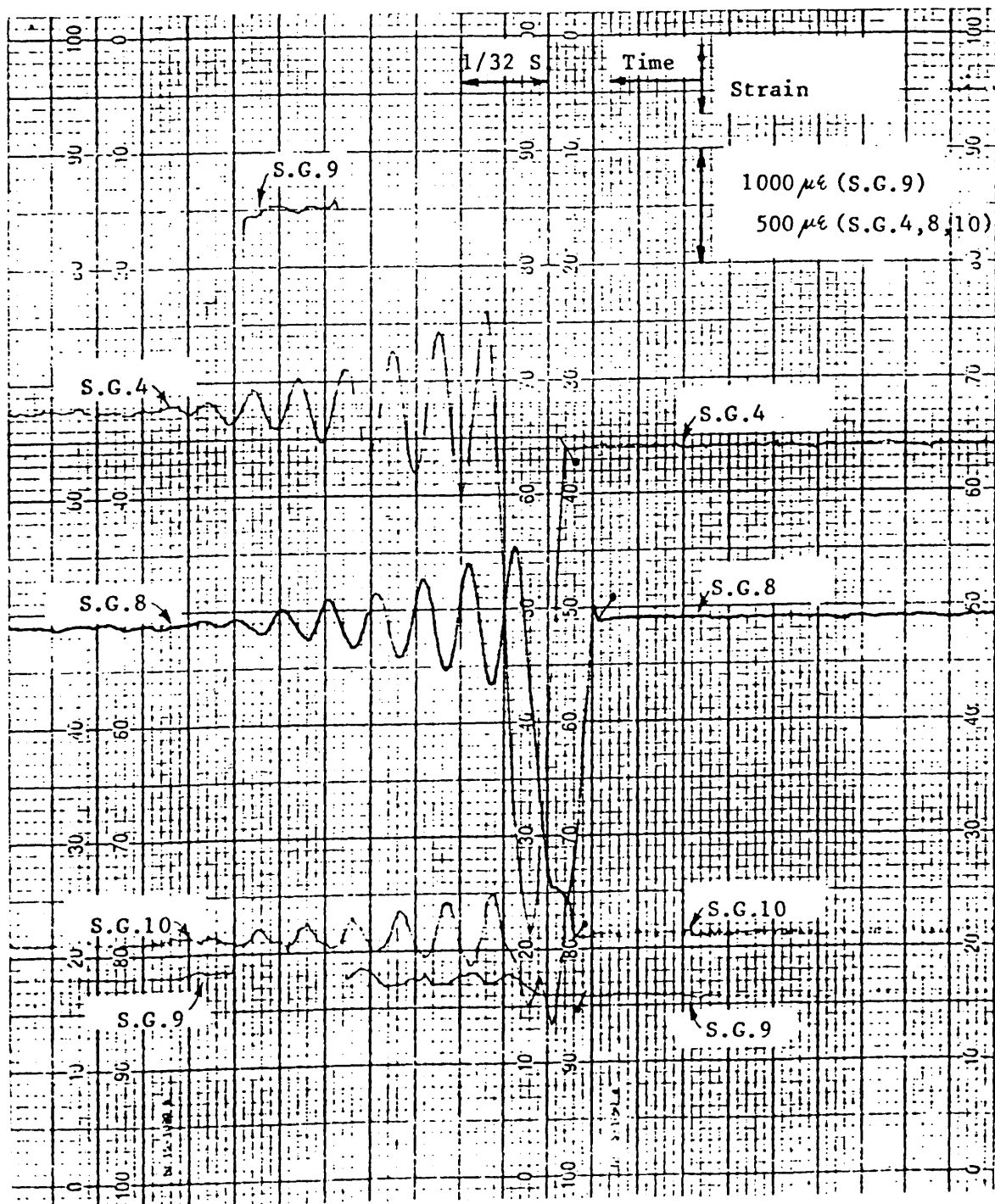
LENGTH(L): 1400 MM

LENGTH for IMPACT TEST(L<sub>i</sub>): 1350 MM

OUTSIDE DIA.: 50.90 MM

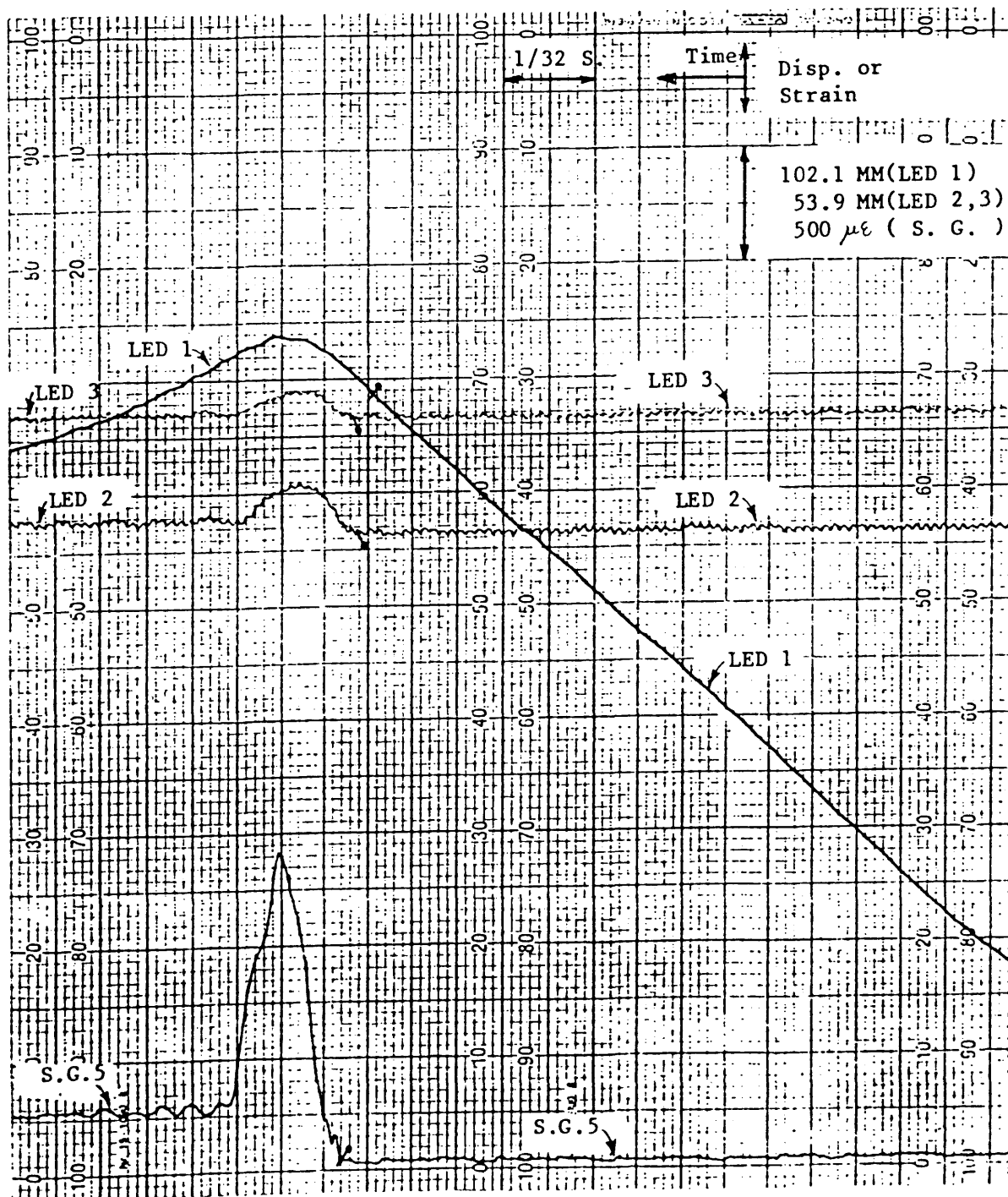
THICKNESS : 2.04 MM

p denotes beginning of contact



DYNAMIC RECORDING RESULTSMODEL : *H<sub>2</sub>*LENGTH(L): *1400* MMLENGTH for IMPACT TEST(L<sub>i</sub>): *1350* MMOUTSIDE DIA.: *50.92* MMTHICKNESS : *2.02* MM

↗ denotes beginning of contact



DYNAMIC RECORDING RESULTSMODEL : H<sub>2</sub>

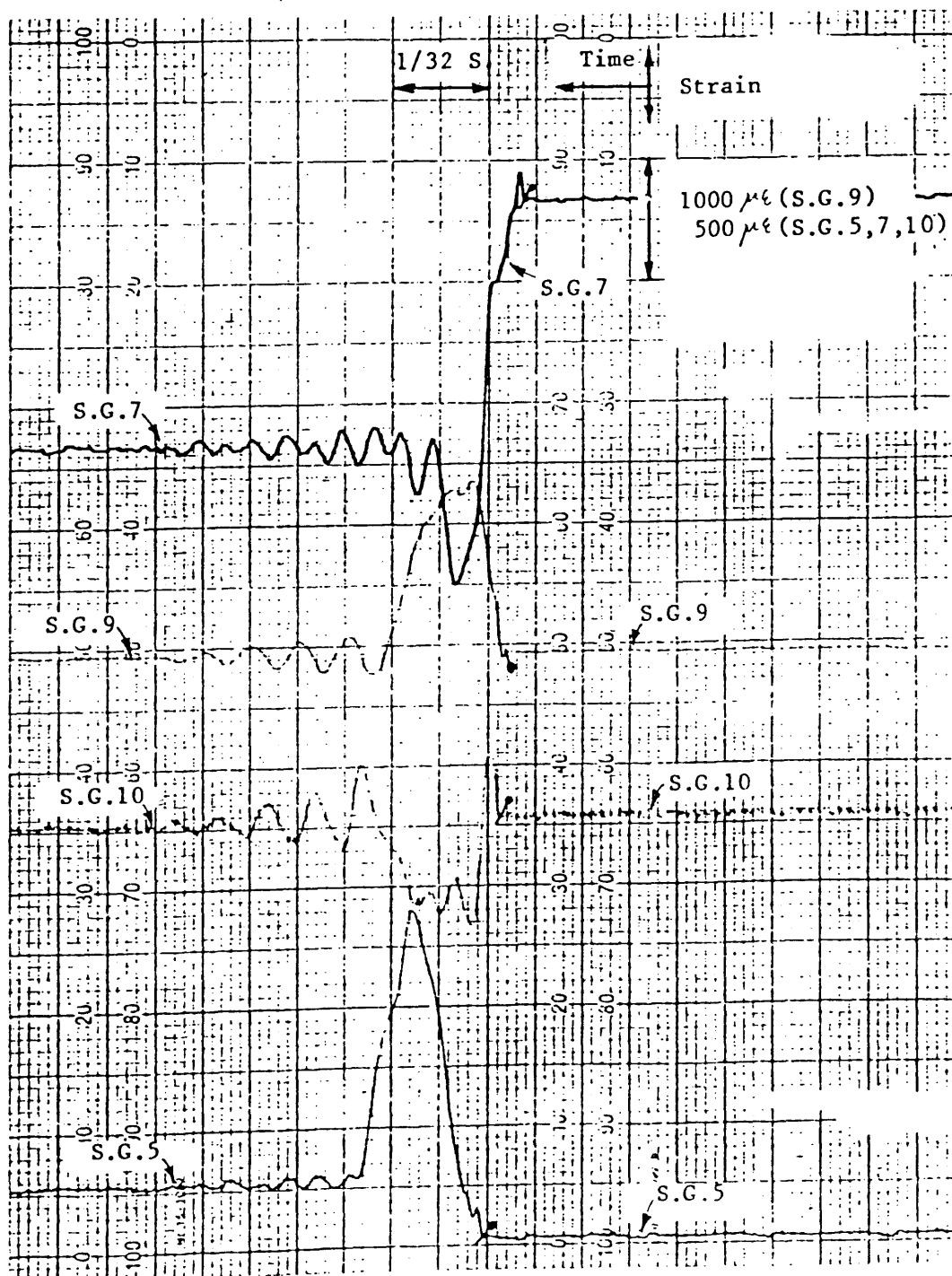
LENGTH(L): 1400 MM

LENGTH for IMPACT TEST(L<sub>i</sub>): 1350 MM

OUTSIDE DIA.: 50.92 MM

THICKNESS : 2.02 MM

p denotes beginning of contact



DYNAMIC RECORDING RESULTSMODEL : *H3*

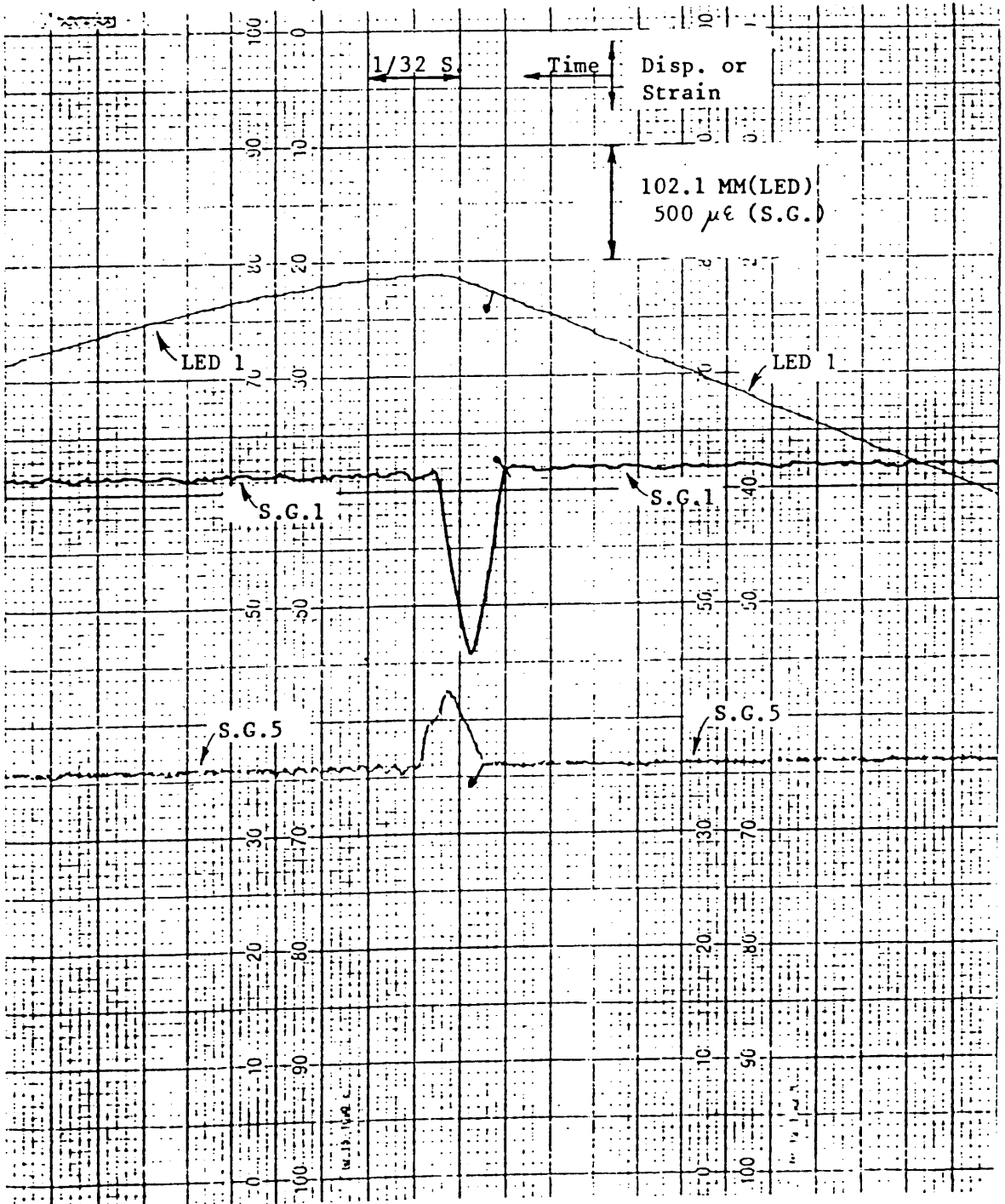
LENGTH(L): 1000 MM

LENGTH for IMPACT TEST(Li): 950 MM

OUTSIDE DIA.: 50.94 MM

THICKNESS : 2.03 MM

• denotes beginning of contact



DYNAMIC RECORDING RESULTS

MODEL : H3

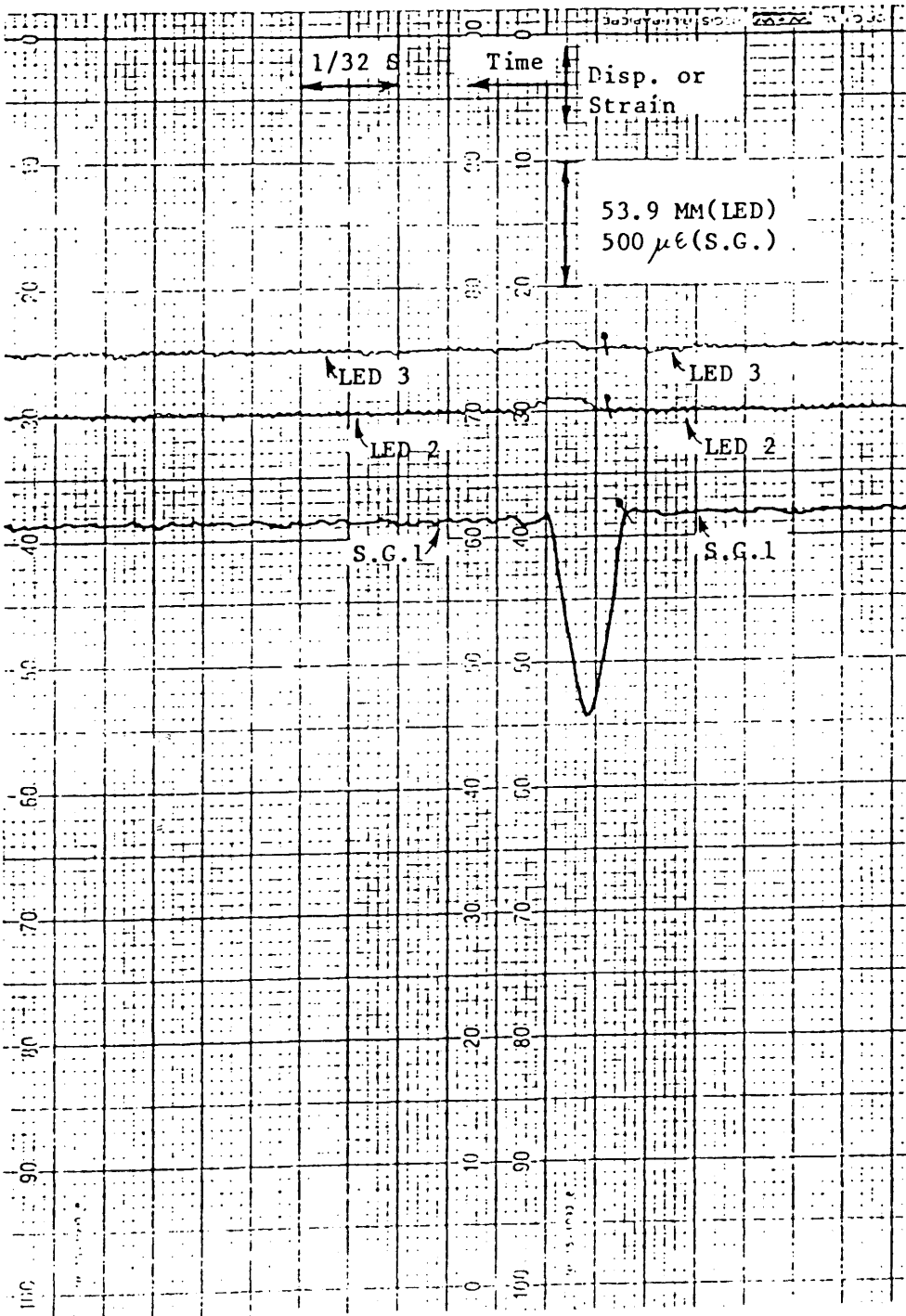
LENGTH(L): 1000 MM

LENGTH for IMPACT TEST(Li): 950 MM

OUTSIDE DIA.: 50.94 MM

THICKNESS : 2.03 MM

p denotes beginning of contact



DYNAMIC RECORDING RESULTS

MODEL : H3

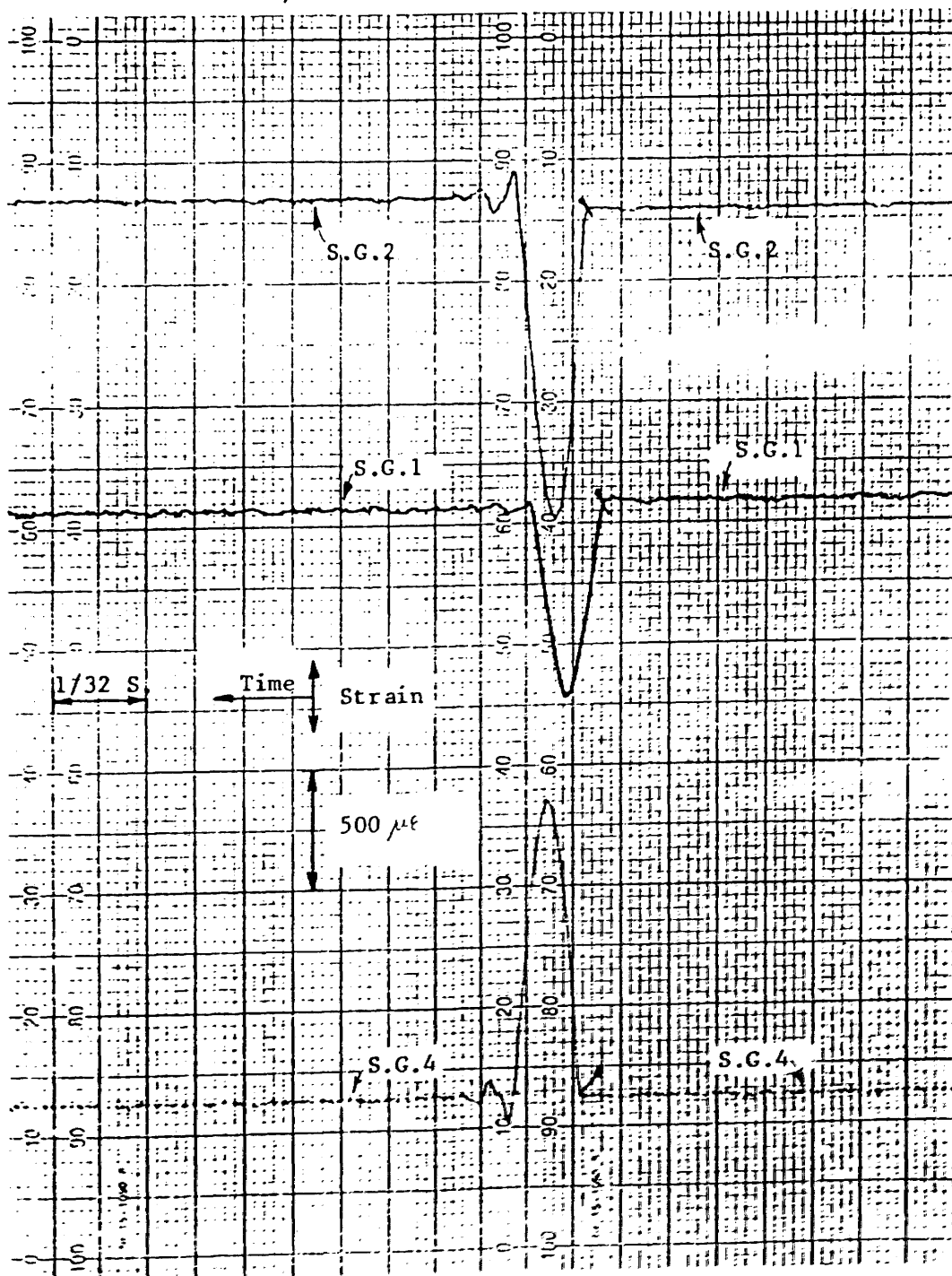
LENGTH(L): 1000 MM

LENGTH for IMPACT TEST(Li): 950 MM

OUTSIDE DIA.: 50.94 MM

THICKNESS : 2.03 MM

/ denotes beginning of contact





### **C. III Extent of Damage Measurements**

**C. III. 1      Extent of Damage Measurements Table**

**C. III. 2      Extent of Damage Plots**

MEASUREMENTS OF EXTENT OF DAMAGE

MODEL : A<sub>3</sub>

o Location of Impact : ( 3.6 MM off Centre toward Bottom, 179° )

o Local Denting Damage ( Depth of Dent ) ( MM )

Location	Centre of Dent	—————→																			MM
		5	10	15	20	25	30	35	40	45	50	60	70	80	90	100	110	120	130	140	
→ toward Top	3.5	2.1	1.4	1.1	0.9	0.8	0.7	0.6	0.5	0.4	0.3	0.1	0.1	0.0							
→ toward Bottom	3.5	2.3	1.6	1.1	1.0	0.8	0.7	0.6	0.5	0.4	0.3	0.1	0.1	0.1	0.0						

o Overall bending Damage ( Out-of-Straightness ) ( MM )

Bottom 0.0 L	0.25L	0.5 L	0.75L	Top 1.0 L
0.0	1.88	3.95	1.99	0.0

Out-of-Straightness at the Impact Point : 4.12 MM

MEASUREMENTS OF EXTENT OF DAMAGE

MODEL : A<sub>4</sub>

o Location of Impact : ( 10.1MM off Centre toward Top, 190° )

o Local Denting Damage ( Depth of Dent ) ( MM )

Location	Centre of Dent															MM				
	5	10	15	20	25	30	35	40	45	50	60	70	80	90	100	110	120	130	140	150
toward Top	3.3	2.2	1.7	1.2	1.1	1.1	0.9	0.8	0.7	0.6	0.4	0.3	0.3	0.2	0.1	0.0				
toward Bottom	3.7	2.5	1.9	1.4	1.3	1.1	1.0	0.8	0.8	0.6	0.4	0.3	0.2	0.2	0.1	0.0				

o Overall bending Damage ( Out-of-Straightness ) ( MM )

Bottom 0.0 L	0.25L	0.5 L	0.75L	Top 1.0 L
0.0	1.90	3.42	2.10	0.0

Out-of-Straightness at the Impact Point : 3.51 MM

MEASUREMENTS OF EXTENT OF DAMAGE

MODEL : B<sub>1</sub>

o Location of Impact : ( 7.0 MM off Centre toward Top, 170° )

o Local Denting Damage ( Depth of Dent ) ( MM )

Location	Centre of Dent	<div>—————→</div>																		MM											
		5	10	15	20	25	30	35	40	45	50	60	70	80	90	100	110	120	130	140	150										
<div>→</div> toward Top	3.1	2.0	1.4	0.9	0.8	0.7	0.6	0.5	0.3	0.2	0.2	0.1	0.0																		
<div>→</div> toward Bottom	3.1	2.0	1.3	1.0	0.9	0.7	0.5	0.4	0.2	0.2	0.2	0.1	0.0																		

o Overall bending Damage ( Out-of-Straightness ) ( MM )

Bottom 0.0 L	0.25L	0.5 L	0.75L	Top 1.0 L
0.0	1.95	3.79	2.16	0.0

Out-of-Straightness at the Impact Point : 3.90 MM

MEASUREMENTS OF EXTENT OF DAMAGE

MODEL : B<sub>3</sub>

o Location of Impact : ( On the Centre of Length, 177° )

o Local Denting Damage ( Depth of Dent ) ( MM )

Location	Centre of Dent	5	10	15	20	25	30	35	40	45	50	60	70	80	90	100	110	120	130	140	150
toward Top	2.8	1.8	1.2	1.0	0.7	0.7	0.6	0.5	0.4	0.3	0.3	0.2	0.1	0.0							
toward Bottom	2.8	1.8	1.2	0.9	0.7	0.6	0.5	0.5	0.5	0.4	0.3	0.3	0.2	0.2	0.1	0.1	0.0				

o Overall bending Damage ( Out-of-Straightness ) ( MM )

Bottom 0.0 L	0.25L	0.5 L	0.75L	Top 1.0 L
0.0	0.97	1.69	0.92	0.0

MEASUREMENTS OF EXTENT OF DAMAGE

MODEL : B<sub>4</sub>

o Location of Impact : ( 7.3 MM off Centre toward Top, 173° )

o Local Denting Damage ( Depth of Dent ) ( MM )

Location	Centre of Dent	MM													
		5	10	15	20	25	30	35	40	45	50	60	70	80	90
toward Top	2.2	1.2	0.8	0.7	0.5	0.4	0.3	0.3	0.1	0.1	0.0				
toward Bottom	2.2	1.5	0.9	0.8	0.6	0.4	0.3	0.3	0.1	0.0	0.0				

o Overall bending Damage ( Out-of-Straightness ) ( MM )

Bottom 0.0 L	0.25L	0.5 L	0.75L	Top 1.0 L
0.0	1.00	2.20	1.15	0.0

Out-of-Straightness at the Impact Point : 2.37 MM

MEASUREMENTS OF EXTENT OF DAMAGE

MODEL : C<sub>1</sub>

o Location of Impact : ( On the Centre of Length, 185° )

o Local Denting Damage ( Depth of Dent ) ( MM )

Location	Centre of Dent	—————																			MM
		5	10	15	20	25	30	35	40	45	50	60	70	80	90	100	110	120	130	140	
<div>→</div> toward Top	2.0	1.3	0.8	0.6	0.5	0.4	0.4	0.3	0.4	0.4	0.3	0.2	0.1	0.1	0.1	0.1	0.1	0.1	0.0		
<div>→</div> toward Bottom	2.0	1.4	0.9	0.7	0.5	0.5	0.4	0.3	0.3	0.3	0.2	0.2	0.2	0.2	0.1	0.1	0.1	0.1	0.0		

o Overall bending Damage ( Out-of-Straightness ) ( MM )

Bottom 0.0 L	0.25L	0.5 L	0.75L	Top 1.0 L
0.0	0.80	1.13	0.56	0.0

MEASUREMENTS OF EXTENT OF DAMAGE

MODEL : C<sub>2</sub>

o Location of Impact : ( On the Centre of Length, 169° )

o Local Denting Damage ( Depth of Dent ) ( MM )

Location	Centre of Dent	MM																			
		5	10	15	20	25	30	35	40	45	50	60	70	80	90	100	110	120	130	140	150
toward Top	10.4	8.2	6.0	5.3	4.4	3.8	3.2	2.9	2.6	2.3	2.0	1.6	1.2	1.0	0.9	0.6	0.5	0.3	0.2	0.1	0.0
toward Bottom	10.4	8.6	6.9	5.3	4.4	3.8	3.2	2.9	2.4	2.3	2.0	1.5	1.2	1.0	0.8	0.6	0.4	0.2	0.2	0.1	0.0

o Overall bending Damage ( Out-of-Straightness ) ( MM )

Bottom 0.0 L	0.25L	0.5 L	0.75L	Top 1.0 L
0.0	7.91	14.96	7.82	0.0



MEASUREMENTS OF EXTENT OF DAMAGE

MODEL : C<sub>3</sub>

o Location of Impact : ( 2.0 MM off Centre toward Top, 178° )

o Local Denting Damage ( Depth of Dent ) ( MM )

Location	Centre of Dent	MM																			
		5	10	15	20	25	30	35	40	45	50	60	70	80	90	100	110	120	130	140	150
→ toward Top	0.5	0.1	0.0																		
→ toward Bottom	0.5	0.3	0.2	0.0																	

o Overall bending Damage ( Out-of-Straightness ) ( MM )

Bottom 0.0 L	0.25L	0.5 L	0.75L	Top 1.0 L
0.0	-0.40	0.17	-0.12	0.0

Out-of-Straightness at the Impact Point : 0.16 MM

MEASUREMENTS OF EXTENT OF DAMAGE

MODEL : C<sub>4</sub>

o Location of Impact : ( On the Centre of Length, 180° )

o Local Denting Damage ( Depth of Dent ) ( MM )

Location	Centre of Dent	5	10	15	20	25	30	35	40	45	50	60	70	80	90	100	110	120	130	140	150
toward Top	6.8	4.7	3.3	2.7	2.1	2.0	1.7	1.5	1.4	1.2	1.0	0.8	0.5	0.4	0.2	0.2	0.1	0.1			
toward Bottom	6.8	5.1	3.7	2.9	2.4	2.0	1.7	1.7	1.5	1.3	1.1	0.8	0.7	0.4	0.3	0.2	0.1	0.0			

o Overall bending Damage ( Out-of-Straightness ) ( MM )

Bottom 0.0 L	0.25L	0.5 L	0.75L	Top 1.0 L
0.0	5.92	12.03	6.27	0.0

MEASUREMENTS OF EXTENT OF DAMAGE

MODEL : D<sub>1</sub>

o Location of Impact : ( On the Centre of Length, 175° )

o Local Denting Damage ( Depth of Dent )																					( MM )
Location	Centre of Dent																			MM	
	5	10	15	20	25	30	35	40	45	50	60	70	80	90	100	110	120	130	140	150	
toward Top	0.2	0.2	0.1	0.0																	
toward Bottom	0.2	0.1	0.1	0.1	0.0																

o Overall bending Damage ( Out-of-Straightness ) ( MM )

Bottom 0.0 L	0.25L	0.5 L	0.75L	Top 1.0 L
0.0	0.16	0.52	0.32	0.0

MEASUREMENTS OF EXTENT OF DAMAGE

MODEL : D<sub>2</sub>

o Location of Impact : ( 12.0 MM off Centre toward Top, 177° )

o Local Denting Damage ( Depth of Dent ) ( MM )

Location	Centre of Dent	5	10	15	20	25	30	35	40	45	50	60	70	80	90	100	110	120	130	140	150
toward Top	6.2	4.1	3.2	2.5	2.2	2.0	1.8	1.6	1.4	1.2	1.1	0.9	0.6	0.4	0.3	0.2	0.1	0.1	0.0		
toward Bottom	6.2	4.8	3.6	2.8	2.3	2.0	1.6	1.4	1.3	1.2	1.1	0.8	0.6	0.4	0.2	0.2	0.1	0.0			

o Overall bending Damage ( Out-of-Straightness ) ( MM )

Bottom 0.0 L	0.25L	0.5 L	0.75L	Top 1.0 L
0.0	3.06	5.53	3.25	0.0

Out-of-Straightness at the Impact Point : 5.87 MM

MEASUREMENTS OF EXTENT OF DAMAGE

MODEL : D<sub>3</sub>

o Location of Impact : ( 16.0 MM off Centre toward Top, 180° )

o Local Denting Damage ( Depth of Dent ) ( MM )

Location	Centre of Dent	5	10	15	20	25	30	35	40	45	50	60	70	80	90	100	110	120	130	140	150
toward Top	5.3	3.8	2.7	2.1	1.8	1.7	1.5	1.2	1.1	1.0	0.8	0.6	0.4	0.4	0.2	0.1	0.1	0.1	0.0		
toward Bottom	5.3	4.0	3.1	2.3	1.9	1.6	1.4	1.2	1.1	0.9	0.8	0.7	0.5	0.3	0.2	0.0					

o Overall bending Damage ( Out-of-Straightness ) ( MM )

Bottom 0.0 L	0.25L	0.5 L	0.75L	Top 1.0 L
0.0	3.81	7.55	4.08	0.0

Out-of-Straightness at the Impact Point : 7.78 MM

MEASUREMENTS OF EXTENT OF DAMAGE

MODEL : D<sub>4</sub>

o Location of Impact : ( On the Centre of Length, 172° )

o Local Denting Damage ( Depth of Dent ) ( MM )

Location	Centre of Dent	5	10	15	20	25	30	35	40	45	50	60	70	80	90	100	110	120	130	140	150
toward Top	9.1	6.8	5.0	3.9	3.5	3.0	2.8	2.4	2.1	1.9	1.7	1.5	1.3	1.1	0.9	0.7	0.4	0.3	0.2	0.1	0.0
toward Bottom	9.1	7.2	5.5	4.3	3.8	3.2	2.9	2.5	2.3	2.0	1.8	1.5	1.3	1.2	1.0	0.7	0.6	0.4	0.2	0.1	0.0

o Overall bending Damage ( Out-of-Straightness ) ( MM )

Bottom 0.0 L	0.25L	0.5 L	0.75L	Top 1.0 L
0.0	10.94	20.70	10.49	0.0

MEASUREMENTS OF EXTENT OF DAMAGE

MODEL : E<sub>3</sub>

o Location of Impact : ( 15.3 MM off Centre toward Top, 183° )

o Local Denting Damage ( Depth of Dent ) ( MM )																				
Location	Centre of Dent																			MM
	5	10	15	20	25	30	35	40	45	50	60	70	80	90	100	110	120	130	140	
<div>→</div> toward Top	0.4	0.2	0.0																	
<div>→</div> toward Bottom	0.4	0.3	0.2	0.1	0.0															

o Overall bending Damage ( Out-of-Straightness ) ( MM )

Bottom 0.0 L	0.25L	0.5 L	0.75L	Top 1.0 L
0.0	0.22	0.40	0.14	0.0

Out-of-Straightness at the Impact Point : 0.51 MM

MEASUREMENTS OF EXTENT OF DAMAGE

MODEL : F<sub>1</sub>

o Location of Impact : ( On the Centre of Length, 180° )

o Local Denting Damage ( Depth of Dent )																					
		( MM )																			
Location	Centre of Dent	MM																			
		5	10	15	20	25	30	35	40	45	50	60	70	80	90	100	110	120	130	140	150
toward Top	O.O																				
toward Bottom	O.O																				

o Overall bending Damage ( Out-of-Straightness ) ( MM )

Bottom 0.0 L	0.25L	0.5 L	0.75L	Top 1.0 L
0.0	0.0	0.0	0.0	0.0



MEASUREMENTS OF EXTENT OF DAMAGE

MODEL : F<sub>1p</sub>

o Location of Impact : ( On the Centre of Length, 191° )

o Local Denting Damage ( Depth of Dent )

( MM )

Location	Centre of Dent	MM													
		5	10	15	20	25	30	35	40	45	50	60	70	80	90
toward Top	0.8	0.4	0.3	0.3	0.3	0.1	0.1	0.1	0.1	0.1	0.0				
toward Bottom	0.8	0.6	0.5	0.3	0.3	0.2	0.1	0.0							

o Overall bending Damage ( Out-of-Straightness )

( MM )

Bottom 0.0 L	0.25L	0.5 L	0.75L	Top 1.0 L
0.0	0.60	1.13	0.27	0.0

MEASUREMENTS OF EXTENT OF DAMAGE

MODEL : F<sub>2</sub>

o Location of Impact : ( 9.0 MM off Centre toward Bottom, 197° )

o Local Denting Damage ( Depth of Dent ) ( MM )

Location	Centre of Dent	5	10	15	20	25	30	35	40	45	50	60	70	80	90	100	110	120	130	140	150
toward Top	2.1	1.4	0.7	0.6	0.4	0.4	0.3	0.3	0.2	0.1	0.1	0.1	0.1	0.1	0.0						
toward Bottom	2.1	1.6	1.0	0.8	0.7	0.6	0.5	0.5	0.5	0.5	0.4	0.3	0.1	0.0							

o Overall bending Damage ( Out-of-Straightness ) ( MM )

Bottom 0.0 L	0.25L	0.5 L	0.75L	Top 1.0 L
0.0	1.13	1.99	1.00	0.0

Out-of-Straightness at the Impact Point : 1.89 MM

MEASUREMENTS OF EXTENT OF DAMAGE

MODEL : F<sub>3</sub>

o Location of Impact : ( 5.5 MM off Centre toward Top, 182° )

o Local Denting Damage ( Depth of Dent ) ( MM )

Location	Centre of Dent															MM				
	5	10	15	20	25	30	35	40	45	50	60	70	80	90	100	110	120	130	140	150
toward Top	0.9	0.5	0.4	0.3	0.2	0.2	0.1	0.1	0.1	0.1	0.1	0.1	0.1	0.0						
toward Bottom	1.0	0.7	0.4	0.3	0.3	0.2	0.2	0.2	0.1	0.1	0.1	0.1	0.1	0.1	0.0					

o Overall bending Damage ( Out-of-Straightness ) ( MM )

Bottom 0.0 L	0.25L	0.5 L	0.75L	Top 1.0 L
0.0	0.68	2.51	1.09	0.0

Out-of-Straightness at the Impact Point : 2.76 MM

MEASUREMENTS OF EXTENT OF DAMAGE

MODEL : G<sub>1</sub>

o Location of Impact : ( 10.8 MM off Centre toward Top, 180° )

o Local Denting Damage ( Depth of Dent ) ( MM )

Location	Centre of Dent	5	10	15	20	25	30	35	40	45	50	60	70	80	90	100	110	120	130	140	150	MM
toward Top	1.7	1.2	0.7	0.5	0.4	0.4	0.2	0.2	0.1	0.1	0.1	0.0										
toward Bottom	1.7	1.1	0.6	0.5	0.4	0.3	0.3	0.3	0.1	0.1	0.1	0.0										

o Overall bending Damage ( Out-of-Straightness ) ( MM )

Bottom 0.0 L	0.25L	0.5 L	0.75L	Top 1.0 L
0.0	0.82	1.63	1.01	0.0

Out-of-Straightness at the Impact Point : 1.73 MM

MEASUREMENTS OF EXTENT OF DAMAGE

MODEL : G<sub>2</sub>

o Location of Impact : ( On the Centre of Length, 192° )

o Local Denting Damage ( Depth of Dent ) ( MM )

Location	Centre of Dent	5	10	15	20	25	30	35	40	45	50	60	70	80	90	100	110	120	130	140	150
toward Top	1.8	1.2	0.8	0.5	0.4	0.3	0.2	0.1	0.0												
toward Bottom	1.8	1.3	0.8	0.4	0.3	0.2	0.1	0.1	0.0												

o Overall bending Damage ( Out-of-Straightness ) ( MM )

Bottom 0.0 L	0.25L	0.5 L	0.75L	Top 1.0 L
0.0	1.78	3.40	1.63	0.0

MEASUREMENTS OF EXTENT OF DAMAGE

MODEL : G<sub>3</sub>

o Location of Impact : ( On the Centre of Length, 192° )

o Local Denting Damage ( Depth of Dent ) ( MM )

Location	Centre of Dent																MM			
	5	10	15	20	25	30	35	40	45	50	60	70	80	90	100	110	120	130	140	150
toward Top	0.1	0.1	0.0																	
toward Bottom	0.2	0.2	0.1	0.0																

o Overall bending Damage ( Out-of-Straightness ) ( MM )

Bottom 0.0 L	0.25L	0.5 L	0.75L	Top 1.0 L
0.0	-0.29	-0.54	-0.86	0.0

MEASUREMENTS OF EXTENT OF DAMAGE

MODEL : H<sub>1</sub>

o Location of Impact : ( 19.5 MM off Centre toward Top, 183° )

o Local Denting Damage ( Depth of Dent ) ( MM )

Location	Centre of Dent	5	10	15	20	25	30	35	40	45	50	60	70	80	90	100	110	120	130	140	150
toward Top	0.3	0.2	0.2	0.1	0.1	0.1	0.0														
toward Bottom	0.3	0.2	0.1	0.1	0.1	0.0															

o Overall bending Damage ( Out-of-Straightness ) ( MM )

Bottom 0.0 L	0.25L	0.5 L	0.75L	Top 1.0 L
0.0	0.12	0.34	0.23	0.0

Out-of-Straightness at the Impact Point : 0.40 MM

MEASUREMENTS OF EXTENT OF DAMAGE

MODEL :H<sub>2</sub>

o Location of Impact : ( On the Centre of Length, 173° )

o Local Denting Damage ( Depth of Dent ) ( MM )

Location	Centre of Dent	MM													
		5	10	15	20	25	30	35	40	45	50	60	70	80	90
toward Top	3.2	1.6	1.4	0.8	0.8	0.4	0.4	0.3	0.3	0.3	0.2	0.1	0.1	0.0	
toward Bottom	3.2	2.4	1.4	0.9	0.7	0.7	0.5	0.3	0.3	0.2	0.1	0.1	0.1	0.0	

o Overall bending Damage ( Out-of-Straightness ) ( MM )

Bottom 0.0 L	0.25L	0.5 L	0.75L	Top 1.0 L
0.0	2.82	6.06	2.35	0.0



MEASUREMENTS OF EXTENT OF DAMAGE

MODEL : H<sub>3</sub>

o Location of Impact : ( On the Centre of Length, 180° )

o Local Denting Damage ( Depth of Dent ) ( MM )

Location	Centre of Dent																				MM										
	5	10	15	20	25	30	35	40	45	50	60	70	80	90	100	110	120	130	140	150											
toward Top	0.05	0.0																													
toward Bottom	0.05	0.0																													

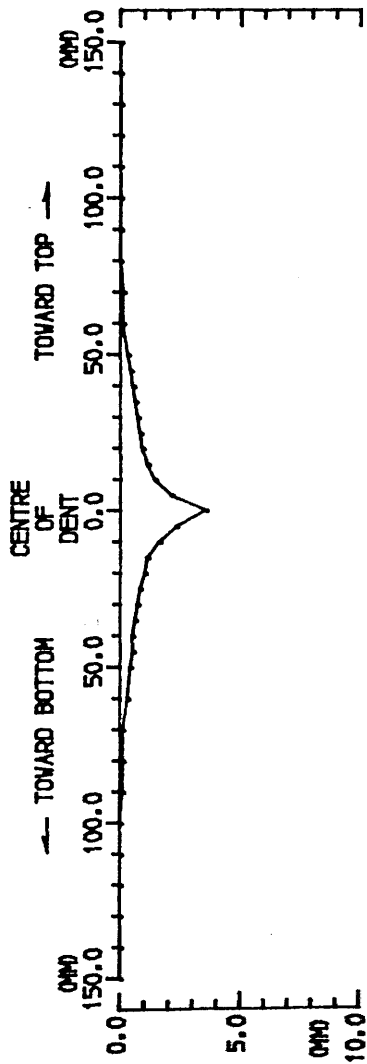
o Overall bending Damage ( Out-of-Straightness ) ( MM )

Bottom 0.0 L	0.25L	0.5 L	0.75L	Top 1.0 L
0.0	0.0	0.01	0.0	0.0

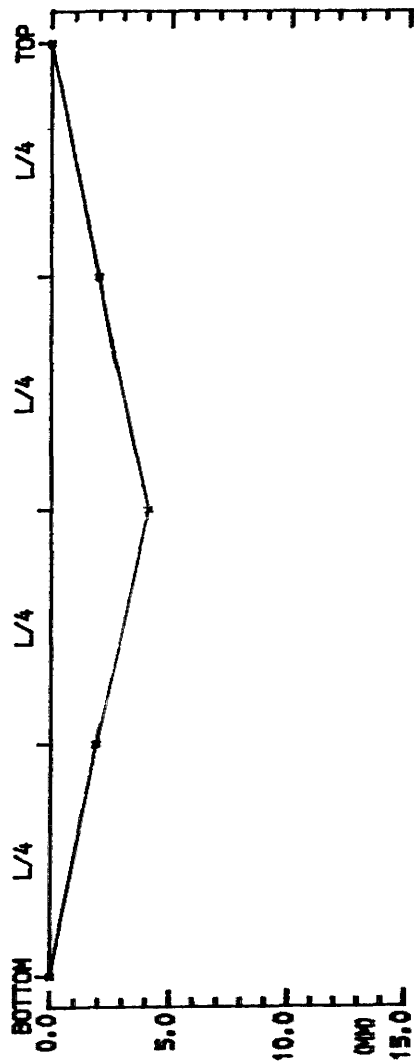
EXTENT OF DAMAGE

MODEL : A3

0 LOCAL DENTING DAMAGE (DEPTH OF DENT)



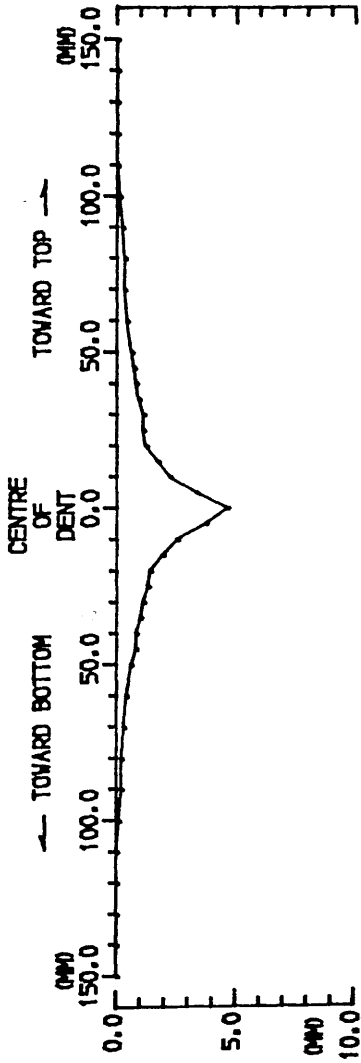
0 OVERALL BENDING DAMAGE (OUT-OF-STRAIGHTNESS)



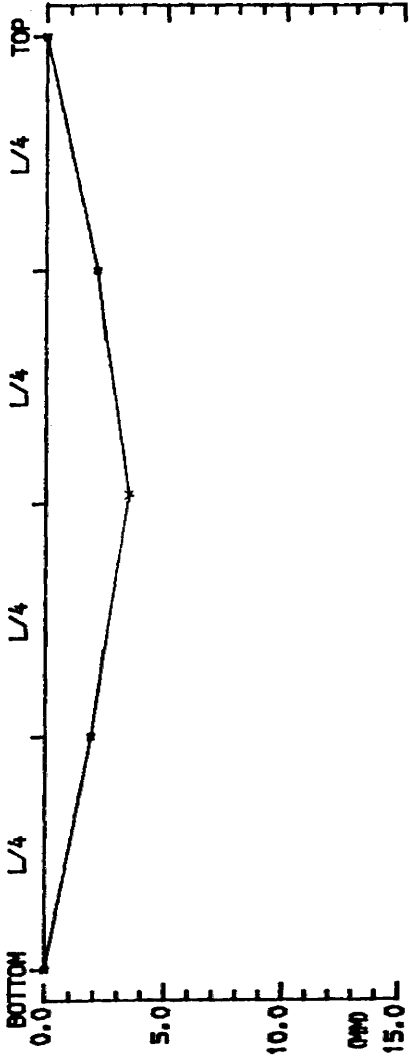
EXTENT OF DAMAGE

MODEL • A4

0 LOCAL DENTING DAMAGE (DEPTH OF DENT)



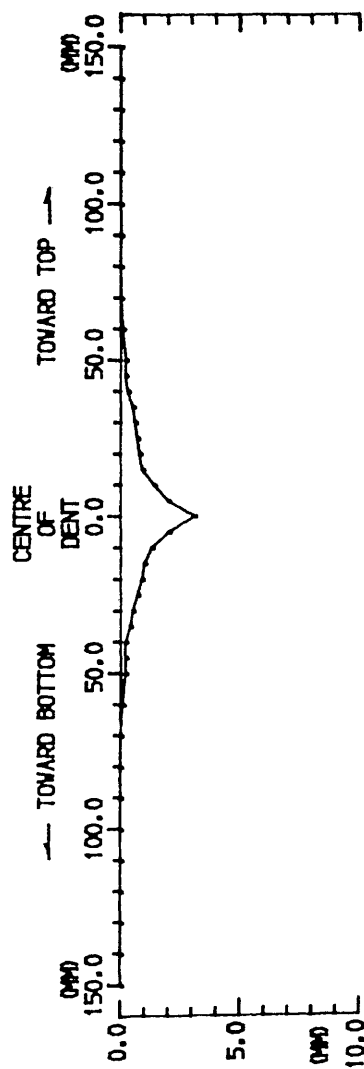
0 OVERALL BENDING DAMAGE (OUT-OF-STRAIGHTNESS)



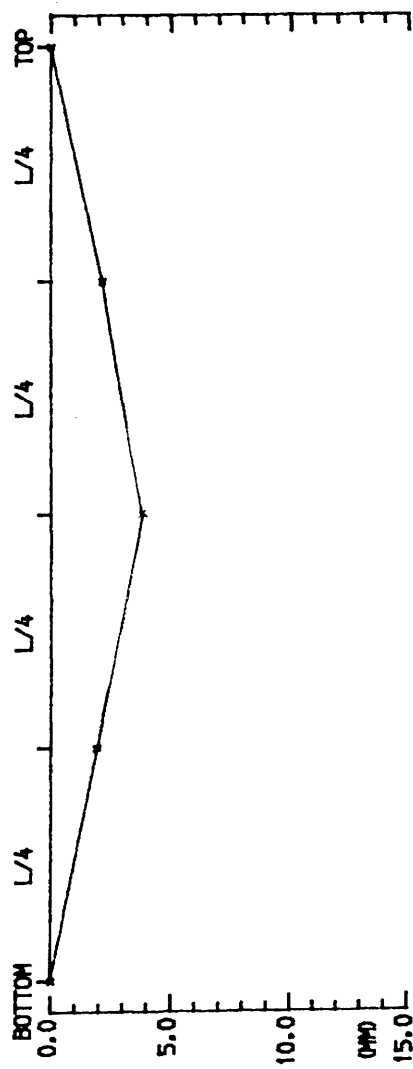
# EXTENT OF DAMAGE

MODEL • B1

0 LOCAL DENTING DAMAGE (DEPTH OF DENT)



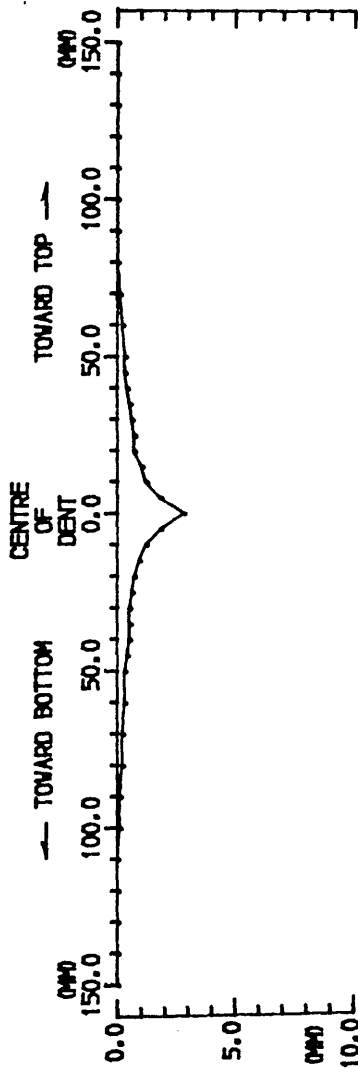
0 OVERALL BENDING DAMAGE (OUT-OF-STRAIGHTNESS)



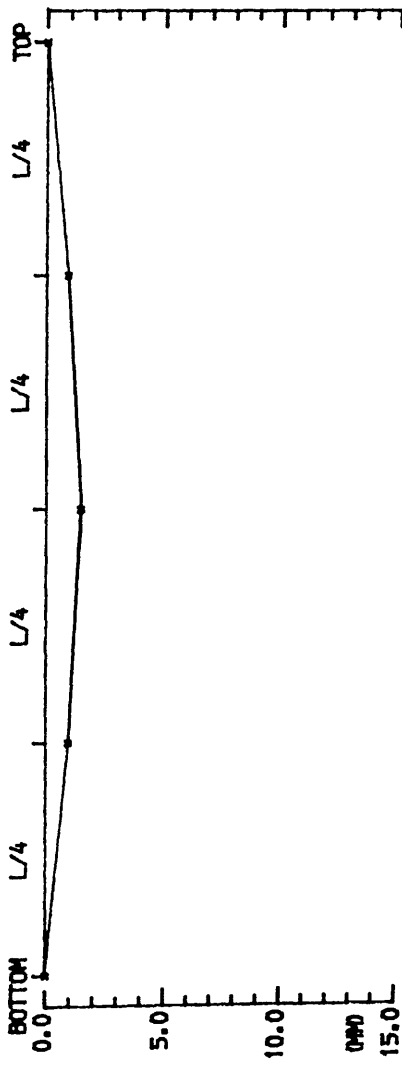
EXTENT OF DAMAGE

MODEL : B3

0 LOCAL DENTING DAMAGE (DEPTH OF DENT)



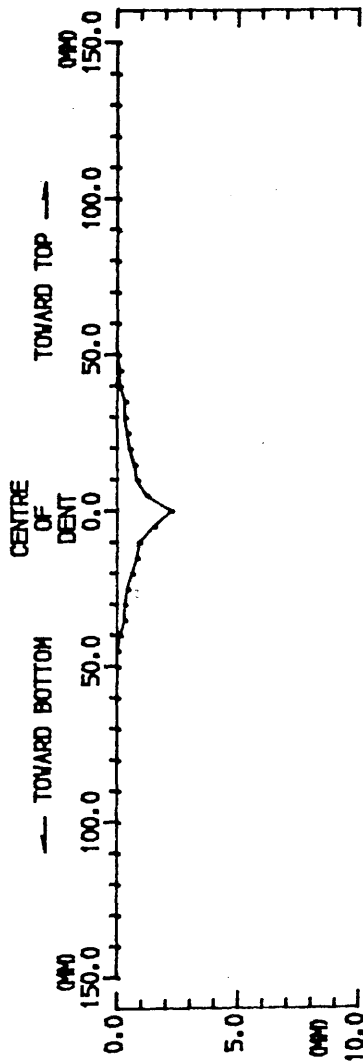
0 OVERALL BENDING DAMAGE (OUT-OF-STRAIGHTNESS)



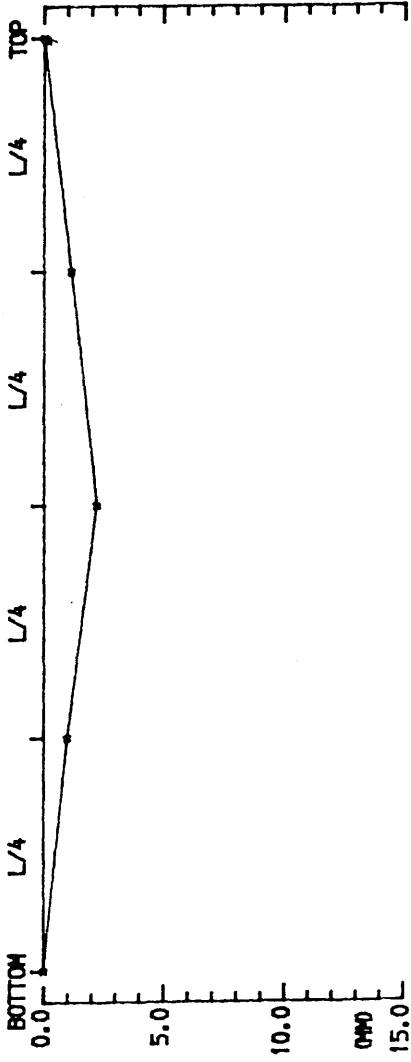
EXTENT OF DAMAGE

MODEL , B4

0 LOCAL DENTING DAMAGE (DEPTH OF DENT)



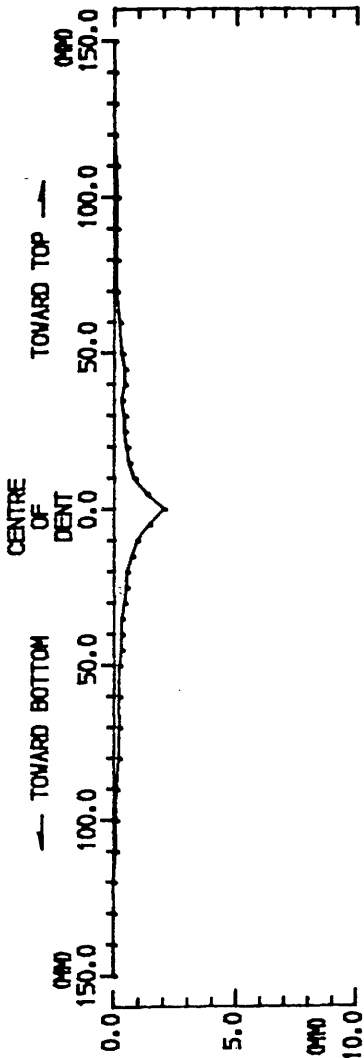
0 OVERALL BENDING DAMAGE (OUT-OF-STRAIGHTNESS)



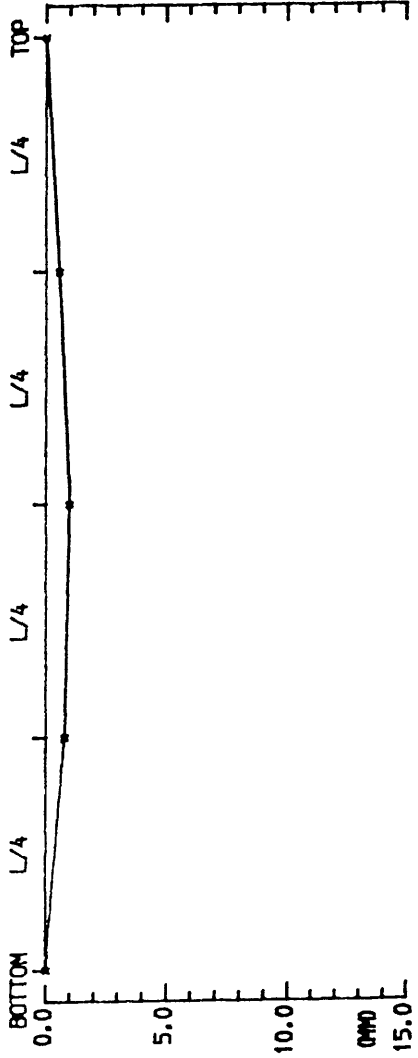
EXTENT OF DAMAGE

MODEL : C1

0 LOCAL DENTING DAMAGE (DEPTH OF DENT)



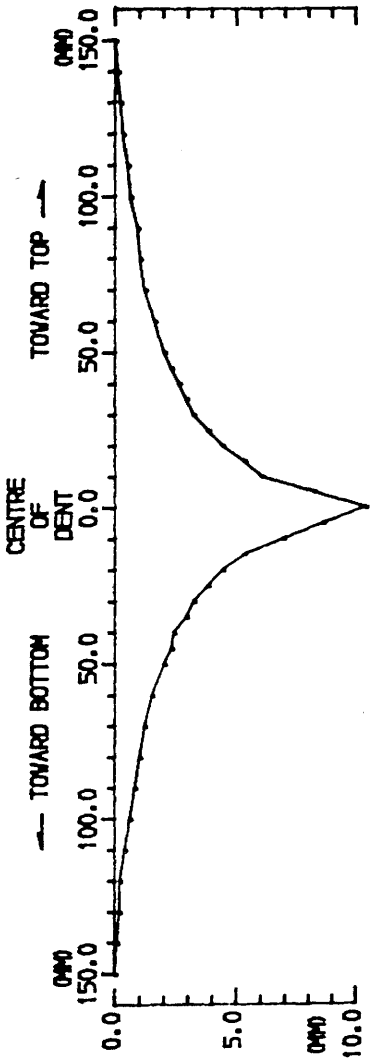
0 OVERALL BENDING DAMAGE (OUT-OF-STRAIGHTNESS)



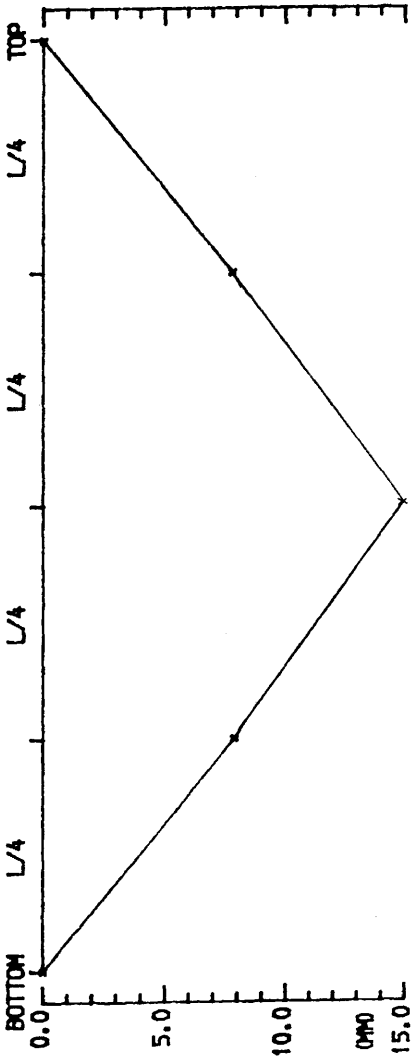
EXTENT OF DAMAGE

MODEL : C2

0 LOCAL DENTING DAMAGE (DEPTH OF DENT)



0 OVERALL BENDING DAMAGE (OUT-OF-STRAIGHTNESS)

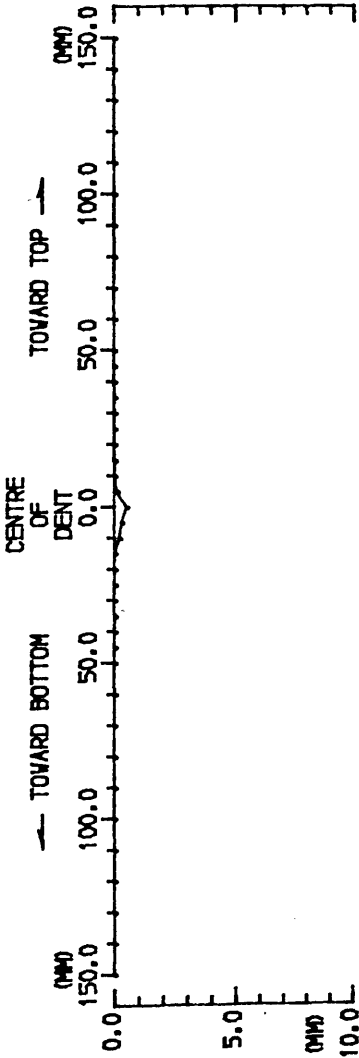




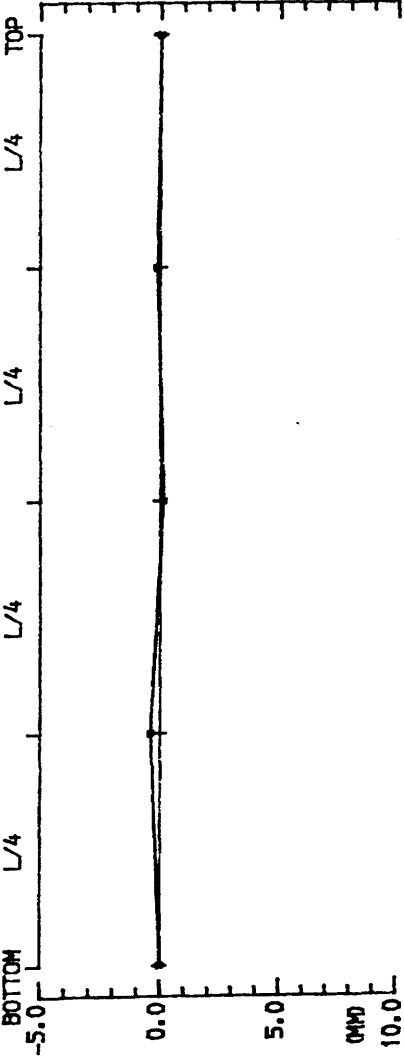
EXTENT OF DAMAGE

MODEL : C3

0 LOCAL DENTING DAMAGE (DEPTH OF DENT)



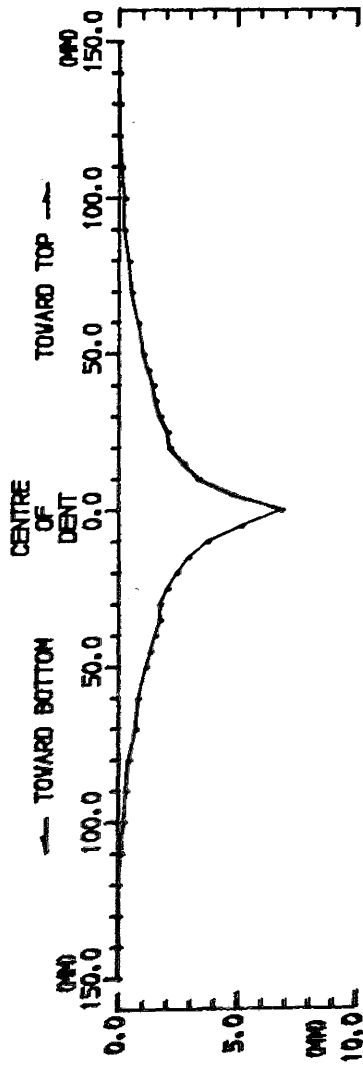
0 OVERALL BENDING DAMAGE (OUT-OF-STRAIGHTNESS)



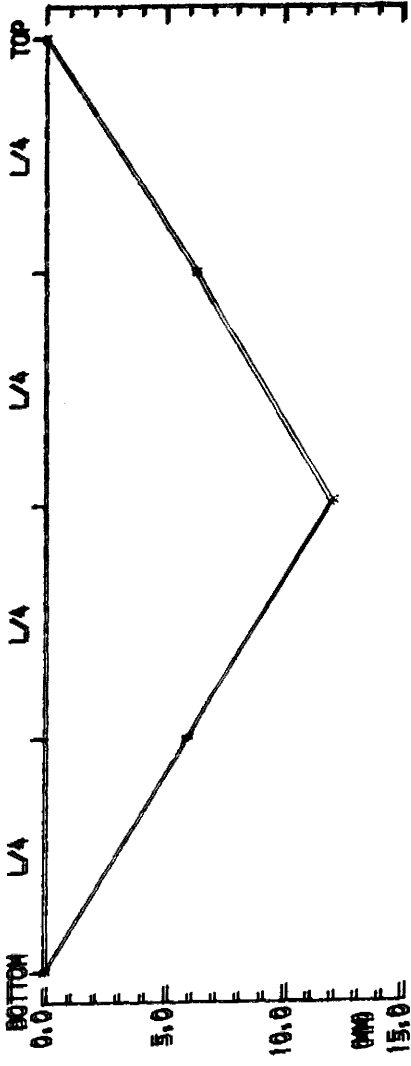
EXTENT OF DAMAGE

MODEL : C4

0 LOCAL DENTING DAMAGE (DEPTH OF DENT)



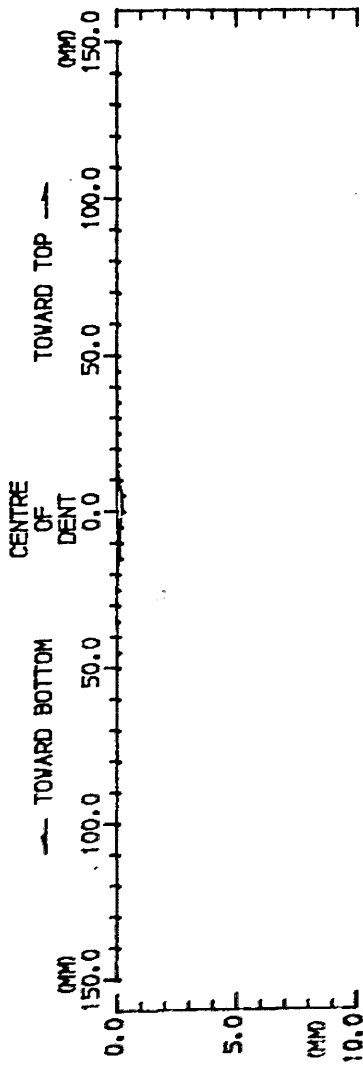
0 OVERALL BENDING DAMAGE (OUT-OF-STRAIGHTNESS)



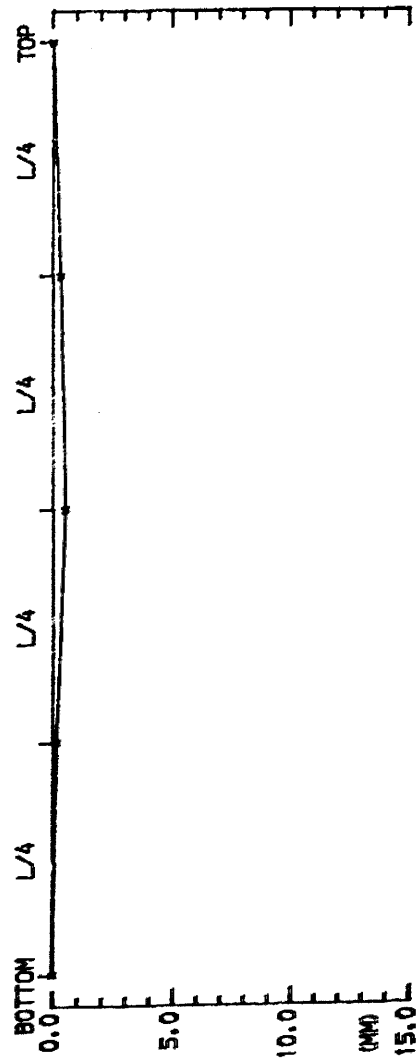
## EXTENT OF DAMAGE

MODEL • D1

0 LOCAL DENTING DAMAGE (DEPTH OF DENT)



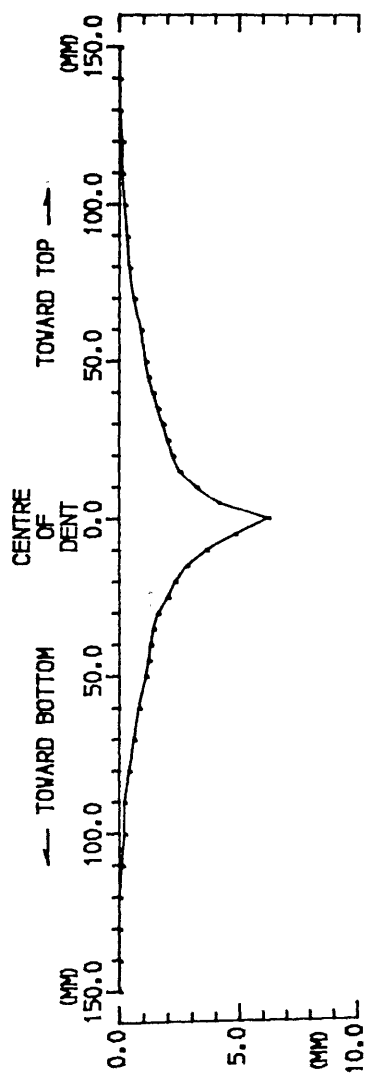
0 OVERALL BENDING DAMAGE (OUT-OF-STRAIGHTNESS)



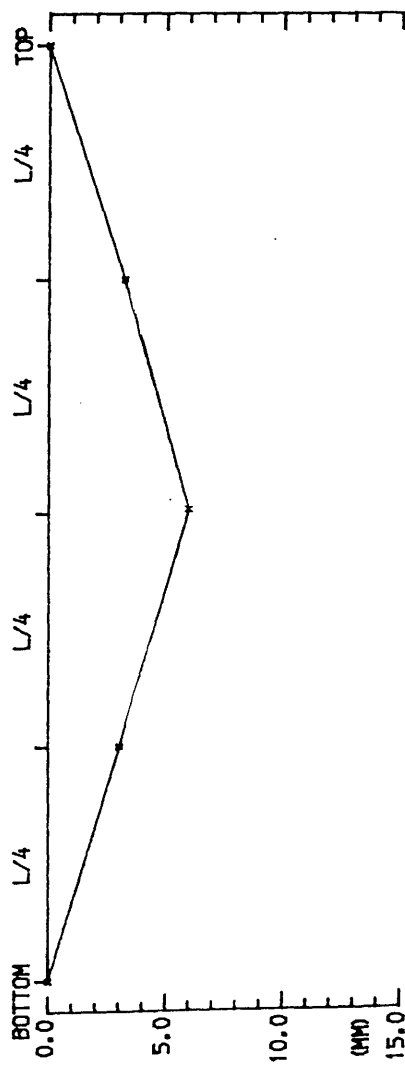
# EXTENT OF DAMAGE

MODEL • D2

0 LOCAL DENTING DAMAGE (DEPTH OF DENT)



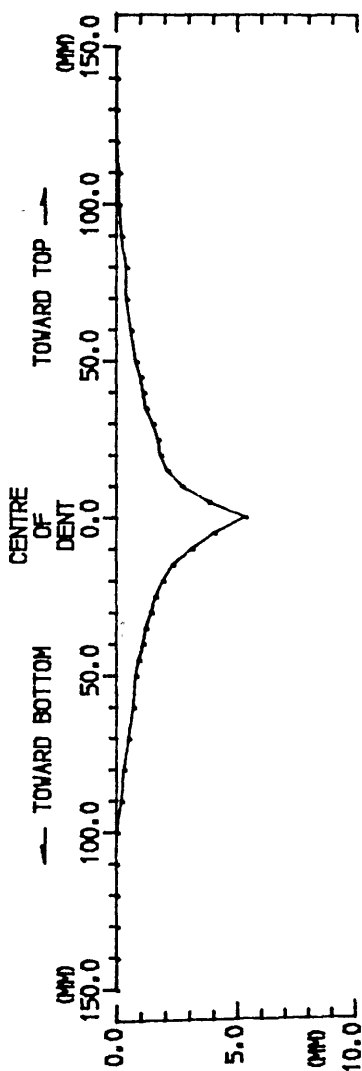
0 OVERALL BENDING DAMAGE (OUT-OF-STRAIGHTNESS)



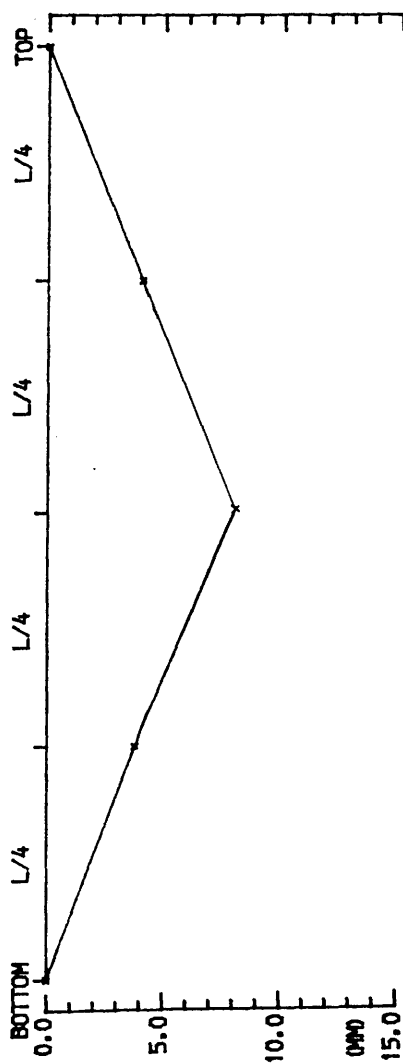
# EXTENT OF DAMAGE

MODEL , D3

0 LOCAL DENTING DAMAGE (DEPTH OF DENT)



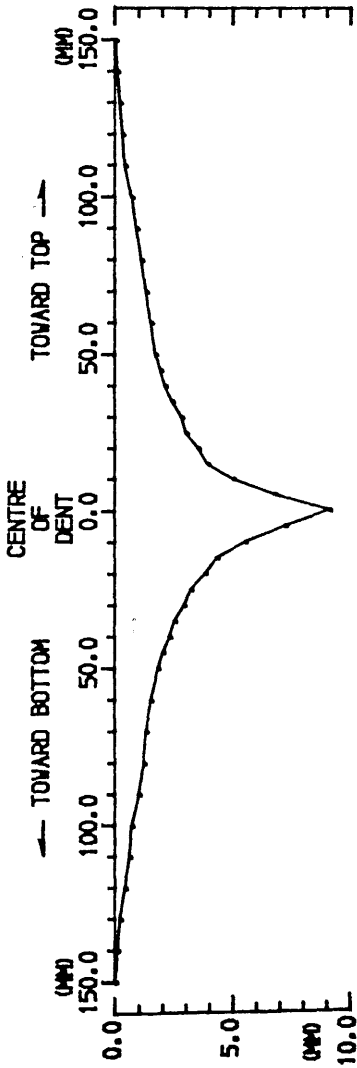
0 OVERALL BENDING DAMAGE (OUT-OF-STRAIGHTNESS)



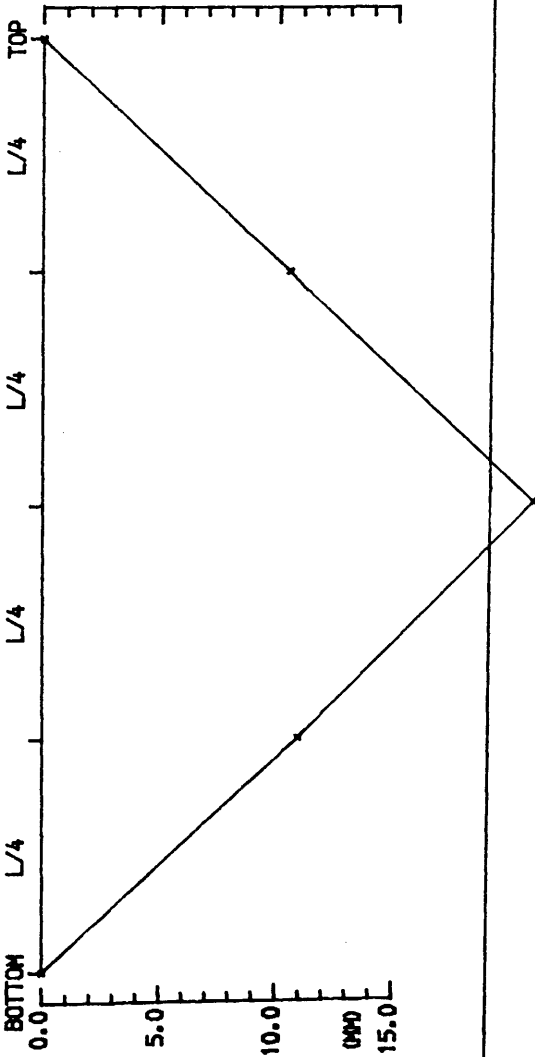
EXTENT OF DAMAGE

MODEL • D4

0 LOCAL DENTING DAMAGE (DEPTH OF DENT)



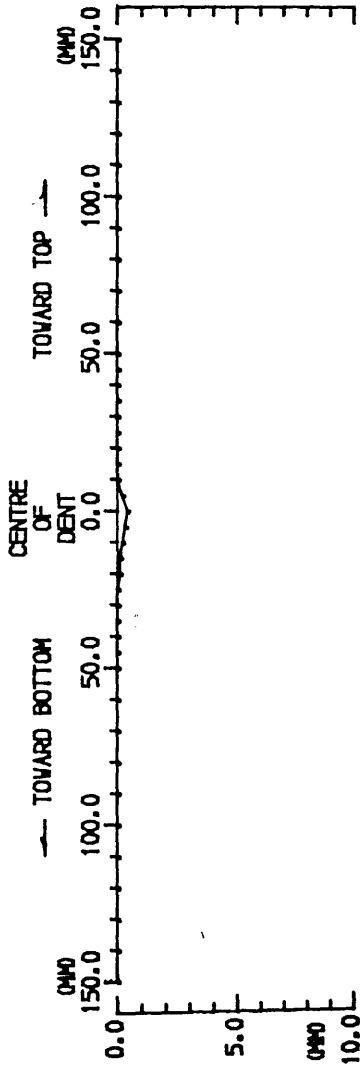
0 OVERALL BENDING DAMAGE (OUT-OF-STRAIGHTNESS)



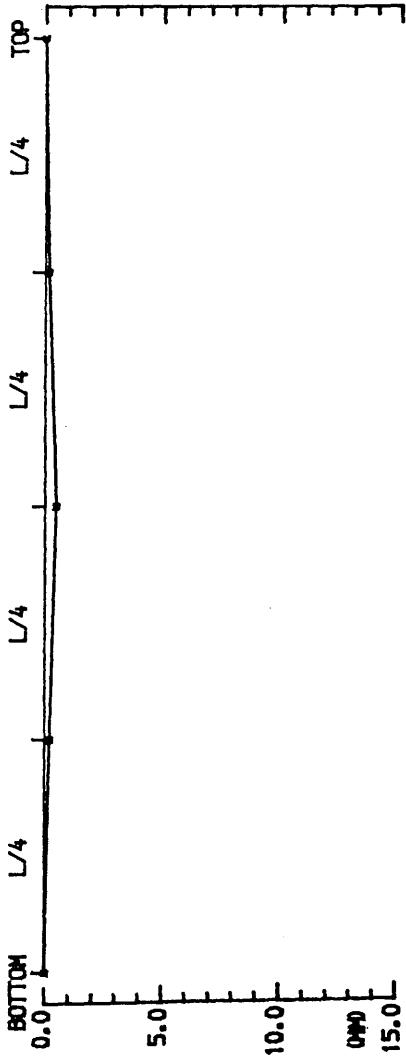
EXTENT OF DAMAGE

MODEL • E3

0 LOCAL DENTING DAMAGE (DEPTH OF DENT)



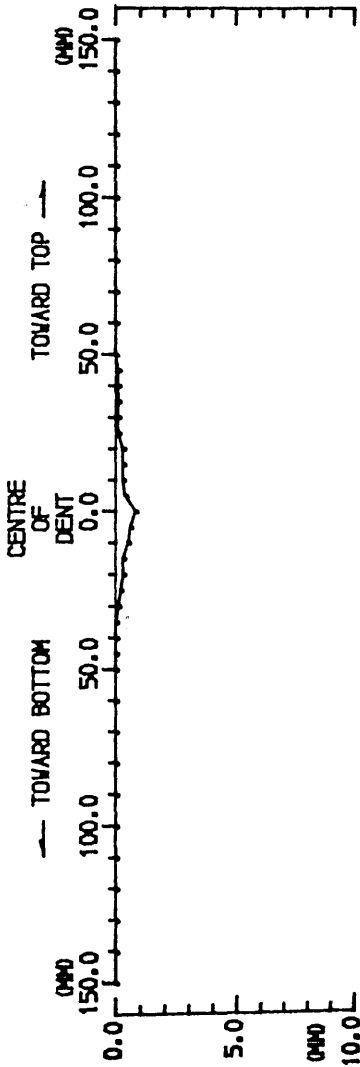
0 OVERALL BENDING DAMAGE (OUT-OF-STRAIGHTNESS)



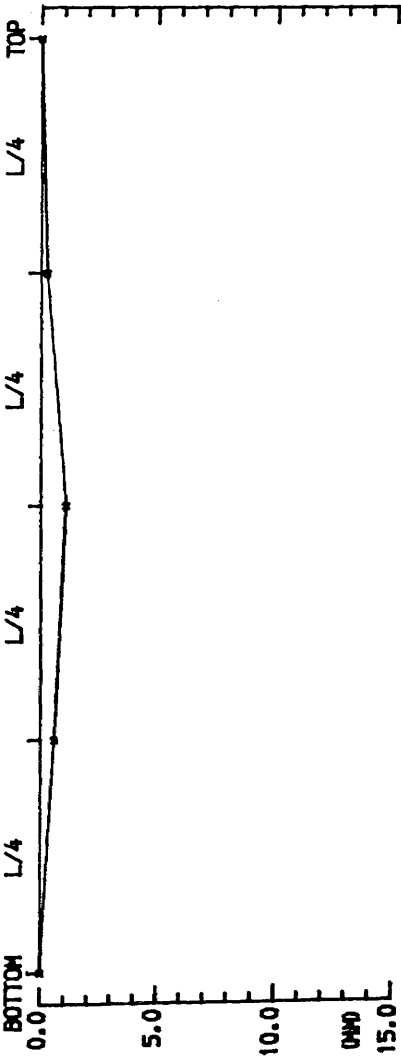
EXTENT OF DAMAGE

MODEL , F1P

0 LOCAL DENTING DAMAGE (DEPTH OF DENT)



0 OVERALL BENDING DAMAGE (OUT-OF-STRAIGHTNESS)

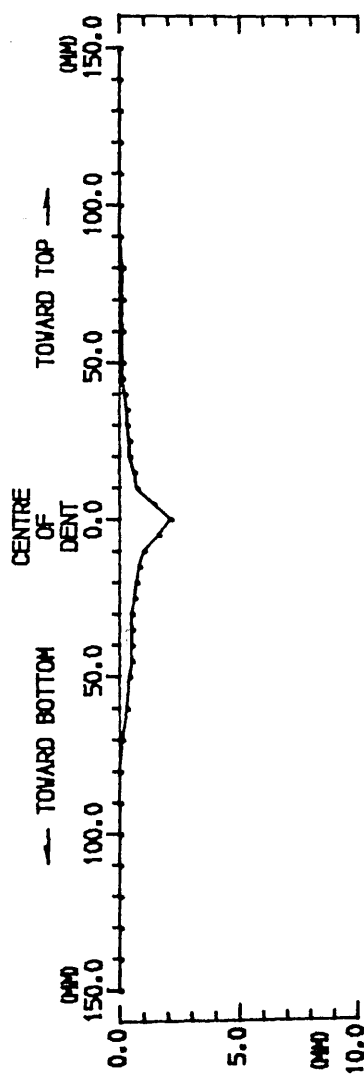




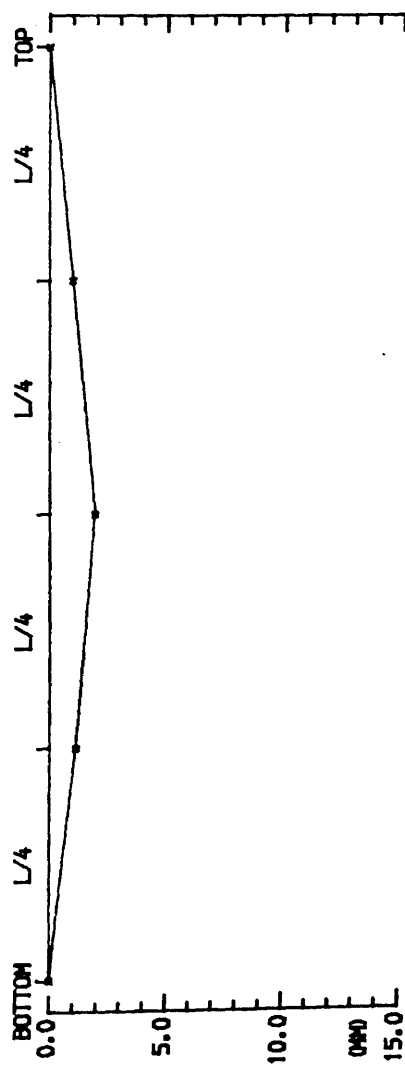
## EXTENT OF DAMAGE

MODEL , F2

0 LOCAL DENTING DAMAGE (DEPTH OF DENT)



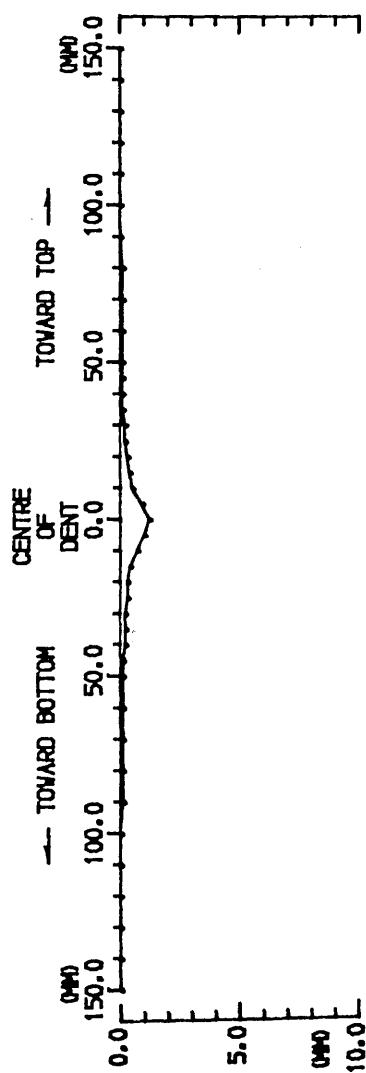
0 OVERALL BENDING DAMAGE (OUT-OF-STRAIGHTNESS)



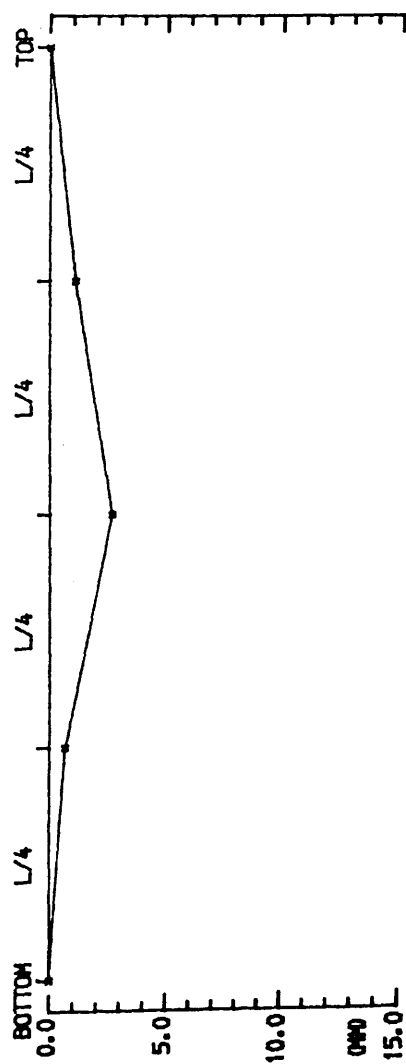
# EXTENT OF DAMAGE

MODEL : F3

0 LOCAL DENTING DAMAGE (DEPTH OF DENT)



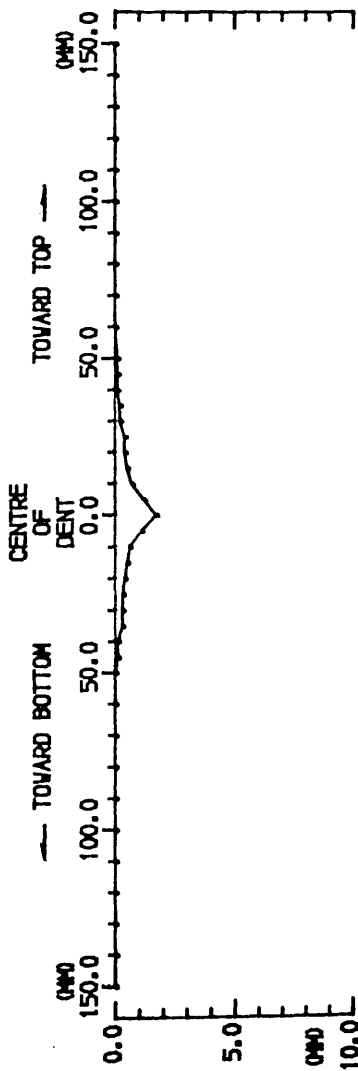
0 OVERALL BENDING DAMAGE (OUT-OF-STRAIGHTNESS)



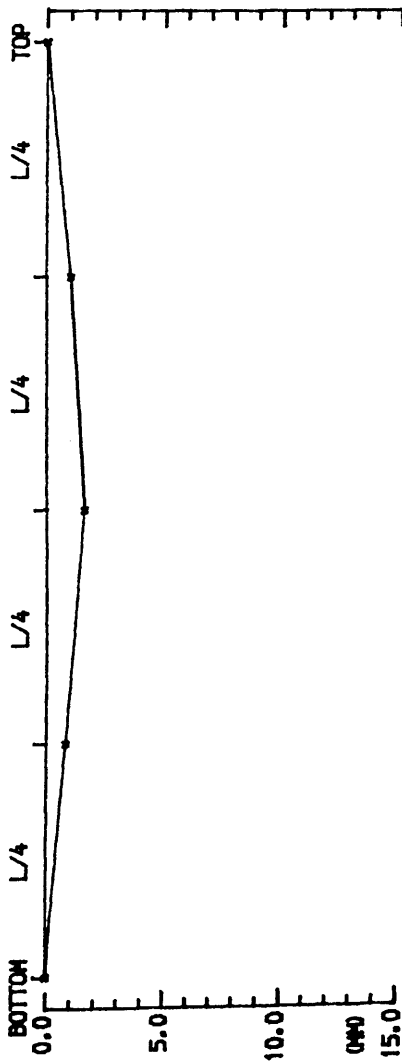
EXTENT OF DAMAGE

MODEL • G1

0 LOCAL DENTING DAMAGE (DEPTH OF DENT)



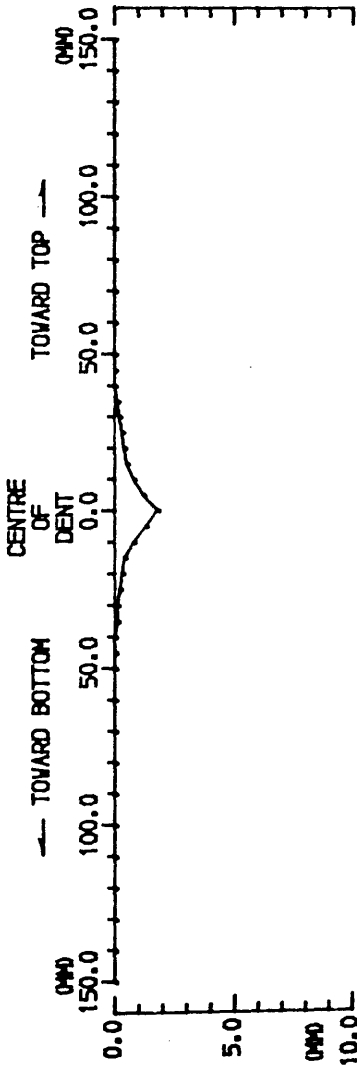
0 OVERALL BENDING DAMAGE (OUT-OF-STRAIGHTNESS)



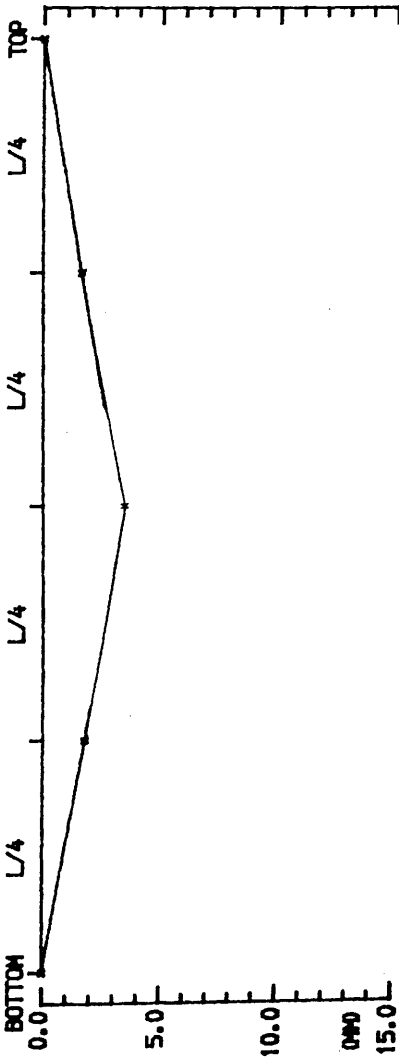
EXTENT OF DAMAGE

MODEL : G2

0 LOCAL DENTING DAMAGE (DEPTH OF DENT)



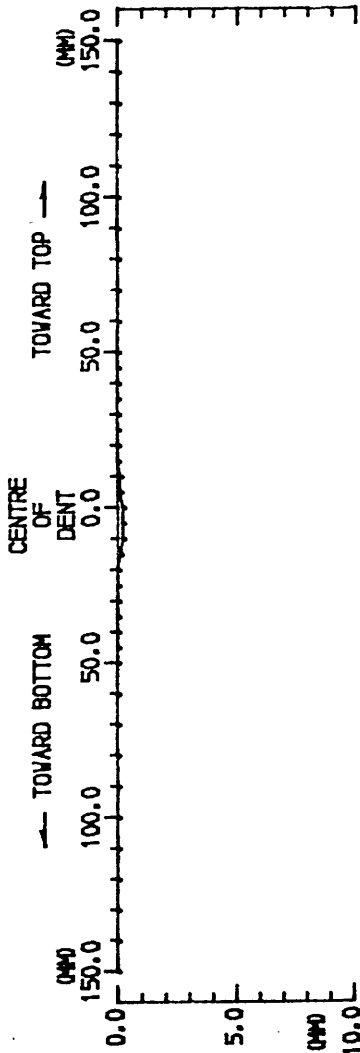
0 OVERALL BENDING DAMAGE (OUT-OF-STRAIGHTNESS)



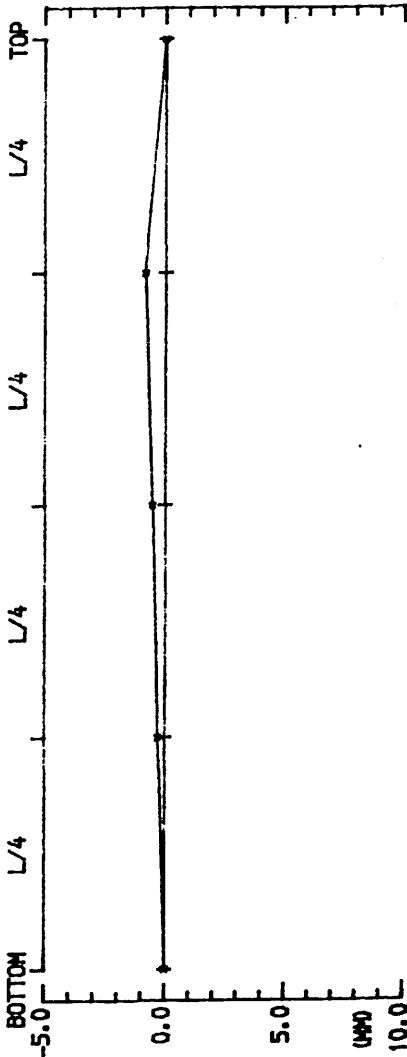
EXTENT OF DAMAGE

MODEL , G3

0 LOCAL DENTING DAMAGE (DEPTH OF DENT)



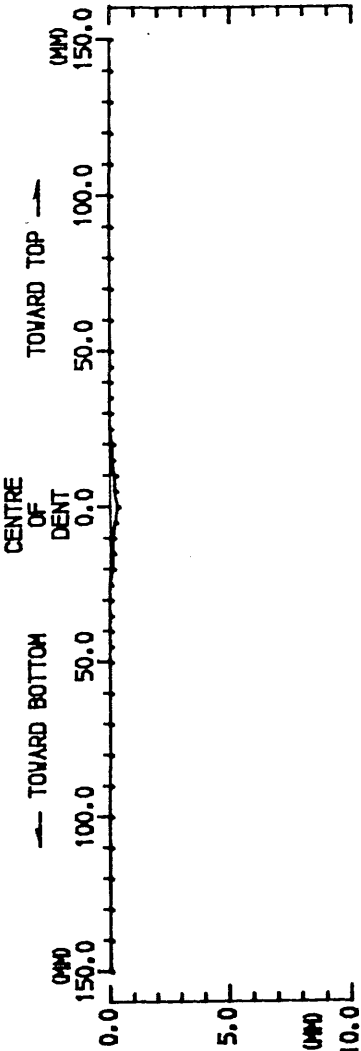
0 OVERALL BENDING DAMAGE (OUT-OF-STRAIGHTNESS)



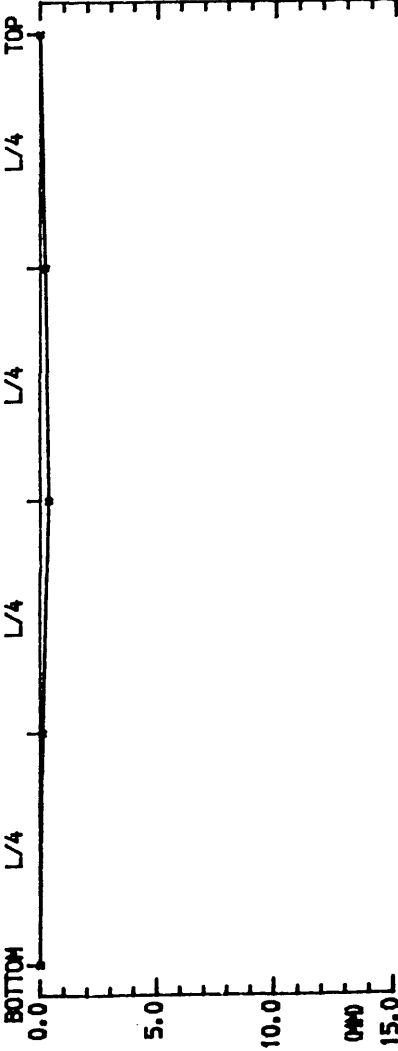
EXTENT OF DAMAGE

MODEL : H1

0 LOCAL DENTING DAMAGE (DEPTH OF DENT)



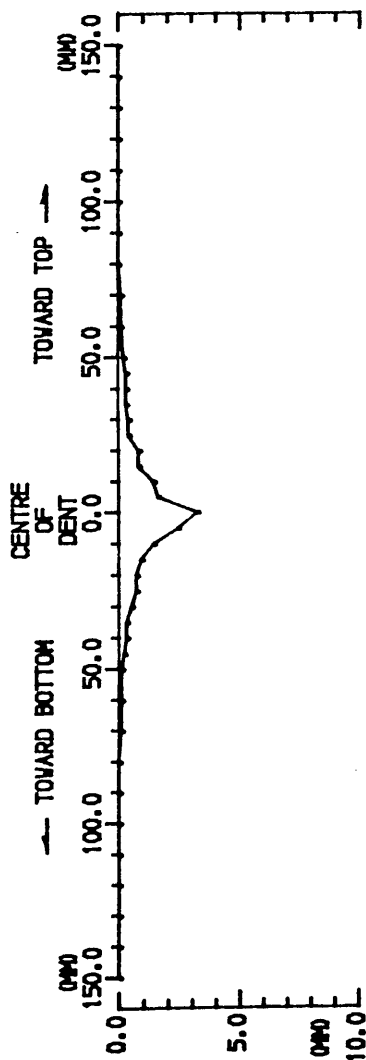
0 OVERALL BENDING DAMAGE (OUT-OF-STRAIGHTNESS)



EXTENT OF DAMAGE

MODEL . H2

0 LOCAL DENTING DAMAGE (DEPTH OF DENT)



0 OVERALL BENDING DAMAGE (OUT-OF-STRAIGHTNESS)

